National Library of Canada

Acquisitions and Bibliographic Services Branch

395 Wellington Street
Ottawa, Ontario
K1A 0N4

Bibliothèque nationale du Canada

Direction des acquisitions et des services bibliographiques

395, rue Wellington
Ottawa (Ontario)
K1A 0N4

Your file Votre référence

Our file Notre référence

NOTICE

The quality of this microform is heavily dependent upon the quality of the original thesis submitted for microfilming. Every effort has been made to ensure the highest quality of reproduction possible.

If pages are missing, contact the university which granted the degree.

Some pages may have indistinct print especially if the original pages were typed with a poor typewriter ribbon or if the university sent us an inferior photocopy.

AVIS

La qualité de cette microforme dépend grandement de la qualité de la thèse soumise au microfilmage. Nous avons tout fait pour assurer une qualité supérieure de reproduction.

S'il manque des pages, veuillez communiquer avec l'université qui a conféré le grade.

La qualité d'impression de certaines pages peut laisser à désirer, surtout si les pages originales ont été dactylographiées à l'aide d'un ruban usé ou si l'université nous a fait parvenir une photocopie de qualité inférieure.

Canada

THE HYDROGEOLOGICAL AND CONTAMINANT TRANSPORT PROPERTIES OF FRACTURED LEDA CLAY IN EASTERN ONTARIO

VINCE O'SHAUGHNESSY

A Thesis

Submitted under the supervision of

Dr. V. K. Garga P. Eng.

in partial fulfilment

of the requirement for the degree of

Master of Applied Science

Department of Civil Engineering
University of Ottawa
Ottawa, Ontario
Canada, K1N 6N5

The Master of Science Program in Civil Engineering is a joint program between the University of Ottawa and the Carleton University, which is administered by the Ottawa-Carleton Institute for Civil Engineering.

ISBN 0-315-82500-6

UNIVERSITÉ D'OTTAWA
UNIVERSITY OF OTTAWA

ABSTRACT

The objectives of the study were to investigate the hydraulic, geochemical and solute or contaminant transport properties of the upper fractured zone at four Leda clay deposits in Eastern Ontario. These four sites are known as NRC, Fallowfield, Renfrew and Casselman.

Physical conditions and depth of fractures of the Leda subsoil was investigated with the use of boreholes and test pits. Piezometers were installed using a conventional auger method and the double-Shelby method developed at the University of Waterloo. Hydrogeological aspects of the upper twelve metres were analyzed using water level fluctuations and variation profiles, hydraulic head and conductivity profiles. A geochemistry analysis was made by measuring the major ions and tritium concentration distribution in groundwater samples obtained from piezometers. Laboratory tests were performed on five Leda clay samples to determine the effective diffusion coefficients and the retardation factors of the major ions.

The results of the study indicated that the upper portion of Leda clay deposits within Eastern Ontario are fractured and hydraulically active. Fractured Leda clay deposits less than 12 metres in depth are highly questionable on their ability to protect any underlying aquifer from surficial or buried contaminants.

ACKNOWLEDGEMENTS

I would like to express my gratitude to my parents and family (Huguette, Maurice, and Marty) for their support, patience and for teaching me the value of a good education. I would like also to thank Dr. Bengt H. Fellenius and Dr. Vinod K. Garga for encouraging me to follow a career in geotechnical engineering. Special thanks are expressed to André D' Astous of Environ Eau, Norm Castonguay of Fondex Ltd., and John Loop of the Department of Geology at the University of Ottawa. Additional gratitude is expressed to Fondex Ltd. for the piezometer installation, and sharing the results of the grain size analysis and the Atterberg limits. My thanks are extended to the support staff of the Civil Engineering Department for their many contributions. Special thanks are expressed to my friends (André, Bob, Mike, Mark, Gille and Denis) for their support and encouragement.

SUMMARY

A large part of Eastern Ontario is covered by surficial Leda clay deposits which overlay many sand, gravel and bedrock aquifers. Leda clay deposits, a part of Champlain Sea clays, vary in thickness from a few metres to over 65 m in places but average 30 metres thick (Karrow, 1972).

Because of their low hydraulic conductivity, many natural clayey till deposits are considered a safe place for waste burial. The protection of the underlying aquifers from contamination is dependent on the nature of these clays. The amount of aquifer protection will depend on thickness, advective and diffusive properties of the clay deposit and most important, the penetration depth of hydraulically active fractures if fractures are present. The upper section of most glacial clayey till deposits in Canada are weathered and fractured. These fractures provide an effective pathway for contaminant migration. At present, little information is available on the hydraulic characteristics and solute or contaminant transport processes in fractured Leda clay deposits.

The objectives of the study were to investigate the hydraulic, geochemical and solute or contaminant transport properties of four Leda clay deposits in Eastern Ontario. These four sites are known as NRC, Fallowfield, Renfrew and Casselman.

The depth to which hydraulically active fractures penetrate are site specific and vary substantially, as revealed by literature review. Grisak and Cherry (1975) reported

hydraulically active fractures to depths of 8 to 10 metres below ground surface for a glaciolacustrine clay deposit in southeastern Manitoba. These clays showed visual evidence of weathering and fractures which extended to 10 metres. Day (1977) studied the clayey Lake Agassiz deposit near the Winnipeg area. He reported hydraulically active fractures which extend from the near ground surface to the till or aquifer at a depth of 10 to 15 m. However, no visual evidence of weathering and fractures were visible from vertical core samples in the bottom 2-4 m of the clayey till deposit. These observations suggest that widely spaced fractures may not be detectable by vertical boreholes.

Keller et al. (1986) performed a long term pumping test on a 18 m thick clayey till deposit which overlies a sand aquifer near Saskatoon, Saskatchewan. A rapid response was observed in all piezometers which indicated that vertical hydraulically active fractures existed throughout the entire clayey till aquitard. However, no visual evidence of fractured clay was observed in core samples collected at depth.

Studies by D'Astous et al. (1989) and Ruland et al. (1991) on a large clayey till deposit in southwestern Ontario demonstrated that vertical fractures can penetrate up to 10 metres depth. The formation of a complex fracture network in clay deposits by desiccation over a long period of time would result in deep widely spaced fractures (Masse et al., 1990).

Foster (1975) and Day (1977) were among the first to conclude that matrix diffusion can play a significant role in the rate and distribution patterns of solute or contaminants where advective transport of solute occurs along fractures. Mathematical models developed by Grisak and Pickens (1980),

Tang et al. (1981), Sudicky and Frind (1982) further acknowledged the strong attenuation capabilities of matrix diffusion process has on contaminant transport through fractured porous medium.

The environmental isotope tritium is often used to establish the depth at which groundwater is hydraulically active. However, many researchers have warned that the lack of tritiated groundwater at a depth does not indicate the absence of open fractures. Its absence could be due to matrix diffusion.

Physical conditions and depth of fractures of the Leda subsoil was investigated with the use of boreholes. In addition, visual inspection of the fracture network was possible at NRC and Fallowfield sites by excavated test pits. Piezometers were installed using the conventional auger method and the double-Shelby method developed at the University of Waterloo. Hydrogeological aspects of the upper 12.0 metres were analyzed using water level fluctuations and variation profiles, hydraulic head and conductivity profiles. The geochemical analysis was made by measuring the major ions and tritium concentration distribution in groundwater samples obtained from piezometers. Geochemical analysis was also performed by squeezing clay samples collected at the NRC site.

Test pits revealed a complex system of fractures, roots, root holes, paleoroots, pores and sand lenses. If these geological features are well interconnected and hydraulically active, they define the active groundwater zone. The many small sand lenses observed at Fallowfield, highly influenced the hydraulic properties of the upper clay. Well defined fractures below a depth of 1.1 m probably controlled the

hydraulic characteristics of the clay deposit at NRC. These fractures extend beyond the base of the test pit at 4.0 m. Fracture spacing steadily increased with increasing depth. The measured fracture spacing varied from one fracture every 40 mm at 1.5 m depth to one fracture every 400 mm at 3.5 m.

Results from water level monitoring, maximum seasonal variations and hydraulic head profiles revealed a highly hydraulically active zone at all four sites. However, the extent of this active zone varies from site to site. The active zone extends to 4.4 metres at NRC and Casselman, to 3.2 metres at Fallowfield, and to 6.0 metres at Renfrew. The highly active zone can be defined as a zone in which fractures are well interconnected, hydraulically active and which is usually easily intercepted by piezometers.

Slug test analysis indicated that hydraulic conductivity values in the upper active zone range from 1.85×10^{-8} to 2.05×10^{-5} m/s. In contrast, the hydraulic conductivity values measured in the deepest piezometers range from 8.20×10^{-10} to 1.40×10^{-9} m/s. This represents a difference of 1 to 4 orders of magnitude. The double-Shelby piezometer installation technique provided higher hydraulic conductivity values in the upper active zone. At greater depths, both types of piezometers gave similar results. Therefore, measured hydraulic conductivity values are highly dependent on the method of analysis used and can be grossly underestimated. Groundwater flow through the highly active zone was measured at rates of 70 to 220 l/h.

Measurements of fracture aperture were only possible through an indirect method, unlike fracture spacing which can be evaluated directly from excavated trenches. Based upon

results from the NRC site, calculated fracture apertures range from 10 to 50 μm. Fracture apertures also decrease with depth. Effective fractured porosities were also determined and varied from 1.02×10^{-4} to 6.22×10^{-4}. Groundwater velocities through Eastern Ontario Champlain Sea clay deposits are dependent on whether or not groundwater movement occurs through fractures. Fracture flow is prevalent in the upper near surface zone where groundwater velocities range from 0.10 to 4.8 m/d. Where intergranular flow occurs, velocities are between 1.11×10^{-6} m/d (0.4 mm/year) and 1.11×10^{-4} m/d (40 mm/year).

The geochemical analysis was best represented by trilinear Piper diagrams. Three hydrochemical facies were observed at the NRC, Fallowfield and Casselman sites while only one facie could be used to represent groundwater at Renfrew. This was probably due to surface salt contamination.

These hydrochemical facies were established for groundwater samples with respect to vertical depth only and were defined as follows:

1) a shallow "active" facie which represents groundwater that has undergone considerable chemical change from its original composition due to fresh water infiltration;

2) a deep "inactive" facie that represents deep groundwaters which did not interact with the near surface groundwaters. The deep groundwaters were completely different in chemical composition from near surface groundwaters. This hydrochemical facie may represent the initial groundwater chemical composition or was subjected to a geochemical change due to only an upward diffusion from the clay bedrock

interface to the upper hydraulic active zone (Desaulniers and Cherry, 1991), and;

3) Intermediate "transition" facie that represents a geochemical transition between the surface and deep groundwaters. This transition zone is usually influenced by fracture flow.

Two different laboratory test were performed on five Leda clay samples. One test involved the placement of a single salt solution (NaCl) in contact with a fully saturated undisturbed clay sample, thus allowing downward chemical migration throughout the sample by diffusion only. The second test involved the placement of deionized water in contact with the undisturbed saturated clay, thus allowing a upward chemical migration by diffusion only. During the testing period which ranged from 15 to 16 days, samples were taken from the source solution and analyzed for chemical species of interest (i.e. Cl^-, Na^+, K^+, Mg^{2+} and Ca^{2+}). At the termination of the test, the soil samples were sectioned to determine the porewater and adsorbed concentrations as a function of depth. From plotted "adsorption isotherms", retardation factors were evaluated and the diffusion coefficients were determined by "back-figuring", a finite differences procedure.

The single salt "adsorption isotherms" are essentially linear. Therefore, the retardation factors were not a function of solute concentration. The "distribution coefficient K_d" was evaluated to determine retardation. However, a concave nonlinear relationship was observed for the deionized water "adsorption isotherm". Thus, the retardation factors were a function of solute concentration.

Cl^- showed little variation in all soil tested from the three sites: Fallowfield, Renfrew, Casselman. The effective diffusion coefficient ranged from 7.0 to 6.0 x 10^{-6} cm^2/s.

Na^+ migration parameters determined from single salt tests samples from Fallowfield and Casselman sites, were in close agreement. Effective diffusion and retardation coefficients ranged from 6.5 to 5.8 x 10^{-6} cm^2/s and 2.22 to 3.60, respectively. Effective diffusion coefficients for Na^+ determined from deionized water tests were about 50% less than those determined from the single salt. This difference was due to increased competition between ion for exchange sites on clay particles.

Ca^{2+} and K^+ had the highest retention for both Renfrew and Fallowfield sites. Effective diffusion coefficients for K^+, Mg^{2+}, Ca^{2+} ranged from 6.0 to 7.5 x 10^{-6} cm^2/s, 3.8 to 4.6 x 10^{-6} cm^2/s and 5.8 to 6.25 x 10^{-6} cm^2/s, respectively. The Renfrew sample showed the highest retention capability since it had the largest CEC value.

Analytical profiles were fitted to the observed field data by using laboratory measured effective diffusion coefficients and retardation factors with advective parameters measured during field investigations. Two different analytical models were used in field simulations. The first model used the Ogata (1970) analytical solution which idealized the clay deposit as a massive homogeneous porous medium. The second model used the Sudicky and Frind (1982) analytical solution which idealized the clay deposit as having parallel, equally spaced vertical fractures with constant apertures.

These analytical models helped to better define the transition zone. The transition zone is usually influenced by fracture flow in which fractures become more widely spaced with increasing depth. Transition zone fracture apertures also decrease with increasing depth due to larger confining stresses. Nevertheless, the fracture network in the transition zone can be continuous and hydraulically active. The transition zone extends to at least 9.0 m at NRC, 7.5 m at Fallowfield, 10.0 m at Casselman and well below 12.0 m at Renfrew. However, the degree of activity within the transitional zone is not easily defined. It is a function of the probability of intercepting one or more fractures or sampling groundwater in close proximity to a fracture. For these reasons, the identification of the active, transition and "inactive" zones has to rely on several investigative techniques.

All field simulations assumed that all available solutes were able to migrate downward. However, some geochemical evidence indicates that strong lateral flushing of solutes has occurred. The geochemical evidence for lateral flushing is the lack of gypsum crystals in fractures, the relatively low sulfate concentration and low sodium exchange capacity in the upper active zone.

The analysis of hypothetical cases in which a surficial aquitard is fully penetrated by continuously open fractures have shown that a fracture network can be an effective pathway for the transport of contaminants to the underlying aquifer. If advective transport along the fractures occurs, penetration time for contaminant into a regional groundwater supply would sharply decrease compared to penetration time determined on the basis of advection and molecular diffusion in unfractured

clay. Even fractured clay deposits of 20 m thick may not protect the surrounding environment from toxic contaminants, especially if a strong hydraulic gradient is present at the site.

The results of the study indicate that surficial glacial clay deposits within eastern Ontario should be considered to be fractured unless demonstrated otherwise. Based upon field evidence, Champlain Sea clay deposits of less than 12.5 m (the maximum depth investigated) are highly questionable in their ability to protect any underlying aquifer from surficial or buried contaminants.

TABLE OF CONTENTS

CHAPTER CONTENTS

Page

Page

Page

Page

LIST OF TABLES

Page

LIST OF FIGURES

Page

CHAPTER 1
INTRODUCTION

1.1 General

Many existing and proposed landfill and waste disposal sites are and will continue to be built on clay deposits. The appropriateness of these sites depends upon the retention capabilities of the clay. Fractures within the clay can be effective pathways for contaminant movement. It is important to estimate the relative thickness of the hydraulically active fractures zone within these clay deposits.

Investigation of glacial clayey till deposits in the interior of Canada reveal that the upper portions are fractured and weathered (Cherry et al., 1975; Day, 1977). They are interconnected and hydraulically active. In the Plains Region, vertical fractures can be hydraulically active to large depths. In Southwestern Ontario and the Montreal area, hydraulic open fractures are usually limited to the upper 10 metres of the clayey till deposit.

In thick silty clay deposits, deep unweathered groundwater are Pleistocene in age, based upon isotopic studies. This would indicate the groundwater flow does not exist in these thick clayey till deposits. In some cases, the underlying unweathered zone behaves hydraulically like a fractured zone in which no apparent visible fractures were observed.

Groundwater in the upper zone typically contains significant levels of post-1952 tritium which is a diagnostic of groundwater recharge. Tritium profiles are useful tools in identifying deep hydraulically active fractures. However,

strong diffusive losses into the clay matrix would result in ^{3}H levels to decline below detection limits well above the depth to which fractures are open and active.

The factors which control fracture spacing and aperture size are still unknown. The consequence of this ignorance is that results are site-specific and should not be related to other areas. The accurate determination of the hydraulically active fractured zone is difficult since it is highly influenced by the method used in piezometer installation, piezometer design, presence of environmental isotopes and mathematical models used for analysis.

1.2 Statement of the Problem

In eastern Ontario, little is known about the hydrogeological behaviour of the upper weathered and fractured zone of the Champlain Sea clay also known as Leda clay. Since much of the reported behaviour of hydrogeological and contaminant transport in fractured clayey deposits have been produced for Southwestern Ontario and the Prairies Region, it is not appropriate to use these results for the Eastern Ontario region because of the different origins of the clay. Also, the depth of open and active fractures, fracture spacing and aperture size, distribution and transport characteristics are a function of the depositional mode, local stress history and environmental changes.

Champlain Sea clay is the most commonly found surficial geological material found in Eastern Ontario and it has been and will be used to contain municipal and industrial wastes. At present, little information is available on the migration of contaminants or solutes through Eastern Ontario clay

deposits. The assessment of the hydrological nature of these clays is an essential first step in the evaluation of potential landfill sites.

1.3 Objectives of the Investigation

The objectives of this research were:

1) to determine the depth of hydraulically active fractured zone at four different sites in Eastern Ontario in terms of hydraulic conductivity and geochemical profiles;

2) to assess the contaminant transport properties of fractured and unfractured Leda clay;

3) to determine the impact of hazardous wastes on the underlying aquifer and the surrounding environment.

1.4 Scope of the Investigation

Four sites located throughout Eastern Ontario within the Western Champlain Sea basin were selected for this research. Two principal sites were subjected to more extensive investigation and analysis. These were located at the National Research Council site in Gloucester and a farmer's field in Fallowfield, Ontario. The other sites were located in the vicinity of the Ottawa region, Renfrew and Casselman, Ontario.

Information on the geochemical and hydrogeological aspects of weathered and unweathered Leda clay was obtained at the principal sites. Here field work consisted of borehole

sampling, a large well pump test, the installation of 12 piezometers in which two different designs were used to evaluate the effects of smearing on the measured hydraulic conductivity values, and the excavation of a test pit for direct geological observation and measurements of fracture spacing and orientation.

The two complementary sites gave information on the geochemical and hydrogeological behaviour of the local clay. This was provided by borehole sampling and a piezometer nest installation.

To evaluate solute or contaminant transport through fractured and unfractured Leda clay, five laboratory tests were performed to evaluate the effective diffusion coefficients and retardation properties of major ions.

Simulation of solute transport through homogenous clay was modelled using the Ogata (1970) solution, for geochemical data obtained from purged piezometers. Also, geochemical and environmental tritium isotope concentration profiles were compared with theoretical curves generated by Sudicky and Frind (1982) analytical solution for a system of vertical parallel fractures.

Based upon field and laboratory investigations, four different scenarios were used to evaluate contaminant migration through fractured and homogeneous Champlain Sea clay and to define a minimum protective thickness of clay.

1.5 Outline of the Thesis

The material presented in this thesis is organized as follows:

* Historical review of field investigation with emphasis on hydrogeological and geochemical behaviour in fractured and unfractured clayey till deposits in Canada.

* Introduction of the basic transport equation for homogeneous saturated medium.

* Introduction of the solute transport equation for fractured media with emphasis on analytical solutions:
  (1) a single fracture using Tang et al. (1981)
  (2) a system of parallel fractures using Sudicky and Frind (1982).

* Controlling parameters for solute migration through fractured porous media.

* Background information on laboratory diffusion test in fully saturated soil for reactive and non reactive solutes.

* Methods of field and laboratory investigation.

* Description of field and laboratory data.

* Discussion of the results.

* Transport analysis.

* Conclusions.

CHAPTER 2

SOLUTE TRANSPORT IN CLAYEY TILL DEPOSITS: A LITERATURE REVIEW

2.1 Introduction

Clayey glacial deposits cover a large region of the interior of North America. These surficial deposits usually overly sand, gravel or bedrock aquifers. Glacial tills are divided into two main regions: The Interior Plain Region of Canada and The Eastern Region of Canada. The Interior Plain is comprised of the southern parts of Manitoba, Saskatchewan and Alberta; while the Eastern Region includes southern Ontario and the St. Lawrence lowlands of eastern Ontario and Quebec. These surficial deposits were formed by the retreat of glaciers and/or the sedimentation in large lakes of glacial meltwater which occurred between 9,500 and approximately 14,000 years ago.

2.1.1 Interior Plain Region

The Interior Plain region of Canada was the first to undergo an extensive field investigation on the nature of groundwater flow in clayey glacial till deposits (Meyboom, 1966; Lissey, 1968; and Rozkowski, 1967). They reported an active groundwater flow system existed in these deposits based upon several tests which included measurements of hydraulic head, mapping of surface salinity and vegetation, and obtaining geochemical profiles from installed piezometers. They did not attribute this activity to the possible presence of fractures even though the presence of vertical fractures was first

reported by Horberge (1952). Nor did Meyboom (1966), Lissey (1968), and Rozkowski (1967) distinguish between weathered and unweathered till deposits. Williams and Farvolden (1967) were the first to associate active groundwater flow regime to the presence of fractures in a weathered clayey till deposit in northeastern Illinois. A number of researchers (Gilliland, 1965; Freeze, 1969; Render, 1970; Vonhof, 1970; Cherry et al., 1971, 1973; and Sloan, 1972) have extended the preliminary work done by Williams and Farvolden (1967) to the Interior Plain. They confirmed that fractures are a integrated physical characteristic property of these types of deposits.

Cherry et al. (1971, 1973) studied a clayey till and clayey glaciolacustrine deposits in the southeastern part of Manitoba, known as the Whiteshell site. At this site, the sandy aquifer is overlaid by a 8-12 metre thick fractured clayey till deposit and the water table is within 3 metres of the surface. The study showed high bulk hydraulic conductivity and high groundwater sulfate content. These results were attributed to the presence of fractures.

A more intensive research on southeastern Manitoba fractured deposits was conducted by Grisak and Cherry (1975), Grisak (1975) and Grisak et al. (1976). From fresh excavated test pits, fractures were observed to a depth of 6.1 m and up to 9.1 m depth in Shelby-Tube samples. These fractures were generally coated with calcite, gypsum crystals or iron oxides. Fracture orientation was mostly vertical or near-vertical. Some fractures extended through several stratigraphic units, including non-till units such as lacustrine silts and clays, and to the underlying aquifer. This was indicated by the measured rapid response of the installed piezometers, when a long-term pumping test of the sandy aquifer was conducted.

A number of tests including the pump test, slug tests on individual piezometers and laboratory permeameter or consolidation tests on intact samples, indicated that the fractured clayey till has a bulk hydraulic conductivity of 10^{-9} m/s which is 2 orders of magnitude higher than the intergranular hydraulic conductivity. Thus, the fracture network controls the effective hydraulic conductivity rather than the intergranular pore spaces.

Grisak (1975) using the parallel plate model developed by Snow (1968) estimated the effective fracture porosity, excluding the intergranular pore spaces, to be between 10^{-4} to 10^{-3}, for the Whiteshell site, as compared to intergranular values ranging from 0.3 to 0.7. The calculated average fracture aperture width was of the order of 10^{-6} to 10^{-5} m. Grisak et al., (1976) estimated fracture flow using the Darcy equation with the Dupuit-Forchheimer assumption with representative values for the hydraulic conductivity K, gradient i, and effective porosity n. The fracture flow velocity ranged from 1.1×10^{-4} m/day (0.04 m/year) to 0.11 m/day (40 m/year) whereas the intergranular velocity through the pore spaces ranged from 1.4×10^{-8} m/d (5×10^{-6} m/year) to 1.4×10^{-6} m/d (5×10^{-4} m/year).

Cherry (1976) studied a proposed municipal landfill site near the City of Winnipeg, Manitoba. The Winnipeg area is underlain by a very permeable regional carbonate rock aquifer. At the proposed site, the bedrock aquifer is overlain by a 2-4 m silty grey till followed by a 12-15 m thick glacial lacustrine clay deposit. A strong downward hydraulic gradient exists throughout the till and clay due to the heavy pumping of the underlying aquifer (Render, 1970).

Results from hydraulic testing of the piezometers indicated that the clay and till exhibited a fractured medium hydraulic response. A geochemical analyses with depth for ^{3}H - tritium, ^{2}H - deuterium and ^{18}O - oxygen-18 was undertaken. Tritium was only detectable in the upper zone of the clay deposit within a maximum depth of 6 m. The concentrations of ^{18}O and ^{2}H typical of Pleistocene water were found at depth in the clay. Since this deposit is highly fractured with a strong downward gradient, high tritium concentrations were expected to be encountered at depth. Foster (1975) reported unusual low levels of tritium in the underlying fractured Chalk bedrock aquifer. He postulated that tritium diffused into the rock matrix and that this process has a great capacity for reducing solute concentration in fracture storage in fractured rock aquifer.

Day (1977) expanded the work done by Cherry to a larger area of Winnipeg. The single-well response tests analyzed by the method of Hvorslev (1951) for the Lake Agassiz and Upper Lake Agassiz deposits gave a mean hydraulic conductivity value of 1.84×10^{-9} m/s. The till deposits near Winnipeg gave a wider range of hydraulic conductivity due mainly to the variation in clay content. The reported average value was 1.5×10^{-7} m/s with a range between 2.5×10^{-10} and 6.4×10^{-7} m/s. Again, these values are several orders higher than the intergranular values measured by consolidation tests. These higher values are attributed to fractures.

The calculated average fracture spacing was 7 to 20 m^{-1} and estimated fracture aperture width ranged from 1.3×10^{-6} to 5.5×10^{-6} m in the clay and 1.4×10^{-6} to 5.0×10^{-6} m in the till. Based upon the Dupuit-Forachеimer assumption, the fracture flow velocities ranged from 0.013 m/d to 2.0 m/d as compared

to the intergranular flow velocities which ranged from 1.0 x 10^{-5} to 5.0 x 10^{-4} m/d.

Day (1977) also observed rapid depletion of tritium and oxygen-18 with depth which was not consistent with the groundwater flow regime (high fracture flow velocities). The simulated vertical profiles of tritium and other solutes using an analytical-numerical model demonstrated the strong attenuation capacity of matrix diffusion even at high fracture flow. Day concluded that diffusion exchange between fractures and the surrounding matrix is the major controlling mechanism of mass transport in fractured porous media of low permeability.

Thus, in predicting solute transport in porous fractured media it is important to consider the properties of both the fractures and the surrounding matrix. Also, the absence of tritiated groundwater at depth does not necessarily indicate the absence of fractures.

Keller (1985) and Keller et al. (1986) studied a site near Saskatoon, Saskatchewan, known as the Dalmeny site. The geology is as follows: 1 to 2 m of sandy, calcareous, brown and very fractured till covers the surface; this zone is underlain by a 10 to 12 m of clayey, silty, calcareous till which is olive to grey in colour. This unit is oxide stained and contains vertical and horizontal fractures spaced about 10 mm apart. Gypsum crystals are found in many fractures; this zone is followed by 6 to 8 m thick unweathered olive to dark grey till which shows no visual evidence of fractures or weathering; and overlies the regional sand aquifer. The weathered and unweathered zones form a stratigraphic unit. The unweathered till is well below the water table.

The aquifer was pumped for 3 days during which the till response was monitored by a detailed set of piezometers installed in both zones. A rapid response was observed in most piezometers including those in the unweathered till unit. This result indicated that the unweathered zone had a strong vertical hydraulic activity. This assumption was further supported by geochemical trends, tritium data, measured seepage fluxes from an ephemeral pond and slug tests which gave values exceeding the laboratory consolidation tests by two orders of magnitude.

The unweathered till at the Dalmeny site has a significant vertical and horizontal fracture permeability. The visual absence of weathered features in many vertical bore holes samples should not be regarded as evidence of a non-active fractured zone.

The Warman site is situated 15 km from the Dalmeny site. Here a large sand and gravel aquifer is protected by a 60 to 70 m thick greyish clayey till (Keller et al., 1989). The upper 5 to 8 m is weathered and oxidized to a pale olive to greyish brown colour. The water table fluctuates seasonally between 1.5 to 2.5 m below ground surface. In contrast to the Delmeny site, the unweathered zone is composed of two different stratigraphic units. The hydraulic properties of the Warman unoxidized tills showed no influence by fractures. The hydraulic conductivity measured on a variety of scales and techniques ranged from 10^{-11} to 10^{-10} m/s. Also, the environmental isotope analyses indicated a residence time from thousands to tens of thousands of years.

The Warman unweathered clayey till may provide good protection for the underlying aquifer against contamination from buried

and ground surface sources for thousands of years compared to the Dalmeny site. Since hydraulic conductive fractures are absent, or if they do exist, they are rare widely spaced and closed due to the large confining stresses.

Hendry (1988) studied three different areas of weathered and unweathered till deposits in southern Alberta. The groundwater flow regime was evaluated by using hydraulic and isotopic techniques which include (^{18}O), (^{2}H) and (^{3}H). The tested areas consisted of 9 to 18 m thick upper weathered zone which is underlain by 10 to 30 m thick unweathered zone. Fractures were only visible in core sample from the upper unit. Analysis of oxygen-18 and deuterium from ground and surface waters revealed minimum recharge of surficial waters to the underlying aquifer; tritiated groundwater was only found in the upper weathered zone. From hydraulic and tritium analysis, the vertical groundwater velocities due to fracture flow are about 0.1 m/year. Velocities range from 2 to 6 m per 1000 years in the unweathered zone. Again, the unweathered clayey till unit shows no evidence of hydraulically conductive fractures.

Van der Kamp et al. (1986) concluded after a 11 year pumping test, a clayey aquitard in southern Saskatchewan exhibited an unfractured flow regime. The maximum penetration of tritium was 5 m below the water table in the weathered zone.

Up to now, only the Dalmeny site has shown a hydraulically responsive fracture flow regime well below its defined weathered zone. This may be due to the rarity of open active fractures with depth or the investigative limitation in acquiring conclusive evidence of their existence.

2.1.2 Southern Ontario

The hydrogeologic nature of the Saint Clair clay plain region around Sarnia, Ontario, has been the main focus of work in Southern Ontario. This plain is relatively flat and covers an area of about 6000 km^2. The Sarnia deposit is composed of beds of silty clay till and fine-grained glaciolacustrine sediments which vary in thickness from 25 to 50 m, with 40 m as an average (Desaulnier et al., 1981). The underlying aquifer is composed of moderately permeable bedrock consisting of fractured Devonian limestone and shale (Sanford, 1973). The clay till is believed to comprise six till sheets of which only two are recognized as mappable units (Fitzerald et al., 1979). The upper till, known locally as the St.Joseph till, is generally 10 to 15 m thick which can be overlain locally by surface deposits of sand and gravel up to 1 m thick (Richards et al., 1984). The St-Joseph till was deposited around 13,000 years ago (Gavernor and Sterpavsky, 1976). This till is underlain by a 30 to 35 m thick silty-clay till containing abundant black shale clasts which is referred to as the Black Shale Till. Fullerton (1980) estimated the age of deposition of the Black Shale Till to be as old as 16,000 years. These tills are composed of 40 to 60% clay (typically 55-60%), 30-40% silt, 5-10% sand and usually less than 5% gravel (Harding, 1986). The mineralogy of the two tills is composed of mainly quartz and minor feldspar while the clay content is composed of abundant dioctahedral illite and trictahedral chlorite (Quigley and Ogunbadejo, 1976).

The water table fluctuates from 1 to 2 m below ground surface. The upper 4 to 6 m of the St.Joseph till has undergone extensive weathering by physical, geochemical and biological processes (D'Astous et al., 1989). Oxidation of the upper

zone has created a very stiff to hard, brown, fissured crust. Desaulnier (1980, 1986) observed vertical fractures to depths of 5 metres in many test pits. Many of these were filled with secondary mineralization of very fine to coarse grained gypsum. Adams (1969) and Rodvang (1987) reported fractures to depths of more than 9 metres in drill core samples. Also, Hanna (1966) observed root holes as deep as 9 metres. Adams (1969) noted variation in the thickness of the weathered zone beneath forested areas in Lambton county due to water removal by deep rooted trees.

Quigley and Ogunbadejo (1976) reported that the clay minerals in Lambton county's clay crust had undergone chemical alteration. The iron chlorite had been destroyed by oxidation to produce up to 15% smectite (swelling clay), and the carbonate content decreased due to fresh water leaching. The intensity and spacing of fractures decreased with depth. A fracture spacing of 14 cm was encountered at 1.5 m depth, while spacing ranged from 0.6 to 1.2 m at 4.6 m depth. The fissures were in nearly two vertical sets oriented more or less at right angles to each other.

Desaulniers et al. (1981) were the first to report an active zone of groundwater circulation in the upper 3 to 5 m due to fractures and deep root holes. This conclusion was based upon hydraulic-head, major-ion and isotopic (oxygen-18, tritium) profiles. Oxygen-18 composition similar to present day atmospheric precipitation and post-1952 tritium levels occurred predominately in the upper fractured till zone. An abrupt change in vertical gradient indicated the bottom of the active zone.

The initial laboratory hydraulic conductivity measurements performed by Desaulniers et al. (1981), Richards et al. (1984) and Harding (1986) in the weathered zone on core samples, and initial recovery data from conventional piezometers gave values similar to those found in the unweathered zone. The measured hydraulic conductivity was of the order of 10^{-10} m/s. These low values for the weathered zone were attributed to the combined effect of smearing of the borehole during drilling and fracture spacing (Bruce, 1987; D'Astous et al., 1989).

A more intensive investigation into properties of the weathered zone near Sarnia was carried out by Ruland et al. (1991) and D'Astous et al. (1989). In order to expose the numerous fissures, D'Astous et al. (1989) had to remove manually the smear and shear zone. Results from a large-diameter well tracer test and some overcored piezometers gave hydraulic conductivities in the range of 10^{-9} to 10^{-7} m/s. These values are 100 and 1,000 times greater than those of unfractured clay and are similar to those documented for the Prairies region.

D'Astous et al. (1989) estimated the average fracture aperture using the Navier-Stokes equation from tracer experiments. It was assumed that each collector was intersected by only one fracture. They reported values of 0.30 and 0.54 millimetres for the shallowest and deepest collectors, respectively. Observations from excavated trenches, indicated fracture spacing to be 5, 10, 30 cm at depths of 2, 3, 4 metres, respectively. Based upon an average hydraulic conductivity of 6.3×10^{-8} m/s and the above spacings, the effective porosity ranged from 2.3×10^{-4} to 7.5×10^{-4} based upon Snow's equation. D'Astous et al. (1989) concluded that fractures and fossil root holes are effective pathways for groundwater flow

and that high volumetric flow can occur even when fracture widths are small. The depth of this activity ranges from 3 to 6 m.

Ruland et al. (1991) obtained tritium profiles with depth for 12 different sites around Sarnia. Post-1952 tritium level greater than 1 T.U. (tritium unit), [1 T.U. represents one ^{3}H atom in 10^{18} atoms of normal hydrogen (^{1}H)], were found at depths ranging from 7.5 to 12 m. Ruland et al. (1991) inferred that tritium probably migrated 1 to 2 metres from the base of open fractures by molecular diffusion.

Ruland (1988) and D'Astous et al. (1989) found that the degree of hydraulic activity in the upper zone can be obtained by correlating water level fluctuations recorded in piezometers with seasonal variations in precipitation. Ruland et al. (1991) proposed that seasonal water level fluctuations greater than 50 cm were caused by fractures. Based upon tritium profiles and water level fluctuations, Ruland (1988) reported that fractures varied from 5 m to more than 10 m in depth at the 12 sites in Lambton County. Direct evidence of fracture flow was observed in test pits at the Tricil site, where water flowed through fractures at rates up to 90 l/h (Ruland, 1988; D'Astous et al., 1989). They recommended that environmental isotopes, tritium and seasonal water level fluctuations are useful tools for evaluation of maximum depth of active fracture flow.

Many municipal landfills and a large landfill for hazardous industrial wastes are located on the St.Clair clay plain. Site specific studies of contaminant migration in Lampton County were first reported in 1977. In order to provide an adequate barrier between the wastes and the underlying

hydrogeologic domain, it is important to determine the contaminant migration characteristics. Goodall and Quigley (1977) investigated the transport of inorganic ions (Ca^{2+}, Mg^{2+}, Na^{+} and K^{+}) below two sanitary landfill sites in Lampton county: Confederation Road and the Blackwell Road. The Confederation Road site is founded on unfissured and intact grey clay below the weathered zone. Analysis from clay core samples taken below the waste suggested that chemical diffusion was the dominant cause of ion migration. The Blackwell Road site is situated on fissured and weathered brown clay crust. Here, Goodall and Quigley (1977) had limited success in fitting a diffusion only model to their data, since vertical fractures had strongly influenced the downward migration of contaminants. Their conclusions were in agreement with results from the western prairie regions reported by Day (1977).

The concentration profiles of sodium and chloride below the Confederation Road site have migrated to a maximum depth of 1.5 metres in 15 years as compared to the estimated advective or seepage concentration fronts of 3 to 5 cm. Heavy metals have migrated only 10 cm indicating rapid field attenuation (Quigley and Rowe, 1986). Also, Yanful and Quigley (1990) evaluated the migration of environmental isotopes such as tritium, oxygen-18 and deuterium below this landfill site. These isotopes are considered conservative since they do not interact with the surrounding soil. Oxygen-18 and deuterium have migrated to a depth of 2.3 metres in a 16 year time period.

Johnson et al. (1989) obtained vertical core samples beneath a 5 year old hazardous waste landfill site operated by Tricil limited located 15 km southwest of Sarnia. The profiles of

chloride and volatile organic compounds obtained in the 40 metres thick unfissured clay were indicative of downward diffusion with no advective influence. The maximum penetration depths of waste-derived chloride and volatile organic compounds were 0.83 m and 0.15 m, respectively. Also, Johnson et al. (1989) predicted that it would take more than 1000 years for waste derived contaminants to reach the underlying aquifer due to the large thickness of the clay barrier.

Recent work by Barone et al. (1991) again indicates that in clay deposits of low hydraulic conductivity or when advective transport is minimal, a contaminant can migrate significantly by simple Fickian diffusion.

Desaulnier (1986) studied the migration of naturally-occurring solutes in these clay deposits. Isotopes and chloride have developed upward-directed concentration profiles. These profiles are consistent with simulation of one-dimensional diffusion models and diffusion times of 12000 to 16000 years. Even though an appreciable downward gradient exists in the unweathered clay till, Desaulnier et al. (1986) proposed that the natural gradient was not large enough to exceed threshold gradients necessary to cause advective flow. Solute or contaminant transport in thick unfractured clay deposits in southern Ontario is a function of the diffusive rate of each species.

A general conclusion based upon these studies is that the thick regional unweathered clay deposit will protect the underlying aquifer from pollution for thousands of years. This assumes that the maximum depth of active hydraulic fractures or groundwater regime is no greater than 10 metres.

This generalization may introduce some uncertainty since all field information pertaining to the unweathered zone has been acquired from vertical boreholes, (core samples and piezometers) which have low probability of intersecting sets of widely spaced fractures (Ruland et al., 1991).

2.1.3 Montreal Region

In Eastern Canada, the Champlain Sea occupied much of the upper St. Lawrence River valley during the late Pleistocene period. This sea was a mixture of fresh and ocean waters. Clay deposits were formed 12,000 years ago as a result of the inland sea. Champlain Sea clay can be as thick as 65 m in places but averages about 30 m (Karrow, 1972). The Champlain Sea sediments are composed of very fine-grained rock flour derived from the Precambrian Shield. The clay mineralogy is composed of an abundance of illite-mica, chlorite and amphibole with small amounts of smectite (Quigley, 1980). Lafleur and Geroux (1983) established for the Montreal region that the upper-zone is now weathered to a depth of 5 m. This zone is active due to fracturing which permits appreciable amounts of groundwater flow. Lafleur et al. (1987) established the hydraulic conductivity of the weathered zone by packer-injection tests in vertical auger holes to be 2 to 4 orders of magnitude higher than that of the unfractured clay beneath this zone. The packer-injection assembly allows the smears zone on the borehole wall caused by augering process to be removed, exposing fractures to the injection test. The unweathered clay has a hydraulic conductivity that ranges from 10^{-11} to 10^{-10} m/s (Tavenas et al., 1983). These deposits have low hydraulic gradients, usually less than 0.1. With low permeability in the unfractured zone, groundwater flow is very

slow (Quigley et al., 1983); Lafleur and Lefebvre, 1980); and Lafleur and Giroux, 1983).

Quigley et al. (1983) and Desaulnier and Cherry (1989) concluded that major-ions and isotopes migration in the thick unfissured clay was predominately by molecular diffusion with no advection. This conclusion was based upon the observation that the original solute concentrations in the porewater were the same as in the Champlain Sea. When the sea retreated, leaching of the upper zone occurred due to infiltration of fresh water (rain and snow). Major ions began to diffuse upwards against the hydraulic gradient which resulted in a gradual increase in concentration with depth. Based upon the one-dimensional diffusive model, Desaulnier and Cherry (1989) predicted that several tens of thousands of years will pass before the vertical distribution of natural solutes in the clay will achieve a steady state.

2.1.4 Eastern Ontario

In Eastern Ontario, only a few research studies have been conducted on the hydrogeological and contaminant transport properties of the weathered, fractured zone of the Champlain Sea Clay also known as Leda Clay. In fact, the Leda Clay has been studied mostly for its geotechnical properties.

Quigley et al. (1989) have undertaken an evaluation on the effect of domestic waste leachate on the hydraulic conductivity of the clay. Three samples in the upper zone were taken at three different locations in the Ottawa-Carleton region. The NRC sample (Montreal road) taken at 1.14 m depth was particularly heavily fractured. By means of laboratory consolidation tests, measured hydraulic conductivity gave

values ranging from 2 x 10^{-10} to 1 x 10^{-7} m/s. The larger value is characteristic of the heavily fractured clay sample. Quigley et al.(1989) indicated that the geotechnical behaviour of Leda clay can be associated with its depositional mode. Fransham and Gadd (1977) established that four different types of deposition environment existed for Leda clay throughout eastern Ontario.

Much of the literature on the hydrogeological properties and contaminant behaviour in fractured clayey deposits have been produced for southwestern Ontario and the Prairies region. Although many of the studies in these regions showed that fracture flow occurs in the unweathered clay up to and exceeding 10 metres depth, it is not correct to use these results for the eastern Ontario clay region because of the different origins of the clay. The Champlain Sea clay is the most commonly foun surficial geological material in eastern Ontario. It has been and will be used to contain municipal and industrial wastes. At present little information is available on the groundwater transport mechanisms through the deposit.

2.2 Geochemical Studies (Hydrogeochemistry of Clayey Till)

The weathered zones of clayey deposits in Western Canada and Southern Ontario, contain relatively high concentration of sulfate (SO_4^{2-}) in the groundwater. Gypsum crystals ($CaSO_4*2H_2O$) are commonly found in fractures.

Sulfate concentrations in the Western Prairies Region of Canada are in the range of 1,000 to 10,000 mg/l, Cherry (1972). But in the unweathered zone, sulfate concentrations are much lower and gypsum and selenite are generally absent.

Henry et al. (1986) studied a fractured till in Southern Alberta, and postulated that sulfate generation was due to the oxidation of very small amounts of solid-phase reduced organic and inorganic sulfur, primarily organic. Oxidation commenced after glacial retreat about 10,000 years ago which exposed the surface to the atmosphere. The infusion of atmospheric oxygen into the weathered zone was most predominant during the dry Altithermal climatic period between 11,000 to 3,000 years BP. This episode lowered the present day water table allowing deeper penetration of oxygen through the fracture network.

Work done by Keller (1987), Keller et al. (1988), Mermut and Arshad (1987) on Saskatchewan tills indicated that oxidation of sulfide minerals such as pyrite (FeS_2) was the predominant source of sulfate. But recent work by Hendry et al. (1989) on oxygen and sulfur isotopes from dissolved sulfate implied that most of the oxygen in sulfates was obtained from groundwaters.

In the weathered tills of Southern Ontario, sulfate is the dominant major-ion but gypsum and selenite crystals in fractures are not ubiquitous as they are in the Plains Region. Results of oxygen and sulfur isotopes from dissolved sulfates in the Sarnia clay plain indicated that the weathered zone (SO_4^{2-}) has been produced by oxidation of solid-phase sulfur, primarily sulfide minerals (Abbott, 1987).

This oxidation process can be approximated by the stoichiometry of pyrite oxidation:

$$FeS_2 + (7/2)O_2 + H_2O = Fe^{2+} + 2SO_4^{2-} + 2H^+$$

Also, sharp drops in sulfate concentration in the unweathered zone can be attributed to sulfate reduction by sulfate

reducing bacteria. The bacteria consumes dissolved SO_4^{2-} and produces HS^- and CO_2. The equation for this reaction can be written as:

$$2CH_2O + SO_4^{2-} = HS^- + 2HCO_3^- + H^+$$

where CH_2O represents organic matter. If this reaction occurs in a calcite and dolomite rich environment, the CO_2 causes calcite to dissolve until calcite and dolomite saturation is attained and buffers the pH in the range of 7 to 8. From Stumm and Morgan (1979), the overall reaction equation can be represented by:

$$2CH_2O + SO_4^{2-} + (1/2)CaCO_3(s) + (1/4)CaMg(CO_3)_2(s) =$$

$$3HCO_3^- + (3/4)Ca^{2+} + (1/4)Mg^{2+} + HS^-$$

2.2.1 Spatial Variability

Keller et al. (1991) reported for the Dalmeny Site, Saskatchewan, that the pattern of hydrogeochemistry was one of dominantly lateral variability (unleached/high sulfate zone adjacent to leached/bicarbonate zone). This was in contrast to the two vertical layered system described by Hendry et al. (1986), where the high-sulfate oxidized till overlies the low-sulfate till. They proposed that two dominant types of hydrogeochemical evolution occur in clayey tills. The first is dominantly a lateral chemical differentiation which occurs in till deposits of less than 20 m in thickness with relatively large vertical permiabilities. The second type is dominantly a vertical chemical differentiation which occurs in thick deposits where vertical permeability is small.

Sulfate genesis is important since it may contribute to the reduction of the bulk volume of the clay fraction through cation exchange involving Na^{+}, Mg^{2+} and Ca^{2+} which may promote fracture development (Henry et al., 1986). Also, since high concentrations of sulfate are generated in the weathered fissured zone, it may serve as a natural tracer for estimating the depth of active zone and/or identifying the extent of contaminant migration in the fractured porous zone and beyond.

2.3 Depth of the Active Zone (Fractures)

The major problem as stated by many researchers is the determination of active fractures below the observable weathered zone. The detection or identification of hydraulically active fractures is usually hampered by investigative techniques and their geological nature. Assessing the depth of active hydrogeological zone is an important parameter in the qualification of solute or contamination migration processes in the weathered and unweathered zones. To estimate the maximum depth of hydraulically-active fractures in the Sarnia clay, (Ruland et al., 1991) proposed that tritium analysis of water samples from piezometers nests installed at various depths and the monitoring of seasonal water level fluctuations be used. Prior to above-ground nuclear testing which started in 1952, background levels of atmospheric tritium in Ontario were low, about 3 to 5 T.U. (Robertson and Cherry, 1989). By 1963 at the end of atomic testing, the measured tritium concentration in the precipitation had increased to several thousands T.U. Since the radioactive decay constant used for tritium is based on a half life of 12.43 years, (Mann et al., 1982), groundwater that has recharged prior to 1952 is expected to have tritium levels below 1.0 T.U.. Therefore, water samples

with tritium values greater than 1 T.U. indicates that some mixing of post 1952 precipitation has occurred.

Using tritium analysis coupled with measured seasonal variation, Ruland et al. (1991) noted that high tritium levels found below the visible weathered zone were associated with relatively large seasonal water level variations, even at depths of 10 m. This result indicated that installed piezometers intersected fractures or were close to fractures. Ruland and co-workers developed a conceptual model in which tritiated heavy rain waters quickly travelled downward through the open dry fractures. The drying of open fractures occurs during dry summer periods when water consumption by evapotranspiration is intense. The sudden flooding of deep dry open fractures will result the diffusion of tritium into the surrounding clay matrix between the fractures, as illustrated in Figure 2.0. Thus, ^{3}H levels in the matrix in which a piezometer is install may provide the evidence for the existence of active fractures. Detectable tritium levels may occur at distances of 1-2 metres from each fracture.

It is important to realize that a piezometer in the clay matrix, even near a fracture, may not have a high hydraulic conductivity value nor show rapid water level response as expected for a piezometer in a zone of active groundwater flow. Also, using only tritium values to infer maximum depth of hydraulically-active fractures is not absolutely correct. Since advection-diffusion processes may cause ^{3}H level to decline below its detection limit well above the depth to which fractures are open and active.

2.4 Piezometer Design and Installation

In the Western Prairie Region of Canada, the piezometer used was a standard standpipe with a permeable tip at the bottom. The installation of the piezometer was achieved by augered boreholes. The hydrologic response, water level fluctuations and hydraulic conductivity in the weathered zone seem to be unaffected by the smearing created by the augering process. Because the fractures are well interconnected and open, borehole reaming to remove smear is not necessary.

In contrast to the Prairie Region, southern Ontario and the Montreal Regions, standard piezometer installation in the weathered zone by augured boreholes rarely showed evidence of hydraulically connected fractures. Lafleur et al. (1987) related the low values of permeability in the weathered zone to the strong influence of smearing. They overcame the boreholes smear problem by means of the reaming and packer-test apparatus. Bruce (1987) and D'Astous et al. (1989) proposed a new method of piezometer installation which minimized the smear and shear zone along the borehole wall caused by drilling. After the initial drilling of the borehole is completed, a cylindrical hole is created at the bottom for the placement of a permeable piezometer tip. This is done by a double-Shelby tube core sampling process, known as the double-Shelby method. The double-Shelby method consists of hydraulically pushing a Shelby tube which is bevelled on the outside, through the centre of the borehole and then removing it. A second but larger Shelby tube is then hydraulically pushed around the first Shelby hole. The void created by the first Shelby tube makes the insertion of the second one easier. The second Shelby tube removes any potentially disturbed zone created by the first Shelby tube.

The second Shelby tube is bevelled on the inside to force the clay cuttings inward during insertion. This minimizes the smear zone around the edges of the hole which allows interconnected fractures to be exposed to the piezometer tip. Early results reported by D'Astous et al. (1989) indicated that the double-Shelby method provided higher hydraulic response than the conventional auger hole method and thus is considered a major improvement. However the level of hydraulic interference caused by this new method is still unknown.

2.5 Theoretical Background

This section discusses the theoretical background to field investigations. These aspects include: hydraulic conductivity, flow velocity in clay, estimation of fracture flow velocities, mass transport of solutes and controlling parameters for solute migration through fractured media.

2.5.1 Hydraulic Conductivity

As seen in the first section of this chapter, accurate determination of the hydraulic conductivity values for fractured and unfractured clayey till deposits are essential. Many researchers have obtained hydraulic conductivity values from laboratory tests, (e.g., Law and Lee, 1981; Tavenas et al., 1983) and/or from single-piezometer response "slug" tests (e.g., Schwartz, 1975; Hendry, 1988; Herzog et al., 1989; D'Astous et al., 1989; and Keller et al., 1989). Accuracy of these tests was directly dependent on the interception of major conductors in clayey till deposits (Keller et al., 1989).

2.5.1.1 Slug Test (Single-Well Response Test)

The single-well response test is the most direct field test method to obtain hydraulic conductivity (K) values, but can only yield values of K, in the vicinity of the permeable tip (well screen). This test involves either bailing or adding water to the piezometer with monitoring of subsequent water level. The analysis of the data can be performed by many procedures as described by Hvorslev (1951), Cooper et al. (1967), Bouwer and Rice (1976) and others. The hydraulic conductivity values from field piezometer slug tests (bailing

of water) are very dependent on installation disturbance, condition of the well screen and sand pack. These tend to reduce the measured K value, (Day, 1977; D'Astous et al., 1989). Thus, hydraulic conductivity values calculated by these methods should generally be considered a minimum.

The analytical method of Cooper et al. (1967) for evaluation of hydraulic conductivity incorporates the storage capacity of the deposit, while the methods of Hvorslev (1951) and Bouwer and Rice (1976) do not. The major difference between the Hvorslev and Bouwer and Rice Methods is the treatment of the effect of the well configuration on the well response. Hvorslev's "shape factors" are based purely upon an analytical approach while Bouwer and Rice use an "effective radius" based upon an electrical resistance network analogue.

In this research, piezometer slug tests results were evaluated using the Hvorslev method with the Bouwer and Rice method as a check. Analysis of results from the pumping test on the two large wells was performed using the Bouwer and Rice (1976) and the Boast and Kirkham (1971) methods. The Hvorslev method allows for quasi-three dimensional response thus allowing a vertical flow component which might exist in a fractured media (Keller et al., 1989).

2.5.1.2 Summary of the Hvorslev Method

The Hvorslev Method assumes that Darcy's Law is valid and that water and soil are incompressible. After the water level is lowered or raised in the piezometer, water will flow into or out of the standpipe through the permeable tip. The water will gradually reestablish equilibrium with the original

potentiometric surface. Basic parameters of a slug test are given in Figure 2.1.

When corrections for piezometer design are taken into account, the recovering rate is proportional to the hydraulic conductivity of the surrounding deposit. These corrections are called Hvorslev's "shape factors".

The corresponding flow into the piezometer, after removal of a slugged volume of water, can be expressed as:

$$Q = FKH = FK(z-y) \qquad (2.1)$$

where F is the shape factor dependent on the shape and dimensions of the piezometer intake; K is the hydraulic conductivity; H is the active head; z is the distance from the potentiometric surface to the water level in the piezometer at t=0 and y is the change in water level in the piezometer after t=0. Disregard of frictional losses caused by the well casing and screen, the volume of flow during an increment of time, dt is determined as:

$$Qdt = Ady \qquad (2.2)$$

where A represents the cross-sectional area of the piezometer. Substitution of equation 2.2 into equation 2.1 results in:

$$\frac{dy}{(z-y)} = \frac{FK}{A}dt \qquad (2.3)$$

The volume of flow, V, required to equalize the active head is:

$$V = AH \tag{2.4}$$

Hvorslev (1951) defines the basic time lag, TL, as the time required for the equalization of the induced pressure difference (H) while the initial flow rate is maintained. That is:

$$TL = \frac{V}{Q} = \frac{AH}{FKH} = \frac{A}{FK} \tag{2.5}$$

and equation 2.3 may then be rewritten as:

$$\frac{dy}{(z-y)} = \frac{dt}{TL} \tag{2.6}$$

Equation (2.6) is the basic differential equation for hydrostatic time lag with the solution:

$$TL = \frac{-t}{\ln(\frac{z-y}{z})} = \frac{-t}{\ln(\frac{H}{H_o})} \tag{2.7}$$

To calculate the basic time lag, the computed ratio H/H_o is plotted versus time on semilogarithmic graph paper, as shown in Figure 2.2. The basic time lag is the time required for 37 percent recovery of the initial water level or active head since $\ln(0.37) = -1$, TL = t at this point. The hydraulic conductivity is calculated by rearranging equation 2.5 as:

$$K = \frac{A}{FT} \tag{2.8}$$

Four different piezometer designs are given in Figure 2.3 as well as their corresponding equations, developed by Hvorslev (1951.) Piezometer design used in this study is represented in Figure 2.3c. Where the length of the piezometer was more than 8 times the radius of the well screen including the permeable sand pack (L/R > 8). Thus, the following formula was applied:

$$K = \frac{r^2 \ln(L/R)}{2LTL} \qquad (2.9)$$

where r is the radius of the piezometer; R is the radius of the well screen and sand pack and L is the length of the well screen. A limitation of Hvorslev's equations is that they are not valid when the sand pack extends above the well screen.

2.5.1.3 Bouwer and Rice Slug Test Theory

The geometry and symbols for the Bouwer and Rice slug test are given in Figure 2.4. The rate of flow of water into the piezometer is based upon the Thiem equation which states:

$$Q = 2\pi KL \frac{y}{\ln(R_e/r_w)} \qquad (2.10)$$

where Q is the volumetric flow rate into the piezometer; K is the hydraulic conductivity; L is the length of well screen; y is the water level difference between the piezometer and the water table; R_e is the effective radial distance over which y is dissipated; and r_w is the radial distance of undisturbed portion of the clay from piezometer center line. After the quick removal of a volume of water from the piezometer, the

corresponding rate of rise dy/dt of the water can be expressed as:

$$\frac{dy}{dt} = \frac{-Q}{\pi r^2} \qquad (2.11)$$

where r is the radius of the piezometer. An equivalent value of r should be used when water level recovery is taken place within the well screen or open section. This value takes into account the porosity and thickness of the sand or gravel pack. After solving equation 2.11 for Q and substituting the result into equation 2.10, and solving it in terms of K yields:

$$K = \frac{r^2 \ln(R_e/r_w)}{2L} \frac{1}{t} \ln \frac{Y_o}{Y_t} \qquad (2.12)$$

where Y_o = y at time zero; and Y_t = y at time t.

Bouwer and Rice used an electrical resistance network analog to determine R_e values for different values of r_w, L, L_w and H as defined in Figure 2.4. The results were then expressed in terms of the dimensionless ratio $\ln(R_e/r_w)$. Two equations were developed, one when $L_w < H$, and the other when $L_w = H$. They were, respectively:

$$\ln \frac{R_e}{r_w} = \left[\frac{1.1}{\ln(L_w/r_w)} + \frac{A+B\ln[(H-L_w)/r_w]}{L/r_w} \right]^{-1} \quad L_w < H \qquad (2.13)$$

and

$$\ln \frac{R_e}{r_w} = \left[\frac{1.1}{\ln(L_w/r_w)} + \frac{C}{L/r_w} \right]^{-1} \quad L_w = H \qquad (2.14)$$

The dimensionless numbers A, B and C are a function of L/r_w and are evaluated from Figure 2.5.

The term $\ln(Y_o/Y_t)/t$ in equation 2.12 is taken as the slope of the best-fitting line through the y versus t points plotted on semilogarithmic paper, as illustrated in Figure 2.6. Since recovery rate slows as the water level reaches equilibrium, data points tend to deviate from the initial established trend. Thus, only the early straight line portion of graph should be used to calculate the hydraulic conductivity value. The Bouwer and Rice Method is applicable provided the geometric factor R_e has been established. Erroneous results can be obtained for small diameter boreholes or piezometers for which the effective well diameter can be inaccurately calculated.

2.5.1.4 Boast and Kirkham Seepage Theory

Boast and Kirkham (1971) solved the water flow problem into a soil cavity of any cylindrical shaped e.g. a large circular pit, in a surrounding water-saturated porous homogenous medium. For a general literature review see Kirkham (1965), relating the flow rate of water, Q, into a pit and the surrounding hydraulic conductivity K of the soil is:

$$Q = WKy \qquad (2.15)$$

where W is a "shape factor". Dividing the "shape factor" W by the radius of the cylindrical hole, r, gives a "dimensionless shape factor" W/r, and dividing equation 2.15 by Kyr results in:

$$\frac{W}{r} = \frac{Q}{Kyr} \qquad (2.16)$$

From Ernst (1950):

$$K\,(m/day) = \frac{-dy}{dt}\,(cm/s)\,xC \qquad (2.17)$$

here C is a shape factor. Then, relating the shape factor and the "dimensionless shape factor" W/r gives:

$$C = \frac{864\,\pi\,a}{(Q/Kyr)\,y} = \frac{864\,\pi\,a}{(W/r)\,y} \qquad (2.18)$$

Their analysis yielded a table of shape factors C for both finite and infinite depth of soil below the augered hole. The determined shape factors C using equation 2.18 were calculated for a wide range of geometries. The hydraulic conductivity is given by multiplying the shape factor C with the observed rate of rise of water in the soil cavity (-dy/dt), as expressed by equation 2.17.

2.5.2 Flow Velocity in Clay

The solute or contaminant migration through the clayey deposit can be evaluated once seepage groundwater velocities are known. The velocity of groundwater through a geological medium can be determined by applying the Dupuit-Forachheimer assumption to Darcy's seepage flux as follows:

$$v = \frac{K}{n_e}\frac{dh}{dl} = \frac{ki}{n_e} \qquad (2.19)$$

where v is the average linear velocity; K is the hydraulic conductivity; (dh/dl) or i is the hydraulic gradient which is defined as the change in hydraulic head over distance and n_e is the effective porosity of the geological medium. The effective porosity is defined as the volume of interconnected pore spaces contributing to flow per unit bulk volume of soil (Gordon, 1986). The effective porosity of a clayey till deposit can be much lower than its total porosity, n, which is defined as the ratio of volume of voids over the total volume of soil (Holtz and Kovacs, 1981).

2.5.3 Estimation of Fracture Flow Velocity

An accurate determination of fracture flow velocity is an important factor in the prediction of long term contaminant transport in the underlying aquifer.

2.5.3.1 Flow in a Single Fracture

Flow through a single fracture can be described as a nonturbulent flow of a viscous incompressible fluid between two parallel plates, neglecting inertial forces. A detailed derivation of the one-dimensional Navier-Stokes equation in the context of Hele-Shaw models is provided by Harr (1962). The average fracture flow velocity can be expressed as:

$$v = \frac{\rho g (2b)^2}{12\mu} \frac{dh}{dl} \qquad (2.20)$$

where v is the average fluid velocity in the fracture; ρ is the fluid density; g is the gravitational constant; 2b is the fracture aperture; (dh/dl) is the hydraulic gradient; μ is the dynamic viscosity of the fluid. Equation 2.20 demonstrates that fracture flow velocity is directly controlled by the fracture aperture.

2.5.3.2 Effective Porosity of Fractured Media

Fracture flow velocity can be estimated from Darcy's law, using equation 2.19, by considering the fractured geological media to behave as an equivalent porous-media continua. The effective porosity of a fractured medium is dependent on fracture location, extent, apertures, roughness, frequency and orientation (Gordon, 1986). In addition Nkedi-Kizza et al. (1983) and Gibb et al. (1985) have found that the effective porosity is a dynamic parameter which is influenced by the fluid velocity and fluid or solute molecular size. Thus, the effective fracture porosity, n_{ef}, is defined as the percentage of volumetric fractures contributing to the flow per bulk volume of soil. Huyakorn et al. (1983) expressed the effective fracture porosity for a system of continuous, planar and identical parallel fractures in the direction of flow as:

$$n_{ef} = \frac{b}{(a+b)} \qquad (2.21)$$

where n_{ef} is the effective fracture porosity; a and b are half the distance between fractures and half the fracture aperture, respectively. Fracture apertures, unlike fracture spacings,

in clayey deposits are practically impossible to measure from visual inspection. Therefor equation 2.21 has limited application since both parameters must be known in advance. The evaluation of the effective fracture porosity neglects the soil's interconnected pore spaces. Since the intergranular hydraulic conductivity is very low, it does not significantly contribute to the groundwater flow compared to the higher permeable fracture network.

Snow (1968) developed an equation relating the permeability of a fractured media to the effective fracture porosity using the theory of flow through parallel plates, as shown in Figure 2.6. The effective fracture porosity of a parallel set of fractures all having the same opening, spacing and bulk hydraulic conductivity can be expressed as:

$$n_{ef} = 5.45\left[\frac{K_i}{\Delta^2}\right]^{1/3} \qquad (2.22)$$

where n_{ef} is the effective fracture porosity; K_i is the intrinsic permeability; Δ is the fracture spacing. The intrinsic permeability represents the properties of the porous medium alone. It is a function of the size and number of openings as well as their degree of interconnection. The intrinsic permeability K_i is related to the hydraulic conductivity K by the relationship:

$$K = K_i\left[\frac{\gamma}{\mu}\right] = K_i\left[\frac{\rho g}{\mu}\right] \qquad (2.23)$$

where ρ is the density of water; g is the gravitational constant and μ is the dynamic viscosity of the fluid. The density and dynamic viscosity of water vary with temperature.

Equation 2.23 can be reduced for the measured groundwater temperature of 8°C to:

$$K = 7.069 \times 10^{4} \ (cm^{-1} s^{-1}) \ K_i \qquad (2.24)$$

where K is expressed in cm/s and K_i is expressed in cm^2. Substituting equation 2.24 into equation 2.22 yields:

$$n_{ef} = 13.2 \times 10^{-2} \left[\frac{K}{\Delta^2} \right]^{1/3} \qquad (2.25)$$

From geometric consideration, the fracture aperture, 2b, can be estimated from the fracture porosity and spacing which results in:

$$b = \frac{n_{ef} \Delta}{2} \qquad (2.26a)$$

or

$$b = 2.77 \times 10^{-2} \left[\frac{K}{\Delta} \right]^{1/3} \qquad (2.26b)$$

The use of equation 2.26b also requires prior knowledge of the hydraulic conductivity and the fracture spacing. There is considerable controversy over the parallel plate model when applied to natural fractures. It can only be considered a qualitative description of flow through real fractures. Real fracture surfaces are rough and in contact with each other at discrete points (Gangi, 1978; Brown, 1987). Fluid flow through natural fractures is expected to take a tortuous path; thus deviations from Snow's cubic law are expected. Tsang (1984) reported that a 1-2 order of magnitude error should

result when neglecting the tortuosity factor. Recent work by Brown (1987), using Reynold's equation and computer simulation of flow between rough surfaces showed that the actual flow between rough surfaces is about 70-90% of that predicted by the parallel plate model.

2.5.3.3 In Situ Characterization of Effective Fracture Porosity

The effective fracture porosity is estimated by using field determined hydraulic conductivity tests, which are very localized related to the scale of interest in hydrologic and contaminant transport modelling. A piezometer may not intersect an open fracture even though the larger area is dominated by a network of fractures. Therefore the calculated effective fracture porosity will reflect more the soil intergranular porosity rather than the large scale equivalent-continuum effective fracture porosity. Thus, accurate evaluation of contaminant transport may be very limited in a discontinuously fractured medium because of strong spatial heterogeneity in fracture frequency.

2.5.4 Mass Transport of Solutes

It is important to correctly assess short and long term effects of contaminant migration through the clay deposit. This is only possible through mathematical prediction which can quantify the potential impact on the underlying aquifer from a contaminant source. Also, the interpretation of chemical and environmental isotopes distribution profiles in the porewater can be useful tools in defining the depth of the active hydraulic zone. The processes by which chemical and environmental isotopes move through porous media are

complex. There are three basic processes governing solute migration in clayey till deposits: diffusion, advection and retardation (adsorption). Diffusion is the process by which dissolved ionic and molecular species in water migrate from a high concentration zone to a lower concentration zone. Advection is the process by which dissolved solutes are transported by moving groundwater. Retardation are chemical and physical processes which limit solute migration.

2.5.4.1 Solute Transport in a Homogenous Porous Formation

Solute transport equation is derived on the basis of conservation of mass. The basic assumptions are that the porous medium is homogenous, isotropic and fully saturated; that steady state flow conditions apply; and that Darcy's law is valid. It is also assumed that the governing equation for physical processes of molecular diffusion and mechanical dispersion can be treated as Fickian type spreading mechanisms. For one-dimensional transport in the z direction, the mass flux (F_z) is given by:

$$F_z = \theta v_z C + \left[-\theta D_z \frac{\partial C}{\partial z}\right] \qquad (2.27)$$

where the first and second terms on the right-hand side represent the advective and dispersive transport mechanisms, respectively where: θ being the volumetric water content or effective porosity; C is the concentration (mass per unit volume of soil); v_z the average seepage velocity in the z direction; D_z is the dispersive term in z direction; z is the distance from the solute source. The negative sign indicates that the movement is in direction of decreasing concentration gradient. The coefficient D_z represents the two dispersive

transport mechanisms: diffusion and dispersion. This is possible since both are treated mathematically in the same way, though both are inherently very different. The D_z parameter is given by:

$$D_z = D_e + D_m \qquad (2.28a)$$

where D_e is the effective diffusion coefficient and D_m is the coefficient of mechanical dispersion for the specie of interest.

The dispersion term can be represented as a linear function of velocity, Bear (1972), Freeze and Cherry (1979) by:

$$D_m = \varsigma v_z \qquad (2.28b)$$

where ς is a dispersivity term which is not a true material property (Gillham and Cherry, 1982).

Since the seepage velocity through unweathered clay is very low, the mechanical dispersion term in equation 2.28a can be neglected (Gillham and Cherry, 1982; Rowe, 1988).

The consideration of mass balance gives:

$$\frac{\partial F_z}{\partial z} = -\left[\theta \frac{\partial C}{\partial t} + \rho_d \frac{\partial S}{\partial t}\right] \qquad (2.29)$$

where $(\partial S/\partial t)$ represents the source or sink term describing geochemical reactions; ρ_d is the dry density of the soil matrix and S represents the adsorption term (weight/weight). A positive sign indicates a source while a negative sign represents a sink.

Combining equations 2.27, 2.28 and 2.29 gives:

$$\frac{\partial C}{\partial t} = \left[D_z \frac{\partial^2 C}{\partial z^2} - v_z \frac{\partial C}{\partial z} \right] + \frac{\rho_d}{\theta} \frac{\partial S}{\partial t} \qquad (2.30)$$

This is known as the advection-dispersive equation for solute transport in one-dimension. It simply states that the increase in solute concentration within a small volume of soil is equal to the increase in mass due to advection and diffusion minus or plus the mass of solute removed or added from solution by the geochemical processes. The sink term ($\partial S/\partial t$) in equation 2.30 is a function of concentration and using the chain rule yields:

$$\frac{\partial S}{\partial t} = \frac{\partial S}{\partial C} \frac{\partial C}{\partial t} \qquad (2.31)$$

If equilibrium conditions are assumed, the adsorbed solute (S) and the porewater concentration can be related by an exponential function, then the rate of adsorption is a function of solute concentration. If the rate of adsorption is independent of the solute concentration, then the absorbtion rate is represented by a linear relationship.

Hence substituting equation 2.31 into equation 2.30 gives:

$$\frac{\partial C}{\partial t} \left[1 + \frac{\rho_d}{\theta} \frac{\partial S}{\partial C} \right] = D_z \frac{\partial^2 C}{\partial z^2} - v_z \frac{\partial C}{\partial z} \qquad (2.32)$$

where $(1+\rho_d \partial S/\theta \partial c)$ is the retardation term (R) and $\partial S/\partial C$ is the buffering capacity B(C) which are determined from laboratory experiments for a given soil and any solute

species. If the buffering capacity B(C) is defined by a linear relationship:

$$\frac{\partial S}{\partial C} = K_d \qquad (2.33a)$$

Where K_d is known as a distribution coefficient. Freeze and Cherry (1979) defined it as the mass of solute adsorbed per unit volume of solids divided by the concentration of solute in solution.
Thus, retardation is expressed as:

$$R = 1 + \frac{\rho_d}{\theta} K_d \qquad (2.33b)$$

Substituting equation 2.33b into equation 2.32 yields:

$$\frac{\partial C}{\partial t} = \frac{D_z}{R} \frac{\partial^2 C}{\partial z^2} - \frac{v_z}{R} \frac{\partial C}{\partial z} \qquad (2.34)$$

If equation 2.34 is subjected to the following initial and boundary conditions:

$C(z,t) = C_b$ for $t < 0$ (2.35a)

$C(z,0) = 0$ for $z > 0$, $t > 0$ (2.35b)

$C(L,t) = C_b$ for $t > 0$ (2.35c)

where C_b represents the background solute concentration with C_o as the initial concentration at $t = 0$. For the above set of initial and boundary conditions, the analytical solution given by Ogata (1970) is:

$$\frac{C(z,t)-C_b}{C_o-C_b} = \frac{1}{2}\,erfc\left[\frac{z-Vt}{2\sqrt{Dt}}\right] + \frac{1}{2}\,e^{\left(\frac{Vz}{D}\right)}\,erfc\left[\frac{z+Vt}{2\sqrt{Dt}}\right] \qquad (2.36)$$

where erfc is the complementary error function; and

$$V = \frac{v_z}{R} \qquad (2.37a)$$

$$D = \frac{D_z}{R} \qquad (2.37b)$$

The Ogata (1970) solution assumes that D is a constant.

2.5.4.2 Transport in Fractured Porous Formations

Field investigations show that the upper zone of clayey glacial deposits in Canada are fractured. These fractures can play an important role since they have the potential for being highly effective pathways for transport of solute or contaminants. According to Grisak and Pickens (1980), Sudicky and Frind (1982), Harrison et al. (1992), the factors which are of considerable importance in transport of solute in fractured media are: (1) diffusion of species from the fracture into the matrix or vis-versa, (2) fracture spacing and aperture size, (3) fracture flow velocity, (4) dispersivity, (5) matrix porosity, and (6) retardation.

2.5.4.2.1 Transport Through a Single Fracture

The derivation of the equation for solute transport through a single fracture has the following assumptions relating to the

geometry and hydraulic properties of the system, as shown in Figure 2.8:

1. That fracture flow velocity is constant.
2. Source concentration is placed at the origin of the fracture and remains constant.
3. That fracture aperture is much smaller than its length.
4. That complete mixing occurs across the fracture width at all times.
5. That solute transport in the matrix is only governed by molecular diffusion.
6. That solute transport along the fracture is much faster than through the surrounding matrix.

The first four assumptions provide the basis for a one-dimensional analysis along the fracture itself. Assumptions five and six allow for the direction of mass flux into the porous matrix due to diffusion only to be taken perpendicular to the fracture axis. These assumptions allow this two-dimensional problem to be treated as two one-dimensional mathematical equations. One equation is for transport along the fracture and another is for transport through the matrix.

For the above assumptions, the differential equation for solute concentration along a fracture with radioactive decay is given by Tang et al. (1981) as:

$$\frac{\partial C}{\partial t} + \frac{v}{R}\frac{\partial C}{\partial z} - \frac{D_z}{R}\frac{\partial^2 C}{\partial z^2} + \lambda C + \frac{q}{Rb} = 0 \qquad 0 \le z \le \infty \qquad (2.38)$$

where C = C(z, t) is the concentration of solute in solution; z is the distance along the fracture; t is time; 2b is the fracture aperture; q is a loss term which will be defined later and v is the fracture flow velocity. The hydrodynamic

dispersive term D_z which represents both mechanical dispersion and molecular diffusion along the fracture's axis is defined by equation 2.28. The radioactive decay constant is expressed as:

$$\lambda = \frac{\ln 2}{t_{1/2}} \qquad (2.39)$$

where $t_{1/2}$ is the half-life of the radioactive solute. The retardation term R represents the effect of adsorption of solute along the fracture face and is assumed to be governed by a linear relationship. It is defined by Freeze and Cherry (1979) as:

$$R = 1 + \frac{K_f}{b} \qquad (2.40)$$

where K_f is the fracture distribution coefficient. It is defined as the mass of solute adsorbed per unit area of surface divided by the concentration of solute in solution.

Chemical adsorption on to the fracture wall and on to the clay matrix are considered separately because of the possibility of different chemical properties.

The diffusive transport of solute perpendicular to the fracture is described by the following differential equation:

$$\frac{\partial C'}{\partial t} - \frac{D'}{R'}\frac{\partial^2 C'}{\partial x^2} + \lambda C' = 0 \qquad b \le x \le \infty \qquad (2.41)$$

where $C' = C'(x, z, t)$ is the concentration of solute in the porous matrix; x is the distance perpendicular to the

fracture's axis. The matrix retardation R' is again assumed to be constant, and is defined as:

$$R' = 1 + \frac{\rho_d}{\theta} K_m \qquad (2.42)$$

where K_m is the porous matrix distribution coefficient. The matrix diffusion coefficient for an isotropic medium is expressed by Bear (1972) as:

$$D' = \tau D_o \qquad (2.43)$$

where τ is the matrix tortuosity and D^o is the molecular diffusion coefficient for a solute in free solution. The loss term q in equation 2.38 is equal to the diffusive flux crossing the fracture / matrix boundary and is expressed by Fick's first law as:

$$q = -\left[\theta D' \frac{\partial C'}{\partial x}\right]_{x=b} \qquad (2.44)$$

Substitution of equation 2.44 into equation 2.38 yields the final expression for solute transport in a fracture, which is:

$$\frac{\partial C}{\partial t} + \frac{v}{R}\frac{\partial C}{\partial z} - \frac{D_z}{R}\frac{\partial^2 C}{\partial z^2} + \lambda C - \left[\frac{\theta D'}{bR}\frac{\partial C'}{\partial x}\right]_{x=b} = 0 \quad 0 \le z \le \infty \qquad (2.45)$$

If the following boundary conditions are applied to equation 2.45:

$$C(0, t) = C_o \qquad (2.46a)$$

$$C(\infty, t) = 0 \qquad (2.46b)$$

$$C(z, 0) = 0 \tag{2.46c}$$

and the following ones to equation 2.41:

$$C'(b, z, t) = C(z, t) \tag{2.47a}$$

$$C'(\infty, z, t) = 0 \tag{2.47b}$$

$$C'(x, z, 0) = 0 \tag{2.47c}$$

where C_o is the source concentration, then the analytical solutions are given by Tang et al. (1981). For the general transient solution for concentration in the fracture is:

$$\frac{C}{C_o} = \frac{\exp(Vz)}{\pi^{1/2}} \int_1^\infty \exp\left[-\xi^2 - \frac{V^2 z^2}{4\xi^2}\right] \exp(-\eta z^2)$$

$$\cdot \left\{\exp(-\lambda^{1/2} Y)\, erfc\left(\frac{Y}{2T} - \lambda^{1/2} T\right)\right.$$

$$\left. + \exp(\lambda^{1/2} Y)\, erfc\left[\frac{Y}{2T} + \lambda^{1/2} T\right]\right\} d\xi \tag{2.48}$$

where

$$V = \frac{v}{2D_z} \tag{2.49a}$$

$$Y = \frac{V^2 \beta^2 z^2}{4A\xi^2} \tag{2.49b}$$

$$T = \left[t - \frac{R z^2}{4 D_z \xi^2} \right]^{1/2} \qquad (2.49c)$$

$$\eta = \frac{\lambda R}{4 D_z \xi^2} \qquad (2.49d)$$

$$l = \frac{z}{2} \left[\frac{R}{D_z t} \right]^{1/2} \qquad (2.49e)$$

$$A = \frac{bR}{\theta (R' D')^{1/2}} \qquad (2.49f)$$

$$\beta^2 = \frac{4RD}{V^2} \qquad (2.49g)$$

The general transient solution for concentration in the porous matrix is:

$$\frac{C'}{C_o} = \frac{\exp(Vz)}{\pi^{1/2}} \int_l^\infty \exp\left[-\xi^2 - \frac{V^2 z^2}{4 \xi^2} \right] \exp(-\eta z^2)$$

$$\cdot \left\{ \exp[-\lambda^{1/2} Y'] \, erfc\left[\frac{Y'}{2T} - \lambda^{1/2} T \right] \right.$$

$$\left. + \exp[\lambda^{1/2} Y'] \, erfc\left[\frac{Y'}{2T} + \lambda^{1/2} T \right] \right\} d\xi \qquad (2.50)$$

where

$$Y' = \frac{V^2 \beta^2 z^2}{4 A \xi^2} + G(x-b) \qquad (2.51a)$$

$$G = \left[\frac{R'}{D'}\right]^{1/2} \qquad (2.51b)$$

The analytical solution for fracture concentration when neglecting longitudinal dispersion in the fracture is:

$$\frac{C}{C_o} = 0 \qquad T' < 0 \qquad (2.52a)$$

$$\frac{C}{C_o} = \frac{1}{2} \exp\left[-\frac{\lambda R z}{V}\right] \left\{ \exp\left[-\frac{\lambda^{1/2} R z}{VA}\right] erfc\left[\frac{z}{2\sqrt{VAT'}} - \lambda^{1/2} T'\right] \right.$$

$$\left. + \exp\left[\frac{\lambda^{1/2} R z}{VA}\right] erfc\left[\frac{z}{2\sqrt{VAT'}} + \lambda^{1/2} T'\right] \right\} \qquad T' > 0 \qquad (2.52b)$$

where

$$T' = \left[t - \frac{R z}{V}\right]^{1/2} \qquad (2.53)$$

The concentration in the porous matrix when $D_z = 0$, can be expressed as:

$$\frac{C'}{C_o} = 0 \qquad T' < 0 \qquad (2.54a)$$

$$\frac{C'}{C_o} = \frac{1}{2}\left[-\frac{\lambda R z}{V}\right]\left\{\exp\left(-\lambda^{1/2} W\right)\ erfc\left[\frac{W}{2T'} - \lambda^{1/2} T'\right]\right.$$

$$\left. + \exp\left(\lambda^{1/2} W\right)\ erfc\left[\frac{W}{2T'} + \lambda^{1/2} T'\right]\right\} \qquad T' > 0 \qquad (2.54b)$$

where

$$W = \frac{Rz}{VA} + G(x-b) \qquad (2.55)$$

If the source concentration remains constant and is radioactive, the concentration gradient will stabilize when the rate of loss due to decay equals the rate at which it enters the system; thus, steady state solutions are achieved. The steady state condition will predict the contaminant's ultimate penetration depth.

The steady state concentration in the fracture is given by:

$$\frac{C}{C_o} = \exp\left\{\left[V - \left(V^2 + \frac{\psi}{D_z}\right)^{1/2}\right] z\right\} \qquad (2.56)$$

where

$$\psi = \lambda + \frac{\theta\,(D'\lambda)^{1/2}}{b} \qquad (2.57)$$

The steady state solution for the porous matrix is:

$$\frac{C'}{C_o} = \exp\left\{\left[V-\left(V^2+\frac{\psi}{D_z}\right)^{1/2}\right]z\right\}\exp\left\{-\left[\frac{\lambda}{D'}\right]^{1/2}(x-b)\right\} \qquad (2.58)$$

The steady state solution for the fracture and matrix always shows an exponential type distribution regardless of the values of V or D_z. The maximum depth of penetration of some concentration level in a fracture can be estimated from equation 2.56. For a concentration of $C/C_o = \delta$, the ultimate penetration depth, $d\delta$, is given as:

$$d\delta = \frac{\ln\delta}{V-(V^2+\psi/D)^{1/2}} \qquad (2.59)$$

2.5.4.2.2 Analytical Solution for a System of Parallel Fractures

The analytical solution presented here was developed by Sudicky and Frind (1982) for a parallel fracture system represented in Figure 2.9. Since the fracture / matrix geometry is symmetrical, only one half of a fracture and one half of the intervening porous matrix need to be considered. The system is governed by the same assumptions and processes as in the single fracture case, Tang et al. (1981). Thus it is expressed by the same mathematical equations (2.38 to 2.45) except that equation 2.41 (which is the expression for diffusion transport into the porous matrix) is now limited by the fracture spacing, 2B, and is redefined as:

$$\frac{\partial C'}{\partial t} - \frac{D'}{R'}\frac{\partial^2 C'}{\partial x^2} + \lambda C' = 0 \qquad b \le x \le B \qquad (2.60)$$

If equation 2.45 is subjected to the following initial and boundary conditions:

$$C(z, 0) = 0 \tag{2.61a}$$

$$C(0, t) = C_o \tag{2.61b}$$

$$C(\infty, t) = 0 \tag{2.61c}$$

and equation 2.60 is subjected to:

$$C'(x, z, 0) = 0 \tag{2.62a}$$

$$C'(b, z, t) = C(z, t) \tag{2.62b}$$

$$\partial C'/\partial x\ (B, z, t) = 0 \tag{2.62c}$$

The general transient solution for fracture concentration is given by Sudicky and Frind (1982) as:

$$\frac{C}{C_o} = \frac{2}{\pi^{3/2}} \exp(Vz) \int_1^\infty \exp\left[-\xi^2 - \frac{V^2 z^2}{4\xi^2} - \frac{R\lambda z^2}{4 D_z \xi^2}\right] \int_0^\infty \frac{\epsilon}{\lambda^2 + \epsilon^4/4} \exp(\epsilon_I)$$

$$\cdot \left\{ \exp(\lambda T) \left[\frac{\epsilon^2}{2} \sin(\epsilon_I) \Big|_T - \lambda \cos(\epsilon_I) \Big|_T \right] \right.$$

$$\left. + \frac{\epsilon^2}{2} \sin(\Omega) + \lambda \cos(\Omega) \right\} d\epsilon\, d\xi \tag{2.63}$$

where

$$\epsilon_r = -\frac{Y\epsilon}{2}\left[\frac{\sinh(\sigma\epsilon) - \sin(\sigma\epsilon)}{\cosh(\sigma\epsilon) + \cos(\sigma\epsilon)}\right] \qquad (2.64a)$$

$$\epsilon_I = \frac{\epsilon^2 t}{2} - \frac{Y\epsilon}{2}\left[\frac{\sinh(\sigma\epsilon) + \sin(\sigma\epsilon)}{\cosh(\sigma\epsilon) + \cos(\sigma\epsilon)}\right] \qquad (2.64b)$$

$$\Omega = \frac{Y\epsilon}{2}\left[\frac{\sinh(\sigma\epsilon) + \sin(\sigma\epsilon)}{\cosh(\sigma\epsilon) + \cos(\sigma\epsilon)}\right] \qquad (2.64c)$$

$$l = \frac{z}{2}\left[\frac{R}{Dt}\right]^{1/2} \qquad (2.64d)$$

$$T = t - \frac{Rz^2}{4D\xi^2} \qquad T \geq 0 \qquad (2.64e)$$

$$G = \left[\frac{R'}{D'}\right]^{1/2} \qquad (2.64f)$$

$$\sigma = G(B-b) \qquad (2.64g)$$

The general transient solution for concentration in the porous matrix given by Davis and Johnston (1984) is:

$$\frac{C'}{C_o} = \frac{2}{\pi^{3/2}} \exp(Vz - \lambda t) \int_1^\infty \exp\left[-\xi^2 - \frac{V^2 z^2}{4\xi^2}\right] \int_0^\infty \epsilon \exp(\epsilon_r)$$

$$\cdot\left\{\frac{\cosh[G\lambda^{1/2}(B-x)]}{(\lambda^2+\epsilon^4/4)\cosh(\sigma\lambda^{1/2})}\left[\frac{\epsilon^2}{2}\sin(\epsilon_I^T)-\lambda\cos(\epsilon_I^T)\right.\right.$$

$$\left.+\exp(\lambda T)\left(\frac{\epsilon^2}{2}\sin(\Omega)+\lambda\cos(\Omega)\right)\right]$$

$$-4\pi\sum_{n=0}^{\infty}\frac{(-1)^n(2n+1)}{[(2n+1)^2\pi^2+4\lambda\sigma^2]}$$

$$\cdot\frac{\cos[(2n+1)\pi(B-x)/(2(B-b))]}{(\kappa^2+\epsilon^4/4)}$$

$$\left.\cdot\left[\frac{\epsilon^2}{2}\sin(\epsilon_I^T)+\kappa\cos(\epsilon_I^T)+\exp(-\kappa T)\left(\frac{\epsilon^2}{2}\sin(\Omega)-\kappa\cos(\Omega)\right)\right]\right\}d\epsilon\,d\xi$$

(2.65)

where

$$\kappa = (2n+1)^2\pi^2/4\sigma^2 \qquad (2.66)$$

When the advective flux is relatively large, longitudinal dispersion along the fracture axis can be neglected (Tang et al., 1981; Sudicky and Frind, 1982). This simplification is useful since dispersivity is a difficult parameter to estimate quantitatively.

The fracture concentration solution when $D_z = 0$ is given by Sudicky and Frind (1982) as:

$$\frac{C}{C_o} = 0 \qquad T^o < 0 \tag{2.67a}$$

$$\frac{C}{C_o} = \frac{1}{\pi} \exp\left[-\frac{R\lambda z}{V}\right] \int_0^\infty \frac{\epsilon}{\lambda^2 + \epsilon^4/4} \exp(\epsilon_r^o)$$

$$\cdot\left[\exp(-\lambda T^o)\left\{\frac{\epsilon^2}{2}\sin(\epsilon_I^o) - \lambda\cos(\epsilon_I^o)\right\}\right.$$

$$\left. + \frac{\epsilon^2}{2}\sin(\Omega^o) + \lambda\cos(\Omega^o)\right] d\epsilon \qquad T^o > 0 \tag{2.67b}$$

where

$$\epsilon_r^o = -\frac{\omega\epsilon}{2}\left[\frac{\sinh(\sigma\epsilon) - \sin(\sigma\epsilon)}{\cosh(\sigma\epsilon) + \cos(\sigma\epsilon)}\right] \tag{2.68a}$$

$$\epsilon_I^o = \frac{\epsilon^2 T^o}{2} - \frac{\omega\epsilon}{2}\left[\frac{\sinh(\sigma\epsilon) + \sin(\sigma\epsilon)}{\cosh(\sigma\epsilon) + \cos(\sigma\epsilon)}\right] \tag{2.68b}$$

$$\Omega^o = \frac{\omega\epsilon}{2}\left[\frac{\sinh(\sigma\epsilon) + \sin(\sigma\epsilon)}{\cosh(\sigma\epsilon) + \cos(\sigma\epsilon)}\right] \tag{2.68c}$$

$$\omega = \frac{\theta (R'D')^{1/2} z}{bV} \tag{2.68d}$$

$$T^{o} = t - \frac{Rz}{V} \qquad (2.68e)$$

The solute concentration in the porous matrix when $D_z = 0$ is given by Davis and Johnston (1984) as:

$$\frac{C'}{C_o} = 0 \qquad T^{o} < 0 \qquad (2.69a)$$

$$\frac{C'}{C_o} = \frac{Co}{\pi} \exp\left[\frac{-R\lambda z}{V}\right] \int_0^{\infty} \epsilon \exp(\epsilon_r) \left\{ \frac{\cosh[G\lambda^{1/2}(B-x)]}{(\lambda^2 + \epsilon^4/4)\cosh(\sigma\lambda^{1/2})} \right.$$

$$\cdot \left[\exp(-\lambda T^{o}) \left(\frac{\epsilon^2}{2} \sin(\epsilon_I^{o}) - \lambda \cos(\epsilon_I^{o}) \right) + \frac{\epsilon^2}{2} \sin(\Omega^{o}) + \lambda \cos(\Omega^{o}) \right]$$

$$-4\pi \exp(-\lambda T^{o}) \sum_{n=0}^{\infty} \frac{(-1)^n (2n+1)}{[(2n+1)^2 \pi^2 + 4\lambda\sigma^2]}$$

$$\cdot \frac{\cos[(2n+1)\pi(B-b)/(2(B-b))]}{(\kappa^2 + \epsilon^4/4)}$$

$$\left. \cdot \left[\frac{\epsilon^2}{2} \sin(\epsilon_I^{o}) + \delta \cos(\epsilon_I^{o}) + \exp(-\delta T^{o}) \left(\frac{\epsilon^2}{2} \sin(\Omega_o) - \delta \cos(\Omega^{o}) \right) \right] \right\} d\epsilon$$

(2.69b)

The steady state solutions given below were defined by Sudicky and Frind (1982). The general steady state solution for concentration in a fracture is:

$$\frac{C}{C_o} = \exp\left\{ Vz\left[1-\left(1+\frac{4}{\gamma}(1+\phi)\right)^{1/2}\right]\right\} \qquad (2.70a)$$

where

$$\gamma = \frac{V^2}{\lambda D_z R} \qquad (2.70b)$$

$$\phi = \frac{\theta (R'D')^{1/2}}{\lambda^{1/2} bR} \tanh(\sigma \lambda^{1/2}) \qquad (2.70c)$$

and the concentration in the matrix is:

$$\frac{C'}{C_o} = \exp\left\{ Vz\left[1-\left(1+\frac{4}{\gamma}(1+\phi)\right)^{1/2}\right]\right\} \frac{\cosh[G\lambda^{1/2}(B-x)]}{\cosh[\sigma\lambda^{1/2}]} \qquad (2.71)$$

Equation 2.70a can be rearranged to give the depth of penetration, $d\delta$, at a predetermined concentration $C/C_o = \delta$. The $d\delta$ value is given by:

$$d\delta = \frac{\delta}{V\left[1-\left(1+\frac{4}{\gamma}(1+\phi)\right)^{1/2}\right]} \qquad (2.72)$$

The steady state solution for the nondispersive case for fracture concentration can be expressed as:

$$\frac{C}{C_o} = \exp\left[-\frac{R\lambda z}{V}(1+\phi)\right] \qquad (2.73)$$

and for the porous matrix in this case is given by:

$$\frac{C'}{C_o} = \exp\left[-\frac{R\lambda z}{V}(1+\phi)\right]\frac{\cosh\left[G\lambda^{1/2}(B-x)\right]}{\cosh\left[\sigma\lambda^{1/2}\right]} \qquad (2.74)$$

The ultimate penetration depth $d\delta$ is given by:

$$d\delta = -\frac{\ln\delta}{\left[-\frac{R\lambda z}{V}(1+\phi)\right]} \qquad (2.75)$$

Although these analytical solutions apply to a highly idealized fracture system, they do provide a basic framework for predicting solute or contaminant migration through porous fractured media and their potential impact on the environment.

2.5.5 Effect of Matrix Diffusion

In clayey till deposits, matrix diffusion has an overwhelming effect on the net solute concentration through the fracture due to the relatively high diffusion coefficients (Day, 1977; Grisak and Perkens, 1980; Harrison et al., 1992). A large diffusion coefficient reduces significantly the net solute fracture velocity.

Grisak and Pickens (1980) showed that the storage capacity of the porous matrix is proportional to the diffusive flux crossing the fracture/matrix interface which decreases with increased contact time. This effect is illustrated in Figure 2.10. This figure shows the gradual utilization of storage capacity of the matrix with contact time and distance from the source. As the matrix storage is fully utilized, the effective solute velocity for a nonreactive species approaches the water velocity.

If the concentration gradient in the fracture/matrix boundary is reversed (higher concentration in the matrix than in the fractures), the diffusive direction would also be reversed. Solutes would migrate by diffusion from the clay matrix into the fracture.

Diffusive flux into the matrix is a function of the matrix storage capacity which is a function of fracture spacing, porosity and geochemical reactions. Porosity is a measure of the physical space available for species storage. Thus, porosity of the matrix controls the rate of volumetric solute concentration in the fracture. The rate of increased concentration in the fracture is much slower for a high porosity medium as compared to a low porosity medium. Therefore, if the matrix porosity is low, minimum solute loss from the fracture would occur. Geochemical reactions remove solutes from the matrix porewater. This maintains a high matrix storage capacity. Thus, the diffusive flux from the fracture into the porous matrix will also remain high. Again, high retardation factor will significantly reduce the effective solute velocity in the fracture.

The importance of matrix diffusion can be reduced significantly if the matrix porosity is very small and/or fracture spacing is extremely small. This would result in a low storage capacity for solutes in the matrix. Also, large fracture aperture or high fracture flow velocity would reduce the diffusive flux. These factors would increase the ratio of solutes transported by the fracture to solutes stored in the matrix (Grisak and Pickens, 1980; Tang et al., 1981; Harrison et al., 1992).

2.5.6 The Effects of Fracture Spacing, Width and Velocity

Since fracture flow velocities are based upon Snow's cubic law equations (2.19, 2.25, 2.26), fracture spacing and aperture size have a direct effect on velocity. However, these effects on solute transport will be illustrated separately for clarity.

Three examples using steady state analytical solutions (Sudicky and Frind, 1982) (equation 2.73) will be used to illustrate the effects of varying the fracture spacing, width and velocity. The environmental isotope tritium will be used as an example. Tritium has the following constant parameters:

$D' = 6.0 \times 10^{-6}$ cm^2/s

$R = R' = 1$

$T_{1/2} = 12.35$ years.

The effective porosity is assumed to be 0.50 which is a typical value for Leda clay around the Ottawa area.

2.5.6.1 Variation in Fracture Spacing

Figure 2.11 illustrates the effect of fracture spacing on solute concentration profile in the fracture. The profiles are based on the following assumptions: steady state, an average fracture velocity of 1.0 m/d, fracture width of 15 μm and fracture spacing ranging from 0.1 to 0.5 m. The maximum penetration depth of solute for the smallest fracture spacing is about 10 m. This is approximately 4 times greater than that given for the largest fracture spacing.

This example shows that fracture spacing has a direct effect on the ultimate penetration of a radioactive solute or

contaminant, since small fracture spacing limits the storage capacity of the finite matrix.

2.5.6.2 Variation in Aperture Size

Figure 2.12 illustrates the effect of aperture size on solute concentration profile in the fracture. The profiles are based on the following assumptions: steady state, an average velocity of 1.0 m/d, a fracture spacing of 0.2 m and fracture aperture ranging from 10 to 100 μm. The maximum penetration depth of solute for the largest aperture width is about 20 m which is approximately 10 times greater than that given by a fracture width of 10 μm.

The reduction of aperture size reduces the amount of solute transported by the fracture. Thus, a greater portion of solute in the fracture is diffused into the clay matrix which results in a concentration profile in the fracture that remains near the input source.

2.5.6.3 Variation in Fracture Flow Velocity

The effect of increasing velocity in the fracture on the concentration profile is illustrated in Figure 2.13. For an aperture width of 15 μm and fracture spacing of 0.4 m and a fracture water velocity ranging from 0.5 to 5.0 m/d, the results indicated that the ultimate penetration depth increased by a factor of 10 when also increasing the velocity by the same factor. The volumetric flux rate increases with velocity, thus the fracture network is capable of transporting more solute per unit time.

2.5.7 Tritium Profiles Generated

The tritium concentration profiles are generated along a fracture for various fluctuating parameters. These are shown in Figures 2.11 to 2.13. The profiles illustrate that post-1952 tritium isotope concentration may not indicate maximum depth of hydraulically active fractured zone. Because of the high losses in tritium concentration in the fracture due to migration into the matrix by diffusion. Also, since tritium has a short half-life, equilibrium is reached quickly. From the above examples, the ultimate penetration depth of tritium can be as little as 2.0 metres, while the fracture network may extend well below this depth.

CHAPTER 3

DIFFUSION IN SATURATED SOILS

3.1 General

In recent years, studies have indicated that diffusion is the controlling transport mechanism for pollutant and natural solute migration through clayey till deposits (e.g. Goodall and Quigley, 1977; Desaulnier et al., 1981, 1982, 1984, 1986, 1989; Crooks and Quigley, 1984; Quigley et al., 1987; Johnson et al., 1989; Shackelford, 1991). Also, migration of contaminants and solutes through fractured porous media, and diffusion into the adjacent clay matrix is an important mechanism (e.g. Day, 1977; Grisak and Pickens, 1980; Tang et al., 1981; Sudicky and Frind, 1982; Harrison et al., 1992).

The contrclling parameters for diffusive transport are the diffusion coefficient (D) and geochemical reactions (S), such as absorption, precipitation, desorption, etc. These parameters depend on the clay's mineralogy, porewater composition, solute species of interest, ionic strength, and biological factors which are not easy to measure. Since these parameters are unique for a given soil, the diffusion coefficient and geochemical reactions are generally determined by laboratory experiments for a given soil. A review of the different types of diffusion, the evaluation of the diffusion coefficient in terms of reactive solutes and a description of the different methods of measurements are given in this chapter.

3.2 Steady-State Diffusion

Diffusion migration of extreme diluted solute occurs in "bulk" or "free" water due to a creation of a chemical potential gradient. In accordance with Fick's first law, diffusion migration in one dimension can be expressed as:

$$f = -D_o \frac{\partial C}{\partial x} \qquad (3.1)$$

where f is the chemical mass flux, C is the solute concentration in the fluid at any point x, x is the direction of transport from the high concentration interface and D_o is the "free-solution" diffusion coefficient.

The "free-solution" diffusion coefficient, D_o, is a complex parameter as it incorporates many influencing factors. This results in a number of expressions. One such expression is the Nerst-Einstein equation (Jost, 1960). This equation expresses the "free-solution" diffusion coefficient at infinite dilution. At this point no interaction between competitive ions occurs. The equation is:

$$D_o = \frac{uR_gT}{N} \qquad (3.2)$$

where R_g is the universal gas constant (8.134 J/mol·k), T is the absolute temperature, N is Avogadro's number (6.022×10^{23} mol^{-1}) and u is the ionic mobility of a particle which is related to the chemical potential or gradient (Robinson and Stokes, 1959).

If the ionic mobility is a function of the limiting ionic equivalent conductance and the viscous resistance of the fluid in accordance with Stokes law (Lerman, 1979), then two more expressions are possible for D_o:

$$D_o = \frac{R_g T \lambda_o}{F^2 |z|} \tag{3.3}$$

and

$$D_o = \frac{R_g T}{6 \pi N \eta r} \tag{3.4}$$

where F is Faraday's constant (96,490 Coulombs/equivalent), $|z|$ is the ionic valence, λ_o is the limiting ionic conductance, η is the viscosity of the fluid and r is the molecular or hydrated ionic radius. Equations 3.3 and 4.4 are known as the Nernst and Einstein-Stokes equations, respectively.

The above equations show that D_o is influenced by many factors: temperature, viscosity of the fluid, ionic radius, solute mass, valence, concentration/dissociation state and the dielectric constant.

Table 3.0 lists several D_o values based upon equation 3.3 using λ_o values from Robinson and Stokes (1959). The D_o values represented here are the maximum values attainable under ideal conditions.

Under nonideal conditions, effects such as electroneutrallity become important. As cations and anions migrate through the solution (fluid), an electrical potential is established

between them (Robinson and Stokes, 1959). Co-diffusion of both ions results as the slower moving ion is accelerated while at the same time the faster moving ion is slowed. Simple electrolyte diffusion values are shown in Table 3.1. They are different than those in Table 3.0 for individual species caused, in part, by electrical potential effects.

Other effects which can become important under certain conditions are interactions between solute-solute and solute-solvent (Jost, 1960).

The effects of temperature on diffusion are important since many laboratory experiments are carried-out at room temperature, around 25 °C, while actual field temperatures can be much lower, i.e. 8°C. Chloride which is often used as a "conservative tracer" in field experiments is highly susceptible to temperature as seen in Figure 3.0. A difference of up to 40% in D_o values can occur due to the effect of temperature alone. This difference can be significant when transposing laboratory determined diffusion coefficient for field predictions. Thus measured diffusion coefficient must be corrected for temperature. An expression relating the diffusion coefficient to temperature change is given by Li and Gregory (1974) as:

$$(D_o\eta)_{T_1} = (D_o\eta)_{T_2} \qquad (3.5)$$

where η is the viscosity of water at the temperature of interest.

3.3 Types of Diffusion

In addition to the above factors which influence D_o, it is also dependent on the type of the diffusion process. The literature reports essentially four types of diffusions. These are the following: (1) self-diffusion, (2) tracer diffusion, (3) salt-diffusion, (4) counter diffusion or interdiffusion (Robinson and Stokes, 1959; Li and Gregory, 1974; Lerman, 1979; Shackelford, 1989; Shackelford and Daniel, 1991). The four types of diffusions are illustrated in Figure 3.1, where the single salts sodium chloride (NaCl) and potassium chloride (KCl) diffuse freely.

True self-diffusion is illustrated in Figure 3.1(a), where the two initial diffusion half-cells have the same concentrations of NaCl without any isotopically different species. The ion movement would be totally random and undetectable. For this reason, self-diffusion coefficient is measured by introducing a small amount of isotopic tracer (^{22}Na) to one of the half-cells. The amount of ^{22}Na introduced must be sufficiently small to avoid a large concentration gradient. This would ensure that the radioactive tracer ($^{22}Na^+$) and Na^+ are not influenced by the chloride anions (ions of the opposite sign). The measured diffusive parameter is known as the "self-diffusion coefficient".

If the isotropic species $^{22}Na^+$ in the self-diffusion case is replaced by a different element such as $^{42}K^+$, while maintaining equal concentrations of NaCl in both half-cells, then self-diffusion now becomes a tracer diffusion test. Tracer diffusion is illustrated in Figure 3.1(b). At infinite dilution both self-diffusion and tracer diffusion are equal.

Salt diffusion is defined as the diffusion of both cations and anions in the same direction which is illustrated in Figure 3.1(c). In this example, only one half-cell contains the single salt (NaCl) solution, this half-cell is placed in direct contact with the other half-cell containing only the solvent, usually distilled water. This allows free movement of both ions.

Counterdiffusion or interdiffusion is depicted in Figure 3.1(d). This process is appropriate to systems in which an opposite chemical potential gradient is established. As illustrated, two half-cells are placed in contact, each containing equal concentration of NaCl and KCl; potassium and sodium ions diffuse in opposite direction to each other. Usually salt diffusion and counterdiffusion occur simultaneously and represents the boundary conditions in contaminant transport.

3.4 Steady-State Diffusion Through Soil

If one of the half diffusion cells in Figure 3.1 is replaced by a soil plug, diffusion into the soil pores would be slower than in free solution. The two main reasons are: (1) restrictive pathways for migration or tortuosity, as illustrated in Figure 3.2; (2) reduction in cross-sectional area due to soil particles.

3.4.1 Reduction in Cross-Sectional Area

When a solute diffuses into a soil medium, the reduction in cross-sectional area is taken into account by modifying equation 3.1:

$$f = -D_o\theta \frac{\partial C}{\partial x} \qquad (3.6)$$

where θ is the volumetric water content, C represents the solute porewater concentration of the species of interest in the soil. The volumetric water content is evaluated from:

$$\theta = nS_r \qquad (3.7)$$

where n is the total porosity of the soil and S_r is the degree of saturation expressed as decimal fraction. The maximum mass flux would occur at fully saturation, when $S_r = 1$.

3.4.2 The Effects of Tortuosity

The restrictive pathways are taken into account by a tortuosity factor, τ, equation 3.6 can now be redefined as:

$$f = -D_o\theta\tau \frac{\partial C}{\partial x} \qquad (3.8)$$

where tortuosity is the actual or effective length of the migration pathway, l_o, divided by the shortest distance (a straight line), l,: $\tau = l_o/l$. Unfortunately, many tortuous paths exist in a given soil, as illustrated in Figure 3.2. Thus one is left with an experimental approach. Tortuosity, τ, has been reported to range from 0.01 to 0.84 for saturated soils and from 0.025 to 0.57 for unsaturated soils (Low, 1981; Rowe et al., 1988; Shackelford and Daniel, 1991).

Other factors influencing the rate of diffusion migration of solute in soil are: (1) the increase in viscosity of water

near the diffuse double layer (DDL) on clay minerals (Kemper et al., 1964); (2) anion exclusion from small porewater spaces due to the DDL (Porter et al.; 1960; van Schaik and Kemper, 1966). Anion exclusion is also referred to as salt filtration, ultrafiltration or membrane filtration (Freeze and Cherry, 1979; Drever, 1982). It has been suggested that anion exclusion may occur in natural clay deposits when the natural soil porosity is reduced below 0.30 (Berner, 1971).

Equation 3.8 can be modified for these additional effects:

$$f = -D_o \theta \tau \mu \xi \frac{\partial C}{\partial x} \qquad (3.9)$$

where ξ is a fluidity factor and μ represents the effects of salt filtration. These extra factors are usually indistinguishable from one another and are usually associated with the tortuosity factor. For this reason, reported values of tortuosity factors values for a given soil type must be used with caution.

The diffusion coefficient through a soil system can now be defined as:

$$D_e = D_o \Gamma \qquad (3.10)$$

where D_e is the true diffusion coefficient through soil or also known as the effective diffusion coefficient and Γ represents all factors influencing D_o:

$$\Gamma = \tau \mu \xi \qquad (3.11)$$

Γ has also been called a "complex tortuosity factor".

For steady-state, diffusion through a soil system is defined by:

$$f = -D_e\theta \frac{\partial C}{\partial x} \qquad (3.12)$$

From steady-state laboratory diffusion tests, the effective diffusion coefficient is evaluated using equation 3.12, while equation 3.10 is used to determine Γ, the "complex tortuosity factor", using an appropriate "free-solution" diffusion coefficient.

3.5 Transient Diffusion

Steady-state diffusion is time independent. In a natural environment steady-state condition may require a long time period to be achieved. Transient diffusion is more practical to evaluate effective diffusion coefficients since it is time dependent. Transient diffusion is based upon Fick's second law which quantifies the change in concentration over distance with time. For a nonreactive solute, Fick's second law can be expressed as:

$$\frac{\partial C}{\partial t} = D_e \frac{\partial^2 C}{\partial x^2} \qquad (3.13)$$

A nonreactive solute is one which does not participate in any chemical and/or biochemical reactions.

For reactive, nondecaying solutes with reversible kinetics, diffusive transport can be expressed as:

$$\frac{\partial C}{\partial t} = D_e \frac{\partial^2 C}{\partial x^2} - \frac{\rho_d}{\theta} \frac{\partial S}{\partial t} \qquad (3.14)$$

where ρ_d is the dry or "bulk" density of the soil, ($\partial S/\partial t$) represents the source or sink term describing geochemical reactions. These geochemical reactions include adsorption, desorption, dissolution, precipitation, oxidation-reduction, ion pairing, radioactive decay and complexation reactions. Usually, only adsorption and desorption are modelled due to the complexity of the other reactions in a soil system. The geochemical reaction term in equation 3.14 is a function of solute concentration and using the chain rule yields:

$$\frac{\partial S}{\partial t} = \frac{\partial S}{\partial C} \frac{\partial C}{\partial t} \qquad (3.15)$$

If equilibrium conditions are assumed, substituting equation 3.15 into 3.14 results in:

$$\frac{\partial C}{\partial t}\left[1 + \frac{\rho_d}{\theta} \frac{\partial S}{\partial C}\right] = D_e \frac{\partial^2 C}{\partial x^2} \qquad (3.16)$$

where ($1+ \rho_d \partial S/\theta \partial C$) is known as the retardation term (R) and $\partial S/\partial C$ is the buffering capacity B(C) of the soil system.

The buffering capacity is determined by laboratory experiments for a given soil and the solute of interest. Substituting (R) into equation 3.16 yields:

$$\frac{\partial C}{\partial t} = \frac{D_e}{R} \frac{\partial^2 C}{\partial x^2} \qquad (3.17)$$

Some researchers couple diffusion with geochemical reactions, where:

$$D_a = \frac{D_e}{R} \qquad (3.18a)$$

so, equation 3.17 becomes:

$$\frac{\partial C}{\partial t} = D_a \frac{\partial^2 C}{\partial x^2} \qquad (3.18b)$$

where D_a is referred as the apparent diffusion coefficient.

The advantage of this simplification is that only one unknown has to be solved; this is usually done when the retardation factor is unknown. Thus, when comparing reported diffusion coefficients for reactive solutes, care must be taken to establish whether the values represent effective or apparent diffusion. In addition retardation factors are characteristic of individual soils; they should not be applied to untested or unknown soils.

3.6 Soil Chemistry

3.6.1 Geochemical Reactions

When a solute reacts with the surrounding soil system or other solutes in solution, the amount of interaction is directly proportional to the buffering capacity B(C). There exist several processes capable of retaining solutes or toxicants in a soil system. These processes, illustrated in Figure 3.3, are as follows: (1) adsorption, (2) chemisorption, (3) passivation, (4) diodochy, (5) precipitation.

3.6.1.2 Adsorption

Adsorption is the process by which a molecule or ion in solution is attracted to a soil's charged surface. The retaining forces are weaker than chemical bonding. This system is weak for solute or contaminant containment, but can be effective for certain species. In the perfect form, adsorption is completely reversible. The chemical retention is usually restricted to cation-dipole interaction, hydrogen bonding or weak charge transfer.

3.6.1.3 Chemisorption

Chemisorption or sorption is the retention of solutes by close-range chemical or physical forces. Sorption in the case of ion retention is attributed to the entrance of ions into lattice vacancies in the mineral's crystal structure. The ion becomes part of the mineral's structure. Also, organic material are strongly adsorbed by organic matter in the soil matrix. Organic ligands have strong retention capacity for heavy metals. Chemisorbed species can often be removed only high temperature treatment.

3.6.1.4 Passivation

Passivation or armouring is a chemical reaction which occurs at the surface of a particle, thus forming a chemical coating. For example, barium in solution will react with gypsum to form a reaction ring of barium sulfate ($BaSO_4$). If the coating or reaction ring adheres to the surface of the particle, then the reaction stops. But, passivation is not a major attenuation process in a natural geological system.

3.6.1.5 Diodochy or Elemental Substitution

Many soil minerals do not have precisely defined chemical compositions which allow a certain percentage of sites in the mineral lattice to be substituted with another ion. Diodochy or elemental substitution is one of the major chemical processes that occur in natural geochemical cycles e.g. mineral alteration in rocks. The principle of elemental substitution is that elements of similar size and charge can substitute for one another. For example, arsenic can interchange for phosphorous in the common phosphate mineral, apatite. Also, zinc and manganese can both substitute for calcium in calcite ($CaCo_3$).

3.6.1.6 Precipitation

Precipitation is the reaction process by solutes, mainly heavy metals, react with other soluble ions (carbonates, sulfates) to form new insoluble compounds. Precipitation is dependent upon specific ion concentration, temperature and pH. Other important phenomena are complexation and oxidation-reduction reactions of metal species in solution. Complexation and oxidation-reduction reactions generally reduce the free metal ion concentration in a solution.

3.6.2 Soil Minerals

The interactions between the soil system and solutes indicate that some soil minerals are charged, either positively or negatively. Since some of the soil matrix colloids or minerals are charged, they adsorb solutes or contaminant species by electrostatic forces (Anderson and Rulsin, 1983; Sposito, 1984). Positive charged species are attracted to

permanent and variable negative charged sites on the clay mineral surfaces.

The total negative charges on minerals are measured by the capacity to exchange cations or CEC (cation exchange capacity). Soil colloids or minerals which can carry a positive or a negative charge are clay minerals - kaolins, illites, chlorites, vermiculites and montmorillonites, soil organics and amorphous minerals - oxides and hydroxides.

Clay minerals are layered silicates. These layered silicates are composed of two types of structural units: silica and cation (alumina) sheets. The silica sheet is a two-dimensional array of Si-O tetrahedra known as the tetrahedral sheet. The second type is a two-dimensional array of cations, usually Al^{3+}, but Mg^{2+}, Fe^{2+} and Fe^{3+} can be fairly common in octahedral coordination with oxygen or hydroxyl anions. These two sheets are the building blocks for clay minerals and are bonded together by shearing layers of oxygens. Some characteristics of clay minerals are presented in Table 3.2.

Soil organic are composed of living organisms, their partly-decomposed and completely transformed remains.

Amorphous minerals are composed of two main groups: oxides and hydroxides. Simple oxides are composed of metallic elements with oxygen such as hematite (Fe_2O_3), ilmenite ($FeTiO_3$), bixbyite ($(Mn, Fe)_2O_3$. Hydroxides are compounds of metallic elements with water or hydroxyl ion (the OH^- radical) such as brucite ($Mg(OH)_2$), bauxite ($Al(OH)_3$), geothite ($HFeO_2$), limonite ($FeO(OH) \cdot nH_2O$.

3.6.3 Origin of Surface Charges in Soils

There are three main origins for surface charge in a mineral assemblage. These are isomorphic substitution, ionic dissolution, and ionization.

3.6.3.1 Isomorphic Substitution

Mineral charges are the result of internal structural imperfections in the crystal lattice, usually found in clay minerals. These imperfections are due to ion substitution or site vacancies. The substitution is usually restricted to lower valence elements for one of higher valency, due to ion size limitations. For example, Al^{3+} interchanges for tetrahedral Si^{4+} and Mg^{2+} or Fe^{2+} substitutes for octahedral Al^{3+}. These types of exchanges lead to a positive deficiency on the mineral structural surface. This results in a permanent negative surface charge on the clay particle (Bohn, 1971; Sposito, 1984).

However, these clays may not display nonamphoteric behaviour since some clay particles edges may be amphoteric, for example, kaolinite (Sposito, 1984; Sparks, 1986). This pH-dependent charge at the crystal edges is quantitatively represented in Figure 3.4. This figure indicates that the change can be either positive, negative or zero depending on the ambient pH.

3.6.3.2 Ionic Dissolution

Ionic dissolution is the process by which the water molecule H_2O is split into H^+ and OH^- during adsorption to a hydroxylated surface. The sign and magnitude of the surface

charge is dependent on the type and amount of excess ions (H^+ or OH^-) adsorbed on to the hydroxylated surface. This type of surface charge is related directly the potential determining ion activity in the bulk solution or pH dependent (Sparks, 1986). Typical minerals which follow this behaviour are oxides and/or hydroxides of Al, Fe, Mn, Si and Ti. Figure 3.5 illustrates the mechanism by which an iron oxide acquires its surface charge.

3.6.3.3 Ionization

The origin of surface charge in organic material is either by dissociation of H^+ from or onto the active organic functional groups. The charge generated can be either positive or negative:

$$R\text{-}COOH \leftrightarrows R\text{-}COO^- + H^+$$

or

$$R\text{-}NH_2 + H_2O \leftrightarrows R\text{-}NH_3^+ + OH^-$$

The type of charge is a function the dissociation constant of each functional group and the ambient pH of the soil system. Examples of organic functional groups are carboxyl, phenolic and aminos.

3.6.4 Permanent Surface Charge

Isomorphic substitution is the primary source of permanent charge in soils. It is the principal origin of negative charges for the 2:1 (e.g. illites, vermiculites) and 2:1:1 (e.g. chlorites) type clay minerals, but is reportedly of

minor importance for the 1:1 type clay minerals such as Kaolins (Bohn, 1971; Sparks, 1986). The source and type of surface charge are given in Table 3.2.

3.6.5 pH-Dependent Surface Charge

Ionic dissolution and ionization are the main source of pH-dependent charges in soils. The total charge on a soil is the algebraic sum of its negative and positive charges. The variation of the net charge with pH is represented in Figure 3.6. One index frequently used for pH-dependent soil is the zero point of charge, ZPC. The ZPC is the pH at which the negative and positive charges on a colloid are equal. The ZPC for the hypothetical soil in Figure 3.6 would be well below a pH value of 3. As mentioned before, the primary source of pH-dependent charge is the gain or loss of H^+ from functional groups on the surface of soil solids. These groups include hydroxyl (OH^-), carboxyl (-COOH), phenolic (C_6H_4OH) and amine ($-NH_2$).

The cation or anion exchange capacity are highly variable values since the system is dependent on pH. The development of negative charges on 2:1 layer silicates (illites and vermiculites) is 5 to 10 percent pH dependent, whereas 50 percent or more developed on 1:1 minerals can be pH dependent (Sposito, 1984; Sparks, 1986). This phenomena is illustrated in Figure 3.7, where the chloride anion Cl^- is retained by kaolinite in acidic conditions. The presence of OH^{2+} on the clay structural edges produces a positive charged soil particle. In alkaline conditions, the functional group changes to OH^- which repels the anion. The ZPC is indicated by the vertical dashed line at a pH of 6.5.

3.6.6 Diffuse Double Layer

In an air-dry soil, the negative charges of the colloid must be counter balanced by cations to maintain electrostatic neutrality. This corresponds to a layer made up of exchangeable cations, CEC, which resides directly on the surface of the colloid. This configuration is named a "Helmholtz double layer".

The presence of water alters the concentration of exchangeable cations because the electrostatic attraction is counteracted by diffusion. This tends to equalize concentration differences in the aqueous phase. The exchangeable cation concentration profile due to these two opposing forces is illustrated in Figure 3.8, for two salt concentrations. As depicted in Figure 3.8, the cation concentration decreases with distance from the negatively charged surface. From Figure 3.8 the cation exchange capacity is proportional to the area between the curves and their corresponding dashed lines.

Increasing the bulk salt solution from C_1 to C_2 reduces the tendency for diffusion away from the colloid's charged surface, thus shrinking the DDL (diffuse double layer) which in turn decreases the CEC. Another factor affecting the extent of the diffused layer is the valence of the counter ion. Assuming that equilibrium concentration remains the same, the DDL decreases with increasing counter-ion valence since higher valence cation are attracted more than lower valence cation. Because of the cation-rich solution near the colloid surface, anion repulsion occurs.

Figure 3.9 illustrates the variation in anion concentration; the anion concentration outside the DDL is higher than if no repulsion occurred. Since the total mass charge must balance, anion repulsion increases the net salt concentration in the bulk solution.

The combined result of cation attraction, anion repulsion and ion diffusion is illustrated in Figure 3.10 for two different initial concentrations.

3.6.7 Cation Retention

The two main mechanisms for cation retention are cation exchange and precipitation. Cation exchange is the predominant process for retention of alkali (group IA) and the alkaline earth metals (group IIA). Precipitation is the predominant mechanism for heavy metals especially in highly carbonated soils.

As seen previously, to maintain electroneutrallity, the counter-ions cannot be separated from the charged surface. But, it is possible to exchange these cations against others. The exchange reaction is totally reversible and can be indicated according to the following expression:

$$SOIL - A^{+} + B^{+} \rightleftharpoons SOIL - B^{+} + A^{+}$$

The total amount of cations held exchangeable by a unit of soil is defined as the cation exchange capacity or CEC. The CEC is usually the sum of Ca^{2+}, Mg^{2+}, K^{+}, Na^{+} and Al^{3+} held originally by the soil system (Kelley, 1948).

3.6.7.1 Cation Selectivity

A major limitation of the DDL theory is the failure to predict selectivity of mineral surfaces for cations of the same valence. Such preference is related to the relative hydrated ion size. The hydrated radius of small ions has greater charge density per unit volume which attracts hydrated water more strongly. Thus, their effective radius becomes much larger than other ions and are consequently held less tightly by the colloid charged surface (Kelley, 1948; Bohn, 1971; and Sparks, 1986). The above generalizations arise from data such as those shown in Table 3.3. The DDL theory indicates that the most important factor relative to the extent of adsorption or desorption is the counter-ion valence (Bohn, 1971; Sposito, 1984). Divalent ions are generally retained more strongly than monovalent ions and trivalent ions are retained even more strongly. The lyotropic series has been proposed to indicate the relative ion replaceability, or ease of removal from specific colloids. For example, the data presented in Table 3.3 could be written in order of relative ion replaceability as:

$$Li^+ = Na^+ > K^+ = NH_4^+ > Rb^+ > Cs^+ = Mg^{2+} > Ca^{2+} > Sr^{2+} = Ba^{2+} > La^{3+} = Al^{3+} > Th^{4+}$$

3.6.7.2 Qualitative Aspects

Thompson (1850) and Way (1850) indicated that cation exchange were reversible, stoichiometric and rapid. Exceptions to the above statement are as follows:

- retention of heavy metals by soil organic matter,

- cation fixation,

- large organic cations which are physically (stoically hindered) from approaching certain interlayer exchange sites,

- in some cases multivalent cations are preferentially adsorbed because they can simultaneously balance several closely adjacent exchange sites.

3.6.7.3 Cation Fixation

Clay minerals of 2:1 structure have tetrahedral surface layers containing "hexagonal" holes between the oxygen atoms. These holes provide a possibility for cations to penetrate into the mineral's structure, provided the ion is small enough. But, smaller the cation, higher is the energy needed to dehydrate the ion. Experience shows that K, Rb, Cs, and also NH_4^+ can make use of this possibility, whereas Na and Li will not (Shainberg and Kemper, 1966).

The most predominant fixation is K-fixation on illite, vermiculite and on weathered mica edges. The potassium ions are held extremely preferentially with respect to other cations, and therefore are largely non-exchangeable. Thus, K-fixation reduces the CEC of the soil systems (Sposito, 1984). It should be mentioned that NH_4, Rb, and Cs are fixed roughly to the same extent as K ions on these clays.

An example of mineral vermiculite exhibiting unusually high preference for magnesium cation is illustrated in Figure 3.11. The dashed line in Figure 3.11 represents no ion preference, the dotted line is the typical case for Ca^{2+} - Mg^{2+} exchange

for clay minerals where as the solid line represents the actual Ca^{2+} - Mg^{2+} exchange for vermiculite. It is obvious that when the concentration of Mg^{2+} is greater than 40 percent in solution, vermiculite shows a pronounced preference for magnesium. This specific adsorption is due to the fact that the hydrated magnesium ion fits so well into the water network between partially expanded sheets of vermiculite.

3.6.7.4 Retention of Cation by Soil Organic

Polymer chains of humus will form complexes with certain cations, particularly heavy metals, which are held in place by covalent bonding (Kelley, 1948; Bohn, 1971). The complexed cation should be considered as part of the solid phase since its presence causes a decrease in the soil's CEC by organic matter. The chemical interactions of these complexes are not well understood (Snoeyink and Jenkins, 1980), but a possible chemical reaction between humic acid and copper is illustrated in Figure 3.12.

The stability of these complexes have been based upon experimental "constants" from which the following series was developed:

$$Cu^{2+} < Fe^{3+} = Pb^{2+} < Ni^{2+} < Co^{2+} < Mn^{2+}$$

This series is given in decreasing stability. These stability "constants" are very sensitive to pH. At a pH of 7 the cations are complexed much more strongly than at lower pH values (Snoeyink and Jenkins, 1980).

3.6.7.5 Cation Exchange Equation

The most general type of cation exchange relationship is a mass reaction of the form:

$$CaX + 2Na^{+} \rightleftharpoons 2NaX + Ca^{2+}$$

resulting in the selectivity coefficient, K_k:

$$K_k = \frac{[(NaX)^2 (Ca^{2+})]}{[(CaX)(Na^{+})^2]}$$

The above equation can be rearranged to:

$$\frac{(NaX)^2}{(CaX)} = K_k \frac{(Na^{+})^2}{(Ca^{2+})}$$

This equation is a Kerr type exchange equation in which Kerr used concentration in place of ion activity. The goal of each equation is to provide a relatively uniform exchange "constant", the selectivity coefficient, K_k, over a wide range of exchangeable cation compositions. The difficulty, as shown in Figure 3.13, is that the selectivity coefficients are approximately constant over a limited concentration range. This limits their practical application, (Bohn, 1971; Sparks, 1986).

3.6.8 Anion Retention

Anions are attracted electrostatically by positively charged sites on layered silicates, hydroxides and oxides minerals in

the same manner as cations are attracted to negatively charged soil colloids. There exist two processes by which anions are restrained by soil particles: (1) nonspecific adsorption, (2) specific adsorption.

3.6.8.1 Nonspecific Adsorption

Nonspecific adsorbed anions are retained by mineral surfaces by electrostatic forces only (Hingston et al., 1968). Figure 3.14(a) illustrates the nonspecific adsorption of chloride and Figure 3.14(b) shows the exchange of one nonspecific adsorbed anion (NO_3^-) for another (Cl^-). Nonspecific anions are readily exchangeable since they are weakly bonded. Exchangeable equations have been developed for such anions in the same manner as those developed for exchangeable cations. The anions Cl^-, NO_3^- and SO_4^{2-} are generally considered to be nonspecific. Table 3.4 indicates typical data for the adsorption of Cl^- and SO_4^{2-} by kaolinitic and montmorillonitic soils. The amount of anions adsorbed increases with the increase in acidity of the soil system. Also, at all pH values, the divalent SO_4^{2-} ion is retained to a greater extent than the monovalent Cl^- ion.

3.6.8.2 Specific Anion Reaction

Some hydrous oxides have a high preference for certain anions. This preference can not be explained by the DDL theory alone. In fact, hydrous oxides can scavenge arsenate, phosphate, molybdate and similar anions from solution with high efficiency (Hingston et al., 1968; Bohn, 1971). Ligand exchange, or anion penetration has been proposed to explain this strong phenomena (Hingston et al., 1968).

Ligand exchange can occur on surfaces initially carrying a net negative, positive or neutral charge. In contrast to nonspecific adsorption which occurs only when the soil colloids carry a net positive charge. Figure 3.15 demonstrates ligand exchange or anion penetration. The oxygen ion on the hydrous oxide surface is replaced by an anion, such as phosphate or fluoride. Maximum adsorption from ligand exchange for weak-acid anions occurs at pH values which are about equal to their equilibrium constants (pK values), as depicted in Figure 3.16.

3.7 Adsorption-Desorption Isotherms

An ideal mathematical model for soil/solute interaction does not exist in view of the following factors: (1) the sheer number of chemical reactions that can take place in a soil system; (2) these reactions are not all well understood, (3) the ability of a soil to attenuate a specific solute or contaminant is site specific.

Soil scientists have developed the experimental procedure of relating solute reaction to a soil through "adsorption isotherms". This simplistic method involves the establishing of the amount of solute (adsorbate) adsorbed or eluted as a function of its equilibrium concentration per unit weight of solid soil (adsorbent). In their strictest forms, adsorption or desorption isotherms do not include secondary reactions such as precipitation since equilibrium conditions must prevail. These isotherms do not model all geochemical reactions. Thus, adsorption or desorption isotherms model only: (1) physical adsorption resulting from van der Waals attractions, (2) chemical adsorption, (3) ion exchange

resulting from electrostatic attraction to charged sites on soil surfaces (Weber, 1975).

Factors influencing adsorption or desorption are:(1) the specific surface area of the mineral assemblage; (2) type and concentration of the solute in question; (3) pH; (4) temperature; (5) the presence of competing ions and the nature of the adsorbent (soil system) (Stumm and Morgan, 1970; Weber, 1972; and Yong, 1985). But adsorption isotherms have long been used to model geochemical reactions and are described by a number of investigators (e.g. Sposito, 1979; Horford, 1978; Karickhoff et al., 1979; Parker et al., 1984; and Conans, 1987).

The experimental procedure involves either batch-equilibrium tests or from direct solute-soil interactions in a standard column test.

The batch-equilibrium test procedure involves the complete mixing of a predetermined ratio of soil and solute of interest for a specific time or until equilibrium is reached at a constant temperature (usually 20°C). The difference between the initial and final solute concentration is the amount adsorbed.

A complete review of the batch-equilibrium test can be found in ASTM Standards ES-10-85 and D4319. The results are plotted on graph paper by showing the mass of solute adsorbed or desorbed per unit mass of soil (S) as a function of the concentration of the solute (C). Typical adsorption isotherms are illustrated in Figure 3.17, which are: a linear relationship (Figure 3.17(a)), a concave nonlinear or Freudlich type (Figure 3.17(b)), a convex nonlinear

relationship (Figure 3.17(c)), or a concave-linear relationship or Langmuir type (Figure 3.17(d)). A nonlinear relationship indicates that the amount adsorbed is a function of solute concentration (Bohn, 1979; Melnyk, 1985; and Schackelford, 1991). From the type of adsorption isotherm relationship, the retardation function, $R(C) = [1+\rho/\theta\ B(C)]$, as well as the buffering capacity, $B(C) = (\partial S/\partial C)$, can be evaluated.

3.7.1 Retardation Functions

3.7.1.1 Linear Relationship

A linear adsorption isotherm is represented by:

$$S = K_d C \tag{3.24a}$$

where S and C are the exchangeable and soluble ions, respectively; K_d is known as the distribution coefficient (Freeze and Cherry, 1979). Linear adsorption isotherms have been used by many researchers to model solute-soil interaction (e.g. Rowe et al., 1985; Quigley et al., 1987).

The buffering capacity is expressed as:

$$B(C) = K_d \tag{3.24b}$$

with the resulting retardation function as:

$$R = 1 + \frac{\rho}{\theta} K_d \tag{3.24c}$$

This expression indicates an infinite sink, which is incorrect since the soil has a limited retention capacity predicted by its CEC value. The effects of retardation on solute transport through the soil remains constant.

3.7.1.2 The Freundlich Equation

The Freundlich equation is an empirical formulation without a theoretical foundation and can be expressed as:

$$S = KC^n \tag{3.25a}$$

where K and n are constants and n > 1, the buffering capacity is expressed as:

$$B(C) = nKC^{n-1} \tag{3.25b}$$

and the retardation function as:

$$R = 1 + \frac{\rho}{\theta} nKC^{n-1} \tag{3.25c}$$

This retardation function implies that the amount of adsorption decreases logarithmically with increase in solute concentration, i.e. there is a decrease in the effect of soil retention as solute migrates through the soil. The limitation of the Freundlich equation is it does not predict a maximum adsorption capacity.

3.7.1.3 The Langmuir Equation

The Langmuir equation is based upon four assumptions:
(1) a constant energy of adsorption;

(2) adsorption takes place on specific sites with no interaction between adsorbate molecules;
(3) the maximum adsorption is equal to only the monolayer capacity of each reactive adsorbent surfaces;
(4) the ion exchange process involves the replacement of a single ion by another single ion.

The Langmuir equation is expressed as:

$$\frac{S}{S_{max}} = \frac{C}{\left[\frac{1}{K_1}\right] + C} \qquad (3.26a)$$

where S_{max} is the maximum adsorption of solute by the solid phase or soil system, and K_1 is a measure of the affinity of sorption sites on soil surfaces. The buffering capacity is expressed as:

$$B(C) = S_{max} \frac{1}{K_1[1/K_1 + C]^2} \qquad (3.26b)$$

and the retardation function is:

$$R = 1 + \frac{\rho}{\theta} \frac{S_{max}}{K_1[1/K_1 + C]^2} \qquad (3.26c)$$

The amount of retardation in a soil system is directly proportional to its S_{max} value. As solute concentration increases, retardation will decrease. And for solute concentrations which exceeds the maximum adsorption value, it will migrate through the soil medium as if uninfluenced by adsorption processes. One limitation of the Langmuir model is that adsorption at different species occurs beyond the monolayer capacity of the soil surface (Adamson, 1963). Also,

the Langmuir equation is limited to the specific range of experimental data and can not be extrapolated to a higher concentration range.

3.7.1.4 A 3 Parameter Relationship

In addition to the above mentioned deficiencies and limitations of the linear, Freundlich and Langmuir models, they also do not include desorption processes. A mathematical relationship expressing both adsorption and desorption processes (Warith, 1987), has the following form:

$$S = \alpha - \beta \exp(-\gamma C) \qquad (3.27a)$$

which is basically an asymptotic regression model; where α, β and γ are constants. This regression model seemed to overcome some of the disadvantages of the previously mentioned models (Warith, 1987). The constant α represents the maximum adsorption capacity of the soil system which is a function of the type of soil and the nature of the solute in question. The constant β represents the initial conditions of the soil system at C = 0,

$$\alpha - \beta = S_o \qquad (3.27b)$$

where S_o is the initial amount adsorbed of a specific species before migration. The constants α and β are dimensionless. The constant γ in equation 3.27a represents the affinity capacity of adsorption sites on soil surfaces for certain solute species. The buffering capacity of the soil is expressed as:

$$B(C) = \beta \gamma \exp(-\gamma C) \qquad (3.27c)$$

and the retardation function is:

$$R = 1 + \frac{\rho}{\theta} [\beta \gamma \exp(-\gamma C)] \qquad (3.27d)$$

The value of B(C) is greater than 0 for all adsorption processes and for desorption B(C) is always less than 0. This adsorption-desorption regression model is again limited to the range for which experimental data are available. Extrapolation to higher concentration may lead to erroneous predictions.

3.8 Method of Measurement

In general, transient methods are used to evaluate the effective diffusion coefficient and the buffering capacity of the soil. Several techniques are available but transient methods can be divided into 3 main categories: (1) column methods, (2) the half-cell method, (3) reservoir methods (e.g. Crooks and Quigley, 1984; Gillham et al., 1984; Rowe et al., 1985, 1988; Shackelford et al., 1989). When the interest is only diffusion migration with no advection, the half-cell and reservoir methods are used. For this reason, other methods will be neglected, for more details reference may be made to Freeze and Cherry (1979), Rowe et al (1988), and Shackelford (1991).

3.8.1 Half-Cell Method

The half-cell method involves the placement of two half-cells, each filled with saturated soil of different initial solution concentrations, together and allowing diffusion to take place. After a predetermined time period, the cells are separated,

the soil is sectioned to determine the resulting concentration profile (Olsen et al., 1965; Gillham et al., 1984). Though this approach has existed for a long time and is preferred by soil scientists, it may not correctly represent initial boundary conditions which exist in natural clay deposits nor for clay barriers at landfill sites. Also, it is difficult to insure a full contact area between the two half-cells which may lead to experimental errors.

3.8.2 Reservoir Methods

The reservoir method is a more appropriate technique for measuring effective diffusion coefficients in clay soils and is based upon methods developed by Mott and Nye (1968), Stoessell and Hanor (1975) and Rowe et al. (1988).

The reservoir method is divided into two groups: double reservoir and single reservoir. Furthermore, the single reservoir method can be separated into two types. The first one is a constant concentration source reservoir over time. The second one is a decreasing concentration source reservoir over time. Both reservoir methods with boundary conditions are illustrated in Figure 3.18.

3.8.2.1 Boundary Conditions

The boundary for the source reservoir which is allowed to decrease as solutes migrate into the soil plug is illustrated in Figure 3.18. It was demonstrated by Rowe and Booker (1985) that the concentration in the source reservoir, C_s, at any time t is a function of the initial concentration of that species C_o, diffusive mass flux across the soil sample, volume

of the reservoir, the cross-sectional area of the soil sample. This boundary condition is expressed as:

$$C_s(t) = C_o - \frac{1}{H_f}\int_0^t f_s(t)\,dt \qquad (3.28)$$

where H_f is the height of solution or leachate in the reservoir which is expressed by:

$$H_f = \frac{V_f}{A} \qquad (3.29)$$

where V_f is the volume of solution or leachate and A is the cross-sectional area of the soil sample. The diffusive mass flux $f_s(t)$ is proportional to the chemical potential across the top of the soil sample $(\partial C(t)/V\partial x)_s$ which is related to Fick's first law, which says:

$$f_s(t) = -\theta D_e\left[\frac{\partial C(t)}{\partial x}\right]_s \qquad (3.30)$$

Two base boundary conditions exist as illustrated in Figure 3.18. If the base is impermeable in such a way to create a zero-flux base boundary condition, Figure 3.18a, can be expressed as:

$$f_b(t) = -\theta D_e\left[\frac{\partial C(t)}{\partial x}\right]_b = 0 \quad for \quad t \geq 0 \qquad (3.31)$$

The second alternative is to have a collection chamber at the base with zero outflow but having an initial solute concentration equal to the background concentration of the sample's porewater, as shown in Figure 3.18b. Thus, as the

solute migrates through the soil sample, it increases its initial concentration in the collection chamber. This increase in concentration $C_b(t)$ with time is represented by:

$$C_b(t) = C_i + \frac{1}{H_c}\int_0^t f_b(t)\,dt \qquad (3.32)$$

where C_i is the initial background concentration which can be zero, H_c is the height of solution in the collection chamber and $f_b(t)$ is the mass flux into the reservoir from the soil at time t, which is defined in the same manner as $f_s(t)$, equation 3.30.

3.8.2.2 Procedure

The procedure concept is illustrated in Figure 3.19 for a single reservoir with zero flux at the base. This method was used to determine both the effective diffusion coefficient and the retardation factor in this research. A chemical gradient is created between the soil surface and the source reservoir. Solute migrates from the source reservoir through the soil and, if present, into the collection chamber; the concentration of solutes in the source reservoir will decrease with time as shown in Figure 3.19(a). At some predetermined time, the test is terminated and the concentration profile through the soil is determined by sectionalizing the sample as shown in Figure 3.19(b). The effective diffusion coefficient D_e is evaluated by fitting a theoretical solution to the experimental curves with prior knowledge of the retardation factor.

3.8.2.3 Advantages and Disadvantages of the Reservoir Method

The advantages are that undisturbed soil samples pertaining to the site of interest can be used for a direct evaluation of both D_e and R parameters. The determined diffusion coefficient is a true diffusion value since v = 0. The test is easier to perform and the testing period is relatively short. Another advantage is the direct determination of adsorption isotherms from undisturbed samples, since sorption values determined from batch equilibrium tests are usually performed at low solids to water ratios. The R value may not reflect solids to porewater ratios typical of the field situation (Voice et al., 1983). Also, boundary conditions between the source reservoir and the soil sample closely resemble field boundary conditions (leachate being contained by clay). However, obtaining a good seal between the soil sample and the plexiglass cylinder or mould can be difficult. An improper seal would allow diffusive flux to occur along the sides of the soil sample, which would result in overpredicting the effective diffusion coefficient.

3.9 Quality Assurance

Quality assurance during laboratory diffusive testing should include a mass balance analysis, pH, electrical conductivity (EC) and temperature measurements. Also, blank tests (control tests) i.e. tests without soil, to evaluate the possible loss of chemical species due to the testing apparatus. The mass balance is performed at the end of the test to determine if there was an experimental error. A mass balance error may indicate another chemical reaction has taking place, such as precipitation. Such losses would result in erroneous interpretation of the experimental data and give a false

effective diffusion coefficient and retardation factor for reactive solutes.

CHAPTER 4
FIELD INVESTIGATIONS

4.0 Geological Setting

4.0.1 General

A large part of eastern Ontario is covered by the Champlain Sea sediments commonly known as Leda clay. The history and properties of the clay soils encountered within the Champlain Sea basin have been the subject of numerous studies and extensive research, but few have studied the hydrogeological characteristics of the upper weathered zone.

Because of the large extent of the Champlain Sea, the nature, depositional environment and resulting properties of Leda clay vary from location and depth. The physical and geochemical properties of Leda clay depends on the local origins and history of the Champlain Sea.

The Champlain Sea was formed during the northerly recession of the Wisconsin ice sheet, around 12 800 BP. As deglaciation occurred, a channel opened up the gulf of the St. Lawrence which permitted the sea to invaded the depressed low lands of the St. Lawrence and the Ottawa valley (Gadd, 1975; Cronin, 1977). Thus, the chemical composition of the early Champlain Sea was probably a mixture of fresh water from glacial ice, rain, and snow and sea water.

The western Champlain Sea basin follows a narrow corridor along the upper Ottawa valley between Arnprior and Point Alexander, covers all of eastern Ontario east of Perth, extends into Quebec bounded to the north by the Ottawa river and southward into the United States along the St-Lawrence River, as depicted in Figure 4.0.

Marine environment terminated around 10,200 BP. Due to isostatic rebound of the earth's crust, fluvial systems developed which allowed drainage of fresh water from the upper great lakes (Gadd, 1962, 1975). Due to these environmental changes, eastern Ontario has six distinct lithofacies (Gadd, 1986). One of the most important and abundant is the offshore marine clay lithofacie, which is composed mainly of clay, silty clay and silts. It may show a rhythmical or cyclical texture and colour-banding and is usually calcareous and fossiliferous. The upper portion contains very fine grained sand lenses or pockets which decrease in frequency and thickness with depth. The upper section is usually mottled or laminated with reddish brown and blueish grey clay which become massive and uniform blue grey clay at greater depth.

A second important lithofacie is a clay/silt deposit resulting from a proto-fluvial system, which eroded the upper part of the original marine deposit. Due to variation in fluvial erosion and subsequent redeposition, the deposit may vary from uniform massive structureless blue grey clay to silty clay deposits. This silty clay deposit contains sand lenses, bars and channel fills. These have sand and silts of non-marine origins which were deposited during channel cutting.

The Champlain Sea deposits are usually underlain by a thin layer of glacial till and then by regional bedrock which may

be either: (1) shale or limestone for deposits found in the St. Lawrence lowlands south of the Ottawa river and west of the Frantenac arch; or (2) marble, quartzite, aluminous gneiss and metavolcanics from the upper Ottawa valley and Gatineau regions.

Champlain Sea clay deposits are composed of two zones: the upper weathered and fractures layer and by a relatively soft, unweathered clay. For the Ottawa area, the upper section in relatively thick deposits is often fissured to depths of 6 metres or more which is well below the observed weathered brown clay which seldom exceeds a depth of 2.0 metres (Eden and Crawford, 1957). Lafleur and Giroux (1983) established open fracture depth of 5 metres for Leda clay deposits around the Montreal region.

The Champlain Sea clay deposits in the upper St-Lawrence river valley are as thick as 65 metres in places but the average is about 30 metres (Karrow, 1972).

4.0.2 Champlain Sea Sediments

The Champlain Sea sediments are composed of very fine-grained rock flour derived from the Precambrian Shield. Investigations of the mineral composition of the Ottawa valley clays, reported for the clay-sized fraction as generally consisting of 40-60% non clay minerals (quartz, feldspar, amphiboles and carbonates). The clay mineral suit is approximately: 20 to 40% illite, 5 to 20% chlorite, and 5 to 10% smectite (swelling mineral) (e.g. Gillott, 1971; Yong et al., 1979; Quigley et al., 1983; Torrance 1988). In a recent study by Quigley et al. (1989) on clays from four different sites in the Ottawa/Carleton region, the clay fraction was

found to consist of abundant quartz, moderate to abundant feldspar, moderate amounts of illite and chlorite and with trace amounts of swelling clays (smectite).

Carbonates are commonly present in Champlain Sea sediments, ranging between zero and 12% with no apparent spatial pattern (Torrance, 1988). Quigley et al. (1989) reported carbonate content between 3 to 7.5% for the Ottawa area. Usually very low carbonate content is found in the upper weathered zone and also in the surface deposits that occurs in parts of the Ottawa Valley where sediments have been eroded and redeposited in a fresh water environment (Gadd, 1962, 1975).

Relatively small amounts of oxides and amorphous materials are present in Leda clays (Torrance, 1988).

4.0.3 Regional Porewater Chemistry

Champlain Sea sediments were initially deposited under near-marine conditions. At the later stages of glacial retreat, brackish conditions existed. But, most of the fine grained sediments were deposited in a mixture of about 33% seawater and 67% freshwater (Desaulniers and Cherry, 1989). The current low salinity of porewater reflects the post depositional removal of salts. The maximum salinity observed is 0.63 N (~36.9%) at 46 m depth at Plaisance Quebec (Torrance, 1988), and the lowest are observed in most near-surface zones (hydraulically active zones). This could be a consequence of salt removal, or it could reflect a low salinity environment during redeposition of sediments due to fluvial erosion.

The typical salt concentration profile (higher salt concentration with increasing depth) can be explained by a combination of leaching and molecular diffusion. The near-surface or weathered zone has been leached by infiltration of fresh rain water. Below this upper zone, salt removal has been accomplished by upward or downward migration of ions by diffusion, or both (Quigley et al., 1983; Torrance, 1988; and Desaulnier and Cherry, 1989).

In general, sodium is the dominant porewater cation, while bicarbonate and chlorite are the dominant anions. Calcium may be the cation with the highest concentration in the upper fractured zone where some weathering beyond leaching has occurred.

In higher salinity environments, the concentrations of magnesium and potassium are higher than calcium. If leaching has occurred, the Mg^{2+} and K^{+} concentration are usually lower than that of calcium.

In general, Leda clay porewater chemistry varies with location, depth and the nature of ionic species over great distance (Torrance, 1988).

4.0.4 Site Condition

The four study sites are located within the Champlain Sea deposit, as illustrated in Figures 4.0 and 4.1. The study sites will be referred as The National Research Council (NRC), Fallowfield, Renfrew and Casselman sites.

4.0.4.1 NRC Site

The NRC site is situated in the north-east of Ottawa as shown in Figure 4.1. The site is located on National Research Council property. This clayey deposit resulted from a proto-fluvial system (GSC, Map 1506A). Most of the property is flat, though bedrock outcroppings are frequent. The intervening valleys are filled with clay. The depth of clay varies, but usually extends beyond 18 metres (Eden and Crawford, 1957).

4.0.4.2 Fallowfield Site

The Fallowfield site is located in Goulburn Township, south-west of Ottawa as shown in Figure 4.1. The clayey deposit of the site is part of the offshore marine clay deposit (GSC Map 1506A). The property used for this research belongs to a local farmer and the field testing are conducted in a corn field. The site topography is flat, with a small creek to the east of the property. The clay deposit is approximately 20 metres in depth (M. Khan, University of Ottawa, personal communications, 1992).

4.0.4.3 Renfrew Site

The Renfrew site is situated 75 km west of Ottawa as shown on Figure 4.1. No official classification exists for this deposit. The study site is located in the south west sector of the city of Renfrew, on the municipal garage property. The site is relatively flat.

4.0.4.4 Casselman Site

The Casselman site is situated 60 km east of Ottawa as shown in Figure 4.1. This clay deposit is a result of a proto-fluvial system, (GSC Map 1507A). The study site is located approximately 15 metres away from the South Nation river. A difference of 15 m in elevation exists between the site and the surrounding plain. The clay deposit at this site is in excess of 26 metres thick (Cherron, 1978).

4.1 Methodology

4.1.1 General

The field investigation involved the collection of data at four sites located throughout eastern Ontario within the Western Champlain Sea basin. All major research activities were conducted at NRC and Fallowfield sites, while Renfrew and Casselman sites were used to obtain complementary information.

The first phase of the field program involved the installation of a piezometer nest and soil sampling on each site. Boreholes were drilled during the period of December 1989 to May 1990. Drilling was conducted by OGS Ltd. of Ottawa, Ontario using a CME 55 continuous flight auger rig. Physical testing of the soil samples was carried out by Fondex Ltd. and by the Geotechnical Engineering Laboratory of University of Ottawa.

Following piezometer installation, water level responses to climatic change were monitored regularly in each piezometer. After the water level had reached equilibrium, hydraulic conductivity tests were conducted at each site by means of the

slug test. An attempt was made to measure hydraulic conductivity with the use of a self-boring permeameter as described by Tavenas et al. (1986). The self-boring equipment, PERMAC model developed by Rocktest Inc., Montreal, was found to be unsuitable for use in cold weather conditions.

Test pits and large well pump tests were also undertaken at the two principal sites.

At each site, the geochemistry was assessed by undertaking chemical analysis of groundwater samples from piezometers at various depths. Also, a profile of porewater chemistry from squeezed core samples was performed for the NRC site. The chemical analysis included the determination of major ion concentrations in solution, pH, conductivity and tritium.

4.1.2 Soil Sampling

Soil sampling was conducted to determine soil type and corresponding physical properties. Samples were taken using the CME continuous sampler and the thin walled Shelby tube. At each site, a 12 metre borehole was drilled using the continuous sampler to obtain a detailed overburden profile and to observe any geological heterogeneity. Soil samples were sent to Fondex Ltd. for the determination of grain size distribution, natural water content and Atterberg limits.

In addition, physical properties such as specific gravity, unit weight, and porosity were determined at the University of Ottawa on soil samples taken using a Shelby tube of 5 cm diameter. Soil samples were also used in diffusion experiments at the University of Ottawa.

4.1.3 Piezometer Installation Techniques

Two different techniques were used to install the piezometers: the conventional augering method and the double-Shelby method developed at the University of Waterloo (D'Astous et al., 1989).

The conventional augering method refers to the installation of the piezometer in a 15 cm diameter augered borehole as illustrated in Figure 4.2. A sand pack was placed around the tip of the piezometer and sealed with 1 m of bentonite. The remainder of the borehole was then filled with a mixture of cuttings, bentonite and concrete.

The double-Shelby piezometer is installed by using two Shelby tubes of different diameters and opposite bevelled edges as shown in Figure 4.3. This method consisted in drilling a borehole with a (83 mm i.d.) hollow-stem auger to 0.5 m above the desired permeable piezometer tip depth. The first shelby tube with a diameter of 51 mm, bevelled on the outside, was hydraulically pushed 0.4 m through the center of the augered hole. The second Shelby tube with a larger diameter of 76mm, bevelled on the inside, was then hydraulically pushed through the center of the first Shelby hole to a depth of 0.5 m.

A detailed piezometer nest was installed at the two principal sites, NRC and Fallowfield. Twelve (12) piezometers were set in twelve boreholes using both installation techniques. Nine (9) piezometers were installed at small intervals in the upper near surface zone, less than 6.0 m deep. Most of these piezometers were set using the double Shelby method, though the conventional augering method was used on two occasions for comparison purposes. The shallow piezometers have a 3.8 cm

diameter and a filter screen length of 0.3 m. For piezometers installed below a depth of 6.0 m, the conventional method was used. These piezometers have a permeable filter tip of 1.5m in length with a corresponding diameter of 25.4 cm.

Piezometers nest of seven (7) and eight (8) piezometers were installed at the two complementary sites, Renfrew and Casselman, respectively. Installation methods, as previously stated, were used. The details of piezometer installation for all four sites are given in Appendix A.

4.1.4 Field Testing

Monitoring of the water levels was conducted periodically after the installation of the piezometer nests. The number of water level readings varied from 19 at complementary sites to 61 at the principal ones. A higher frequency of readings was taken at all sites during 1990 with only seasonal measurements taken during 1991. All piezometers reached equilibrium within one month after their installation.

Hydraulic head profiles were obtained following the survey of the piezometers. All piezometers were referenced to an arbitrary bench mark of 100 metres.

In-situ hydraulic conductivity tests were conducted on all piezometers at all four sites using the slug test (rising head method). The analysis of the data was performed using both the Hvorslev method (1951) and the Bouwer and Rice method (1976).

Daily rainfall data for 1990 were obtained from Environment Canada for the monitoring station at the Ottawa International Airport.

In addition to borehole logging, a test pit was excavated at each of the principal sites. These test pits were used to observe the geological features of the upper weathered zone. Typically, the excavations were to 3.8 and 4.0 m below ground surface.

Finally, a 15 cm diameter monitoring well was placed in each test pit as schematically shown in Figure 4.4. This monitoring well was later used to conduct a pump test. Well recovery data were analyzed using methods established by Bouwer and Rice (1976) and Boast and Kirkham (1971).

4.1.5 Geochemistry

4.1.5.1 General

Chemical analysis were carried out on groundwater samples obtained from selected piezometers at all four sites. Porewater samples obtained from soil samples were also analyzed for the NRC site. The chemical analysis included the determination of major ion concentrations in solution, pH, conductivity, tritium and exchangeable cations in porewater samples only.

4.1.5.2 Water Sampling at Piezometers

The selected piezometers were initially purged. After the piezometers had recovered, water samples were collected using a one-way valve pump placed at the end of a tygon tube which

was operated by a manual jerking motion. Each piezometer was pumped with its own tygon tube, and after each sample collection, the valve was cleaned with distilled water. The initial discharge was used to rinse the tubing and the 125 ml high density polyethylene sample bottle. The sample bottles were then transported back to the laboratory and filtered by centrifuge (IEC Model B-20) immediately. The samples were kept refrigerated at 4 °C until tested. pH, conductivity and alkalinity were measured after filtration.

4.1.5.2 Water collection by squeezing

In addition to water samples taken from piezometers, porewater squeezed from core samples from NRC was also analyzed. The major-ion chemistry obtained was compared with the results from chemical analysis of the piezometer water. Soil samples were collected during the piezometer installation. The soil samples were also extracted from the Shelby tubes back at the laboratory. The samples were then sectioned, wrapped in saran wrap, waxed and stored in a cold room that was maintained at 4 °C to slow the rate of sediment aging (Lessard and Mitchell, 1985).

The soil samples were squeezed using a modified 5 cm floating-ring oedometer, schematically illustrated in Figure 4.5. Core samples were unwrapped and cut with the floating-ring's sharp edge. The outer edges were quickly trimmed, a glass micro fibre filter paper was placed at the base , while a rubber stopper was placed on top. This system would allow water migration in one direction only.

A maximum of 2 MPa squeezing pressure was gradually applied for approximately 1 hr. The squeezing was conducted at a laboratory temperature of (20 +/- 1°C).

Previous research into hyperfiltration due to pressure effects during squeezing, concluded that pressures of up to 4.83 MPa (700 psi) caused negligible chemical change to extruded porewater (e.g. Manheim, 1966; Kalil and Goldhaber, 1973; Manheim and Sayles, 1974; Patterson et al., 1978; and Rodvang, 1987).

Because squeezing produces very small volumes of porewater, extreme care was used when assembling the squeezing apparatus to minimize the potential for contamination. Between squeezing runs, all squeezer parts were washed thoroughly with ordinary tap water, then were soaked and rewashed in deionized water and finally oven dried to remove all possible chemicals and clay particles.

4.1.5.3 Water analysis

All water analyses were performed at the Geochemistry Laboratory of the University of Ottawa. Cation (Na^+, K^+, Mg^{2+}, Ca^{2+}) concentrations were measured using a Thermo Jarwell Ash Atomic Scan (ICP-AES, Inductively Couple Plasma Atomic Emission Spectrometer). Anions (Cl^-, SO_4^{2-}) concentrations were measured using a Waters 880 High Pressure Liquid Chromatography system with conductivity detector.

Alkalinity was measured from a standard acid titration test with H_2SO_4 to a pH of 4.3. Conductivity was analyzed by a Radiometer Copenhagen type CDM22 conductivity meter. pH was measured using a Fisher Accumet pH meter, model 210.

A charge balance was done to verify the quality of the data and as a check that all major ions were identified.

The cation exchange capacity (CEC) and exchangeable cations were determined by washing soil samples with silver thiourea solution (Chhabra, 1975).

An alkalinity test was not possible on the porewater squeezed from the samples due to the small amounts produced.

Tritium analysis was undertaken on groundwater samples by the Alberta Environmental Center, Environmental Isotopes Section, located in Vergreville, Alberta.

4.2 Results

4.2.1 Site Geology

The local geology was obtained for each site by drilling a continuously sampled 12 m borehole. The results of the borehole samples and the complete borehole profile are presented in Appendix B. The observed overburden stratigraphy for each site is given in the logs.

4.2.1.1 NRC

The stratigraphic profile at the NRC site consists of an upper 4m thick stratified, brown and grey, silty clay with a stiff consistency. Traces of roots and oxidation bands were observed in the upper section. Underlying the upper layer is a 0.5 metre thin, soft, grey silty clay band. Below 4.60 m depth, the grey silty clay is generally stiff. Traces of organic matter and marine shells were observed beyond 10.0 m depth.

Grain size distributions and Atterberg limits were conducted on three samples at the following depths: 2.2, 5.2, and 11.3 metres. Grain size distribution curves are presented in Figure 4.6a. The percentage of clay fraction varies from 50 to 74%. The percentage of clay fraction decreases with depth. The Atterberg limits and clay fraction versus depth for all four sites are presented in Figure 4.6b.

A detailed water content profile is given in Figure 4.7, for the NRC site only. The water content ranged from 39 to 93%. As depicted in Figure 4.7, the water content steadily increases to reach the maximum value of 93% at a depth of 5.5

m, and slowly decreases to a value of 57% at 12.2 m depth. The water content exceeds the liquid limit below 5.0 m, indicating a sensitive clay.

Based upon Casagrande's plasticity chart, the upper 5 m of the clay deposit has a high plasticity, while the deeper clay has medium plasticity.

This clay deposit has a specific gravity, Gs, of 2.80.

4.2.1.2 Fallowfield

The soil stratigraphy at the Fallowfield site consists of an upper 2.3m thick brown silty clay with some pebbles and traces of oxidation. This stratigraphic unit is soft and wet and is interbedded with numerous sand lenses. A transition zone is found between 2.3 and 4.5 metres depth, this zone consists of stratified brown and grey clay with sporadic sand lenses and roots. Underlying the transition unit, the clay deposit becomes a grey silty clay, relatively soft and wet.

Grain size distribution curves are presented in Figure 4.8 for samples taken at 2.1, 5.2 and 11.3 metres. The test results indicate that the clay deposit is a silty clay with the clay fraction ranging approximately between 45 to 65%. The percentage of clay fraction increases with depth, contrary to the NRC site.

The water content for the three samples varies from 34% to a maximum of 49.5%. The water content showed a steady increase with depth. The liquid limit decreases with depth while the plastic limit remains fairly constant throughout the first 12

metres (see Figure 4.6b). The water content with depth exceeds the liquid limit indicating a sensitive clay.

This deposit can be characterized as a medium plastic inorganic clay, based upon Casagrande's plasticity chart.

This clay deposit has a specific gravity of 2.80.

4.2.1.3 Renfrew

The soil profile is comprised of a 1.45m thick brown silty clay layer which is underlaid by 3.9m thick laminated silty clay layer. This unit is composed of stratified brown and grey silty clay with some pebbles. A grey silty clay, generally hard, with inclusions of soft and wet layers is found below the stratified unit.

Grain size distribution curves are represented in Figure 4.9 for three samples collected at 2.1, 5.2 and 11.3 m. The test results indicate that the percentage of clay fraction is fairly constant with depth, ranging between 55 and 60%. This deposit is classified as a silty clay.

There was little variation in water content throughout the clay deposit, ranging from 38 to 46%. The liquid and plastic limit also remained fairly constant throughout the deposit. The liquid limit is surpassed by the water content only below 10.0 m depth (see Figure 4.6b.).

From Casagrande's plasticity chart, this deposit can be characterized as clay of medium plasticity.

This clay deposit has a specific gravity of 2.70.

4.2.1.4 Casselman

The soil stratigraphy at the Casselman site consist of a 0.6 m thick topsoil overlying a 4.9 m thick brown silty clay layer. The brown clay is generally stiff. Inclusions of sand and silt are present in this brown clay unit which becomes more reddish-brown at 2.5m depth. Below 5.5m depth, a stiff greyish silty clay is found to the borehole completion. Traces of organic matter are found at 6.0m depth.

Grain size distribution curves are presented in Figure 4.10 for three samples taken at 2.1, 5.2 and 11.3 metres depth. The test results indicated that the clay fraction increased dramatically between 2.1 and 5.2m, from 32 to 69%. The clay fraction increases to 75% at 11.3m depth. The upper part of the deposit differs significantly in grain size containing more silt and fine sand size particles (see Figure 4.6b).

The water content varied from 23 to 73%. The water content showed a steady increase with depth. A sensitive clay is found at greater depth similar to the three sites.

From Casagrande's plasticity chart, this clay deposit can be characterized as a medium to high plasticity clay.

This clay deposit has a specific gravity of 2.70.

4.2.2 Test Pit Observations

In addition to borehole drilling, a test pit was excavated at each of the principal sites. These test pits allowed for direct observation of the physical features of the upper weathered zone. The details of test pit observations for each

site are provided in Appendix C. A short summary is given in the following sections.

4.2.2.1 NRC Site

The NRC test pit was oriented 15 degrees northwest from the magnetic North, along its long axis. It was excavated by backhoe to a depth of 4.0 metres. The maximum width of the excavation was 1.6 m with a corresponding length of 11.0 m. A photograph showing the geological features of the upper weathered crust is given in Figure 4.11.

The following is a summary of the observations given in Appendix C.

- A zone composed of oxidized silty, grey-brown clay extends from the surface to an approximate depth of 1.3m. Oxidized reddish clay bands with maximum width equal to 10 mm are present to a depth of 2.7 m. A 10 mm organic layer was observed at 0.55 m below ground surface. From 2.0 to 4.0 m, the clay matrix is greyish and very stiff.

- Root systems are found to a depth of 2.0 m and paleoroots were observed to a depth of 4.0 m. The greatest density of paleoroots occurs between 2.0 and 3.5 m.

- Fractures became observable below a depth of 1.1m and extended to the bottom of the excavation (4.0 m). The fractures were very distinctive below 2.5 m where they become long and planar. Below 2.5 m, the fractures divide the clay matrix into large tabular blocks which extend to the bottom of the pit.

- Fracture spacing with depth is represented in Figure 4.12. The fracture spacing increased with depth, ranging from one fracture every 4 cm at 1.5 m depth to one fracture per 40 cm at 3.5 m depth. The average length of fractures is given in Figure 4.13. The average length of fissures ranges from 1 to 5 cm at depth of 1.5m to over 50 cm at 2.5 m.

- The contact zone between the fractures becomes more moist and granular with depth, indicating increasing hydraulic activity. Water flow was observed in some fissures below a depth of 2.5 m. The water infiltrated into the test pit at a rate of approximately 70 l/hr.

- Fracture orientation data are summarized in the stereographic representation in Figure 4.14. From the polar representation, four fracture orientations were observed. These orientations are: 176, 205, 268, and 304 degrees from the magnetic North, to sets of fractures almost 90° from each other. Fracture dips ranged from 70 to 90 degrees with the highest concentrations between 80 and 90 degrees.

4.2.2.2 Fallowfield Site

The Fallowfield test pit was excavated by backhoe to a depth of 3.8 m. It was oriented, along its axis, 75 degrees southwest from the magnetic North. The length and width of the excavation were 8.5 m and 1.9 m, respectively. A photograph showing the geological features of the upper weathered crust is given in Figure 4.15.

The following is summary of the observations given in Appendix C.

- A zone composed mainly of oxidized light brown silty clay extends from the surface to an approximate depth of 2.0m. Mineral alteration and/or oxidation around roots, root holes, fractures and small pores are found between 0.2 and 2.0m. Between 1.4 and 3.25 m in depth, the clay matrix is interbedded with 26 fine sand layers. These sand beds range from 1 to 12 mm in thickness. Organic bands are found between 3.25 and 3.8 m in depth.

- The sudden change in the colour of the clay matrix from light brown to grey at a depth 2.0 m, may indicate the extent of oxidation that has taken place. The root system extends to a depth of 2.5 m.

- Above the water table, measured at 1.0m depth, the fractures are distinctive. The fracture spacing varied from one fracture every 1.5 mm at 0.5 m depth to one fracture per 5 mm at 1.0 m depth. Below the water table, the fracture was obscured due to the nature of the soil conditions. The clay, being very wet and soft obscured observation of any distinctive fracture faces, unlike at the NRC site where the upper clay is very stiff. Small pores or canals were visible below the water table. These features may represent fracture intersections in which water can percolate easily. The density of both fractures and pores with depth is represented in Figure 4.16. The pore density decreased with depth, ranging from 100 per 100cm^2 at 1.5m depth to none at a depth of 3.5m.

- Most of the water flow was observed entering the pit through the small sand beds which were very active. The measured flow was evaluated approximately at 220 l/hr.

- As mentioned above, fractures are not well defined and seemed to have a random orientation. But, while the trench was being excavated, the southern wall failed to retain its vertical form. This failure revealed four possible fracture faces. These fracture faces ranged from 1.8 to 2.9 m in depth. Two faces had a horizontal distance of 15 cm, while the other two had a width of 50 cm. Their dips were all vertical with the following orientations: 220, 222, 275 and 280 degrees from the magnetic North.

4.2.3 Physical Hydrogeology

4.2.3.1 Groundwater Conditions

4.2.3.1.1 NRC

The piezometers at the NRC site were installed in February 1990. Water level monitoring started shortly after piezometer installation. Water level measurements for the upper piezometers were not possible, during the winter months, due to freezing of ground water. The ground water level measurements and corresponding head levels are given in Tables 4.1 and 4.2. The water table fluctuated seasonally by 1.2 m, from lying on the ground surface in the fall of 1990 to a depth of 1.2 m in early August 1991.

Water level fluctuations with time are shown in Figure 4.17 and unfiltered water level elevations with time are given in

Appendix D. Also, water level variations with depth for selected time intervals are shown in Figure 4.18. These two figures indicate that all piezometers respond to seasonal variation in climatic conditions. High ground water levels are observed in late spring and fall whereas the lower levels occur during the dry summer months. Water levels in the upper 4.5 m follow each other closely and seem to respond to short term precipitation events. The deeper piezometers seem to fluctuate to seasonal variations only and do not respond to short term precipitation events. Daily rainfall records for the year 1990, recorded at the Ottawa International Airport are provided on Figure 4.19.

The maximum difference in water level variations with depth is illustrated in Figure 4.20. Variations in the order of 1.1 m are recorded for piezometers installed in the upper 4.5 m. The maximum variations decrease with increasing depth ranging from 0.81 m at a depth of 6.1 m to 0.42 m at a depth of 12.2 m.

Hydraulic head profiles for selected times are illustrated in Figure 4.21. There exist a small upward hydraulic gradient, measured at 0.04, in the upper 4.5 metres of the deposit in the fall (October, November) and early spring (April, May). In the summer months, the hydraulic gradient is negligible to depths of up to 7.4 m (August 91). A downward hydraulic gradient was observed for the rest of the profiles. From the average hydraulic head profile in Figure 4.22, an average downward gradient of 0.084 existed between 4.4 and 6.5 m and a higher average gradient of 0.12 was measured below 7.4 m.

The change in hydraulic gradients indicated between 6.4 and 7.4 metres depths for August, October and November can be

attributed to the interference of piezometer screen and sand pack between instruments.

The hydraulic responses for both types of piezometer designs (auger hole and "double-Shelby"), installed at depths of 3.0m and 6.1m, are also illustrated in Figures 4.18, 4.20 and 4.21. At a depth of 3.0m, a small but noticeable difference in water levels and hydraulic heads is observed, while at 6.1 metres, both types of instruments show comparable results.

4.2.3.1.2 Fallowfield

Water level readings commenced January 15, 1990 and ended on August 3, 1991. The resulting water table levels are given in Table 4.3. The corresponding hydraulic heads are provided in Table 4.4. The water table fluctuated seasonally by 1.08m. The highest value measured near the ground surface at 0.25m depth in the late fall of 1990 while the lowest value measured at a depth of 1.33m in August 1991.

Water level fluctuations with time are shown in Figure 4.23 and unfiltered water level elevations with time are given in Appendix D. Also, water level variation with depth for selected time intervals are shown in Figure 4.24. These two figures indicate that all piezometers respond to seasonal variations in precipitation. Again, high ground water tables are observed in late spring and fall whereas the low levels occur during the dry summer months. Water levels in the upper 3.2 metres (PZ-8 to PZ-12) follow each other closely and seem to respond to short term precipitation events, see Figure 4.19. Piezometer PZ-7 at a depth of 3.7m has similar short-term response in water level variations to the piezometers above it but does not reach the same water level elevations.

Piezometers installed below 3.7 metres show only seasonal trends.

The maximum difference in water level variations with depth is illustrated in Figure 4.25. Variations in the order of 1.1 m are recorded for piezometers installed in the upper 3.2 m. There is a marked decline in variation differences between 3.2 m and 4.3 m. Below this depth, of 4.3m, maximum differences decrease steadily from 0.68 m to 0.37 m.

Hydraulic head profiles for selected intervals are given in Figure 4.26. A non-uniform downward hydraulic gradient existed throughout the profiles during spring and fall, except between 6.0 and 7.5 metres, where the data shows an upward gradient. An upward gradient is well developed in the summer months above a depth of 9.9 m, with an average value of 0.32. The lowest downward gradients are found in the upper 3.2m, ranging from 0.005 to 0.017. The highest downward gradients are found between 3.2 and 4.3 m, and range from 0.1 to 0.62. From the average hydraulic head profile in Figure 4.27. An average downward hydraulic gradient of 0.024 was calculated between 4.3 and 12.1 m.

A comparison between both piezometer installation techniques for depths of 3.0 m and 4.3 m is also illustrated in Figures 4.24, 4.25 and 4.26. The results from all three graphs show little variation for both methods. However, a difference of 13 cm in the hydraulic head is noted for September 27, 1990 with the auger hole piezometer having a higher water level elevation.

4.2.3.1.3 Renfrew

Water level readings were taken 20 times in all piezometers since their installation in February 1990 until August 1991. The ground water level measurements and corresponding hydraulic head levels are given in Tables 4.5 and 4.6. The water table fluctuated seasonally by 1.11 m. The highest water table level was recorded at 0.17 m in the fall of 1990, while the lowest was measured at 1.36m in the summer 1991.

Water level fluctuations with time are shown in Figure 4.28 and water level variation with depth for selected intervals are shown in Figure 4.29. Figures 4.28 and 4.29 indicate that all piezometers respond to seasonal surface groundwater fluctuations with peak values occurring during the spring and autumn months and low values recorded in summer. Water level elevations recorded at 9.15m (PZ-2) were higher than at 8.4m (PZ-3). It should be noted that the slotted piezometer, PZ-2, extends from 9.15 to 7.65m whereas, PZ-3, extends from 8.4 to 8.1m. Water levels in the upper 5.9 m follow each other closely .

Figure 4.30 shows the maximum measured variation in groundwater levels with depth which range from 1.05m to 1.14m in the upper 8.4m. Piezometers at 9.15 m and 12.2 m show smaller variations of 0.90 m and 0.50 m, respectively.

Hydraulic head profiles in Figure 4.31 show a general downward trend with depth. The registered gradient in the upper 5.9 m is small, with an average value of 0.02. The average hydraulic head profile is given in Figure 4.32. Between 5.9 m and 12.2 m the average downward gradient is 0.25. The upward gradient indicated between 8.4 and 9.15 m could be

attributed to the sand pack of PZ-2 (9.15m) which extends above PZ-3 (8.4 m).

4.2.3.1.4 Casselman

Water level readings were taken in all piezometers 19 times between April 1990 to August 1991. The groundwater level measurements and corresponding hydraulic heads are given in Table 4.7 and 4.8. The water table varied seasonally from 0.5m depth in the spring and fall to 2.9 m depth in August, 1991.

Water level fluctuations with time are shown in Figure 4.33 and the water level variation with depth for selected intervals are shown in Figure 4.34. Water levels show a seasonal response by piezometers at all depths with peak values recorded in the Spring and Fall and lower values occurring in the summer months.

Piezometers located in the upper 4.40 m register the same water level elevations and response to groundwater fluctuations.

Large variations in water levels in excess of 2.4 m were measured in the upper 4.4 m. Maximum variation decreased dramatically below 4.4 m depth, ranging from 0.60 m at 6.4m to 0.42 m at 12.2 m. Maximum water level variations are shown in Figure 4.35.

Hydraulic head profile in Figure 4.36 demonstrates that a strong downward gradient exists at this site. In the upper 4.4 m, a gradient of 0.035 was calculated. Between 4.4 m and 6.4 m a strong gradient ranging from 0.47 to 1.18 has been

registered. A non-existent gradient is found between 6.4 and 9.1 m in the spring and fall, but an upward gradient is recorded during the dry summer months. The average hydraulic head profile plotted on Figure 4.37 which shows an average gradient between 4.4m and 12.2m of 0.40.

Again, both types of piezometers installed at depths of 3.0m and 4.4m show little discrepancies in measured data.

4.2.3.2 Determination of Hydraulic Conductivity Values

Determination of all hydraulic conductivity values were performed by rising head tests (slug test). This involved the removal of a known volume of water from the piezometer below its equilibrium level. This method was employed to preserve the natural chemical and isotropic characteristics of the groundwater in each piezometer. Response data were plotted in the manner outline by Hvorslev (1951). Only the corresponding straight line portion of the graphs was used for analysis. Tests involving the addition of water were not performed.

Since all plotted response data have a straight line segment, the assumptions inherent to both methods of Hvorslev (1951) and Bouwer and Rice (1976) are valid. This result would imply that fracture storage has relatively unimportant effect during the localized, short-term stress imposed by the response test. The plotted graphs for all piezometers are given in Appendix D.

4.2.3.2.1 NRC Site

Results of hydraulic conductivity analysis are presented in Table 4.9 with a reference made to the type of piezometer

installation. Hydraulic conductivity (K) values range from a maximum of 3.9×10^{-7} m/s to a minimum of 8.2×10^{-10} m/s, a difference in excess of two orders of magnitude. From the hydraulic conductivity profile shown in Figure 4.38, the higher K values ($> 10^{-8}$ m/s) were obtained in the upper 4.4 metres of the clay deposit. A marked decrease was observed at 6.1 m depth, with K becoming fairly constant with depth, ranging from 8.2×10^{-10} to 1.7×10^{-9} m/s.

Caution needs to be exercised when analyzing slug test data in a relatively impervious medium using the Bouwer and Rice (1976) method, since the depth of this medium was not established in this investigation.

The effects of piezometer design on hydraulic conductivity values were investigated at 3.0 and 6.0 metres depth. At 3.0m the double-Shelby installation technique produced higher hydraulic conductivity values, up to two orders of magnitude. But, no significant difference between the two methods is observed at 6.0 m.

At the NRC site, hydraulic conductivity ranged from 2.26×10^{-6} to 2.64×10^{-6} m/s based upon the large well recovery data. The results are presented in Table 4.10, with the two methods of analysis employed: Bouwer and Rice (1976) and Boast and Kirkham (1971). Also the recovery data for the large well are presented in Figure 4.39. Only the straight line portion of the plotted curve was used in the analysis. Hydraulic conductivities based upon the large well test are approximately 10 times larger than those obtained by the double-Shelby method between depths of 2 and 3 metres.

4.2.3.2.2 Fallowfield Site

Results of rising head tests for each piezometer are presented in Table 4.11, with reference made the type of piezometer used. The hydraulic conductivity profile is given on Figure 4.40. The hydraulic conductivities ranged from a maximum of 5.4×10^{-5} m/s at a depth of 2.10 m to a minimum of 1.07×10^{-9} m/s at 12.50 m. The higher values (10^{-5} to 10^{-6} m/s) were measured in the upper 3.70 metres of the deposit. A sharp decrease occurs between 3.70 and 4.30 m depth. Where the K values decrease from 1.2×10^{-6} m/s to 3.4×10^{-9} m/s, a difference of three orders of magnitude. In general, a linear reduction of the hydraulic conductivity was observed below 4.30 m depth.

Again, a comparison between the two piezometer installation techniques was investigated at depth of 3.0 and 4.4 metres. At a depth of 3.0 m, the augered piezometer gave a hydraulic conductivity value of 3.2×10^{-7} m/s while the double-Shelby method reported a value of 7.60×10^{-6} m/s. The double-Shelby piezometer produced much higher hydraulic conductivity values, similar to the NRC site. At 4.4 m depth, no significant difference in the K values was noticeable between the two installation methods.

The results of hydraulic conductivity tests performed on the large well are presented in Table 4.10. The analysis performed by the Boast and Kirkham (1971) method produced a slightly higher value of 8.10×10^{-6} m/s than the Bouwer and Rice (1976) method. Their technique reported a K value of 3.61×10^{-6} m/s. These two values compare favourably with measured hydraulic conductivity values, in the upper 3.0 m, by

the double-Shelby technique. The well recovery data are plotted on Figure 4.41.

4.2.3.2.3 Renfrew Site

Hydraulic conductivity values measured from field tests are presented in Table 4.12, and the corresponding profile is provided on Figure 4.42. Hydraulic conductivity values ranged from 2.05 x 10^{-5} m/s at a depth of 4.60 m to 1.3 x 10^{-9} m/s at 12.20 m. There is a marked decrease in the K values between 4.60 and 5.90 m, with a 3 orders of magnitude difference. In the upper 3.0 metres of the deposit, the hydraulic conductivity varied from 1.96 to 5.24 x 10^{-7} m/s, a difference of 2 orders of magnitude compared to the value obtained at 4.60 m and a one order of difference to the K value at 5.90 m. This difference increases to two orders of magnitude below 8.4 metres. Between 5.90 m and 8.40 m, the conductivity decreases linearly with depth. From 8.4 m to 12.2 m, the hydraulic conductivity was relatively uniform, ranging from 1.30 to 2.75 x 10^{-9} m/s.

No comparison was performed at this site between the two piezometer installation techniques.

4.2.3.2.4 Casselman Site

Field test results for hydraulic conductivity evaluated for the Casselman site are provided in Table 4.13. The hydraulic conductivity profile is plotted on Figure 4.43. Values ranged from a high of 1.4 x 10^{-7} m/s to a low of 1.4 x 10^{-9} m/s, a difference of about two orders of magnitude. In general, the higher conductivities are found in the upper 6.40 m of the clay deposit. Below this depth, a steady decrease in the

hydraulic conductivity values was observed. No distinctive pattern exist in the upper fractured clay, as compared to the other three sites.

At a depth of 4.40 metres, the auger piezometer gave a slightly lower hydraulic conductivity value (9.33×10^{-8} m/s), compared to the double-Shelby piezometer (1.19×10^{-7} m/s).

4.2.3.2.5 Comparison Between All Four Sites

Hydraulic conductivity profiles for the four sites are presented in Figure 4.44. The data show a general decrease in conductivity values with depth, although each site is inherently different. In the upper fractured zone, hydraulic conductivity values ranged from 1.85×10^{-8} to 2.05×10^{-5} m/s. The hydraulic conductivity in the upper 6.0 metres are highly scattered. At all four sites, the conductivity encountered at the deepest installed piezometers fall within a small span, between 8.20×10^{-10} to 1.40×10^{-9} m/s.

4.2.3.3 Estimation of Fracture Aperture

The estimation of fracture apertures was based on Snow's method (1968). Snow's method required prior knowledge of fracture spacing and hydraulic conductivity. The fracture spacing for the two principle sites was obtained through test pit observations. No direct observations of fracture spacing were available for the two minor sites. NRC fracture spacings were assumed to be characteristic of upper fractured Leda clay deposits at the two minor sites. Also the hydraulic conductivity profiles for the two minor sites and the NRC site were relatively similar.

The estimated fracture widths, at the NRC site, ranged from a maximum of 54μm to a minimum of 10 μm. These results are based upon fracture spacings presented in Figure 4.12 and the hydraulic conductivity values provided in Table 4.10, for the upper 6.1 metres of the deposit. A fracture spacing of 1 m was assumed at 6.1 metres depth, based upon observation in southwestern Ontario by Ruland et al. (1991).

For the Fallowfield site, the estimated fracture apertures varied from 20 to 120 μm in the upper 4.3 m of the deposit. A fracture spacing of 1 m was assumed at 4.3 metres. The effects of sand lenses were not taken into account.

The largest fracture width found at the Renfrew site was estimated at 200 μm at a depth of 4.60 metres. This value was calculated using an assumed fracture spacing of 25 cm. Excluding this measured value, fracture apertures ranged between 14 and 44 μm.

At the Casselman site, the estimated fracture widths were in the range of 14 to 46 μm.

4.2.3.4 Porosity

The effective fractured porosity at all four sites was estimated using an equation developed by Snow (1968), Equation 2.25. Again, the fracture spacings observed at the NRC site were assumed to represent fracture conditions at the two minor sites. Fractured porosity was only determined for the upper zone, as defined by the higher hydraulic conductivity values. The calculated effective fracture porosity excludes the intergranular pore spaces.

4.2.3.4.1 NRC Site

The effective fractured porosities of the upper weathered zone are presented in Table 4.14. In the upper 4.4 m of the deposit, the effective fractured porosity ranged from 1.02 x 10^{-4} at 3.48 m to 6.22 x 10^{-4} at 1.45 m.

The intergranular porosity is also given in Table 4.14, for depths between 6.3 and 12.2 m. The effective unfractured porosity decreased with depth, from 0.69 to 0.61.

4.2.3.4.2 Fallowfield Site

The fractured porosity of the upper 4.30 metres of the deposit is given in Table 4.15, where the effective fractured porosity varied from 2.80 x 10^{-5} to 1.28 x 10^{-2}.

The intergranular porosity ranged from 0.54 at 4.40 m depth to 0.58 at 12.50 m depth.

4.2.3.4.3 Renfrew Site

Based on NRC conditions, the estimated porosities are presented in Table 4.16. The porosity of the fractured media ranged from a maximum of 1.30 x 10^{-3} to a minimum of 2.20 x 10^{-5}.

The intergranular porosity is fairly constant at 0.56.

4.2.3.4.4 Casselman Site

Test results for measured porosities at the Casselman site are provided in Table 4.17. Based upon NRC conditions, fractured

porosities ranged from 8.90×10^{-5} to 8.60×10^{-4}. The lowest value was evaluated at a depth of 9.15 metres.

The intergranular effective porosity was relatively uniform below 6.4 m, ranging from 0.64 to 0.67.

4.2.3.5 Estimation of Flow Velocities

The velocities of groundwater through fractured and unfractured clay were determined by applying the Dupuit-Forachheimer Assumption to the Darcy seepage flux model, equation 2.19, and substituting the appropriate porosity value. Also, fracture flow velocities were determined by using the parallel plate model, equation 2.20.

4.2.3.5.1 NRC Site

Groundwater velocities are summarized in Table 4.14. Fracture flow velocities in the clay deposit were in the range of 0.117 to 4.593 m/d. The highest value was obtained at a depth of 3.10 metres. The average fracture velocity (equations 2.19 and 2.20) between depths of 0.91 and 6.10 metres was 1.1 and 1.4 m/d, respectively.

The parallel plate model gave similar results.

Groundwater velocities through unfractured clay, calculated using the intergranular porosities, were between 9.1 and 25.7 $\times 10^{-6}$ m/d (0.33 and 0.94 cm/a) at gradients of 0.084 and 0.12, respectively.

4.2.3.5.2 Fallowfield Site

Table 4.15 represents the groundwater velocities at the Fallowfield site. Fracture flow velocities varied from 0.10 to 4.8 m/d, with the highest value found at a depth of 2.10 m. Again, the parallel plate model gave similar results.

The average fracture flow velocity, based upon both equations, was approximately 1.80 m/d, for the upper 4.30 m.

The intergranular groundwater velocities were between 1.11 and 81 x 10^{-6} m/d (0.04 and 2.95 cm/a) from gradients of 0.007 and 0.024, respectively.

4.2.3.5.3 Renfrew Site

Test results for groundwater velocities measurements, at the Renfrew site, are presented in Table 4.16. Fracture flow velocities, for the upper 8.40 m, varied from a maximum of 27m/d at a depth of 4.60 m to a minimum of 0.13 m/d at 8.40 m. The parallel plate model gave lower velocities by an approximate factor of 2.

The average fracture flow velocity for the upper 8.40 m, based upon equation 2.19, was 5.87 m/d.

Groundwater velocities through unfractured clay were estimated between 43.3 and 110.7 x 10^{-6} m/d, using gradients of 0.22 and 0.26, respectively, or 1.58 to 4.04 cm per year.

4.2.3.5.4 Casselman Site

Groundwater velocities are summarized in Table 4.17. Fracture flow velocities in the upper 9.15 metres of the clay deposit, ranged from 0.25 to 2.40 m/d.

Whereas the intergranular velocities varied between 4.14×10^{-5} m/d to 7.81×10^{-3} m/d at gradients of 0.23 and 0.40, respectively. The highest values were reported at a depth of 6.40 metres.

The average fracture flow velocity between 1.3 and 9.15 m depth, using Equation 2.19, was approximately 0.90 m/d. The parallel plate values tended to be less than those estimated using equation 2.19.

Based upon hydraulic conditions only, fractured and unfractured zones for this site were not well defined, compared to the other three sites. Consequently, overlapping of both zones is shown in Table 4.17.

4.2.4 Geochemistry

The determination of major ion concentrations, pH, conductivity and tritium concentrations were undertaken at all four sites for selected depths. In addition, porewater analysis was performed on squeezed clay samples taken from the NRC site. The porewater analysis included the determination of pH, adsorbed cations and major ions, excluding HCO_3^-.

4.2.4.1 Groundwater (Piezometer Sampling)

4.2.4.1.1 NRC Site

The evaluation of major ion concentrations, pH and conductivity was undertaken on groundwater samples obtained from six piezometers (PZ-1,2,4,6,8 and 11), ranging in depth from 1.45 to 12.20 m. Tritium concentrations were measured on samples from five piezometers (PZ-1,4,6,9 and 11). The geochemical results are presented in Table 4.18.

The major cation concentration profiles are given on Figure 4.45. The overall predominant cation in solution is Na^+, followed in decreasing order by Ca^{2+}, Mg^{2+} and K^+. Sodium concentration increases with depth where it ranges from 0.78 M/m^3 at 2.95 m to 6.31 M/m^3 at 12.20 m. Potassium concentration is fairly constant with a slight increase with depth, ranging from 0.10 to 0.33 M/m^3. Calcium is the predominant cation in the upper 3 metres, maximum of 2.47 M/m^3 at 1.45 m, but decreases significantly below 6.1 m and is present only in small concentrations at greater depths. Magnesium has a higher concentration of 0.67 M/m^3 near the surface, but decreases to very low concentrations below 3.0 m.

Below this depth, Mg^{2+} concentration remains fairly constant ranging between 0.38 and 0.21 M/m^3.

The most predominant anion in solution is Cl^-, followed in decreasing order by HCO_3^- and SO_4^{2-}, as shown in Figure 4.46. A strong Cl^- concentration of 3.66 M/m^3 is found near the surface but decreases significantly to 1.94 M/m^3 at 2.95 m. Below 2.95 m depth, chloride increases to a maximum of 4.37 M/m^3 at 12.20 m. HCO_3^- shows a steady increase with depth, with a maximum concentration of 3.50 M/m^3 at 12.20 m. Sulfate concentrations are higher in the upper 4.3 m of the clay deposit, ranging from 0.65 to 1.19 M/m^3, but drop dramatically to very low levels below 6.10 metres.

Variations in conductivity with depth are presented in Figure 4.47. The highest value of 750 mmhos is found near the surface at 1.45 m. Then it decreases to the lowest level of 370 mmho's at 6.10 m, and increases to 580 mmhos at 12.20 metres. An anomaly to the above trend occurs at 4.40 m, where the conductivity increases to 520 mmhos. Overall, the groundwater is not highly conductive.

The pH of the groundwater increases with depth, from 6.8 at 1.45 metres to 7.6 at 12.20 metres. This indicates a neutral environment, as shown in Figure 4.48.

Interactions between groundwater chemistry and the surrounding environment can be illustrated using the Piper trilinear diagram developed by Hill (1940) and Piper (1944). The diagram distinguishes bodies of groundwaters that differ in their chemical composition. The term hydrochemical facies is used to describe these compositional differences.

The major ion data were used to obtain the Piper trilinear diagram presented in Figure 4.49. Three (3) hydro chemical facies can be observed and are as follows:

1) shallow "active" facie (1.45 and 2.95 m);
2) intermediate "transition" facie (4.4, 6.1 and 9.1 m), and;
3) deep "inactive" facie (12.2 m).

Groundwater at 9.1 m depth could also be classified in the deep "inactive" facie. The diagram shows that shallow and deep groundwaters are distinctive, separate and do not interact. The "transition" facie is well defined between 4.0 and 9.0 metres depth, which indicates some mixing between deep and shallow groundwaters. The chemical composition of the groundwater shifts along a relatively straight line. This is due to a decrease in the Mg^{2+}/Ca^{2+} and SO_4^{2-}/HCO_3^- ratios with increasing depth.

The tritium profile with depth is plotted in Figure 4.50. The highest tritium concentration of 34 T.U. is found near the surface at 1.45 m. Below this depth, tritium concentrations decreases to 24 T.U. at 4.4 m and are lower than the detection limits (<1.0 T.U.) below 6.10 m.

4.2.4.1.2 Fallowfield Site

The determination of major ion concentrations, pH and conductivity was undertaken on groundwater samples obtained on six piezometers (PZ-1,2,4,6,9 and 11) ranging in depth from 1.6 to 12.50 m. Tritium concentration profile was evaluated by sampling five piezometers (PZ-1,3,5,8 and 11). The geochemistry results are presented in Table 4.19.

Profiles of the major cations are provided in Figure 4.51. Sodium is the predominant cation in solution, followed in decreasing order by Ca^{2+}, Mg^{2+} and K^{+}. Na^{+} concentration ranges from 1.91 M/m^3 at 1.60 m depth to 16.09 M/m^3 at 12.50 m depth. Sodium concentration increases sharply from 2.65 M/m^3 at 3.0 m to 14.52 M/m^3 at 6.10 m. It continues to increase with depth. Calcium and magnesium have higher concentrations in the upper zone of the deposit. But both decrease significantly below 4.40 m. Potassium concentrations are very low, but tend to increase in concentration with depth.

Profiles of major anions are presented in Figure 4.52. The predominant anion in solution is Cl^{-}, followed in decreasing order by HCO_3^{-} and SO_4^{2-}. Sulfate is present only in low levels, with higher concentrations found in the upper 4.40 metres. Sulfate shows the same trend as Mg^{2+} and Ca^{2+}, a pronounced decrease in concentration between 3.0 and 6.0 m. Chloride concentrations range from a minimum of 3.46 M/m^3 at 1.60 m to a maximum of 13.52 M/m^3 at 12.50 metres. The Cl^{-} profile is similar to the sodium profile with a significant increase in concentration between 3 and 6.1 metres and with maximum values between 9.9 and 12.50 m. Bicarbonate shows a steady increase in concentration with depth, ranging from 3.45 to 5.90 M/m^3. Concentration strength and generated profiles indicate that salt is predominantly NaCl.

The conductivity varies from 658 mmhos at 1.60 m, increases to 1650 mmhos at 9.90 m and decreases to 1550 mmhos at 12.50 metres. The conductivity profile is plotted on Figure 4.53. The conductivity profile fundamentally indicates high dissolved ion content below 6.10 m depth. The conductivity profile follows the same trends as sodium and chloride.

The pH profile is illustrated in Figure 4.54. The pH increases from 7.2 at 1.60 m to 8.0 at 6.10 m then decreases to 7.5 at 12.50 m depth. The pH values indicate a neutral environment.

The Piper trilinear diagram presented in Figure 4.55 is produced from the major ion data. Three hydrochemical facies can be observed and are as follows:

1) shallow "active" facie (1.6 and 3.0 m);
2) intermediate "transition" facie (4.4 m) and;
3) deep "inactive" facie (6.10, 9.90 and 12.50).

The diagram indicates that no mixing of groundwaters in the upper "active" zone and the deep "inactive" zone has occurred. Since both facies are distinctive and separate. The groundwater chemistry at 4.4 m depth indicates that some mixing of both shallow and deep waters has taken place. This shift in chemical composition of the water is due to a decrease in the Mg^{2+}/Ca^{2+} ratios and an increase in the Cl^{-}/HCO_3^{-} ratios with increasing depth.

Tritium concentration with depth is presented on Figure 4.56. The highest tritium level of 31 T.U. occurs at 1.60 m with no significant change at 3.0 m. Below this depth, a rapid decline in tritium concentration occurs from 30 T.U. to 0.9 T.U.. Tritium concentrations fall below pre-1952 levels (<1.0 T.U.) below 7.6 metres.

The tritium profile at Fallowfield between 4.40 and 7.60 metres is not well established due to the lack of experimental data.

4.2.4.1.3 Renfrew Site

The determination of major ion concentrations, pH and electrical conductivity was performed on groundwater samples obtained from six piezometers (PZ-1,2,3,5,6 and 8). Tritium profile was determined by sampling groundwater on four piezometers (PZ-1,3,4 and 6). The geochemical results are presented in Table 4.20.

Plotted profiles of the major cations are given on Figure 4.57. The most predominant cation in solution is sodium, followed in decreasing order by Ca^{2+}, Mg^{2+} and K^{+}. Na^{+} concentrations range from 11.39 M/m^3 at 1.50 m to 1.74 M/m^3 at 9.15 m depth. Here, high sodium concentrations are found near the surface, decrease with increasing depth to 9.15 m; and increases slightly at 12.20 metres. Calcium concentrations are fairly constant in the upper 6 metres, ranging from 3.17 to 3.94 M/m^3. Between 6.0 and 9.15 m, Ca^{2+} levels drop significantly from 3.69 to 0.93 M/m^3 and continues to decrease with depth. Calcium concentration levels in the upper 6.0 m are stronger than magnesium, but the opposite is seen at 9.15 and 12.2 metres. Mg^{2+} show decreasing concentration with increasing depth, ranging from 3.56 to 1.10 M/m^3. K^{+} is present in the groundwater in very small amounts. Potassium concentration levels tend to increase with depth, ranging from 0.10 to 0.38 M/m^3.

Major anion profiles are presented in Figure 4.58. As with the other sites, the predominant anion in solution is Cl^{-}, followed in decreasing order by HCO_3^{-} and SO_4^{2-}. Sulfate is founded in relatively small concentration levels. SO_4^{2-} profile is fairly constant with depth, ranging from 0.20 to 0.53 M/m^3. High chloride concentrations are observed in the

upper 4.6 m, ranging from 19.71 to 20.98 M/m^3. A sharp decrease occurs between 4.60 and 9.15 metres, where Cl^- profile varies from 19.71 to its lowest level of 3.41 M/m^3. HCO_3^- concentrations seem to decrease linearly with depth.

The Na^+ and Cl^- profiles are similar with maximum concentrations occurring at 1.50 m and a minimum level occurring at 9.15 metres.

Conductivity profile is provided on Figure 4.59. A steady decrease in the electrical conductivity is observed between 1.50 m and 9.15 m. The conductivity varied from 4100 to 660 mmhos. This low value was measured at 12.20 metres depth. The conductivity profile is similar in form to that of Cl^- and Na^+ profiles.

The pH of the groundwater, as shown in Figure 4.60, increases from 6.5 at 1.5 m to 7.7 at 12.2 m, indicating a neutral environment.

The Piper trilinear diagram for Renfrew geochemical data is presented in Figure 4.61. This diagram shows no appreciable chemical differences between groundwaters at different depths. It could be concluded that only one hydrochemical facie exist or that some mixing of upper groundwaters (1.50 to 5.90 m) and lower groundwaters (9.15 and 12.20 m) has occurred.

Figure 4.62 shows tritium concentration profile with depth. The highest tritium concentration of 38 T.U. is found at 5.90m depth. Below this depth, tritium levels decrease significantly to 2 T.U. at 9.15 m and increases slightly to 3 T.U. at 12.2 m. The tritium profile is not well defined due to limited experimental points.

4.2.4.1.4 Casselman Site

The major ion concentrations, pH and electrical conductivity were determined on groundwater samples obtained from six piezometers (PZ-1,2,3,5,6 and 8). The tritium profile was assessed by measuring concentrations on four groundwater samples (PZ-1,3,5 and 7). The results of geochemical analysis are presented in Table 4.21.

The major cation profile is given in Figure 4.63. Similar to the other three sites, Na^+ is the dominant cation in solution, followed in decreasing order by Mg^{2+}, Ca^{2+} and K^+. Sodium concentrations varies from a minimum of 0.97 M/m^3 at 1.30 m to a maximum of 12.96 M/m^3 at 12.20 m. Sodium levels increase greatly between 4.40 and 6.40 metres. Calcium with a concentration of 2.50 M/m^3 is the predominant cation at a depth of 1.30 m, but decreases to low levels below 9.15 m. Magnesium and calcium have different profiles but have concentrations in the same range. Mg^{2+} is more dominant than Ca^{2+} between 3.05 and 12.20 m. Magnesium concentrations are fairly constant between 1.30 and 6.40 m depth, ranging from 1.05 to 1.34 M/m^3. Below 6.40 m depth, Mg^{2+} concentrations drop to low levels. Very little potassium is found in the deposit. K^+ tends to increase in concentration with increasing depth.

The predominant anion in solution is HCO_3^-, followed closely by Cl^-, as illustrated by Figure 4.64. Sulfate is the less dominant anion in solution. HCO_3^- concentration ranges from 2.00 M/m^3 at the shallowest depth of 1.3 m to 6.6 M/m^3 at 12.2m. Cl^- is the dominant anion in the upper 3.0 metres of the deposit. Below 3.0 m, chloride has a similar profile to HCO_3^-, but with lower concentrations. Higher sulfate

concentrations are found in the upper 6.40 m, ranging from 0.89 to 1.25 M/m^3. Below 6.40 m, sulfate concentrations are very low.

Na^+, HCO_3^- and Cl^- profiles are similar, indicating a marked increase in concentration between 4.40 and 6.40 m. Their maximum concentrations are observed at 12.20 metres. The Ca^{2+}, Mg^{2+} and SO_4^{2-} profiles are similar indicating a sharp decrease in concentration between 6.40 and 9.15 metres.

The electrical conductivity varies from 610 to 640 mmhos for the upper 4.40 m and from 960 to 1200 mmhos between 6.40 and 12.20 metres. The conductivity profile, as illustrated in Figure 4.65, parallels that of Na^+, HCO_3^- and Cl^- with a marked increase between 4.40 and 6.40 metres.

The pH profile plotted in Figure 4.66 increases from 6.6 at 1.30 m to 8.3 at 12.20 m which indicates a neutral environment.

The Piper trilinear diagram is presented in Figure 4.67. Again, three (3) hydrochemical facies are possible as follows:

1) Shallow "active" facie (1.30 to 4.40 m);
2) intermediate "transition" facie (6.40 m), and;
3) deep "inactive" facie (9.15 and 12.20 m).

Another hydrochemical scheme is possible, the shallow "active" facie is only found at 1.30 m and samples from 3.05 to 6.40 metres represent the "transition" facie. However, both schemes indicate that deep groundwaters are distinct and separable from those found near the surface, with a transition zone were mixing of both facies occurs.

Tritium concentration with depth is plotted on Figure 4.68. The highest tritium concentration of 34 T.U. is observed at 4.40 m depth. Below this depth, tritium levels decrease to 17 T.U. at 6.40 m and to less than 1 T.U. at 12.20 m. The tritium profile is not well defined between 6.40 m and 12.20 m depth, since no measurable concentrations were obtained.

4.2.4.1.5 Comparison Between All Four Sites

A comparison of major cation concentration profiles between all four sites is provided on Figures 4.69 through 4.72

All sodium profiles (Figure 4.69) show a marked increase in concentration around a depth of 6.0 metres, except at Renfrew. Sodium concentrations range from 0.78 to 3.18 M/m^3 in the upper zones of the clay deposits. The deepest samples has a sodium concentration range between 6.31 and 16.09 M/m^3. The highest Na^+ levels are observed at Fallowfield while the lowest are found at NRC. The Renfrew profile shows the reverse trend, decreasing concentration with increasing depth.

All calcium profiles (Figure 4.71) indicate a decrease in concentration with increasing depth. The Renfrew site has the highest Ca^{2+} levels, while the other three sites fall within the same range. Excluding the Renfrew site the calcium concentration range from 0.69 to 2.50 M/m^3 in the upper weathered zone and decrease to low levels, between 0.19 and 0.25 M/m^3.

All Mg^{2+} profiles (Figure 4.72) decrease in concentration with increasing depth. Excluding the Renfrew site, magnesium concentrations varied in the upper fractured zone between 0.34

to 1.44 M/m^3 and became fairly uniform below 9.0 m, ranging from 0.20 to 0.49 M/m^3.

All K^+ profiles, see Figure 4.70, show an increase in concentration with depth. Potassium concentration in solution is very low at all four site, ranging from 0.03 to 0.43 M/m^3.

Renfrew cation profiles are anomalous, except for potassium.

A comparison of major anions concentration profiles between all four sites is presented in Figures 4.73 to 4.75.

Chloride profiles (Figure 4.73) increase in concentration with increasing depth, except at the Renfrew site which showed the opposite trend. Excluding the Renfrew site, the upper active zone varies in chloride concentration from 1.94 to 4.70 M/m^3, while ranging between 4.37 to 13.52 M/m^3 at the deepest sampling point (~12.2 m). Fallowfield has the highest concentration levels at depth while NRC has the lowest.

Bicarbonate concentrations (Figure 4.75) increase with increasing depth, except at the Renfrew site which shows the opposite trend. HCO_3^- concentration levels, omitting Renfrew, in the upper 2.0 metres, range from 1.70 to 3.45 M/m^3. While just below 12.0 metres, it varies from 3.50 to 6.60 M/m^3. NRC has the lowest overall levels.

All sulfate profiles generated (Figure 4.74) showed higher concentrations in the upper weathered zone and decreased to very low levels at depth. Below a depth of 8.0 metres, SO_4^{2+} concentrations become uniform and range between 0.07 and 0.23 M/m^3.

The Renfrew site presents an anomaly, in the Cl^- and HCO_3^- concentration profiles.

Tritium profiles for all four sites are provided in Figure 4.76. Tritium concentrations range between 30 and 38 T.U. in the upper 6.0 metres. Tritium levels decrease below 1.0 T.U. at 12.20 m for NRC, Fallowfield and Casselman sites, while tritium levels, at the Renfrew site, drop to 2.0 T.U. at 12.20 m.

4.2.4.2 Porewater Analysis (Squeezed Clay Samples)

Seven clay samples from the NRC site were analyzed. The geochemical data obtained are presented in Table 4.22.

Figure 4.77 represents the major cation profiles. Sodium is the predominant cation in solution, followed in decreasing order by Ca^{2+}, K^+ and Mg^{2+}. Sodium concentrations ranged from 1.14 M/m^3 at 1.70 m depth to 6.65 M/m^3 at 12.50 m. Sodium profile shows a significant increase in concentration below 4.00 m depth.

Calcium and magnesium decrease in concentration with increasing depth and are only found a very low amounts at 12.50 m. The highest K^+ concentration of 0.42 M/m^3 occurs at 1.70 m. Between 2.60 m and 12.50 m, potassium levels vary from 0.20 to 0.31 M/m^3.

Cl^- and SO_4^{2-} concentration profiles are provided in Figure 4.78. Chloride concentrations range from 2.25 M/m^3 at 1.70 m depth to 3.66 M/m^3 at 12.50 m. Chloride shows a steady increase with depth, below 5.50 metres. Sulfate profile shows a gradual decrease in concentration between 1.7 and 4.0 m, and

become fairly constant between 5.50 and 12.50 metres, ranging from 0.07 to 0.11 M/m^3.

The pH of the porewater, as illustrated in Figure 4.79, shows an inconsistent increase with depth. The pH ranges from 7.0 at 1.70 m to 8.3 at 8.15 m depth. The results suggest that a neutral environment exist in the upper 6.0 metres, which becomes slightly alkaline below 8.15 m.

A comparison between porewater and groundwater concentration profiles for Na^+, K^+, Mg^{2+}, Ca^{2+}, Cl^- and SO_4^{2-} are presented in Figures 4.80 through 4.85. Porewater and groundwater concentration profiles show similar trends but vary in strength. Variations in ion concentrations are more pronounced in the upper 6.0 metres, but become more consisted with increasing depth. Generally, porewater profiles tend to be more smooth and uniform with depth.

The cation exchange capacity (CEC) with depth for the NRC site is plotted in Figure 4.86. The CEC is fairly consistent between 1.70 and 8.15 metres, ranging from 30 to 39 meq/100 g of dry soil. The CEC increases between 44 to 55 meq/100 g at 12.5 m depth.

The exchangeable cation profiles for the NRC site are presented in Figures 4.87 to 4.90. Calcium is the predominant adsorbed cation, followed in decreasing order by Mg^{2+}, Na^+ and K^+. Sodium, potassium and magnesium all show an increase in the amount adsorbed below 6.0 metres. Calcium adsorption is fairly constant between 1.70 and 8.15 m, and then increases dramatically at 12.50 metres.

The sodium-adsorption ratio (SAR) and the exchangeable sodium percentage (ESP) profiles are presented in Figure 4.91. The percentage of adsorbed sodium on the clay exchange sites increase with depth. ESP and SAR values are most pronounced below 4.0 m depth. The results indicate that in the upper 4.0m of the clay deposit, Na^+ occupies between 2 to 4% of the exchange sites, while at 12.20 m, sodium occupies 8 and 16%. The SAR and ESP values are similar to one another, except at 12.50 metres, where the SAR is approximately twice the ESP value.

Adsorption isotherms for all four major cation are presented in Figures 4.92 through 4.95. Two adsorption relationships best represented the experimental data: a linear relationship (equation 3.24a) and the 3 parameter relationship (equation 3.27a). Na^+, K^+ and Ca^{2+} showed an increase in adsorption with increased porewater concentrations. But magnesium showed an "apparent" desorption with increased porewater concentrations, see Figure 4.94.

CHAPTER 5
LABORATORY STUDY

5.1 General

In order to fulfil the research objective, a laboratory study was undertaken to complement the field investigation to insure a full evaluation of the retention capabilities of Eastern Ontario clay deposits. In clay deposits, correct effective diffusion coefficients and retardation factors are essential for good field modelling and predictions. The scope of the laboratory study is:

(1) to determine characteristics of Leda clay at the four sites;

(2) to investigate the buffering capacities of Leda clay in terms of inorganic species;

(3) to evaluate the diffusive properties of inorganic species in undisturbed samples of Champlain Sea clay.

5.2 Materials and Methods

Undisturbed soil samples with no visible fissures were selected for diffusive testing. Originally, seven diffusion tests were performed, two from NRC and three from Fallowfield, one each from Renfrew and Casselman, but the two NRC samples were nullified due to improper chemical analysis.

The soil samples were collected during piezometer installation. At the four sites, Shelby tube samples of 5 cm diameter were removed at the desired depth, capped and sealed with masking tape upon collection. On the day of collection,

the core samples were sent to the University of Ottawa laboratory. The samples were sectioned, wrapped tightly in several layers of Saran wrap, waxed and stored in a cool-room which was maintained at 4°C to slow the rate of sediment aging (Lessard and Mitchell, 1985).

5.2.1 Soil Properties

The two soil samples from the Fallowfield site consisted of soft grey silty clay from depths of 3.0 and 3.6 m. Renfrew sample was a stiff grey silty clay from a depth of 4.2 m and the Casselman sample collected at 4.6 m depth was a stiff brownish grey silty clay. The geotechnical index characteristics, porewater chemistry and cation exchange properties of all five soil samples are given in Tables 5.0 to 5.3.

5.2.1.1 Physical Properties

Liquid limits were determined for all clay samples using the Cassagrade apparatus (ASTM D4318) and the plastic limits using the ASTM D4318 recommended procedures. All moisture contents were determined by oven drying the soils at a temperature of ~110°C for over twenty-four hours (ASTM D2216). The Specific gravity was evaluated by volumetric flask procedures according to ASTM D854.

The sieve analysis was performed by Fondex limited from original field samples.

Fallowfield samples had moisture contents of 42 and 41 percent which approximately equalled their liquid limit of 41 percent. Renfrew and Casselman samples had moisture contents of 37 and

47 percent which were below their corresponding liquid limits of 44 and 58 percent. The specific gravity varied from 2.76 for Fallowfield samples to 2.70 for the Renfrew and Casselman specimens. The Fallowfield samples reported the lowest percentage of clay fraction at 40% while Casselman had the highest at 64%.

5.2.1.2 Soil and Porewater Chemistry

The chemical analysis included the determination of major porewater cation concentrations (Na^+, K^+, Mg^{2+} and Ca^{2+}), pH and chloride content. The soil samples were mechanically squeezed using a modified floating-ring oedometer. A maximum of 2 MPa squeezing pressure was applied for approximately 1 h. The squeezing was conducted at a laboratory temperature of 20 ± 1°C.

All water analyses were done at the University of Ottawa geochemistry laboratory. Cation (Na^+, K^+, Mg^{2+}, Ca^{2+} and Ag^{2+}) concentrations were measured using a Thermo Jarwell Ash Scan, ICP-AES (Inductively Couple Plasma Atomic Emission Spectrometer). Chloride concentrations were measured using a Waters 880 High Pressure Liquid Chromotograph with Conductivity Detector. pH was measured using a Fisher Accumet pH meter, Model 210.

The cation exchange capacity (CEC) and exchangeable cation were determined by a single wash of dry pulverized soil ranging from 0.2 to 0.4 g in 40 ml of silver thiourea solution. This solution was mechanically shaken for 24 h. at room temperature of 20 ± 1 °C in 40 ml plastic centrifuge tubes. The mixture was then centrifuged and the supernatant

analyzed. A minimum of three soil samples for each tests was performed to ensure representative results.

The pH for the Fallowfield samples (tests 1, 2 and 4) was slightly alkaline at 7.8. The most predominant cation in solution was Na^+, followed in decreasing order by Ca^{2+}, Mg^{2+} and K^+. The sodium adsorption ratio (SAR) ranged from 17 to 25%. The Fallowfield samples reported the lowest CEC values which varied from 22.6 to 28.7 meq per 100 g of dry soil with calcium as the highest exchangeable cation followed in decreasing order by Mg^{2+}, K^+ and Na^+.

The Renfrew sample (Test #3) had a neutral pH of 7.0. The most predominant cation in solution was Ca^{2+}, followed in decreasing order by Na^+, Mg^{2+} and K^+. SAR value indicated that Na^+ would occupy 13.4% of exchange sites on the clays minerals surfaces. The Renfrew CEC values ranged from 44.4 to 55.6 meq per 100 g of dry soil with calcium as the most predominant exchangeable cation followed in decreasing order by Mg^{2+}, K^+ and Na^+.

The Casselman sample (Test #5) had a porewater pH of 7.3 and the lowest ion concentrations of all the tested samples. Again, the most predominant cation in solution was sodium followed in decreasing order by Mg^{2+}, Ca^{2+} and K^+. It had a SAR value of 15.3%. The CEC values varied from 47.9 to 56.3 meq per 100 g of dry soil with again calcium as the highest exchangeable cation followed in decreasing order by Mg^{2+}, K^+ and Na^+.

The results of silver thiourea exchange for the five tests indicated that no unmeasured species are present in Leda clay,

since the sum of the exchangeable cation yielded values close to the CEC values for each sample.

The reported high CEC values for Renfrew and Casselman samples are due in part to their high percentage of clay fraction, ~60% as compared to ~40% for Fallowfield samples.

Quigley et al. (1989) reported that high CEC values for Leda clay can be associated with the presence of swelling clay smectite (montmorillonite), due to the oxidation weathering of chlorite. They reported several CEC values, varying from 14.0 to 31.8 meq/100 g. Warith (1987) reported CEC values for Champlain Sea clay around the Montreal area, ranging from 60 to 85 meq/100 g of dry soil with Ca^{2+} as the highest exchangeable cation followed by Mg^{2+}, K^{+} and Na^{+}.

The spread in CEC for both Renfrew and Casselman samples may be due, in part, to the dissolution of calcite and/or dolomite in the supernatant by silver thiourea (Barone et al., 1989).

5.2.2 Experimental Procedure

The experimental model consisted of a hollow plexiglass cylinder 0.5 cm thick, with an outside diameter of 4.5 cm, and a total length of 20 cm. A stainless steel cutting shoe with an inside diameter of 4.5 cm was fitted to the end of the plexiglass tube. Next, the soil sample, 5 cm in diameter, was pressed into the cylinder by a mechanical pressing device to an approximate length of 6.0 cm. Once the specimen was in place, a visual examination was undertaken to ensured a proper seal between the clay sample and the cylinder wall had been achieved. An impermeable plexiglass plate was sealed at the base of the test apparatus by using a silicone seal bond.

Then, a 14 cm high source solution was placed directly above the soil sample. To prevent leakage or losses due to evaporation, the plexiglass top plate was fitted with rubber "O" rings and vacuum grease was applied around the stir stick. The stir stick was provided to ensure proper mixing of the source solution during testing. This was done manually each day and before reservoir sampling. The diffusion cell assembly is schematically shown in Figure 5.0. A photograph of the experimental set up is shown in Figure 5.1(a), while Figure 5.1(b) gives a view of the different parts of the cell.

After each test apparatus was assembled properly, it was placed in a controlled environmental chamber at a constant temperature of 20 ± 1°C.

During diffusion testing, the source solution concentration was monitored periodically (usually at 2 day intervals) by withdrawing a 0.5 ml sample by pipette through the sampling port, as shown in Figure 5.0. These source solution samples were analyzed for the species of interest in order to monitor source concentration variations with time. At the end of testing, the last source reservoir sample was taken. The final total weight of the diffusion cell apparatus with soil sample was measured and the diffusion cell was disassembled. The testing period varied from 15 to 16 days which was found to be sufficient time for migration to take place.

The soil samples were extruded and sectioned into approximately four equal slices. These four slices provided the vertical distribution of both soluble and adsorbed of selected chemical constituents. Each slice was weighed, wrapped in saran wrap before extrusion of porewater by squeezing. After squeezing, the sectioned samples were

allowed to air dry, pulverized and passed through a No 200 sieve for extraction analysis with silver thiourea. The entire sectioning and squeezing were performed in the same day at room temperature (20 ± 1°C).

A mass balance was performed for species of interest to check against any possible losses, such as precipitation, cation fixation, experimental error, etc. In order to perform a mass balance calculation, it is necessary to know the total mass flux from or into the source reservoir (Ct), and the total amount of each element retained: soluble (Cs) and adsorbed (Ca).

The different elements involved in a mass balance calculation are schematically illustrated in Figure 5.2, and are as follows:
(1) the mass in the source reservoir is a function of the area of the concentration curve bounded by the initial concentration and the volume of source solution, (Ct);
(2) the retained ions are a function of: (a) the area bounded by the initial and migration profile which gives the total soluble ions (Cs), (b) the area bounded by the initial and final adsorbed concentration which gives the total adsorbed ions (Ca).
Thus, Ct must equal Cs + Ca plus or minus any sinks (precipitation) or sources (elution).

5.3 Data Analysis

The effective diffusion coefficients were determined by "back-figuring" with an explicit finite difference program. The

finite difference equation for the differential equation 3.17 is:

$$\frac{C_i^{j+1} - C_i^j}{\Delta t} = \frac{D_e}{R} \frac{C_{i+1}^j - 2C_i^j + C_{i-1}^j}{\Delta z^2} \qquad (5.0)$$

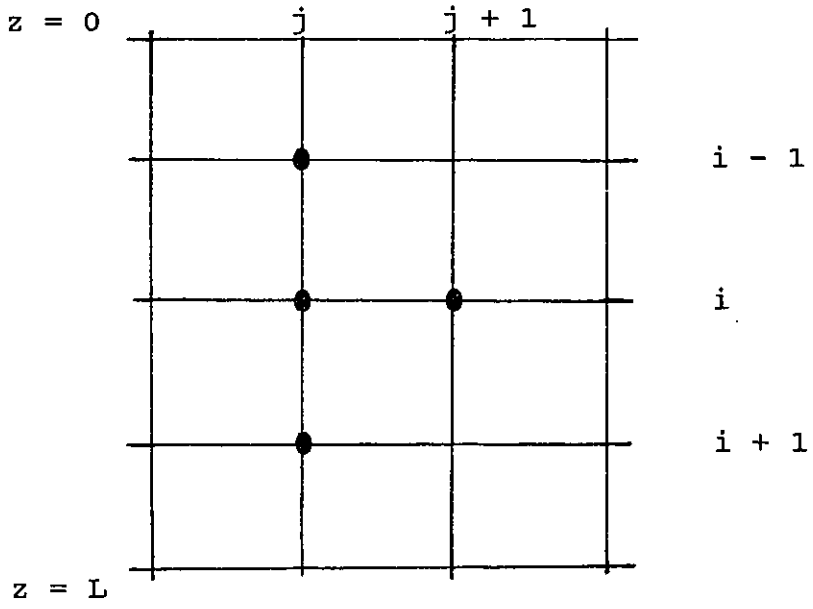

The finite difference scheme is valid for mesh points in the interior domain of the solution, the boundary values are specified by Equations 3.28 and 3.31.

A computer program written on Lotus 123 spreadsheet was developed to compute the effective diffusion coefficient from experimental data.

The retardation factors were evaluated separately, by plotting "adsorption isotherms".

5.4 Diffusion Test Program

Two different tests were performed on the five Champlain Sea clay test samples. The results are summarized in Table 5.4. One test involved the placement of a single salt solution (NaCl) in contact with a fully saturated undisturbed sample. This allowed downward chemical migration by diffusion only throughout the sample. The second test involved the placement of deionized water in contact with the undisturbed fully saturated sample. This allowed an upward chemical migration by diffusion only into the source reservoir. The testing period varied from 15 to 16 days.

The two deionized tests were used to investigate the in-situ diffusion properties of the natural clay. These tests were also used to observe the variations in migration characteristics due to chemical interactions as compared with the single salt test (Quigley et al., 1987; Barone et al., 1989).

The single salt tests were performed to determine the effects of a large chemical gradient which can be established at the interface between the landfill leachate and the clay barrier.

5.5 Experimental Results and Interpretation

5.5.1 Mass Balance

The results of the mass balance calculations are presented in Table 5.5. They fall within an approximate absolute range of 10 to 33%. The deionized water tests had the highest mass balance error of 33%, while the single salt had the lowest at 9.6%.

Based upon results obtained during control tests on the diffusion apparatus, no significant sources or sinks were observed. The discrepancies in the mass balance can be attributed to the following:

(1) the natural scatter of the data;
(2) cation fixation;
(3) improper or incomplete extraction of adsorbed cation;
(4) incorrect dilution for chemical analysis;
(5) small sample size;
(6) the effects of biomass interference which would consume such elements as K^+, Ca^{2+} and other ions in the soil system.

An incomplete extraction of adsorbed cations can greatly influence the results of mass balance since in most cases adsorbed cation represented the highest portion of the total mass of the specie. Thus, relatively small error in adsorbed cation determination can greatly affect the initial and the final conditions. This might explain the relative constant error found for each test (test 1 ~20%, test 3 ~15%).

Samples had to be diluted for chemical analysis due to the relatively small amounts sampled from the source solution and from porewater extraction during squeezing. An improper dilution could be another factor that could give rise to a relatively constant mass balance error.

5.5.2 Adsorption Isotherm

The relationships between soluble and adsorbed cations for all five tests are presented in Figures 5.3 to 5.7. For clarity, the single salt models will be presented first, followed by deionized water models.

Since the charged clay minerals of Leda clay are composed mainly of illites, chlorites and smectites which have permanent negative charges (no positive charges on clay surfaces with decrease in pH of the soil system), and that diffusion test was performed in a neutral environment (pH~7), it was assumed that anion (chloride) adsorption would not be operative.

For the single salt models in which sodium was the only cation of interest, two adsorption relationships that best represented the experimental data were a linear relationship (equation 3.24a) and the 3 parameter relationship (equation 3.27a). The Langmuir model was impractical, since no direct input of maximum adsorption was observed. The linear and 3 parameter relationships with the experimental data are shown in Figures 5.3 to 5.5.

The linear relationship represented the best fit; thus retardation was independent of solute concentration. The "distribution coefficient" K_d was evaluated and substituted into equation 3.24c to calculate the corresponding retardation factor.

The retardation factors for sodium ranged from 2.22 to 3.60, with the Casselman soil sample having the highest value. For the two Fallowfield samples, there were no appreciable differences (2.22 and 2.67).

Figures 5.6a to 5.6d and 5.7a to 5.7d give the relationship between soluble and adsorbed cations for Na^+, K^+, Mg^{2+}, and Ca^{2+} for the deionized water tests. The plotted data indicate a nonlinear relationship for all results. The 3 parameter and

the linear relationship are shown on these figures for comparison.

The Langmuir model in most cases overestimated the adsorption values in the vicinity of low concentrations. It also could not model the "apparent" desorption of Mg^{2+} and Ca^{2+} in test 1, as depicted in Figures 5.6c and 5.6d.

Since the adsorption isotherm are nonlinear in principal, retardation is a function of the equilibrium concentration. Thus, the 3 parameters were evaluated by Least Square Regression and were substituted into equation 3.27d to determine the range of retardation factors for each cation.

In equations 3.27, the parameter α represents the maximum adsorption capacity of the soil system for a specific ion, Table 5.6 summarizes the α values for Test #1 & #3 for Fallowfield and Renfrew, respectively. From Table 5.6, calcium in both cases is the most preferred cation followed in decreasing order by magnesium, potassium and sodium. Test #1 reported much lower values for Mg^{2+} and Ca^{2+} than in Test #3. A possible explanation is the higher adsorption of Mg^{2+} and Ca^{2+} at lower solute concentrations. This phenomenon gives the appearance of desorption with increase in solute concentration. However, since no actual high concentration flushing of the sample by Mg^{2+} and Ca^{2+} was performed, it is impossible relate these observations to true elution of each species. For this reason it is identified as an "apparent" desorption trend. The calculated parameters are only valid for the observed concentration range.

Quigley et al. (1989) reported elution of magnesium and calcium for some Ottawa area clays. However, Yong et al.

(1986) found sodium elution occurred in Leda clays from the Montreal region.

Since retardation factors are a function of solute concentration, the following ranges show the maximum difference between the lowest and the highest observed solute concentration. Sodium had a retardation factor for Fallowfield (test 1) ranging from 1.50 to 1.56, and for Renfrew (Test 3), from 2.0 to 2.1.

Calcium retardation factors for both tests, fell within the same ranges. Fallowfield had a calcium range between 17 to 33 while Renfrew gave a range of 18 to 32. Calcium tended to be the highest retarded cation, if no elution occurs. Potassium had the highest retardation factor of 48 at very low solute concentration at 3 mg/l in test 3.

Based upon calculated retardation factors in both diffusion models, the relative mobility of each of the cation for all tested soils was found to be:

(1) $Na^{+} > Mg^{2+} > K^{+} > Ca^{2+}$ (no elution)

(2) $Ca^{2+} > Mg^{2+} > Na^{+} > K^{+}$ (with elution)

These basic trends were also observed for Southern Ontario clays by Rowe et al. (1988), Quigley et al. (1989) and Barone et al. (1989).

The highest overall retention of cations was observed for the Renfrew sample. This is not surprising since it had one of the highest CEC.

The retardation factors for the deionized water models for sodium are about 40% lower than for the single salt model. This difference is due to the higher degree of competition for exchange sites when multi-cations migrate together.

A summary of retardation factors used to calculate the effective diffusion coefficients for each species of interest is provided in Table 5.7. Since chloride is assigned zero adsorption, the retardation factor equals 1.

5.5.3 Effective Diffusion Coefficients

5.5.3.1 Single Salt Tests

The three single salt model results are illustrated in Figures 5.8(a & b) to 5.10(a & b), respectively. For each test performed, the source solution reservoir concentration decreased with time, while porewater and adsorbed concentrations increased above background levels, thus indicating diffusive migration of sodium and chloride.

The theoretical concentration versus-depth profile determined using the finite difference scheme were fitted by "least square regression" to the measured porewater concentration versus-depth profile, source concentration with time and adsorbed cation concentration versus depth profile for best fit.

Chloride and sodium gave relatively good theoretical fits. All three chloride profiles yielded similar effective diffusion coefficients, ranging from 6.8 to 7.0 x 10^{-6} cm^2/s, which are well below the Cl^- "free diffusion" coefficient reported in Table 3.0.

The effective diffusion coefficient for sodium varied from 5.8 to 6.5 x 10^{-6} cm^2/s. The larger value was reported for Fallowfield while the lowest value was shown for Casselman.

5.5.3.2 Deionized Water Tests

As illustrated in Figures 5.11(a to e) and 5.12(a to e), all four cations and chloride appear to have migrated by diffusion into the source reservoir. This results in an increase in concentration with time in the source reservoir.

The measured porewater concentration has decreased below background levels for all species in both Tests (#1 & #3). The adsorbed concentrations for all cations in Test #3 (Renfrew sample) and for sodium and potassium in Test 1 (Fallowfield sample) have decreased below or have remained near the original background levels. Calcium and magnesium in Test #1 showed an increase in retention as illustrated in Figures 5.11d and 5.11e.

The deionized water tests showed great scatter in adsorption data as shown in Figures 5.11(b to e) and 5.12(b to e), which depicts the previous mentioned extraction problem. Even with this variability in adsorption, trends are nevertheless clear; adsorption either increases or decreases with depth.

The corresponding effective diffusion coefficients for each species are in good agreement with each other. Chloride ion gave 6.0 and 6.5 x 10^{-6} cm^2/s, and the cations: sodium, potassium, magnesium and calcium yielded values of 3.4 & 4.0 x 10^{-6} cm^2/s, 6.0 & 7.5 x 10^{-6} cm^2/s, 3.8 & 4.6 x 10^{-6} cm^2/s, 5.8 & 6.25 x 10^{-6} cm^2/s, respectively. All effective diffusion coefficients are given in Table 5.7.

The order of the D_e value for each model is as follows:

$$D_e(Cl) \approx D_e(K) > D_e(Ca) > D_e(Mg) > D_e(Na) \quad \text{(deionized water)}$$

$$D_e(Cl) > D_e(Na) \quad \text{(single salt)}$$

The results for the deionized water series are almost exactly opposite to the order of mobility predicted by the retardation factors. Though, reported "self-diffusion" coefficients from Table 3.0, gives Cl^- the highest mobility followed closely by K^+, then in decreasing order, Na^+, Ca^{2+} and Mg^{2+}.

5.5.4 Comparing the Two Diffusion Models

Comparing the two diffusion model results was only possible for Na^+ and Cl^- ions. Sodium effective diffusion coefficients were about 50% lower for the deionized water model as compared to the NaCl model. This is probably due to more cation competition and interaction between solutes and clay mineralogy.

Chloride effective diffusion coefficients were fairly constant in both models and in the five test soils, ranging from 6.0 to 7.0×10^{-6} cm^2/s for a maximum difference of 15%. Thus chloride, a conservative specie, was not effected by either the composition of the source solution or the test used.

The deionized water and single salt models represent two different types of diffusion. NaCl model represents counterdiffusion since cations not present in the source solution migrated upwards into the reservoir, as illustrated in Figure 5.13. In contrast the deionized water model represents salt diffusion.

5.5.5 Comparison of D_e and R Values with Previous Results

As mentioned in Chapter 3, effective diffusion coefficients and retardation factors are dependent on several factors such as: type of soil, source solutions, initial and final boundary conditions, type of diffusion, modelling procedure, etc. For these reasons a quantitative analysis should be used when comparing results,

5.5.5.1 Retardation Factors

The retardation factors reported in Table 5.8 for sodium, potassium, magnesium and calcium ranged from 1.50 to 3.60, 17.2 to 48, 4.8 to 12.4 and 17 to 33, respectively.

Reported retardation factors for southern Ontario clays, based upon a distribution coefficient K_d, showed: sodium varying from 1.4 to 2.9, potassium varied from 5.4 to 19, magnesium approximately equalling 11, and calcium ranging from 6.2 to 13.8 (Rowe et al., 1988; Barone et al., 1989).

It is of interest to compare the retardation factors found in this study with those from Leda clay in the Montreal region. Consequently, the retardation factors were calculated using the experimental data reported by Warith (1987). The analyses yielded a range for Na^+, K^+, Mg^{2+} and Ca^{2+} of 8.5 to 10, 48 to 128, 17 to 97, and 10 to 120, respectively.

The soil retention capabilities are highly influenced by the soil mineralogy and the CEC value. The rather low R values for southern Ontario clays are expected since the CEC for these clays is 3 to 5 times lower than eastern Ontario Leda clays. Warith (1987) reported that CEC for the Montreal area

Leda clay varied from 60 to 85 meq/100 g which is approximately 2 to 3 times higher and is reflected in the higher R values.

The calculate R values for eastern Ontario fall within this spread and shows the same trends, with Ca^{2+} and K^{+} as the highest retained cation, while Na^{+} is the most mobile.

5.5.5.2 Effective Diffusion Coefficients

The D_e values for Cl^{-} reported in Table 5.7 varied from 6.0 to 7.0 x 10^{-6} cm^2/s. Johnson et al. (1989) indicated that Cl^{-} in saturated clayey soils ranged from 2.0 to 6.0 x 10^{-6} cm^2/s. The D_e values reported in the literature tend to lie between 2.0 x 10^{-6} cm^2/s to 1.0 x 10^{-5} cm^2/s when Cl^{-} diffuses in saturated clays, silty clays and sand:bentonite mixtures (e.g. Gillham et al., 1984; Crooks and Quigley, 1984; Rowe et al., 1988; Shackelford, 1988; Barone et al., 1989). Therefore, the calculated effective diffusion coefficients for Cl^{-} are in excellent agreement with previous findings.

The D_e values for Na^{+}, K^{+}, Mg^{2+} and Ca^{2+} reported in Table 5.7 varied from 3.4 to 6.5 x 10^{-6} cm^2/s, from 6 to 7.5 x 10^{-6} cm^2/s, from 3.8 to 4.6 x 10^{-6} cm^2/s, and from 5.8 to 6.25 x 10^{-6} cm^2/s, respectively. Typically, D_e for major cation, Na^{+}, K^{+}, Mg^{2+} and Ca^{2+} in saturated glacial marine clays fall within a narrow range, between 9.0 x 10^{-7} cm^2/s and 7.0 x 10^{-6} cm^2/s. More specifically for silty clays, Na^{+} ranged from 2.5 to 5.7 x 10^{-6} cm^2/s, K^{+} ranged from 5.0 to 7.5 x 10^{-6} cm^2/s, Mg^{2+} ranged from 2.0 to 4.0 x 10^{-6} cm^2/s and Ca^{2+} varied from 1.0 to 3.8 x 10^{-6} cm^2/s (e.g. Li and Gregory, 1974; Crooks and Quigley, 1984; Warith, 1987; Rowe et al., 1988; Barone et al., 1989).

The cation effective diffusion coefficients are in good agreement with the previous findings, though they tend to be slightly high.

The higher calculated D_e values can be associated with the naturally high porosity of the undisturbed samples. High porosity would reduce the tortuous path undertaken by the ions as they migrate through the soil. The lesser the soil particles restrict the free moving ion, closer the D_e coefficient will approach the "free-solution" diffusion coefficient (D^*), as expressed by equation 3.10.

The difference in cation D_e values may be due to the varying retardation for the deionized model, which tended to be conservative. The adsorption analysis did not always give a perfect fit, due to the natural scatter of the experimental data.

Overall, the experimental results and analysis reported in this study are consistent with previous findings given in the literature.

CHAPTER 6

FIELD MODELLING

6.1 General

In order to evaluate the effects of various parameters on the groundwater transport process, theoretical profiles were generated from analytical solutions and then compared to field data.

A number of major ions (Na^+, K^+, Mg^{2+}, Ca^{2+}, Cl^-, HCO_3^-, SO_4^{2-}) were sampled up to an approximate depth of 12 metres at each of the four sites. With the exception of the Renfrew site, Na^+, K^+, Cl^- and HCO_3^- concentration profiles increased with depth. The results suggest that higher concentrations of these ions exist below 12.0 m depth. Desaulniers and Cherry (1989) reported for a Champlain Sea clay deposit near Montreal that maximum ion concentrations occurred at the clay-bedrock interface except for sulfate. Only downward migration of some major ions and tritium into the clay deposit were modelled. No upward migration profiles of Na^+, K^+, Cl^- and HCO_3^- were generated. Since the exact thickness of the clay is not known at the NRC, Renfrew and Casselman sites, no geochemical data are available regarding the clay-bedrock interface.

6.2 Conceptual Models

Two conceptual models were used to evaluate quantitatively the effects of various parameters on the groundwater transport process. The first model assumed that the clay section below

the observed active zone behaves like a massive, unfractured porous medium. The second model assumes that hydraulically active vertical fractures exist throughout the silty clay deposit. In the first case, the vertical solute migration is controlled by both advection and diffusion. In the second model, the solute migration in a fractured porous media is influenced by fracture aperture, fracture spacing and the degree of efficiency in which groundwater is transported through the fracture network.

6.3 Downward Migration Using the First Conceptual Model

6.3.1 Major Ion Profiles

The higher concentrations of Ca^{2+}, Mg^{2+} and SO_4^{2-} in the near surface zone are due to oxidation production. These concentrations are attributed, for the most part, to the oxidation of iron sulfide which produces iron hydroxide and sulfuric acid. The production of H^+ causes the dissolution of carbonate minerals in the silty clay deposit. Pyrite oxidation and carbonate dissolution cause Ca^{2+}, Mg^{2+} and SO_4^{2-} concentrations to rise and the pH to decrease. The oxidation of the upper portions of the Champlain Sea clay deposit was assumed to begin around the beginning of the dry Hypsithermal Period, 11,500 BP.

Downward migration theoretical profiles were generated using the Ogata (1970) solution, for times of 10,000 years. These theoretical profiles were generated using laboratory determined effective diffusion coefficients with the corresponding retardation factors. The effective diffusion coefficient were adjusted to field temperatures of 8°C using

the relationship developed by Li and Gregory (1974) (equation 3.5).

At the Renfrew site, sodium and chloride have higher concentrations in the upper section. This high concentration could be due, in part, to road salt (mainly NaCl) contamination, since the Renfrew site is situated on the grounds of the Renfrew Town garage were road salt is stored. The Renfrew Town garage was built in 1960 (Township of Renfrew Registry Office). Theoretical profiles, at the Renfrew site, for Na^+ and Cl^- were generated for times of 30 years.

The Ogata (1970) solution assumes that the clay is a semi-infinite medium which is fully saturated and homogeneous. Also, the modelling assumes that porosity, hydraulic conductivity, hydraulic gradient and diffusion coefficients have remained constant throughout the Holocene Period (Desaulniers, 1986). The starting point for matching each measured concentration profile to a theoretical transport profile was the depth at which the ion reached its maximum concentration. The analysis assumes that the peak concentration point has remained constant throughout the Holocene Period.

6.3.1.1 NRC Site

Based on field evidence presented earlier, the lower limit of the active groundwater zone was assumed to be at an approximate depth of 4.4 m. The results of profile matching for Mg^{2+}, Ca^{2+} and SO_4^{2-} for the NRC site are presented in Figures 6.0 to 6.2. For all three major ions, peak concentrations were found well above 4.40 m.

The measured calcium concentration at 12.20 m depth was assumed to represent background level. This background level was subtracted from all data points. The calcium theoretical profile in Figure 6.0 gave a best fit by using a D_e value of 5.8×10^{-6} cm^2/s, a retardation factor of 25 and a zero advective groundwater velocity.

Two theoretical profiles for magnesium are given in Figure 6.1. Again, a background concentration was assumed to exist at 12.20 m depth. The profiles were generated by using an effective diffusion coefficient of 3.8×10^{-6} cm^2/s with two different retardation factors of 6 and 10. A groundwater velocity of zero gave the best fit.

Desaulniers (1986) reported sulfate concentration levels approaching zero at the clay-bedrock interface for Champlain Sea clays, due to sulfate reduction. In a marine environment, rich in organic matter, SO_4^{2-} is consumed by sulfate reducing bacteria which in turn produce HS^- and CO_2. For this reason SO_4^{2-} was adjusted for a zero background level. Since sulfate parameters were not evaluated during laboratory testing, an apparent diffusion coefficient, D_a (D_e/R), was determined based upon field data. This parameter couples effective diffusion with geochemical reactions. A D_a value of 4.0×10^{-7} cm^2/s seemed to give the best fit, with a groundwater velocity of zero (Figure 6.2). A tortuosity factor of 0.35 (equation 3.10) was calculated from chloride migration profiles. It was assumed that chloride was a conservative tracer (R=1). Multiplying the D_o value given in Table 3.0, for sulfate, by the tortuosity factor (τ) gave an effective diffusion coefficient of 3.7×10^{-6} cm^2/s. SO_4^{2-} retardation factor based upon equation 3.18a was approximately 9.

6.3.1.2 Fallowfield Site

The active groundwater zone is assumed to extend to a depth of 3.20 m. The results of profile matching for Ca^{2+}, Mg^{2+} and SO_4^{2-} are shown in Figures 6.3 to 6.5. All peak ion concentrations were found just below the active zone. For all three ions, best fits for diffusion profiles were obtained using an average linear groundwater velocity of zero.

The Mg^{2+} and Ca^{2+} measured concentration profiles (Figure 6.3) may represent a combination of both the upward diffusion from bedrock and the downward diffusion from the weathered zone. For this reason, calcium and magnesium were not adjusted to a zero background value.

Two calcium profiles were generated using an effective diffusion coefficient of 5.8×10^{-6} cm^2/s and retardation factors of 17 and 25. These are plotted in Figures 6.3.

Two magnesium profiles as shown in Figure 6.4 were generated using a D_e value of 3.8×10^{-6} cm^2/s and retardation factors of 4 and 12.

Sulfate concentrations were assumed to approach zero at greater depth (Figure 6.5). The two sulfate theoretical profiles, as shown in Figure 6.5, were generated using apparent diffusion coefficients of 1.50×10^{-7} cm^2/s and 5.0×10^{-7} cm^2/s. These two D_a value corresponded to the retardation factors of 7 and 24 respectively.

6.3.1.3 Renfrew Site

Based upon field evidence, the active groundwater zone was assumed to extend to a depth of 6.0 metres. Calcium, magnesium and sulfate theoretical profiles were generated by diffusion only (V=0). The theoretical profiles for Mg^{2+} Ca^{2+} and SO_4^{2-} are presented on Figures 6.6 to 6.8.

The Renfrew Piper trilinear diagram showed no distinctive difference in chemical composition between shallow and deep groundwaters. For this reason, Ca^{2+} was adjusted for a zero background level. The calcium concentration remains fairly constant throughout the active zone. The starting point for profile matching was at the base of the active zone. Two theoretical calcium profiles are given in Figure 6.6, for a D_e value of 6.25×10^{-6} cm^2/s and retardation factors of 25 and 40.

The peak concentration for magnesium occurred at a depth of 1.50 metres, well within the active zone. It was assumed that Mg^{2+} had a background concentration level of 1.0 M/m^3. A retardation factor of 9 with a D_e value of 4.6×10^{-6} cm^2/s gave the best theoretical fit. This is shown in Figure 6.7.

The sulfate theoretical profile is given in Figure 6.8. The best fit was achieved by assuming a SO_4^{2-} background level at 12.20 metres, and with an apparent diffusion coefficient of 3.0×10^{-7} cm^2/s.

Sodium and chloride were assumed to have migrated downwards for 30 years due to road salt contamination. Since the lowest concentration for both species was observed at a depth of 9.15

m, it was assumed that this concentration at this depth represented initial background levels.

The chloride theoretical profile is provided in Figure 6.9. A best fit was achieved by using a effective diffusion coefficient of 6.0 x 10^{-6} cm^2/s, retardation factor of 1, and an average linear groundwater velocity of 15 cm/a.

The results of profile matching of Na^+ are shown in Figure 6.10. The best fit was obtained by using D_e value of 4.0 x10^{-6} cm^2/s, a retardation factor of 2 and an average groundwater velocity of 25 cm/a.

6.3.1.4 Casselman Site

Based on field evidence presented earlier, the lower limit of the active groundwater zone was assumed at an approximate depth of 4.50 metres. The results of profile matching for Ca^{2+} and SO_4^{2-} are presented on Figures 6.11 and 6.12, respectively. Best fits for Ca^{2+} and SO_4^{2-} were obtained by assuming a groundwater velocity of zero. No magnesium profile have been presented here, since a theoretical match to the constant field data with depth was not found.

A background concentration level for calcium was assumed to exist at 12.20 m depth. This value was adjust to a zero background value. A D_e value of 6.0 x 10^{-6} cm^2/s with a corresponding retardation factor of 30 gave the best theoretical match to the observed calcium field data.

SO_4^{2-} was assumed to have a background concentration level near zero. This best fit theoretical profile was generated by using an apparent diffusion coefficient of 5.0 x 10^{-7} cm^2/s.

6.3.2 Tritium Profiles

Tritium occurs in the hydrogeologic cycle from natural and anthropogenic sources. In Canada, atmospheric testing of ^{3}H levels in atmospheric precipitation began in Ottawa in 1952 (Brown, 1961). The monthly tritium levels for the Ottawa area between 1952 and 1986 (International Atomic Energy Agency, IAEA, 1986) is provided in Figure 6.13.

Prior to above-ground nuclear testing which began in 1952, background levels of atmospheric tritium in eastern Ontario were low, ranging from 3 to 5 T.U. (Robertson and Cherry, 1989). By the end of atomic testing, tritium concentrations in rain and snow had increased sharply, reaching a peak value of approximately 6,000 T.U. Present day tritium precipitation levels throughout eastern Ontario are generally less than 50 T.U.

Tritium concentration levels measured in the precipitation at Ottawa were converted to a one year average step function for the period of 1952 to 1991. The yearly step function was then divided into 4 equal time sections, simulating the four seasons (winter, spring, summer, fall). In the winter months, the ground surface remains frozen around the Ottawa area. This results in a zero tritium concentration flux into the groundwater. Thus, for the winter months a tritium step function equal to zero was used. The radioactive decay constant used for tritium is based on a half life of 12.43 years (Mann et al., 1982).

Tritium migration profiles were generated using an explicit finite difference scheme which has the following form:

$$\frac{C_i^{j+1} - C_i^j}{\Delta t} = \frac{D_e}{R} \frac{C_{i+1}^j - 2C_i^j + C_{i-1}^j}{\Delta Z^2} - \frac{V}{R} \frac{C_{i+1}^j - C_{i-1}^j}{2\Delta Z} - \lambda C_i^j \qquad (6.0)$$

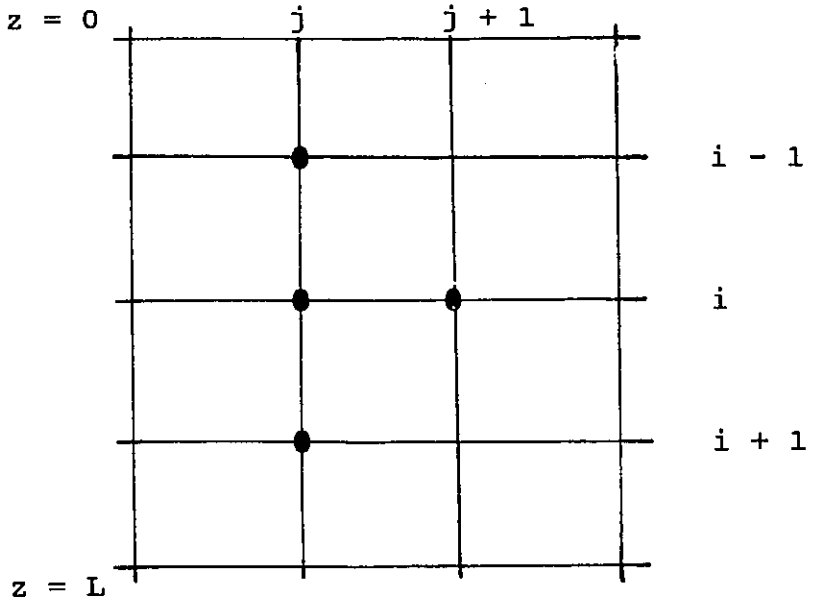

The scheme is valid for all mesh points in the interior domain of the solution, the boundary values are specified by the tritium input function (summation of all step functions) and a background level of zero.

Theoretical profiles were obtained by substituting the proper D_e for tritium which produced the best match to the field data.

6.3.2.1 NRC Site

The simulated tritium profile for the NRC site is given in Figure 6.14. The tritium input function was placed at the ground surface, since tritium levels greater than background levels (<1 T.U.) were only observed in the assumed active zone. This solution was generated using two different groundwater velocities while maintaining the effective diffusion coefficient constant at 4.8 x 10^{-6} cm^2/s. A groundwater velocity of 30 cm/a was used in the upper active zone while a zero groundwater velocity was assumed in the unfractured zone. This simulated tritium profile gave a tritium concentration range, in the upper active zone, between 20 and 40 T.U.

6.3.2.2 Fallowfield Site

A theoretical tritium profile is presented on Figure 6.15, where the depth of the active zone is assumed to be at 3.2 m. The tritium input function was placed at the active-inactive interface, since tritium concentration levels in the active zone were fairly constant. Placing the tritium input function at the base of the active zone assumes that tritium was transported instantaneously to this depth during precipitation events.

Very small groundwater velocities were measured at depth during the field investigations. For this reason, only a diffusive profile was generated below the active zone. As seen in Figure 6.15, an effective diffusion coefficient of 4.8 x 10^{-6} cm^2/s gave the best fit.

To illustrate the effect of changing the depth at which the tritium input function is placed, a diffusion only profile was generated. This profile was based on assuming that the depth of the active zone was 3.0 metres. Figure 6.16 shows the best fit, this profile was generated by using an effective diffusion coefficient of 6.4 x 10^{-6} cm^2/s.

Thus, placing the tritium input function at 3.0 metres depth instead of 3.2 metres increased the D_e value by a factor of 1.34.

6.3.2.3 Renfrew Site

Two theoretical tritium profiles were generated for the Renfrew site, as illustrated on Figures 6.17 and 6.18. The first assumed that a threshold gradient was operative at this site. This resulted in a zero groundwater velocity. When downward migration of tritium was assumed to be controlled by diffusion only, a D_e coefficient of 11.2 x 10^{-6} cm^2/s gave the best theoretical fit. The second simulation used an average groundwater velocity of 2.0 cm/a. This velocity value was measured during field investigations at depth of 8.40 metres. As seen on Figure 6.18, the best theoretical fit when using a groundwater velocity of 2.0 cm/a was achieved by using a D_e coefficient of 4.8 x 10^{-6} cm^2/s. In both cases, the tritium input function was placed at the base of the active zone which was assumed to be at 5.90 metres.

6.3.2.4 Casselman Site

Two tritium simulations are given on Figures 6.19 and 6.20. The theoretical profile in Figure 6.19 was generated by placing the tritium input function at the base of the active

zone which was assumed to be at 4.40 metres. If tritium migration was assumed to be diffusive only, the best fit was achieved by using an effective diffusion coefficient of 14.40 x 10^{-6} cm^2/s.

Measured groundwater velocities at 6.40 m depth ranged between 160 to 285 cm/a. These velocities were to high to produce any theoretical profiles which matched the observed field data. An effective diffusion coefficient of 4.8 x 10^{-6} cm^2/s was assumed to be operative at this site. The tritium input function was placed at a depth of 4.0 m. By "back-figuring", a linear groundwater velocity of 3.5 cm/a gave the best fit. This groundwater velocity approached measured values at 12.20 metres depth during field investigations.

6.4 Downward Migration Analyses Using the Second Conceptual Model

6.4.1 Theoretical Profiles for Some Major Ions

Theoretical profiles for solute transport in a fractured porous media were generated by analytical solutions presented by Sudicky and Frind (1982). These analytical solutions are for a system of idealized series of smooth, parallel fractures with constant aperture and spacing. A steady state flow field is specified. The source solution is placed only at the entrance of each fracture. Solute diffusion into the adjacent matrix is performed perpendicular to the vertical fracture axis.

Due to the measured high fracture flow velocities encountered at all four sites, the term ϕ/γ [equations 2.70 (a) and (b)] was less than 0.02, thus both the general and the

nondispersive solutions would give essentially the same results (Sudicky and Frind, 1982). For this reason, the nondispersive solution [equations 2.67 (a) and (b)] were used to generate the theoretical profiles for the selected ions. This analytical solution was much easier to solve since it involved the evaluation of only one integral.

Only the downward migration of weathering products were modelled. Oxidation was assumed to have produced constant source concentrations over a period of 10,000 years. Also, theoretical profiles were generated for sodium and chloride at the Renfrew site, for a period of 30 years due to salt contamination. It was assumed that salt contamination occurred at a constant concentration.

Ion concentrations at the ground surface were determined by extrapolating field data to the surface. Effective diffusion coefficients, effective porosities and matrix retardation factors were predetermined through laboratory and field experiments reported earlier.

6.4.1.1 NRC Site

The theoretical calcium profiles were derived assuming a concentration at ground surface of 3.47 M/m^3 and the calcium concentration at 12.20 metres depth was assumed to represent the initial background level. All Ca^{2+} profiles were generated using a D_e coefficient of 5.8×10^{-6} cm^2/s, an effective porosity of 0.65, and a matrix retardation factor of 30.

To show the effects of fracture flow velocity, fracture aperture and spacing, each of these variables were varied and the results plotted.

Figure 6.21 shows the effects of varying the fracture flow velocity from 0.25 to 1.30 m/d. These three theoretical profiles were generated using a fracture spacing of 0.50 metres and a fracture aperture of 30 μm. These three parameters fall within the field observations.

A velocity of 1.30 m/d represents the average value calculated for the assumed active zone. The fracture flow velocity which gave the best fit was 0.25 m/d. This value fell within the lower estimated range at the NRC site, see Table 4.14.

Figure 6.22 shows the effects of varying fracture spacing while maintaining a fracture flow velocity of 1.30 m/d and a fracture aperture of 30 μm. The fracture spacing ranged from 0.80 to 2.0 m. A constant fracture spacing of 2.0 m gave the best fit. This fracture spacing was not supported by direct field observations.

The sensitivity of solute migration to fracture aperture is illustrated on Figure 6.23. The fracture aperture ranged from 10 to 50 μm while the fracture velocity and spacing were maintained at 1.30 m/d and 0.50 μm, respectively. These fracture apertures were very small, only slightly larger than the average diameter of human hair. A fracture aperture of 10 μm gave the closet fit to the observed field data. This value represented the smallest fracture width estimated at the NRC site.

Figures 6.21 to 6.23 demonstrated that several possible combinations of fracture flow velocities, fracture apertures and spacings could produce theoretical profiles which closely match the observed field data.

Theoretical profiles were produced for SO_4^{2-} by using a D_e coefficient of 3.71 x 10^{-6} cm^2/s and a matrix retardation factor of 2. A SO_4^{2-} concentration level of 1.45 M/m^3 at the surface was assumed and that background concentration was near zero. The two generated theoretical profiles are shown on Figure 6.24. A best fit was produced by using a fracture flow velocity of 0.04 m/d, a fracture spacing of 0.50 m and a fracture aperture of 20 μm. This low velocity was not measured during field investigations.

The sulfate theoretical profile demonstrated the some of mathematical restrictions of the analytical solution when dealing with low reactive solutes for very long time periods. The difference in fracture flow velocities between calcium and sulfate was probably due to the much lower soil retention capacity for sulfate. For these reasons, only calcium theoretical profiles were generated at the Fallowfield and Casselman sites. At the Renfrew site, only sodium and chloride were generated for a time period of 30 years.

6.4.1.2 Fallowfield Site

The theoretical calcium profiles at the Fallowfield site were generated using an effective diffusion coefficient of 5.8 x 10^{-6} cm^2/s, a matrix effective porosity of 0.55 and a matrix retardation factor of 25. A concentration of 2.60 M/m^3 was assumed at the ground surface. Calcium concentrations were adjusted for a zero background level.

Two theoretical profiles are given on Figure 6.25. The first profiles was generated using the average fracture flow velocity measured in the upper active zone of 1.85 m/d, a fracture spacing and aperture of 1.0 m and 70 μm,

respectively. The second profile was generated using parameters measured in the field at a depth of 0.80 metres. These measured parameters were a fracture flow velocity of 0.14 m/d, a fracture spacing of 0.01 m and a fracture width of 20 μm.

6.4.1.3 Renfrew Site

Only theoretical profiles for sodium and chloride were generated for the Renfrew site. Sodium and chloride profiles were produced by assuming that fracture spacings observed at the NRC site were also characteristic of upper fracture Leda clay deposits. Since no direct evidence was obtained at this site. Migration of solutes along a fracture has occurred for at least 30 years.

Theoretical sodium profiles were generated by using a D_e coefficient of 4.0 x 10^{-6} cm^2/s, a matrix effective porosity 0.55, a matrix retardation factor of 2, an average fracture flow velocity of 5.9 m/d, a fracture spacing of 0.40 m, and the fracture aperture was varied from 20 to 40 μm. A Na^+ concentration level of 12.0 M/m^3 at the ground surface was assumed and the concentration level at a depth of 9.15 m represented initial background conditions. Three theoretical sodium profiles are provided on Figure 6.26. The observed field data fall within the three theoretical profiles.

Chloride theoretical profiles were generated using the same fracture parameters as those used for sodium except for the matrix effective diffusion coefficient and the matrix retardation factor. The D_e coefficient and retardation factor used for chloride migration were 6.0 x 10^{-6} cm^2/s and 1, respectively. A concentration of 22.0 M/m^3 was assumed at the

ground surface and a background concentration level of 2.0 M/m^3 was also assumed. Two theoretical profiles are presented in Figure 6.27. Two different fracture apertures of 20 and 40μm were used.

6.4.1.4 Casselman Site

The Ca^{2+} theoretical profile at the Casselman site was generated using a D_e coefficient of 5.8 x 10^{-6} cm^2/s, a matrix effective porosity of 0.65, and a matrix retardation factor of 25. A calcium concentration level of 3.20 M/m^3 at the ground surface was assumed. It was also assumed that the Ca^{2+} concentration level at a depth of 12.20 m was assumed to represent initial background value. As illustrated on Figure 6.28, a combination of a fracture flow velocity of 0.50 m/d, a fracture spacing of 0.50 m and a fracture aperture of 22 μm gave a good match to the field data. These three parameters fell within their previously measured field ranges.

6.4.2 Theoretical Tritium Profiles

Tritium theoretical profiles in a fractured porous media were generated by analytical solutions presented by Sudicky and Frind (1982). The exact analytical solutions are only valid for a constant source strength.

Only steady state solutions presented by Sudicky and Frind (1982) were used. Since peak tritium concentration levels in atmospheric precipitation occurred in the early 1960's and coupled with the relatively high radioactive decay of tritium, it was assumed that steady state conditions have been reached by 1991. A constant source strength of 40 T.U. at the top was assumed for the analysis. This assumption would produce a

conservative tritium profile and allow a better estimate to which depth fractures were active and open.

In all tritium simulations, an effective matrix diffusion coefficient of 5.0 x 10^{-6} cm^2/s and a matrix retardation factor of 1 were used. This D_e value falls within the lower boundaries reported in the literature, e.g. Ruland et al. (1989), Yanful and Quigley (1990), Shackelford (1991).

6.4.2.1 NRC Site

Two theoretical tritium profiles are given in Figure 6.29. The first profile was produced by using a fracture flow velocity of 3.5 m/d, a fracture spacing and aperture of 0.05 m and 20 μm, respectively. These 3 parameters gave the best match for field data in the upper 4.0 metres. The second profile was generated using a fracture flow velocity of 3.0 m/d, a larger fracture spacing of 0.1 m while maintaining the fracture aperture at 20 μm. The second profile fell below tritium detection limits at an approximate depth of 12.0 metres.

In Figure 6.30, two theoretical profiles were combined together to form one profile. This combination gave the best match to the measured field data which no single theoretical profile could do. Combining two profiles allowed more freedom in terms of fracture spacing and aperture size. As observed in the test pits, fracture spacing increased with depth.

In Figure 6.30, a theoretical profile was generated to match field data below 3.5 metres depth by using a fracture flow velocity of 3.5 m/d, observed fracture spacing of 0.40 m and a fracture width of 20 μm. A second profile was generated to

match field data above 3.5 m depth by using a fracture flow velocity of 3.5 m/d, observed fracture spacing of 0.05 m and a fracture aperture of 20 μm. These two theoretical profiles were then superimposed on each other at a depth of 3.5 m. The relative concentrations were adjusted accordingly to achieve a continuous curve. This combination was possible since the relative concentration at 3.5 m depth reached 0.8 within a few years. Thus, the steady state assumption was still valid for the second theoretical profile generated below 3.5 metres. Also presented on Figure 6.30 is the tritium concentration at the centre line of the clay matrix block.

6.4.2.2 Fallowfield Site

Two theoretical tritium profiles are presented on Figure 6.31. The first generated profile matched the field data in the upper 3.0 metres of the clay deposit. It was produced by using a fracture flow velocity of 4.0 m/d, a fracture spacing and aperture size of 0.1 m and 40 μm, respectively. The second profile was generated by decreasing the fracture flow velocity to 0.50 m/d while maintaining the same fracture spacing and aperture. The tritium levels dropped below detection limits around 9.0 metres depth, for the second profile.

No single theoretical profile came close to matching the measured field data. A combination of two theoretical profiles were merged into a single profile which closely match the field data. This theoretical profile is provided in Figure 6.32. To match the field data below 3.0 m, a profile was generated using a fracture flow velocity of 4.0 m/d, a fracture spacing of 0.50 m and a fracture aperture of 20 μm. This profile was superimposed on the first profile generated

on Figure 6.31 at a depth of 3.2 metres. The tritium concentration along the centre line of the clay matrix is also given on Figure 6.32.

6.4.2.3 Renfrew Site

The tritium concentration profile along a fracture and at the centre line of the clay matrix block is given on Figure 6.33. This figure represents the combination of two theoretical profiles at a depth of 6.0 metres. This solution was generated by using a fracture flow velocity of 30 m/d, a fracture spacing of 0.20 m and fracture aperture size of 50 μm, for the upper 6.0 metres. Below this depth, the fracture flow velocity was decreased to 8 m/d, the fracture spacing was increased to 2.0 m and the fracture aperture was decreased to 20 μm. This theoretical profile fell below tritium detection limits around a depth of 14.0 m.

6.4.2.4 Casselman Site

The tritium concentration along a fracture and at the centre line of the clay matrix block is presented on Figure 6.34. This figure represents the combination of two theoretical profiles at a depth of 4.40 m. This solution was achieved by using a fracture flow velocity of 15 m/d, a fracture spacing of 0.40 m and a fracture aperture of 40 μm for the upper 4.40 metres of the clay deposit; and a fracture flow velocity of 5.0 m/d, a fracture spacing of 1.0 m and a fracture aperture of 20 μm below 4.40 metres. This theoretical profile predicted that tritium levels fell below detection limits around a depth of 12.0 metres.

A discussion of the validity of the two models is presented in Chapter 8.

CHAPTER 7

PREDICTION CASES

7.1 General

Field simulations were restricted to downward migration of weathered products and tritium. Thus, field simulations did not predict migration rates for eluted solute species in an unfractured porous media nor did they predict migration of a conservative solute in a fractured porous media.

Eluted and/or non-reactive solutes are very important since they represent contaminants with the greatest mobility. Five hypothetical cases were studied; 4 out of the 5 cases involved the placement of a landfill site on fractured clay. The fractured cases involved the prediction of the migration of a non-reactive solute while the unfractured case includes the migration of some eluted species. Schematic physical representation for the five hypothetical cases is shown on Figure 7.0.

7.2 Transport through Unfractured Porous Media

Contaminant transport through an unfractured clay deposit is represented in Case 1. The landfill site was underlain by 20 metres thick unfractured clay. Prediction migration profiles for Na^+, K^+, Mg^{2+}, Ca^{2+} and Cl^- were based upon effective diffusion coefficients and retardation factors obtained during the laboratory experiments. The individual D_e coefficients were corrected to a field temperature of 8 °C. A downward

average linear groundwater velocity of 2.0 cm/a existed at the site. It was assumed that elution of Mg^{2+} and Ca^{2+} from the soil exchange sites occurred during leachate migration (Quigley et al., 1989). Major ion concentrations in the landfill site were typical of domestic waste leachate (Barone et al. 1989):

Na^{+} = 955 mg/L,
K^{+} = 400 mg/L,
Mg^{2+} = 290 mg/L,
Ca^{2+} = 250 mg/L,
Cl^{-} = 1000 mg/L.

7.3 Contaminant Transport Through Fractured Porous Media

Contaminant transport through a fractured porous media is represented in cases 2 to 5. Only a conservative specie, chloride, was modelled. In all cases, a D_e coefficient of 6.0 x 10^{-6} cm^2/s, an effective matrix porosity of 0.50 and a retardation factor of 1 were used.

In case 2, the landfill was placed over a fractured clay deposit of 20 metres thick. The deposit had a small fracture spacing of 0.15 m, a fracture aperture of 20 μm and a fracture flow velocity of 2.0 m/d.

In case 3, the fracture spacing was increased to 0.40 m while the remaining parameters were unchanged for case 2.

In case 4, the fracture spacing and aperture were increased to 1.0 m and 50 μm, respectively. The fracture flow remained constant at 2.0 m/d.

The landfill site in case 5 was underlaid by a 10 m thick clay deposit in which a single fracture connected the landfill leachate to the bedrock aquifer. This fracture had a flow velocity of 5.0 m/d and an aperture of 10 μm.

7.4 Results

7.4.1 Predictions for Case 1

Prediction periods of 25 to 100 years were used for Mg^{2+}, Ca^{2+} and Cl^{-}. A prediction periods of 50 to 100 were made for Na^{2+} while only a period of 100 years was made for K^{+}. Prediction results for each solute species is presented in Figures 7.1 to 7.5.

The results showed that calcium had the deepest penetration after 100 years, at 9.0 metres. While potassium which had the highest retention had only migrated to less than 2.0m depth. Chloride, the conservative specie, had migrated to 8.0 metres depth after 100 years.

7.4.2 Predictions for Cases 2 to 5

Prediction periods of 25 to 100 years were used for cases 2 to 4, while a prediction periods of 50 to 500 years were used for case 5. Prediction results for cases 2 to 5 are presented in Figures 7.6 to 7.9, respectively.

For case 2, the relative concentration of contaminant entering the underlying bedrock aquifer after 100 years was approximately 0.37 (37% of leachate concentration). While a relative concentration of 0.05 had entered the bedrock aquifer after 100 years for cases 3 and 4. A C/Co value of 0.05,

although low, can be of great environmental significance for many contaminants (Harrison et al., 1992).

For the single fracture case, it had taken over 500 years for the relative concentration to reach 0.025 at the clay-bedrock interface. However, this result was based on that contaminants were only transported by the single fracture. In fact, migration would also occur through the clay matrix by advection and diffusion. This would greatly reduce the matrix storage capacity which, in turn, would result in an increase in the volumetric contaminant flux transported by the fracture. Therefore, the arrival time of contaminant in the underlying aquifer could be significantly reduced.

The above predictions are not absolute because of the simplifying assumptions and estimates made for the parameters required in the solution of the mathematical models employed. Nevertheless, these predictions are useful tools for better understanding of the hydrogeological setting and the impact of hazardous wastes on the surrounding environment.

CHAPTER 8

DISCUSSION

8.1 Geology

The variability of physical properties of Leda clay in Eastern Ontario has been demonstrated by the geological investigations at four different sites. One of these regional heterogeneities was the clay content variations. At NRC and Renfrew sites, high clay percentages ranging from 60 to 74% were found for the upper two metres. Whereas at the Fallowfield and Casselman sites clay content was only 32 to 45%, respectively. The trend in clay content with depth also varied at all four sites. NRC reported a decrease in clay content with depth. At Fallowfield and Casselman, the percentage increased with depth, and the clay percentage at Renfrew remained fairly constant.

The depth at which the Leda clay became sensitive also varied from site to site. Sensitive clay was encountered at an approximate depth of 5.2 m at both NRC and Fallowfield sites while at the two minor sites, sensitive clay was observed below 11.0 metres.

The examination of borehole samples and test pits excavated at Fallowfield and NRC permitted direct visual observation of clay weathering and the existence of fractures.

From borehole logs, geological features such as roots, root holes and oxidation were observed at all sites. But, no

visible fractures were recorded in the borehole logs. The identification of thin fractures in cores was inherently difficult due to the lack of geochemical weathering features. The maximum depth of observed oxidation bands was 4.50 metres at NRC and Fallowfield and 5.50 metres at the two minor sites. In the literature review on Canadian clays, fractures extend well below the observed weathered zone, reaching depths over 10.0 metres (Ruland et al., 1991). Eden and Crawford (1957) observed fractures below 6.0 m depth for Leda clay deposits around the Ottawa area.

Test pits revealed a complex system of fractures, roots, root holes, paleoroots, pores and sand lenses. The depth at which these features are interconnected and hydraulically active can define the active groundwater zone.

The geological features observed in each test pit were inherently different. Above the water table, 1.0 m depth, fractures were so closely spaced that they gave the clay a granular texture. Below the water table, the clay was soft which could explain the observed small pore like features rather than well defined fractures. These pores seemed to be interconnected with the sand lenses and root holes. The number of pores per cm^2 decreased with increasing depth, ranging from 1 per cm^2 at 1.0m depth to 1 per 10 cm^2 at 3.0 m. Below 3.5 m, the clay became massive and devoid of any weathering features.

In contrast to the Fallowfield site, the NRC test pit revealed well defined fractures below a depth of 1.1 metres. The stiff clay encountered in the upper 4.5 m at this site may have resulted in a fractured network formation. Fractures extended beyond the base of the test pit at 4.0 metres. Fracture

spacing steadily increased from one fracture every 4 cm at 1.5 m depth to one fracture every 40 cm at 3.5 m.

Ruland et al. (1991) reported fracture spacings ranging from one fracture every 50 cm to one fracture every 2 m for southwestern Ontario clay deposits. D'Astous et al. (1989) observed fracture spacings from excavated trenches ranging up to a maximum of 1.0 m at a depth of 5.0 metres.

The length of fractures varied considerably, some exceeding 50 cm. Paleoroots were common on fracture surfaces. Fracture dips were near vertical, ranged from 70 to 90 degrees and relatively easy to measure. However, fracture orientations were cumbersome to measure. These measured fracture orientations may be highly influenced by test pit orientation, since only the fractures parallel to the test pit wall would open due to stress relief caused by the excavated pit (Vorauer and Harding, 1986).

The measured high flow rates of 70 l/h at NRC and 220 l/h at Fallowfield, entering the freshly excavated test pits were indicative of groundwater flow through a zone of well interconnected fractures, sand lenses, root holes and pores. The higher value reported for Fallowfield was probably due to a high number of small sand lenses. In comparison, Ruland et al. (1991) registered flow rates of up to 90 l/h for excavated test pits in southwestern Ontario. Based upon the above results, a highly hydraulic active zone exist to a greater depth than 4.0 m at NRC, and up to 3.5 m at Fallowfield.

Observation from test pits indicated a decrease in the number of fractures with depth. However, a definition of the exact cut-off depth below which no fractures exist is not possible.

The probability of intersecting widely spaced vertical fractures (1 fracture every 2 m) with conventional drilling program of vertical boreholes is very small. Ruland et al. (1991) reported a less then 10% chance of intersecting fractures which are spaced at every 2 m.

8.2 Hydrogeology

8.2.1 Physical Aspects

Water level fluctuations with time (Figures 4.17, 4.23, 4.28, 4.33) gave a good indication regarding the depth and degree of the hydrogeological activity in the upper weathered, fractured clay. Piezometers at all depths were found to respond to seasonal variations in climatic events. Piezometers installed in the upper near surface zone showed a significant response to short term precipitation events. These shallow piezometers also showed similar trends in water level variations with time. The above results indicated that the upper sections at four sites are fractured and hydraulically active, but most importantly, these fractures are hydraulically well interconnected and open. Therefore, using water level data with respect to precipitation events, a highly active zone extends to a depth of 4.4 metres at NRC and Casselman, 3.2 metres at Fallowfield and to at least 6.0 metres at Renfrew.

Below this highly active zone, water level fluctuations became less sensitive to short term climatic changes and showed a more progressive change from dry to wet seasons. Water level responses in the deeper piezometers seemed to lag behind the surface water level variations. These phenomena may indicate that the piezometers installed below the highly active zone did not directly intersect open fractures or that these

piezometers were not hydraulically connected with the upper zone.

The maximum difference in water levels during seasonal climatic changes illustrate well the hydraulically active zone. The maximum water level variation profiles (Figures 4.20, 4.25, 4.30, 4.35) were relatively straight in the upper weathered and highly fractured zone. This again suggests that the fracture network near the surface, is well interconnected, opened, and hydraulically active.

Maximum seasonal variation on the order of 110 cm was recorded in the upper 4.4 m at NRC and 3.2 m at Fallowfield. At the Renfrew site, a maximum seasonal variation in the order of 120 cm was observed in the upper 6.0 metres. A value in excess of 240 cm was recorded in the upper 4.40 m at Casselman. This latter large difference may have been influenced by strong horizontal gradients which would exist at the Casselman site due to the sloping topography.

The variation in maximum seasonal piezometric heads was significantly reduced just below the active zone and continued to decrease with depth. This could indicate a reduction in the contribution of groundwater flow by open fractures or that the influence of fractures were reduced due to the increase in fracture spacing with increasing depth.

Ruland et al. (1991) suggested that seasonal water level fluctuations of half a metre or more were indicative of fractures and active groundwater flow zone, in the clayey till plains of southwestern Ontario. A value of 50 cm in Leda clay may indicate those piezometers which were influenced by fractures which displayed strong spatial heterogeneity in

fracture frequency. Using this criterion, the depth at which fractures and other geological features as roots, root holes and sand lenses have a strong influence on the hydraulic properties of Leda clay are 11.0 metres at NRC and Casselman, 9.5 metres at Fallowfield and below 12.0 metres at Renfrew. If the criterion for fracture flow is increased to 70 cm, the revised depths are now 7.5 m at NRC, 4.40 m at Fallowfield, 11.0 m at Renfrew and 6.5 m at Casselman. However, there is no clear evidence that a maximum fluctuation value of 50 cm or greater would be representative of fractured groundwater flow in Leda clay deposits in eastern Ontario. The water level fluctuations are influenced by climatic events, geological composition and hydraulic properties of the glacial clayey till deposits in question.

Jarrett and Eden (1970) reported a maximum seasonal fluctuation difference of 37 cm at the clay bedrock interface, at an approximate depth of 30 metres. Their study was performed on a Leda clay deposit in eastern Ottawa, near the Ottawa river. Thus, fluctuation values of less than 50 cm could represent typical seasonal variation in intact, massive Leda clay deposits in eastern Ontario. Jarrett and Eden (1970) suggested that seasonal water level variation below a depth of 10 metres could be more influenced by the underlying moraine/bedrock aquifer than from surficial rain water infiltration.

Hydraulic head profiles (Figures 4.22, 4.26, 4.31, 4.36) were nearly all vertical near the ground surface which resulted in the development of very small hydraulic gradients. These small gradients in a silty clay deposit would only be possible if weathering features such as fractures, roots, root holes, pores, and sand lenses were hydraulically interconnected and

were the dominant pathways for groundwater movement. The hydraulic gradients were negligible to an approximate depth of 7.4 m at NRC, 3.70 m at Fallowfield, 6.0 m at Renfrew and 4.40 m at Casselman. It is important to note, that from the average hydraulic head profile for Fallowfield, an almost vertical hydraulic head existed between 1.6 m and 7.6 m, excluding the value observed at 6.1 m. Below these active zones, an average downward gradient existed. These average downward gradients ranged at all four sites from 0.024 below 4.3 m at Fallowfield to 0.40 below 4.4 m at Casselman.

An upward gradient was well developed in the summer months at the Fallowfield site. This negative hydraulic gradient could be attributed to the lack of precipitation during the summer months coupled with evapotranspiration from the corn crop. This resulted in a decrease in the measured hydraulic head in all piezometers installed above 7.6 m. Thus, roots may extent to this depth. D'Astous et al. (1989) reported similar findings for a corn field at the Trichl site, in southern Ontario.

Hydraulic conductivity profiles for the four sites are presented in Figure 4.44. In the upper fractured and active zone, hydraulic conductivity values ranged from 1.85×10^{-8} to 2.05×10^{-5} m/s for values measured by the double-Shelby method. The hydraulic conductivity values in the upper active zone were highly scattered, represented by a three order of magnitude difference in K value alone. These high values were associated with the direct fracture intersection or with a more hydraulic conductive sand lense as observed at Fallowfield.

The hydraulic conductivities found in the upper active and fractured zones were approximately 1 to 4 orders of magnitude higher than those evaluated for clays beneath this zone. The hydraulic conductivity measured in the deepest piezometers ranged from 8.20×10^{-10} to 1.40×10^{-9} m/s. Tavenas et al. (1983) reported that hydraulic conductivity values ranging from 10^{-11} to 10^{-10} m/s were associated with unfractured, massive Leda clays. These observations for eastern Champlain Sea clay deposits support earlier findings by Lafleur and Geroux (1983), Lafleur et al. (1987) and Desaulniers and Cherry (1989), indicated that the hydraulic conductivity in the upper near surface zone is controlled by a fracture network rather than the intergranular pore spaces. Higher hydraulic conductivities in the upper fractured zone were also reported for the western Canadian Plains and southwestern Ontario glacial clayey till deposits (e.g. Grisak, 1976; Day, 1977; Keller, 1989; Desaulniers et al., 1981; D'Astous et al., 1989).

The wide variation in hydraulic conductivity values may reflect different local geological history, vegetation, borehole smearing and the probability of intersecting widely spaced and opened fractures with a 7.6 cm diameter vertical borehole.

Based upon hydraulic conductivity profiles, a highly conductive zone extends to a depth of 4.4 m at NRC, 3.7 m at Fallowfield, 6.0 m at Renfrew and 6.4 m at Casselman.

Quigley et al. (1989) reported a hydraulic conductivity value for a highly fractured clay sample from the NRC grounds to be greater than 10^{-7} m/s. Partial remoulding of the fractured clay sample resulted in a reduction of the hydraulic

conductivity to 4.8 x 10^{-9} m/s. Complete remoulding resulted in a further reduction by two orders of magnitude. These results indicate the important effects of smearing or remoulding on measured in-situ hydraulic conductivity values in fractured clay.

Further evidence of the effects of smearing were observed when comparing the two different piezometer installation techniques used in the present study. In the upper fractured zone at NRC, smearing by augering reduced the hydraulic conductivity by two orders of magnitude. Below the highly active zone, only marginal differences were observable at all four sites. This may indicate that the double-Shelby method was more effective in reducing smearing effects in the upper stiff clays, but had only limited success in the more softer and sensitive clays found at depth. However, similar results could have occurred due to the increase in fracture spacing with depth which produced no measurable effect on the test results or that smearing had little effect on less permeable clays. Nevertheless, the double-Shelby technique reduces the effects of smearing along the borehole wall caused by drilling; similar findings were reported by D'Astous et al. (1989).

At the Fallowfield site, hydraulic conductivity values determined from the large diameter well pump test were in good agreement with the double-Shelby test results. However, at the NRC site, two orders of magnitude difference was recorded for the large diameter well. This increase was probably due to the opening of fractures during excavation as a result of stress release or due to the combined effects of intersecting a large number of open fractures. These results re-enforce the importance of properly intersecting hydraulically active

fractures. The many small sand lenses probably control the hydraulic properties of the upper active zone at Fallowfield as compared to the many fractures observed at NRC.

The observation of fractures in test pits provided a direct method for determining fracture spacing, whereas fracture apertures can only be estimated through indirect methods such as that proposed by Snow (1968). The aperture of fractures cannot be measured directly in the field due to the change in initial stress conditions, and also, a direct in-situ method for measuring fracture apertures does not exist. Estimations of fracture apertures by an indirect approach on surficial clayey till deposits of glacial origins in Canada, ranged from 10 to 50μm (Grisak 1975; Day, 1977; D'Astous et al., 1989). Fracture apertures calculated for the NRC site fall within this range. The fracture spacings at the NRC site were easily observable and measurable, therefore these results may be considered as reliable.

No test pits were available for the Renfrew and Casselman sites. Assuming the fracture spacings observed at the NRC site, the largest fracture aperture was 200 μm for the Renfrew site.

The many small sand lenses at Fallowfield exerted a great influence on the evaluation of fracture apertures.

The effective porosity of fractured clay was also determined using methods developed by Snow (1968). Again, the NRC site gave the most reliable results where the effective fractured porosity ranged from 1.02×10^{-4} to 6.22×10^{-4}. D'Astous et al. (1989) reported an effective fractured porosity ranging from 2.3 to 7.5×10^{-4} for fractured clay deposits found in

southwestern Ontario. These results were based upon an average hydraulic conductivity value of 6.3 x 10^{-8} m/s and fracture spacings ranging from 5 to 30 cm. Grisak (1975) found an effective fractured porosity of 2.5 x 10^{-4} for a clayey till located at Pinawa, Manitoba.

Groundwater velocity through fractures at all four sites ranged from 0.10 to 4.8 m/d (1.16 x 10^{-6} to 5.55 x 10^{-5} m/s). The abnormally high value found at Renfrew of 27 m/d (3.1 x 10^{-4} m/s) was excluded. This extreme value was probably due to a large number of sand lenses, since no direct observations were possible to confirm its cause. Intergranular or unfractured groundwater velocities ranged from 0.0004 m/year to 0.04 m/year (1.27 x 10^{-11} to 1.28 x 10^{-9} m/s) at all sites. Grisak (1976) and Day (1977) reported fracture flow velocities for western glacial clayey till deposits to range from 1.1 x 10^{-4} to 2.0 m/d (1.27 x 10^{-9} to 2.3 x 10^{-5} m/s).

The above results demonstrate that fractures can yield fairly high volumetric flow rates even at very small fracture apertures and at relatively large fracture spacings. Fractures are an important pathway for solute or contaminant migration in fractured Leda clay.

8.2.2 Geochemical Aspects

8.2.2.1 Major Ions

The chemical analysis indicated that sodium is the predominant cation in solution for Leda clays, while chloride is the more dominant anion in solution. A prominent feature of the major ion profiles was the gradual increase in concentration of Na^+, K^+, Cl^-, HCO_3^- with depth, with the exception of the Renfrew

site. Calcium and magnesium were dominant in the upper weathered sections but decreased significantly in concentration below this upper zone. Carbonates were variable between sites. They were dominant at NRC and Casselman and were only moderately dominant at Fallowfield and Renfrew. All SO_4^{2-} profiles gradually decreased from maximum concentration levels in the upper active zone to values less than 0.23 M/m^3 below 8.0 m depth. These major ion trends are typical of Leda clay deposits as reported by Torrance (1988).

The Fallowfield and Casselman geochemical profiles could be indicative of sedimentation in a saline water (marine) environment. The low salt concentration throughout the NRC ion profile could represent clay sedimentation in a fresh water environment or strong downward fresh water leaching. The Renfrew site, as frequently stated earlier, showed geochemical abnormality when compared to the other three sites. Renfrew clay sediments could have originally been deposited in a non-marine environment which was later contaminated from recent groundwater salts.

The interpretation of the geochemical analysis and chemical trends were limited due to the fact that major ion concentrations below 12.0 metres remained unknown for each site.

The porewater salinity is best represented by the electrical conductivity profile. The conductance of fresh rain water is around several tens of microsiemens (μmhos) while it is several hundreds of thousands of microsiemens for deep marine sediments (Freeze and Cherry, 1979). The highest conductivity was observed at Fallowfield for depths greater than 9.0

metres. A low conductivity environment was measured throughout the upper 12.2 metres at the NRC site.

The high hydraulic activity in the near surface zone resulted in a strong mixing of mineralized clay porewater with fresh rain waters. This mixing produced a low salinity environment, except for the Renfrew site. The salinity levels in the upper active zone at Renfrew were too high to be representative of fresh water leaching. The electrical conductivity values measured at depths of 9.2 and 12.2 metres fell within the range of conductivity values measured for the near surface zones at the other three sites. Similar observations were made with respect to sodium and chloride ions. A possible explanation for this abnormality is the ground surface contamination by road salt (NaCl) which was assumed to be stored in close proximity to the piezometer nest.

The trilinear Piper plots gave the best representation of the nature of the groundwater geochemistry. Three hydrochemical facies were observed at NRC, Fallowfield and Casselman while only one facie could be used to represent Renfrew's groundwater.

These hydrochemical facies were established for groundwater samples with respect to vertical direction only and were defined as follows:

1) a shallow "active" facie which represented groundwater which has undergone considerable chemical change from its original composition due to fresh water infiltration;

2) a deep "inactive" facie which represented deep groundwaters which did not interact with the near surface

groundwaters and were completely different in chemical composition. This hydrochemical facie may represent the initial groundwater chemical composition or was subjected to a geochemical change due only to an upward diffusion from the clay bedrock interface to the upper hydraulic active zone (Desaulniers and Cherry, 1991), and;

3) Intermediate "transition" facie which represented a geochemical transition between the surface and deep groundwaters. This transition zone may have been influenced by fracture flow; or, it was the result of an upward or downward advective and diffusive transport mode or both.

A more in-depth explanation of the observed chemical trends in the transition zone will be discussed later.

Based upon trilinear Piper diagrams, major ion profiles and electrical conductivity profiles, the highly active groundwater zone extends to 3.0 m, 3.0 m and 4.4 m for the NRC, Fallowfield and Casselman sites, respectively. The transition zone ranges to at least 6.1 m at Fallowfield, to 9.0m at NRC and to 6.4 m at Casselman. In the case of Renfrew, the presence of relatively young salts at ground surface and the subsequent downward infiltration indicate that the active zone here ranges between 6.0 and 8.0 m and that the transition zone extends well below 12.0 m.

8.2.2.2 Tritium

Groundwater having a tritium concentration below 1.0 T.U. indicates that groundwater recharge has occurred prior to 1953 (Freeze and Cherry, 1979; Robertson and Cherry, 1989). Therefore, groundwater with tritium value greater than 1.0

T.U. indicates that post 1952 precipitation has migrated to that depth.

The maximum tritium concentration level was observed at Renfrew at a depth of 5.9 m (38 T.U.). NRC and Fallowfield had their maximum tritium levels near the ground surface, whereas at Casselman it occurs at a depth of 4.4 m. Tritium concentrations for these three sites ranged between 31 and 34 T.U. This result would indicate that tritium concentration in the precipitation over the Ottawa area has been fairly uniform.

Tritium infiltration has occurred well below the ground surface. Post-1952 recharge of groundwater indicated by ^{3}H concentration levels occurred at depths of 4.4 m and 4.3 m at NRC (24 T.U.) and Fallowfield (14 T.U.), respectively, at 6.4m for Casselman (17 T.U.) and at 12.2 m for Renfrew (3 T.U.), respectively. Tritium concentration levels decreased below 1.0 T.U. at 6.10m, 7.60 m and 12.20 m at the NRC, Fallowfield, and Casselman sites, respectively. The maximum depth investigated at Renfrew was 12.20 metres.

The table below provides a summary of the depth at which the "active zone" is defined by different investigative techniques.

Site	Physical (m)	Geochemical (m)	Tritium, relatively constant value (m)	Tritium <1.0 T.U. (m)
NRC	4.4	3.0	4.4	6.1
Fallowfield	3.2	3.0	3.2	6.1
Renfrew	6.0	9.0	6.0	---
Casselman	4.4	4.4	4.4	9.0

8.2.2.3 Geochemical Diagenesis

The main geochemical processes in Leda clays reported by Desaulniers and Cherry (1989) are sulphate reduction, carbonate mineral dissolution and cation exchange.

The sharp drop in dissolved SO_4^{2-} concentrations below the upper weathered zone and the increase in HCO_3^- concentrations with depth can be attributed to sulfate reduction by sulfate reducing bacteria. The bacteria consume dissolved SO_4^{2-} and produce HS^- and CO_2. If this reaction occurs in the presence of calcite and dolomite, the CO_2 cause calcite to dissolve and produce HCO_3^- until the calcite and dolomite saturation point is achieved. This will buffer the pH of the pore water solution in the range of 7 to 8.

Higher groundwater sulfate levels in the upper active zone is probably produced by oxidation of sulfide minerals and perhaps some sulphur-bearing organic matter. However, the production

levels of SO_4^{2-} were about one order lower in magnitude than those reported for the Western Plains and southwestern Ontario by Hendry et al. (1986), Keller (1987), and Desaulniers et al. (1981). Gypsum ($CaSO_4 \cdot 2H_2O$) crystals were absent in both test pits excavated in the present investigation, while they were commonly found in the Western Plains and southwestern Ontario. Desaulniers and Cherry (1989) reported similar findings for the Varennes site near Montreal. Calcium generally occurred at higher concentration levels than magnesium on a per mole basis and that the sites may contain very little exchangeable Na^+ (Figure 4.87) in the upper weathered and fractured zone. These factors may suggest that an active lateral groundwater flushing is more predominant; or else, for some reason, the rate of sulfur oxidation process is slower in the upper weathered zones than those of southwestern Ontario and the Western Plain region.

8.2.2.4 Porewater Analysis From Squeezed Clay Samples

In general, the inorganic chemistry of porewater squeezed from clay samples was similar to those collected from piezometers with variations in concentration strength. This would indicate that the bentonite seals used in piezometer installations did not cause significant contamination of groundwater samples collected from piezometers; and the clay samples did not undergo any aging prior to being squeezed. To prevent sediment aging, clay samples must be maintained at in-situ temperature, sealed from oxygen and squeezed shortly after collection according to Lessard and Mitchell (1985). Sediment aging results in an increase in all major ion porewater concentrations, except for chloride. The application of a maximum pressure of 2.0 MPa did not induce hyperfiltration of any major ion.

Porewater analysis from squeezed clay samples was only performed for the NRC site. Variations in ion concentration between squeezed porewater and groundwater collected from piezometers were more pronounced in the upper 6.0 m; however, they became more consistent with increasing depth. The variation in the upper 6.0 m may be because squeezed core samples probably represented the clay matrix porewater chemistry, while the samples collected from piezometers represented groundwater chemistry stored in the fracture network.

8.3 Field Modelling of Solute Transport

8.3.1 Major Ions

Two different models were used in field simulation of major ion profiles: an advective and diffusive model and a fracture flow model. Both models assumed that a constant source was generated throughout the Holocene Period and that no other geochemical evolution other than those currently observed in the Leda clay deposits have occurred. As before, the Renfrew site was the exception. Field simulations were limited by the fact that no exact initial solute concentrations were known and that solute concentration profiles were limited to the upper 12.0 m of the deposit.

The fracture model used in field simulations attempted to represent a complex series of fractures with different spacings, orientations, aperture sizes, and with a set of parallel fractures with a constant aperture. It was assumed that this fracture model would behave similar to field fracture flow and solute migration.

Therefore, the fracture flow model should be considered an approximation to the hydraulic characteristics of a fracture network that can exist in the Leda clay deposits. For these reasons, several different profiles were generated using different parameters relative to field observations of fracture spacings, aperture and flow velocity. The various simulations of fracture geometry are realistic and consistent with field observations.

A limitation of the fracture flow model is the assumption that the fracture network was created just after glacial retreat, about 10,000 years ago, while in reality the fracture network was probably created over a longer time period.

The best fits for the advective and diffusive profiles were obtained by using an average groundwater velocity of zero at all four sites with the exception of two simulations at Renfrew. At Renfrew, a theoretical match to the chloride and sodium profiles required the incorporation of a groundwater velocity of 15 cm/a and 25 cm/a, respectively.

The existence of no advective term during field simulation may indicate that a threshold gradient is operative in Leda clays. From laboratory studies on clayey deposits, Law and Li (1981) found that hydraulic gradients greater than 0.29 were sometimes necessary to induce advective flow. However, the magnitude of this threshold gradient will vary with each clay deposit (Desaulniers, 1986). The measured hydraulic gradients were less than 0.29 at all sites with the exception of Casselman (0.40).

Theoretical sulfate profiles were generated using an apparent diffusion coefficient. The relatively high retardation factor

for SO_4^{2-} evaluated from this profile could be attributed to sulfate reduction by sulfate reducing bacteria. The Ogata (1970) and Sudicky and Frind (1982) analytical solutions may not be valid since these reduction may not be uniform and constant with respect to time. For this reason theoretical sulfate profiles should be judged with caution.

The shape and the depth of solute penetration produced by the diffusive model at NRC were to some degree representative of the actual concentration distribution, even though, not all data points fell within a reasonable range for a good theoretical fit. Also, these diffusive profiles were only possible if no downward advective flow occurred in the highly active zone. This conclusion is not supported by the estimation of the depth of the active zone from field data.

The fracture flow profiles generated for calcium at NRC were representative of the actual concentration distribution. However, the predicted penetration depths were over estimated. By comparing the two different models, it was established that the transition zone at NRC extends to at least 9 m depth. This transition zone behaves more as a fractured porous medium with some continuous fractures throughout the entire 9 m.

Sulfate reduction was the probable problem in producing a proper theoretical fractured flow profile for sulfate for the NRC site.

Both theoretical profiles generated by the fracture flow model for calcium at Fallowfield were representative of actual field data. The diffusive model gave a better fit in terms of shape and penetration depth. However, field concentration distribution in terms of relative concentration was highly

subjective, since initial ion concentrations were assumed to be close to zero.

Based upon field simulations, the transition zone at Fallowfield extends to at least 7 m. It seems to be controlled predominantly by downward diffusion. The actual concentration distribution is the possible result of a combination of both downward and upward diffusive process (Torrance, 1988; Desaulniers and Cherry, 1989).

The Renfrew field data were assessed using the two analytical models. Only the fractured porous medium model accurately simulated actual field data. This leads to the conclusion that the upper section of the clay deposit at Renfrew is fractured throughout its entire 12.0 m thickness. The transition zone at Renfrew may extend well beyond 12.0 m.

The Casselman field data were assessed by using the two analytical models. The results indicate that the fracture flow model better simulated field data in the upper 6.4 m. While the diffusive model accurately predicted the penetration depth. Based upon the above results, the transition zone at Casselman extends to at least 6.4 metres and is influenced by fracture flow.

The field modelling results can be extrapolated to assess the potential impact of contamination migration through Leda clays on the underlying aquifer.

Migration of contaminants through unfractured, massive clay deposits is controlled by simple downward diffusion, so long as threshold gradient is in effect. If these unfractured clay deposits are relatively thick, greater than 10 m, it would

take several thousand years for reactive contaminants, such as calcium and potassium, to enter the underlying aquifer. However, the presence of strong advective groundwater flow coupled with non-reactive contaminants, such as chloride, would consistently reduce breakthrough time to the underlying aquifer. Therefore, the retention capabilities of the clay deposit would be greatly reduced.

The results of solute migration through a fractured porous medium indicated that for highly reactive contaminants, such as calcium, the penetration depth can be small, even over a period of 10,000 years. However, contaminant movement predictions for a fractured porous medium are highly subjective since they are strongly influenced by the fracture network geometry and aperture size. As seen from field simulations, several combinations of fracture spacing, aperture and fracture flow velocity can produce theoretical curves which closely match the observed field data. Therefore, contaminant migration through a fractured porous media can only be quantified.

Fracture flow profiles demonstrated the high attenuation capability of the diffusive process into the surrounding Leda clay matrix. The fracture analytical model demonstrated that theoretical profiles were particularly sensitive to small changes in fracture apertures (see Figure 6.23). The reduction of aperture size greatly reduces the amount of solute or contaminant transported by the fracture. As the fracture aperture is decreased, a greater portion of solute in the fracture diffuses into the clay matrix which results in a decrease in chemical or contaminant flux transported by the fracture.

It was also demonstrated that fracture spacing plays a significant role in the transport of solute and contaminants in a porous fractured medium. Under a given gradient, fracture spacing and aperture size control the fracture flow velocity. These parameters significantly effect the ratio of contaminant concentration and total mass flux between fracture and matrix.

The effectiveness of fractured Leda clay to attenuate contaminants is significantly reduced when dealing with low and non-reactive solutes, as seen from the Renfrew simulations for sodium and chloride. After only 30 years, Na^+ and Cl^- have migrated well beyond a depth of 12.0 metres (Figure 6.26 and 6.27).

Again, chloride and sodium theoretical profiles demonstrated the important role diffusion plays between the fracture and the adjacent porous matrix in the solute transport process, even at a fracture flow velocity of 5.9 m/d.

Both analytical models assumed that all weathering products have migrated downward. However, as seen from the geochemical analysis, strong lateral flushing may have occurred. This would result in underestimating the environmental impact of contaminants on the underlying aquifer and an erroneous estimation of transport properties of solutes.

8.4.3.2 Tritium

The tritium concentration profiles were also analyzed using the two different models. Absolute values as predicted by both analytical models were subject to error due to approximation, which was required in order to satisfy the

analytical solution. However, the necessary parameters were underestimated to produce conservative theoretical profiles. Generated theoretical tritium profiles were a very useful tool in estimating the depth to which fractures are open and active.

The theoretical profile generated using an advective and diffusive model at NRC fitted the observed field data reasonably well (Figure 6.14). This theoretical profile was produced by using a downward groundwater velocity of 0.30 m/year in the upper 4.40 m coupled with an effective diffusion coefficient of 4.8×10^{-6} cm^2/s. Below 4.40 metres, a threshold gradient was assume to be in effect which resulted in a zero groundwater velocity. An effective diffusion coefficient of 4.8×10^{-6} cm^2/s gave the best fit. The goodness of fit for this analytical model may indicate that strong lateral flushing of tritium has occurred at this site since the upper 4.40 m is highly fractured and hydraulically active. Therefore, tritiated rain waters may be transported more laterally in the upper active zone than directly downwards.

A combination of two theoretical fracture flow profiles gave the best simulation for tritium at NRC. This composite profile indicates that fractures may penetrate to a depth of 12.0 metres. They also indicate the presence of highly active zone in the upper 3.5 m, and that this hydraulic activity decreases with depth due to the increase in fracture spacing and/or a decrease in fracture aperture due to increasing confining stresses.

The tritium data at the Fallowfield site indicated a sharp decrease in concentration below 4.0 m. Comparison between

both theoretical models show that transport below a depth of 3.2 m can be either downward diffusion or by fracture flow. The calculated effective diffusion coefficient ranged from 4.8 x 10^{-6} cm^2/s to 6.4 x 10^{-6} cm^2/s. These values were similar to those reported by Desaulniers (1986) and Yanful and Quigley (1990).

The diffusive theoretical curves were generated assuming an input function of atmospheric tritium concentration which varied with time. This input function may not be totally valid for the interface at the bottom of the active groundwater zone. Therefore, theoretical diffusive profiles may not be a true representation of actual field conditions. The combination of two theoretical profiles generated by fracture analysis indicate that fractures may penetrate to a depth of 7.5 m and that a highly active zone existed in the upper 3.2 m.

Simulation of tritium transport profiles at the Renfrew site, considering the silty clay deposit as a massive unfractured porous medium, did not come close in matching the observed field data, either in shape or in penetration depth. But, the fracture theoretical profile gave a reasonable good fit (Figure 6.33). This figure indicates that the clay deposit may be continuously fractured beyond a depth of 12 metres. Also, a very high hydraulic active groundwater zone exists in the upper 6 m.

For the Casselman site, both analytical models gave a good fit to the actual concentration distribution. Comparison of Casselman field data to the first analytical model shows that transport below a depth of 4 metres can be dominated by an advective and diffusive transport. The calculated groundwater

velocity and effective diffusion coefficient were 3.5 cm/a and 4.8×10^{-6} cm^2/s, respectively. Also, simple diffusion gave a good fit, in this case a D_e value of 14.40×10^{-6} cm^2/s was evaluated.

The fracture flow analytical model provided evidence that the upper 12 m could be considered fractured at Casselman. The theoretical profiles shown on Figure 6.34, demonstrate that a highly active zone exist in the upper 4.4 m. Below this depth, fractures become more widely spaced and decrease in aperture size.

Predictions based upon tritium theoretical profiles should be used with caution due to the lack of field data points below the observed active zone. Also, the tritium profile for a fracture network may not show the maximum depth of the transition zone or hydraulically active fractures due to the high storage capacity of the Leda clay matrix and the relatively short half-life of tritium.

It was demonstrated again, that the diffusive process between fractures and the adjacent matrix plays an important role in the solute transport process in a fractured porous medium.

8.4 Predictions

The contaminant transport process was evaluated through five hypothetical cases. Lateral flushing was not simulated. The first case for contaminant migration was evaluated for massive, intact Leda clay in which calcium and magnesium were eluted from the clay exchange sites. This first hypothetical case predicts that a clay barrier with a minimum thickness of

10 metres would result in a zero contaminant flux in the underlying aquifer after 100 years.

Cases 2 to 4 assessed contaminant transport in a network of idealized vertical fractures in a Leda clay deposit. These vertical fractures extended from the base of the landfill to the underlying aquifer in a 20 metre thick clayey aquitard. However, no field evidence was found which showed that eastern Ontario Leda clays were fractured beyond a depth of 12.0 m.

Case 5 assessed contaminant impact by a single vertical fracture which connected the landfill leachate to the underlying aquifer in a 10 m thick Leda clay deposit.

The sensitivity analysis showed that considerable degradation of water quality in the underlying aquifer would occur with in a few decades to several hundreds of years. These cases are clear evidence that fractures are the controlling pathways for contaminant migration from the leachate source to the underlying aquifer. The sensitivity analysis also demonstrated that deep, widely spaced vertical fractures which fully penetrate the clayey aquitard are important features when assessing the environmental impact of a landfill site. However, these widely spaced fractures will be very difficult to detect or to identify during conventional field investigations. These could still be undetectable even using the most up-to-date investigative techniques.

One of the major implications of the results of these hypothetical prediction cases is that the clay deposits of less than 20 m thick may not provide the necessary protection against hazardous materials entering the regional groundwater

system. Even one fully penetrating vertical fracture may limit the suitability of a site.

The analytical models assumed a constant source concentration, but in actual fact, dilution of contaminants species in a landfill would occur during a 100 year life span due to removal by the leachate collection system and contaminant migration into the clay barrier (conservation of mass) (Rowe, 1990). Also, the hypothetical cases presented here represent some of the many permutations possible among fracture spacings, apertures and advective velocities .

CHAPTER 9

CONCLUSIONS

The results of this research showed that the physical and geochemical properties of Leda clay encountered at four sites in eastern Ontario within the Western Champlain Sea basin vary for each location. From test pit observations, physical and geochemical hydrogeology analyses showed that the upper section of Leda clay deposits in eastern Ontario are weathered, fractured and are relatively pervious.

Slug tests analyzed using Hvorslev method indicated that the field hydraulic conductivity values in the upper sections are several orders of magnitude higher than the typical hydraulic conductivity values found at depth. In the upper fractured zone, hydraulic conductivity values range from 1.85×10^{-8} to 2.05×10^{-5} m/s. The hydraulic conductivity encountered at the deepest installed piezometers fall within a small range, between 8.2×10^{-10} and 1.4×10^{-9} m/s.

Based upon the NRC test pit observations, fracture spacing steadily increases with depth, ranging from one fracture every 4 cm at 1.5 m depth to one fracture every 40 cm at 3.5 m. Fracture apertures also decrease with depth. Using NRC results, the calculated fracture apertures ranged from 10 to 50 μm. The calculated effective fractured porosities ranged from 1.02×10^{-4} to 6.22×10^{-4}.

Groundwater velocities through eastern Ontario Leda clay deposits are dependent on whether or not the flow occurs

through the fractures. Fracture flow is prevalent in the upper near surface zone where groundwater velocities range from 0.10 to 4.8 m/d. Where intergranular flow occurs, velocities lie between 1.11×10^{-6} m/d (0.04 cm/a) and 1.11×10^{-4} m/d (4.04 cm/a). Groundwater flow through the active zone was measured at rates of .07 to .22 m^3/h entering the two excavated test pits.

Hydrogeological methods of investigation such as water level fluctuations, hydraulic head, hydraulic conductivity, major ions and tritium profiles with depth are useful tools in identifying the depth to which the clay deposit is hydraulically highly active. These methods alone are not sufficiently accurate to determine the maximum depth to which open fractures and secondary featured provide pathways for groundwater flow in Leda clay. Mathematical models are necessary to establish this maximum depth.

Leda clay deposits can be divided into three hydrogeological and geochemical zones. They are an upper active zone, "inactive" zone and a transition zone. The upper active zone contains a well interconnected flow network of fractures, pores, roots, root holes, sand lenses etc. and displays the highest level of hydraulic activity. The "inactive" zone consist of deep clays which may contain relatively old groundwaters and where the transport mode is considered to be primarily intergranular advection and diffusion. The transition zone separates the upper active and "inactive" zones. It is characterized by flow in fractures which are more widely spaced and have smaller apertures then those in the upper active zone and the fracture network may be continuous and open. The identification of these three zones should be based on several investigative techniques.

The depth of these hydrogeological zones are site specific and are quite variable between sites. At NRC, the highly active zone extends to 4.4 metres, at Fallowfield to 3.2 metres, at Casselman to 4.4 metres and Renfrew to 6.0 metres in depth. At these sites, the transition zone extends to at least 9.0 m at NRC, to 7.5 m at Fallowfield, to 10.0 m at Casselman and to below 12.0 m at Renfrew. The hydrogeological zones are influenced by the local geological features and depositional modes.

An analysis of five hypothetical cases showed that landfills in fractured Leda clay deposits of less than 20 metres thick may not protect the surrounding environment from toxic contamination; especially, if a strong downward hydraulic gradient is present at the site. The landfill site should be designed with synthetic liner and a leachate collection system for clay deposits of less than 20 thick such as to provide sufficient protection to an important regional groundwater supply.

From laboratory experiments, effective diffusion coefficients for Na^+, K^+, Mg^{2+}, Ca^{2+}, and Cl^- were evaluated and range from 3.4 to 6.5 x 10^{-6} cm^2/s, 6.0 to 7.5 x 10^{-6} cm^2/s, 3.8 to 4.6 x 10^{-6} cm^2/s, 5.8 to 6.25 x 10^{-6} cm^2/s and 6.5 to 7.0 x 10^{-6} cm^2/s, respectively. Retardation factors for Na^+, K^+, Mg^{2+}, and Ca^{2+} range from 1.5 to 3.6, 17 to 48, 4.8 to 12.4, and 17 to 33, respectively. Based upon calculated retardation factors, chloride is the most mobile ion in solution while calcium and potassium are highly attenuated by Leda clay. The Renfrew site showed the highest retention capability since it has the highest CEC value.

Since the matrix diffusion process may cause tritium level to decline below the detection limit well above the depth to which fractures are open and active, the use of tritium values to infer maximum depth of hydraulically-active fractures may not be scientifically accurate.

Several different investigative techniques were necessary to evaluate the hydraulic, geochemical and transport properties of Leda clay deposits in Eastern Ontario.

The lack of gypsum crystals in fractures, relatively low sulfate concentrations and low sodium exchange capacity in the upper active zone may indicate that lateral groundwater flushing in this zone has been extensive. This aspect requires further evaluation.

RECOMMENDATIONS FOR FUTURE RESEARCH

Additional research is required to better define and understand the transition zone. Such an investigation should include a higher degree of instrumentation below the active zone combined with more in-depth analysis into the spatial distribution of natural solutes and environmental isotopes at closer intervals.

This study has indicated that strong lateral flushing occurred in the upper active zone. Horizontal flow properties of fractured Leda clays can be an important feature when dealing with contamination migration.

The physical, geochemical and hydrogeological properties of Leda clay below 12.0 m at each of the four sites used in this thesis require investigation.

There appears to be a need to develop less restrictive mathematical models, and investigative techniques which make greater use of inclined boreholes.

REFERENCES

REFERENCES

ABBOTT, D., 1987. The origin of sulfate and the isotope geochemistry of sulfate-rich shallow groundwater in the St. Clair clay plain, southwestern Ontario. M.Sc. Thesis, Department of Earth Science, University of Waterloo, Waterloo, Ontario.

ADAMS, J.I., 1969. Effect of groundwater levels on stress history of the St. Clair till deposit: Discussion. Canadian Geotechnical Journal, Vol. 7, pp. 190-193.

ADAMSON, A.W., 1963. Physical chemistry of surfaces. Wiley Interscience, John Wiley and Sons, Inc, New York, 747 p.

ANDERSON, M. A., and RUBIN, A. J., 1981. Adsorption of inorganics at solid-liquid interface. Ann Arbor Science Plublishers Inc., Michigan, 357 p.

BARONE, F.S., MUCKLOW, J.P., QUIGLEY, R.M., and ROWE, R.K., 1991. Contaminant transport by diffusion below an industrial landfill site. In: First Canadian Conference on Environmental Geotechnics. The Canadian Geotechnical Society, Montreal, Quebec.

BARONE, F.S., YANFUL, E.K., QUIGLEY, R.M., and ROWE, R.K., 1989. Effect of multiple contaminant migration on diffusion and adsorption of some domestic waste contaminants in a natural clayey soil. Canadian Geotechnical Journal, Vol. 26, pp. 189-198.

BEAR, J., 1972. Dynamics of fluids in porous media. American Elsevier, New York, N.Y.

BELANGER, J.R., and HARRISON, J.E, 1980. Region geoscience information: Ottawa-Hull. Geological Survey Paper 77-11. The Geological Survey of Canada.

BERKOWITZ, B., BEAR, J., and BRAESTER, C., 1988. Continuum models for contaminant transport in fractured porous formations. Water Resources Research, Vol. 24, No. 8, pp. 1225-1236.

BERNER, R.A., 1971. Principles of chemical sedimentology. McGraw-Hill, Inc., New York, N.Y.

BOAST, C.W., and KIRKHAM, D., 1971. Auger hole seepage theory. Soil Science Society of America Proceedings, Division S-1, Soil Physics, Vol. 35, No. 3, pp. 365-373.

BOHN, H.L., MCNEAL, B.L., and O'CONNOR, G.A., 1971. Soil chemistry. John Wiley and Sons, New York, 329 p.

BOUWER, H., and RICE, R.C., 1976. A slug test for determining hydraulic conductivity of unconfined aquifers with completely or partially penetrating wells. Water Resources Research, Vol. 12, pp. 423-428.

BOUWER, H., 1989. The Bouwer and Rice slug test: an update. Ground Water, Vol. 27, No. 3, pp. 304-309.

BROWN, R.M., 1961. Hydrology of tritium in the Ottawa Valley. Geochimica Cosmochmica Acta, Vol. 21, pp. 199-216.

BROWN, S.R., 1987. Fluid flow through rock joints: The effects of surface roughness. Journal of Geophysical Research, Vol. 92, No. B2, pp. 1337-1347.

BRUCE, J.R.G., 1987. Investigation of nature of the fractured till at the Lampton Generating Station. M.Sc. Project, Department of Earth Sciences, University of Waterloo, Waterloo, Ontario.

CHAPUIS, R.P., 1989. Shape factors for permeability tests in boreholes and piezometers. Ground Water, Vol. 27, No. 5, pp. 647-654.

CHARRON, J.E., 1978. Hydrochemical study of groundwater flow in the interstream area between the Ottawa and St. Lawrence Rivers. Inland Water Directorate, Water Resources Branch, Ottawa, Canada, Scientific Series No. 76.

CHERRY, J.A., 1972. Geochemical process in shallow groundwater flow systems in five ares in southern Manitoba, Canada. Proceedings, XXIV International Geological Congress. Montreal, Section 11, pp. 208-221.

CHERRY, J. A., 1976. Hydrogeologic conditions at the proposed Northeast Park Sanitary Landfill Site. Unpublished report prepared for: The Waterworks, Waste, and Disposal Division, Winnipeg, Manitoba, pp. 1-40.

CHERRY, J.A., 1989. Hydrogeologic contaminant behaviour in fractured and unfractured clayey deposits in Canada. International Symposium on Contaminant Transport in Groundwater, April 4-6, Germany.

CHERRY, J.A., BESWICK, B.T., CLISTER, W.E., and LUTCHMAN, M., 1971. Flow patterns and hydrochemistry of two shallow groundwater regimes in the Lake Agassiz basin, southern Manitoba. In: Geoscience Studies in Manitoba. A.E. Turnock (Editor), Geological Association of Canada Special Paper No.9, pp. 321-332.

CHERRY, J.A., GRISAK, G.E., and CLISTER, W.E., 1973. Hydrogeologic studies of a subsurface radioactive waste management site in west-central Canada. Proceedings International Symposium on Underground Waste Management and Artificial Recharge, AAPG-USGS, New Orleans, J. Braunstein (Editor), 1, pp. 436-467.

CHHABRA, R., PLEYSIER, J., and CREMER, A., 1975. Cation exchange capacity and exchangeable cations in soil: A new method. Proceedings to the International Clay Conference, pp. 439-449.

COMANS, R.N., 1987. Adsorption, desorption and isotopic exchange of cadmium on illite: evidence for complete reversibility. Water Resources Research Vol. 12, No. 12, pp. 15573-1576.

COOPER, H.H., BREDEHOEFT, J.D., and PAPADOPULOS, I.S., 1967. Response of a finite-diameter well to an instantaneous change of water. Water Resources Research, Vol. 3, No. 1, pp. 263-269.

CRAWFORD, C.B., and EDEN, W.J., 1965. A comparison of laboratory results with in-situ properties of Leda clay. Proceedings, 6th International Conference on Soil Mechanics and Foundation Engineering, Montreal, Quebec, 1, pp. 31-35.

CRONIN, T.M., 1977. Late-Wisconsin marine environments of the Champlain valley (New York, Quebec). Quaternary Research, Vol. 7, pp. 238-253.

CROOKS, V.E., and QUIGLEY, R.M., 1984. Saline leachate migration through clay: A comparative laboratory and field investigation. Canadian Geotechnical Journal, Vol. 21, pp. 349-362.

D'ATOUS, A.Y., RULAND, W.W., BRUCE, J.R.G., CHERRY, J.A., and GILLHAM, R.W., 1989. Fracture effects in the shallow groundwater zone in weathered Sarnia area clay. Canadian Geotechnical Journal, Vol. 26, No. 1, pp. 43-56.

DAVIS, G.B., and JOHNSTON, C.D., 1984. Comment on "Contaminant transport in fractured porous media: Analytical solutions for a system of parallel fractures" by E.A. Sudicky and E.O. Frind. Water Resources Research, Vol. 20, No. 9, pp. 1321-1322.

DAY, M.J., 1977. Analysis of movement and hydrochemistry of groundwater in fractured clay and till deposits of the Winnipeg area, Manitoba. M.Sc. Thesis, Department of Earth Sciences, University of Waterloo, Waterloo, Ontario.

DESAULNIERS, D.E., 1980. Origin, age and movement of pore water in argillaceous sites in southwestern Ontario. M.Sc. Thesis, Department of Earth Sciences, University of Waterloo, Waterloo, Ontario.

DESAULNIERS, D.E., CHERRY, J.A., and FRITZ, P., 1981. Origin, age and movement of pore water in argillaceous Quaternary deposits at four sites in Southwestern Ontario. Journal of Hydrology, Vol. 50, pp. 231-257.

DESAULNIERS, D.E., 1986. Groundwater origin, geochemistry and solute transport in three major glacial clay plains of East-Central North America. Ph.D. Thesis, Department of Earth Science, University of Waterloo, Waterloo, Ontario.

DESAULNIERS, D.E. and CHERRY, J.A., 1989. Origin and movement of groundwater and major ions in a thick deposit of Champlain Sea clay near Montreal. Canadian Geotechnical Journal, vol. 26, pp. 80-89.

DREVER, J.I., 1982. The geochemistry of natural waters. Prentice-Hall, Inc., Englewood Cliffs, New York.

EDEN, W.J., and CRAWFORD, C.B., 1957. Geotechnical properties of Leda clay in the Ottawa area. In: Poceedings of the 4th International Conference on Soil Mechanics and Foundation Engineering, Vol 1, pp. 22-27.

EDEN, W.J., and LAW, K.T., 1980. Comparison of undrained shear strength results obtained by different test methods in soft clays. Canadian Geotechnical Journal, Vol. 17, No. 3, pp. 369-381.

ERNST, L.F., 1950. A new formula for the calculation of the permeability factor with the auger hole method. Agricultural Experiment Station T.N.O., Groningen, The Netherlands. (Translated from the Dutch by Herman Bouwer, Cornell University, Ithaca, N.Y. 1955.)

FETTER, C.W., 1988. Applied hydrogeology. Second Edition. Merrill Publishing Company, Columbus, Ohio, 592 p.

FITZGERALD, W.D., JANICKI, D., and STORRINSON, D.J., 1979. Sarnia-Brights Grove area, southern Ontario, Ontario Geological Survey Preliminary map, P-2222.

FOSTER, S.S.D., 1975. The chalk groundwater tritium anomaly - a possible explanation. Journal of Hydrology, vol. 25, pp. 159-165.

FRANSHAM, P.B., and GADD, N.R., 1977. Geological and geomorphological controls of landslides in Ottawa Valley, Ontario. Canadian Geotechnical Journal, Vol. 14, pp. 531-539.

FREEZE, R.A., 1969. Hydrology of the Good Spirit Lake Drainage basin, Saskatchewan, A Preliminary Analysis. Inland Waters Branch, Environment Canada, Technical Bulletin, No. 14, pp. 1-36.

FREEZE, R.A. and CHERRY, J.A., 1979. Groundwater. Prentice-Hall, Englewood Cliffs, New Jersey.

FULLERTON, D.S., 1980. Preliminary correlations of Post-Erie interstadial events. (16,000-10,000 radio carbon years before present), Central and eastern Great Lakes region and Hudson, Champlain and St. Lawrence Lowlands, United States and Canada. United States Geological Survey, Professional Paper 1089, 2 charts, 52 p.

GADD, N.R., 1962. Surficial geology of the Ottawa map area, Ontario and Quebec. Geological Survey of Canada, Paper 62-16.

GADD, N.R., 1975. Geology of Leda clay. Mass Wasting, E. Yatsu et al. (Editors), Geographical Publication No. 4, University of Guelph, Guelph, Ontario. Geo Abstracts Limited. University of East Anglia, Norwhich England, pp. 137-152.

GADD, N.R., 1986. Lithofacies of Leda clay in the Ottawa Basin of the Champlain Sea. Geological Survey of Canada, Paper 85-21.

GANGI, A.F., 1978. Variation of whole and fractured porous rock permeability with confining pressure. International Journal of Rock Mechanics and Mining Science Geomechanics Abstracts, Vol. 15, pp. 249-257.

GIBB, J., BARCELONA, M., RITCHEY, J., and LAFAIVRE, M., 1985. Effective porosity of geologic materials. Proceedings, 11th Annual Research Symposium Land Disposal of Hazardous Waste. U.S. Environmental Protection Agency Report No. EPA/600/9-85/013, pp. 190-197.

GILLILAND, J. A., 1965. Geological and groundwater investigation for the Portage Diversion, Province of Manitoba. Department of Mines and Natural Resources, Water Control and Conservation Branch.

GILLHAM, R.W., and CHERRY, J.A., 1982. Contaminant migration in saturated unconsolidated geologic deposits. Geophysical Society of America, Special Paper 189, pp. 31-62.

GILLHAM, R.W., ROBIN, M.L.J., DYTYNYSHYN, D.J., and JOHNSTON, H.M., 1984. Diffusion of nonreactive and reactive solutes through fine-grained barrier materials. Canadian Geotechnical Journal, Vol. 21, pp. 541-550.

GILLOT, J., 1971. Mineralogy of Leda clay. Canadian Mineralogist, Vol. 10, pp. 767-811.

GOODALL, D.C., and QUIGLEY, R.M., 1977. Pollutant migration from two sanitary landfill sites near Sarnia, Ontario. Canadian Geotechnical Journal, Vol. 14, pp. 223-236.

GORDON, M.J., 1986. Dependence of effective porosity on fracture continuity in fractured media. Ground Water, Vol. 24, No. 4, pp. 446-452.

GRAVENOR, C.P., and STUPAVSKY, M., 1977. Magnetic, physical and lithologic properties and age of till exposed along the east cost of Lake Huron, Ontario. Canadian Journal of Earth Sciences, Vol. 13, pp. 1655-1666.

GRISAK, G.E., 1975. The fracture porosity of glacial till. Canadian Journal of Earth Sciences, Vol. 12, pp. 513-515.

GRISAK, G.E., and CHERRY, J.A., 1975. Hydrologic characteristics and response of fractured till and clay confining a shallow aquifer. Canadian Geotechnical Journal, Vol. 12, pp. 23-43.

GRISAK, G.E., and CHERRY, J.A., VONHOF, J.A., and BLUMELE, J.P., 1976. Hydrogeologic and hydrochemical properties of fractured till in the interior plains region. In: Glacial Till, Proceedings of Symposium. Ottawa 1975, R.F. Legget (Editor), Royal Society of Canada, Special Publication No. 12, pp. 304-335.

GRISAK, G.E., and PICKENS, J.F., 1980. Solute transport through fractured media: 1. The effects of matrix diffusion. Water Resources Research, Vol. 16, pp. 719-730.

GRISAK, G.E., and PICKENS, J.F., 1981. An analytical solution for solute transport through fractured media with matrix diffusion. Journal of Hydrology, Vol. 52, pp. 47-57.

GRISAK, G.E., and PICKENS, J.F., and CHERRY, J.A., 1980. Solute transport through fractured media: 2. Column study of fractured till. Water Resources Research, Vol. 16, pp. 731-739.

HANNA, T.H., 1966. Engineering properties of glacial-lake clays near Sarnia, Ontario. Ontario Hydro Research Quarterly, 3rd Quarter, pp. 1-12.

HARDING, D.W.R., 1986. An investigation of the effective stress-permeability relationship for a fracture clay till near Sarnia, Ontario. M.Sc. Thesis, Department of Earth Sciences, University of Waterloo, Waterloo, Ontario.

HARR, M.E., 1962. Groundwater and Seepage. McGraw-Hill, New York, 315 p.

HARRISON, E.A., SUDICKY, E.A., and CHERRY, J.A., 1992. Numerical analysis of solute migration through fractured clayey deposits into underlying aquifers. Water Resources Research, Vol. 28, No. 2, pp. 515-526.

HENDRY, M.J., 1982. Hydraulic conductivity of a glacial till in Alberta. Ground Water, Vol. 20, pp. 162-169.

HENDRY, M.J., CHERRY, J.A., and WALLICK, E.I., 1986. Origin of groundwater sulfate in a fractured till in an area of Southern Alberta, Canada. Water Resources Research, Vol. 22, pp. 45-61.

HENDRY, M.J., 1988. Hydrogeology of clay till in a Prairie Region of Canada. Ground Water, Vol. 26, pp. 607-614.

HENDRY, M.J., KROUSE, H.R., and SHAKUR, M.A., 1989. Interpretation of oxygen and sulfur isotopes from dissolved sulfates in tills of southern Alberta, Canada. Water Resources Research, Vol. 25, No. 3, pp. 567-572.

HERZOG, B.L., GRIFFIN, R.A., STOHR, C.J., FOLLMER, L.R., MORSE, W.J., and SU, W.J., 1989. Investigation of failure mechanisms and migration of organic chemicals at Wilsonville, Illinois. Ground Water Monitoring Revue, Vol. 9, pp. 82-89.

HINGSTON, F.J., ATKINSON, R.J., POSNER, A.M., and QUIRK, J.P., 1968. Specific adsorption of anions on goethite. Nature, Vol. 215, pp. 1459-1461.

HOLTZ, R.D., and KOVACS, W.D., 1981. An introduction to geotechnical engineering. Prentice-Hall Inc., New York, 780p.

HORBERG, L., 1952. Pleistocene drift sheets in the Lethbridge region, Alberta, Canada. Journal of Geology, Vol. 60, pp. 303-329.

HORFORD, I.C.R., 1978. Soil adsorption phenomena and the Langmuir Equation. Soil Science Society America Proceedings, Vol. 42, pp, 986-987.

HUYAKORN, P., LESTER, B., and MERCER, J., 1983. An efficient finite element technique for modelling transport in fractured porous media. 1. Single species transport. Water Resources Research, Vol. 19, No. 3, pp. 841-854.

HVORSLEV, M.J., 1951. Time lag and soil permeability in groundwater observations. Waterways Experiment Station, Bulletin No. 36, Corps of Engineers, U.S. Army, Vicksburg, Mississippi.

JARRET, P.M., and EDEN, M.J., 1970. Groundwater flow in Eastern Ottawa. Canadian Geotechnical Journal, Vol. 7, pp. 326-333.

JOHNSON, R.L., CHERRY, J.A., and PANKOW, J.F., 1989. Diffusive contaminant transport in natural clay: A field example and implications for clay-lined waste disposal sites. Environmental Science and Technology, Vol. 23, pp. 340-349.

JOST, W., 1960. Diffusion in solids, liquids, and gases. Academic Press, New York, N.Y.

KALIL, E.K., and GOLDHADER, M., 1973. A sediment squeezer for removal of pore waters without air contact. Journal of Sedimentary Petrology, Vol. 43, pp. 553-557

KARASKAKI, K., LONG, J.C.S., and WITHERSPOON, P.A., 1988. Analytical models of slug tests. Water Resources, Research. Vol. 24, pp. 115-126.

KARICKHOFF, S.W., BROWN, D.S., and SCOTT, T.A., 1979. Sorption of hydrophobic pollutants on natural sediments. Water Resources Research, Vol. 13, pp. 421-428.

KARROW, P.F., 1972. The Champlain SEa and its sediments. In Soils in Canada, Geological, Redological and Engineering Studies. R.F. Legget (Editor), Royal Society of Canada Special Publication No. 3, pp. 97-107.

KELLER, C.K., 1985. Hydrogeology of fractured clayey till confining a shallow san aquifer near Saskatoon, Saskatchewan. M.Sc. Thesis, Department of Earth Sciences, University of Waterloo, Waterloo, Ontario.

KELLER, C.K., VAN DER KAMP, G., and CHERRY, J.A., 1986. Fracture permeability and groundwater flow in clayey till near Saskatoon, Saskatchewan. Canadian Geotechnical Journal, Vol. 23, pp. 229-240.

KELLER, C.K., 1987. Controls on patterns of groundwater flow and major-ion occurrence in two deposits of clayey till near Saskatoon, Saskatchewan. Ph.D. Thesis, Department of Earth Sciences, University of Waterloo, Waterloo, Ontario.

KELLER, C.K., VAN DER KAMP, G., and CHERRY, J.A., 1988. Hydrogeology of two Saskatchewan tills: 1. Fractures, bulk permeability, and spatial variability of downward flow. Journal of Hydrology, Vol. 101, pp. 97-121.

KELLER, C.K., VAN DER KAMP, G., and CHERRY, J.A., 1989. A multiscale study of the permeability of a thick clayey till. Water Resources Research, Vol. 25, pp. 2299-2317.

KELLER, C.K., 1991. Hydrogeochemistry of a clayey till 2. Source of CO_2. Water Resources Research, Vol. 27, No. 10, pp. 2555-2564.

KELLER, C.K., VAN DER KAMP, C., and CHERRY, J.A., 1991. Hydrogeochemistry of a clayey till 1. Spatial variability. Water Resources Research, Vol. 27, No. 10, pp. 2543-2554.

KELLEY, W.P., 1948. Cation exchange in soils. American Chemical Society Monograph No. 109. Reinhold, New York, 144p.

KEMBLOWSKI, M.W., and KLEIN, C.L., 1988. An automated numerical evaluation of slug test data. Ground Water, Vol. 26, pp. 435-438.

KEMPER, W.D., MAASLAND, D.E.L., and PORTER, L.K., 1964. Mobility of water adjacent to mineral surfaces. Soil Science society America Proceedings, Vol. 28, pp. 164-167.

KIRKHAM, D., 1965. Seepage of leaching water into drainage ditches of unequal water level heights. Journal of Hydrology, Vol. 3, pp. 207-224.

KONRAD, J.M., and LAW, K.T., 1987. Undrained shear strength from piezocone tests. Canadian Geotechnical Journal, Vol. 24, pp. 392-405.

LAVENTURE, R.S., and WARKENTIN, B.P., 1965. Chemical properties of champlain sea sediments. Canadian Journal of Earth Sciences, Vol. 2, pp. 299-308.

LAW, K.T., and LEE, C.F., 1981. Initial gradient in a dense glacial till. Paper presented at 10th International Conference of Soil Mechanics and Foundation Engineers, Stockholm, June 15-19.

LAFLEUR, J., and LEFEBVRE, G., 1980. Groundwater regime associated with slope stability in the Champlain Sea deposits. Canadian Geotechnical Journal, Vol. 17, pp. 44-53.

LAFLEUR, J., and GIROUX, F., 1983. Permeabilité in situ des argiles superficielles de la mer Champlain. Bulletin de l'association internationale de géologie de l'ingénieur, Paris, No. 26-27, pp. 453-459.

LAFLEUR, J., GIROUX, F., and HUOT, M., 1987. Field permeability of the Champlain Sea crust. Canadian Geotechnical Journal, Vol. 24, pp. 581-589.

LERMAN, A., 1979. Geochemical processes - water and sediment environments. John Wiley and Sons, Inc., New York, N.Y.

LESSARD, G., and MITCHELL, J.K., 1985. The causes and effects of aging in quick clays. Canadian Geotechnical Journal, Vol. 22, pp. 335-346.

LI, Y.H., and GREGORY, S., 1974. Diffusion of ions in sea water and in deep sea sediments. Geochimica et Cosmochimica Acta, Vol. 38, pp. 703-714.

LISSEY, A., 1968. Surficial mapping of groundwater flow systems with application to the Oak River Basin, Manitoba. Ph.D. Thesis, Department of Geological Sciences, University of Saskatchewan, Saskatoon, 141 p.

LOCAT, J., LEFEBVRE, G., and BALLIVY, G., 1984. Mineralogy, chemistry and physical properties interrelationships of some sensitive clays from Eastern Canada. Canadian Geotechical Journal, Vol. 21, pp. 530-540.

LOW, P.F., 1981. Principals of ion diffusion in clays. Chemistry in the soil environment, ASA Special Publication No. 40, American Society for Agronomy, Madison, Wisconsin, pp. 31-45.

MALONE, P.G., and LARSON, R.J., 1983. Scientific basis of hazardous waste immobilization. In: Hazardous and Industrial Solid Waste Testing: Second Symposium, ASTM STP 805, R.A. Conway and W.P. Gulledge (Editors), American Society for Testing and Materials, pp. 168-177.

MALOSZEWSKI, P., and ZUBER, A., 1985. On the theory of tracer experiments in fissured rocks with a porous matrix. Journal of Hydrology, Vol. 79, pp. 333-358.

MANHEIM, F.T., 1966. A hydraulic squeezer for obtaining interstitial water from consolidation and unconsolidated sediments. United States Geological Survey Professional Paper 550-C, pp. 256-261.

MANHEIM, F.T., 1974. Comparative studies on extraction of sediment interstitial waters: Discussion and comment on the current state of interstitial water studies. Clays and Clay Minerals, Vol. 22, pp. 337-343.

MANN, W.B., URTERWEGER, M.P., and COURSEY, B.M., 1982. Comments on the NBS tritiated-water standards and their use. International Journal of Applied Radiation Isotopes, Vol 33, pp. 383-386.

MASS, C.W., MCKAY, L., SIMS, J., SUDICKY, E.A., and UNGER, A., 1990. Hydrogeology of desiccated fractured clays. Abstract, EOS Trans. AGU, Vol. 71, No. 43, pp. 1345.

MELNYK, T.W., 1985. Effects of sorption behaviour on contaminant migration. Report AECL-8390, Atomic Energy of Canada Limited, Whiteshell Nuclear Research Establishment, Pinawa, Manitoba, Canada.

MERMUT, A.R., and ARSHAD, M.A., 1987. Significance of sulfide oxidation in soil salinization in southeastern Saskatchewan, Canada. Soil Sciences Society of America Journal, Vol. 51, pp. 247-251.

MEYBOOM, P., 1966. Unsteady groundwater flow near a willow ring in hummocky moraine. Journal of Hydrology, Vol. 4, pp. 38-62.

MOTT, C.J.B., and NYE, P.H., 1968. Contribution of adsorbed strontium to its self-diffusion in a moisture-saturated soil. Soil Science, Vol. 105, No. 1, pp. 18-23.

NKEDI-KIZZA, P., BIGGAR, J., VAN GENUCHTEN, M., WIERENGA, P., SELIM, H., DAVIDSON, J., and NIELSON, D., 1983. Modelling tritium and chloride-36 transport through an aggregated oxisol. Water Resources Research, Vol. 19, No. 3, pp. 691-700.

OGATA, A., 1970. Theory of dispersion in a granular medium. United States Geological Survey Professional Paper, No. 411(I).

OLSEN, S.R., KEMPER, W.D., and VAN SCHAIK, J.C., 1965. Self-diffusion coefficients of phosphorous in soil measured by transient and steady-state methods. Proceedings, Soil Science Society of America, Vol. 29, No. 2, pp. 154-158.

OVERBEEK, J.T.G., 1952. Electrochemistry of the Double Layer. Colloid Science, Vol. 1, pp. 115-193.

PANDIT, N.S., and MINER, R.F., 1986. Interpretation of slug test data. Ground Water, Vol. 24, pp. 743-749.

PARKER, L.V., JENKINS, T.F., and FOLEY, B.T., 1984. Impact of slow-rate land treatment on ground water quality. United States Environmental Protection Agency, Report EPA 600-2/84-097.

PATTERSON, R.J., FRAPE, S.K., DYKES, L.S., and MCLEOD, R.A., 1978. A coring and squeezing technique for the detailed study of subsurface water chemistry. Canadian Journal of Earth Sciences, Vol. 15, pp. 162-169.

PAYNE, B.R., 1972. Isotope hydrology. Advances in Hydrosciences, Vol. 8, pp. 95-138.

PORTER, L.K., KEMPER, W.D., JACKSON, R.D., and STEWART, B.A., 1960. Chloride diffusion in soils as influenced by moisture content. Soil Science Society America Proceedings, Vol. 24, pp. 400-403.

QUIGLEY, R.M., 1980. Geology, mineralogy, and geochemistry of Canadian soft soils: a geotechnical perspective. Canadian Geotechnical Journal, Vol. 22, pp. 238-241.

QUIGLEY, R.M., and OGUNBADEJO, T.A., 1976. Till geology, mineralogy and geotechnical behaviour, Sarnia, Ontario. In: Glacial Till, R.F. Legget (Editor). The Royal Society of Canada: Ottawa, Canada, Special Publication No. 12, pp. 336-345.

QUIGLEY, R.M., GWYN, Q.H.J., WHITE, O.L., ROWE, R.K., HAYNES, J.E., and BOHDANOWICZ, P.A., 1983. Leda clay from deep boreholes at Hawkesbury, Ontario. Part 1. geology and geotechnique. Canadian Geotechnical Journal, Vol. 20, pp. 288-298.

QUIGLEY, R.M., HAYNES, J.E., BOHDANOWICZ, P.A., and GWYN, Q.H.J., 1985. Geology, geotechnique, mineralogy and geochemistry of Leda clay from deep boreholes, Hawkesbury area, Prescott County. Ontario Geological Survey, Study 29, 128 p.

QUIGLEY, R.M., and ROWE, R.K., 1986. Leachate migration through clay below a domestic waste landfill, Sarnia, Ontario, Canada: chemical interpretation and modelling philosophies. Hazardous and industrial solid waste testing and disposal: Sixth Volume, ASTM STP 933, D. Lorenzen, R.A. Conway, L.P. Jackson, A. Hamza, C.L. Pecket, and W.J. Lacy, (Editors), American Society for Testing and Materials, Philadelphia, pp. 93-103.

QUIGLEY, R.M., YANFUL, E.K., and FERMANDEZ, F. 1987. Ion transfer by diffusion through clayey barriers. Geotechnical practice for waste disposal, Special Publication No 13, R.D. Woods (Editors), ASCE, New York, N.Y., pp. 137-158.

QUIGLEY, R.M., FERNANDEZ, F., and OHIKERE, C., 1989. Clay leachate compatibility study. Hydraulic conductivity of Ottawa/Carleton "Leda" Clay barrier soils permeated with domestic waste leachate. Final report to Ontario Ministry of Environment, Ottawa, Ontario (Project # 299 PL).

RENDER, F.W., 1970. Geohydrology of the metropolitan Winnipeg area as related to groundwater supply and construction. Canadian Geotechnical Journal, Vol. 7, pp. 243-274.

RICHARD, S.H., and GADD, N.R., 1976. Surficial geology, Russell, Ontario. Geological Survey of Canada, Open File 367.

RICHARD, S.H., 1982. Surficial geology, Ottawa, Ontario-Quebec. Geological Survey of Canada, Map 1506A.

RICHARD, S.H., 1982. Surficial geology, Russell, Ontario. Geological Survey of Canada, Map 1507A.

RICHARDS, R.A., SOBANSKI, A.A., and NUMAN, J.P., 1984. Tricil (Sarnia) Limited Township of Moore Waste Disposal site hydrogeologic investigation. Report submitted to Tricil Limited, Hydrology Consultants, Toronto, Ontario, 560 p.

ROBERTS, J.R., CHERRY, J.A., and SCHWARTZ, F.W., 1982. A case study of a chemical spill: polychlorinated biphenyls 1, History distribution and surface translocation. Water Resources Research, Vol. 18, pp. 525-534.

ROBERTSON, W.D., and CHERRY, J.A., 1989. Tritium as an indicator of recharge and dispersion in a groundwater system in Central Ontario. Water Resources Research, Vol. 25, No. 6, pp. 1097-1109.

ROBERTSON, W.D., CHERRY, J.A., and SUDICKY, E.A., 1991. Groundwater contamination from two small septic systems on sand aquifers. Ground Water, Vol. 29, No. 1, pp. 82-92.

ROBINSON, R.A., and STOKES, R.H., 1959. Electrolyte solutions, 2nd Edition, Butterworths Scientific Publications, London, England.

RODRIGUES, C.G., 1988. Late Quaternary invertebrate faunal association and chronology of the Western Champlain Sea Basin. N.R. Gadd (Editor). The Late Quaternary Development of the Champlain Sea Basin. Geological Association of Canada, Special Paper No. 35, pp. 155-176.

RODVANG, S.J., 1987. Geochemistry of the weathered zone of a fractured clayey deposit in southwestern Ontario. M.Sc. Thesis, Department of Earth Sciences, University of Waterloo, Waterloo, Ontario.

ROWE, R.K., 1988. Eleventh Canadian geotechnical colloquium: Contaminant migration through groundwater - the role of modelling in the design of barriers. Canadian Geotechnical Journal, Vol. 25, pp. 778-798.

ROWE, R.K., 1990. Fractured till: Its implications for contaminant impact assessment. In: Proceedings Annual Conference and 1st Biennial Environmental Speciality Conference. Canadian Society For Civil Engineering, Hamilton, Ontario, pp. I-667-688.

ROWE, R.K., and BOOKER, J.R., 1985. 1-D pollutant migration in soils of finite depth. Journal of Geotechnical Engineering, ASCE, Vol. 111, No. 4, pp. 479-499.

ROWE, R.K., and BOOKER, J.R., 1991. Modelling of two-dimensional contaminant migration in a layered and fractured zone beneath landfills. Canadian Geotechnical Journal, Vol. 28, pp. 338-352.

ROWE, R.K., CAERS, C.J., and BARONE, F., 1988. Laboratory determination of diffusion and distribution coefficients of contaminants using undisturbed clayey soil. Canadian Geotechnical Journal, Vol. 25, pp. 108-118.

ROZKOWSKI, A., 1967. The origin of hydrochemical patterns in hummocky moraine. Canadian Journal Earth Sciences, Vol. 4, pp. 1065-1092.

RUDOLPH, D.L., CHERRY, J.A., and FARVOLDEN, R.N., 1991. Groundwater flow and solute transport in fractured lacustrine clay near Mexico City. Water Resources Research, Vol. 27, pp. 2187-2201.

RULAND, W.W., 1988. The depth of fractures in a weathered clayey till in Lampton County, Ontario. M.Sc. Thesis, Department of Earth Sciences, University of Waterloo, Waterloo, Ontario.

RULAND, W.W., CHERRY, J.A., and FEENSTRA, S., 1991. The depth of fractures and active groundwater flow in a clayey till plain in southwestern Ontario. Ground Water, Vol. 29, No. 3, pp. 405-417.

SANFORD, B.V., 1973. Geology of the Toronto-Windsor area, Ontario. Geological map.

SCHRAUF, T.W., and EVANS, D.D., 1986. Laboratory studies of gas flow through a single natural fracture. Water Resources Research, Vol. 22, No. 7, pp. 1038-1050.

SCHWARTZ, F.W., 1975. Hydrogeologic investigation of a radioactive waste management site in southern Alberta. Canadian Geotechnical Journal, Vol. 12, pp. 349-361.

SCHWARTZ, F.W., CHERRY, J.A., and ROBERTS, J.R., 1982. A case study of chemical spill: polychlorinated biphenyls: 2, Hydrogeological conditions and contaminant migration. Water Resources Research, Vol. 18, pp. 535-545.

SHACKELFORD, C.D., 1988. Diffusion of inorganic chemical wastes in compacted clay. Ph.D. Thesis, Department of Civil Engineering, University of Texas, Austin, Texas.

SHACKELFORD, C.D., 1991. Laboratory diffusion testing for waste disposal - A review. Journal of Contaminant Hydrology, Vol. 7, pp. 177-217.

SHACKELFORD, C.D., DANIEL, D.E., and LILJESTRAND, H.M., 1989. Diffusion of inorganic chemical species in compacted clay soil. Journal of Contaminant Hydrology, Vol. 4, pp. 441-473.

SHACKELFORD, C.D., and DANIEL, D.E., 1991. Diffusion in saturated soil. I: Background. Journal of Geotechnical Engineering, Vol. 117, No. 3, pp. 467-483.

SHACKELFORD, C.D., and DANIEL, D.E., 1991. Diffusion in saturated soil. II: Results for compacted clay. Journal of Geotechnical Engineering, Vol. 117, No. 3, pp. 485-506.

SHAINBERG, I., and KEMPER, W.D., 1966. Hydration status of adsorbed cations. Soil Science Society America Proceedings. Vol. 30, pp. 707-713.

SLOAN, C.E., 1972. Groundwater hydrogeology of prairie potholes in North Dakota. United States Geological Survey, Professional Paper 585-C.

SMITH, L., and SCHWARTZ, F.W., 1984. An analysis of the influence of fracture geometry on mass transport in fractured media. Water Resources Research, Vol. 20, pp. 1241-1252.

SNOEYINK, V.L., and JENKINS, D., 1980. Water chemistry. John Wiley & Sons, Inc. 463 p.

SNOW, D.T., 1968. Rock fracture spacings, openings and porosities. Journal of Soil Mechanics Foundation Division, American Society of Civil Engineers, Vol. 94, pp. 73-91.

SODERMAN, L.G., and KIM, Y.D., 1970. Effect of groundwater levels on stress history of the St. Clair clay till deposit. Canadian Geotechnical Journal, Vol. 7, pp. 173-187.

SPARKS, D.L., 1986. Soil physical chemistry. CRC Press, Boca Reton, Florida, 308 p.

SPOSITO, G., 1979. Derivation of the Langmuir Equation for ion exchange reactions in soils. Soil Science Society America Proceedings, Vol. 43, pp. 197-198.

SPOSITO, G., 1984. The surface chemistry of soils. Oxford University Press, New York, 234p.

STREETER, V.L., and WYLIE, E.B., 1981. Fluid Mechanics First SI Metric Edition. McGraw-Hill Ryerson Limited.

STOESSELL, R.K., and HANOR, J.S., 1975. A nonsteady state method for determining diffusion coefficients in porous media. Journal of Geophysical Research, Vol. 80, No. 36, pp. 4979-4982.

STUMM, W., and MORGAN, J.J., 1979. Aquatic Chemistry. Wiley-Interscience, New York.

SUDICKY, A.E., and FRIND, E.O., 1982. Contaminant transport in fractured porous media: Analytical solutions for a system of parallel fractures. Water Resources Research, Vol. 18, pp. 1634-1642.

SUDICKY, E.A., and MCLAREN, R.G., 1992. The Laplace Transform Galerkin technique for large-scale simulation of mass transport in discretely fractured porous formations. Water Resources Research, Vol. 28, pp. 499-514.

TANG, D.H., FRIND, E.O., and SUDICKY, E.A., 1980. Contaminant transport in fractured porous media: Analytical solution for a single fracture. Water Resources Research, vol. 17, pp. 555-564.

TAVENAS, F., JEAN, P., LEBLOND, P., and LEROUEIL, S., 1983. The permeability of natural soft clays, II, Permeability characteristics. Canadian Geotechnical Journal, Vol. 20, pp. 645-660.

THOMPSON, H.S., 1850. On the absorbent power of soils. Journal Royal Agricultural Society, Vol. 11, pp. 68-74.

TORRANCE, J.K., 1988. Mineralogy, pore-water chemistry, and geotechnical behaviour of Champlain Sea and related sediments. In: The Late Quaternary Development of the Champlain Sea Basin, N.R. Gadd (Editor). Geological Association of Canada, Special Paper, No. 35, pp. 259-275.

TSANG, Y.W., 1984. The effect of tortuosity on fluid flow through a single fracture. Water Resources Research, Vol. 20, No. 9, pp. 1209-1215.

TSANG, Y.W., and TSANG, C.F., 1987. Channel model of flow through fractured media. Water Resources Research, Vol. 23, No. 3, pp. 467-479.

VAN DER KAMP, G., MAATHIUS, G.H., and MENELEY, W.A., 1986. Bulk permeability of a thick till overlying a buried valley near Weyburn, Saskatchewan. In: Third Proceedings of Canadian hydrogeology Conference, Saskatoon, Saskatchewan. International Association of Hydrogeologists, Canadian National Chapter, April 20-23, pp. 90-101.

VAN SCHAIK, J.C., KEMPER, W.D., and OLSEN, S.R., 1966. Contribution of adsorbed cations to diffusion in clay-water systems. Soil Science Society America Proceedings, Vol. 30, pp. 17-22.

VENNARD, J.K., and STREET, R.L., 1982. Elementary fluid mechanics. John Wiley & Sons, Inc. 685 p.

VOICE, T.C., RICE, C.P., and WEBER, W.O., 1983. Effect of solids concentration on the sorptive partitioning of hydrophobic pollutants in aquatic systems. Environmental Science and Technology, Vol. 17, pp. 513-518.

VONHOF, J.A., 1970. Patterns of joints in Pleistocene sediments. In: Geological Association of Canadian Mining Association, Canada, Programme and Abstracts, Annual Meetings August 30-September 2, 1970, Winnipeg, Canada, pp. 53.

VORAUER, A.G., HARDING, D.W., DUSSEAULT, M.B., and CHERRY, J.A., 1986. The nature of near-surface fractures in clay tills of southwestern Ontario. Proceedings, 3rd Canadian Hydrogeological Conference, Saskatoon, Saskatchewan, PP. 101-115.

WARITH, M.A., 1987. Migration of leachate solution through clay soil. Ph.D. Thesis, Department of Civil Engineering and Applied Mechanics, McGill University, Montreal, Quebec.

WAY, J.T., 1850. On the power of soils to adsorb manure. Journal Royal Agricultural Society, Vol. 11, pp. 313-379.

WEBER, W.J., 1975. Physicochemical processes for water quality control. Wiley Interscience, John Wiley and Sons, Inc., New York, 640 p.

WILLIAMS, R.E., and FARVOLDEN, R.N., 1967. Effects of joints on groundwater movement in till. Journal of Hydrology, Vol. 5, pp. 163-170.

WYLIE, A., and WOOD, T.R., 1990. A program to calculate hydraulic conductivity using slug test data. Ground Water, Vol. 28, No. 5, pp. 783-786.

YANFUL, E.K., and QUIGLEY, R.M., 1990. Tritium, oxygen-18, and deuterium diffusion at the Confederation Road landfill site, Sarnia, Ontario, Canada. Canadian Geotechnical Journal, Vol. 27, No. 3, pp. 271-275.

YONG, R.N., 1985. Interaction of clay and industrial waste - A summary review. Proceedings, Second Annual Canadian/American Conference on Hydrogeology: Hazardous Wastes in Groundwater. Co-sponsored by NWWA and Alberta Research Council, Banff, Alberta, pp. 189-200.

YONG, R.N., SETHI, A.J., and LAROCHELLE, P., 1979. Significance of amorphous material relative to sensitivity in some Champlain clays. Canadian Geotechnical Journal, Vol. 16, pp. 511-520.

YONG, R.N., WARITH, M.A., and BOONSINSUK, P., 1986. Migration of leachate solution through clay liner and substrate. In: Hazardous and Industrial Solid Waste Testing and Disposal: Sixth Volume. ASTM STP 933, D. Lorenzen, R.A. Conway, L.P. Jackson, A. Hamza, C.L. Perket, and W.J. Lacy, (Editors), American Society for Testing and Materials, Philadelphia, pp. 208-225.

TABLES

Table 3.0. Self-Diffusion Coefficient for Representative Ions at Infinite Dilution in Water at 25 ^{0}C [after Shackelford and Daniel (1991)]

Anion (1)	$D_0 \times 10^{-10}$ (m^2/s) (2)	Cation (3)	$D_0 \times 10^{-10}$ (m^2/s) (4)
OH^-	52.8	H^+	93.1
F^-	14.7	Li^+	10.3
Cl^-	20.3	Na^+	13.3
Br^-	20.8	K^+	19.6
I^-	20.4	Rb^+	20.7
HCO_3^-	11.8	Cs^+	20.5
NO_3^-	19.0	Be^{2+}	5.98
SO_4^{2-}	10.6	Mg^{2+}	7.05
CO_3^{2-}	9.22	Ca^{2+}	7.92
-	-	Sr^{2+}	7.90
-	-	Ba^{2+}	8.46
-	-	Pb^{2+}	9.25
-	-	Cu^{2+}	7.13
-	-	Fe^{2+a}	7.19
-	-	Cd^{2+a}	7.17
-	-	Zn^{2+}	7.02
-	-	Ni^{2+a}	6.79
-	-	Fe^{3+a}	6.07
-	-	Cr^{3+a}	5.94
-	-	Al^{3+a}	5.95

[a] Values from Li and Gregory (1974)

Table 3.1. Limiting Free-Solution Diffusion Coefficients for Representative Simple Electrolytes at 25 ^{0}C [after Robinson and Stokes (1959)]

Electrolyte (1)	$D_0 \times 10^{-10}$ (m^2/s) (2)
HCl	33.36
HBr	34.00
LiCl	13.66
LiBr	13.77
NaCl	16.10
NaBr	16.25
NaI	16.14
KCl	19.93
KBr	20.16
KI	19.99
CsCl	20.44
$CaCl_2$	13.35
$BaCl_2$	13.85

Table 3.2. Characteristics of some Clay Minerals.

Clay	Lattice Discrip-tion	C.E.C. (meq/100g)	Source of Charges	Charges
Kaolins	1:1 strong H-bonding	5 - 15	lateral broken edges (hydroxyl)	variable
illites	1:2 strong K-bonding	25	isomorphic substitution and a few broken edges	mostly permanent
chlorites	2:1:1 strong bonding	10 - 40	isomorphic substitution	permanent
vermicu-lites	1:2 weak Mg-bonding	100 - 150	isomorphic substitution	permanent
montmoril-lonites	1:2 very weak bonding	80 - 100	isomorphic substitution and some broken edges	mostly permanent

Table 3.3. Relation of Ion Charge and Ion Size to Ion Retention [after Jenny and Reintemeier (1935) from *J. Phys. Chem.* 39:593-604]

Ion	Crystallographic (Dehydrated) Radius (mm)	% Released by NH_4^+ or K^+
Li^+	0.068	68
Na^+	0.097	67
K^+	0.133	49
NH_4^+	0.143	50
Rb^+	0.147	37
Cs^+	0.167	31
"H^+" (Al^{3+})	(?)	15
Mg^{2+}	0.066	31
Ca^{2+}	0.099	29
Sr^{2+}	0.112	26
Ba^{2+}	0.134	27
Al^{3+}	0.051	15
La^{3+}	0.102	14
Th^{4+}	0.102	2

Table 3.4. Adsorption of Cl^- and SO_4^{2-} by a Kaolinitic and of Cl^- by a Montmorillonitic Soil in Relation to pH [after Bear (1964) from *Chemistry of the Soil*, ACS Monograph Series No. 160]

Kaolinitic Soil (mmole sorbed kg^{-1})			Montmorillonitic Soil (mmole sorbed kg^{-1})	
pH	Cl^-	SO_4^{2-}	pH	Cl^-
7.2	0	0	6.8	0
6.7	3	10	5.6	0
6.1	11	27	4.0	0.5
5.8	24	36	3.0	1
5.0	44	52	2.8	4
4.0	60	-		

Table 4.1. Measured Water Levels at the NRC Site.

DEPTH	(metres)	12.2	9.1	7.4	6.1	6.4	4.4	3.5	3	3.1	2.2	1.5	0.7
DATE	DAYS	PZ-1	PZ-2	PZ-3	PZ-4	PZ-5	PZ-6	PZ-7	PZ-8	PZ-9	PZ-10	PZ-11	PZ-12
2/13/90	1	1.85	0.99	0.93	0.92	1.26	0.34	0.30	0.45	0.39			0.29
2/21/90	8	1.68	0.90	0.89	0.81	0.98	0.57	0.46	0.50	0.67			
3/2/90	17	1.66	0.94	0.89	0.80	0.87	0.50	0.42	0.46	0.54			
3/12/90	27	1.68	1.00	0.97	0.85		0.72	0.67	0.67	0.58			
4/12/90	58	1.69	1.15	0.78	0.68	0.71							
4/16/90	62	1.68		0.86	0.67	0.70	0.18			0.20		0.40	0.20
4/23/90	69		1.19	0.83	0.68	0.71	0.25	0.17	0.40	0.25	0.42	0.23	0.23
5/2/90	78	1.76	1.19	0.87	0.72	0.74	0.41	0.31	0.34	0.48	0.48	0.45	0.39
5/7/90	83	1.74	1.31		0.94		0.52	0.42		0.56	0.55	0.53	0.50
5/21/90	97	1.73	1.23	1.01	1.15	1.17	0.21	0.16	0.26	0.21	0.22	0.21	0.29
7/9/90	146	1.94	1.61	1.37	1.24	1.25	1.10	1.06	1.06	1.11	1.10	1.07	
7/31/90	168	1.90	1.54	1.12	1.16	1.16	0.69	0.64	0.62	0.68	0.68	0.64	0.68
8/8/90	176					1.16	0.28	0.20	0.60	0.28	0.28	0.25	0.44
8/14/90	182			1.18		1.12	0.35	0.23	0.39	0.30	0.28	0.26	0.40
8/17/90	185	1.96	1.56	1.10	1.14	1.08	0.33	0.28	0.31	0.35	0.33	0.28	0.33
8/20/90	188	1.91	1.50	1.01	1.14	1.03	0.26	0.21	0.25	0.28	0.27	0.26	0.29
8/22/90	190	1.90	1.48	0.98	1.07	1.01	0.32	0.32	0.28	0.38	0.36	0.31	0.32
8/24/90	192	1.90	1.45	0.97	1.02	0.98	0.47	0.50	0.38	0.56	0.55	0.49	0.44
8/27/90	195	1.88	1.43	0.97	1.01	0.97	0.60	0.62	0.52	0.68	0.66	0.61	0.56
8/28/90	196	1.88	1.46	1.01	1.02	0.97	0.65	0.65	0.57	0.70	0.67	0.60	0.59
8/29/90	197	1.88	1.45	1.02	1.02	0.97	0.65	0.49	0.57	0.51	0.42	0.30	0.55
8/30/90	198	1.88	1.45	1.04	1.03	0.98	0.64	0.61	0.58	0.66	0.61	0.55	0.54
9/5/90	204	1.88	1.45	1.14	1.11	1.02	0.93	0.91	0.84	0.96	0.94	0.90	0.78
9/7/90	206	1.88	1.47	1.18	1.15	1.05	0.95	0.92	0.90	0.97	0.95	0.90	0.81
9/10/90	209	1.89	1.50	1.21	1.18	1.07	0.97	0.94	0.93	0.99	0.98	0.93	0.86
9/12/90	211	1.89	1.50	1.21	1.20	1.10	0.84	0.73	0.85	0.78	0.75	0.70	0.77
9/14/90	213	1.89	1.51	1.20	1.20	1.10	0.81	0.76	0.80	0.81	0.80	0.76	0.76

Table 4.1. Continued.

9/18/90	217	1.91	1.53	1.20	1.20	1.11	0.85	0.84	0.82	0.90	0.89	0.86	0.79
9/24/90	223	1.90	1.53	1.20	1.18	1.12	0.60	0.43	0.64	0.46	0.41	0.31	0.55
10/1/90	230	1.87	1.46	0.99	1.03	1.04	0.23	0.13	0.23	0.18	0.20	0.20	0.26
10/3/90	232	1.86	1.40	0.95	0.99	1.00	0.21	0.14	0.18	0.20	0.20	0.21	0.22
10/11/90	240	1.72	1.27	0.75	0.77	0.77	0.09	0.00	0.05	0.03	0.06	0.09	0.1
10/15/90	244	1.69	1.17	0.71	0.70	0.73	0.07	0.01	0.05	0.08	0.10	0.10	0.07
10/19/90	248	1.65	1.18	0.66	0.67	0.67	0.07	0.00	0.03	0.07	0.08	0.09	0.07
10/22/90	251	1.65	1.18	0.66	0.65	0.67	0.09	0.06	0.06	0.10	0.11	0.12	0.10
10/24/90	253	1.63	1.18	0.65	0.64	0.65	0.11	0.08	0.08	0.14	0.14	0.14	0.1
10/25/90	254	1.62	1.15	0.66	0.65	0.65	0.12	0.08	0.09	0.14	0.14	0.12	0.1
10/26/90	255	1.62	1.14	0.65	0.64	0.64	0.12	0.08	0.09	0.15	0.14	0.12	0.11
10/29/90	258	1.61	1.12	0.65	0.62	0.63	0.10	0.00	0.08	0.07	0.09	0.10	0.09
10/30/90	259	1.60	1.11	0.62	0.62	0.62	0.08	0.03	0.07	0.09	0.10	0.10	0.10
10/31/90	260	1.60	1.11	0.64	0.61	0.60	0.09	0.05	0.07	0.10	0.11	0.11	0.10
11/1/90	261	1.61	1.11	0.64	0.62	0.60	0.11	0.06	0.09	0.12	0.12	0.12	0.11
11/2/90	262	1.60	1.10	0.63	0.62	0.61	0.11	0.07	0.09	0.14	0.14	0.11	0.11
11/5/90	265	1.60	1.10	0.62	0.61	0.60	0.12	0.08	0.09	0.14	0.13	0.11	0.09
11/6/90	266	1.58	1.09	0.60	0.60	0.59	0.10	0.00	0.07	0.06	0.06	0.09	0.09
11/8/90	268	1.59	1.09	0.62	0.60	0.59	0.09	0.04	0.07	0.08	0.10	0.11	0.10
11/9/90	269	1.59	1.09	0.60	0.59	0.57	0.08	0.05	0.06	0.09	0.11	0.12	0.10
11/12/90	272	1.57	1.08	0.59	0.59	0.57	0.08	0.03	0.04	0.12	0.10	0.11	0.09
11/14/90	274	1.58	1.08	0.59	0.59	0.56	0.11	0.09	0.08	0.15	0.14	0.12	0.11
11/16/90	276	1.54	1.06	0.58	0.58	0.55	0.09	0.04	0.05	0.09	0.10	0.10	0.09
11/21/90	281	1.55	1.04	0.59	0.58	0.55	0.12	0.07	0.09	0.12	0.12	0.12	0.10
11/23/90	283	1.52	1.02	0.56	0.56	0.54	0.08	0.01	0.07	0.07	0.08	0.10	0.10
11/28/90	288	1.51	1.00	0.55	0.55	0.53	0.08	0.00	0.05	0.06	0.07	0.10	0.09
11/30/90	290	1.53	1.02	0.57	0.55	0.53	0.08	0.04	0.06	0.08	0.10	0.10	0.10
12/5/90	295		1.04	0.75		0.54	0.10	0.06	0.08	0.10	0.12	0.12	0.11
12/17/90	307		1.13	0.76		0.68	0.35	0.33	0.35	0.38	0.37	0.30	0.35
1/9/91	330	1.55	1.07	0.71	0.71	0.65	0.50						
3/25/91	405	1.64	1.14	0.71	0.72								
5/30/91	471	1.68	1.24	0.90	0.91	0.83	0.49	0.18	0.49	0.24	0.23	0.24	0.55
7/17/91	519	1.88	1.55	1.33	1.31	1.23	1.17	1.16		1.23	1.20	1.20	
8/3/91	536	1.93	1.60	1.34	1.36	1.30	1.14	1.13		1.2	1.19	1.18	

Table 4.2. Measured Hydraulic Heads (masl) at the NRC Site.

DEPTH	(metres)	12.2	9.1	7.4	6.1	6.4	4.4	3.5	3	3.1	2.2	1.5	0.7
DATE	DAYS	PZ-1	PZ-2	PZ-3	PZ-4	PZ-5	PZ-6	PZ-7	PZ-8	PZ-9	PZ-10	PZ-11	PZ-12
2/13/90	1	95.67	96.54	96.56	96.54	96.14	97.00	97.01	96.89	96.94			96.96
2/21/90	8	95.84	96.63	96.60	96.65	96.42	96.77	96.85	96.84	96.66			
3/2/90	17	95.86	96.59	96.60	96.66	96.53	96.84	96.89	96.88	96.79			
3/12/90	27	95.84	96.53	96.52	96.61		96.62	96.64	96.67	96.75			
4/12/90	58	95.83	96.38	96.71	96.78	96.69							
4/16/90	62	95.84		96.63	96.79	96.70	97.16			97.13		96.88	97.05
4/23/90	69		96.34	96.66	96.78	96.69	97.09	97.14	96.94	97.08	96.90	97.05	97.02
5/2/90	78	95.76	96.34	96.62	96.74	96.66	96.93	97.00	97.00	96.85	96.84	96.83	96.86
5/7/90	83	95.78	96.22		96.52		96.82	96.89		96.77	96.77	96.75	96.75
5/21/90	97	95.79	96.30	96.48	96.31	96.23	97.13	97.15	97.08	97.12	97.10	97.07	96.96
7/9/90	146	95.58	95.92	96.12	96.22	96.15	96.24	96.25	96.28	96.22	96.22	96.21	
7/31/90	168	95.62	95.99	96.37	96.30	96.24	96.65	96.67	96.72	96.65	96.64	96.64	96.57
8/8/90	176					96.24	97.06	97.11	96.74	97.05	97.04	97.03	96.81
8/14/90	182			96.31		96.28	96.99	97.08	96.95	97.03	97.04	97.02	96.85
8/17/90	185	95.56	95.97	96.39	96.32	96.32	97.01	97.03	97.03	96.98	96.99	97.00	96.92
8/20/90	188	95.61	96.03	96.48	96.32	96.37	97.08	97.10	97.09	97.05	97.05	97.02	96.96
8/22/90	190	95.62	96.05	96.51	96.39	96.39	97.02	96.99	97.06	96.95	96.96	96.97	96.93
8/24/90	192	95.62	96.08	96.52	96.44	96.42	96.87	96.81	96.96	96.77	96.77	96.79	96.81
8/27/90	195	95.64	96.10	96.52	96.45	96.43	96.74	96.69	96.82	96.65	96.66	96.67	96.69
8/28/90	196	95.64	96.07	96.48	96.44	96.43	96.69	96.66	96.77	96.63	96.65	96.68	96.66
8/29/90	197	95.64	96.08	96.47	96.44	96.43	96.69	96.82	96.77	96.82	96.90	96.98	96.70
8/30/90	198	95.64	96.08	96.45	96.43	96.42	96.70	96.70	96.76	96.67	96.71	96.73	96.71
9/5/90	204	95.64	96.08	96.35	96.35	96.38	96.41	96.40	96.50	96.37	96.38	96.38	96.47
9/7/90	206	95.64	96.06	96.31	96.31	96.35	96.39	96.39	96.44	96.36	96.37	96.38	96.44
9/10/90	209	95.63	96.03	96.28	96.28	96.33	96.37	96.37	96.41	96.34	96.34	96.35	96.39
9/12/90	211	95.63	96.03	96.28	96.26	96.30	96.50	96.58	96.49	96.55	96.57	96.58	96.48
9/14/90	213	95.63	96.02	96.29	96.26	96.30	96.53	96.55	96.54	96.52	96.52	96.53	96.49

Table 4.2. Continued.

9/18/90	217	95.61	96.00	96.29	96.26	96.29	96.49	96.47	96.52	96.43	96.43	96.42	96.46
9/24/90	223	95.62	96.00	96.29	96.28	96.28	96.74	96.88	96.70	96.87	96.91	96.97	96.70
10/1/90	230	95.65	96.07	96.50	96.43	96.36	97.11	97.18	97.11	97.15	97.12	97.08	96.99
10/3/90	232	95.66	96.13	96.54	96.47	96.40	97.13	97.17	97.16	97.13	97.12	97.07	97.03
10/11/90	240	95.80	96.26	96.74	96.69	96.63	97.25	97.31	97.29	97.30	97.26	97.19	97.15
10/15/90	244	95.83	96.36	96.78	96.76	96.67	97.27	97.30	97.29	97.25	97.22	97.18	97.18
10/19/90	248	95.87	96.35	96.83	96.79	96.73	97.27	97.31	97.31	97.26	97.24	97.19	97.18
10/22/90	251	95.87	96.35	96.83	96.81	96.73	97.25	97.25	97.28	97.23	97.21	97.16	97.15
10/24/90	253	95.89	96.35	96.84	96.82	96.75	97.23	97.23	97.26	97.19	97.18	97.14	97.15
10/25/90	254	95.90	96.38	96.83	96.81	96.75	97.22	97.23	97.25	97.19	97.18	97.16	97.15
10/26/90	255	95.90	96.39	96.84	96.82	96.76	97.22	97.23	97.25	97.18	97.18	97.16	97.14
10/29/90	258	95.91	96.41	96.84	96.84	96.77	97.24	97.31	97.26	97.26	97.23	97.18	97.16
10/30/90	259	95.92	96.42	96.87	96.84	96.78	97.26	97.28	97.27	97.24	97.22	97.18	97.15
10/31/90	260	95.92	96.42	96.85	96.85	96.80	97.25	97.26	97.27	97.23	97.21	97.17	97.15
11/1/90	261	95.91	96.42	96.85	96.84	96.80	97.23	97.25	97.25	97.21	97.20	97.16	97.14
11/2/90	262	95.92	96.43	96.86	96.84	96.79	97.23	97.24	97.25	97.19	97.18	97.17	97.14
11/5/90	265	95.92	96.43	96.87	96.85	96.80	97.22	97.23	97.25	97.19	97.19	97.17	97.16
11/6/90	266	95.94	96.44	96.89	96.86	96.81	97.24	97.31	97.27	97.27	97.26	97.19	97.16
11/8/90	268	95.93	96.44	96.87	96.86	96.81	97.25	97.27	97.27	97.25	97.22	97.17	97.15
11/9/90	269	95.93	96.44	96.89	96.87	96.83	97.26	97.26	97.28	97.24	97.21	97.16	97.15
11/12/90	272	95.95	96.45	96.90	96.87	96.83	97.26	97.28	97.30	97.21	97.22	97.17	97.16
11/14/90	274	95.94	96.45	96.90	96.87	96.84	97.23	97.22	97.26	97.18	97.18	97.16	97.14
11/16/90	276	95.98	96.47	96.91	96.88	96.85	97.25	97.27	97.29	97.24	97.22	97.18	97.16
11/21/90	281	95.97	96.49	96.90	96.88	96.85	97.22	97.24	97.25	97.21	97.20	97.16	97.15
11/23/90	283	96.00	96.51	96.93	96.90	96.86	97.26	97.30	97.27	97.26	97.24	97.18	97.15
11/28/90	288	96.01	96.53	96.94	96.91	96.87	97.26	97.31	97.29	97.27	97.25	97.18	97.16
11/30/90	290	95.99	96.51	96.92	96.91	96.87	97.26	97.27	97.28	97.25	97.22	97.18	97.15
12/5/90	295		96.49	96.74		96.86	97.24	97.25	97.26	97.23	97.20	97.16	97.14
12/17/90	307		96.40	96.73		96.72	96.99	96.98	96.99	96.95	96.95	96.98	96.90
1/9/91	330	95.97	96.46	96.78	96.75	96.75	96.84						
3/25/91	405	95.88	96.39	96.78	96.74								
5/30/91	471	95.84	96.29	96.59	96.55	96.57	96.85	97.13	96.85	97.09	97.09	97.04	96.70
7/17/91	519	95.64	95.98	96.16	96.15	96.17	96.17	96.15		96.10	96.12	96.08	
8/3/91	536	95.59	95.93	96.15	96.10	96.10	96.20	96.18		96.13	96.13	96.10	

Table 4.3. Measured Water Levels at the Fallowfield Site.

DEPTH	(metres)	12.5	9.9	7.6	6.1	4.3	4.4	3.7	3.2	3.0	2.1	1.65	0.8
DATE	DAYS	PZ-1	PZ-2	PZ-3	PZ-4	PZ-5	PZ-6	PZ-7	PZ-8	PZ-9	PZ-10	PZ-11	PZ-12
1/15/90		1.31	1.20	1.22	1.63	1.28	1.43	1.23	1.20	1.19	1.19	1.19	
2/13/90	29	1.23	1.03	0.89	0.99	0.82	0.81	0.69	0.70	0.69	0.67	0.69	0.69
2/14/90	30	1.21	1.02	0.92		0.81	0.80	0.69	0.61	0.61	0.59	0.60	0.63
3/2/90	46	1.18	0.98	0.82	1.09	0.98	0.90	0.90	0.90	0.90	0.86	0.80	
3/15/90	59	1.08	0.99	0.88	1.03	0.85	0.85	0.40	0.28	0.27	0.25	0.26	0.26
4/10/90	85	1.12	0.95	0.64	0.93	0.77	0.77	0.76	0.66	0.65	0.62	0.63	0.70
4/12/90	87	1.09	0.95	0.84	0.92	0.74	0.74	0.58	0.60	0.60	0.57	0.59	0.59
5/23/90	128	0.98	0.88	0.86	0.91	0.81	0.80	0.73	0.72	0.71	0.68	0.70	0.68
6/21/90	157	1.13	0.99		1.47	1.17	1.15	1.28	1.26	1.26	1.23	1.25	
7/9/90	175	1.22	1.10	1.12	1.22	1.30	1.30	1.38	1.35	1.35	1.32	1.33	
7/31/90	197	1.24	1.12	1.05	1.23	1.13	1.09	1.10	1.03	1.02	0.99	1.00	
8/8/90	205		1.28	1.11		1.20		1.07	1.03	1.02	0.99	1.00	
8/14/90	211	1.35	1.16	1.07		1.18		1.11	1.03	1.01	0.99	1.00	
8/17/90	214	1.31	1.15	1.05		1.13	1.11	1.08	1.06	1.05	1.02	1.03	
8/20/90	217	1.31	1.15	1.09	1.42	1.14	1.12	1.15	1.13	1.12	1.10	1.10	
8/22/90	219	1.31	1.15	1.09	1.32	1.15	1.13	1.19	1.17	1.17	1.13	1.14	
8/27/90	224	1.31	1.15	1.06	1.25	1.17	1.14	1.26	1.24	1.24	1.21	1.22	
9/5/90	233	1.33	1.15	1.08	1.23	1.15	1.12	1.17	1.14	1.14	1.10	1.12	
9/7/90	235	1.33	1.15	1.05	1.23	1.14	1.11	1.18	1.16	1.15	1.12	1.13	
9/10/90	238	1.34	1.16	1.09	1.22	1.16	1.14	1.23	1.20	1.20	1.17	1.18	
9/11/90	239	1.33	1.15	1.09	1.23	1.17	1.15	1.19	1.06	1.05	1.10	1.02	
9/12/90	240		1.15		1.23		1.17	1.13	1.07	1.05	1.10	1.02	
9/13/90	241		1.19		1.23		1.19	1.16	1.10	1.10	1.05	1.06	
9/14/90	242		1.21	1.09	1.22		1.19	1.16	1.11	1.10	1.06	1.07	
9/17/90	245		1.20	1.13	1.22		1.20	1.24	1.20	1.20	1.15	1.16	
9/18/90	246		1.20	1.15	1.22		1.20	1.23	1.18	1.17	1.13	1.14	
9/24/90	252	1.35	1.16	1.11	1.22		1.17	1.05	0.86	0.85	0.81	0.82	

Table 4.3. Continued.

9/27/90	255	1.35	1.18	1.09	1.22	1.17	1.06	0.90	0.83	0.82	0.80	0.81	
10/3/90	261	1.32	1.13	0.96	1.16	0.90	0.83	0.70	0.70	0.70	0.68	0.69	0.68
10/5/90	263	1.22	1.00	0.80	1.02	0.75	0.70	0.62	0.55	0.56	0.51	0.53	0.53
10/11/90	269	1.19	0.96	0.77	0.95	0.71	0.68	0.51	0.40	0.40	0.39	0.39	0.38
10/22/90	280	1.15	0.88	0.68	0.84	0.61	0.60	0.64	0.62	0.63	0.60	0.62	0.60
10/24/90	282	1.15	0.87	0.67	0.84	0.62	0.62	0.69	0.65	0.66	0.62	0.63	0.63
10/25/90	283	1.15	0.87	0.68	0.84	0.65	0.62	0.70	0.68	0.68	0.67	0.66	0.64
10/26/90	284	1.13	0.87	0.69	0.82	0.64	0.63	0.70	0.67	0.68	0.65	0.66	0.67
10/29/90	287	1.11	0.86	0.68	0.82	0.67	0.66	0.68	0.60	0.60	0.57	0.59	0.58
10/30/90	288	1.10	0.86	0.70	0.82	0.68	0.68	0.65	0.60	0.61	0.59	0.60	0.59
10/31/90	289	1.10	0.86	0.73	0.82	0.68	0.68	0.68	0.63	0.64	0.61	0.62	0.63
11/2/90	291	1.10	0.85	0.67	0.83	0.68	0.67	0.69	0.66	0.66	0.63	0.65	0.65
11/3/90	292	1.08	0.85	0.68	0.82	0.68	0.66	0.70	0.67	0.67	0.64	0.65	0.67
11/5/90	294	1.07	0.84	0.68	0.81	0.68	0.67	0.70	0.65	0.65	0.62	0.63	0.63
11/6/90	295	1.05	0.81	0.62	0.80	0.67	0.63	0.57	0.34	0.33	0.30	0.31	0.31
11/7/90	296	1.06	0.84	0.67	0.81	0.66	0.64	0.53	0.52	0.52	0.49	0.50	0.50
11/8/90	297	1.07	0.83	0.68	0.82	0.65	0.62	0.60	0.58	0.59	0.56	0.58	0.29
11/10/90	299	1.05	0.80	0.65	0.80	0.65	0.62	0.62	0.55	0.55	0.52	0.53	0.25
11/12/90	301	1.04	0.81	0.63	0.78	0.64	0.62	0.64	0.62	0.62	0.60	0.61	0.32
11/14/90	303	1.03	0.80	0.69	0.81	0.65	0.64	0.69	0.66	0.67	0.63	0.64	0.36
11/16/90	305	1.01	0.79	0.64	0.77	0.65	0.64	0.69	0.65	0.65	0.63	0.64	0.36
11/19/90	308	1.01	0.79	0.67	0.78	0.68	0.67	0.68	0.62	0.64	0.61	0.62	0.35
11/23/90	312	0.99	0.77	0.62	0.78	0.66	0.65	0.60	0.49	0.49	0.45	0.46	0.47
11/28/90	317	0.96	0.75	0.62	0.75	0.64	0.62	0.62	0.54	0.55	0.52	0.53	0.53
11/30/90	319	0.96	0.75	0.68	0.78	0.66	0.65	0.65	0.62	0.62	0.60	0.61	0.61
12/5/90	324	0.96	0.80	0.65		0.69	0.66	0.68	0.64	0.64	0.62	0.62	0.62
12/20/90	339	0.97	0.83	0.74		0.83	0.82	0.81	0.77	0.77	0.75	0.75	
1/9/91	359	0.94	0.80	0.75	0.88	0.80	0.80	0.88	0.86	0.86	0.84	0.85	
3/25/91	434	0.94	0.80		0.83	0.62	0.61	0.46	0.28		0.24	0.26	
5/30/91	500	0.88	0.77	0.69	0.86	0.75	0.72	0.78	0.75	0.75	0.72	0.73	
7/17/91	548	1.11	0.97	0.97	1.06	1.15	1.14	1.30	1.26	1.27	1.24	1.25	
8/3/91	565	1.25	1.09	1.12	1.20	1.26	1.24	1.39	1.35	1.35	1.32	1.34	

Table 4.4. Measured Hydraulic Heads (masl) at the Fallowfield Site.

DEPTH	(metres)	12.5	9.9	7.6	6.1	4.3	4.4	3.7	3.2	3	2.1	1.65	0.8
DATE	DAYS	PZ-1	PZ-2	PZ-3	PZ-4	PZ-5	PZ-6	PZ-7	PZ-8	PZ-9	PZ-10	PZ-11	PZ-12
1/15/90	1	98.36	98.46	98.44	98.04	98.40	98.27	98.46	98.47	98.50	98.49	98.48	
2/13/90	29	98.44	98.63	98.77	98.68	98.86	98.89	99.00	98.97	99.00	99.01	98.98	98.98
2/14/90	30	98.46	98.64	98.74		98.87	98.90	99.00	99.06	99.08	99.09	99.07	99.04
3/2/90	46	98.49	98.68	98.84	98.58	98.70	98.80	98.79	98.77	98.79	98.82	98.87	
3/15/90	59	98.59	98.67	98.78	98.64	98.83	98.85	99.29	99.39	99.42	99.43	99.41	99.41
4/10/90	85	98.55	98.71	99.02	98.74	98.91	98.93	98.93	99.01	99.04	99.06	99.04	98.97
4/12/90	87	98.58	98.71	98.82	98.75	98.94	98.96	99.11	99.07	99.09	99.11	99.08	99.08
5/23/90	128	98.69	98.78	98.80	98.76	98.87	98.90	98.96	98.95	98.98	99.00	98.97	98.99
6/21/90	157	98.54	98.67		98.20	98.51	98.55	98.41	98.41	98.43	98.45	98.42	
7/9/90	175	98.45	98.56	98.54	98.45	98.38	98.40	98.31	98.32	98.34	98.36	98.34	
7/31/90	197	98.43	98.54	98.61	98.44	98.55	98.61	98.59	98.64	98.67	98.69	98.67	
8/8/90	205		98.38	98.55		98.48		98.62	98.64	98.67	98.69	98.67	
8/14/90	211	98.32	98.50	98.59		98.50		98.58	98.64	98.68	98.69	98.67	
8/17/90	214	98.36	98.51	98.61		98.55	98.59	98.61	98.61	98.64	98.66	98.64	
8/20/90	217	98.36	98.51	98.57	98.25	98.54	98.58	98.54	98.54	98.57	98.58	98.57	
8/22/90	219	98.36	98.51	98.57	98.35	98.53	98.57	98.50	98.50	98.52	98.55	98.53	
8/27/90	224	98.36	98.51	98.60	98.42	98.51	98.56	98.43	98.43	98.45	98.47	98.45	
9/5/90	233	98.34	98.51	98.58	98.44	98.53	98.58	98.52	98.53	98.55	98.58	98.55	
9/7/90	235	98.34	98.51	98.61	98.44	98.54	98.59	98.51	98.51	98.54	98.56	98.54	
9/10/90	238	98.33	98.50	98.57	98.45	98.52	98.56	98.46	98.47	98.49	98.51	98.49	
9/11/90	239	98.34	98.51	98.57	98.44	98.51	98.55	98.50	98.61	98.64	98.58	98.65	
9/12/90	240		98.51		98.44		98.53	98.56	98.60	98.64	98.58	98.65	
9/13/90	241		98.47		98.44		98.51	98.53	98.57	98.59	98.63	98.61	
9/14/90	242		98.45	98.57	98.45		98.51	98.53	98.56	98.59	98.62	98.60	
9/17/90	245		98.46	98.53	98.45		98.50	98.45	98.47	98.49	98.53	98.51	
9/18/90	246		98.46	98.51	98.45		98.50	98.46	98.49	98.52	98.55	98.53	
9/24/90	252	98.32	98.50	98.55	98.45		98.53	98.64	98.81	98.84	98.87	98.85	

Table 4.4. Continued.

9/27/90	255	98.32	98.48	98.57	98.45	98.51	98.64	98.79	98.84	98.87	98.88	98.86	
10/3/90	261	98.35	98.53	98.70	98.51	98.78	98.87	98.99	98.97	98.99	99.00	98.98	98.99
10/5/90	263	98.45	98.66	98.86	98.65	98.93	99.00	99.07	99.12	99.13	99.17	99.14	99.14
10/11/90	269	98.48	98.70	98.89	98.72	98.97	99.02	99.18	99.27	99.29	99.29	99.28	99.29
10/22/90	280	98.52	98.78	98.98	98.83	99.07	99.10	99.05	99.05	99.06	99.08	99.05	99.07
10/24/90	282	98.52	98.79	98.99	98.83	99.06	99.08	99.00	99.02	99.03	99.06	99.04	99.04
10/25/90	283	98.52	98.79	98.98	98.83	99.03	99.08	98.99	98.99	99.01	99.01	99.01	99.03
10/26/90	284	98.54	98.79	98.97	98.85	99.04	99.07	98.99	99.00	99.01	99.03	99.01	99.00
10/29/90	287	98.56	98.80	98.98	98.85	99.01	99.04	99.01	99.07	99.09	99.11	99.08	99.09
10/30/90	288	98.57	98.80	98.96	98.85	99.00	99.02	99.04	99.07	99.08	99.09	99.07	99.08
10/31/90	289	98.57	98.80	98.93	98.85	99.00	99.02	99.01	99.04	99.05	99.07	99.05	99.04
11/2/90	291	98.57	98.81	98.99	98.84	99.00	99.03	99.00	99.01	99.03	99.05	99.02	99.02
11/3/90	292	98.59	98.81	98.98	98.85	99.00	99.04	98.99	99.00	99.02	99.04	99.02	99.00
11/5/90	294	98.60	98.82	98.98	98.86	99.00	99.03	98.99	99.02	99.04	99.06	99.04	99.04
11/6/90	295	98.62	98.85	99.04	98.87	99.01	99.07	99.12	99.33	99.36	99.38	99.36	99.36
11/7/90	296	98.61	98.82	98.99	98.86	99.02	99.06	99.16	99.15	99.17	99.19	99.17	99.17
11/8/90	297	98.60	98.83	98.98	98.85	99.03	99.08	99.09	99.09	99.10	99.12	99.09	99.38
11/10/90	299	98.62	98.86	99.01	98.87	99.03	99.08	99.07	99.12	99.14	99.16	99.14	99.42
11/12/90	301	98.63	98.85	99.03	98.89	99.04	99.08	99.05	99.05	99.07	99.08	99.06	99.35
11/14/90	303	98.64	98.86	98.97	98.86	99.03	99.06	99.00	99.01	99.02	99.05	99.03	99.31
11/16/90	305	98.66	98.87	99.02	98.90	99.03	99.06	99.00	99.02	99.04	99.05	99.03	99.31
11/19/90	308	98.66	98.87	98.99	98.89	99.00	99.03	99.01	99.05	99.05	99.07	99.05	99.32
11/23/90	312	98.68	98.89	99.04	98.89	99.02	99.05	99.09	99.18	99.20	99.23	99.21	99.20
11/28/90	317	98.71	98.91	99.04	98.92	99.04	99.08	99.07	99.13	99.14	99.16	99.14	99.14
11/30/90	319	98.71	98.91	98.98	98.89	99.02	99.05	99.04	99.05	99.07	99.08	99.06	99.06
12/5/90	324	98.71	98.86	99.01		98.99	99.04	99.01	99.03	99.05	99.06	99.05	99.05
12/20/90	339	98.70	98.83	98.92		98.85	98.88	98.88	98.90	98.92	98.93	98.92	
1/9/91	359	98.73	98.86	98.91	98.79	98.88	98.90	98.81	98.81	98.83	98.84	98.82	
3/25/91	434	98.73	98.86		98.84	99.06	99.09	99.23	99.39		99.44	99.41	
5/30/91	500	98.79	98.89	98.97	98.81	98.93	98.98	98.91	98.92	98.94	98.96	98.94	
7/17/91	548	98.56	98.69	98.69	98.61	98.53	98.56	98.39	98.41	98.42	98.44	98.42	
8/3/91	565	98.42	98.57	98.54	98.47	98.42	98.46	98.30	98.32	98.34	98.36	98.33	

Table 4.5. Measured Water Levels at the Renfrew Site.

DEPTH	(metres)	12.2	9.2	8.4	5.9	4.6	3.1	1.5
DATE	DAYS	PZ-1	PZ-2	PZ-3	PZ-4	PZ-5	PZ-6	PZ-7
2/19/90	1	2.39	1.18			0.64		0.90
3/7/90	16	2.55	1.44	2.00	0.77	0.77	0.77	0.74
3/15/90	24	2.53	1.27	1.53	0.45	0.28	0.37	0.25
6/5/90	106	2.22	1.19	1.18	0.72	0.73	0.73	0.56
7/9/90	140	2.19	1.15	1.21	0.64	0.64	0.69	0.62
8/8/90	170	2.40	1.44	1.89	1.41	1.01	1.47	1.02
8/15/90	177	2.45	1.51	1.53	1.05	1.01	1.05	1.03
8/24/90	186	2.48	1.43	1.54	0.87	0.89	0.95	0.91
9/5/90	198	2.48	1.38	1.48	0.80	0.83	0.89	0.86
9/12/90	205				0.95	0.97	1.03	0.99
9/14/90	207				0.99	1.00	1.01	1.02
9/19/90	212				1.07	1.09	1.15	1.11
10/9/90	232	2.37	1.10	1.42	0.43	0.22	0.29	0.26
10/22/90	245	2.17	0.80	1.09	0.17	0.17	0.24	0.21
11/19/90	273	2.09	0.80	0.98	0.18	0.19	0.26	0.23
12/7/90	291	2.00	0.77	0.89	0.20	0.23	0.28	0.25
3/26/91	400	2.24	0.75	0.99				
5/30/91	465	2.04	0.88	0.98	0.47	0.49	0.52	0.46
7/17/91	513	2.50	1.51	1.51	1.16	1.19	1.22	1.15
8/3/91	530	2.69	1.65	1.69	1.29	1.31	1.36	1.26

Table 4.6. Measured Hydraulic Heads (masl) at the Renfrew Site.

DEPTH	(metres)	12.2	9.2	8.4	5.9	4.6	3.1	1.5
DATE	DAYS	PZ-1	PZ-2	PZ-3	PZ-4	PZ-5	PZ-6	PZ-7
2/19/90	1	96.91	98.13			98.64		98.42
3/7/90	16	96.75	97.87	97.28	98.49	98.51	98.56	98.58
3/15/90	24	96.77	98.04	97.75	98.81	99.00	98.96	99.07
6/5/90	106	97.08	98.12	98.10	98.54	98.55	98.60	98.76
7/9/90	140	97.11	98.16	98.07	98.62	98.64	98.64	98.70
8/8/90	170	96.90	97.87	97.39	97.85	98.27	97.86	98.30
8/15/90	177	96.85	97.80	97.75	98.21	98.27	98.28	98.29
8/24/90	186	96.82	97.88	97.74	98.39	98.39	98.38	98.41
9/5/90	198	96.82	97.93	97.80	98.46	98.45	98.44	98.46
9/12/90	205				98.31	98.31	98.30	98.33
9/14/90	207				98.27	98.28	98.33	98.30
9/19/90	212				98.19	98.19	98.18	98.21
10/9/90	232	96.93	98.21	97.86	98.83	99.06	99.04	99.06
10/22/90	245	97.13	98.51	98.19	99.09	99.11	99.09	99.11
11/19/90	273	97.21	98.51	98.30	99.08	99.09	99.07	99.09
12/7/90	291	97.30	98.54	98.39	99.06	99.05	99.05	99.07
3/26/91	400	97.06	98.56	98.29				
5/30/91	465	97.26	98.43	98.30	98.79	98.79	98.81	98.86
7/17/91	513	96.80	97.80	97.77	98.10	98.09	98.11	98.17
8/3/91	530	96.61	97.66	97.59	97.97	97.97	97.97	98.06

Table 4.7. Measured Water Levels at the Casselman Site.

DEPTH	(metres)	12.2	9.2	6.4	4.4	4.4	3.1	2.9	1.3
DATE	DAYS	PZ-1	PZ-2	PZ-3	PZ-4	PZ-5	PZ-6	PZ-7	PZ-8
6/5/90	1	4.57	3.56	3.60	1.14	1.15	1.19	1.17	1.08
7/10/90	35	4.47	3.87	3.93	2.14	2.07	2.16	2.12	
8/3/90	59	4.59	3.88	3.98	2.01	1.94	2.01	2.02	
8/9/90	65	4.66	3.86	3.93	1.53	1.48	1.55	1.58	
8/14/90	70	4.66	3.86	3.93	1.36	1.48	1.46	1.58	0.85
8/23/90	79	4.71	3.87	3.94	1.52	1.44	1.55	1.58	
8/30/90	86	4.76	3.90	3.98			1.87	1.90	
9/4/90	91	4.82	3.97	4.08	2.09	2.03	2.11	2.13	
9/10/90	97	4.84	3.99	4.08	2.25	2.20	2.25	2.28	
9/21/90	108	4.90	4.03	4.12	2.50	2.45	2.47	2.53	
10/4/90	121	4.77	3.77	3.84	1.34	1.32	1.39	1.45	1.30
10/15/90	132	4.72	3.36	3.44	0.71	0.69	0.68	0.73	0.60
10/22/90	139		3.51	3.58	0.79	0.88	0.77	0.83	0.70
11/9/90	157	4.76	3.48	3.51	0.54	0.68	0.64	0.71	0.68
11/18/90	166	4.65	3.41	3.45	0.35	0.49	0.44	0.50	0.50
12/14/90	192	4.75	3.49	3.55		0.90	0.87	0.92	0.87
3/25/91	293	4.03	2.72	2.76	0.47	0.46	0.41	0.48	
5/17/91	346	4.45	3.14	3.55	2.60	2.63	2.56	2.53	
8/3/91	424	4.63	3.34	3.83	2.91	2.93	2.82	2.88	

Table 4.8. Measured Hydraulic Heads (masl) at the Casselman

DEPTH	(metres)	12.2	9.2	6.4	4.4	4.4	3.1	2.9	1.3
DATE	DAYS	PZ-1	PZ-2	PZ-3	PZ-4	PZ-5	PZ-6	PZ-7	PZ-8
6/5/90	1	93.48	94.48	94.49	96.98	97.00	96.98	97.03	97.13
7/10/90	35	93.58	94.17	94.16	95.98	96.08	96.01	96.08	
8/3/90	59	93.46	94.16	94.11	96.11	96.21	96.16	96.18	
8/9/90	65	93.39	94.18	94.16	96.59	96.67	96.62	96.62	
8/14/90	70	93.39	94.18	94.16	96.76	96.67	96.71	96.62	97.36
8/23/90	79	93.34	94.17	94.15	96.60	96.71	96.62	96.62	
8/30/90	86	93.29	94.14	94.11			96.30	96.30	
9/4/90	91	93.23	94.07	94.01	96.03	96.12	96.06	96.07	
9/10/90	97	93.21	94.05	94.01	95.87	95.95	95.92	95.92	
9/21/90	108	93.15	94.01	93.97	95.62	95.70	95.70	95.67	
10/4/90	121	93.28	94.27	94.25	96.78	96.83	96.78	96.75	96.91
10/15/90	132	93.33	94.68	94.65	97.41	97.46	97.49	97.47	97.61
10/22/90	139		94.53	94.51	97.33	97.27	97.40	97.37	97.51
11/9/90	157	93.29	94.56	94.58	97.58	97.47	97.53	97.49	97.53
11/18/90	166	93.40	94.63	94.64	97.77	97.66	97.73	97.70	97.71
12/14/90	192	93.30	94.55	94.54		97.25	97.30	97.28	97.34
3/25/91	293	94.02	95.32	95.33	97.65	97.69	97.76	97.72	
5/17/91	346	93.60	94.90	94.54	95.52	95.52	95.61	95.67	
8/3/91	424	93.42	94.70	94.26	95.21	95.22	95.35	95.32	

Table 4.9. Hydraulic Conductivity Versus Depth at the NRC site.

Depth (m)	Hydraulic Conductivity (m/s)	
	Hvorslev (1951)	Bouwer & Rice (1976)
0.91	1.13×10^{-8}	1.16×10^{-9}
1.45	7.04×10^{-8}	
2.18	1.04×10^{-7}	3.14×10^{-8}
2.95	3.25×10^{-9} #	
3.10	3.89×10^{-7}	1.14×10^{-7}
3.48	2.58×10^{-8}	
4.34	7.92×10^{-8}	3.20×10^{-8}
6.10	1.78×10^{-9} #	
6.35	1.72×10^{-9}	
7.39	8.52×10^{-10}	
9.14	1.49×10^{-9} #	
12.19	8.20×10^{-10} #	

Note: The piezometers were installed by Double Shelby method except for # which were augered.

Table 4.10. Hydraulic Conductivity Measured at the Large Wells.

SITE	METHOD OF ANALYSIS	
	BOUWER & RICE (1976)	BOAST & KIRKHAM (1971)
FALLOWFIELD	3.61×10^{-6} m/s	8.10×10^{-6} m/s
NRC	2.26×10^{-6} m/s	2.64×10^{-6} m/s

Table 4.11. Hydraulic Conductivity Versus Depth at the Fallowfield Site.

Depth (m)	Hydraulic Conductivity (m/s)	
	Hvorslev (1951)	Bouwer & Rice (1976)
0.80	2.00×10^{-7}	2.11×10^{-6}
1.60	3.10×10^{-5}	7.52×10^{-6}
2.10	5.37×10^{-5}	1.14×10^{-5}
3.00	3.17×10^{-7} #	
3.20	7.60×10^{-6}	4.73×10^{-7}
3.70	1.22×10^{-6}	5.79×10^{-7}
4.30	3.36×10^{-9}	
4.40	4.35×10^{-9} #	
6.10	6.00×10^{-9}	
7.60	2.20×10^{-8} #	
9.90	1.94×10^{-9} #	
12.50	1.07×10^{-9} #	

Note: The piezometers were installed by Double Shelby method except for # which were augered.

Table 4.12. Hydraulic Conductivity Versus Depth at the Renfrew Site.

Depth (m)	Hydraulic Conductivity (m/s)	
	Hvorslev (1951)	Bouwer & Rice (1976)
1.50	1.96×10^{-7}	3.50×10^{-8}
3.05	5.24×10^{-7}	1.22×10^{-7}
4.60	2.05×10^{-5}	5.65×10^{-6}
5.90	1.85×10^{-8}	8.08×10^{-9}
8.40	1.64×10^{-9}	
9.15	2.75×10^{-9} #	
12.20	1.29×10^{-9} #	

Note: The piezometers were installed by Double Shelby method except for # which were augered.

Table 4.13. Hydraulic Conductivity Versus Depth at the Casselman Site.

Depth (m)	Hydraulic Conductivity (m/s)	
	Hvorslev (1951)	Bouwer & Rice (1976)
1.30	2.36×10^{-7}	4.32×10^{-8}
2.90	2.01×10^{-8}	
3.05	3.95×10^{-8}	1.11×10^{-8}
4.40	9.33×10^{-8} #	3.23×10^{-8}
4.40	1.19×10^{-7}	4.90×10^{-8}
6.40	1.46×10^{-7}	8.16×10^{-8}
9.15	1.68×10^{-8} #	
12.20	1.40×10^{-9} #	

Note: The piezometers were installed by Double Shelby method except for # which were augered.

Table 4.14. Measured Porosities and Velocities at the NRC Site.

Fractured Zone

Depth (m)	Effective Porosity (x 10^{-6}) n_{ef}^{*}	Velocity (m/d) v^{1}	v^{t}
0.91	332	0.139	0.117
1.45	622	0.487	0.411
2.18	491	0.869	0.732
3.10	347	4.593	3.868
3.48	102	1.029	0.867
4.34	149	2.174	1.831
6.10	22	0.319	0.268
Average Fracture Flow Velocity:		1.4	1.1

Unfractured Zone

			Velocity[a] (m/d)	
	Effective Porosity n_e	Gradient used	0.084	0.12
	(x 10^{-6})			
6.35	0.69		18.0	25.7
7.39	0.68		9.1	12.9
9.14	0.66		16.4	23.4
12.19	0.61		9.9	14.1

* Effective porosity based upon Equation 2.25

v^{1} Parallel plate model, Equation 2.20
Gradient,i, (= 0.12 used)

v^{t}: ($v = Ki/n_{ef}^{t}$) Gradient,i, (= 0.04 used)

a: ($v = Ki/n_e$)

Table 4.15. Measured Porosities and Velocities at the Fallowfield Site.

Depth (m)	Effective Porosity (x 10^{-6}) n_{ef}^{*}	Velocity (m/d) v^{1}	v^{t}
Fractured Zone			
0.80	1292	0.127	0.134
1.60	12787	1.999	2.095
2.10	9674	4.555	4.795
3.20	2737	2.278	2.400
3.70	590	1.696	1.786
4.30	28	0.097	0.103
Average Fracture Flow Velocity:		1.80	1.80

	Effective Porosity n_e	Gradient used	Velocity[a] (m/d) 0.007	0.024
Unfractured Zone				
			(x 10^{-6})	
4.40	0.54		4.87	16.7
6.10	0.56		6.51	22.3
7.60	0.56		23.6	81.0
9.90	0.57		2.05	7.02
12.50	0.58		1.11	3.80

* Effective porosity based upon Equation 2.25

v^{1} Parallel plate model, Equation 2.20
Gradient,i, (= 0.024 used)

v^{t}: ($v = Ki/n_{ef}^{*}$) Gradient,i, (= 0.01 used)

a: ($v = Ki/n_e$)

Table 4.16. Measured Porosities and Velocities at the Renfrew Site.

Depth (m)	Fractured Zone: Effective Porosity (x 10^{-6}) n_{ef}^{t}	Velocity (m/d) v^{l}	v^{t}
1.50	808	0.166	0.419
3.05	707	0.507	1.281
4.60	1303	10.760	27.185
5.90	92	0.137	0.347
8.40	22	0.053	0.127
Average Fracture Flow Velocity:		2.3	5.9

Unfractured Zone: Depth (m)	Effective Porosity n_e	Gradient used	Velocity[a] (m/d) 0.22	0.26
			(x 10^{-6})	
8.40	0.54		57.5	67.9
9.15	0.56		93.7	110.7
12.20	0.56		43.3	51.2

* Effective porosity based upon Equation 2.25

v^{l} Parallel plate model, Equation 2.20
Gradient,i, (= 0.26 used)

v^{t}: ($v = Ki/n_{ef}^{t}$) Gradient,i, (= 0.02 used)

a: ($v = Ki/n_e$)

Table 4.17. Measured Porosities and Velocities at the Casselman Site.

Depth (m)	Effective Porosity (x 10^{-6})	Velocity (m/d)	
	Fractured Zone		
	n_{ef}^{*}	v^{1}	v^{2}
1.30	860	0.328	0.829
2.90	238	0.101	0.254
3.05	298	0.158	0.400
4.40	431	0.330	0.834
6.40	183	0.953	2.409
9.15	89	0.225	0.569
Average Fracture Flow Velocity:		0.35	0.90

Depth (m)	Effective Porosity n_e	Gradient used	Velocity[a] (m/d) 0.23	0.40
	Unfractured Zone			
			(x 10^{-6})	
6.40	0.65		4493	7808
9.15	0.64		523	909
12.20	0.67		41.4	71.2

* Effective porosity based upon Equation 2.25

v^{1} Parallel plate model, Equation 2.20
Gradient,i, (= 0.40 used)

v^{2}: ($v = Ki/n_{ef}^{*}$) Gradient,i, (= 0.035 used)

a: ($v = Ki/n_e$)

Table 4.18. Geochemical Results for the NRC Site.

Depth (m)	Ca^{++}	Mg^{++}	Na^{+}	K^{+}	Cl^{-}	SO_4^{--}	HCO_3^{-}	^3H	pH	Conductivity
				(M/m^3)				TU[1]		mmho
1.45	2.47	0.62	1.70	0.12	3.66	1.19	1.70	34	6.8	750
2.95	1.50	0.41	0.78	0.10	1.94	0.65	1.90	31	7.3	410
4.34	1.00	0.34	3.18	0.14	2.40	1.00	2.10	24	7.5	520
6.10	0.57	0.38	2.48	0.19	2.17	0.22	2.10	.9	7.6	370
9.14	0.37	0.33	4.57	0.33	3.77	0.10	2.50	--	7.9	450
12.20	0.20	0.21	6.31	0.28	4.37	0.07	3.50	.9	7.6	580

1 - Tritium Units, 1 TU represents one ^3H atom in 10^{18} atoms of normal hydrogen (^1H).

Table 4.19. Geochemical Results for the Fallowfield Site.

Depth (m)	Ca^{++}	Mg^{++}	Na^{+}	K^{+} (M/m^3)	Cl^{-}	SO_4^{--}	HCO_3^{-}	^3H TU[1]	pH	Conductivity mmho
1.60	1.95	1.11	1.91	0.09	3.46	0.52	3.45	31	7.2	658
3.00	2.15	1.44	2.65	0.16	4.70	0.70	4.25	30	7.7	735
4.40	1.00	1.03	8.13	0.31	8.45	0.43	4.30	14	8.0	1090
6.10	0.30	0.49	14.52	0.36	12.39	0.22	5.20	.9	8.0	1540
9.90	0.27	0.41	15.70	0.41	12.76	0.20	5.90	--	7.6	1650
12.50	0.25	0.37	16.09	0.43	13.52	0.16	5.20	.8	7.5	1550

1 - Tritium Units, 1 TU represents one ^3H atom in 10^{18} atoms of normal hydrogen (^1H).

Table 4.20. Geochemical Results for the Renfrew Site.

Depth (m)	Ca^{++}	Mg^{++}	Na^{+}	K^{+} (M/m^3)	Cl^{-}	SO_4^{--}	HCO_3^{-}	^3H TU[1]	pH	Conductivity mmho
1.50	3.94	3.56	11.39	0.10	20.98	0.52	3.75	--	6.5	4100
3.05	3.17	3.24	10.22	0.19	20.00	0.34	3.40	37	6.9	3450
4.60	3.87	3.13	8.26	0.16	19.71	0.41	3.20	--	7.1	2910
5.90	3.69	2.39	4.40	0.18	12.67	0.53	2.80	38	7.2	1850
9.15	0.93	1.25	1.74	0.23	3.41	0.23	2.20	2	7.6	660
12.20	0.62	1.10	2.04	0.38	3.66	0.20	1.75	3	7.7	650

1 - Tritium Units, 1 TU represents one ^3H atom in 10^{18} atoms of normal hydrogen (^1H).

Table 4.21. Geochemical Results for the Casselman Site.

Depth (m)	Ca^{++}	Mg^{++}	Na^{+}	K^{+} (M/m^3)	Cl^{-}	SO_4^{--}	HCO_3^{-}	^3H TU[1]	pH	Conductivity mmho
1.30	2.50	1.05	0.97	0.03	2.90	1.25	2.00	--	6.6	640
3.05	0.90	1.27	2.86	0.04	2.25	0.94	2.50	30	6.8	610
4.40	0.69	1.34	2.12	0.09	2.08	0.43	3.15	34	7.3	640
6.40	1.10	1.15	9.57	0.21	5.27	0.89	6.15	17	7.7	1200
9.15	0.28	0.47	10.09	0.23	5.07	0.21	5.75	--	8.1	960
12.20	0.19	0.39	12.96	0.27	6.48	0.10	6.60	.8	8.3	1160

1 - Tritium Units, 1 TU represents one ^3H atom in 10^{18} atoms of normal hydrogen (^1H).

Table 4.22. Results of Porewater Analysis, NRC Site.

Depth (m)	Ca^{++}	Mg^{++}	Na^{+}	K^{+}	Cl^{-}	SO_4^{--}	pH
			(M/m^3)				
1.70	1.27	0.23	1.14	0.42	2.25	0.87	7.00
2.60	1.07	0.32	1.26	0.20	2.68	0.71	7.05
4.00	0.70	0.31	1.78	0.26	2.51	0.17	7.73
5.50	0.62	0.36	3.26	0.28	2.56	0.11	7.25
8.15	0.25	0.15	4.09	0.31	3.10	0.07	8.30
12.50	0.15	0.09	6.65	0.31	3.66	0.11	8.13

Table 5.0. Soil Description: Physical and Chemical Properties
TEST #1 & 2, FALLOWFIELD

PROPERTY	METHOD OF MEASUREMENT	VALUE OBTAINED
Specific gravity	ASTM D854	2.76
Moisture content (%)	ASTM D2216	42
Saturation (%)		100
Porosity (%)		54
Dry density (g/cm)		1.27
Liquid limit (g/g)	ASTM D4318	41
Plasticity index (g/g)	ASTM D4318	19
Sieve analysis		
Silt (0.002-0.075 mm)	ASTM D1140	50
Clay (<0.002 mm)	ASTM D1140	40
Cation exchange capacity (meq/100 g dry wt.)		23.0-26.5[‡]
pH of porewater		7.8
Background ion concentration (porewater, mg/l)		
Cl^-		181
Na^+		240-252[‡]
K^+		22
Mg^{++}		100
Ca^{++}		260
Exchangeable cations (meq/100 g dry wt.)		
Na^+		0.58-0.60[‡]
K^+		0.35-1.08
Mg^{++}		1.85-2.60
Ca^{++}		20.21-23.0
SAR		17.8%

‡ Range of analysis

Table 5.1. Soil Description: Physical and Chemical Properties
TEST #4, FALLOWFIELD

PROPERTY	METHOD OF MEASUREMENT	VALUE OBTAINED
Specific gravity	ASTM D854	2.76
Moisture content (%)	ASTM D2216	41
Saturation (%)		100
Porosity (%)		53
Dry density (g/cm)		1.29
Liquid limit (g/g)	ASTM D4318	41
Plasticity index (g/g)	ASTM D4318	19
Sieve analysis		
Silt (0.002-0.075 mm)	ASTM D1140	50
Clay (<0.002 mm)	ASTM D1140	40
Cation exchange capacity (meq/100 g dry wt.)		22.6-28.71[†]
pH of porewater		7.8
Background ion concentration (porewater, mg/l)		
Cl^-		270
Na^+		310
K^+		27
Mg^{++}		94
Ca^{++}		207
Exchangeable cations (meq/100 g dry wt.)		
Na^+		0.75-0.80[†]
K^+		0.56-0.67
Mg^{++}		1.96-2.72
Ca^{++}		19.26-24.61
SAR		25.2%

[†] Range of analysis

Table 5.2. Soil Description: Physical and Chemical Properties Test #3, Renfrew

PROPERTY	METHOD OF MEASUREMENT	VALUE OBTAINED
Specific gravity	ASTM D854	2.70
Moisture content (%)	ASTM D2216	37
Saturation (%)		100
Porosity (%)		50
Dry density (g/cm)		1.35
Liquid limit (g/g)	ASTM D4318	44
Plasticity index (g/g)	ASTM D4318	20
Sieve analysis		
Silt (0.002-0.075 mm)	ASTM D1140	42
Clay (>0.002 mm)	ASTM D1140	58
Cation exchange capacity (meq/100 g dry wt.)		44.4-55.6[†]
pH of porewater		7.0
Background ion concentration (porewater, mg/l)		
Cl^-		1050
Na^+		230
K^+		10
Mg^{++}		130
Ca^{++}		460
Exchangeable cations (meq/100 g dry wt.)		
Na^+		0.53-0.55[†]
K^+		0.78-1.02
Mg^{++}		6.27-6.75
Ca^{++}		36.50-47.37
SAR		13.4%

[†] Range of analysis

Table 5.3. Soil Description: Physical and Chemical Properties Test #5, Casselman

PROPERTY	METHOD OF MEASUREMENT	VALUE OBTAINED
Specific gravity	ASTM D854	2.70
Moisture content (%)	ASTM D2216	47
Saturation (%)		100
Porosity (%)		56
Dry density (g/cm)		1.19
Liquid limit (g/g)	ASTM D4318	58
Plasticity index (g/g)	ASTM D4318	29
Sieve analysis		
Silt (0.002-0.075 mm)	ASTM D1140	36
Clay (<0.002 mm)	ASTM D1140	64
Cation exchange capacity (meq/100 g dry wt.)		47.90-56.34[†]
pH of porewater		7.3
Background ion concentration (pore-water, mg/l)		
Cl^-		210
Na^+		90
K^+		7
Mg^{++}		35
Ca^{++}		34
Exchangeable cations (meq/100 g dry wt.)		
Na^+		0.58-0.61[†]
K^+		1.00-1.34
Mg^{++}		6.50-7.90
Ca^{++}		39.40-46.83
SAR		15.3%

[†] Range of analysis

Table 5.4. Diffusion Testing Program

Test serie	Site & depth	Source leachate (initial concn.)	Duration of test (days)
1	Fallowfield (3.0 m)	deionized water, $C_0 = 0$	16
2	Fallowfield (3.0 m)	Single salt NaCl, C_0: $Na^+ = 755$ (mg/l) $Cl^- = 1220$ (mg/l)	15
3	Renfrew (4.2 m)	Deionized water, $C_0 = 0$	16
4	Fallowfield (3.6 m)	Single salt NaCl, C_0: $Na^+ = 792$ (mg/l) $Cl^- = 1290$ (mg/l)	15
5	Casselman (4.6 m)	Single salt NaCl, C_0: $Na^+ = 755$ (mg/l) $Cl^- = 1220$ (mg/l)	16

Table 5.5. Summary of Mass Balance Calculations

Test Series	Soil	Specie	Mass Balance[1] (%)
1 Deionized Water	Fallowfield	Cl	23.8
		Na	20.7
		K	20.5
		Mg	33.1
		Ca	15.2
3 Deionized Water	Renfrew	Cl	15.0
		Na	15.3
		K	13.1
		Mg	9.6
		Ca	12.6
2 Single Salt	Fallowfield	Na	10.9
		Cl	11.7
4 Single Salt	Fallowfield	Na	15.3
		Cl	13.0
5 Single Salt	Casselman	Na	14.1
		Cl	13.7

[1] Only average values given here.

Sample Calculation:

Mass Flux (Ct) = 20 mg

Additional Soluble Ion (Cs) = 9 mg

Additional Adsorbed Ion (Ca) = 8 mg

Mass Balance Error = $\{1 - [(Cs + Ca)/Ct]\} \times 100$

$= \{1 - [(9 + 8)/20]\} \times 100 = 15\%$

Table 5.6. Summary of α Values For Test #1 & 3

Species	α	
	Test 1, Fallowfield	Test 3, Renfrew
Na	0.0005	0.0005
K	0.0008	0.0006
Mg	0.0002[†]	0.001
Ca	0.003[†]	0.012

[†] shows "apparent" desorption

Table 5.7. Effective Diffusion coefficients and Retardation Factors

Test series	Species	Diffusion coefficient ($\times 10^{-6}$ cm^2/s)	Retardation factor
1	Cl^-	6.5	1
	Na^+	3.4	1.5-1.6[‡]
	K^+	6.0	17.2-22.8
	Mg^{++}	3.8	12.4-4.9[‡]
	Ca^{++}	5.8	33-17[‡]
2	Cl^-	7.0	1[†]
	Na^+	6.5	2.2
3	Cl^-	6.0	1
	Na^+	4.0	2.0-2.1[‡]
	K^+	7.5	36-48
	Mg^{++}	4.6	4.8-8.1
	Ca^{++}	6.25	18-32.
4	Cl^-	7.0	1[†]
	Na^+	6.0	2.7
5	Cl^-	6.8	1[†]
	Na^+	5.8	3.6

[†] Retardation factor = $R = 1 + \rho K/\theta$.

[‡] Retardation factor = $R = 1 + (\rho/\theta)(\beta\gamma\exp(-\gamma c))$, where R is a function of solute concentration (C). The range given is due to the maximum difference between lowest and highest solute concentrations.

[‡] Indicates that greater adsorbtion occurs at the lower solute concentrations, and may indicate possible elution of the species.

FIGURES

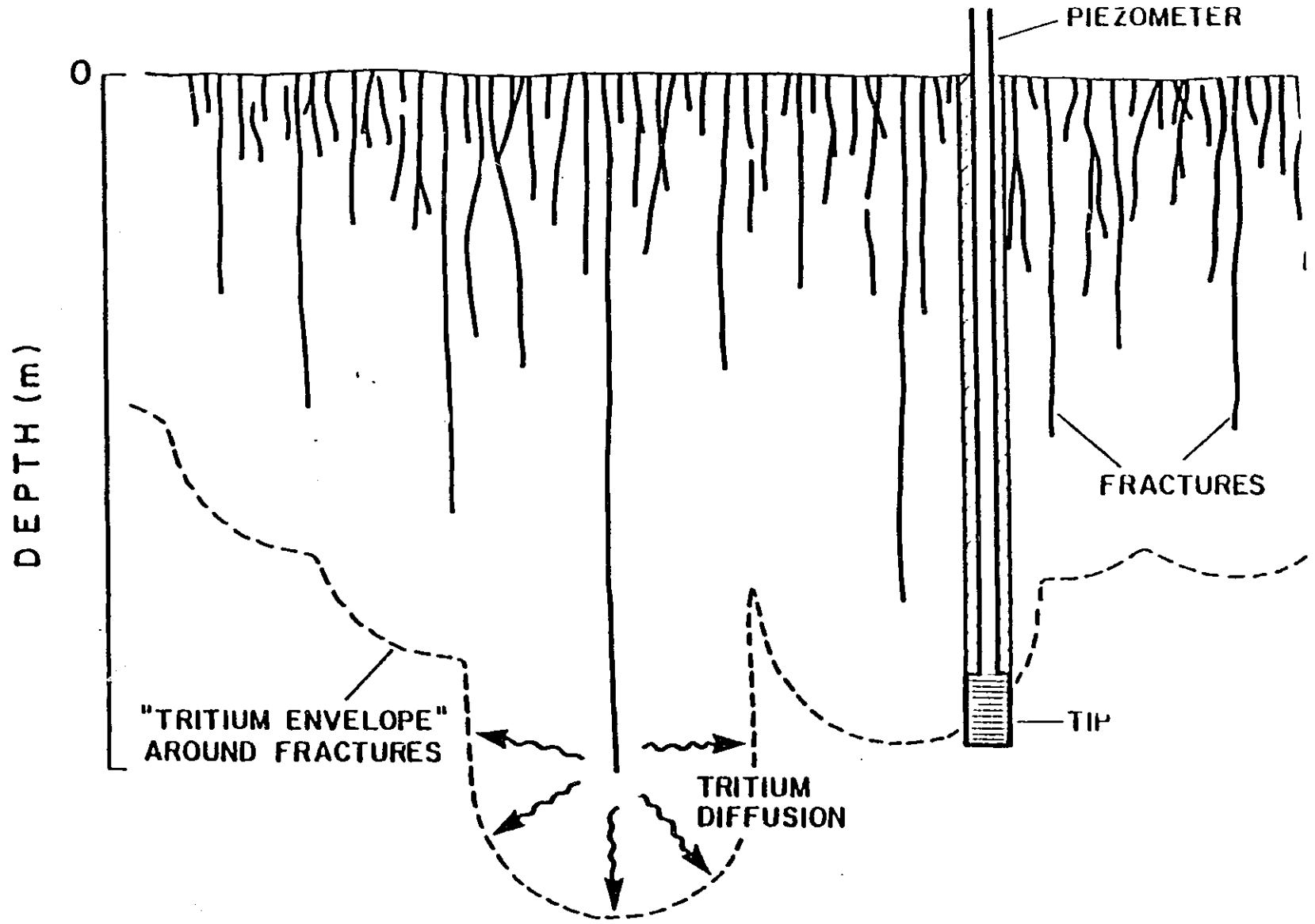

Figure 2.0. A Conceptual Model after Ruland et al. (1989) for Tritium Distribution in a Fractured Clay Deposit

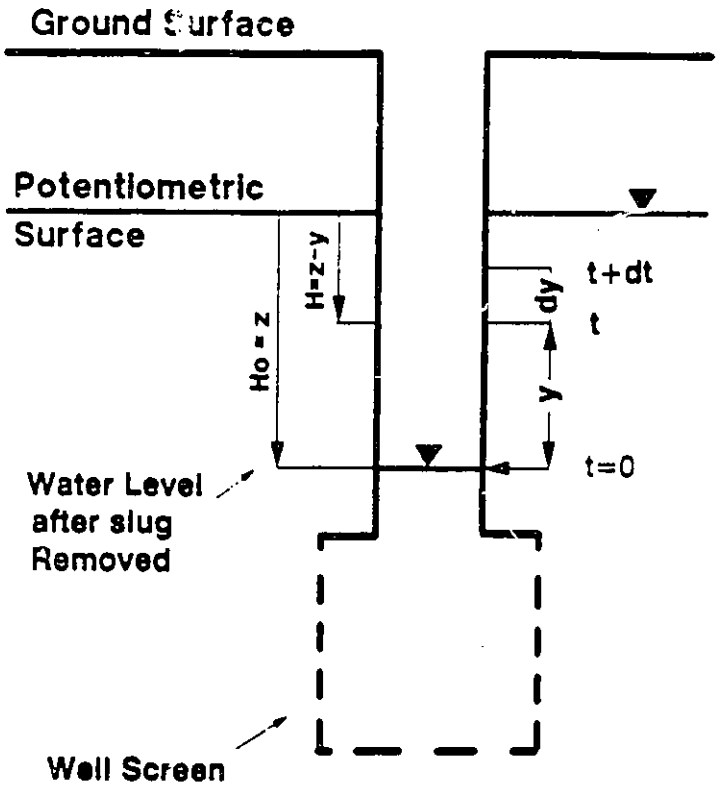

Figure 2.1. The Basic Definitions for the Hvorslev Slug Test Method [after Wylie and Wood (1990)]

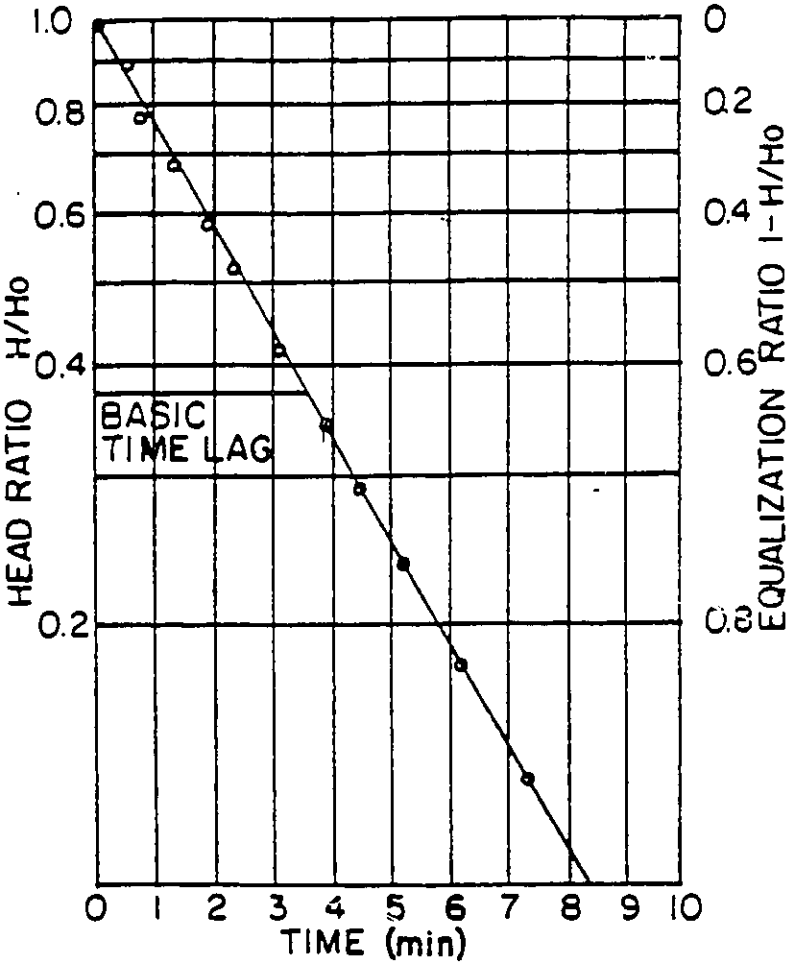

Figure 2.2. The Semilog Graph Used to Calculate the Basic Time Lag [after Hvorslev (1951)]

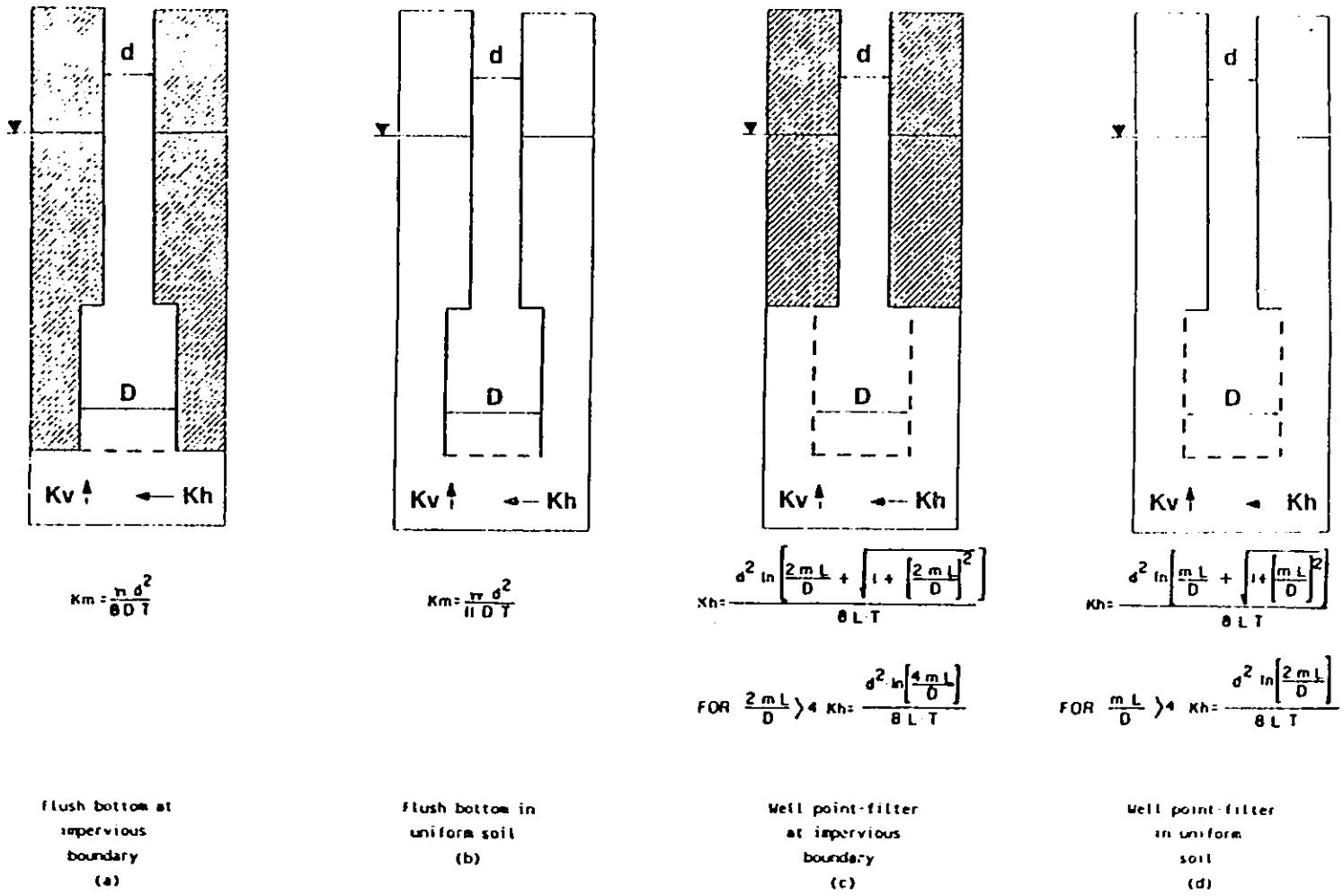

Figure 2.3. Formulas for Different Boundary Conditions Used to Calculate Hydraulic Conductivity [after Hvorslev (1951)]

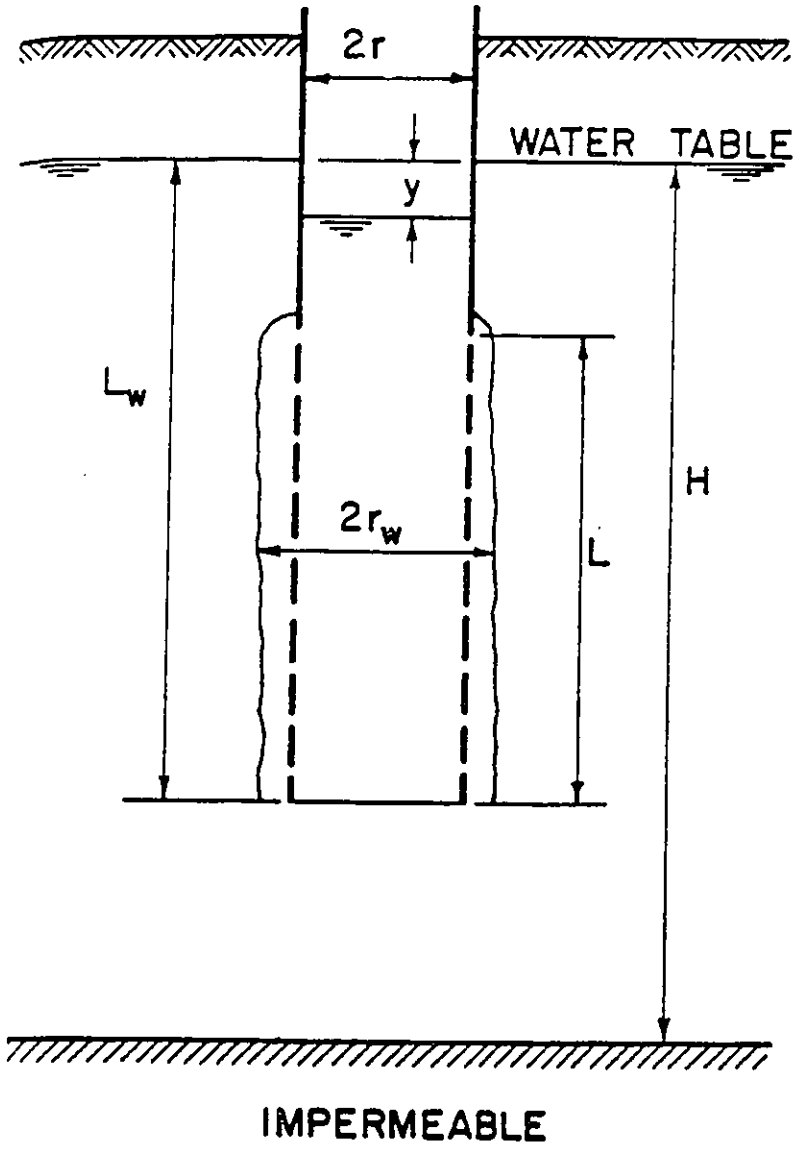

Figure 2.4. Geometry and Symbols Used for the Bouwer and Rice Slug Test for a Partially Screened Well in an Unconfined Aquifer with Gravel Pack [after Bouwer (1989)]

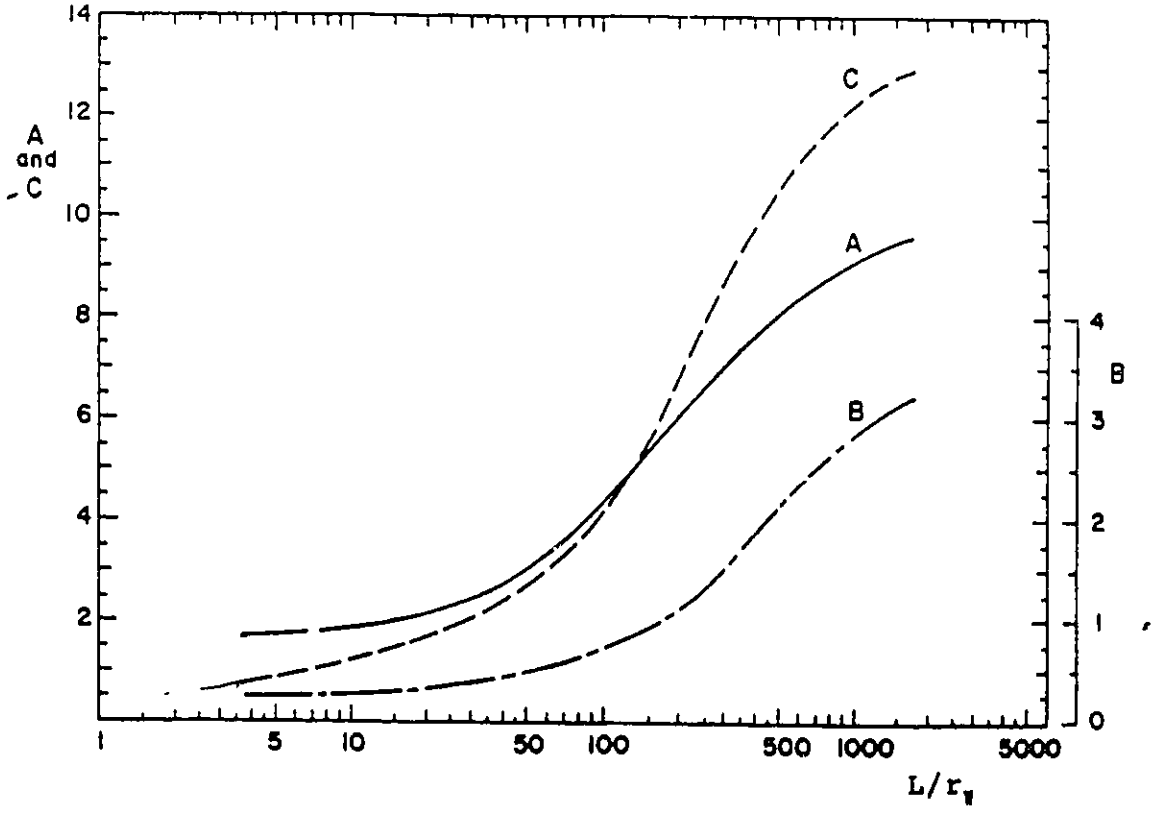

Figure 2.5. Bouwer and Rice Curves Relating the Coefficients A, B, and C to L/r_e [after Bouwer and Rice (1976)]

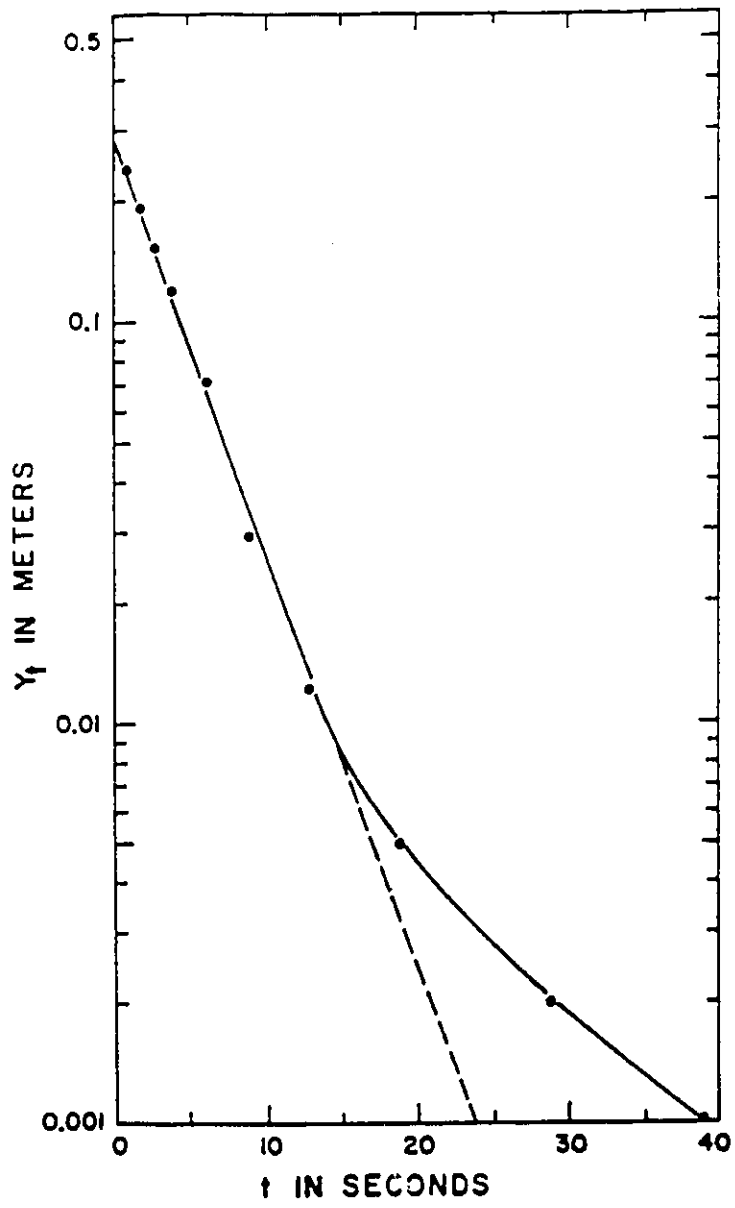

Figure 2.6. Graph of Log Y_t Versus t for the Bouwer and Rice Slug Test [after Bouwer (1989)]

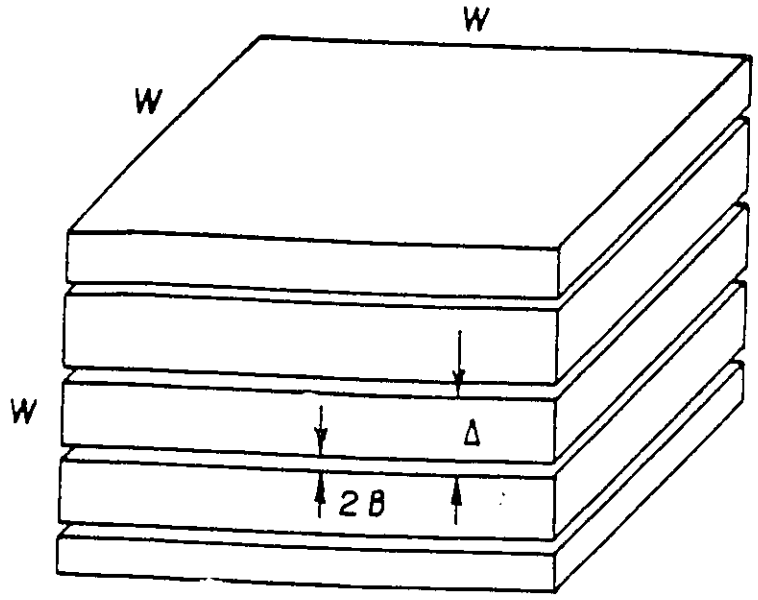

Figure 2.7. Snow's Parallel Plane Fractured Model [after Snow (1968)]

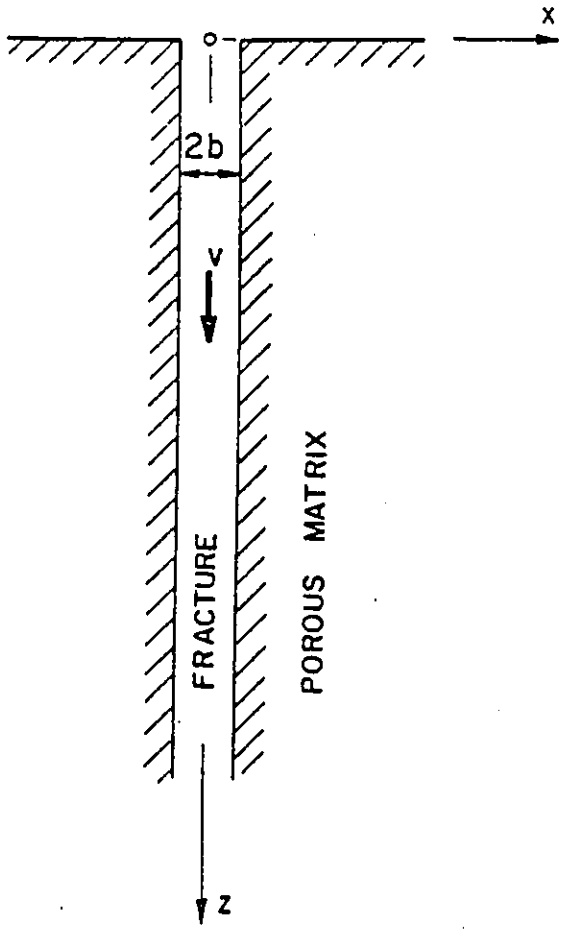

Figure 2.8. A Single Fracture-Matrix System [after Tang (1981)]

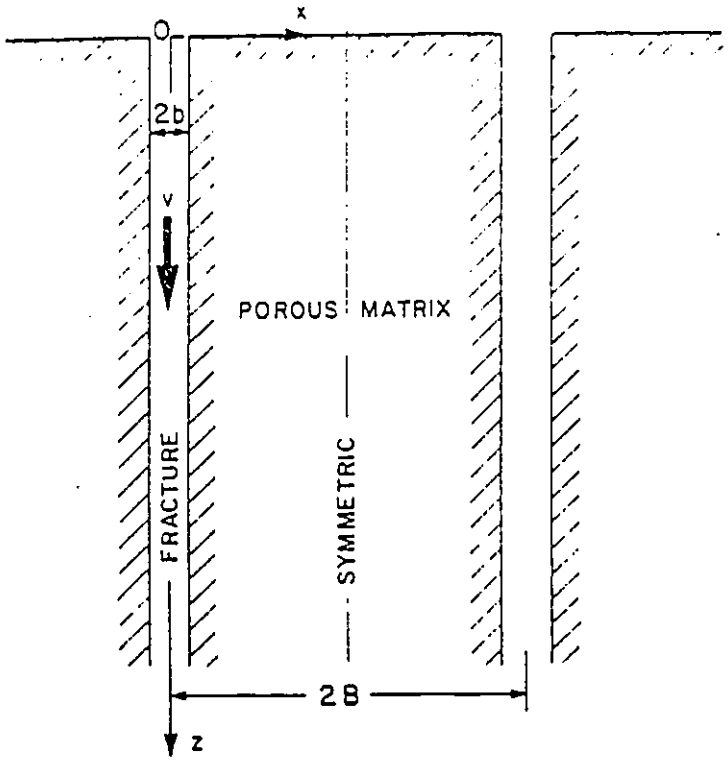

Figurer 2.9. A Parallel Fracture-Matrix System [after Sudicky and Frind (1982)]

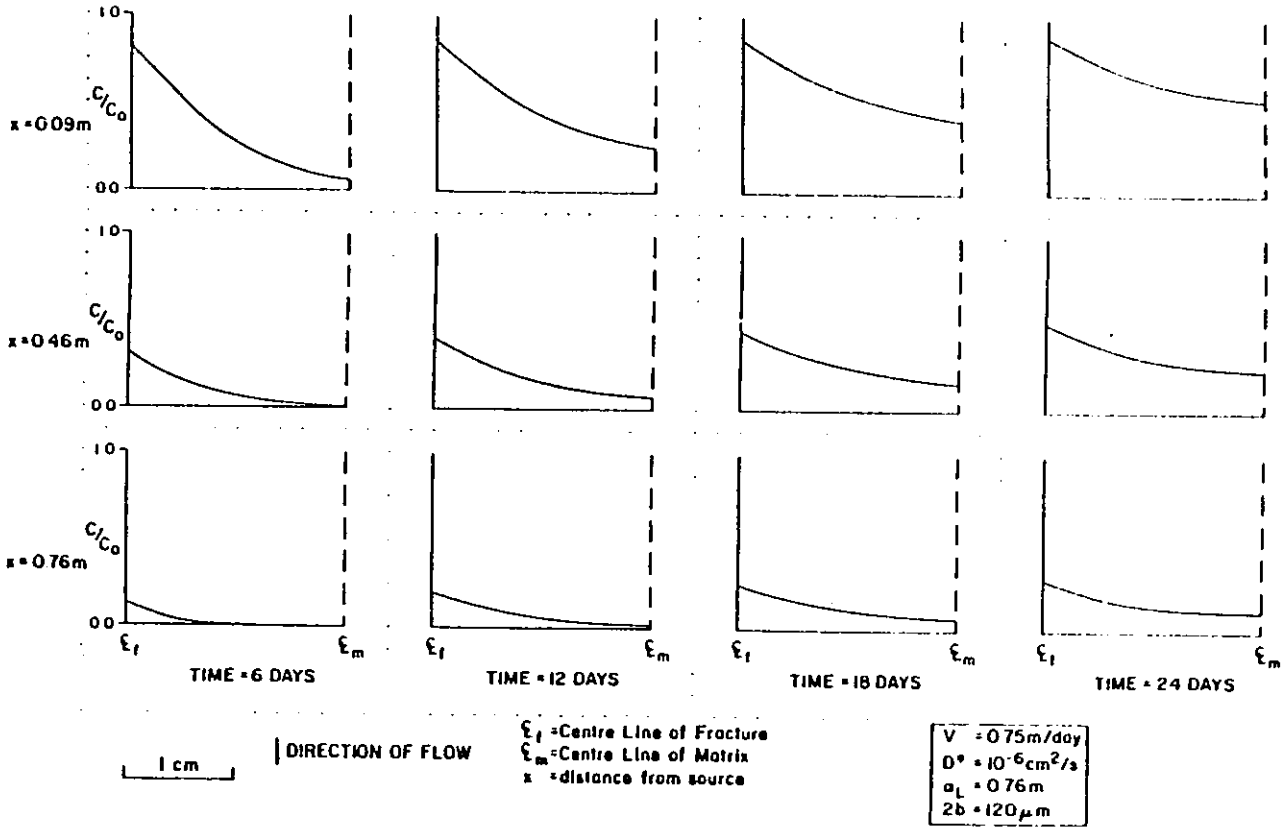

Figure 2.10. Matrix Concentration Profile at Various times and Location from Source, Demonstrating the Gradual Utilization of Matrix Storage Capacity [after Grisak and Pickens (1980)]

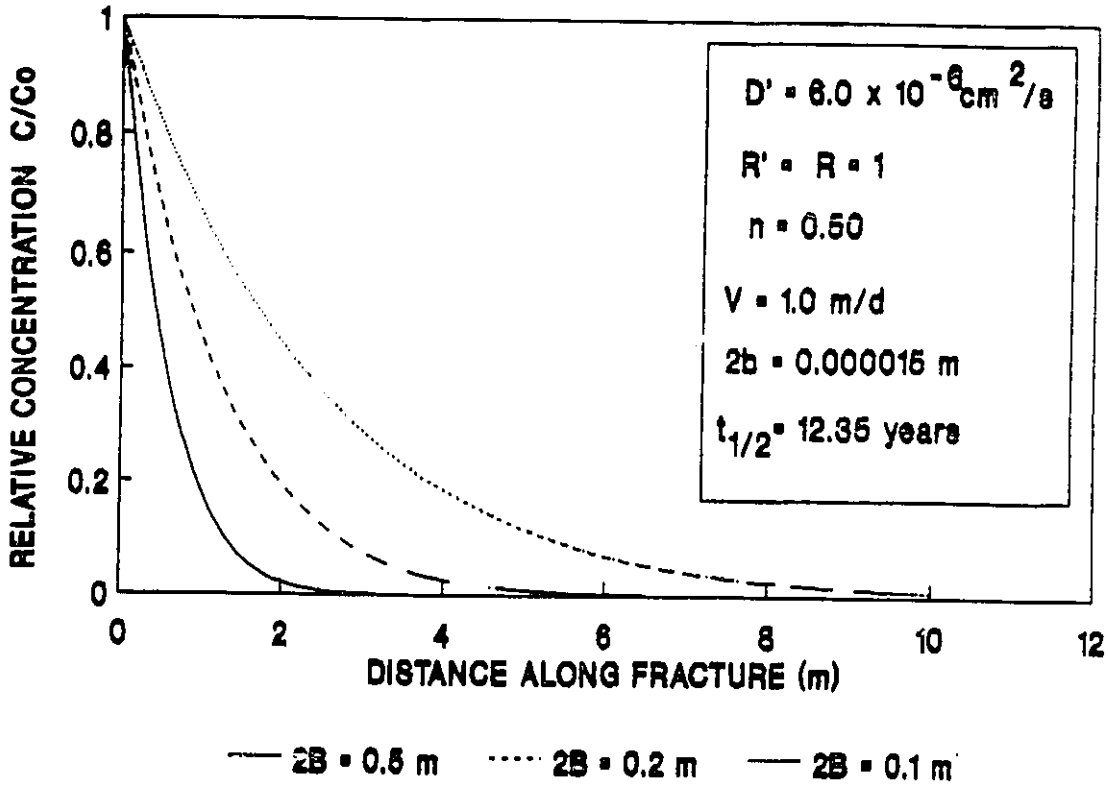

Figure 2.11. Comparison of Tritium Concentration Profile Along a Fracture at Steady State with Variation in Fracture Spacing Only

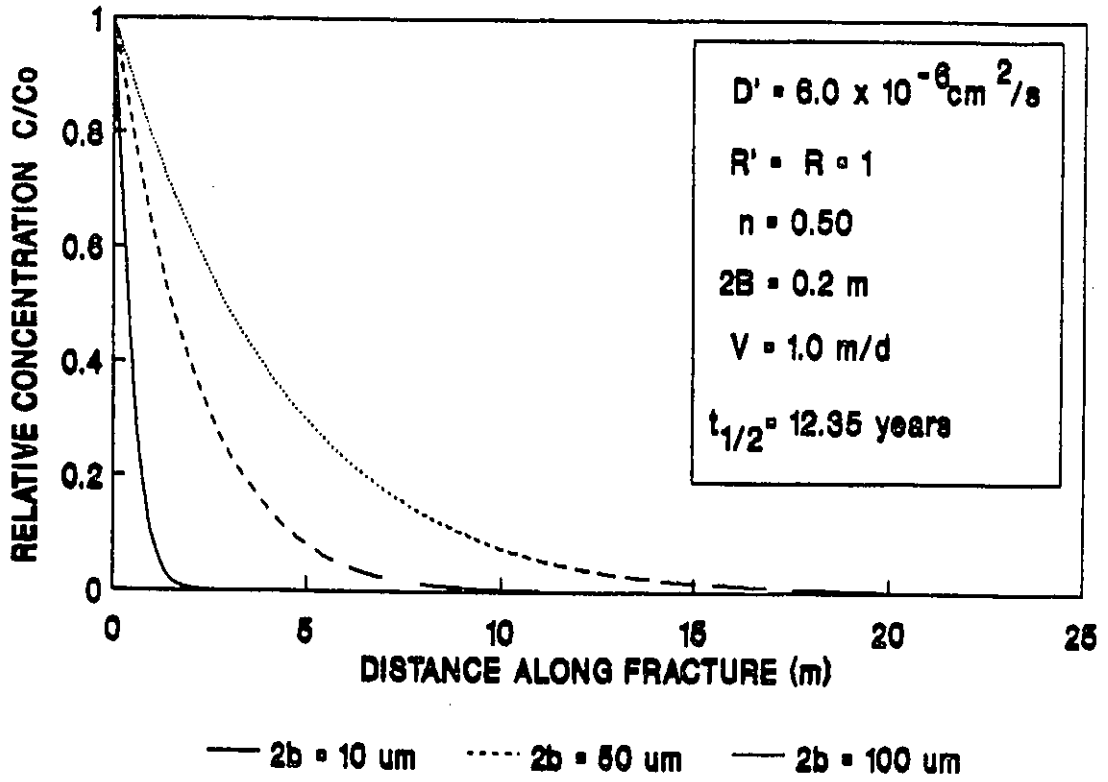

Figure 2.12. Comparison of Tritium Concentration Profile Along a Fracture at Steady State with Variation in Fracture Width Only

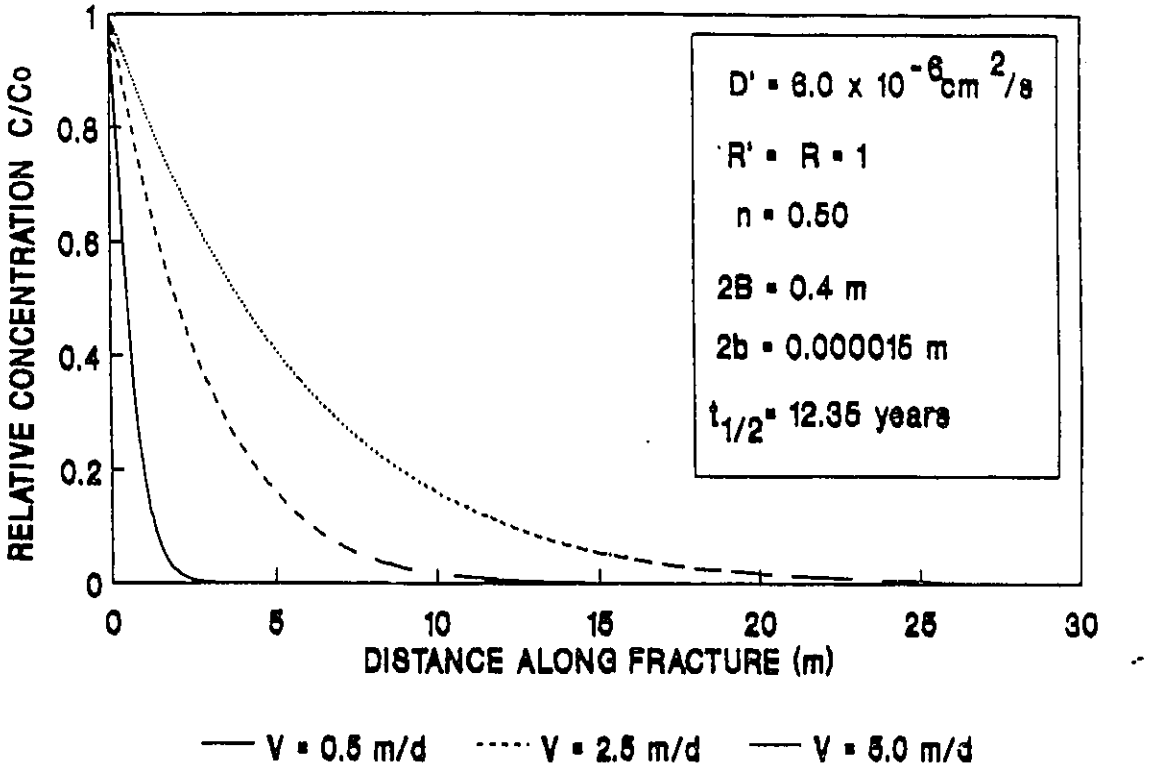

Figure 2.13. Comparison of Tritium Concentration Profile Along a Fracture at Steady State with Variation in Fracture Velocity Only

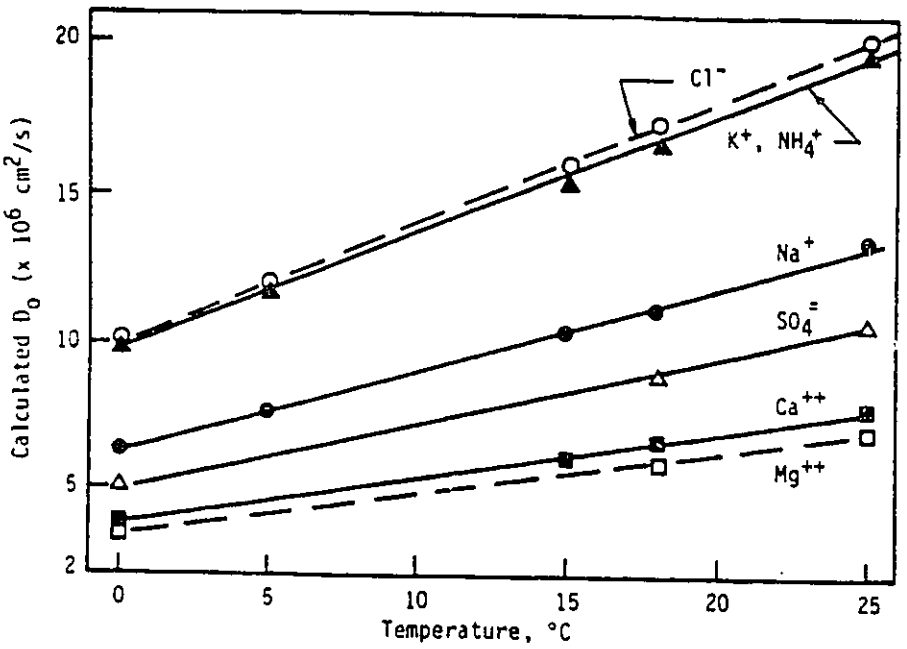

Figure 3.0. Relationship Between "Free Solution Diffusion" coefficient and Temperature [after Quigley et al. (1987)]

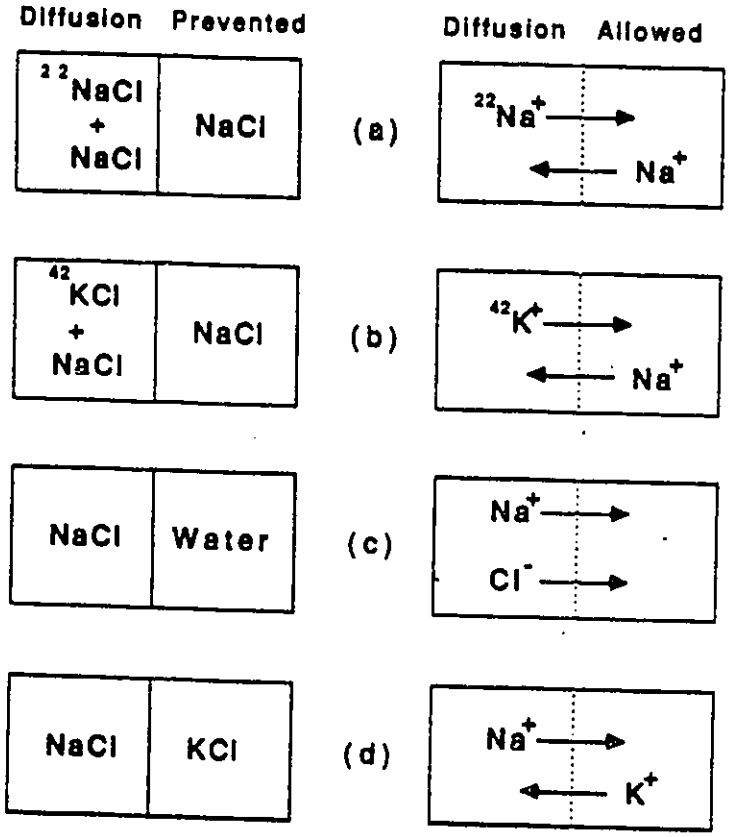

Figure 3.1. Different Diffusion Systems:(a)Self-Diffusion; (b)Tracer Diffusion; (c)Salt Diffusion; (d)Counterdiffusion [after Shackelford (1988)]

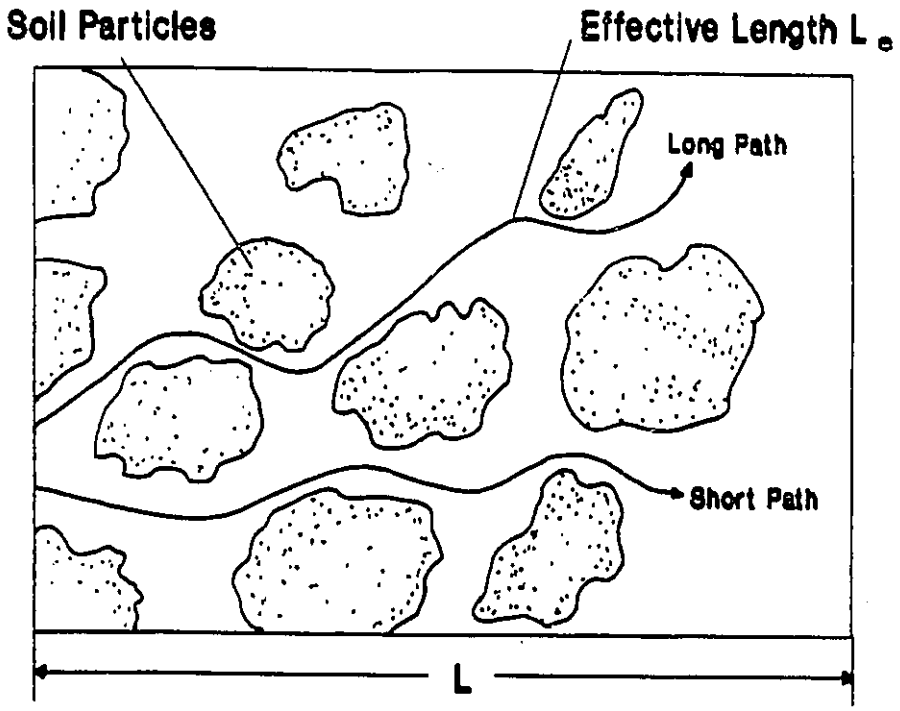

Figure 3.2. Concept of Tortuous Pathway in a Soil Sample with Different Flow Paths

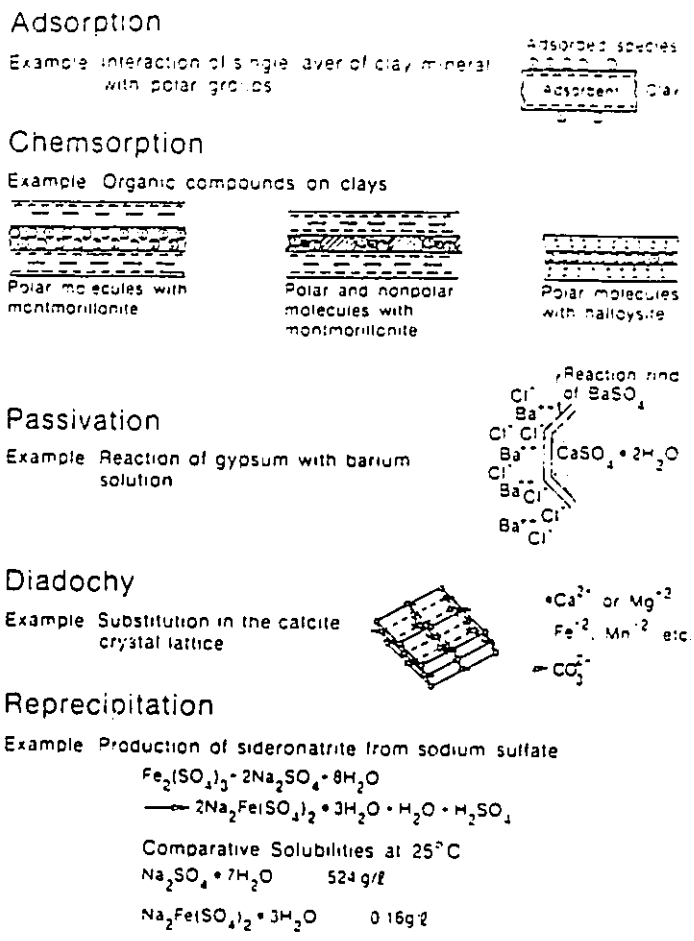

Figure 3.3. Possible Soil Retention Mechanisms [after Malone and Larson (1983)]

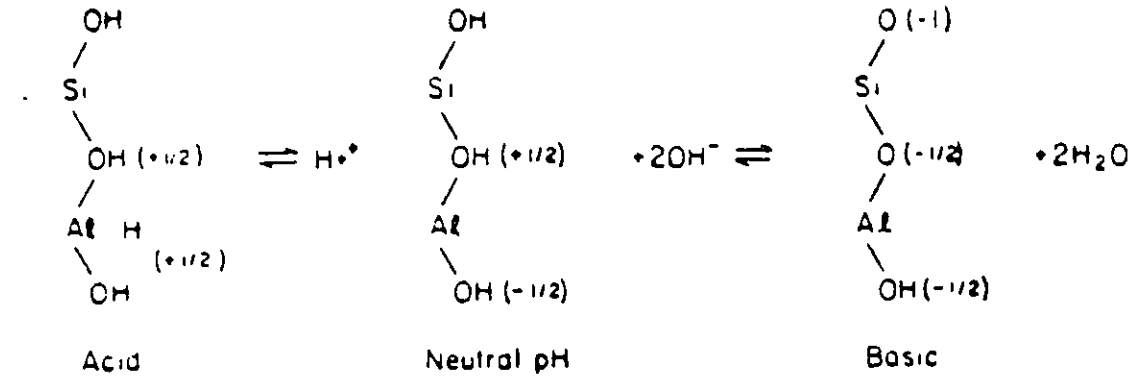

Figure 3.4. Representation of pH-Dependent Charges on Kaolinite's Broken Edges [after Schofield and Samson (1953)]

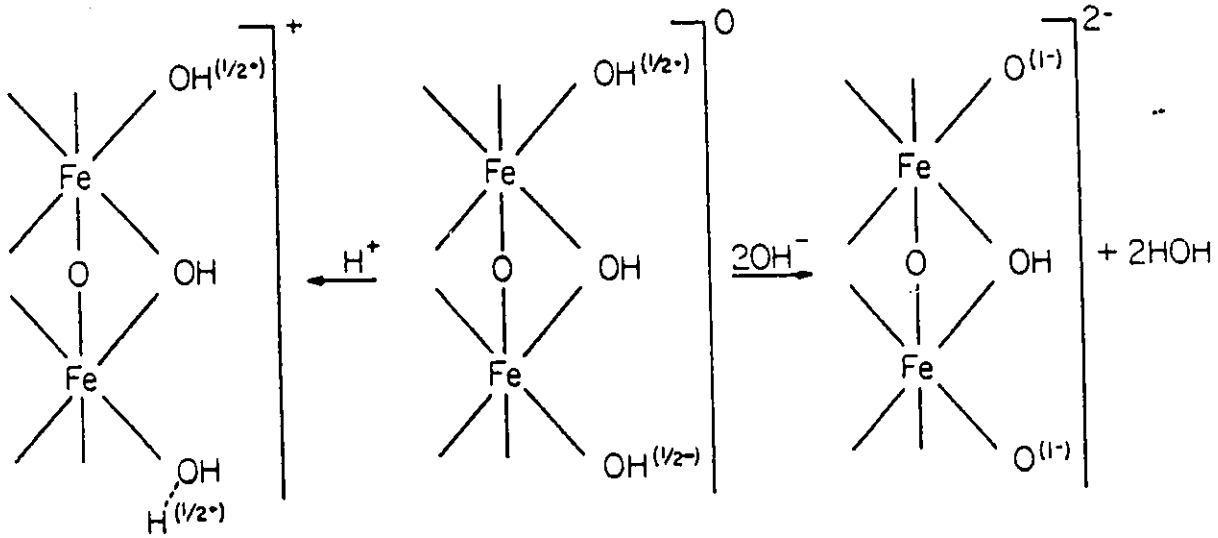

Figure 3.5. Schematic Representation of Charged Reactions and Zero Point Charge of a Iron Oxide in which Ion Dissolution Is the Charge Generating Process [after Sparks (1986)]

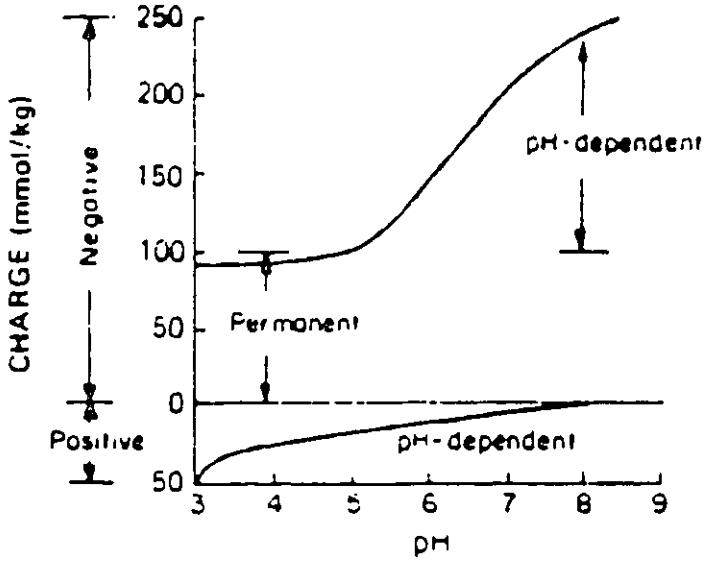

Figure 3.6. Representative Change in Total Soil Charge, Negative and Positive, with pH [after Guenzi (1974)]

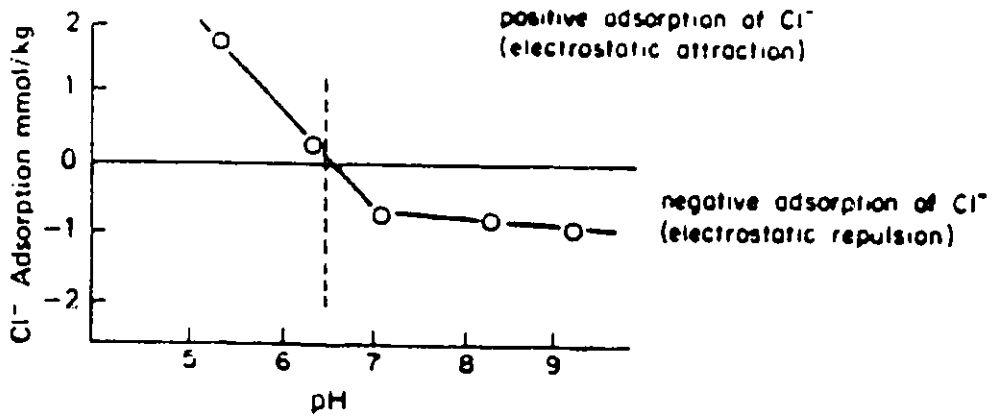

Figure 3.7. Adsorption of Chloride by Kaolinite at Various pH Values [after Schofield and Samson (1953)]

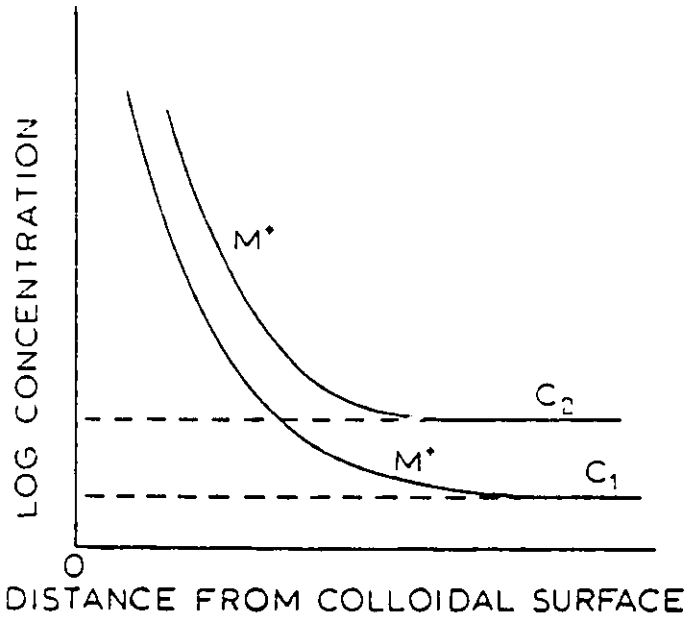

Figure 3.8. The Distribution of Two Different Cation Concentrations Away from a Negatively Charged Soil Surface, With the Effects of Anion Repulsion Neglected. The C.E.C. Is the Area Between the Curves and Their Corresponding Dashed Lines [after Sparks (1986)]

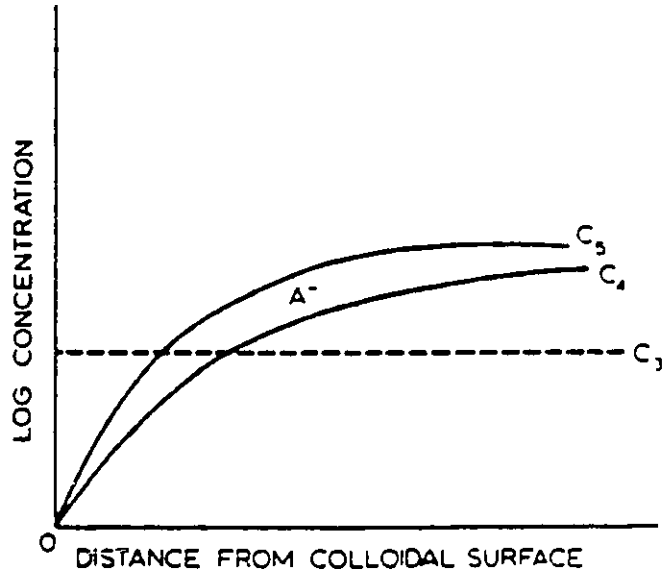

Figure 3.9. Distribution of Anions Near a Negatively Charged Soil Surface at Two Different Concentrations, Disregarding Cation Effects [after Sparks (1986)]

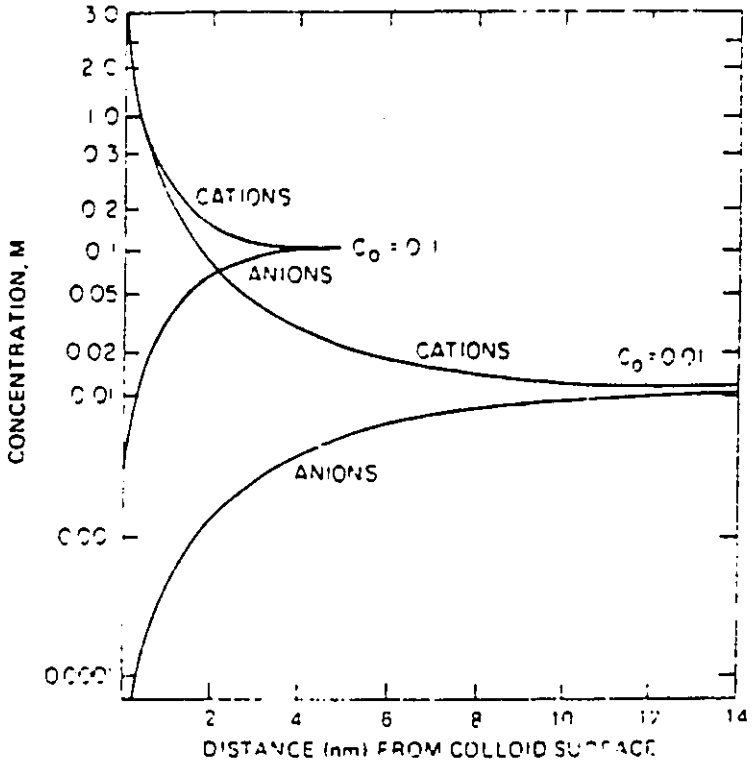

Figure 3.10. Distribution of Monovalent Cation and Anions Near the Charged Soil Surface of a Montmorillonite Particle [after Nielson et al. (1972)]

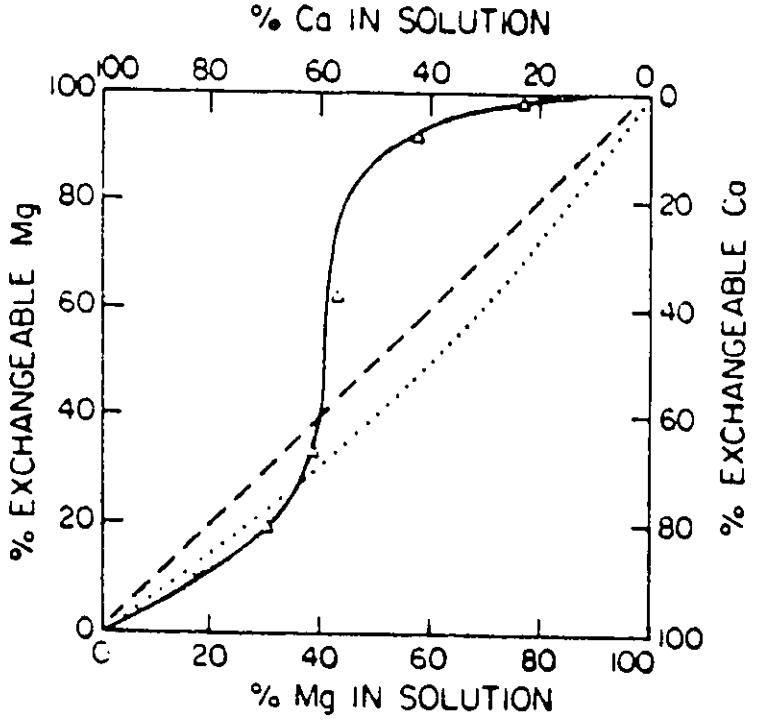

Figure 3.11. Ca-Mg Exchange in a Vermiculite Suspension. The Dashed Line Represents No Preference [after Peterson et al. (1965)]

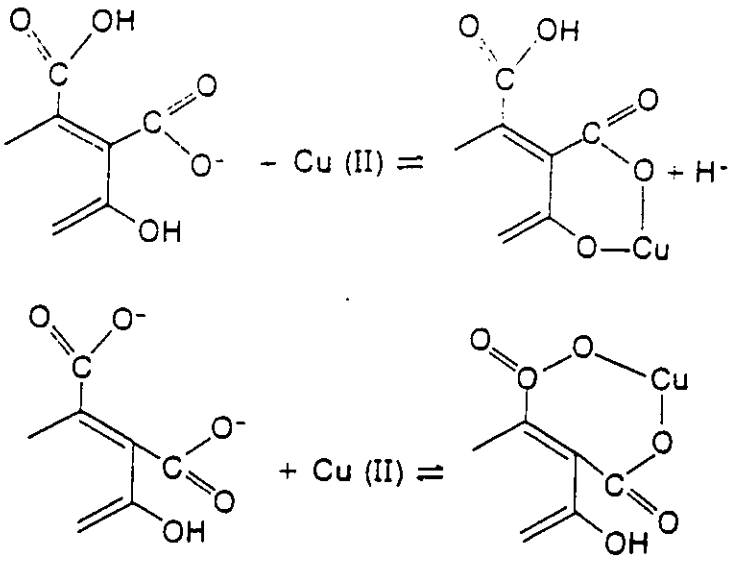

or

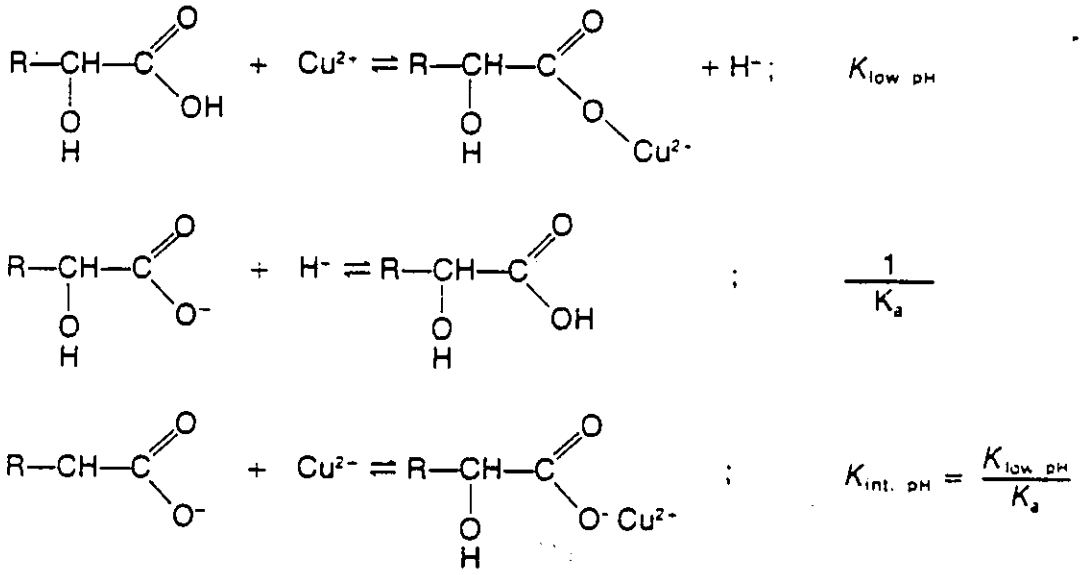

Figure 3.12. Organic Ligand Complexation with Heavy Metals [after Snoeyink and Jenkins (1980)]

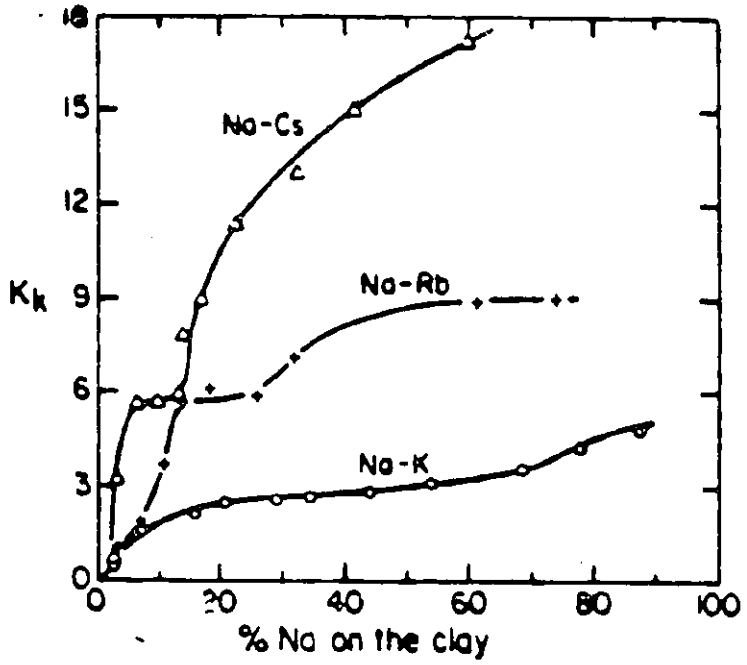

Figure 3.13. Variation in the Selectivity Coefficient K_k for an Attapulgite Clay [after Marshall and Garcia (1959)]

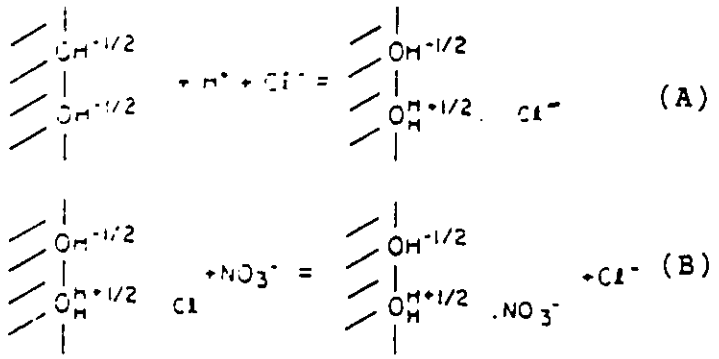

Figure 3.14. Nonspecific Anion Reactions at a Soil-Solution Interface:(A) Adsorption, (B) Anion Exchange [after Hingston et al. (1967)]

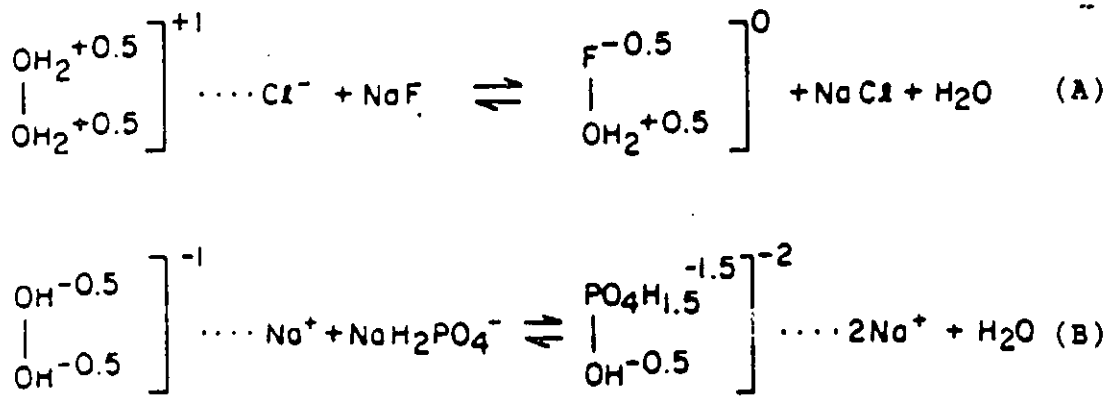

Figure 3.15. Specific Anion Reaction at a Solid-Solution Surface: (A) Neutralization, (B) Ionization of a Proton [after Hingston et al. (1968)]

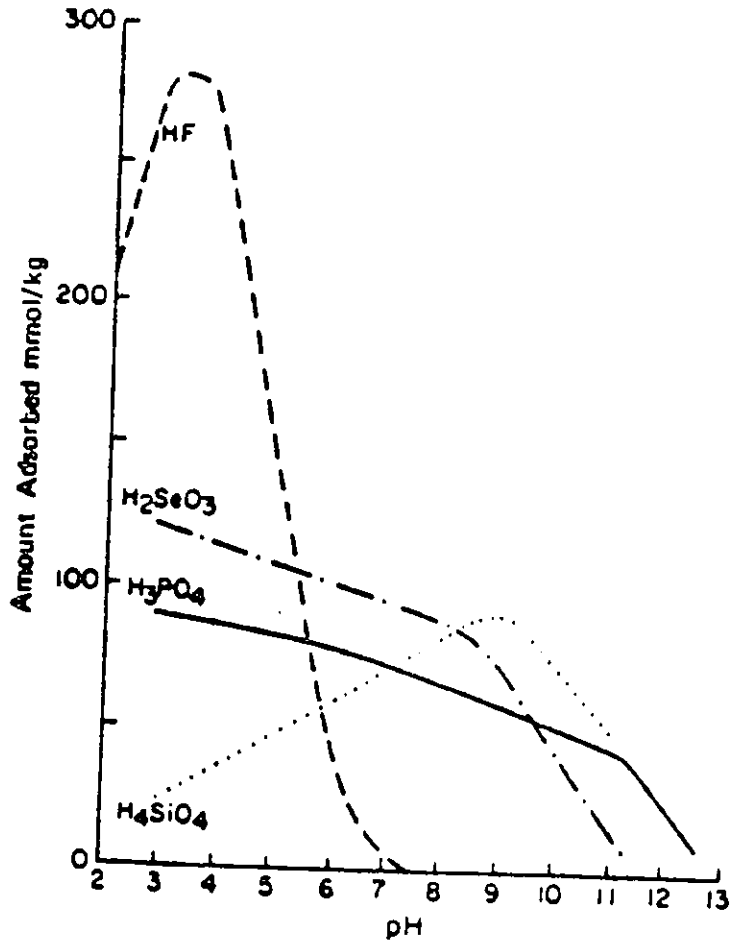

Figure 3.16. The Adsorption of Three Oxyacids and Fluoride on Goethite as a Function of pH. HF, pk = 3.45; H_2SeO_3, pK_2=8.35; H_3PO_4, pK_1=2.12, pK_2=7.21, pK_3=12.67; H_4SiO_4, pK_1=9.66 [after Hingston et al. (1968)]

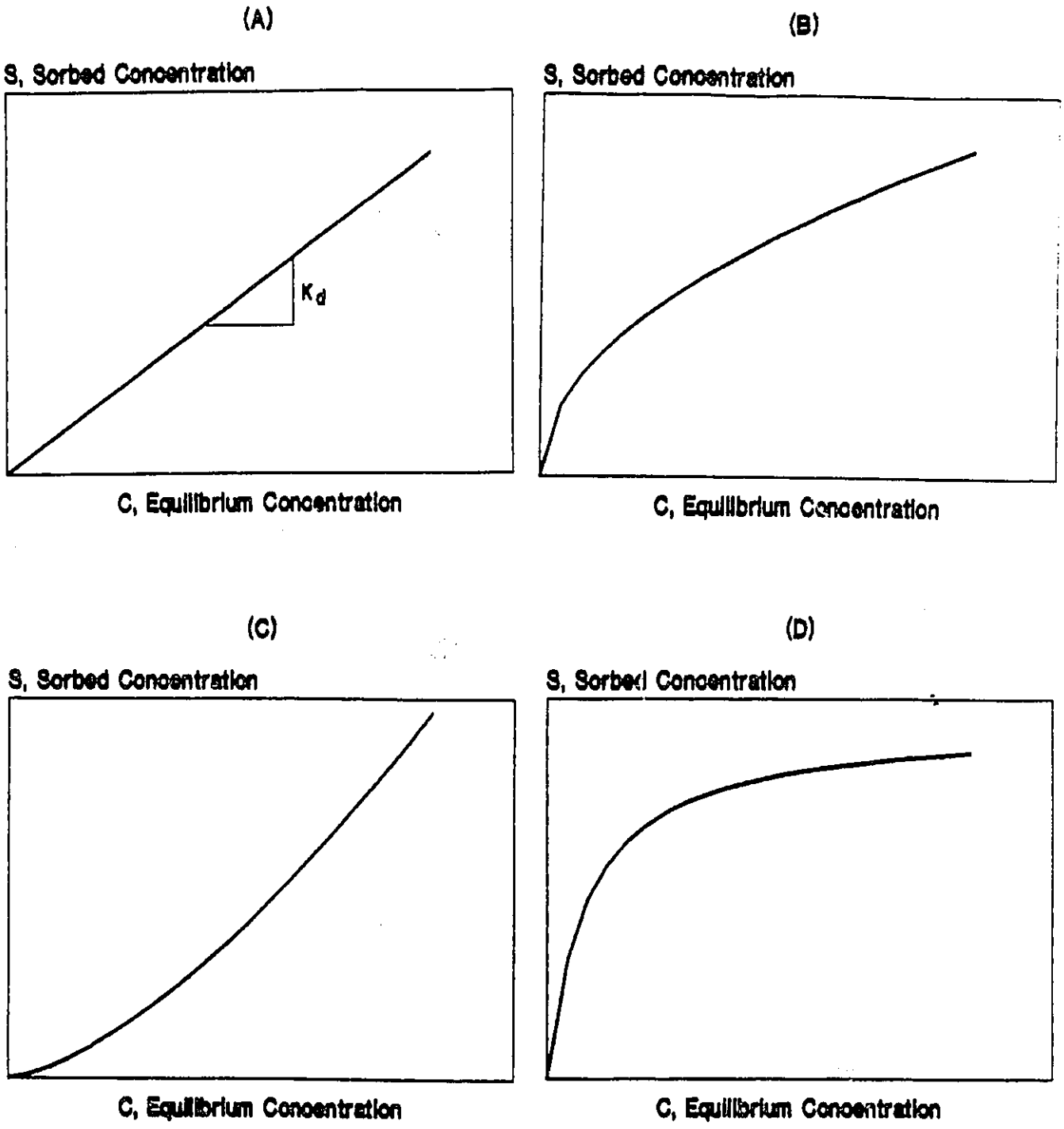

Figure 3.17. General Types of Adsorption Isotherms:(A)Linear; (B)Concave Nonlinear or Freundlich Type; (C)Convex Nonlinear; (D)Concave-Linear or Langmuir Type

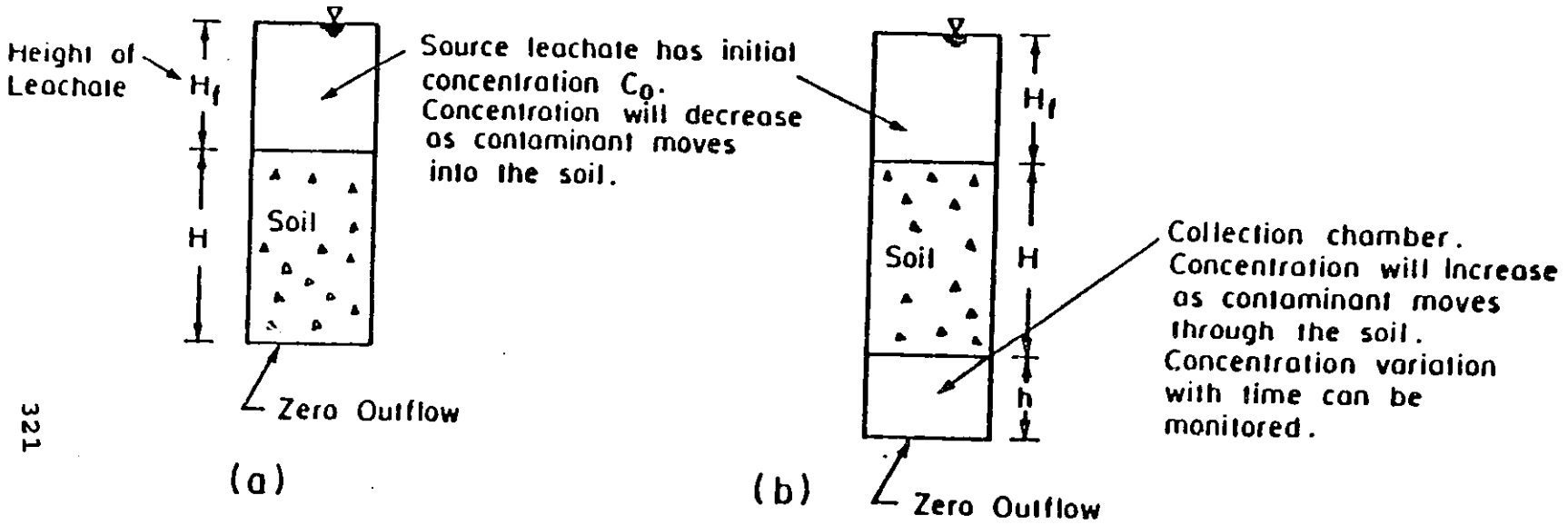

Figure 3.18. Schematic Representation of Two Different Boundary Conditions for Pure Diffusion Tests: (A) Zero Flux at the Base (B) Migration into a Collection Chamber [after Rowe et al. (1988)]

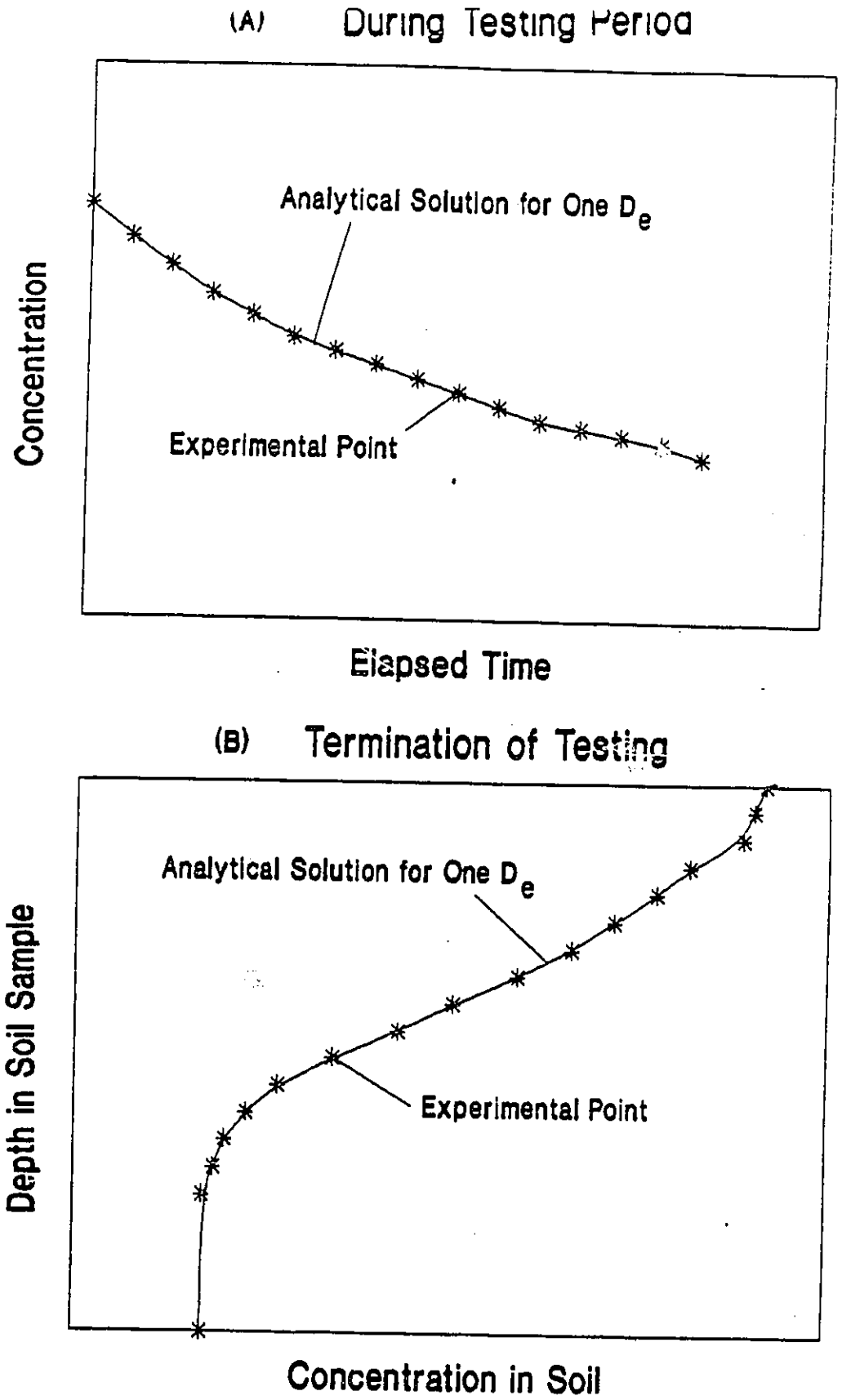

Figure 3.19. Schematic Illustration of Reservoir Method for Measuring Effective Diffusion:(A) Concentration in the Source Reservoir with Time; (B) Concentration Profile in the Soil Sample after Termination of Test [after Rowe et al. (1988)]

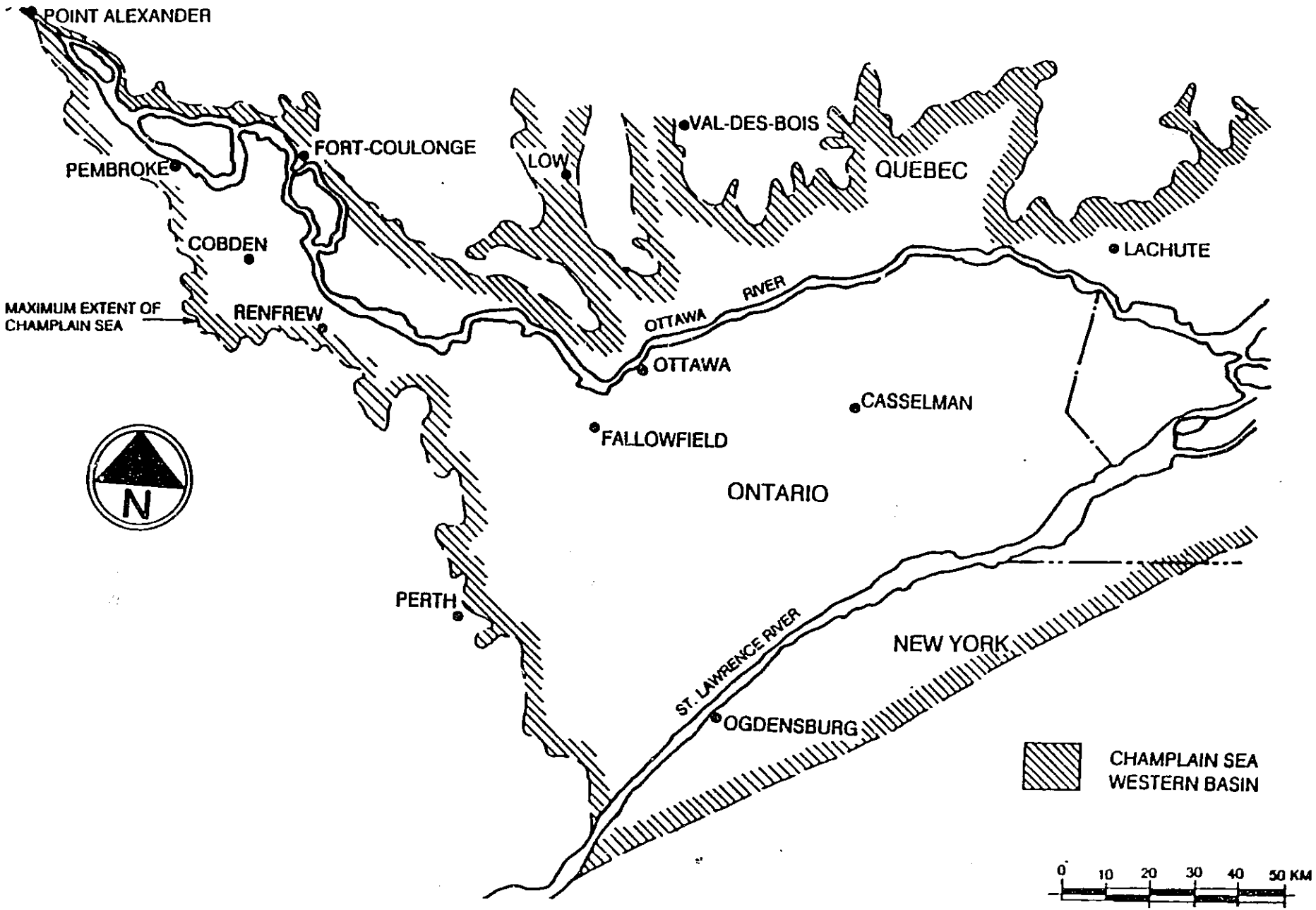

Figure 4.0. The extent of the Western Champlain Sea basin, (after Rodrigues, 1988).

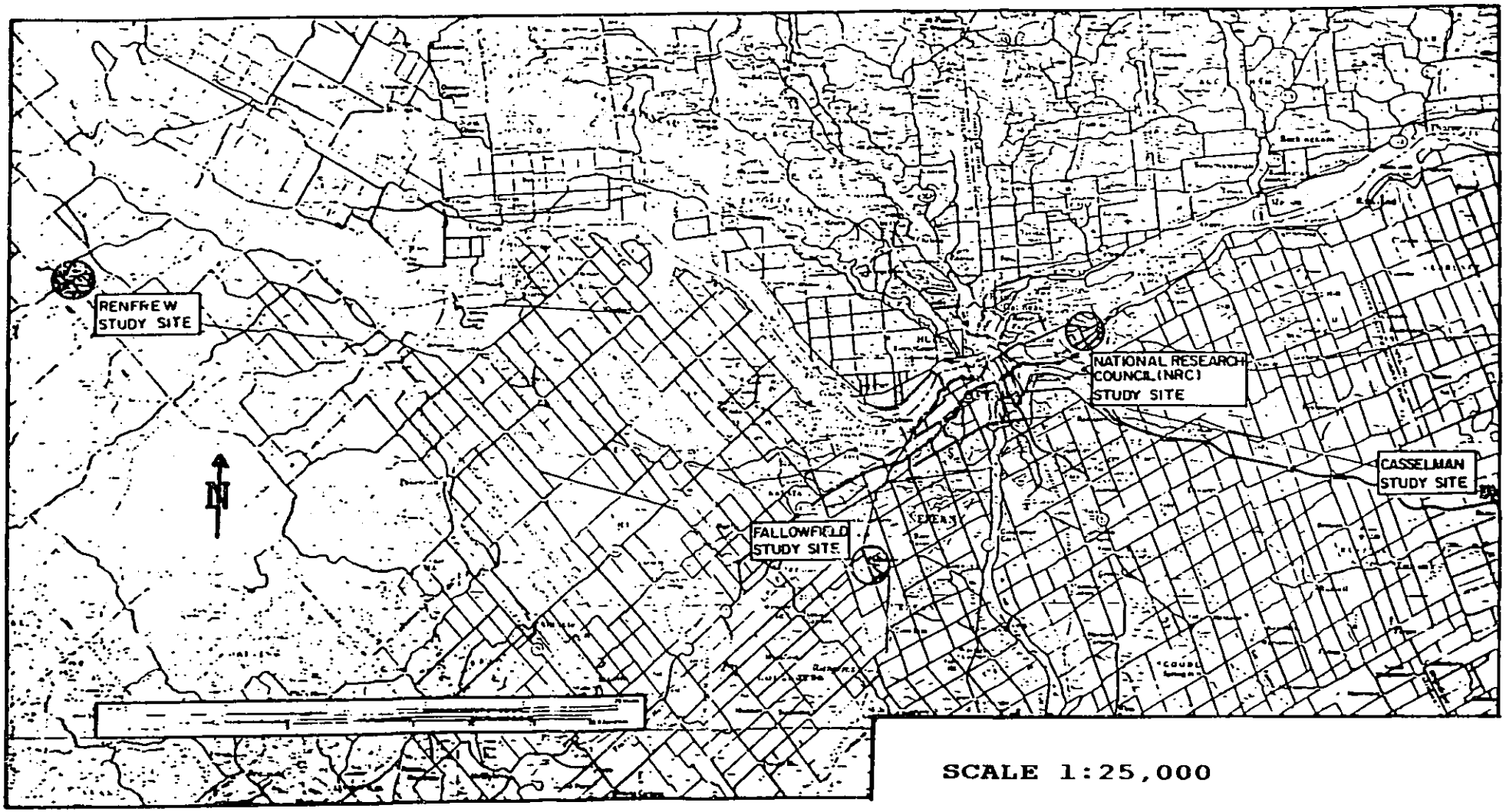

Figure 4.1. Locations of the four study sites.

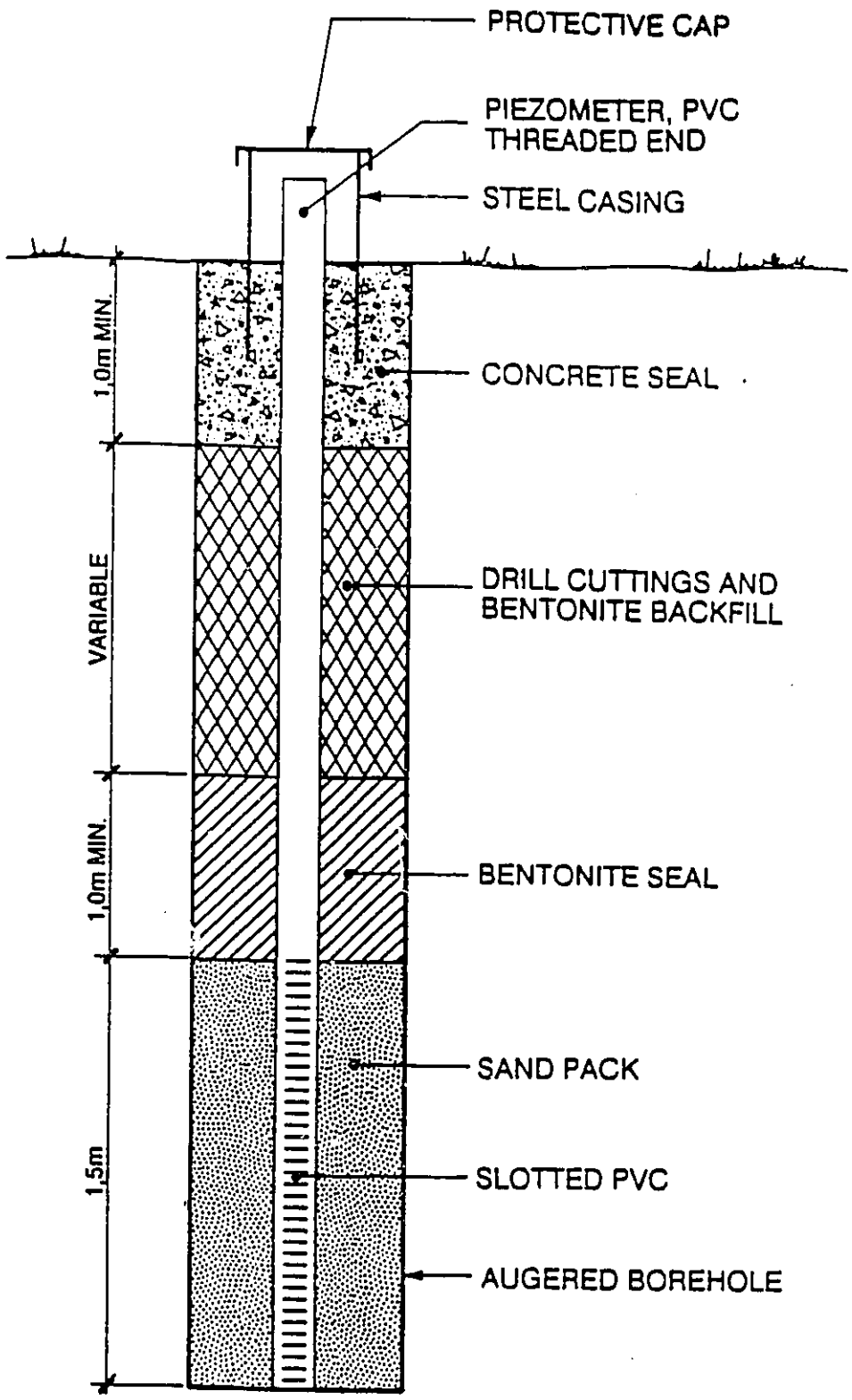

Figure 4.2. Typical borehole piezometer installation technique (courtesy of Fondex Ltd.).

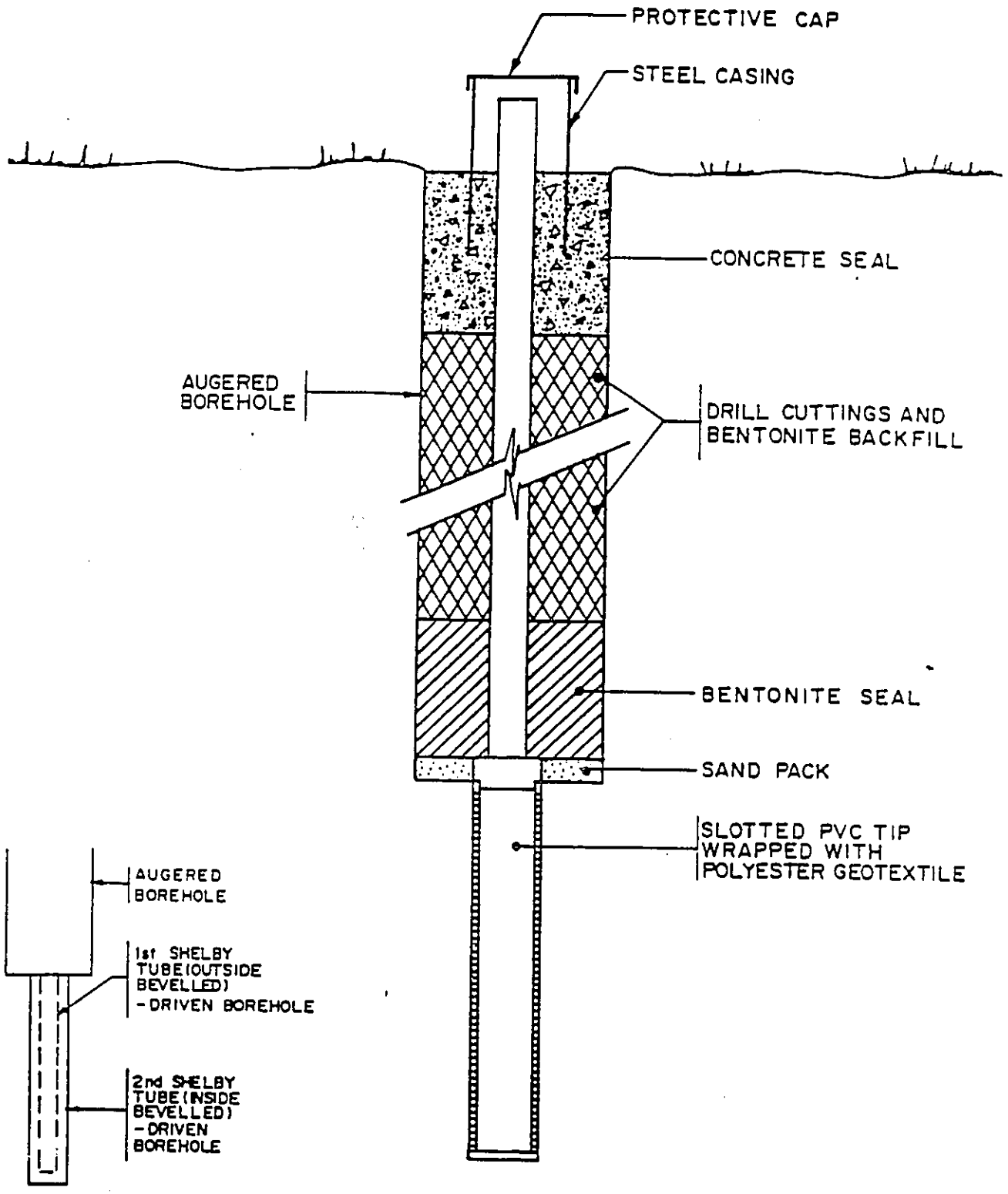

Figure 4.3. Typical double-Shelby installation technique (courtesy of Fondex Ltd.).

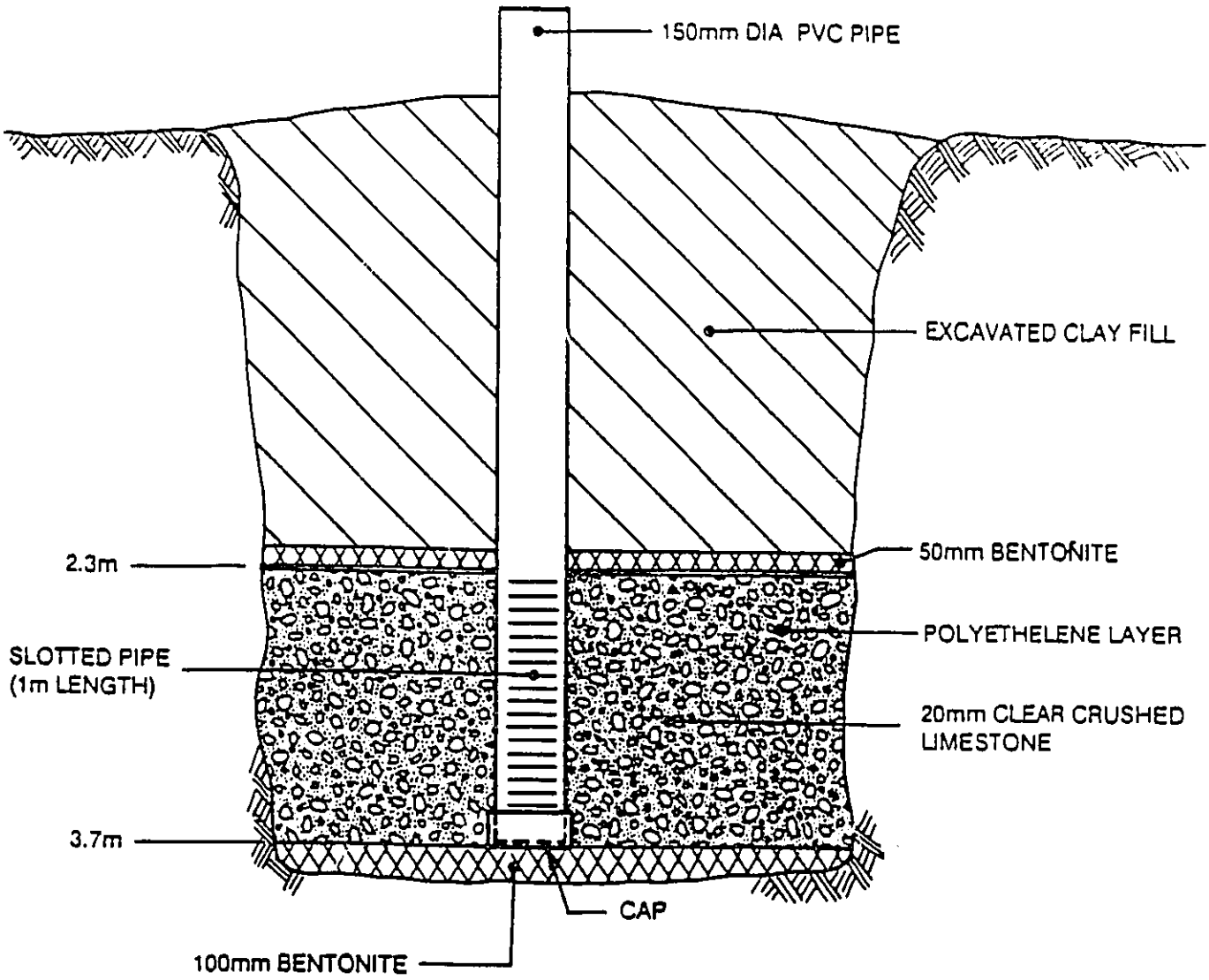

Figure 4.4. Typical large well installation, NRC and Fallowfield (courtesy of Fondex Ltd.).

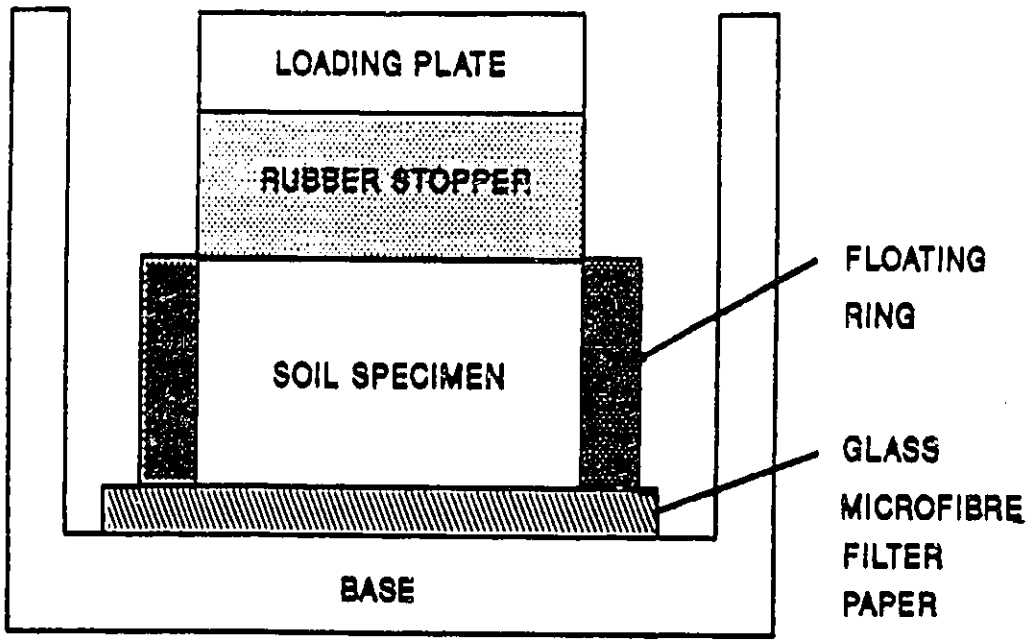

Figure 4.5. Schematic representation of the modified oedometer squeezing apparatus.

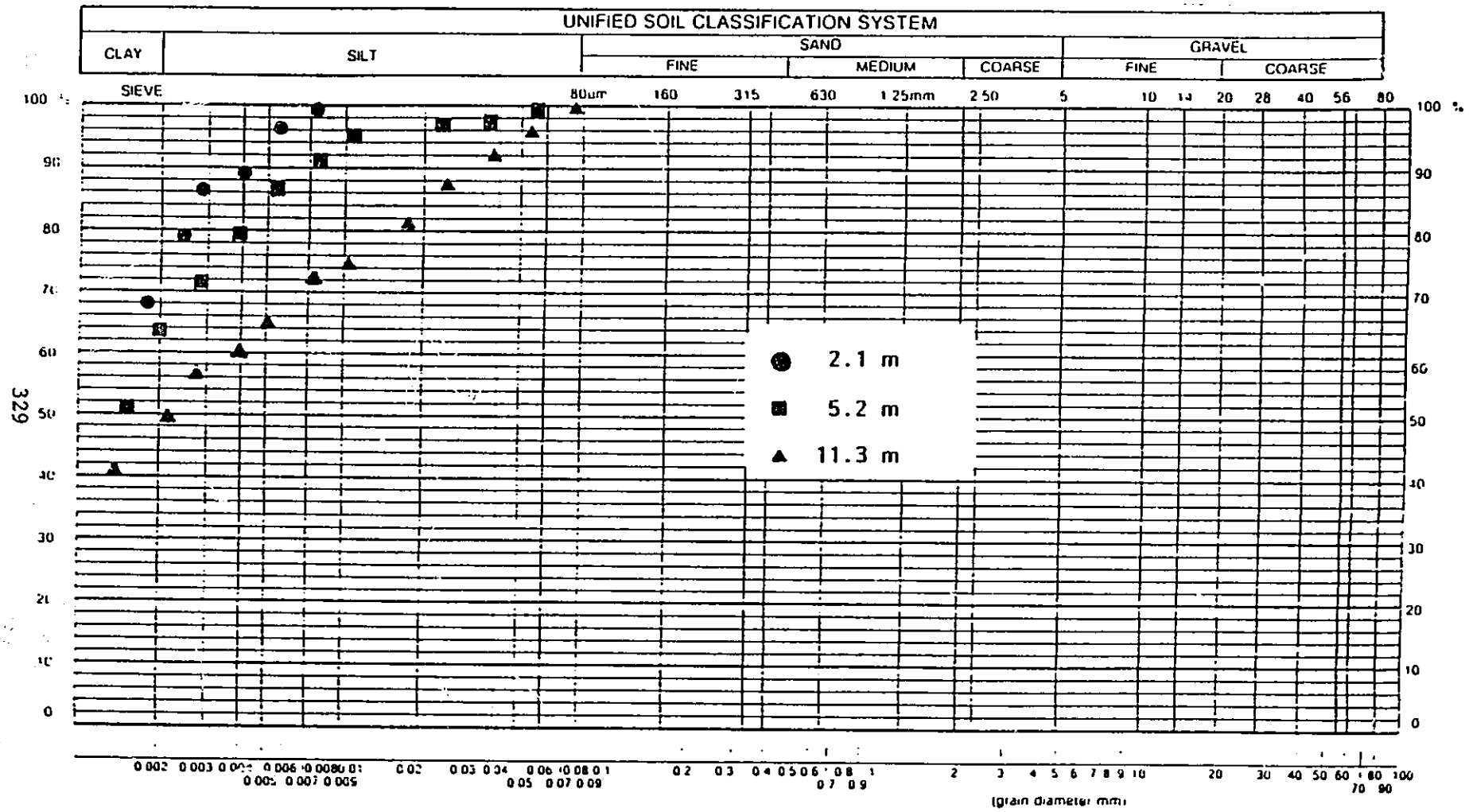

Figure 4.6a. Grain size distribution curves for the NRC site.

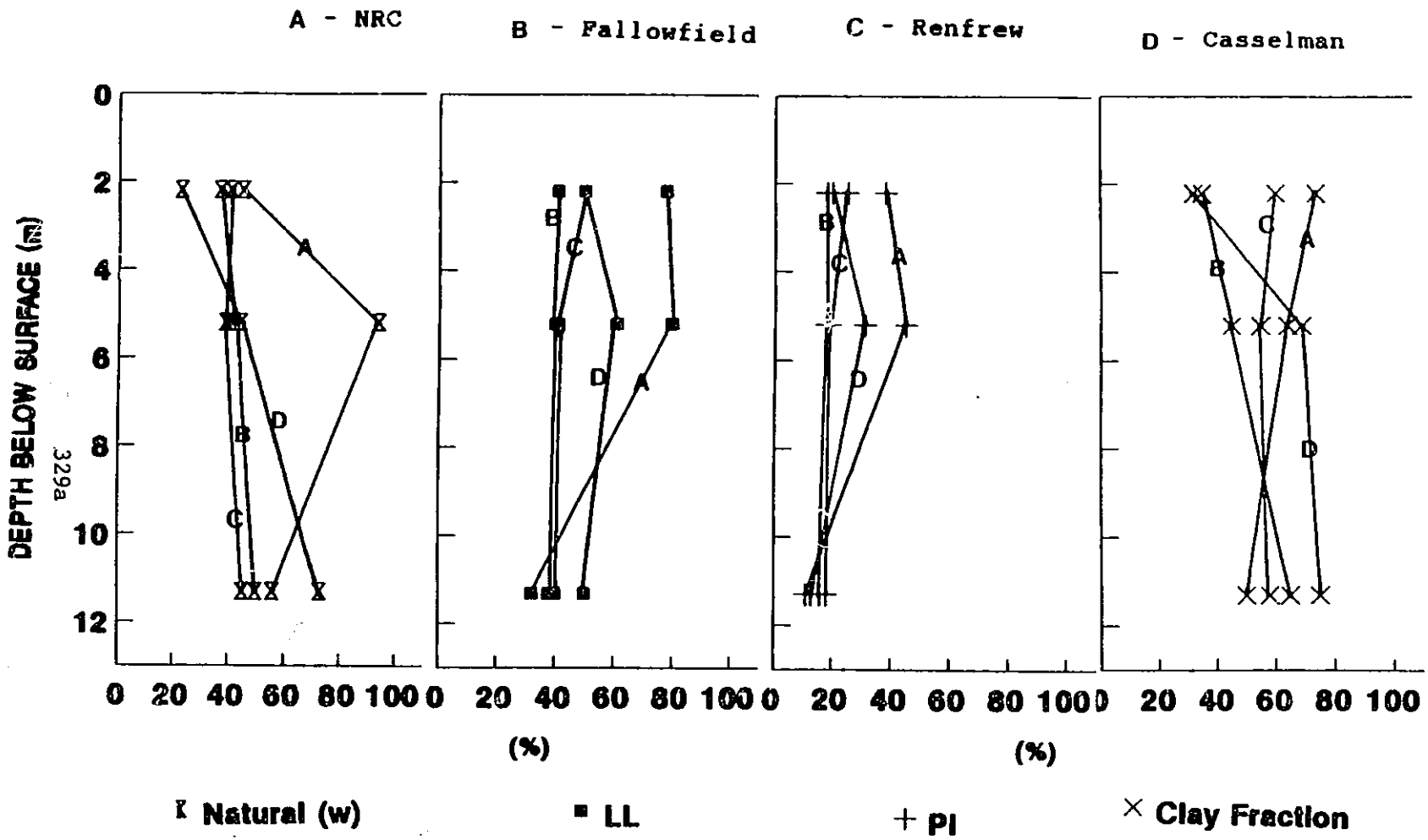

Figure 4.6b. Water content, liquid limit, plasticity index and clay fraction variation with depth at four sites.

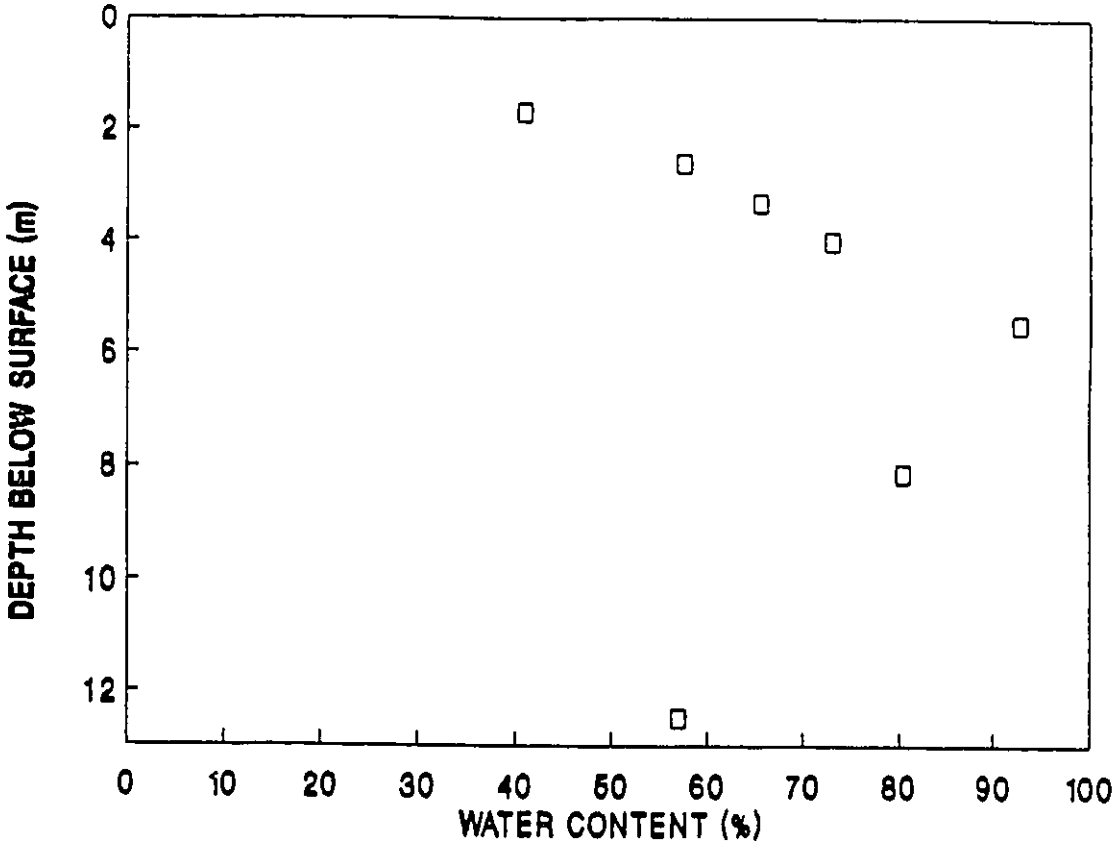

Figure 4.7. Water content profile for selected depths, NRC site.

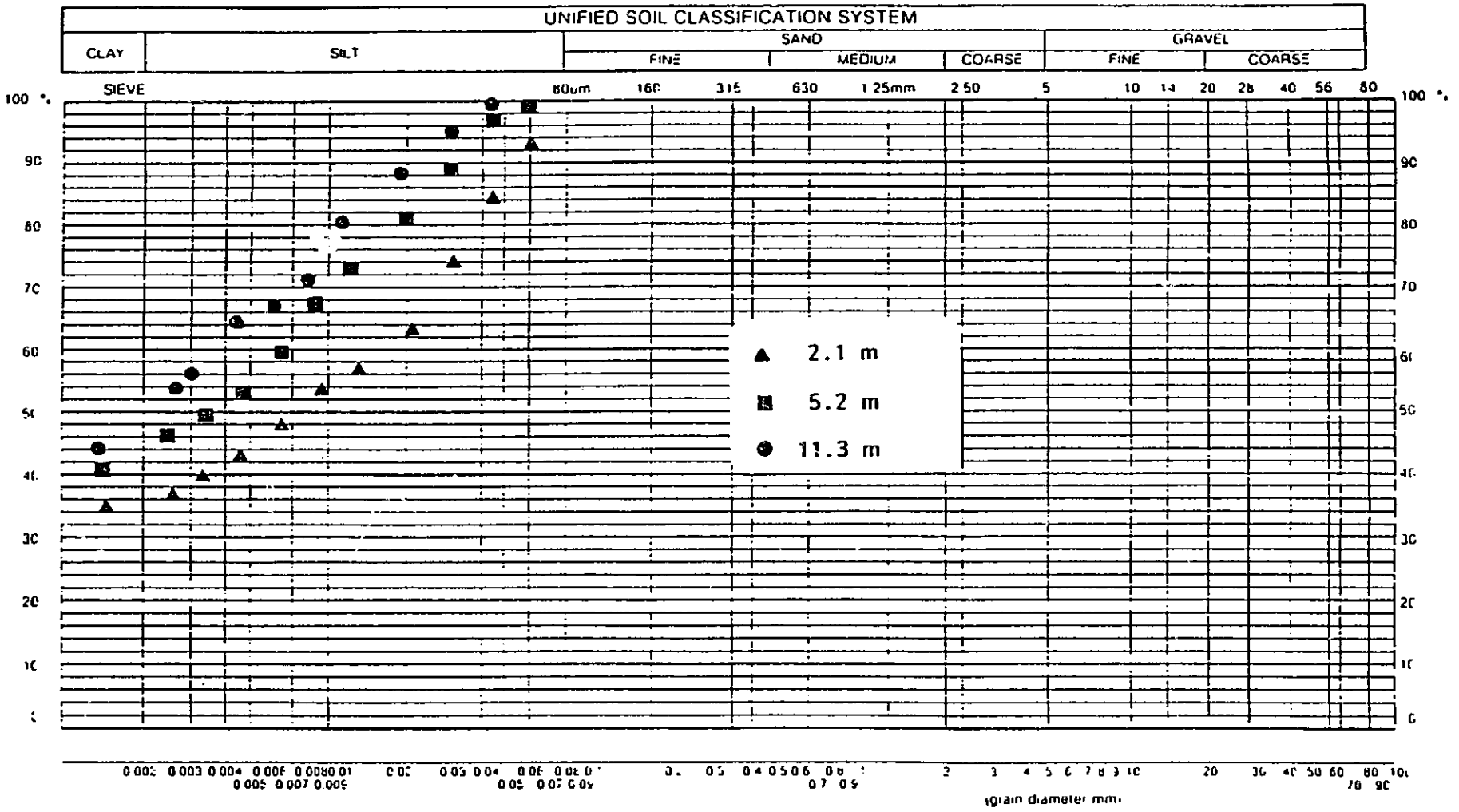

Figure 4.8. Grain size distribution curves for the Fallowfield site.

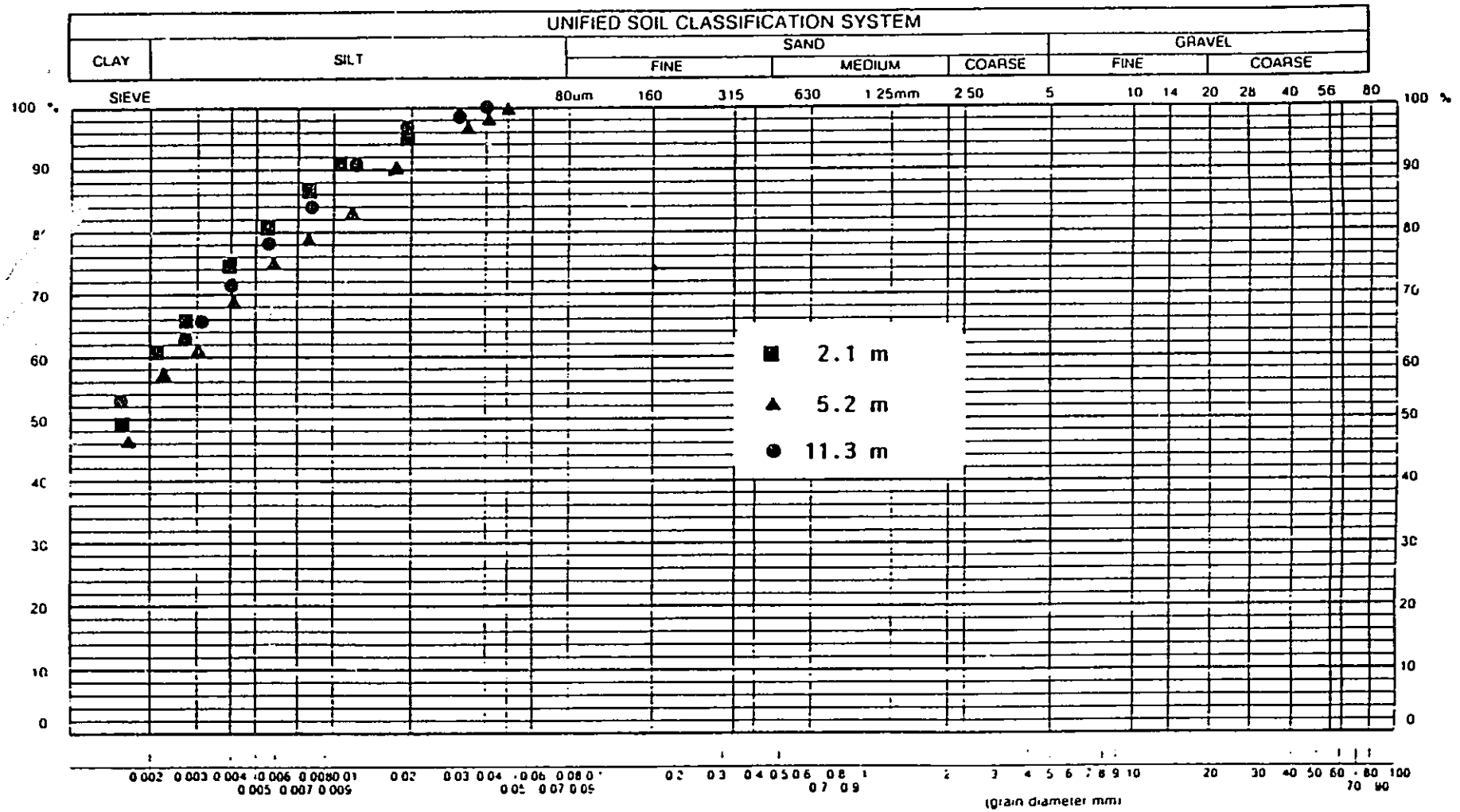

Figure 4.9. Grain size distribution curves for the Renfrew si[illegible].

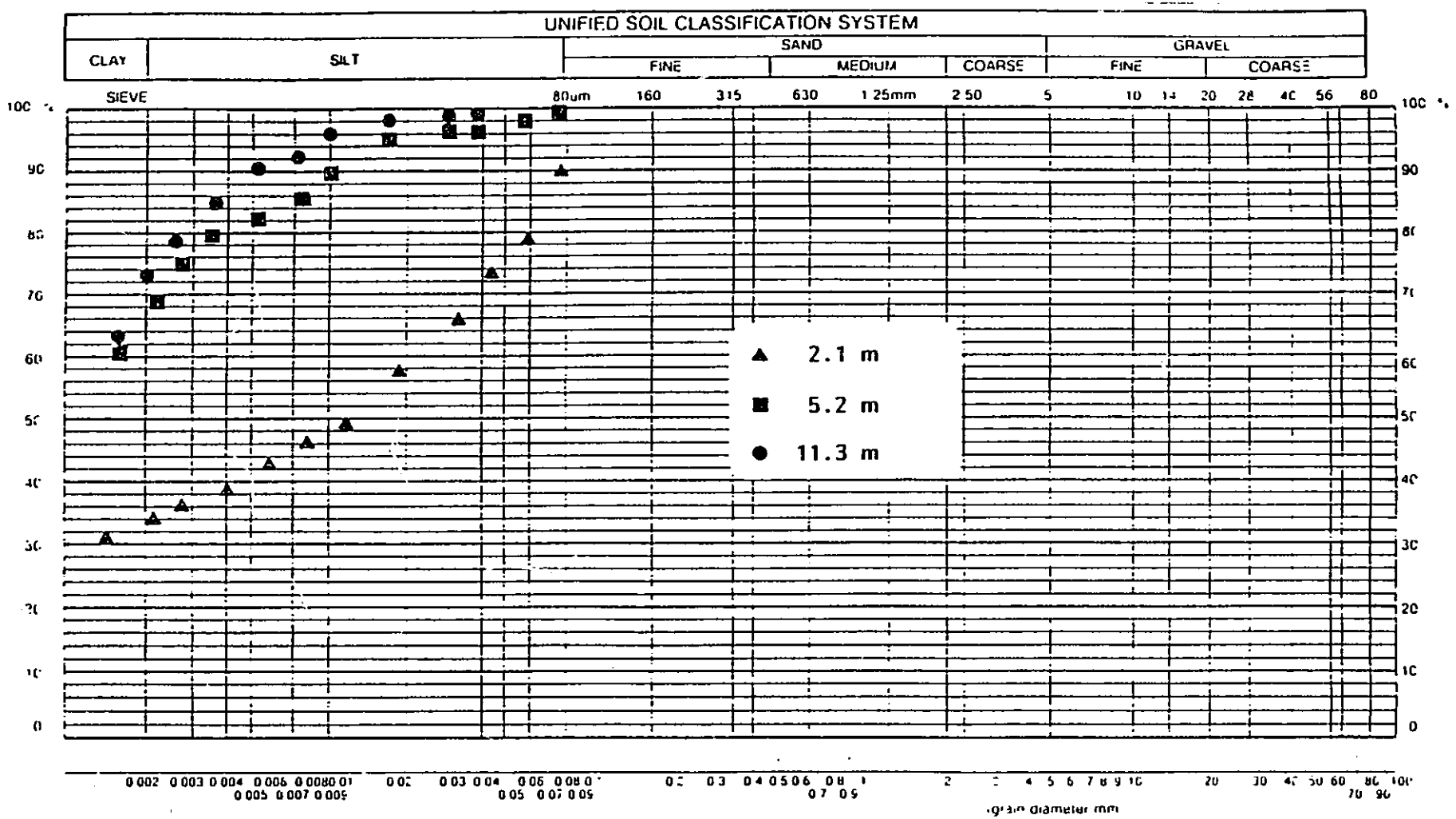

Figure 4.10. Grain size distribution curves for the Casselman site.

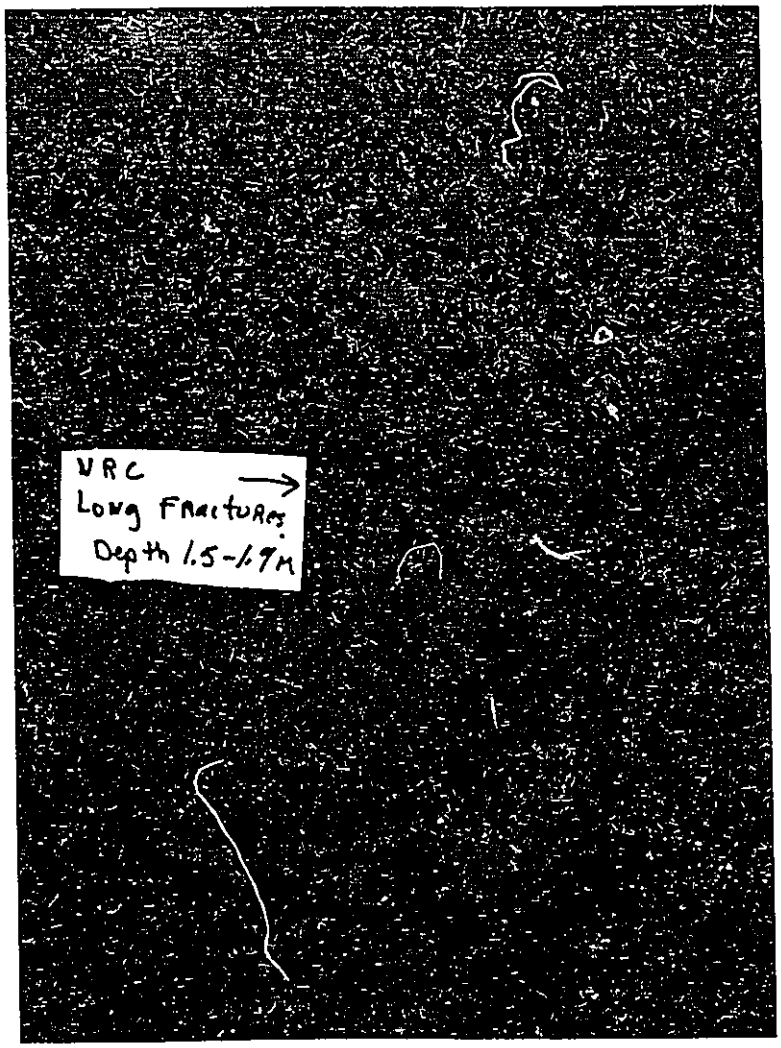

(A)

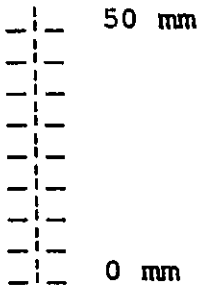

Scale for photograph (A)

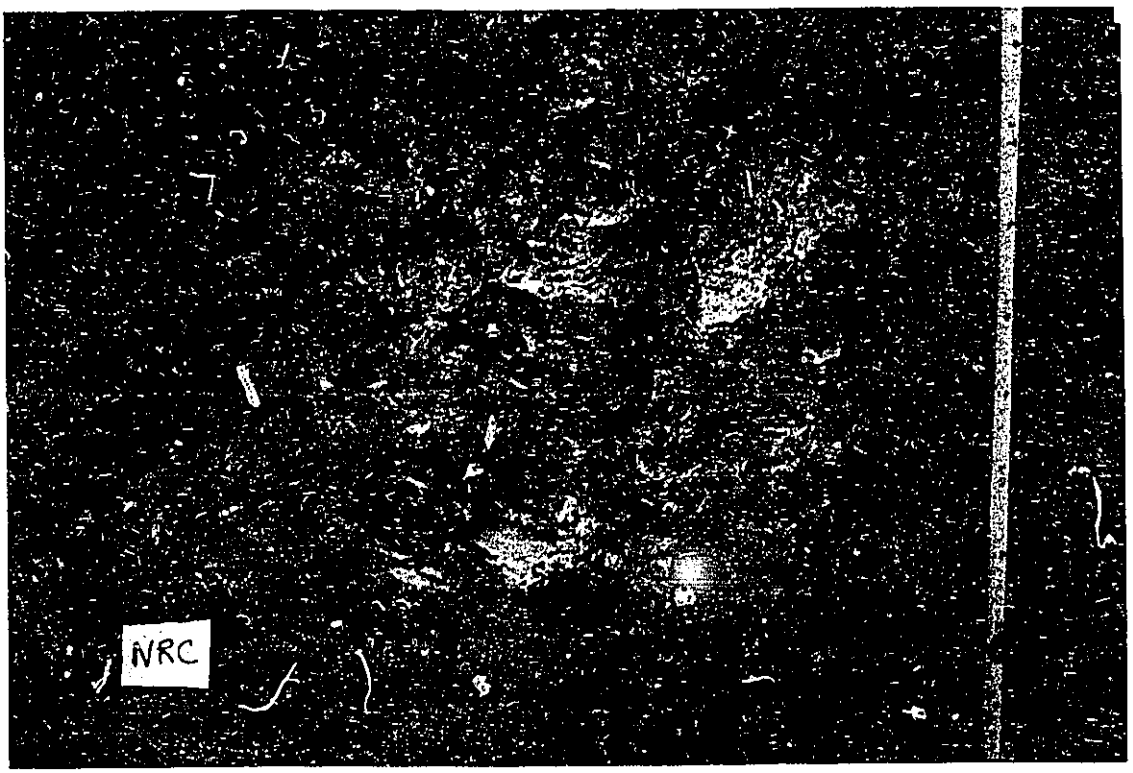

(B)

Figure 4.11. Photographs of the NRC test pit.

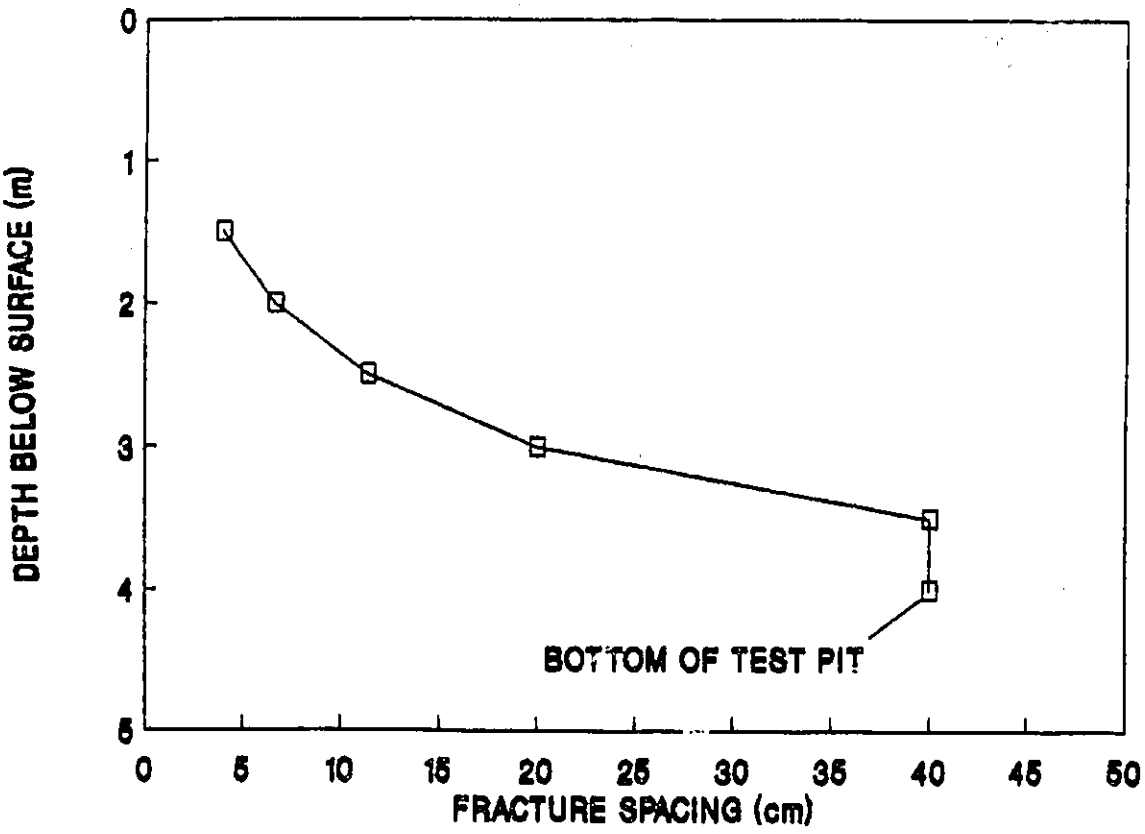

Figure 4.12. Fracture spacing with depth at the NRC site.

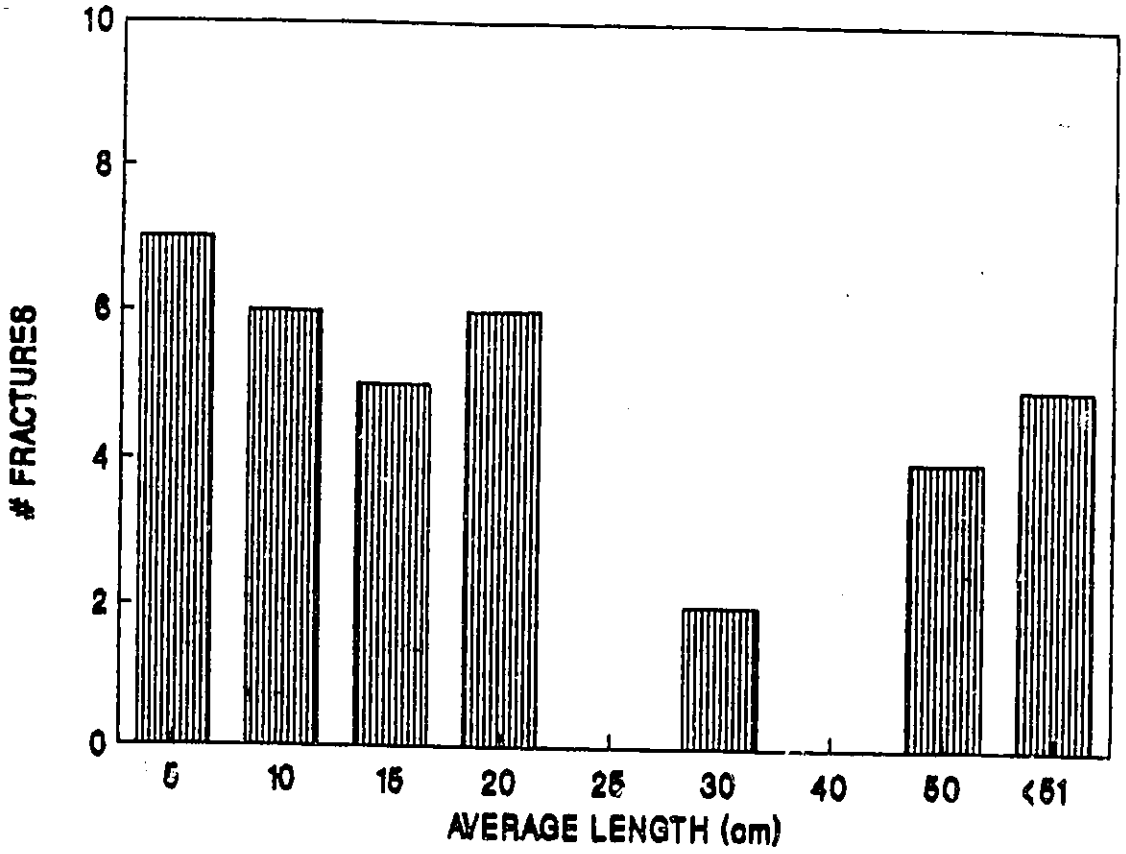

Figure 4.13. Average length of fractures at the NRC site from 0 to 4 m depth.

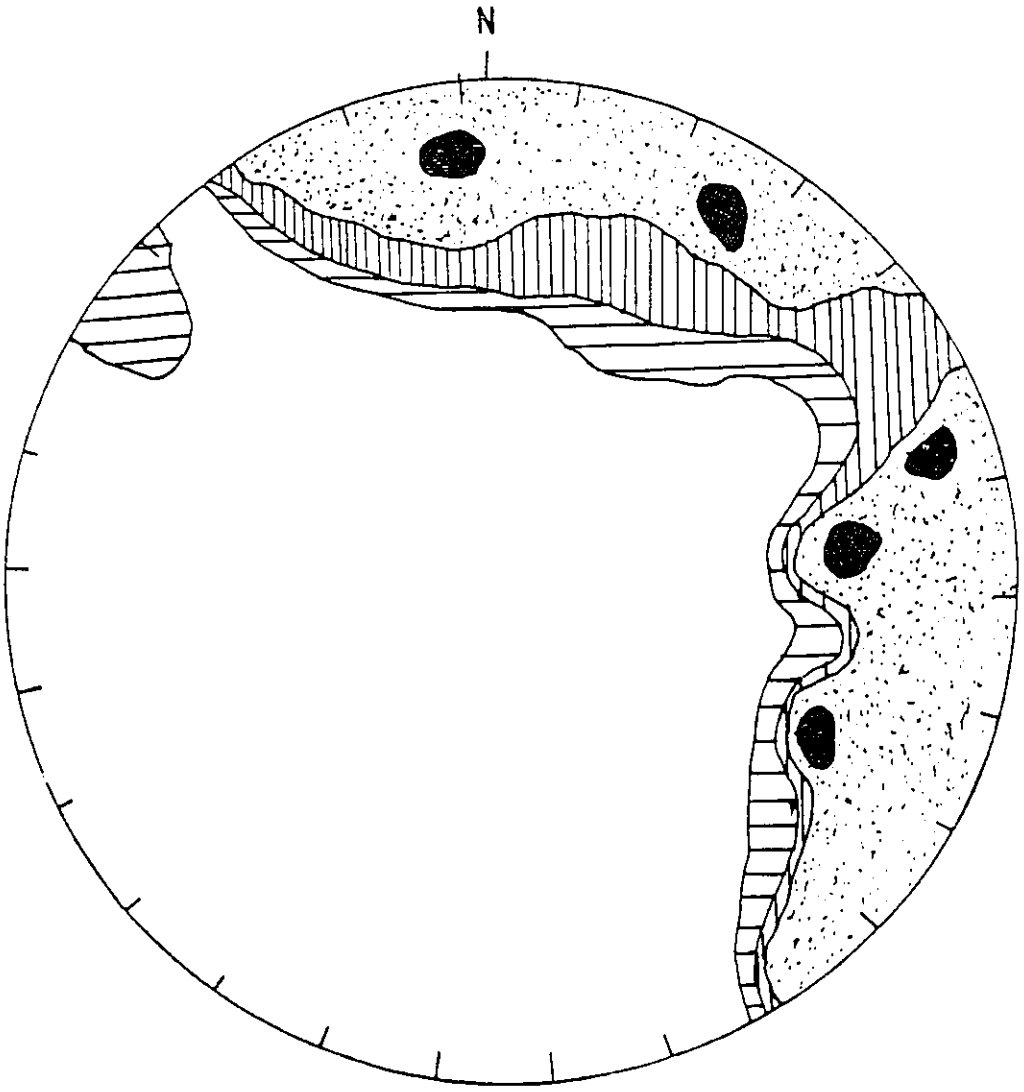

Figure 4.14. Stereographic representation of fractures at the NRC site.

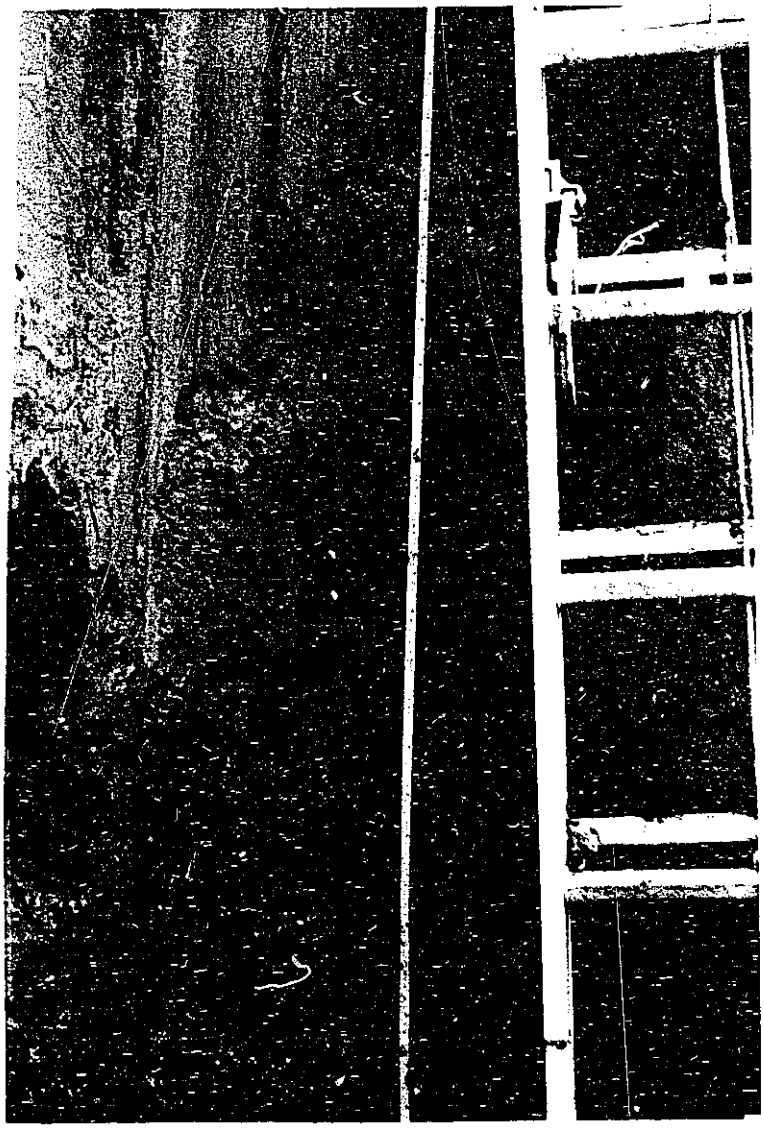

Figure 4.15. A photograph of the Fallowfield test pit.

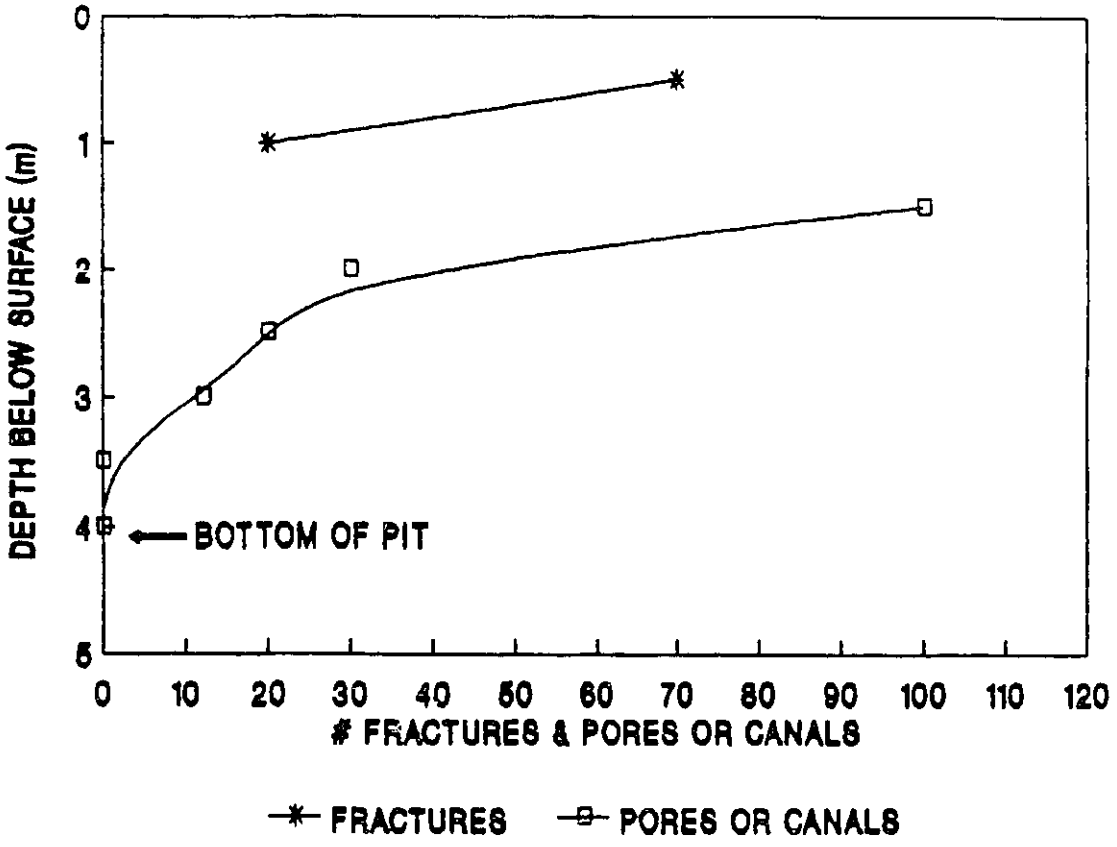

Figure 4.16. The number of fractures and pores or canals per 100 cm^2 with depth, at the Fallowfield site.

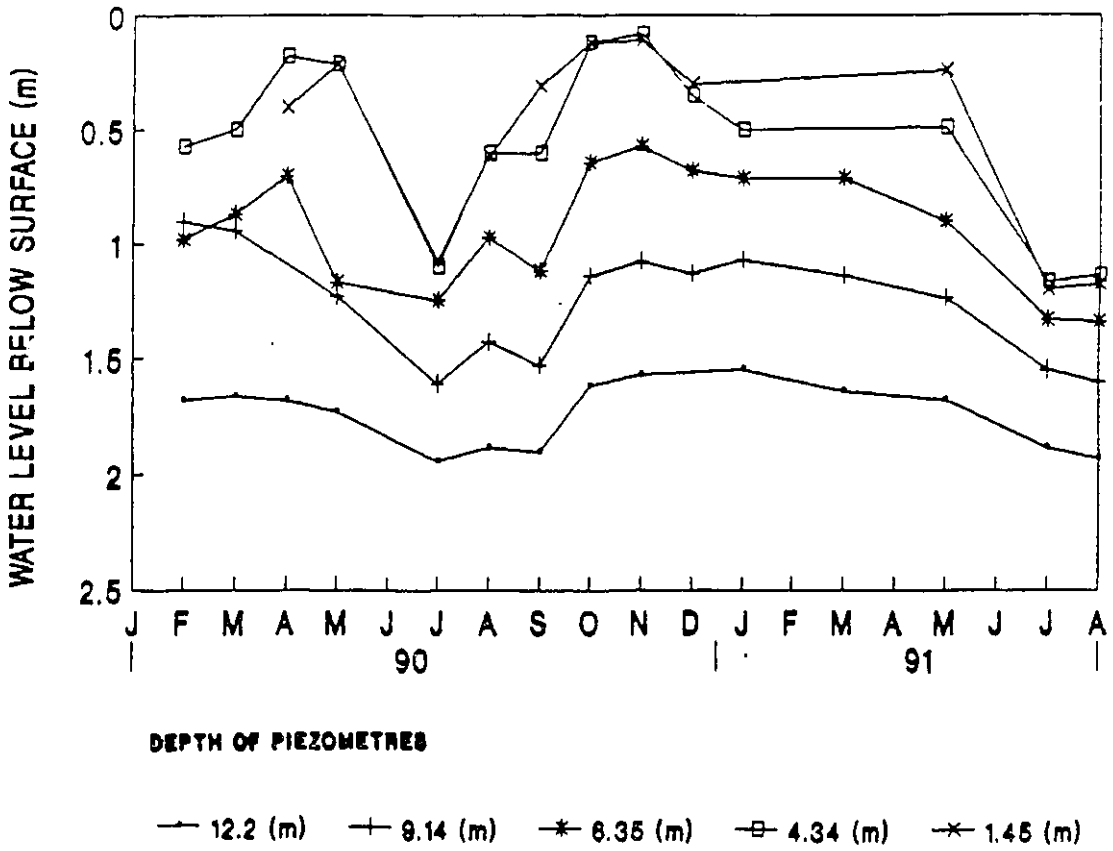

Figure 4.17. Water level fluctuations with time for selected piezometers, NRC site.

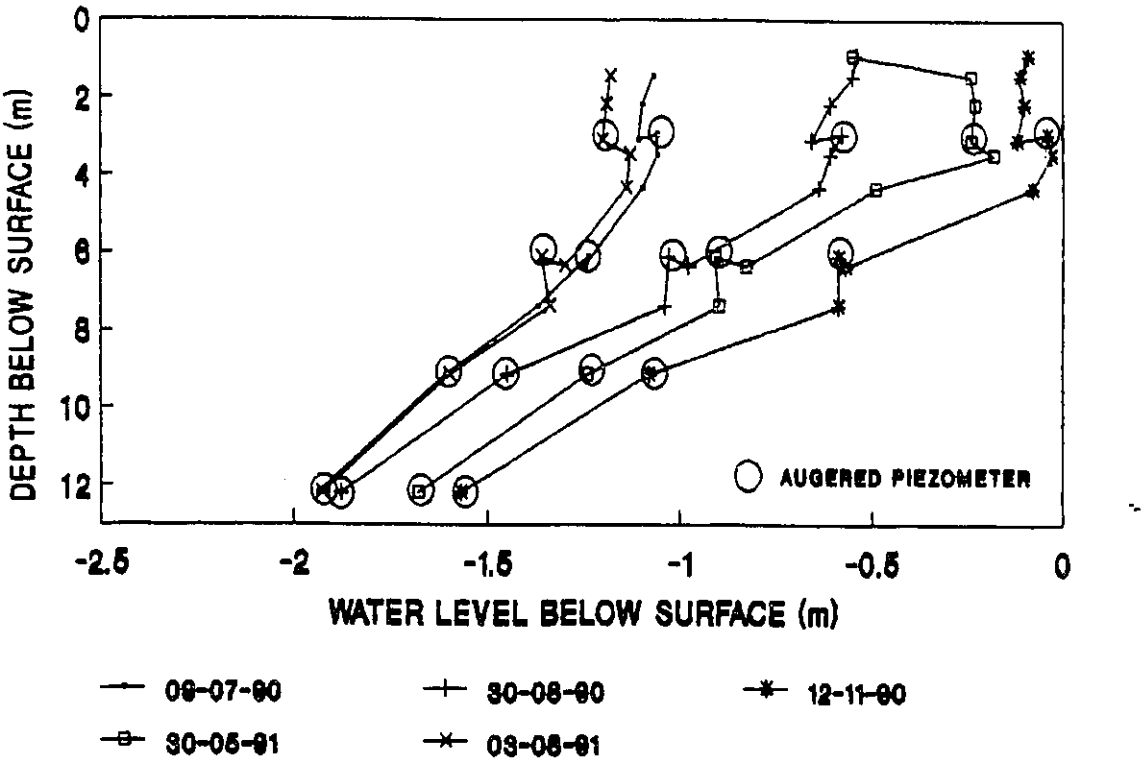

Figure 4.18. Water level variation profiles at the NRC site.

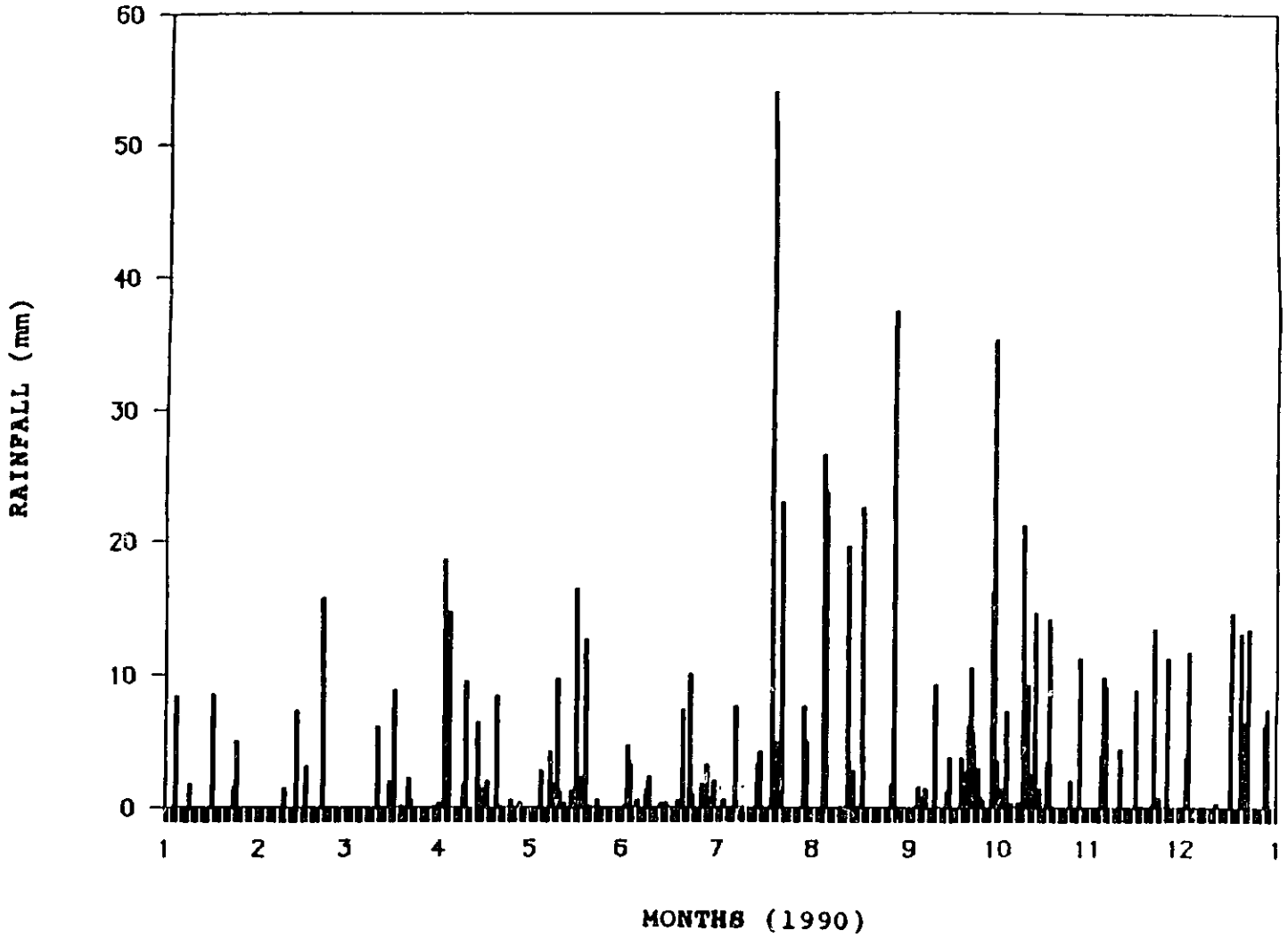

Figure 4.19. Daily rain fall record for the year 1990 at Ottawa International Airport.

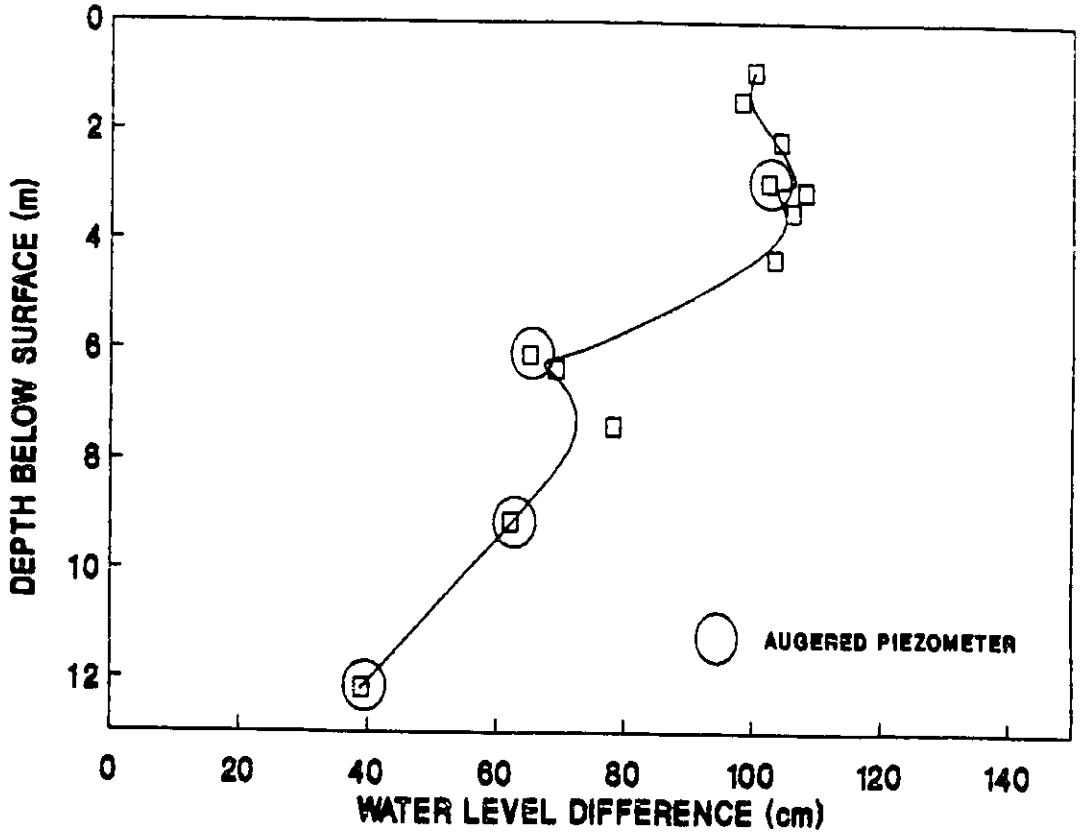

Figure 4.20. Maximum difference in water levels with depth, NRC site.

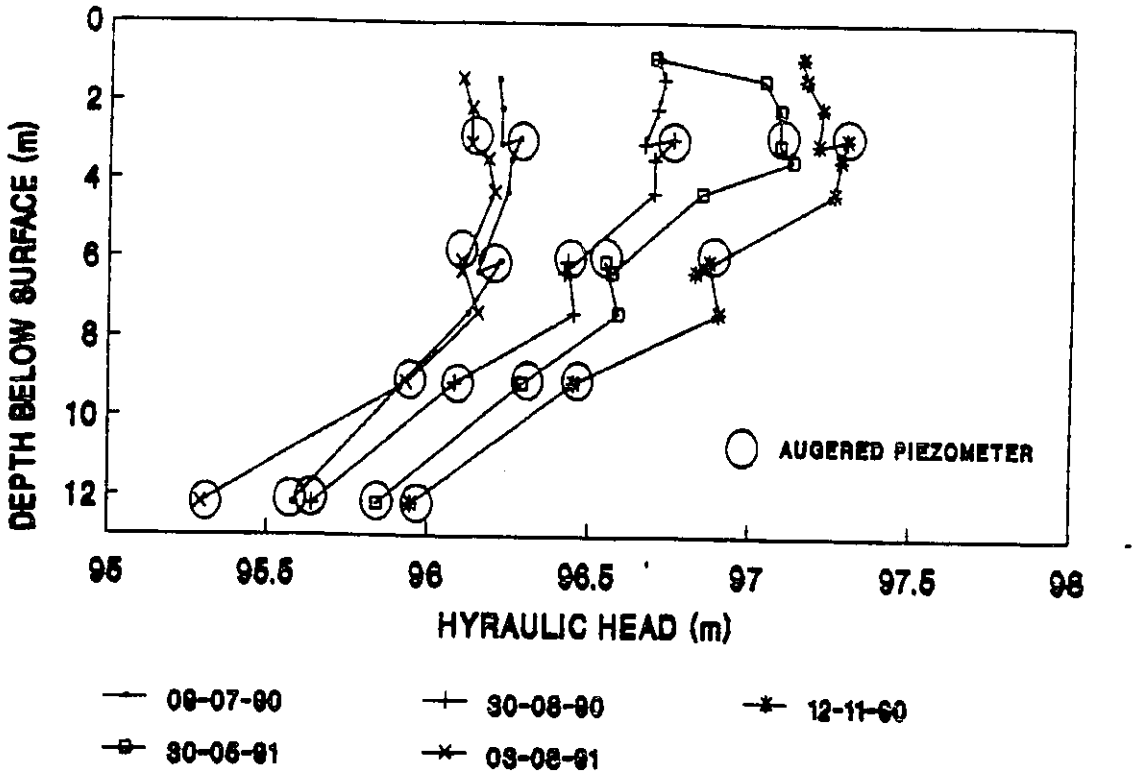

Figure 4.21. Hydraulic head variation profiles at the NRC site (ground surface elevation of 100 masl).

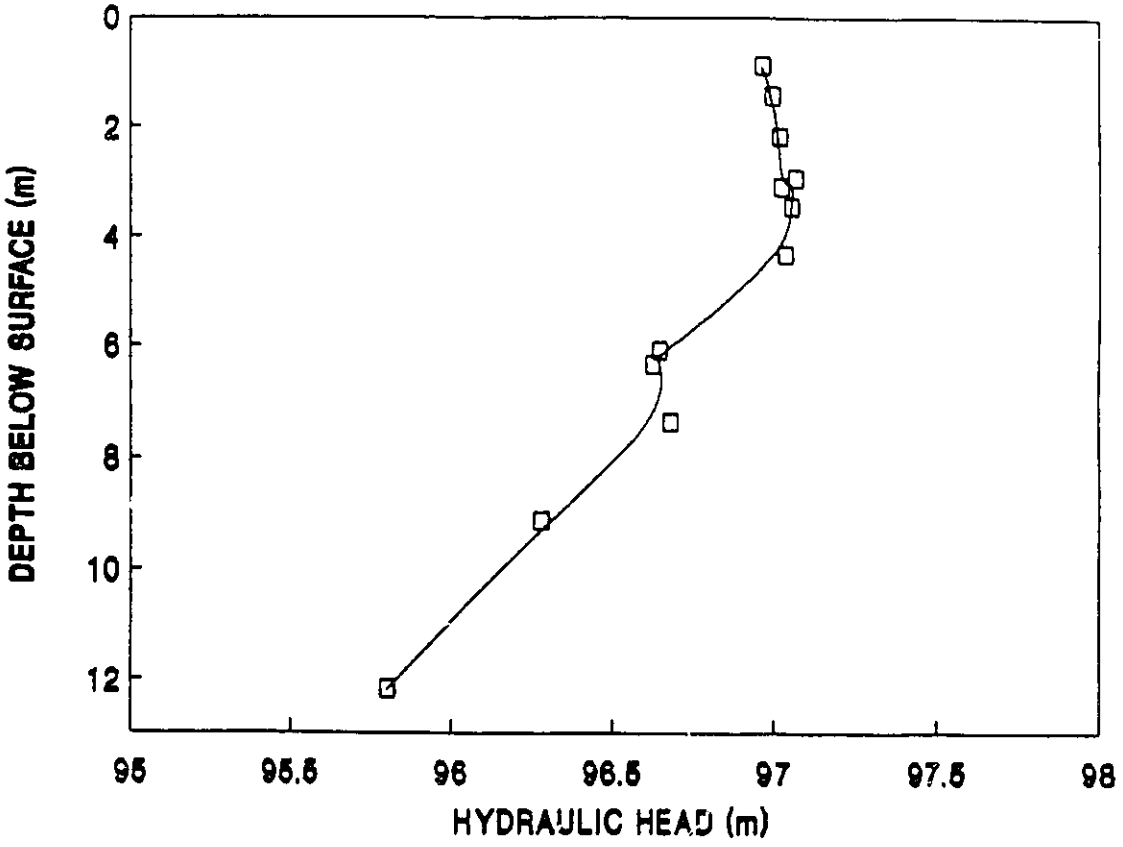

Figure 4.22. The average hydraulic head profile at the NRC site

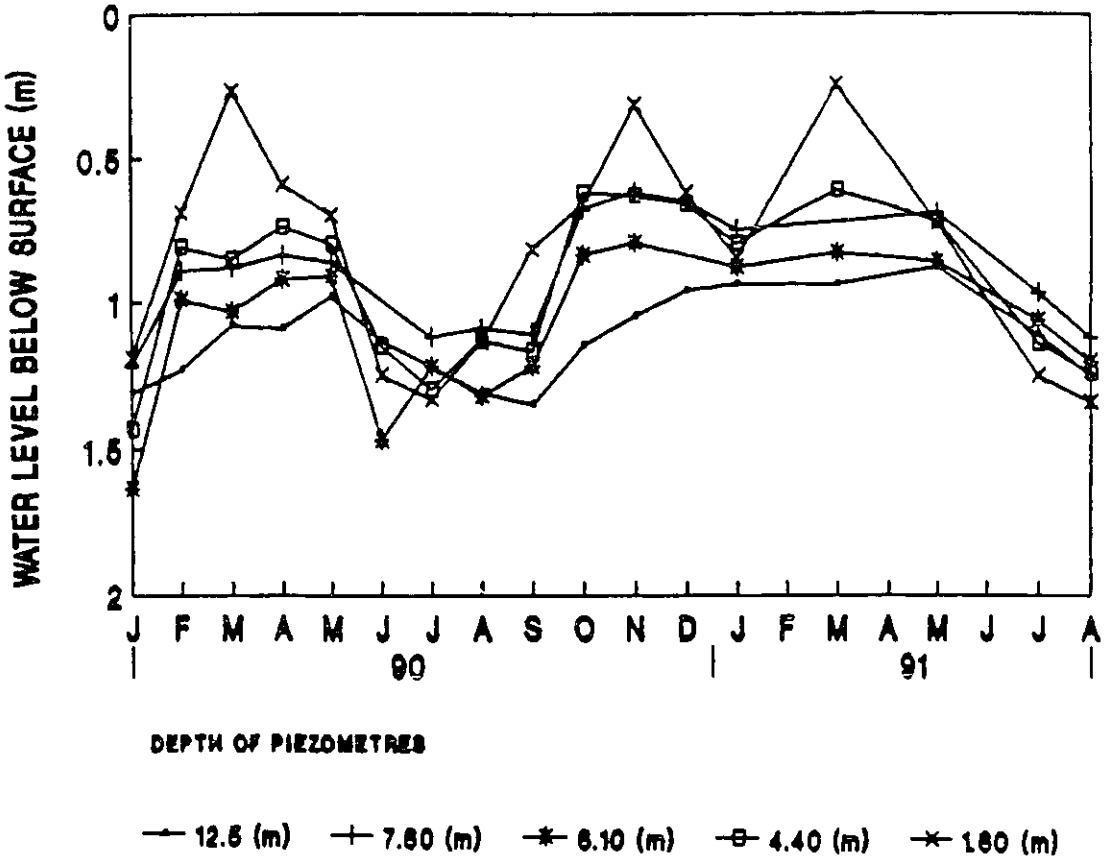

Figure 4.23. Water level fluctuations with time for selected piezometers, Fallowfield site.

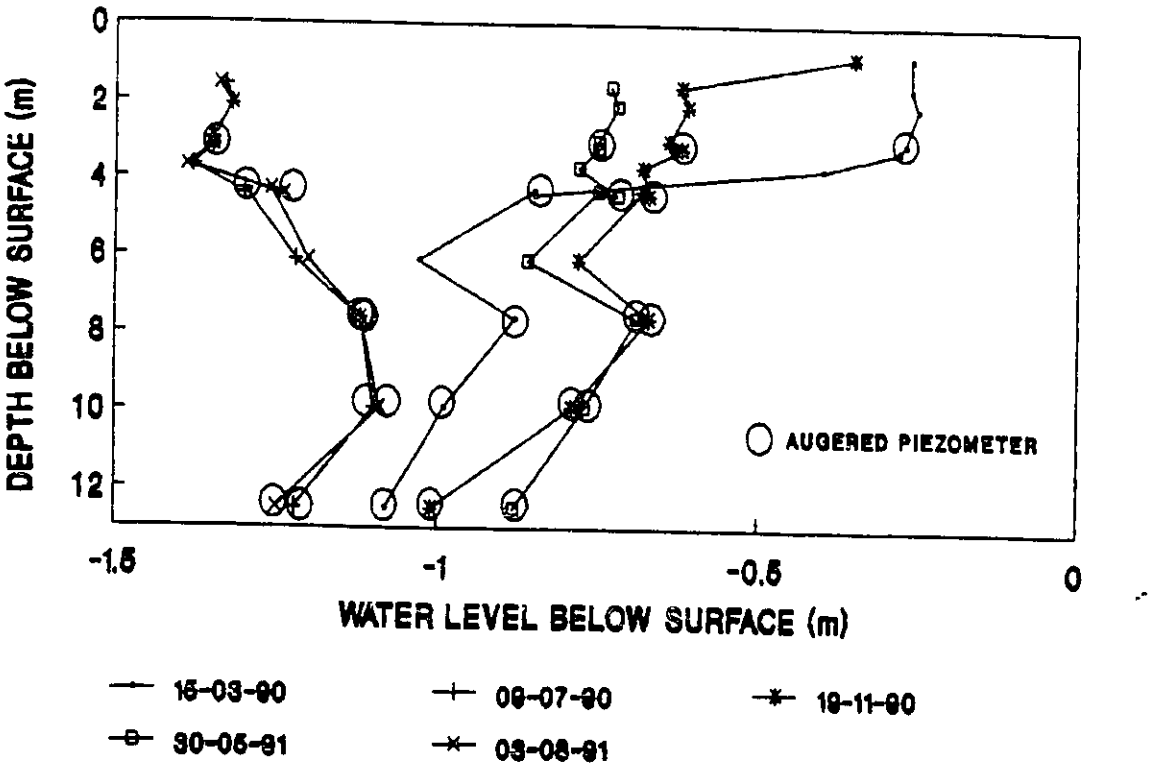

Figure 4.24. Water level variation profiles at the Fallowfield site.

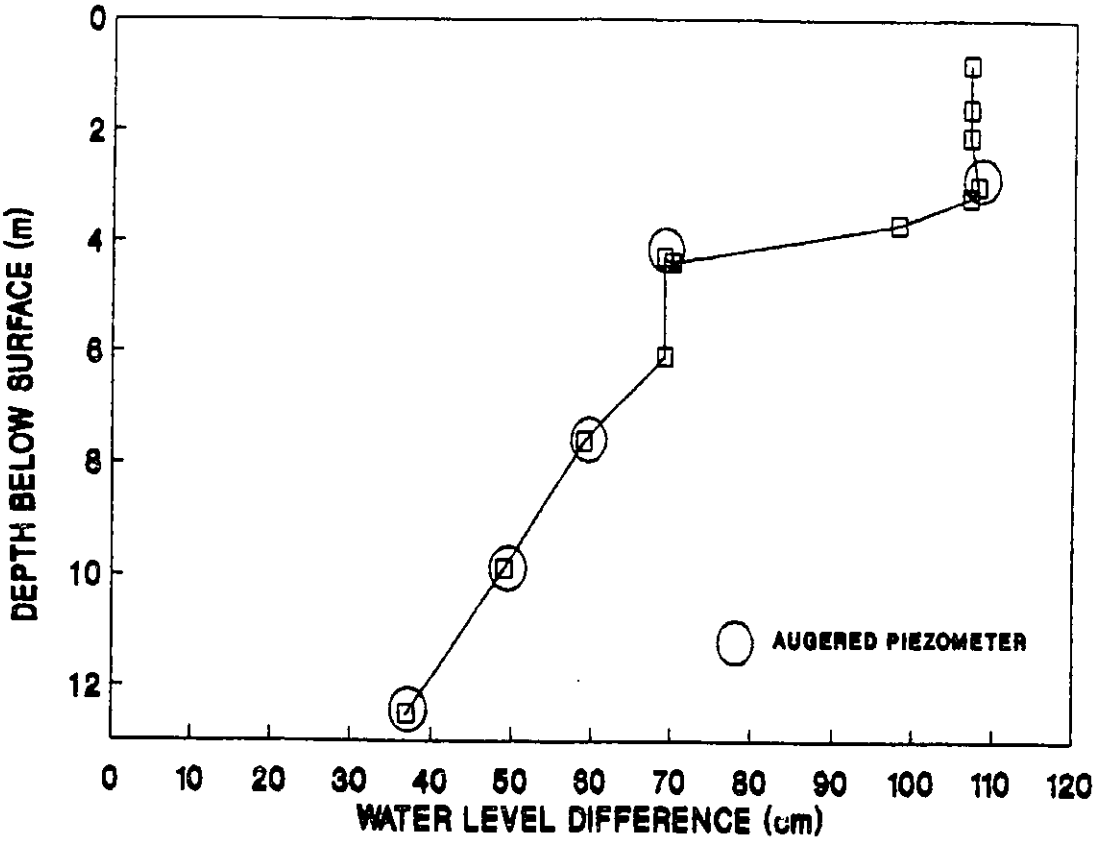

Figure 4.25. Maximum difference in water levels with depth, Fallowfield site.

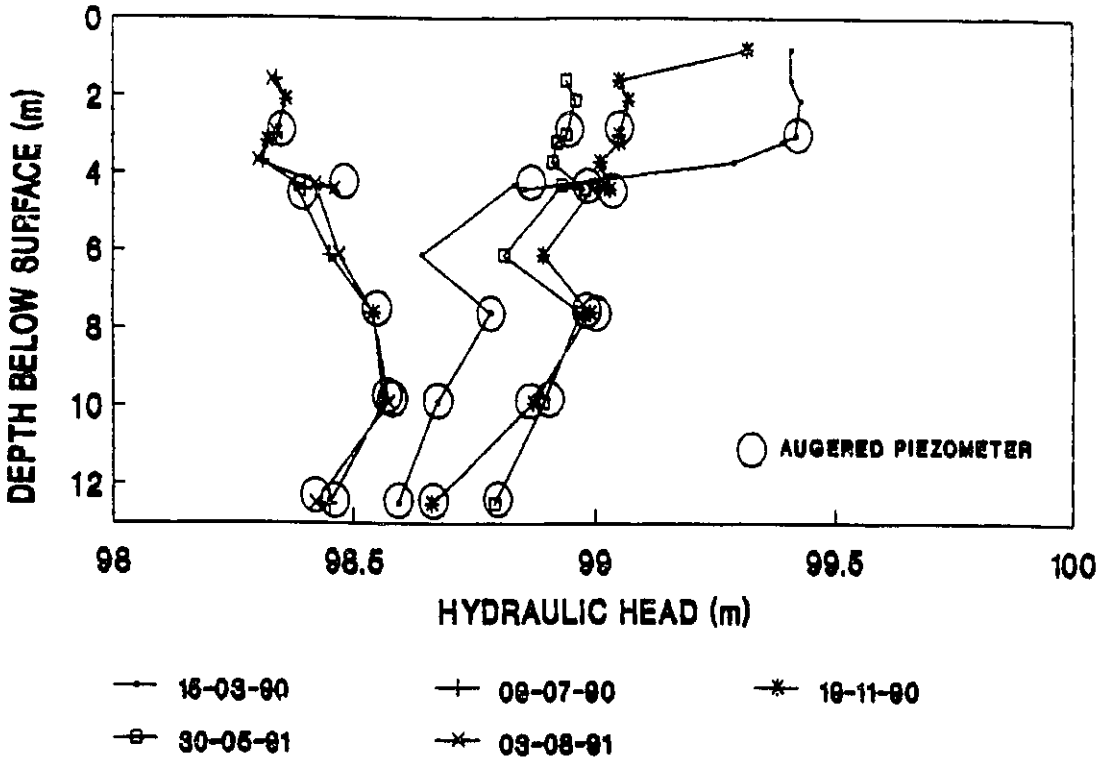

Figure 4.26. Hydraulic head variation profiles at the Fallowfield site (ground surface elevation of 100 masl).

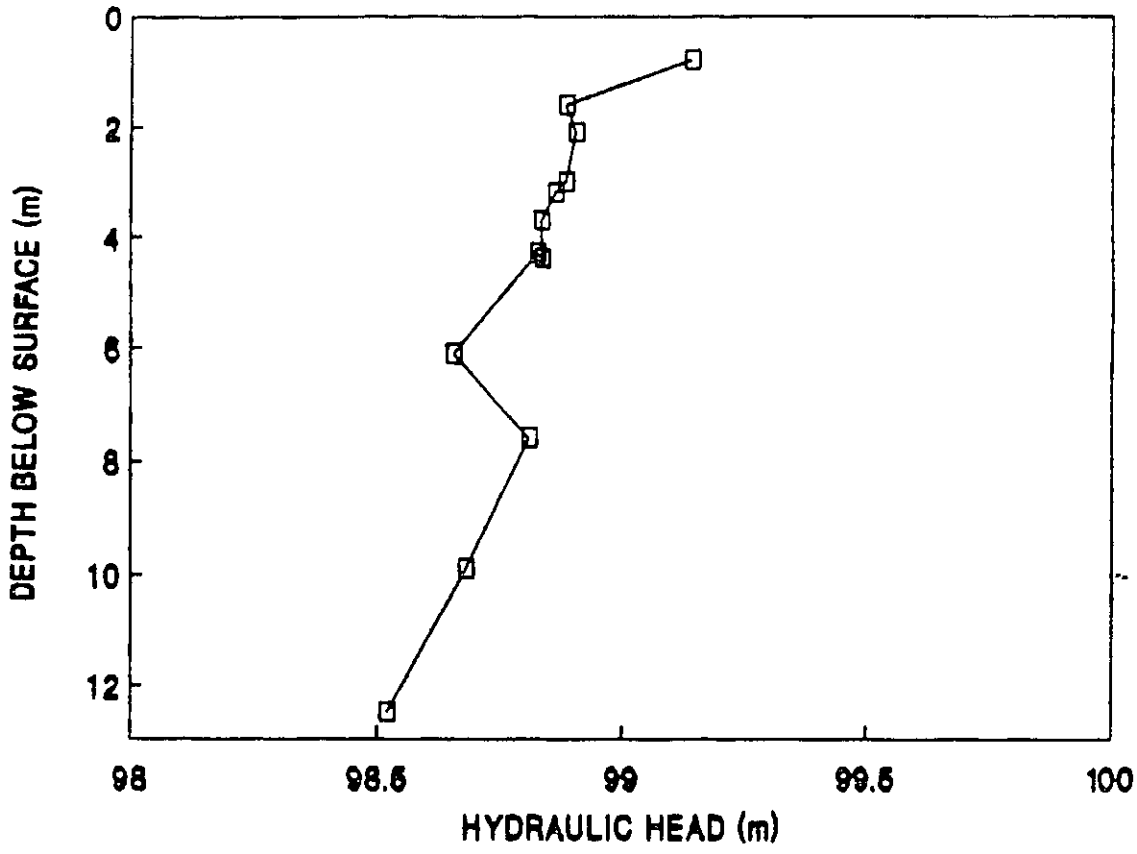

Figure 4.27. The average hydraulic head profile at the Fallowfield site.

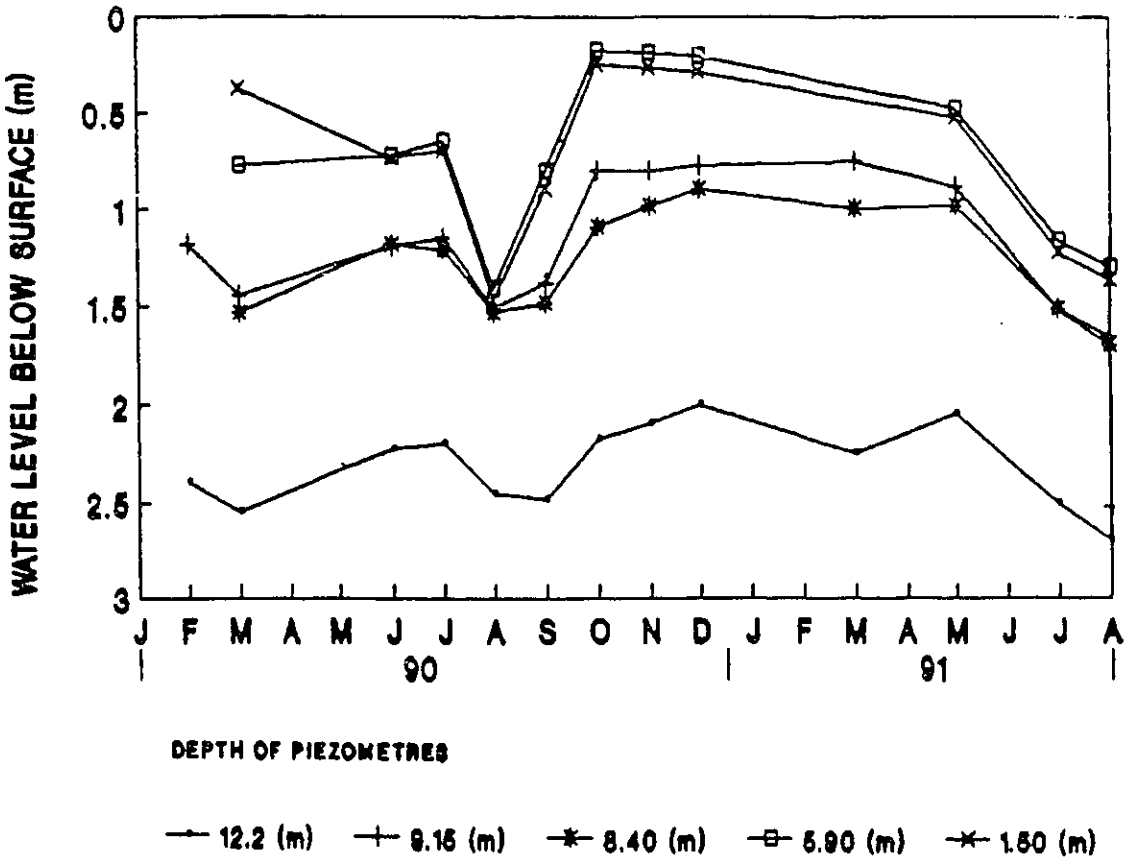

Figure 4.28. Water level fluctuations with time for selected piezometers, Renfrew site.

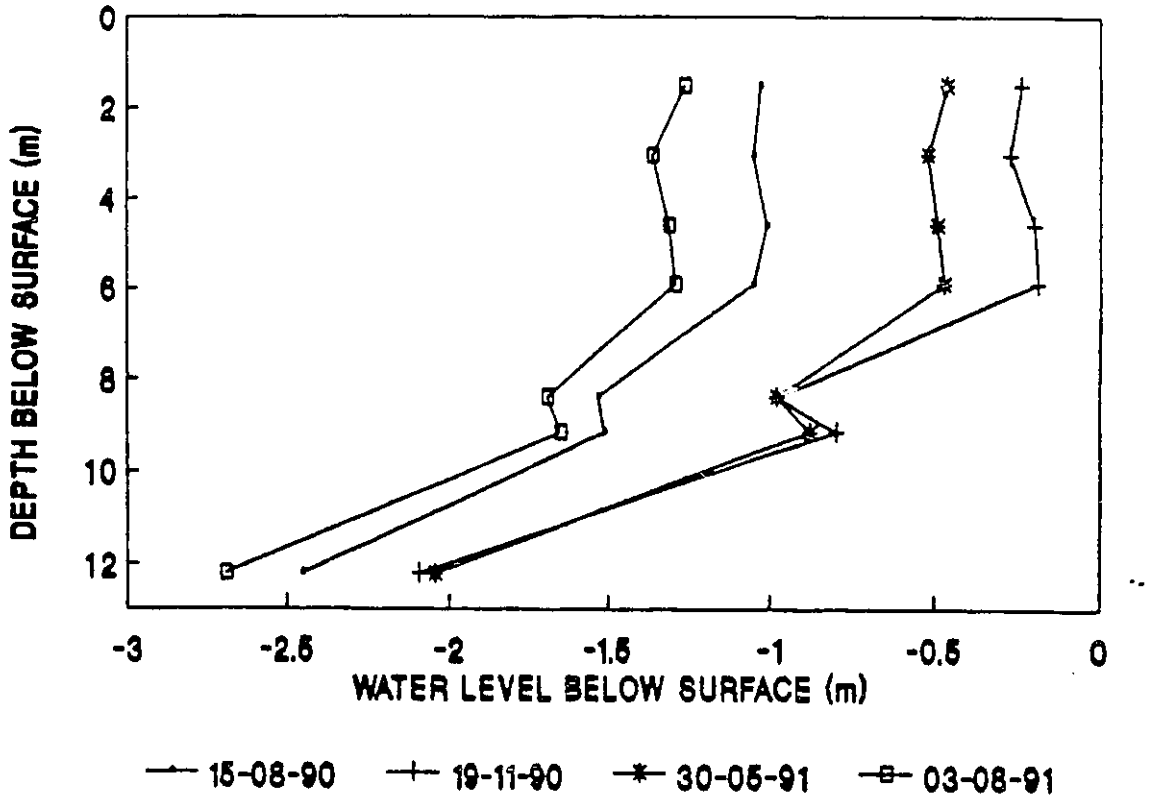

Figure 4.29. Water level variation profiles at the Renfrew site.

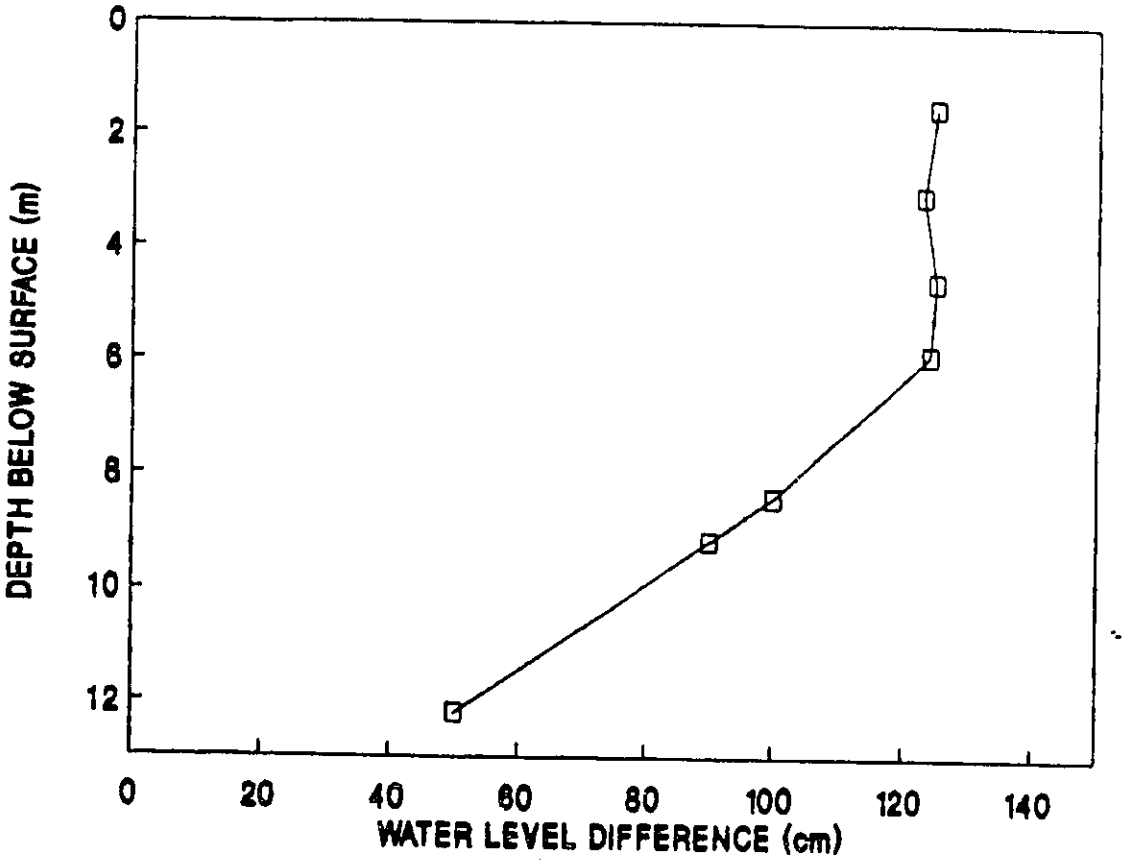

Figure 4.30. Maximum difference in water levels with depth, Renfrew site.

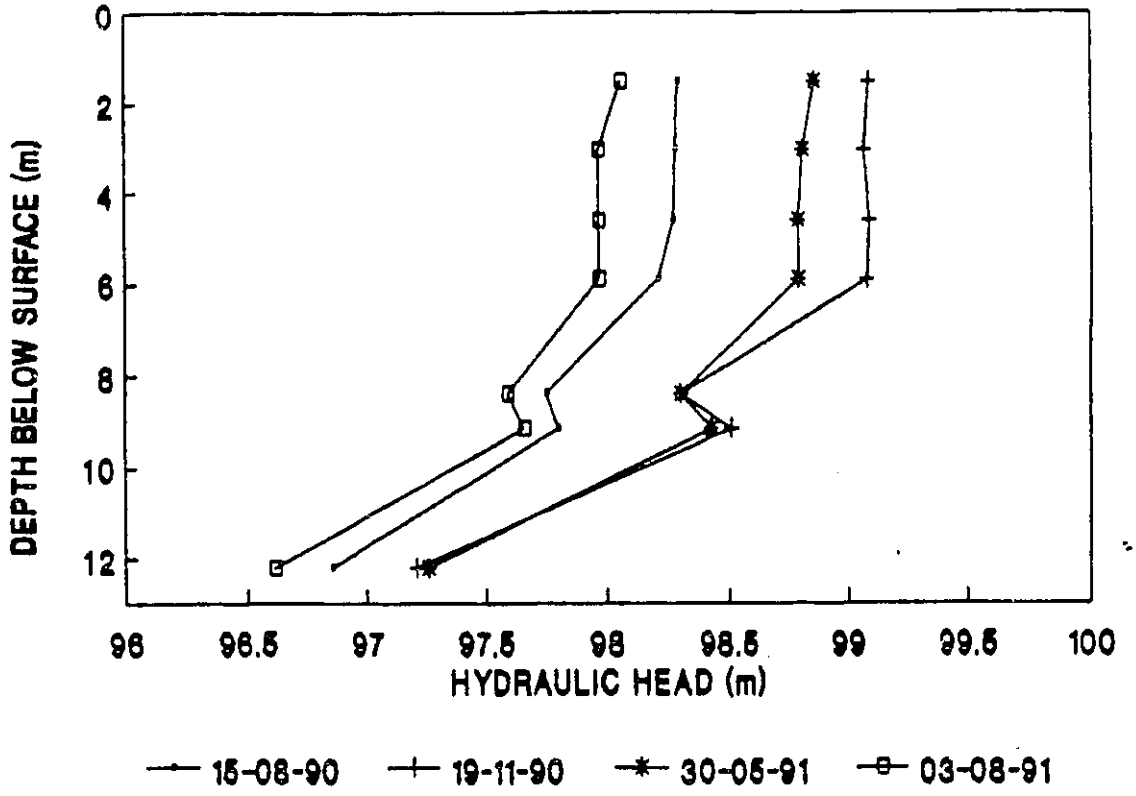

Figure 4.31. Hydraulic head variation profiles at the Renfrew site (ground surface elevation of 100 masl).

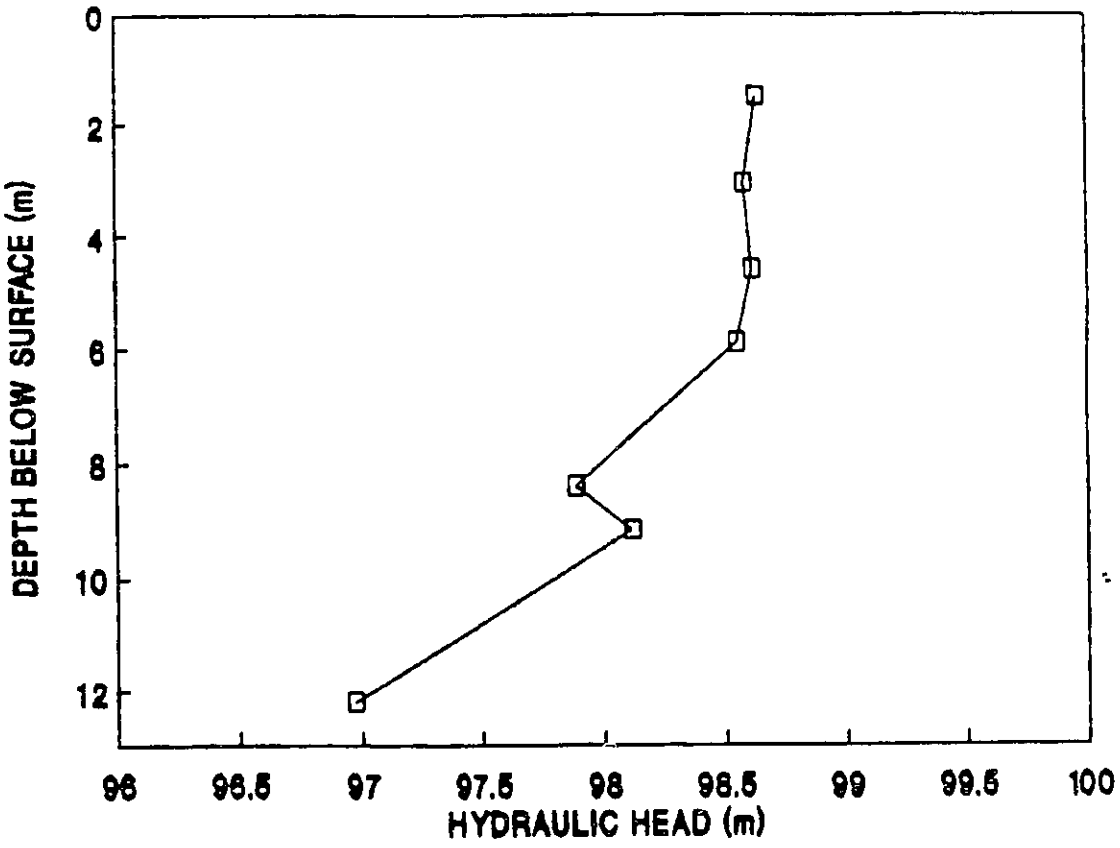

Figure 4.32. The average hydraulic head profile at the Renfrew site.

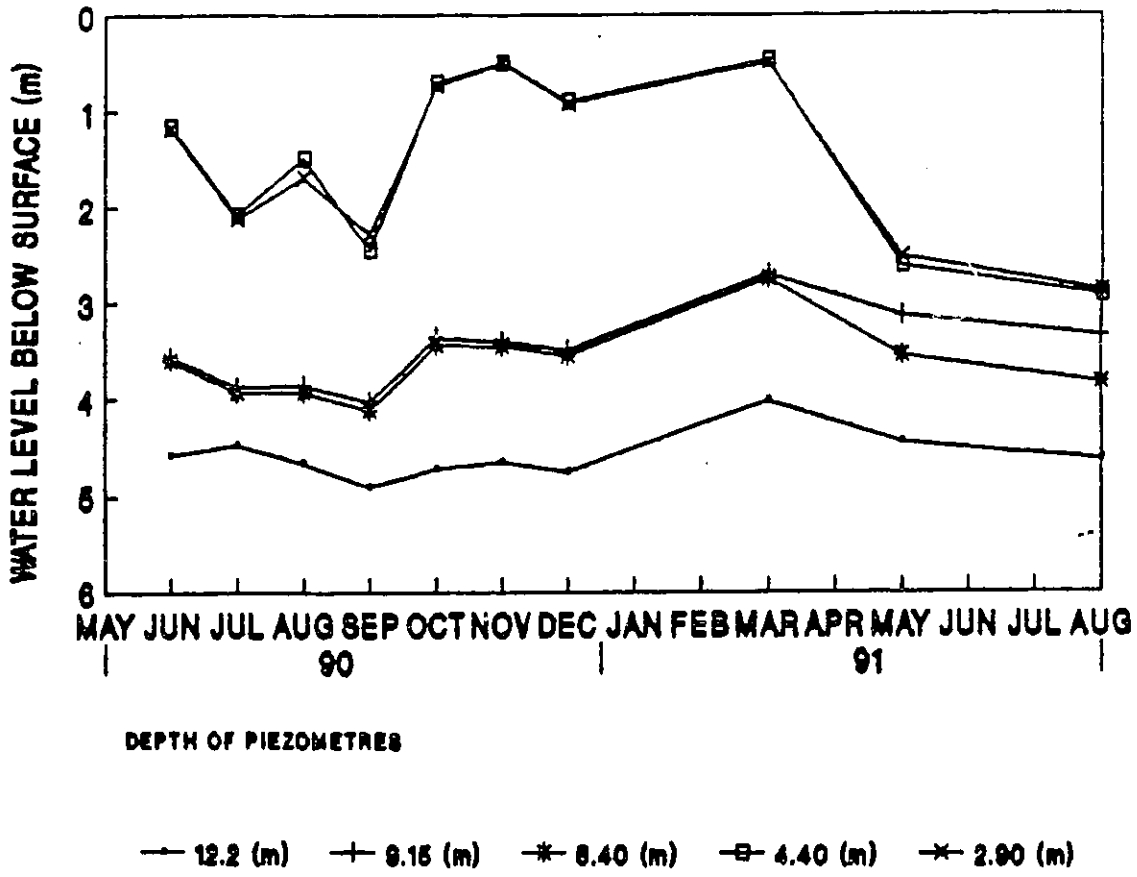

Figure 4.33. Water level fluctuations with time for selected piezometers, Casselman site.

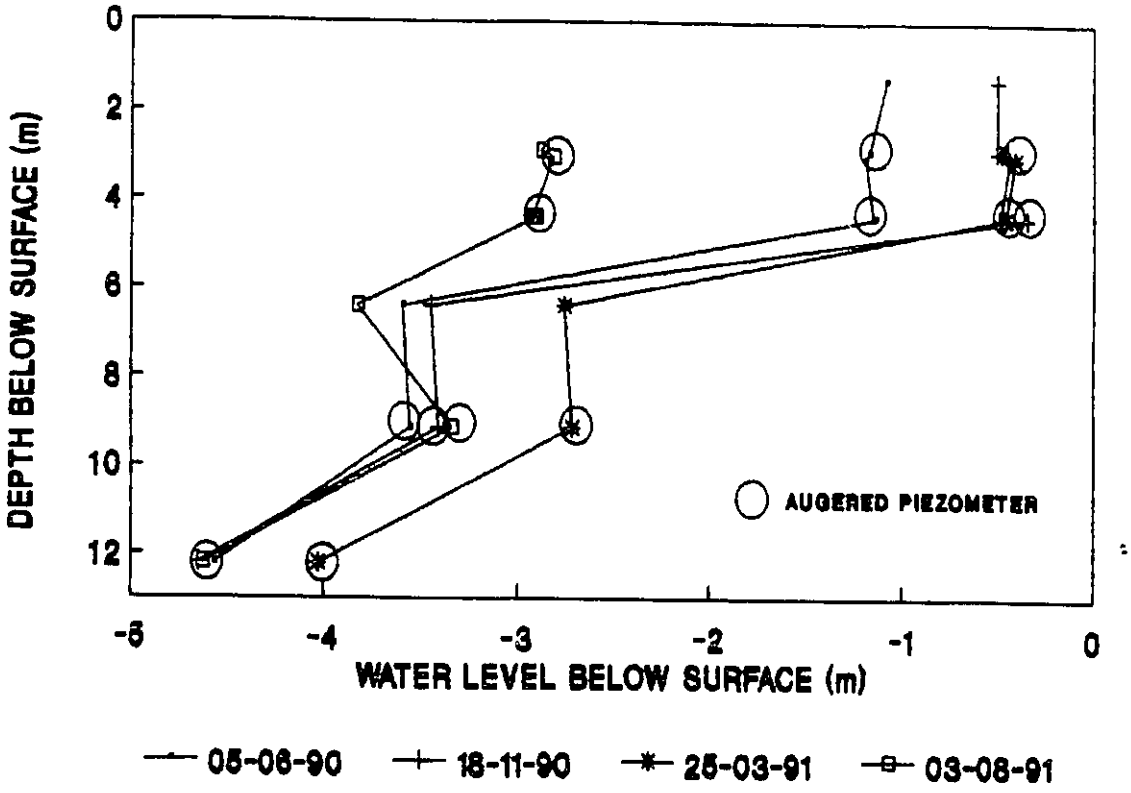

Figure 4.34. Water level variation profiles at the Casselman site.

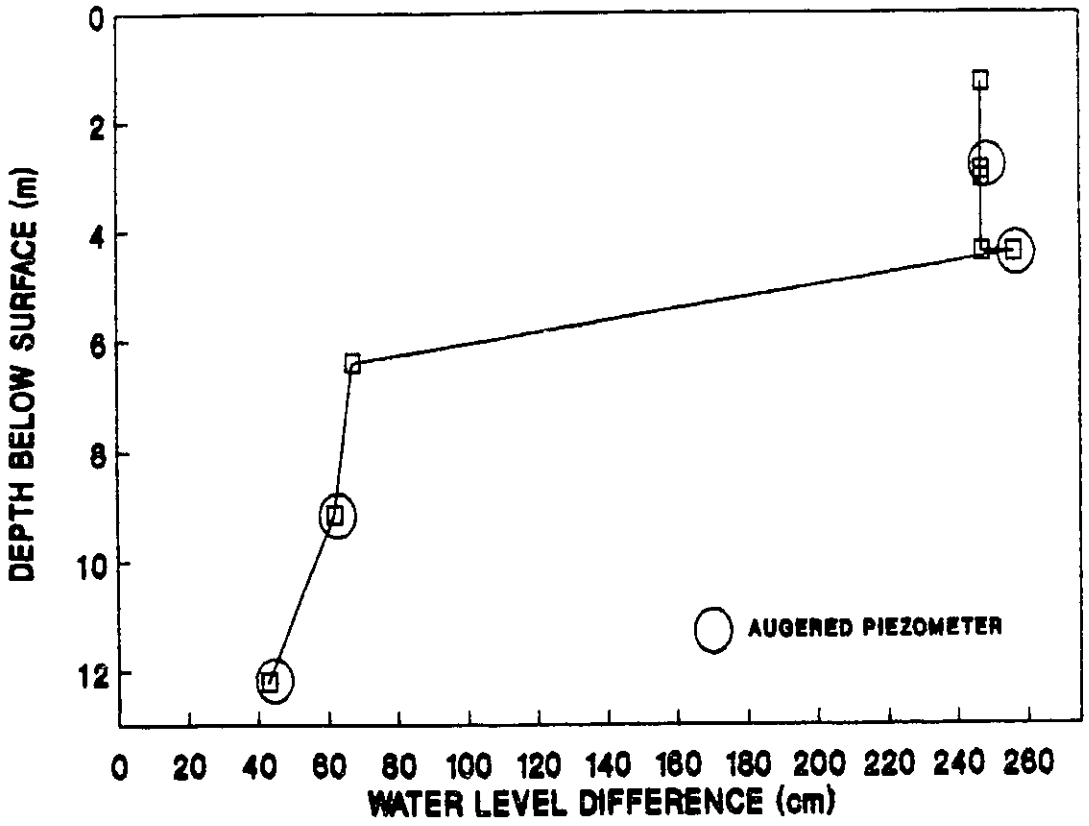

Figure 4.35. Maximum difference in water levels with depth, Casselman site.

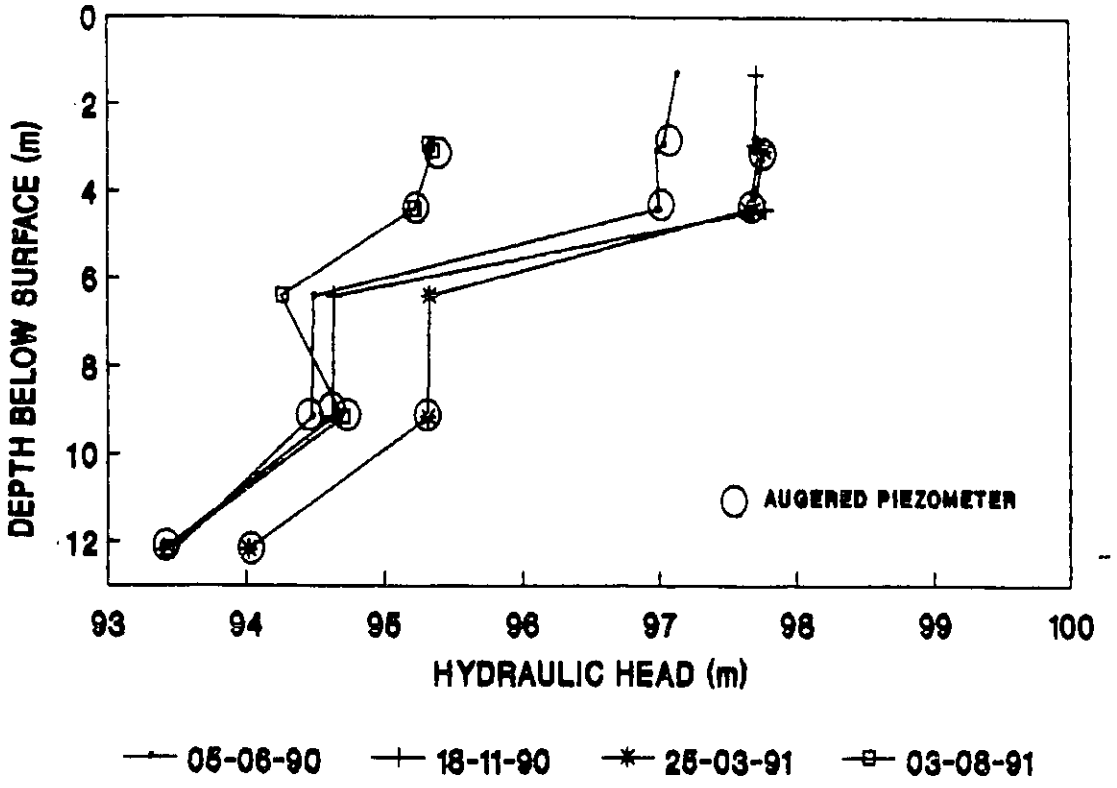

Figure 4.36. Hydraulic head variation profiles at the Casselman site (ground surface elevation of 100 masl).

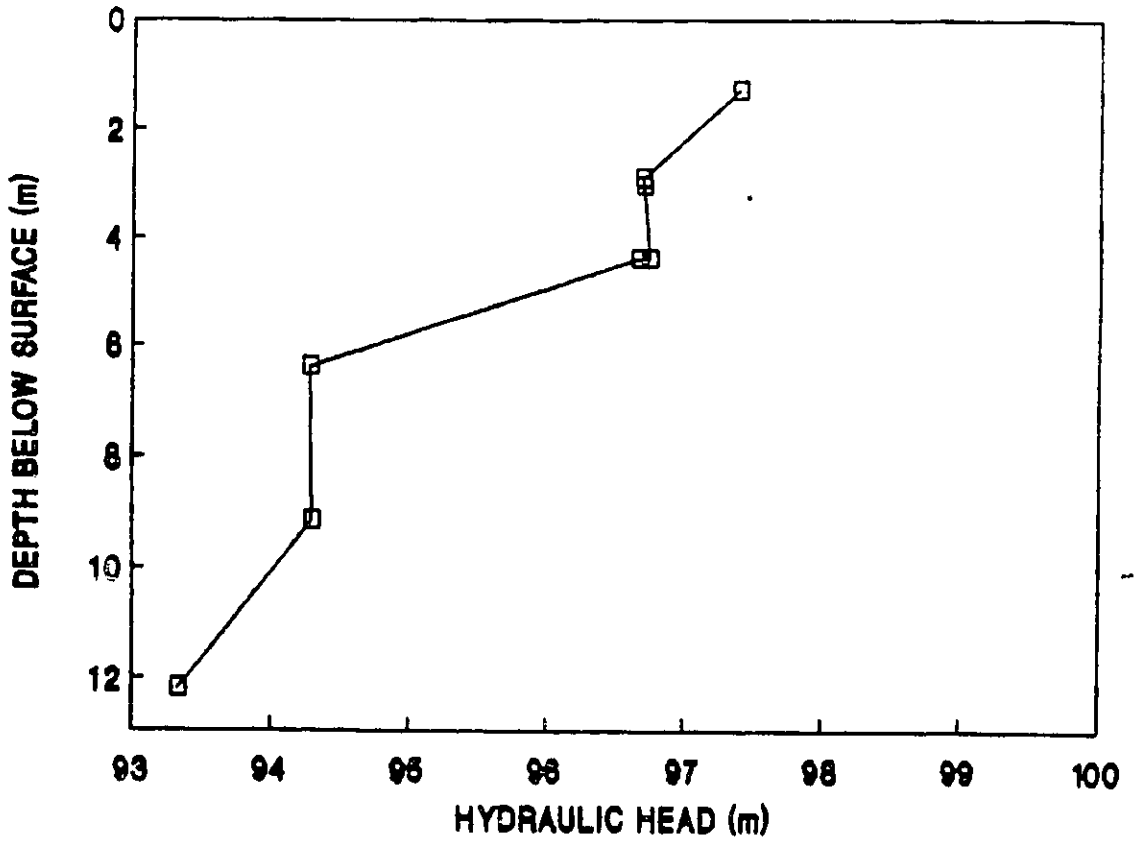

Figure 4.37. The average hydraulic head profile at the Casselman site.

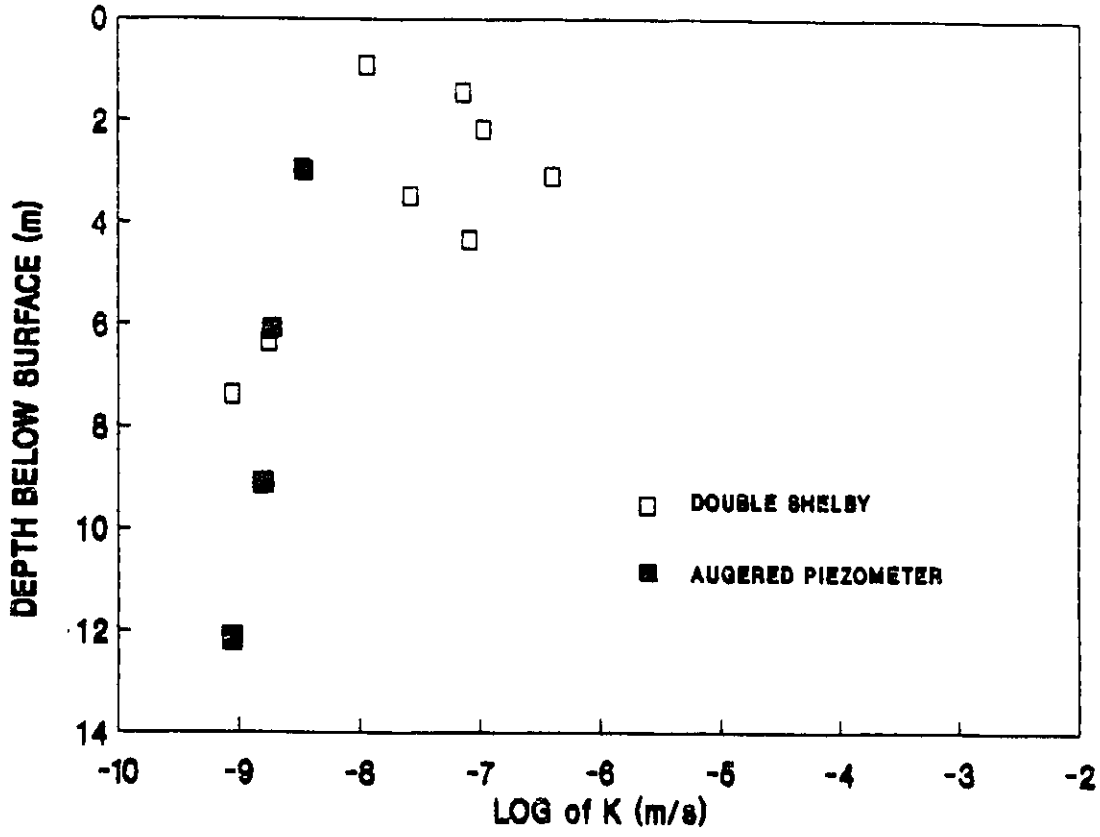

Figure 4.38. The hydraulic conductivity profile at the NRC site, Hvorslev method (1951).

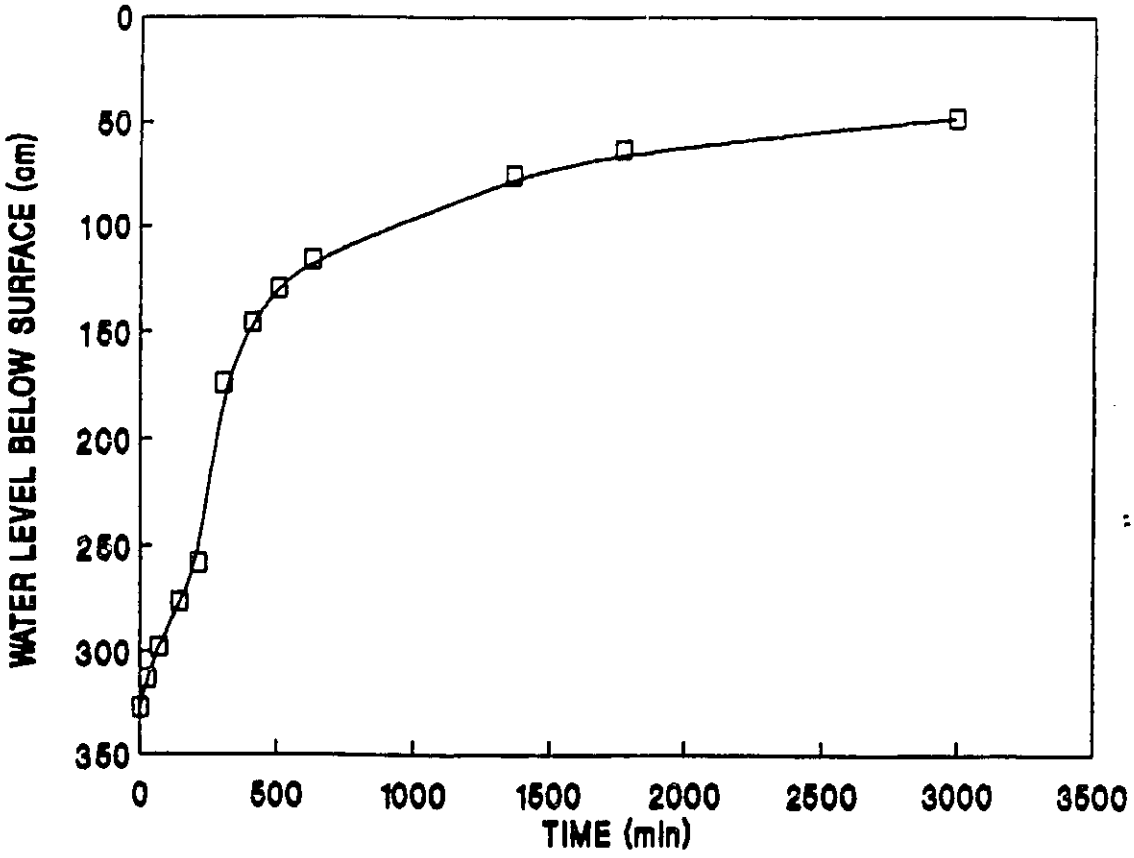

Figure 4.39. The large well recovery data, NRC site.

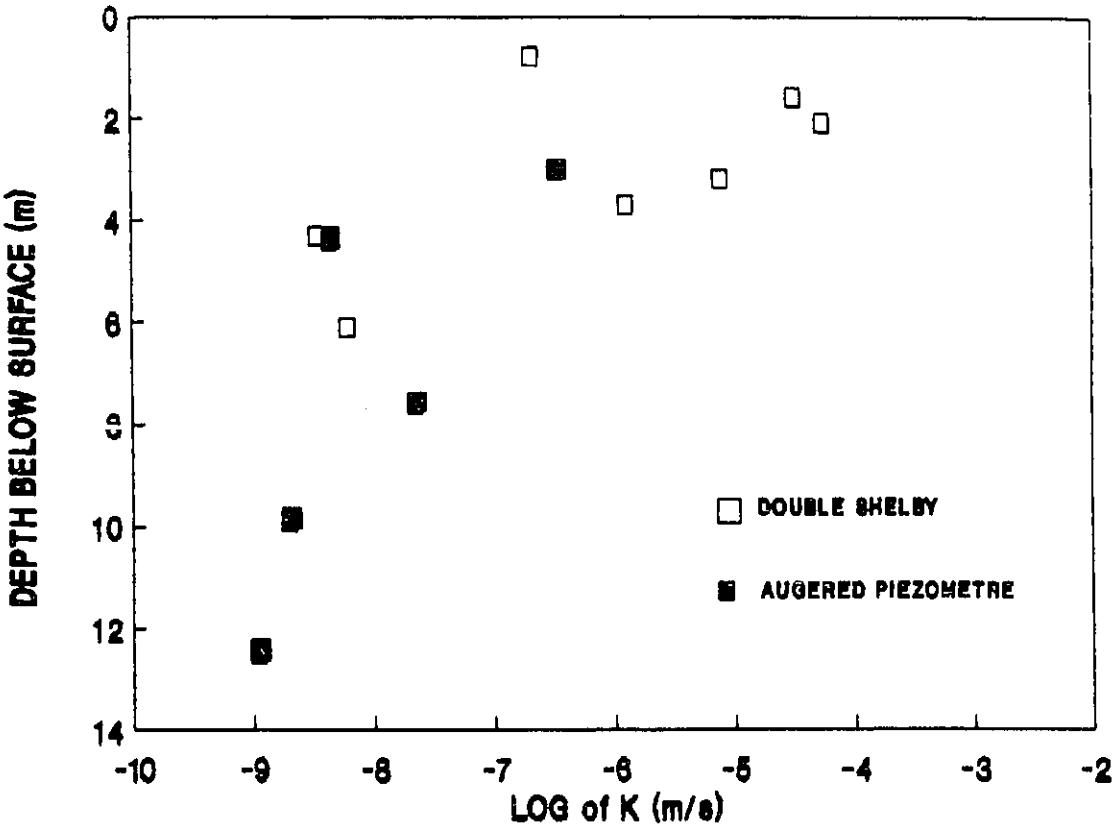

Figure 4.40. The hydraulic conductivity profile at the Fallowfield site, Hvorslev method (1951).

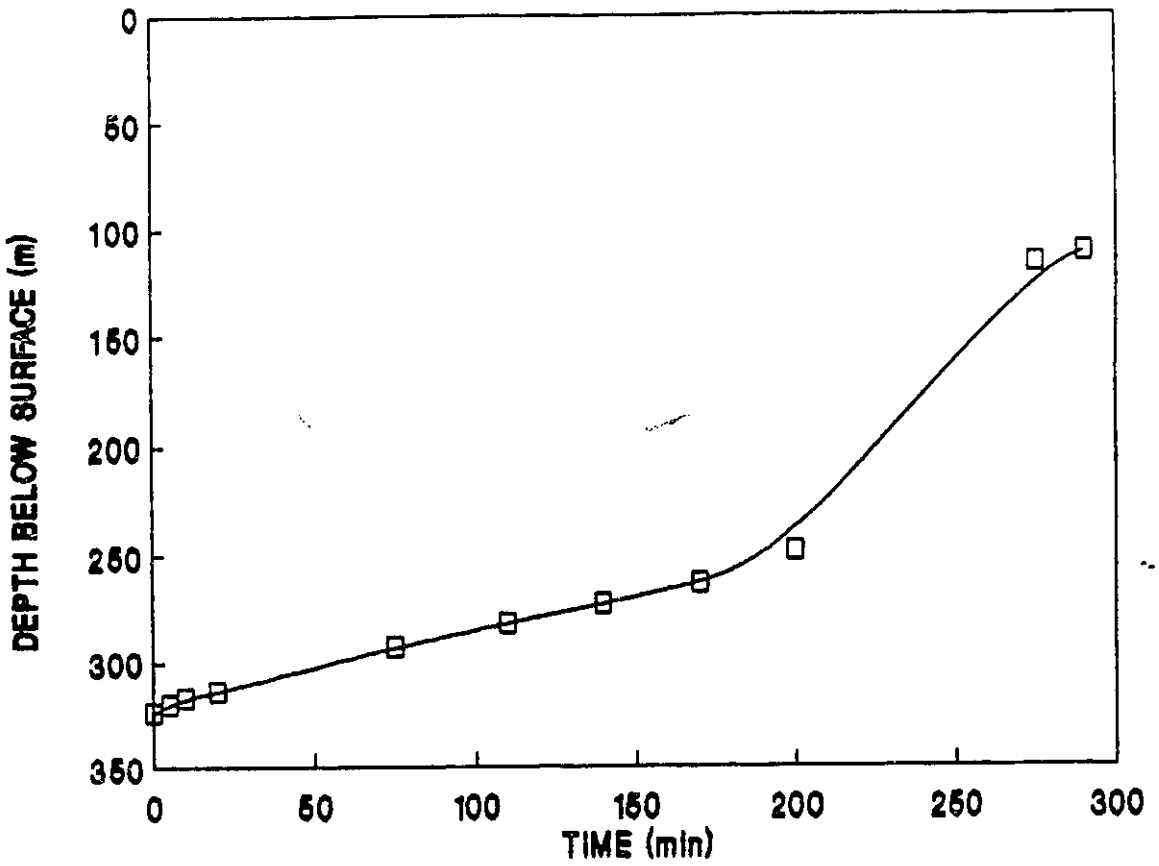

Figure 4.41 The large well recovery data, Fallowfield site.

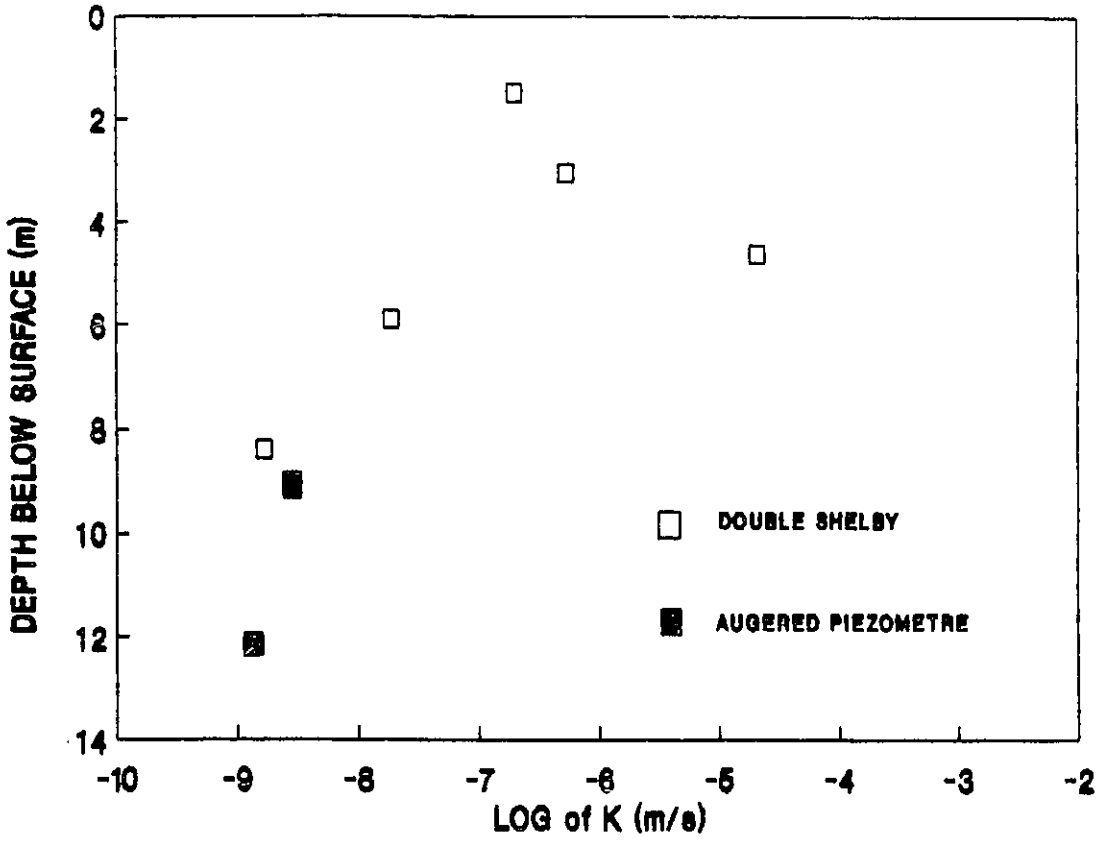

Figure 4.42. The hydraulic conductivity profile at the Renfrew site, Hvorslev method (1951).

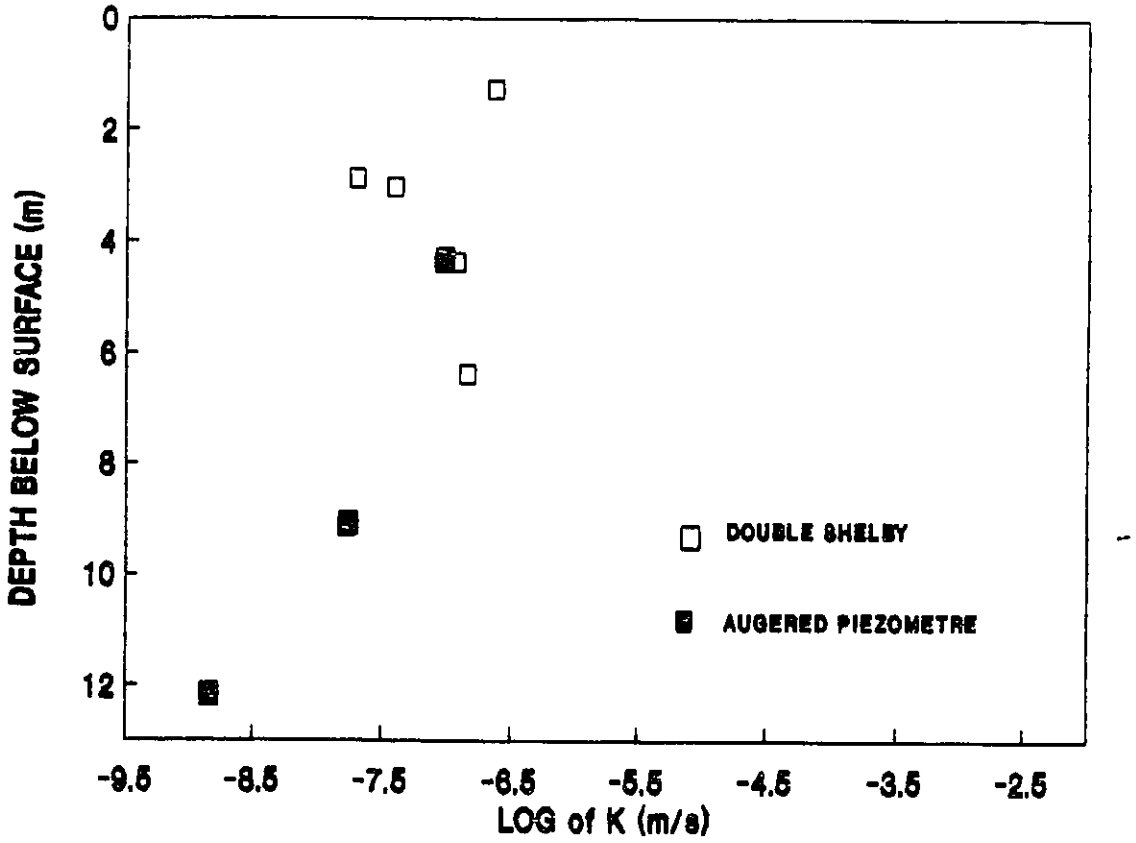

Figure 4.43. The hydraulic conductivity profile at the Casselman site, Hvorslev method (1951).

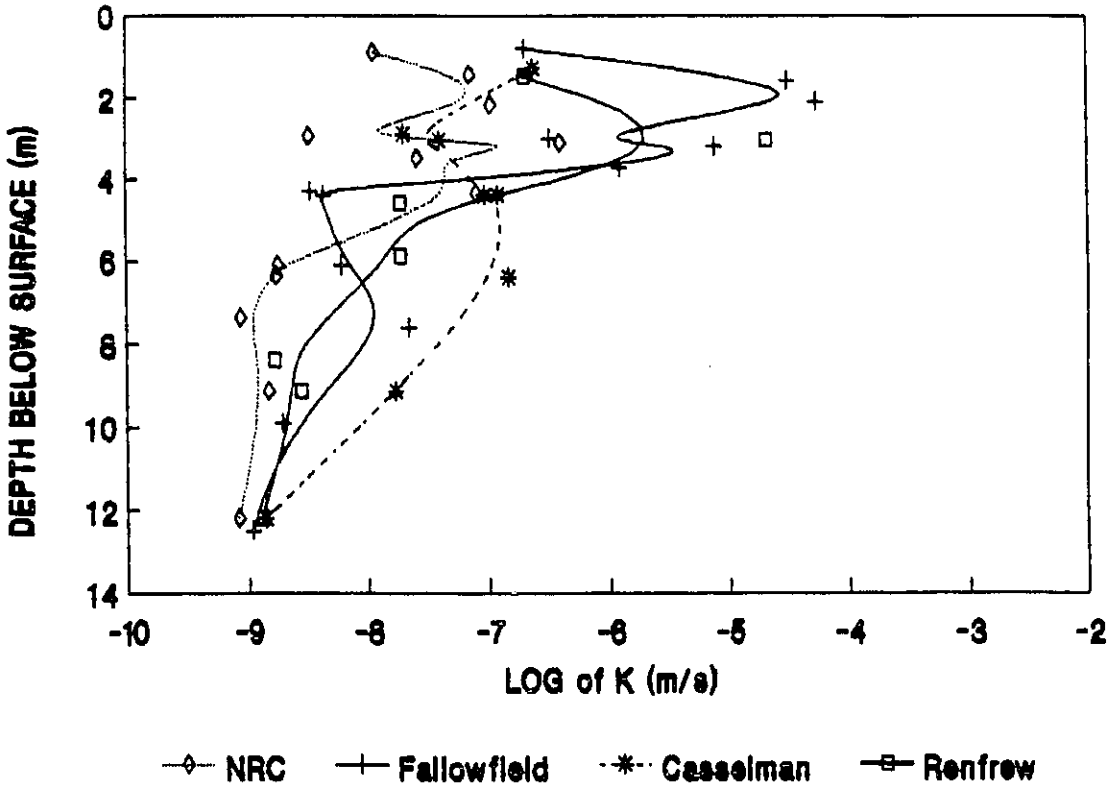

Figure 4.44. The hydraulic conductivity profiles at all four sites, Hvorslev method (1951).

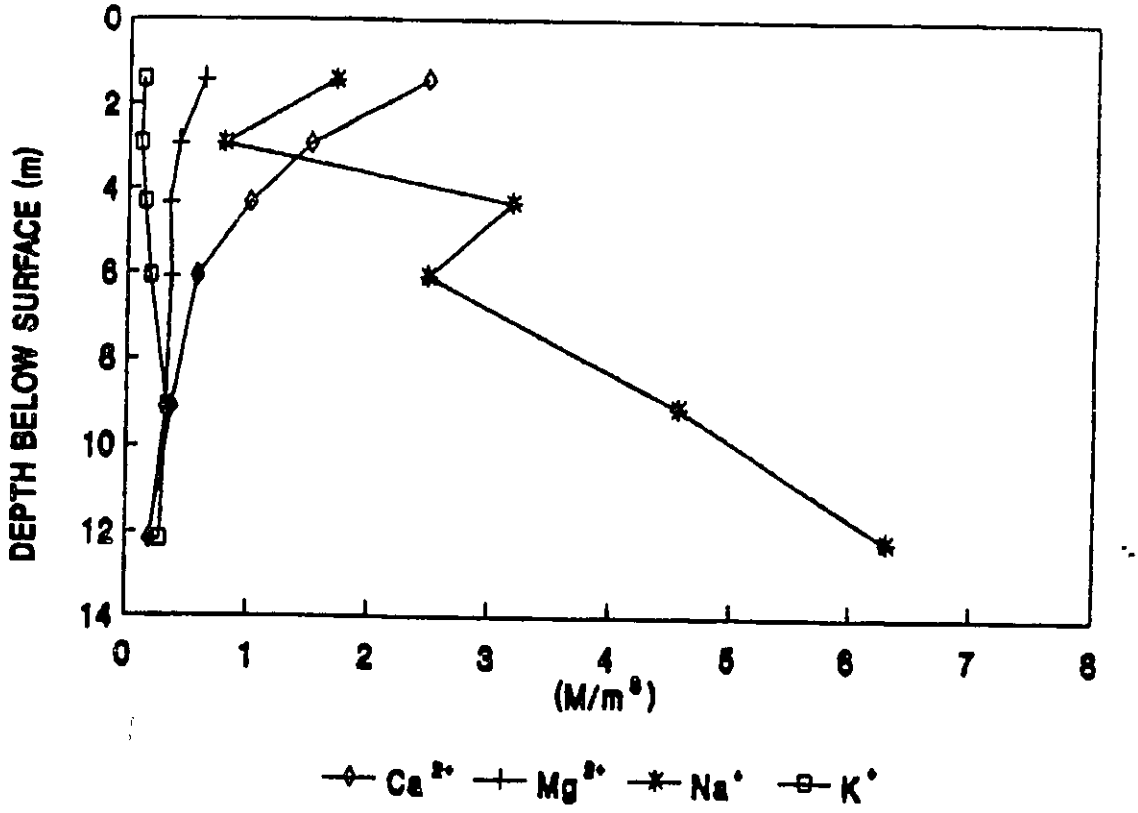

Figure 4.45. The major cation profiles at the NRC site.

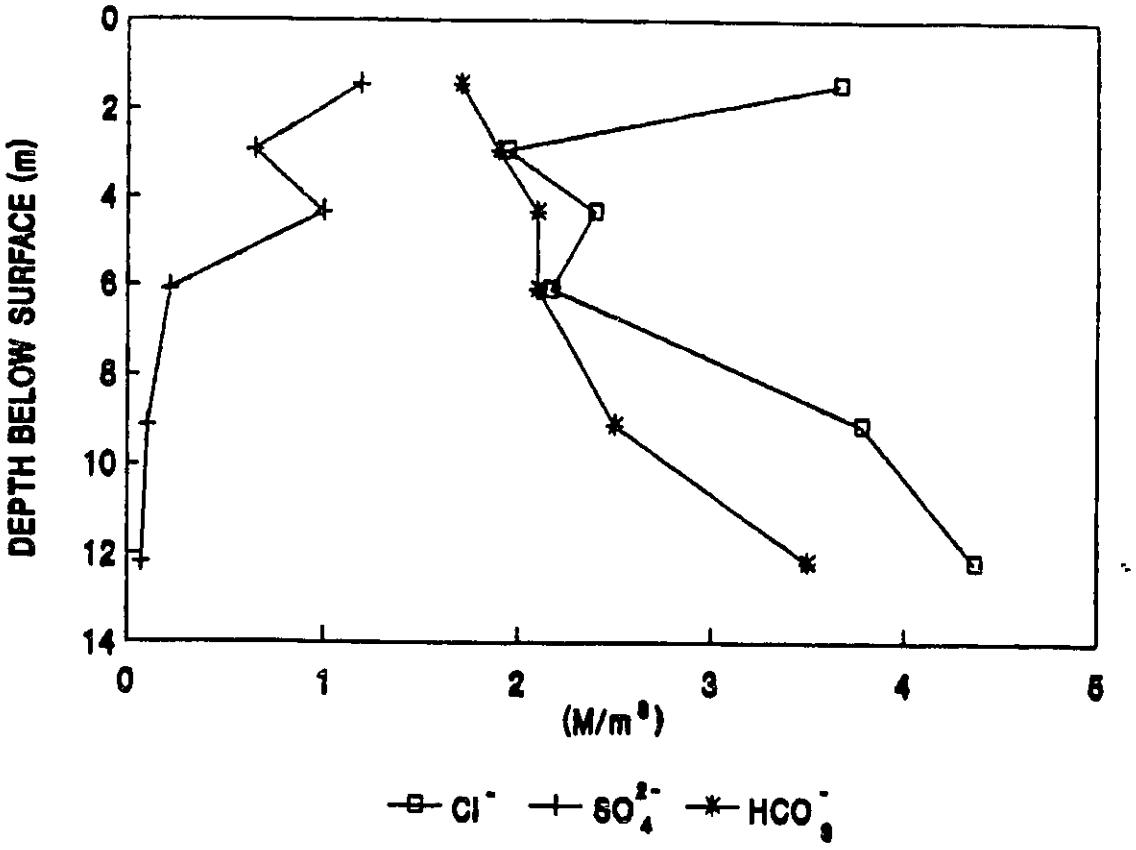

Figure 4.46. The major anion profiles at the NRC site.

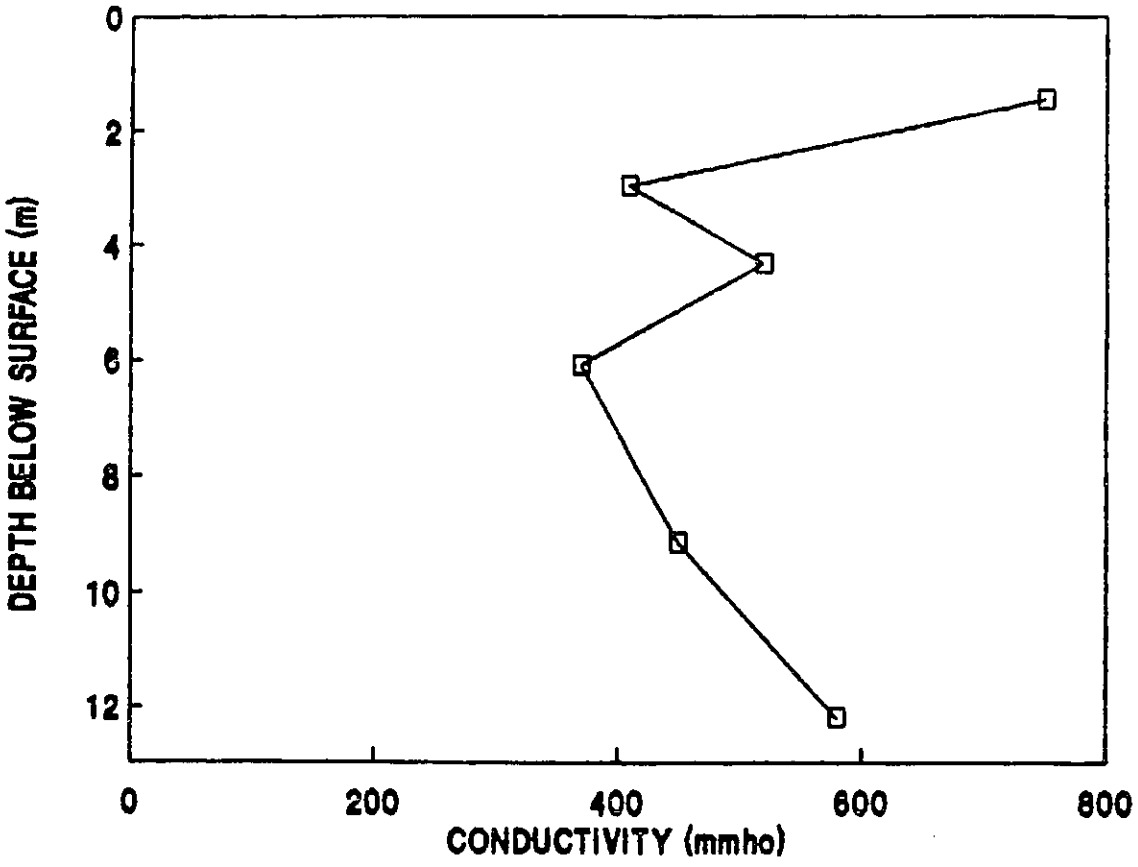

Figure 4.47. The electrical conductivity profile at the NRC site.

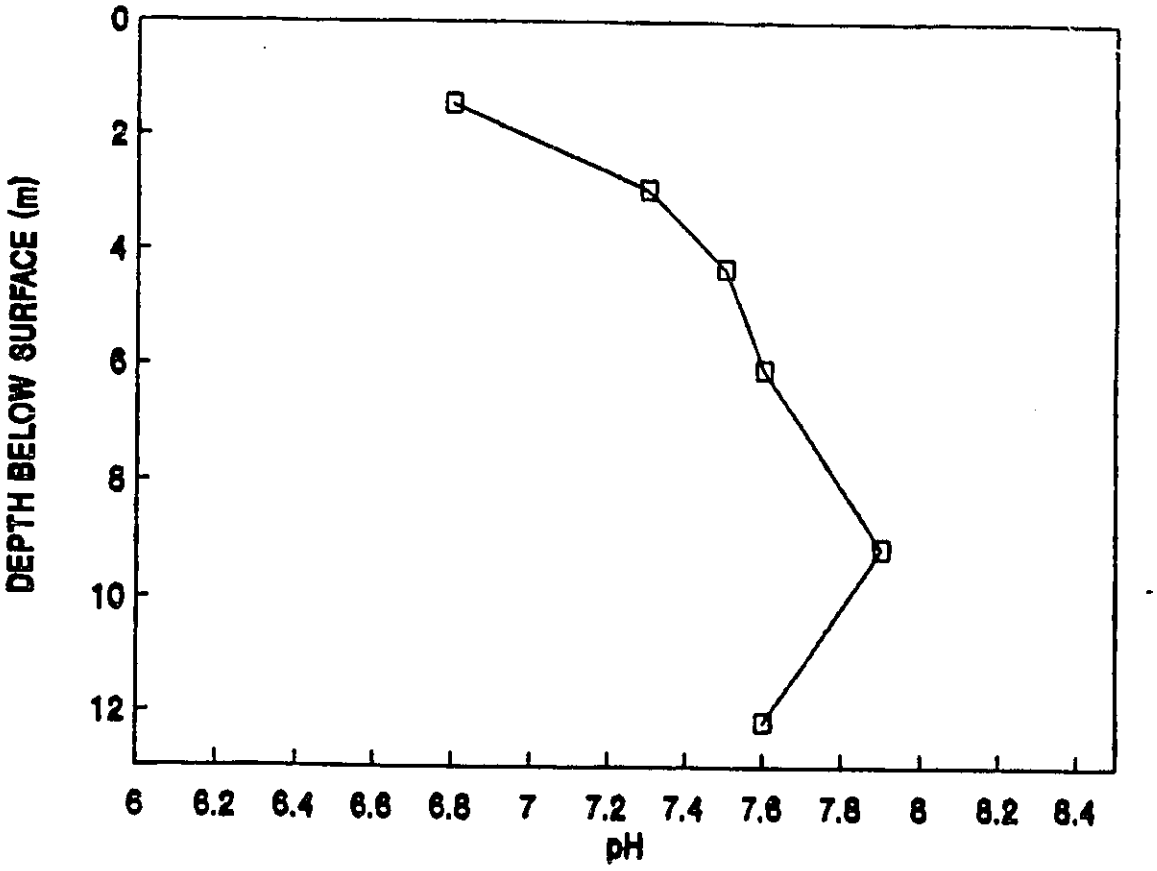

Figure 4.48. pH versus depth at the NRC site.

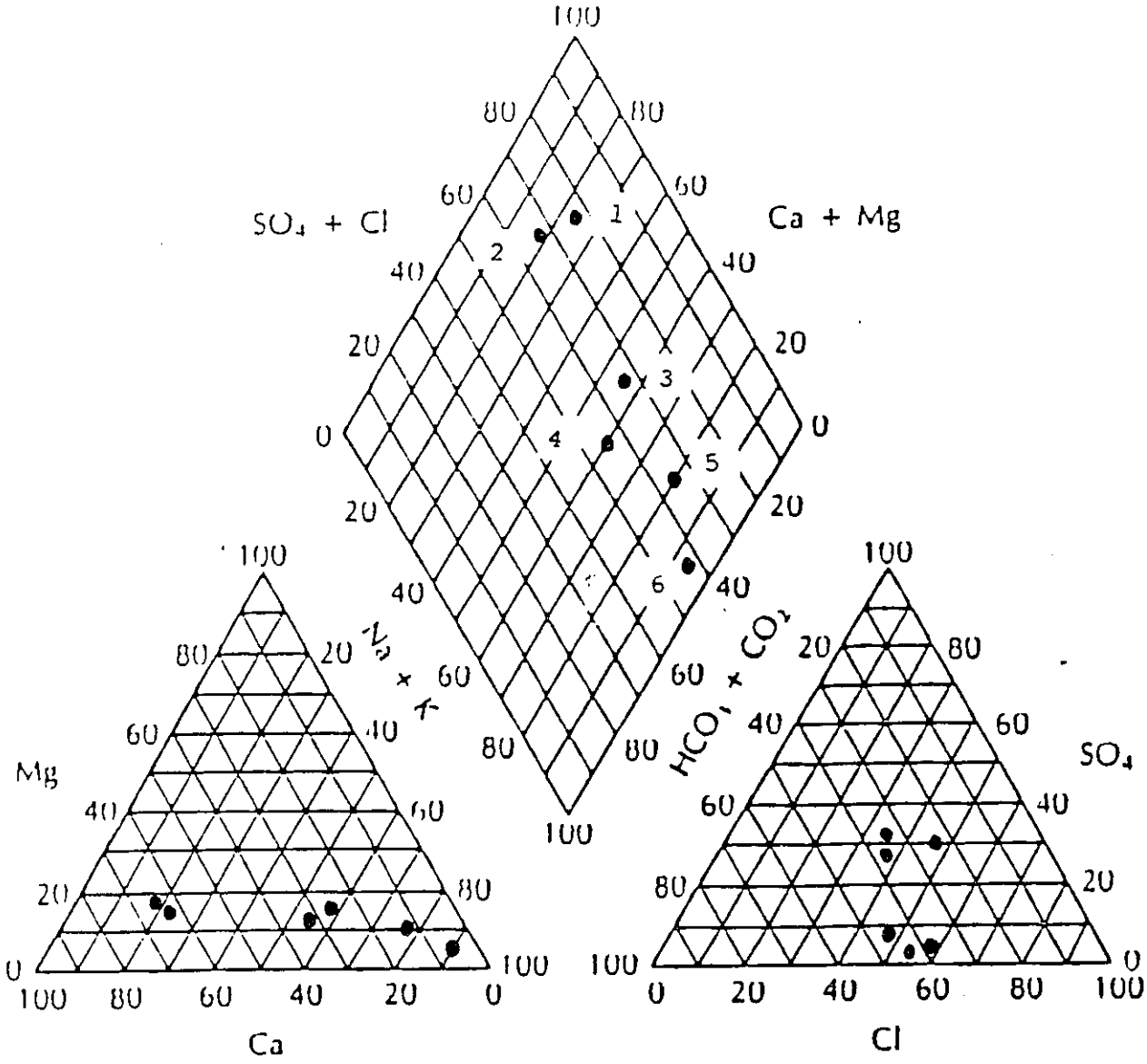

Figure 4.49. Trilinear diagram of water analysis from the NRC site.

SAMPLE DEPTH (m)

1 - 1.45

2 - 2.95

3 - 4.40

4 - 6.10

5 - 9.15

6 - 12.20

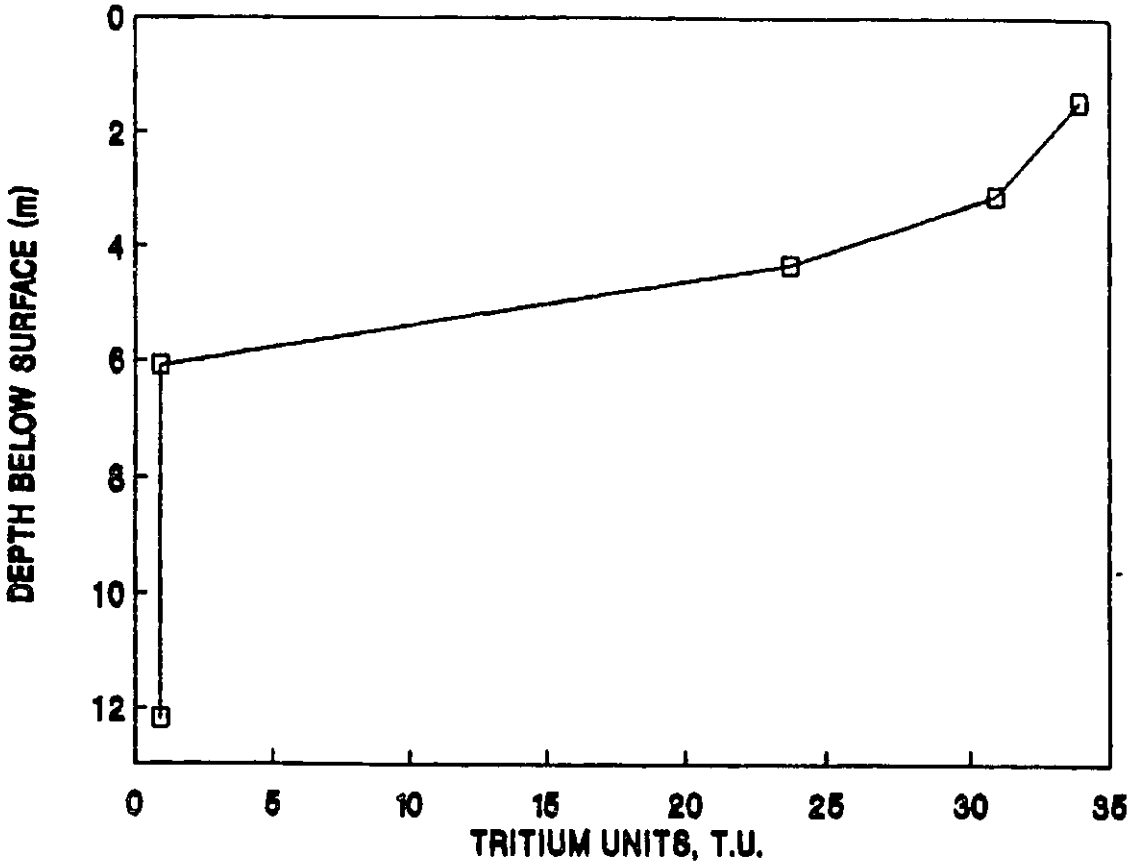

Figure 4.50. Tritium profile at the MRC site.

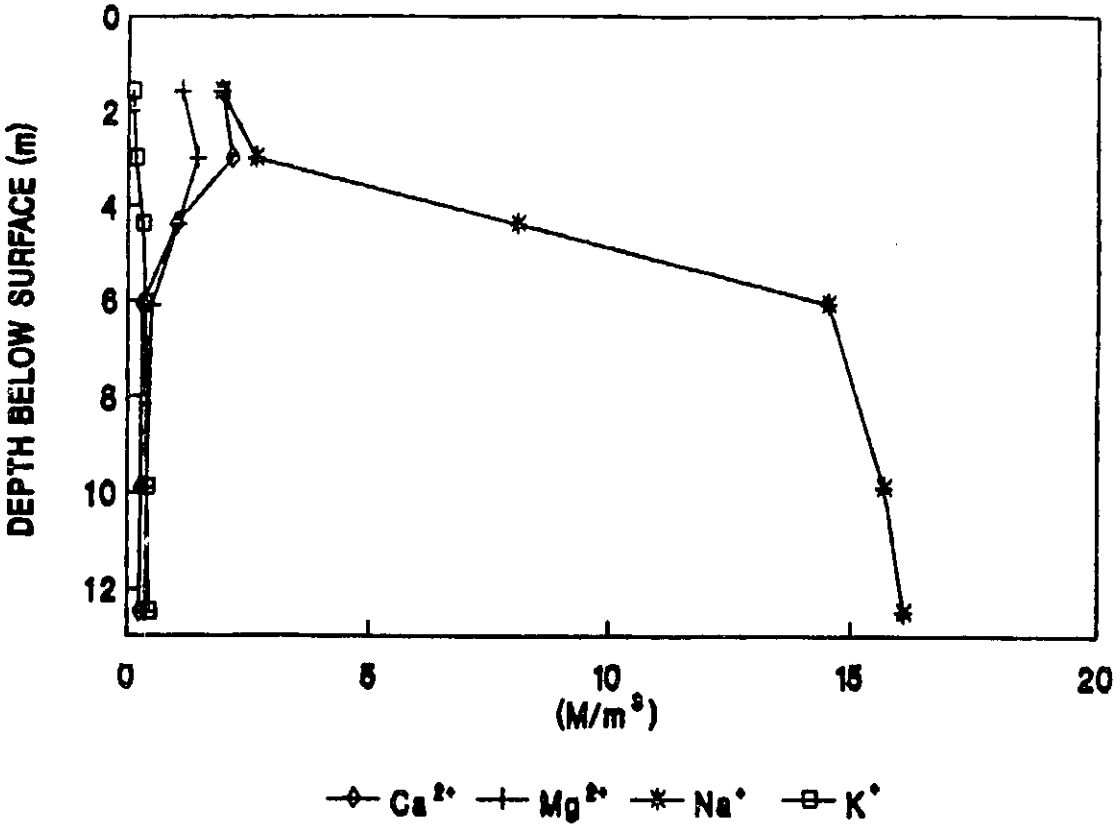

Figure 4.51. The major cation profiles at the Fallowfield site.

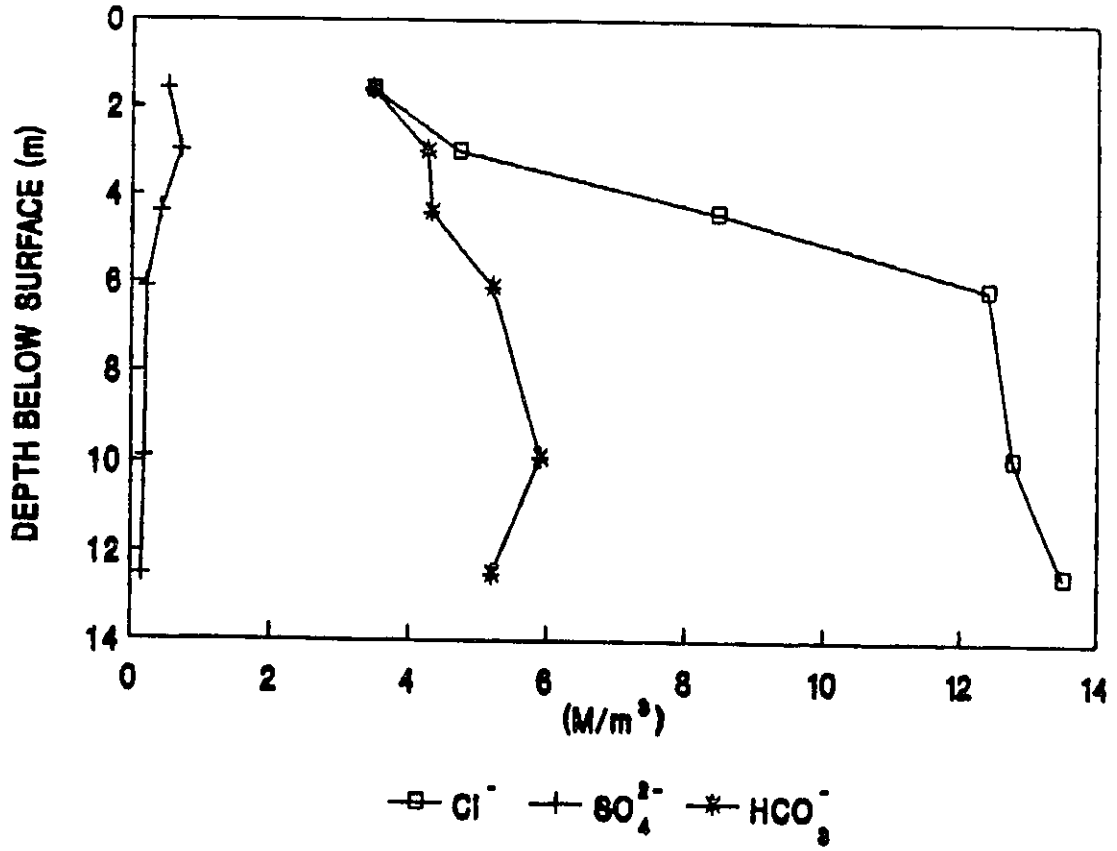

Figure 4.52. The major anion profiles at the Fallowfield site.

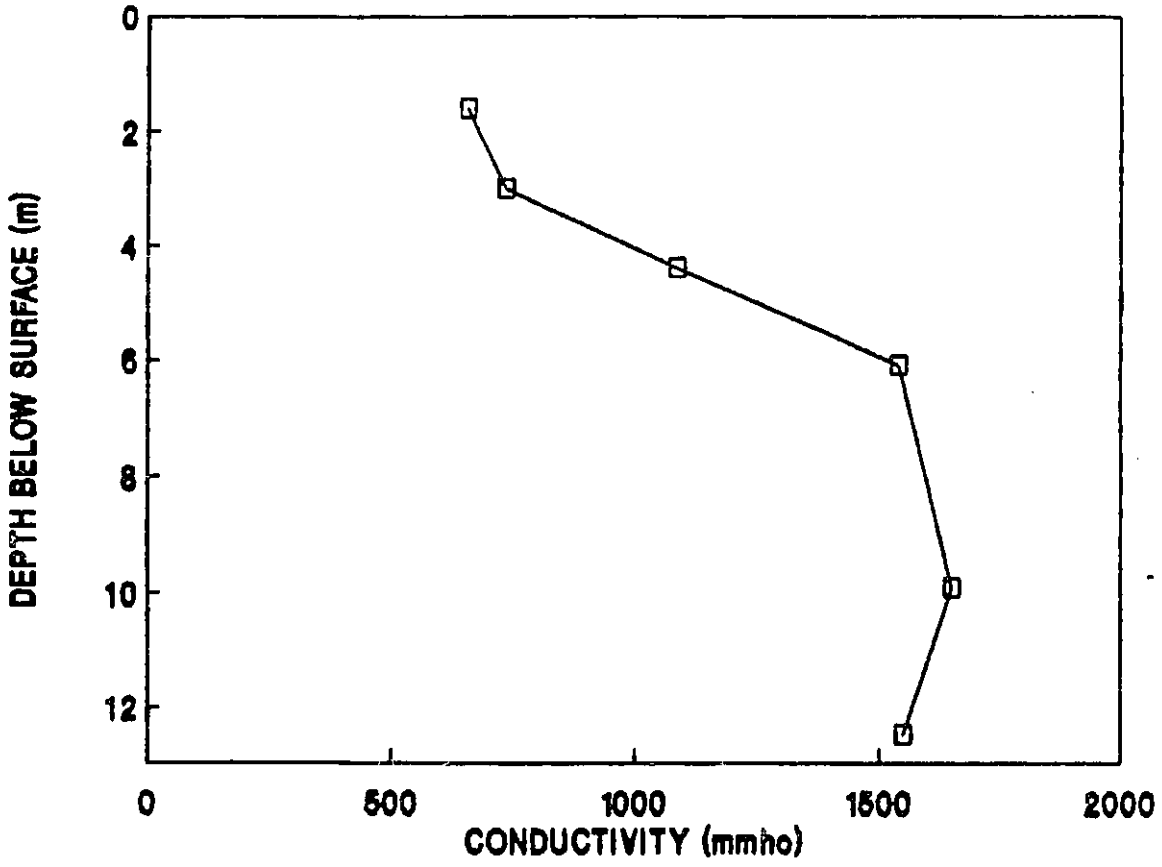

Figure 4.53. The electrical conductivity profile at the Fallowfield site.

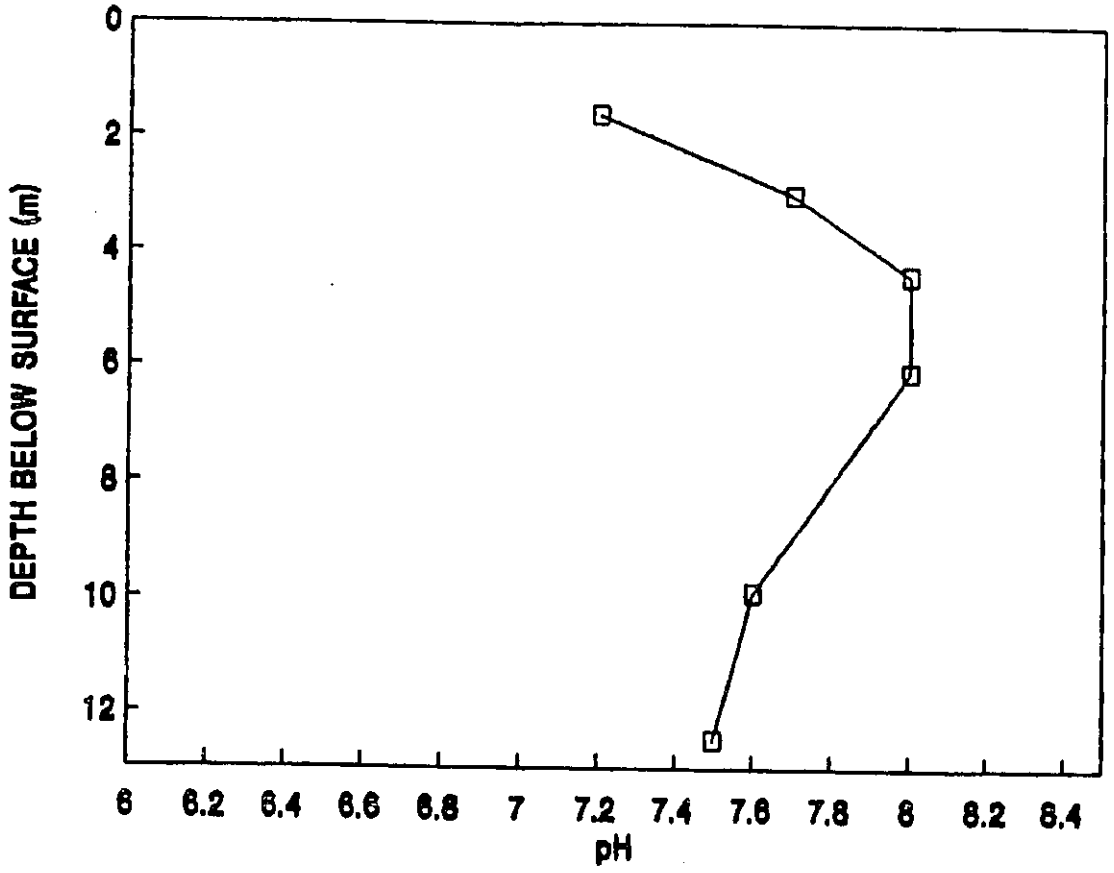

Figure 4.54. pH versus depth at the Fallowfield site.

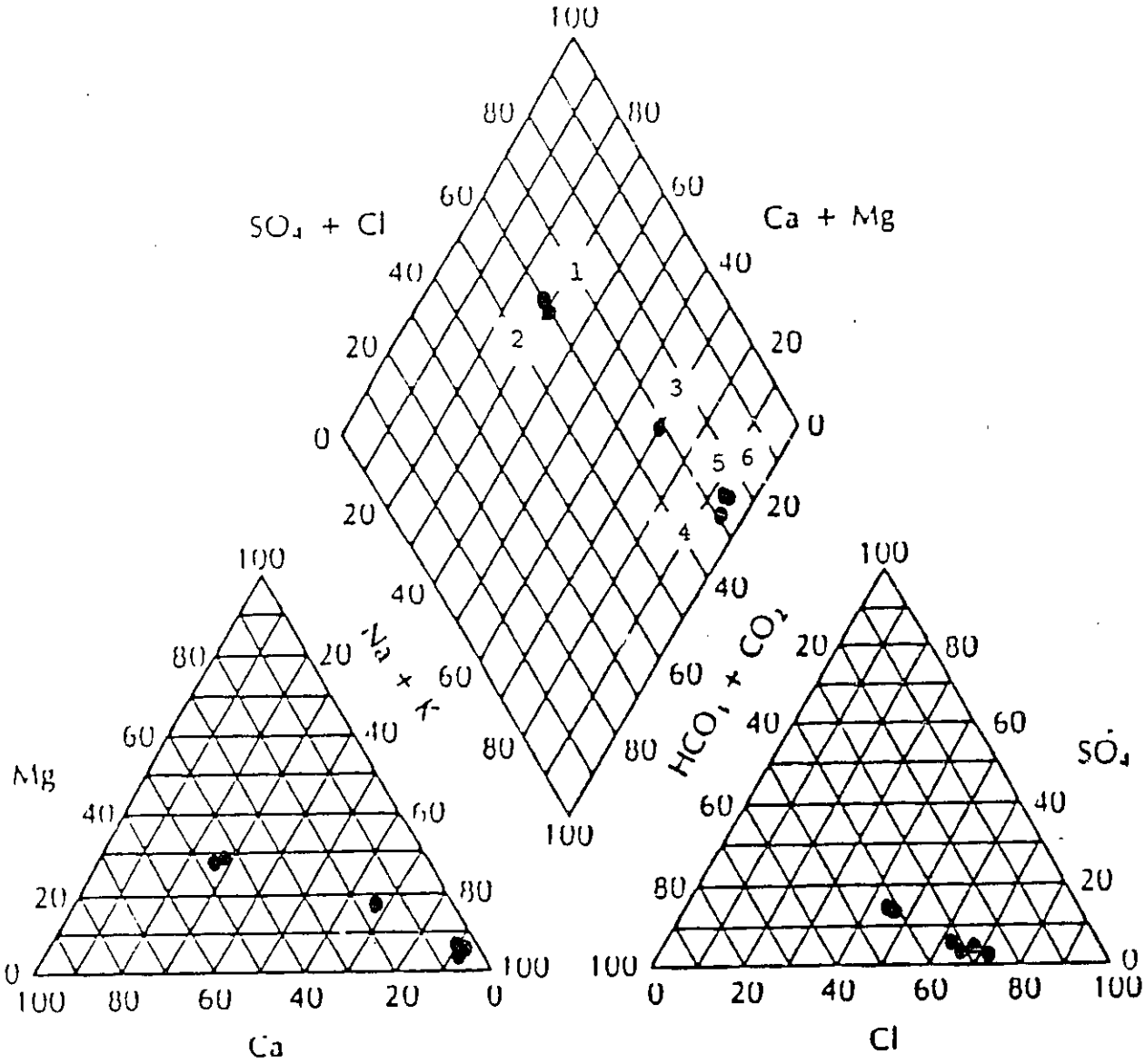

Figure 4.55. Trilinear diagram of water analysis from the Fallowfield site.

SAMPLE DEPTH (m)

1 - 1.60

2 - 3.00

3 - 4.40

4 - 6.10

5 - 9.90

6 - 12.50

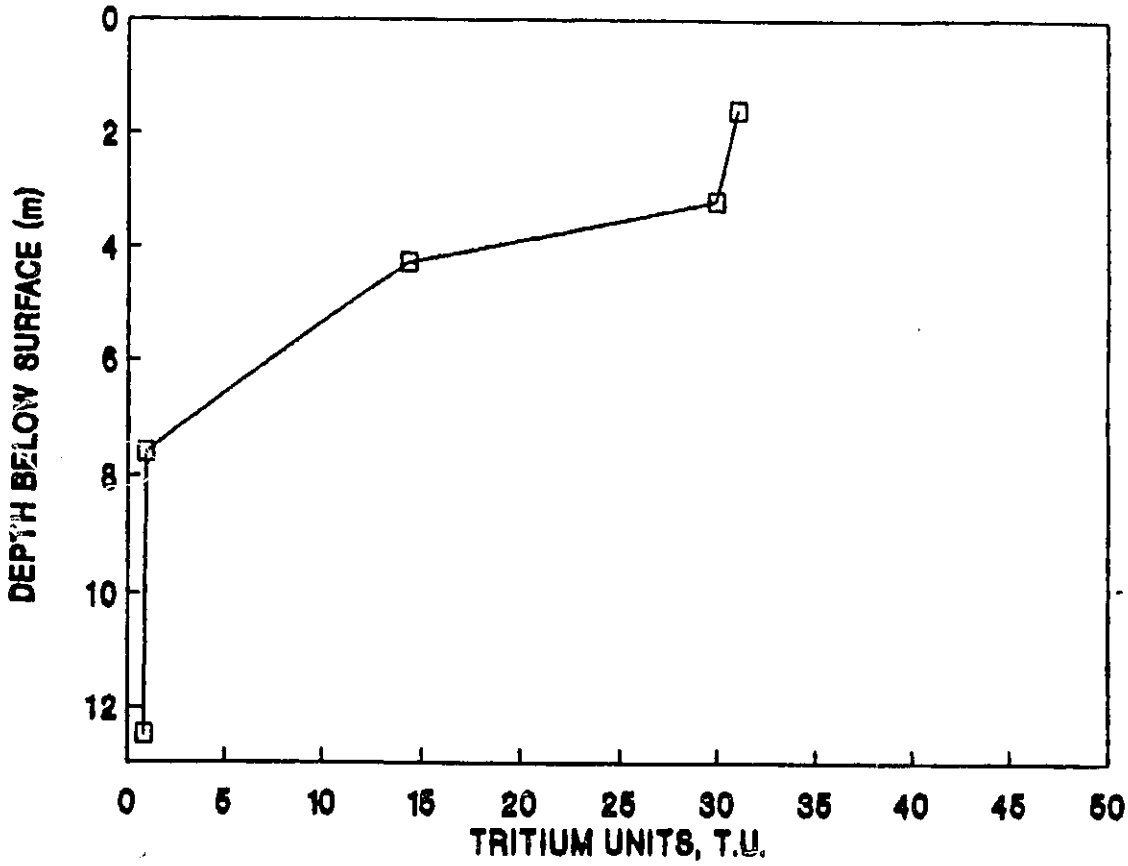

Figure 4.56. Tritium profile at the Fallowfield site.

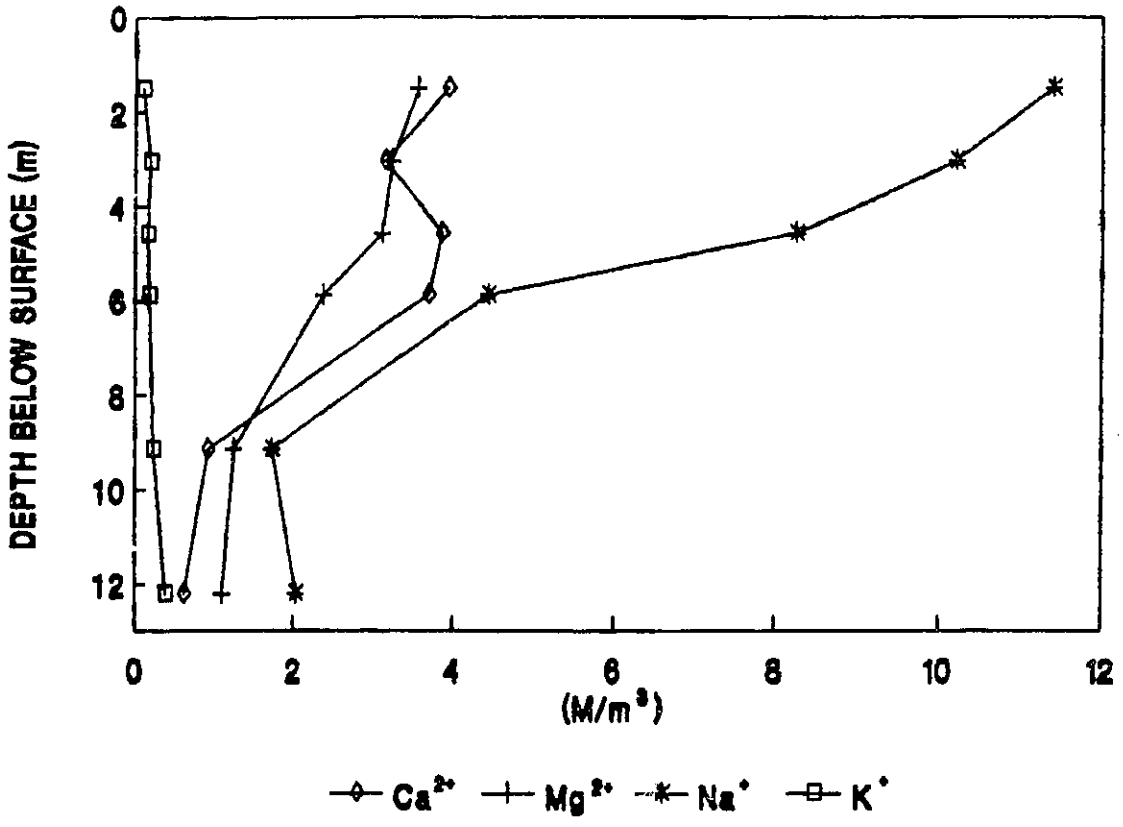

Figure 4.57. The major cation profiles at the Renfrew site.

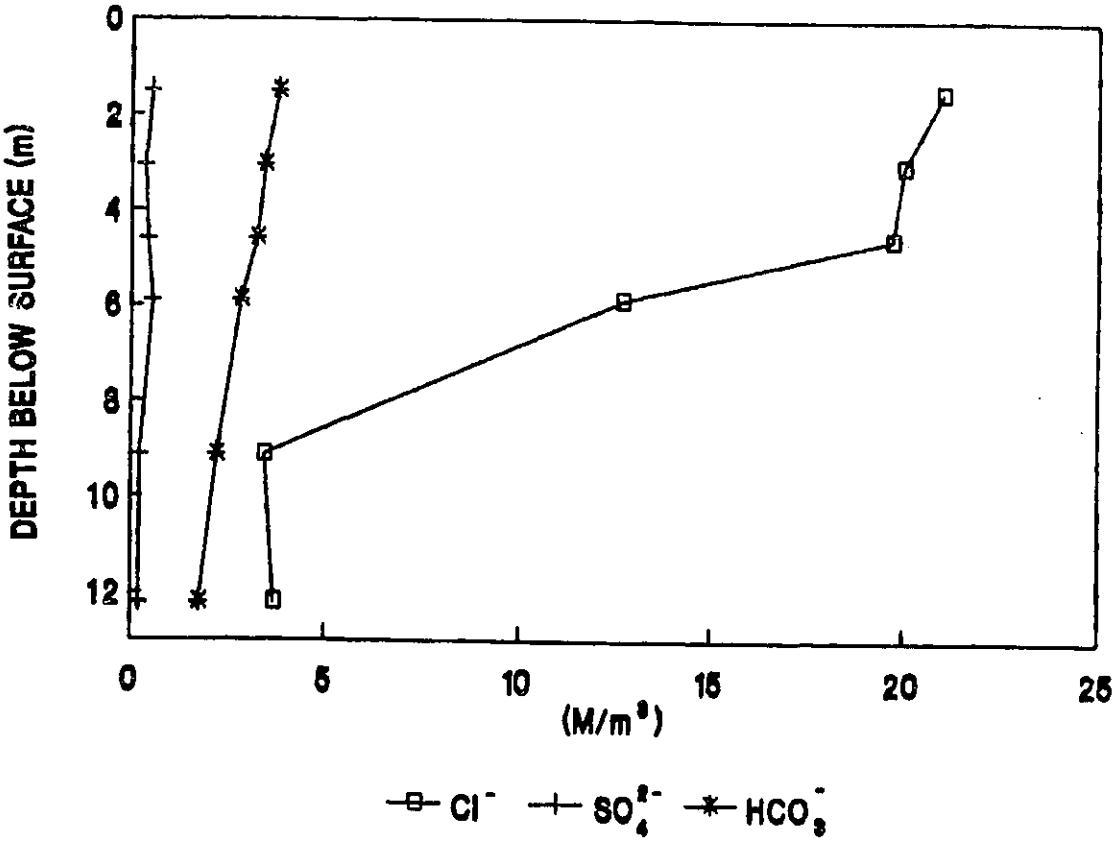

Figure 4.58. The major anion profiles at the Renfrew site.

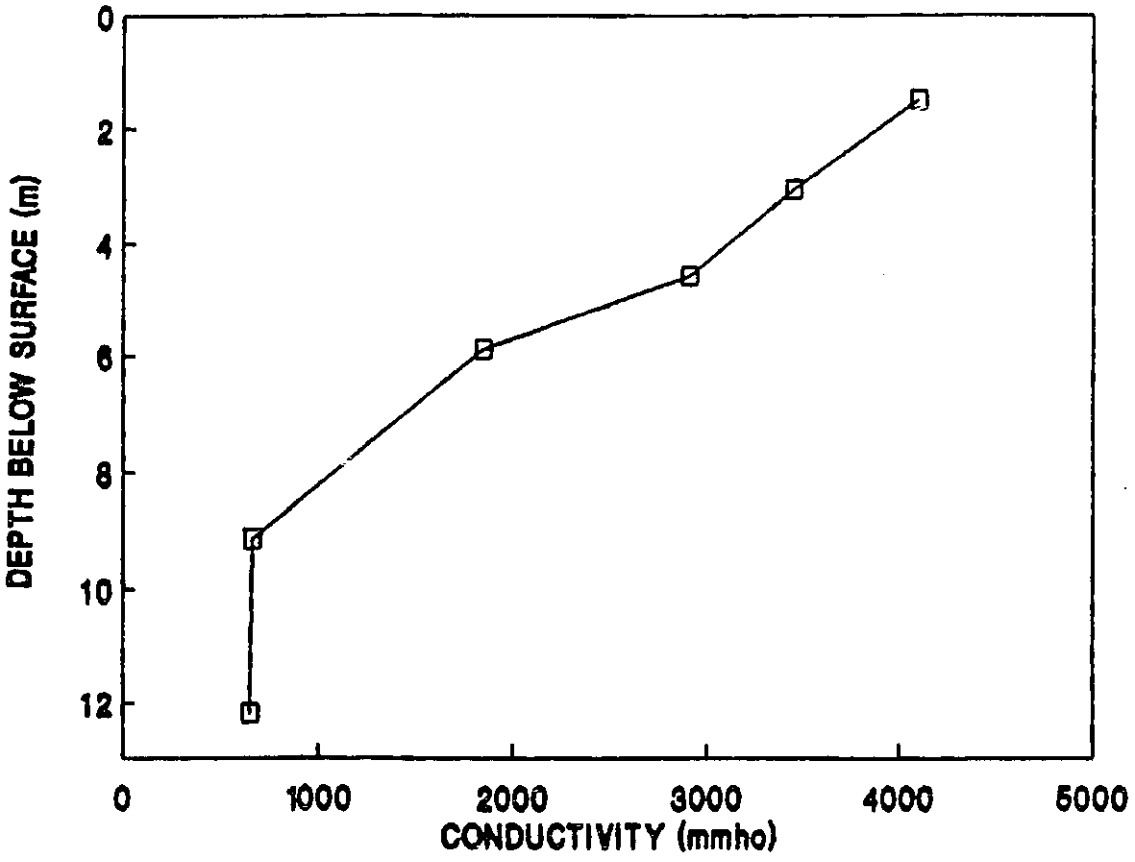

Figure 4.59. The electrical conductivity profile at the Renfrew site.

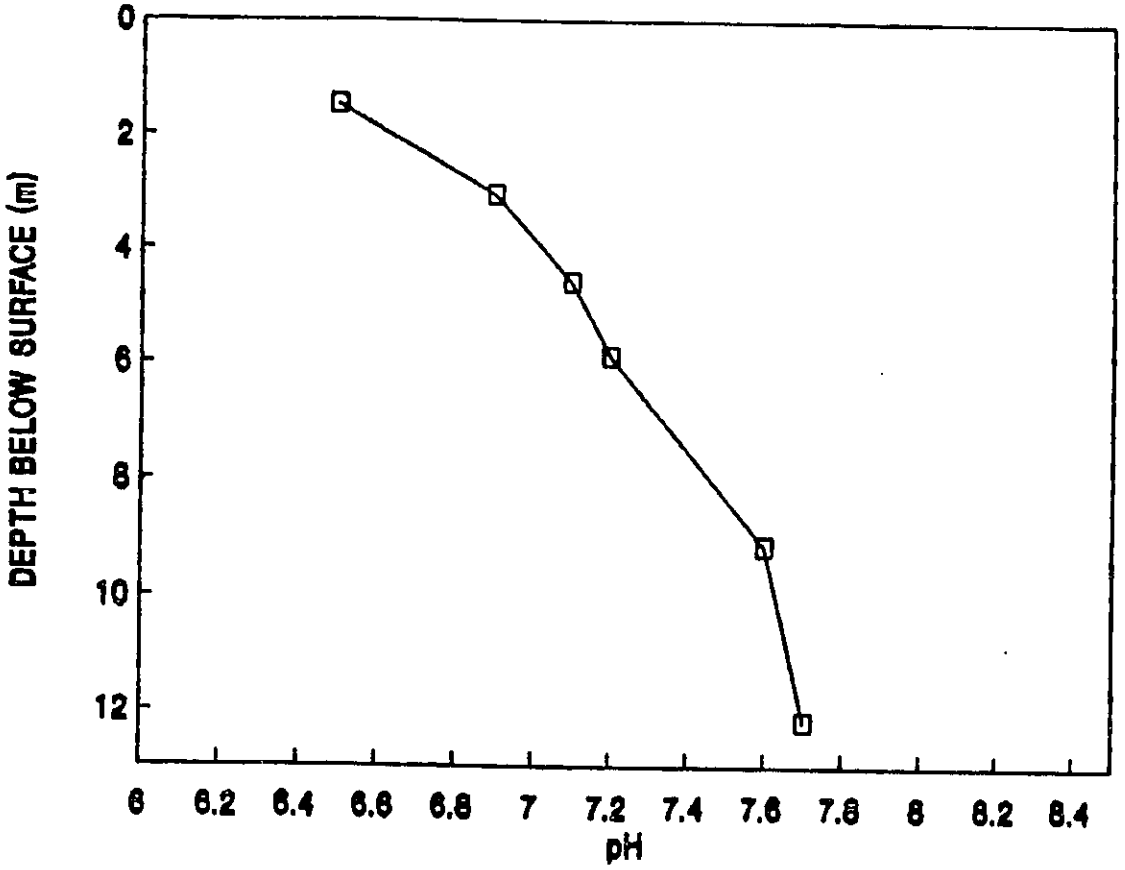

Figure 4.60. pH versus depth at the Renfrew site.

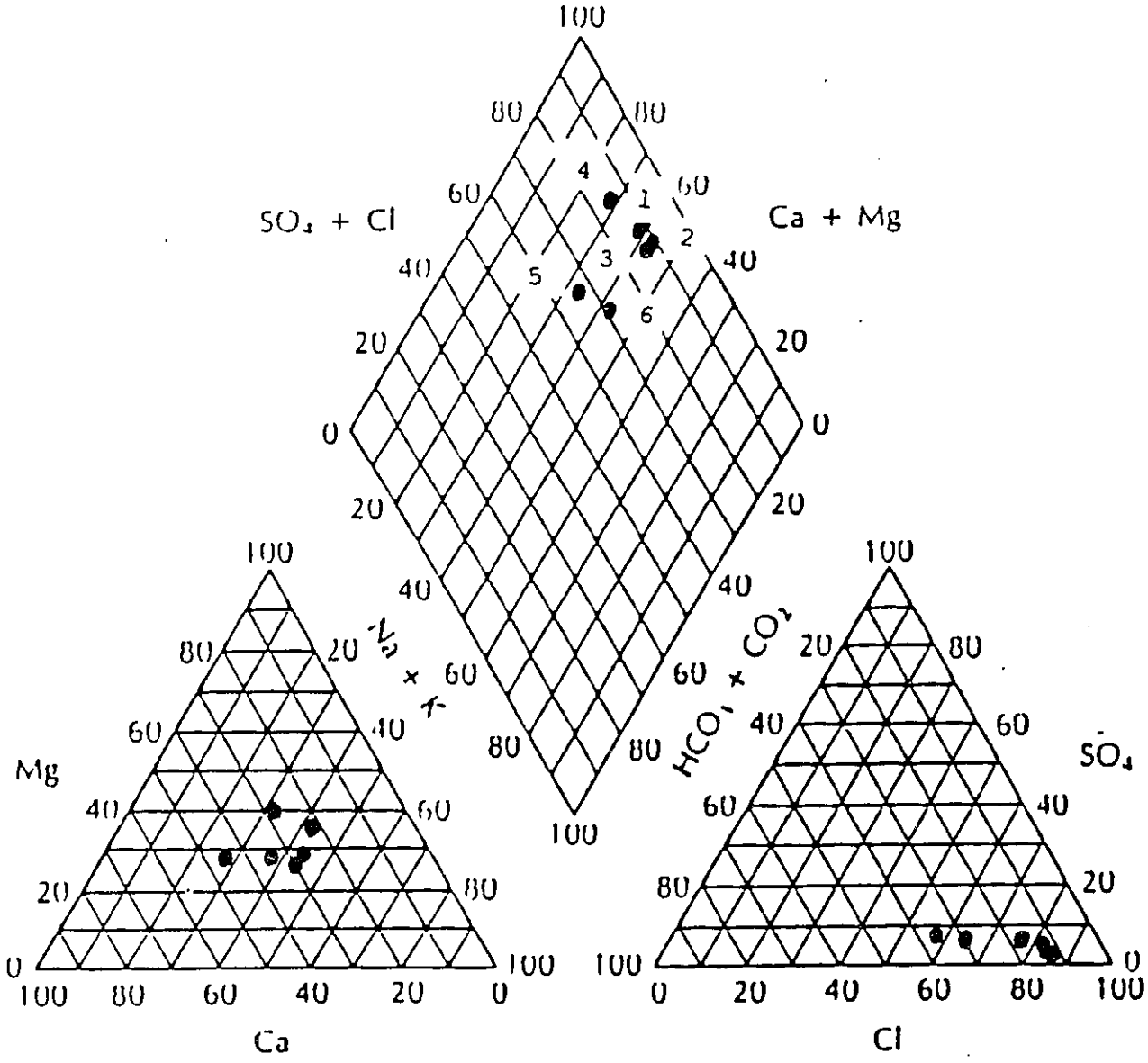

Figure 4.61. Trilinear diagram of water analysis from the Renfrew site.

SAMPLE DEPTH (m)

1 - 1.50

2 - 3.05

3 - 4.60

4 - 5.90

5 - 9.15

6 - 12.20

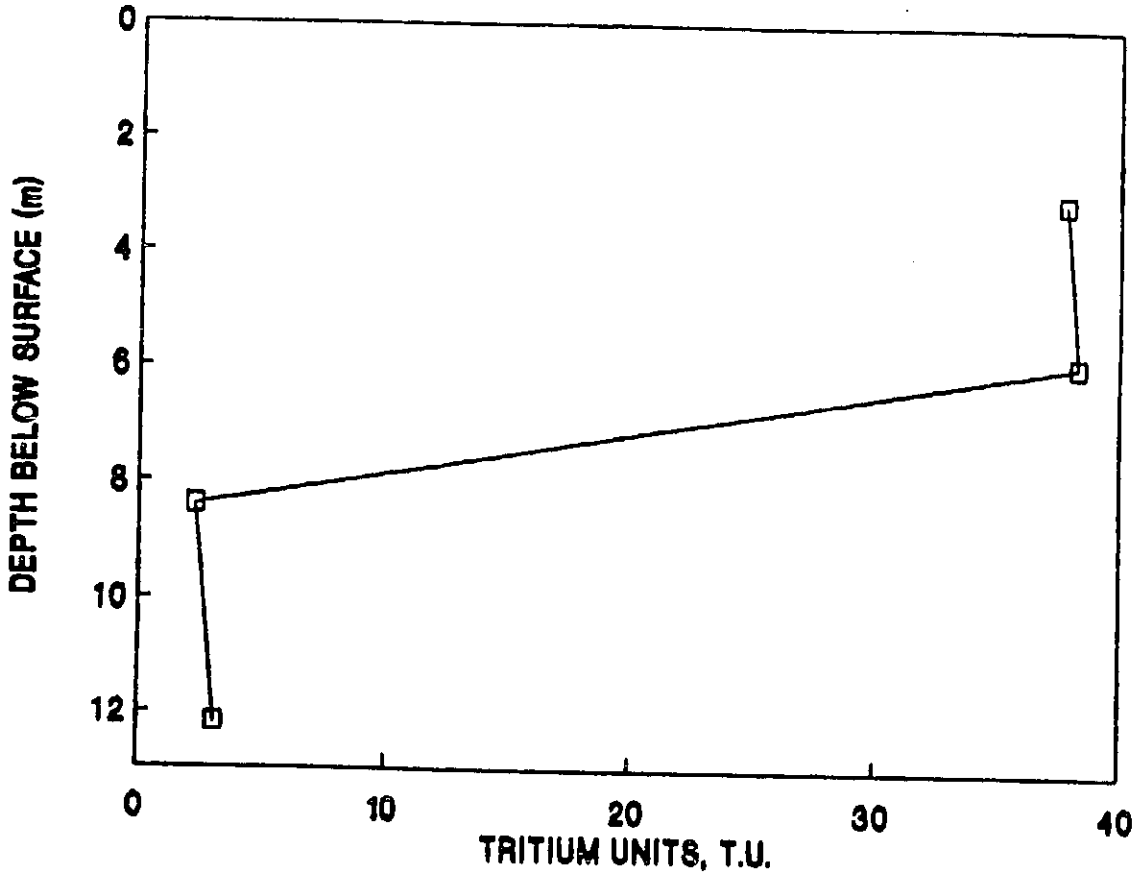

Figure 4.62. Tritium profile at the Renfrew site.

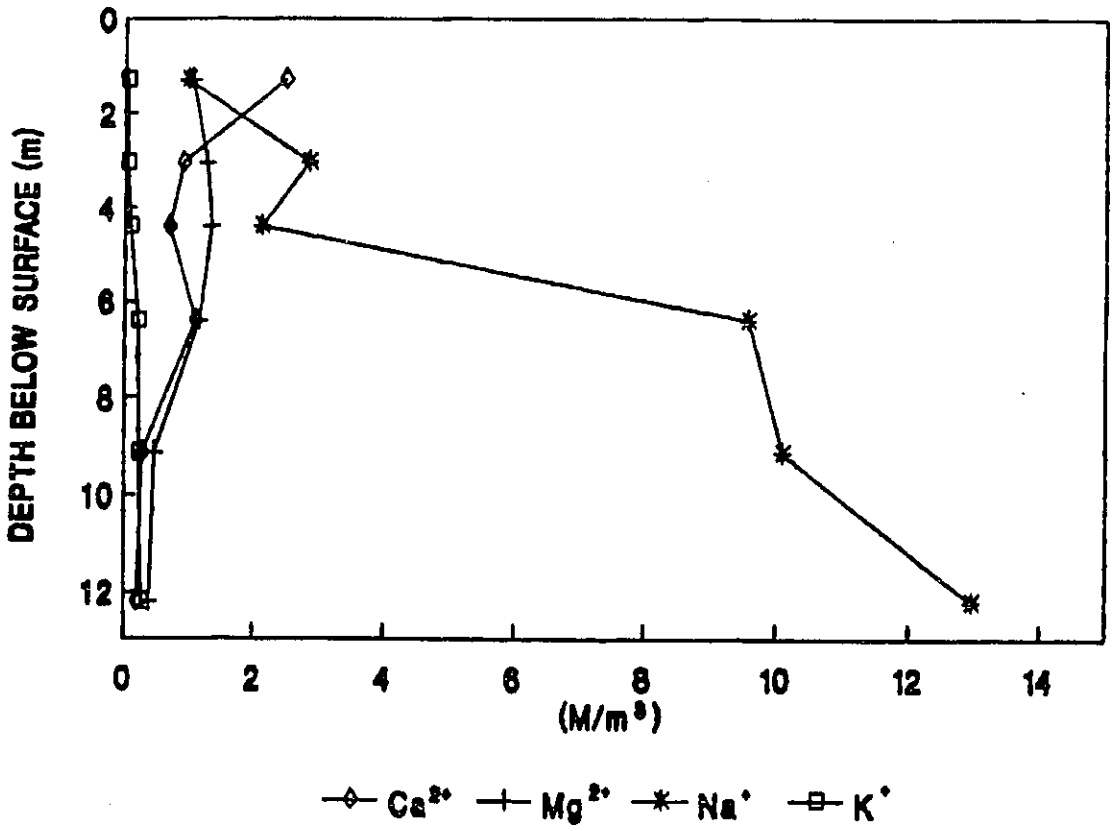

Figure 4.63. The major cation profiles at the Casselman site.

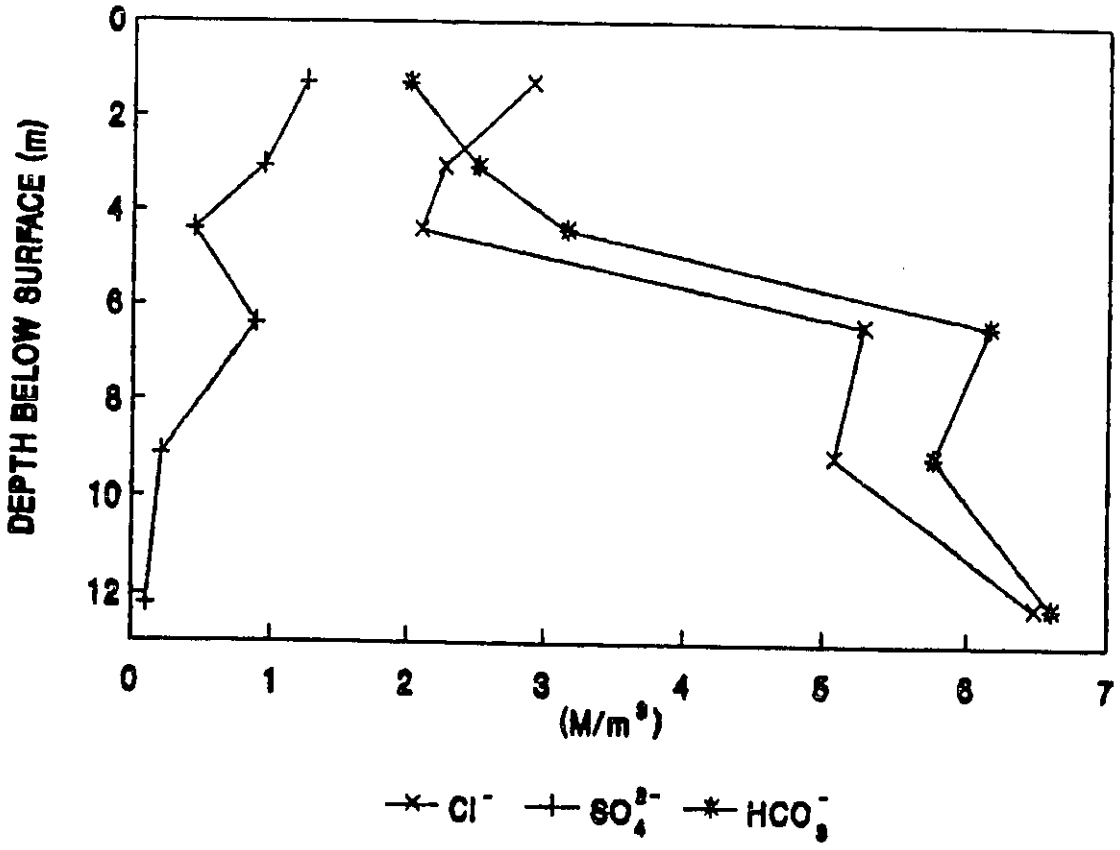

Figure 4.64. The major anion profiles at the Casselman site.

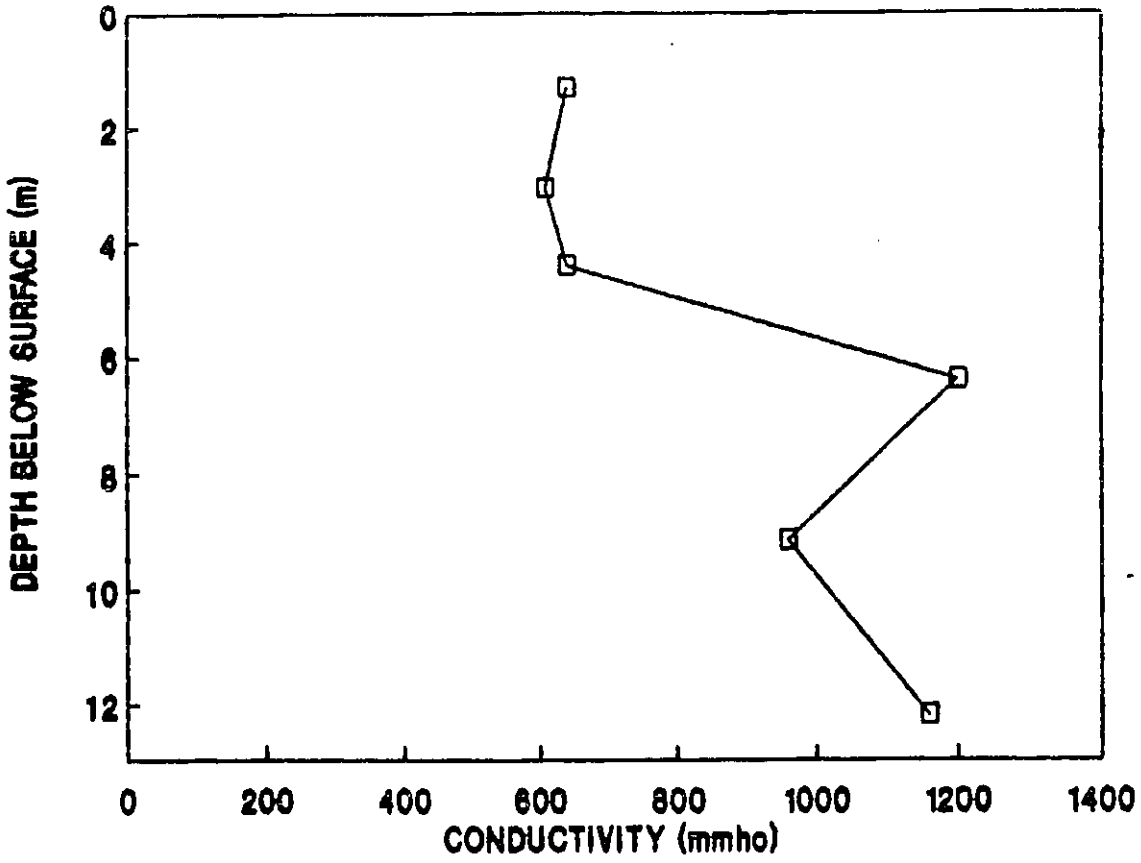

Figure 4.65. The electrical conductivity profile at the Casselman site.

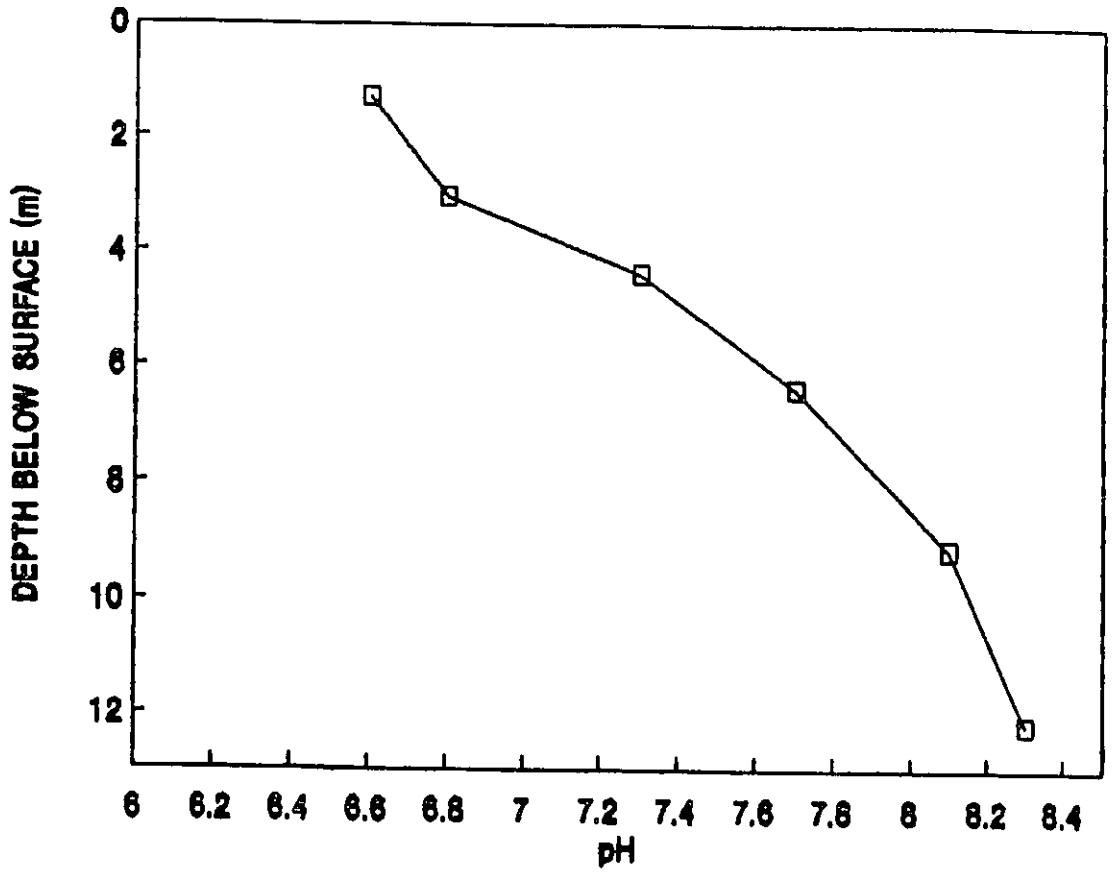

Figure 4.66. pH versus depth at the Casselman site.

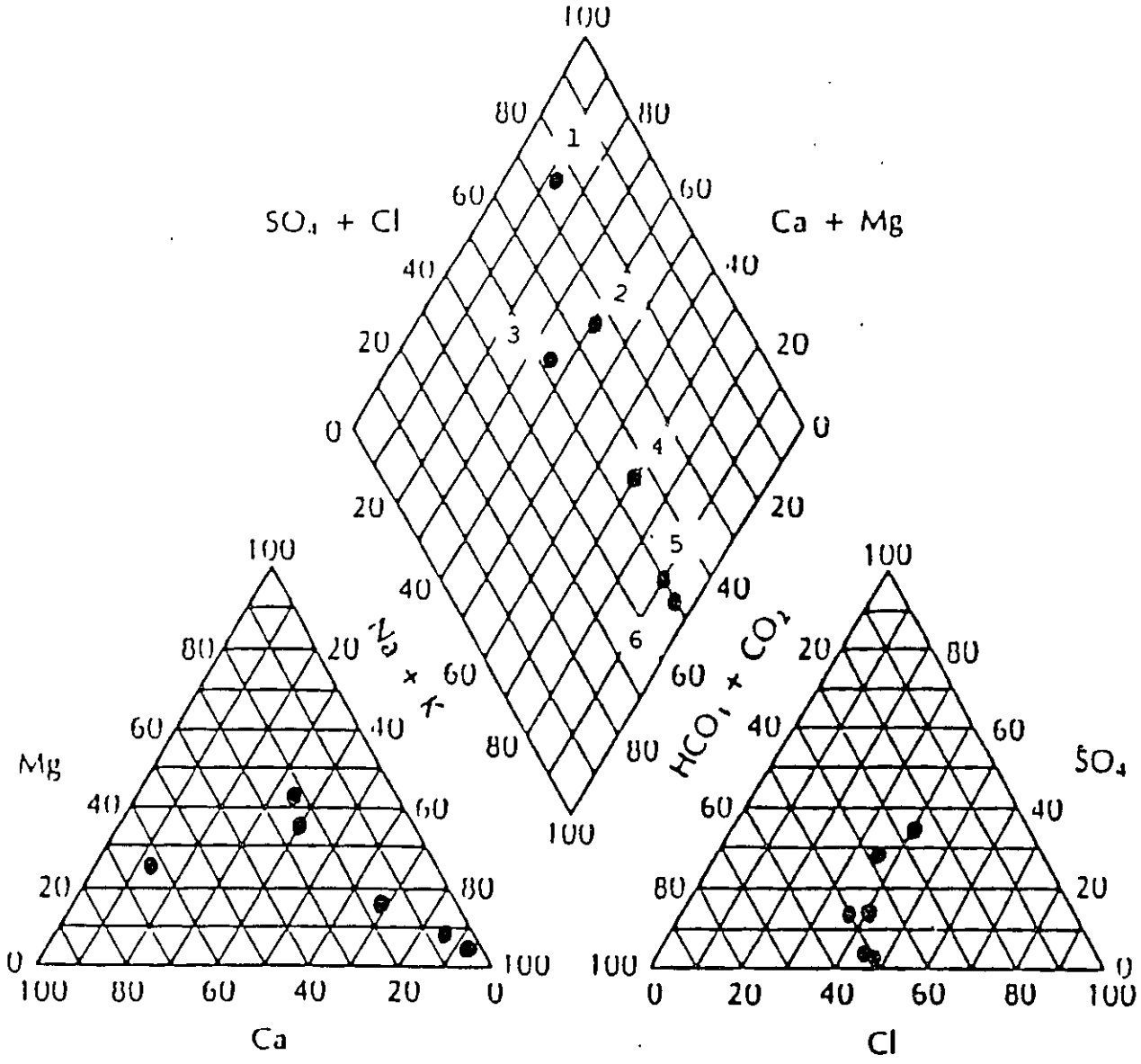

Figure 4.67. Trilinear diagram of water analysis from the Casselman site.

SAMPLE DEPTH (m)

1 - 1.30

2 - 3.05

3 - 4.40

4 - 6.40

5 - 9.15

6 - 12.20

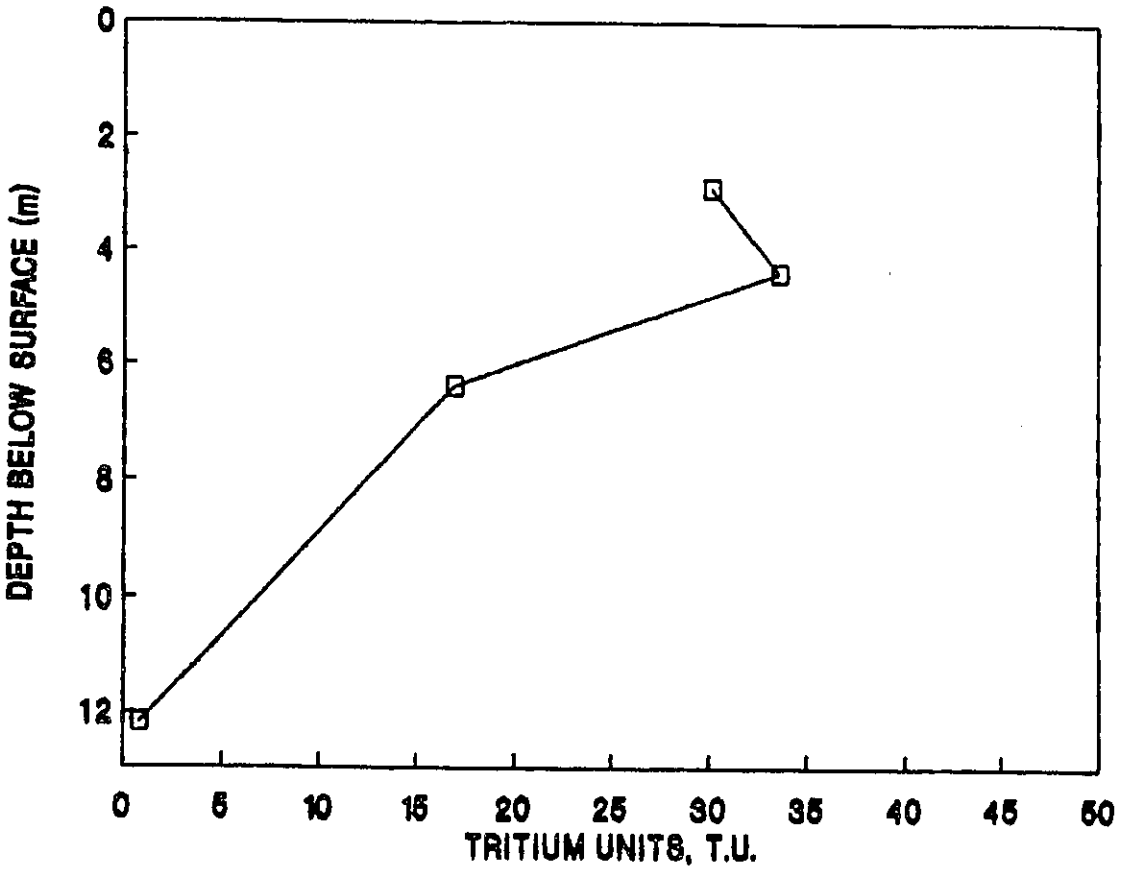

Figure 4.68. Tritium profile at the Casselman site.

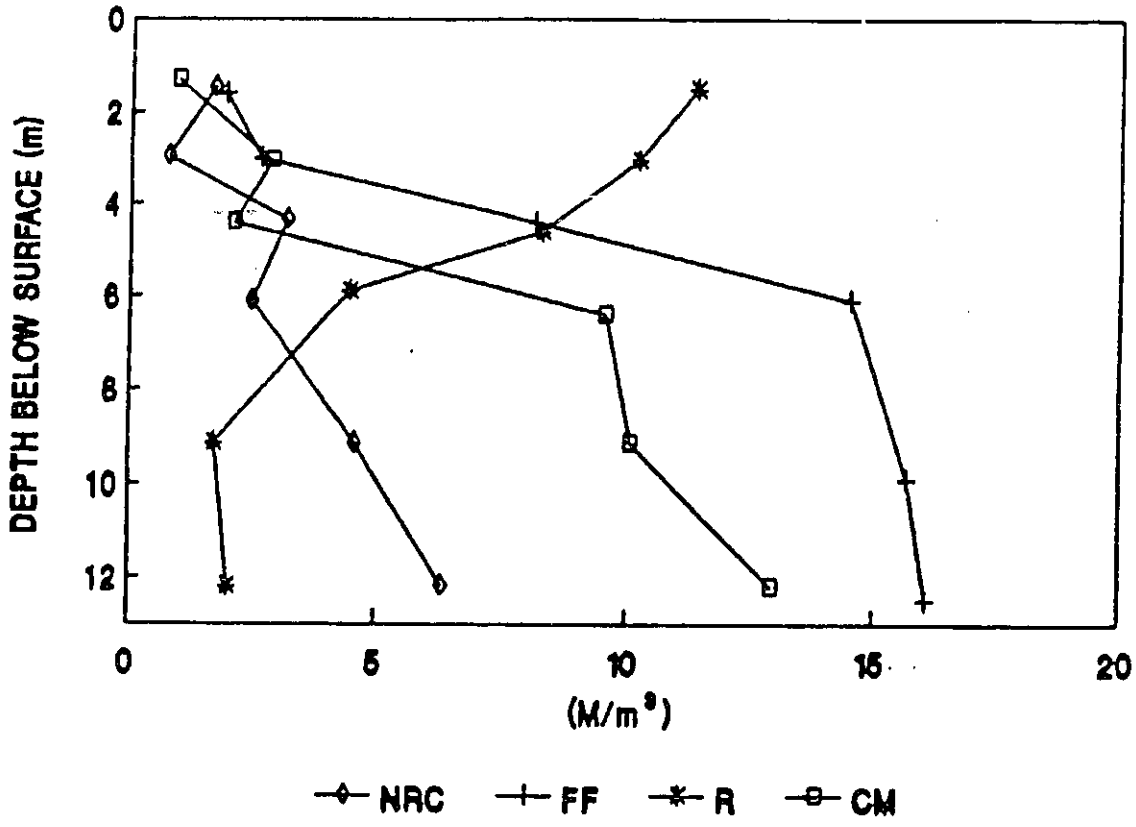

Figure 4.69. Sodium concentration profiles at all four sites (legend abbreviations, Fallowfield:FF, Renfrew:R, Casselman:CM).

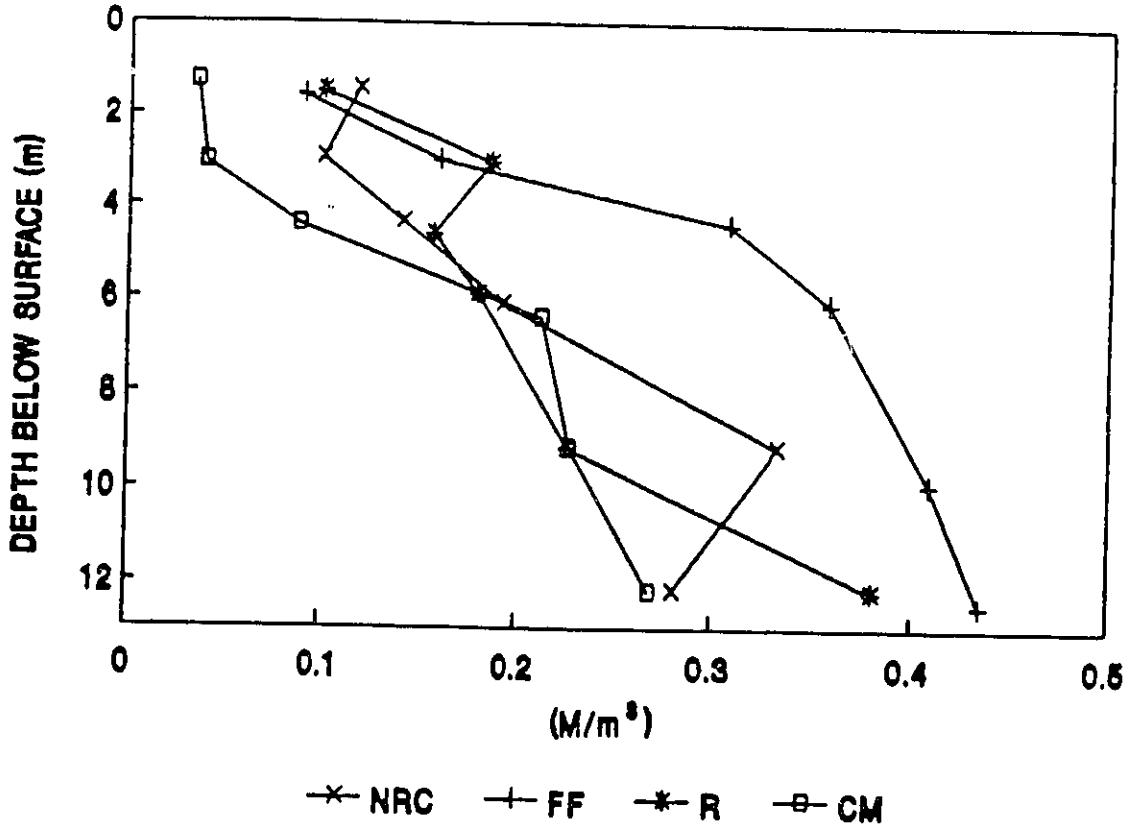

Figure 4.70. Potassium concentration profiles at all four sites (legend abbreviations, Fallowfield:FF, Renfrew:R, Casselman:CM).

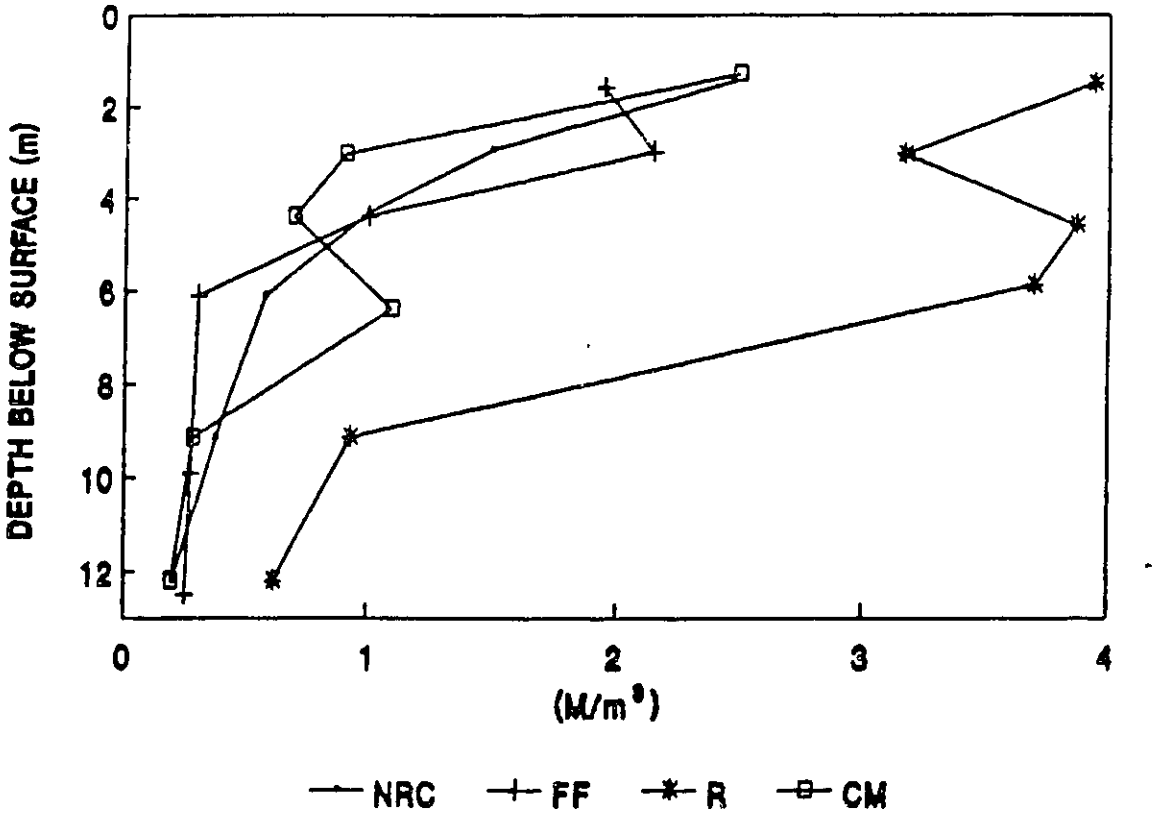

Figure 4.71. Calcium concentration profiles at all four sites (legend abbreviations, Fallowfield:FF, Renfrew:R, Casselman:CM).

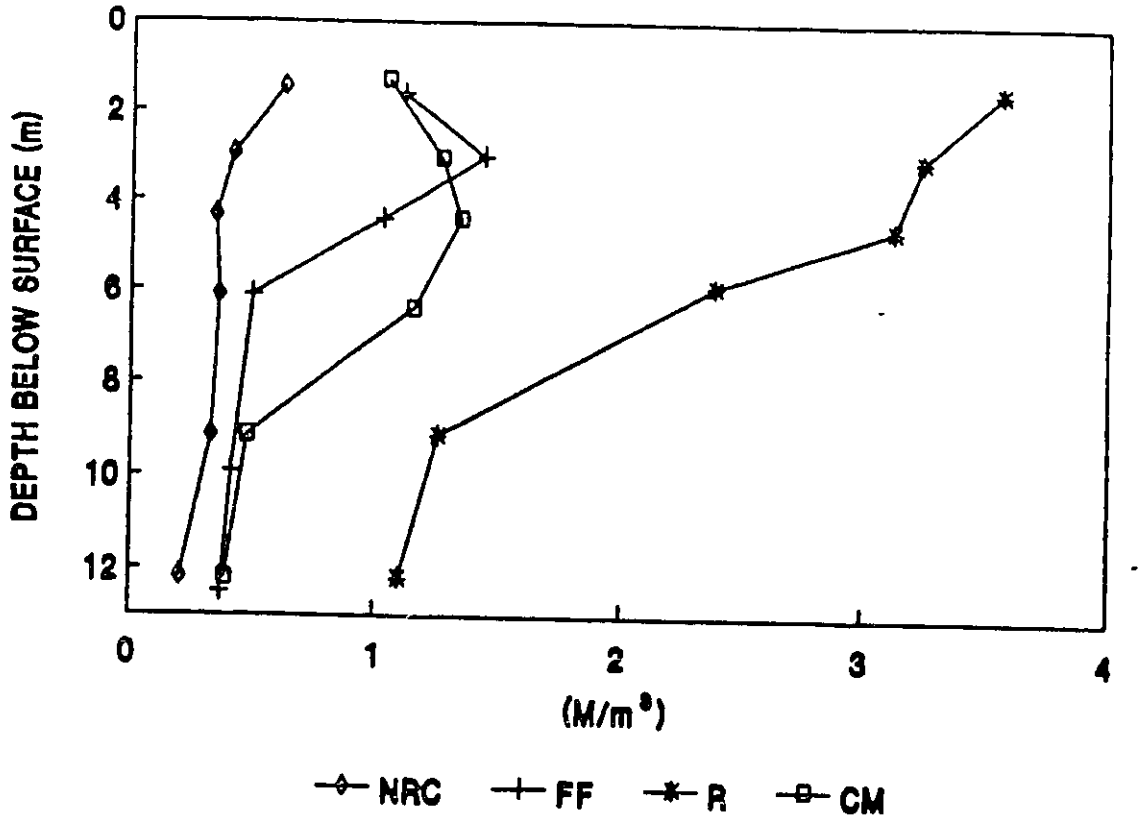

Figure 4.72. Magnesium concentration profiles at all four sites (legend abbreviations, Fallowfield:FF, Renfrew:R, Casselman:CM).

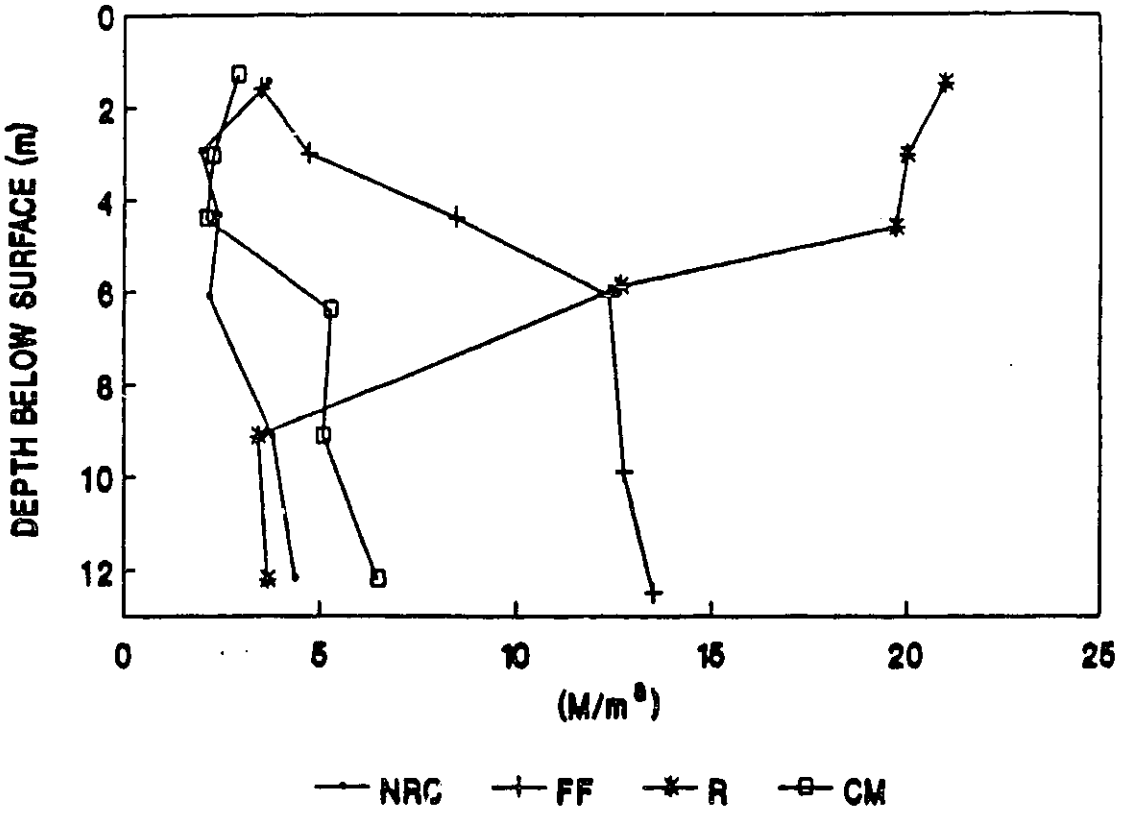

Figure 4.73. Chloride concentration profiles at all four sites (legend abbreviations, Fallowfield:FF, Renfrew:R, Casselman:CM).

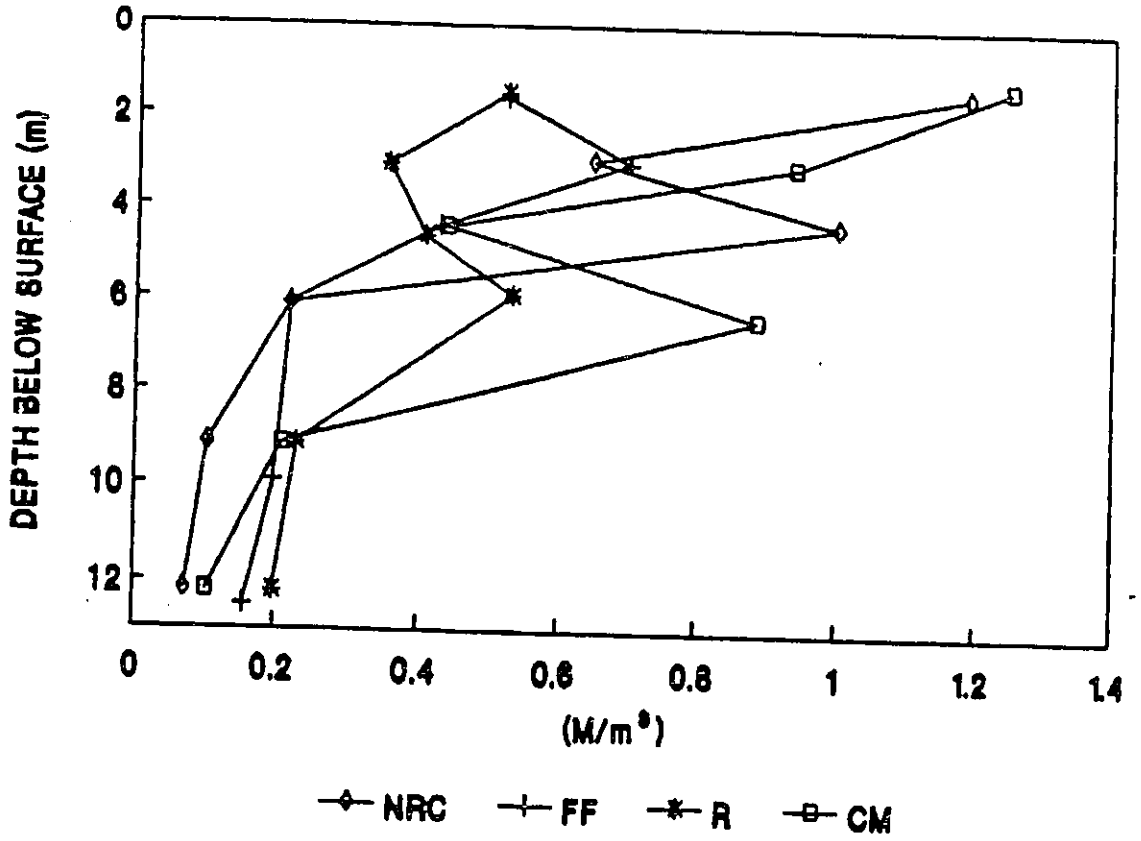

Figure 4.74. Sulfate concentration profiles at all four sites (legend abbreviations, Fallowfield:FF, Renfrew:R, Casselman:CM).

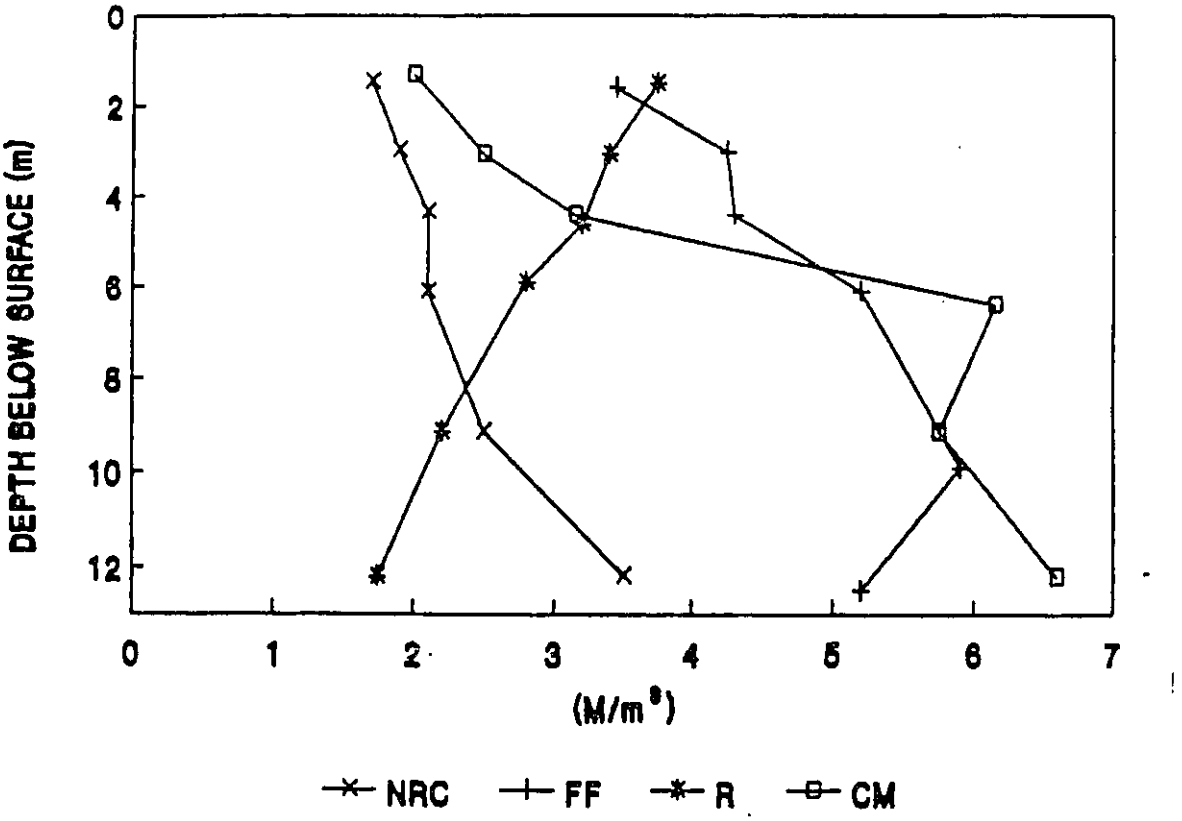

Figure 4.75. Bicarbonate concentration profiles at all four sites (legend abbreviations, Fallowfield:FF, Renfrew:R, Casselman:CM).

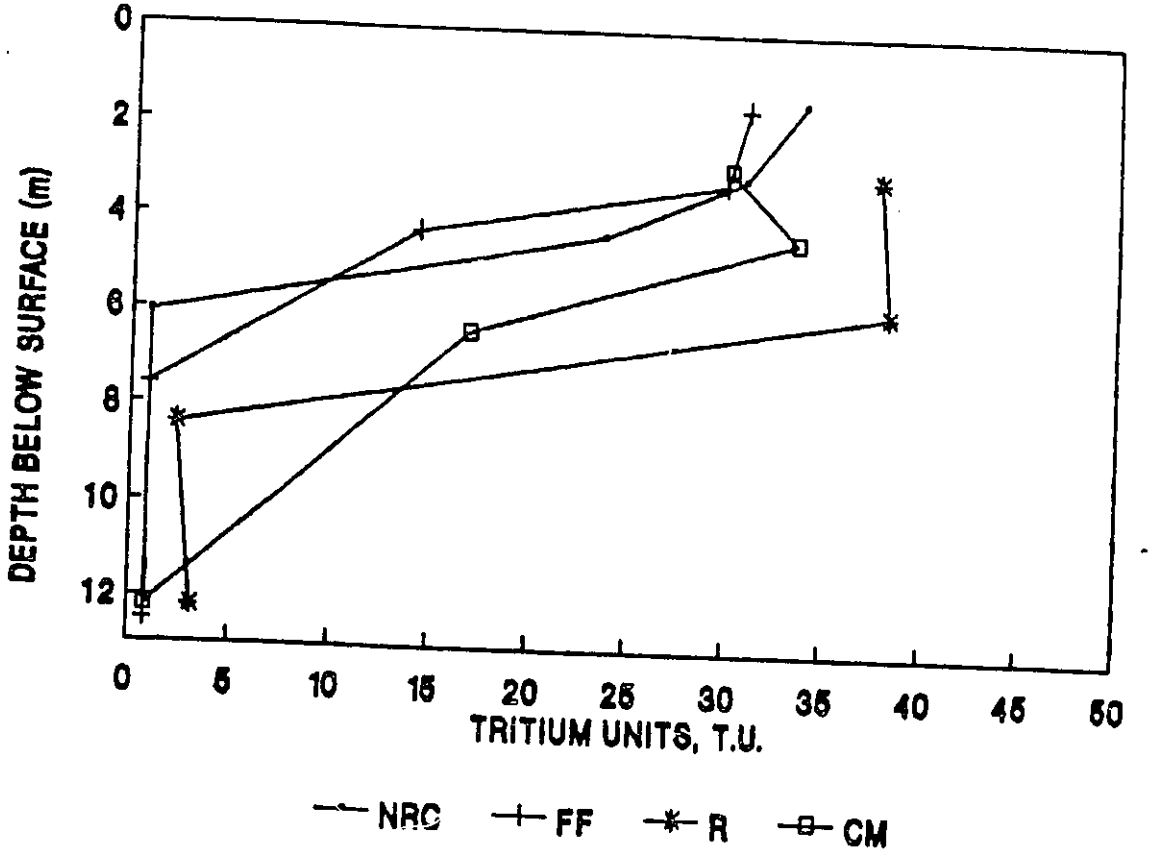

Figure 4.76. Tritium concentration profiles at all four sites (legend abbreviations, Fallowfield:FF, Renfrew:R, Casselman:CM).

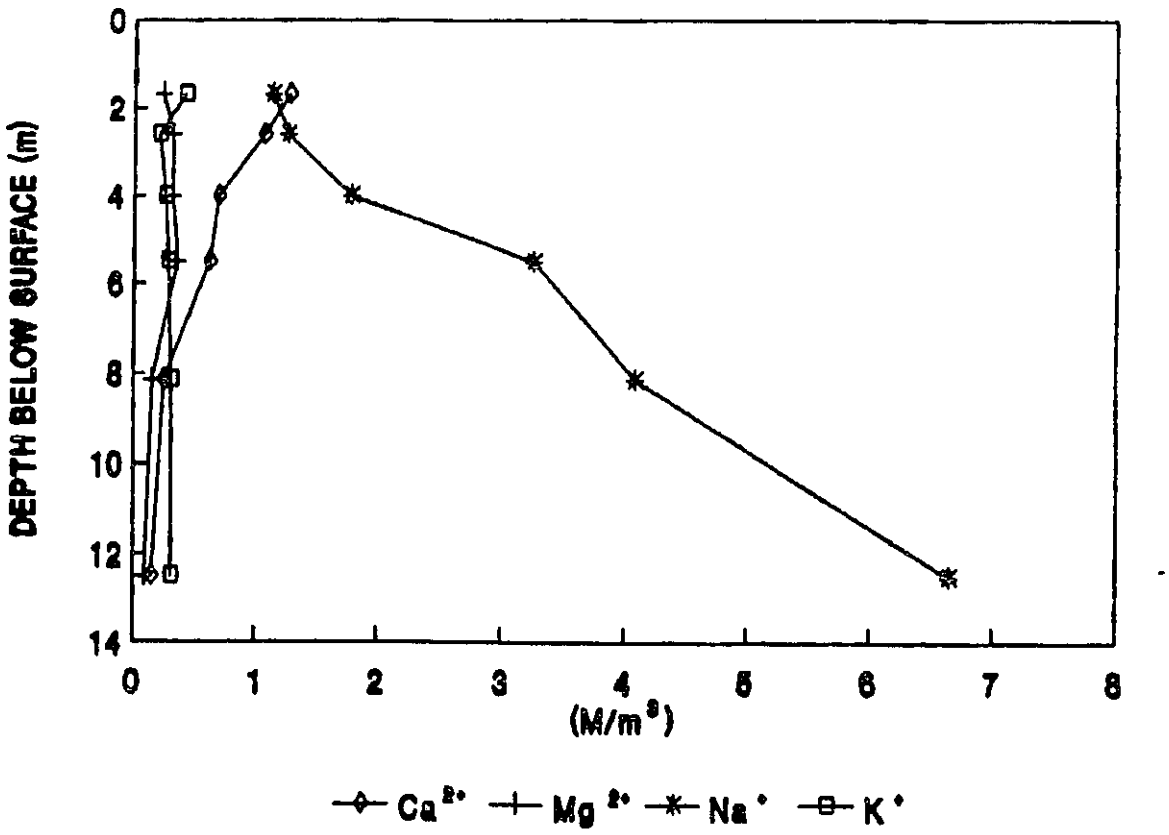

Figure 4.77. The major cation profiles produced by squeezed clay samples at the NRC site.

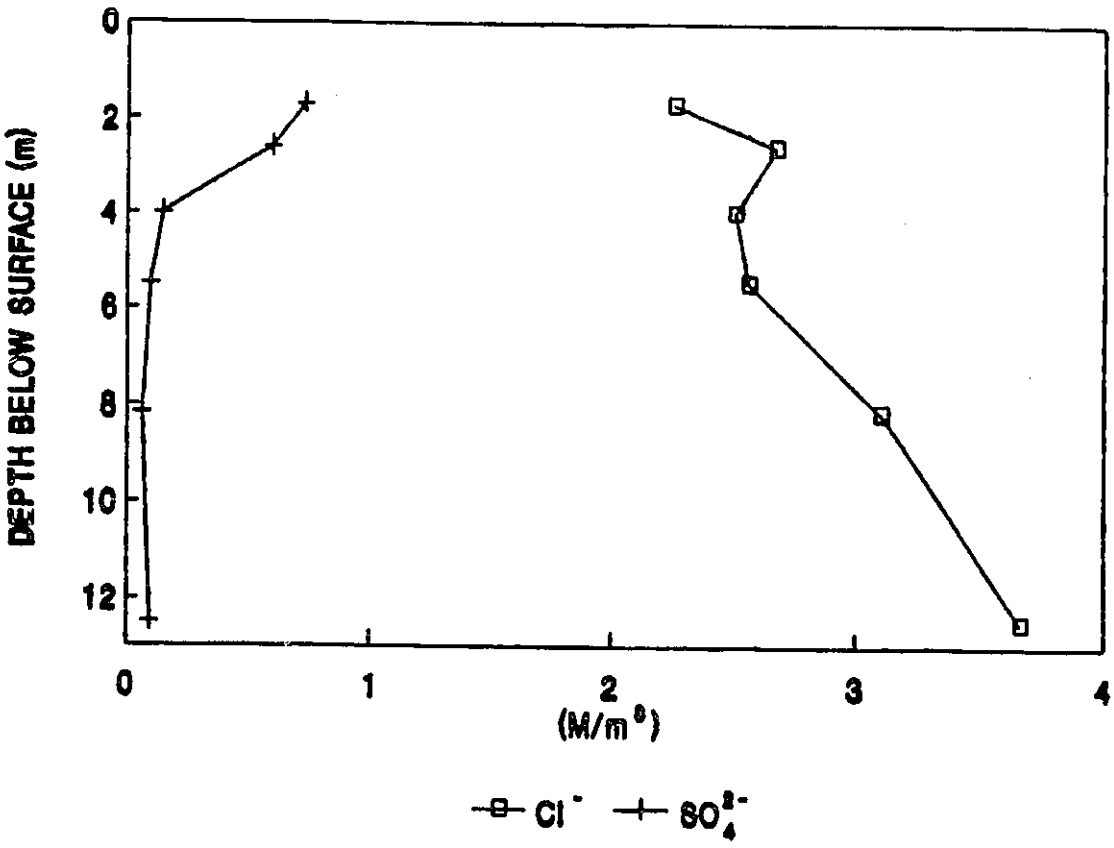

Figure 4.78. The major anion profiles produced by squeezed clay samples at the NRC site.

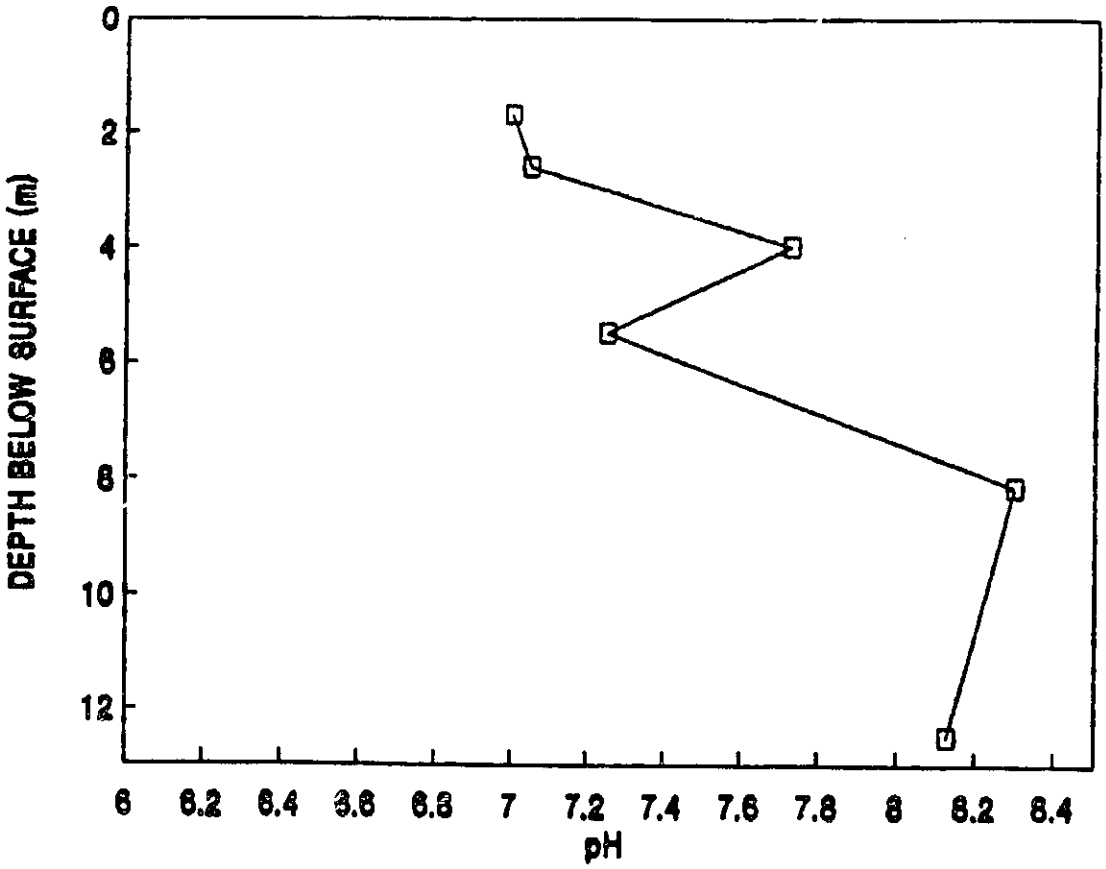

Figure 4.79. pH versus depth for squeezed clay samples at the NRC site.

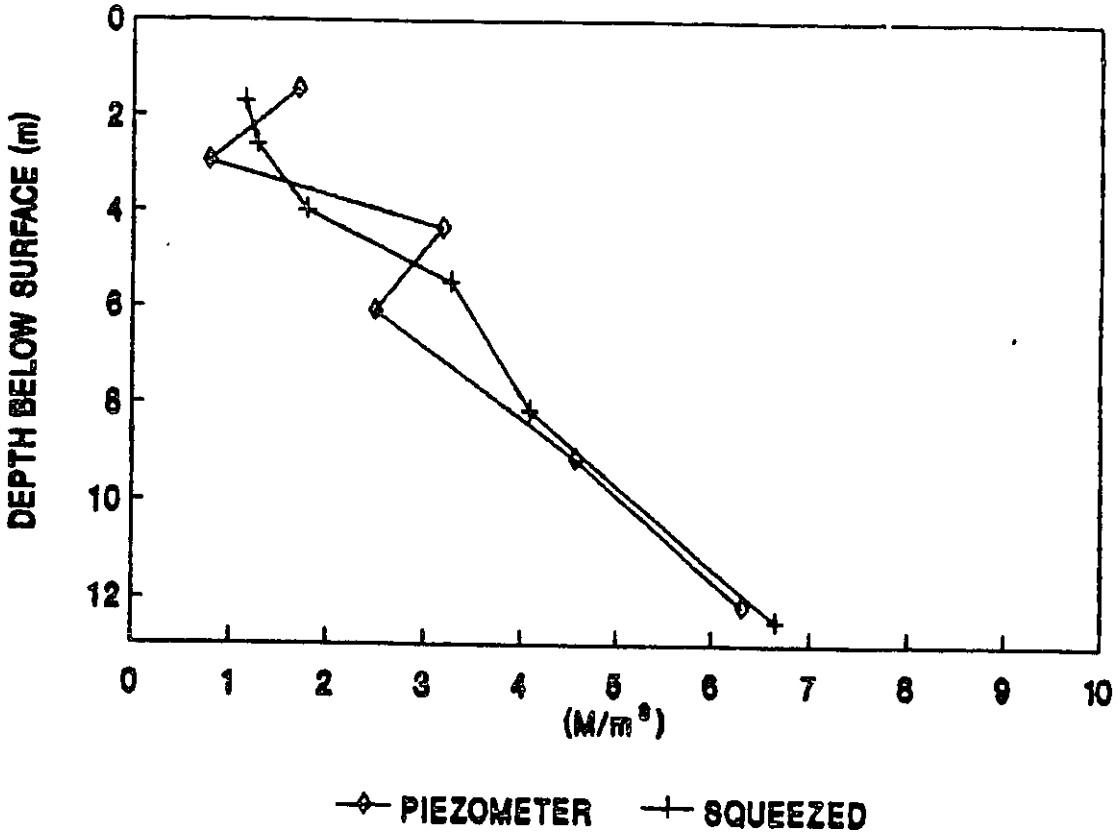

Figure 4.80. Comparison of sodium profiles between squeezed and bailed piezometer porewater, NRC site.

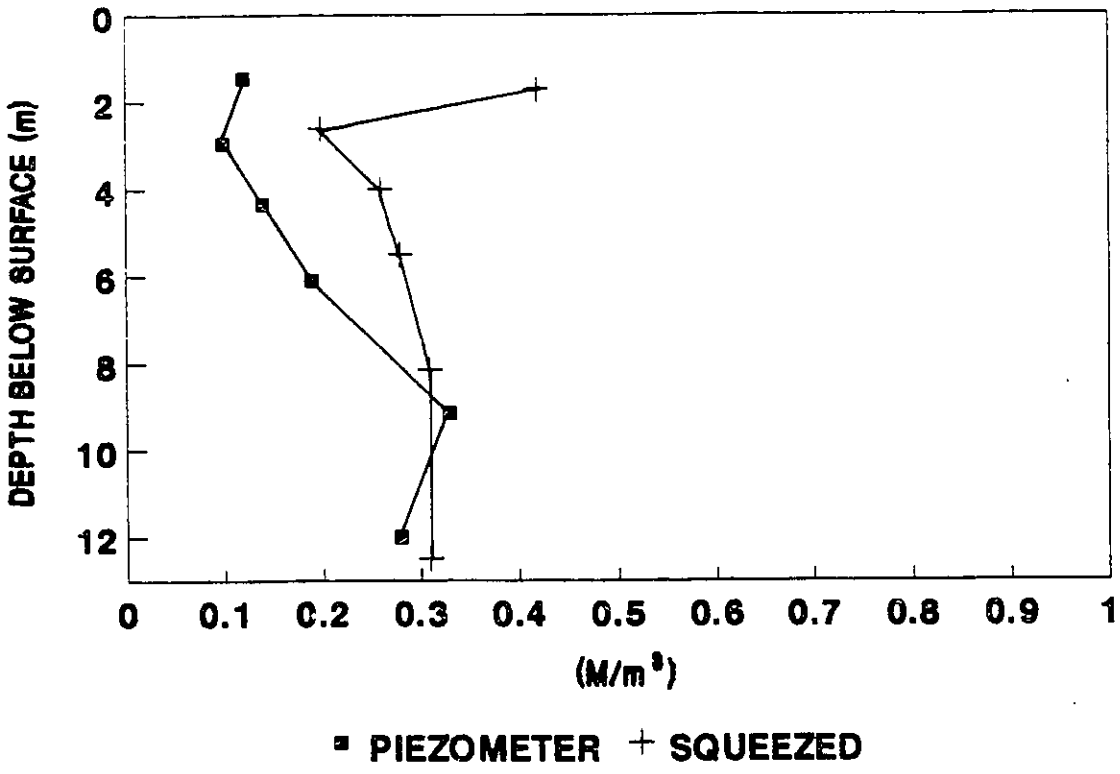

Figure 4.81. Comparison of potassium profiles between squeezed and bailed piezometer porewater, NRC site.

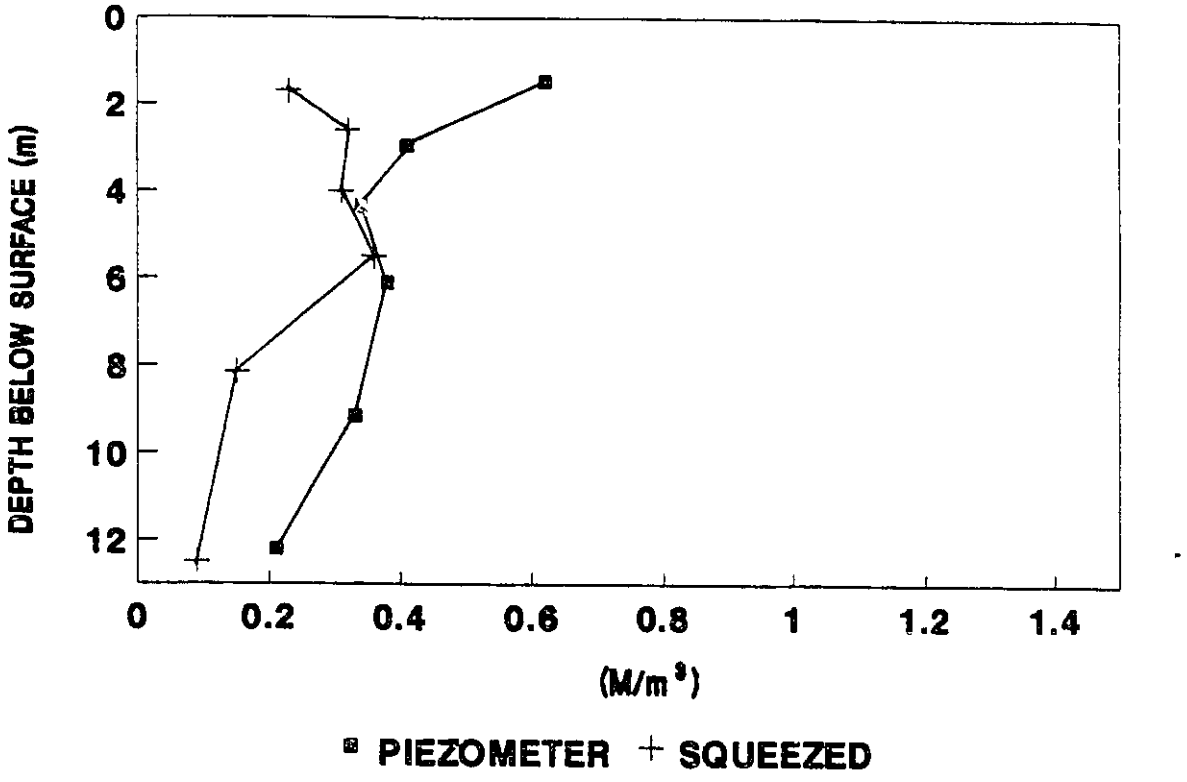

Figure 4.82. Comparison of magnesium profiles between squeezed and bailed piezometer porewater, NRC site.

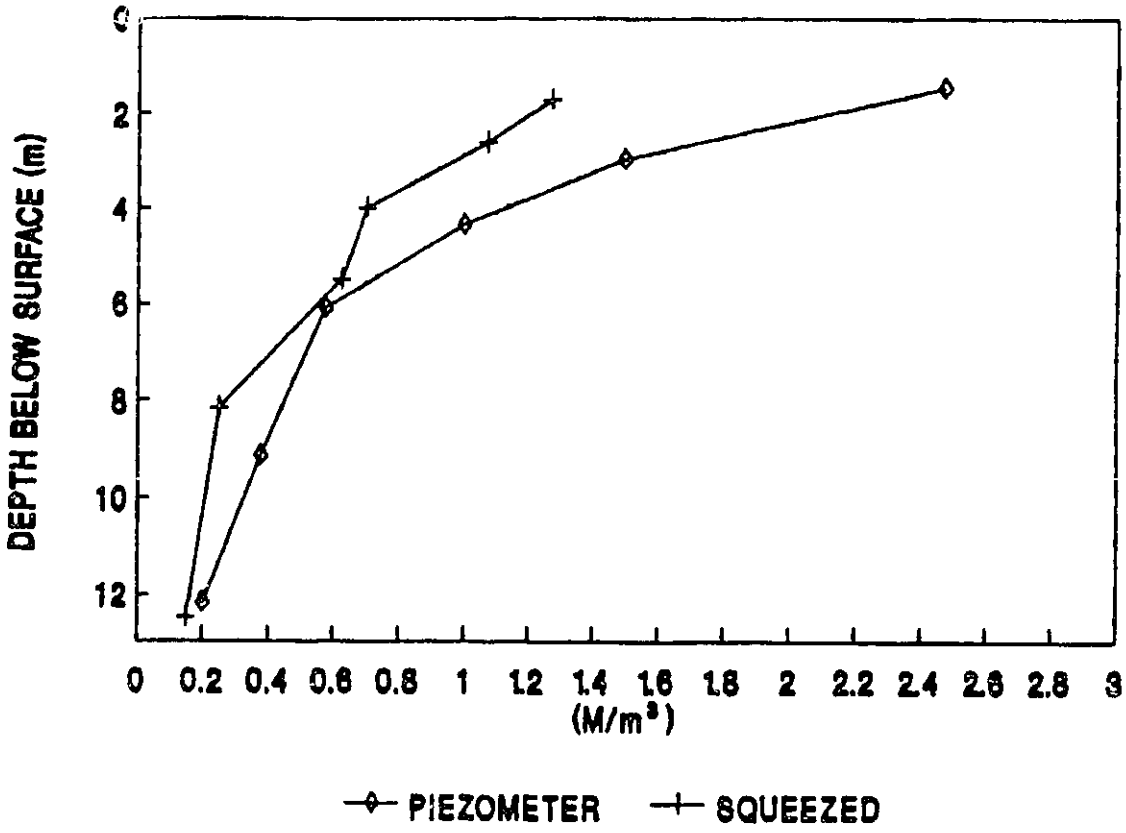

Figure 4.83. Comparison of calcium profiles between squeezed and bailed piezometer porewater, NRC site.

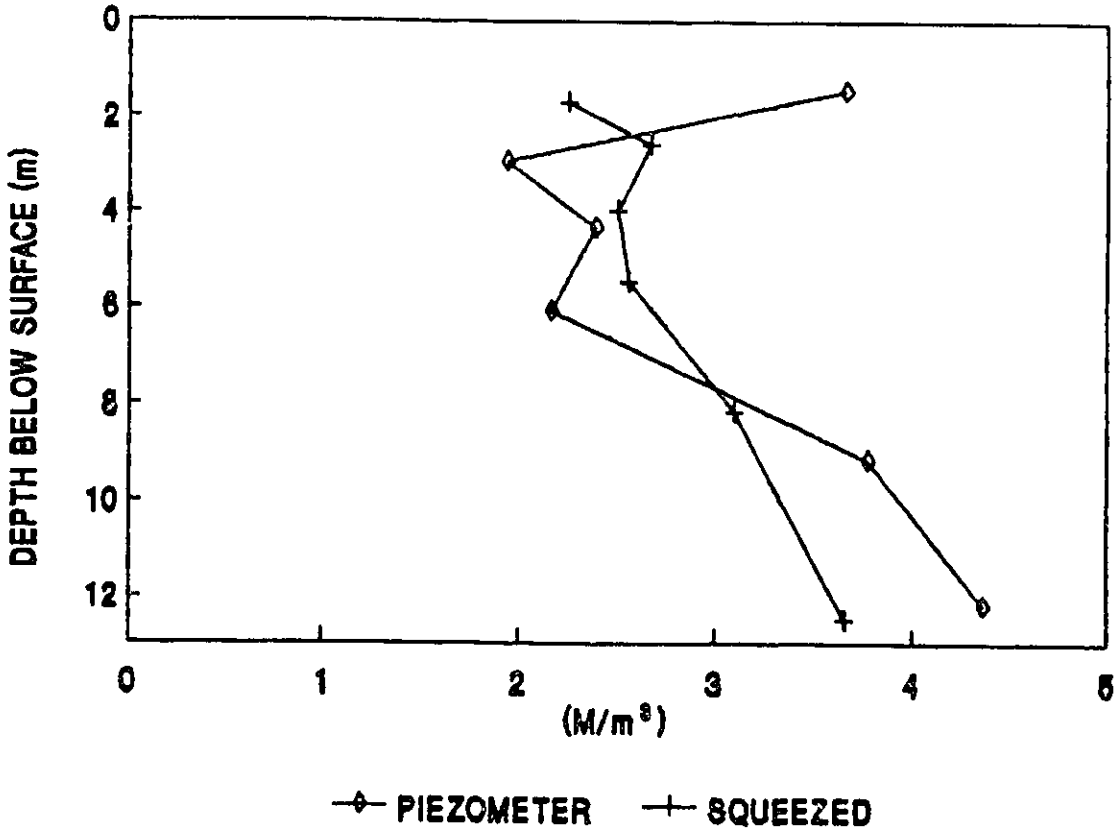

Figure 4.84. Comparison of chloride profiles between squeezed and bailed piezometer porewater, NRC site.

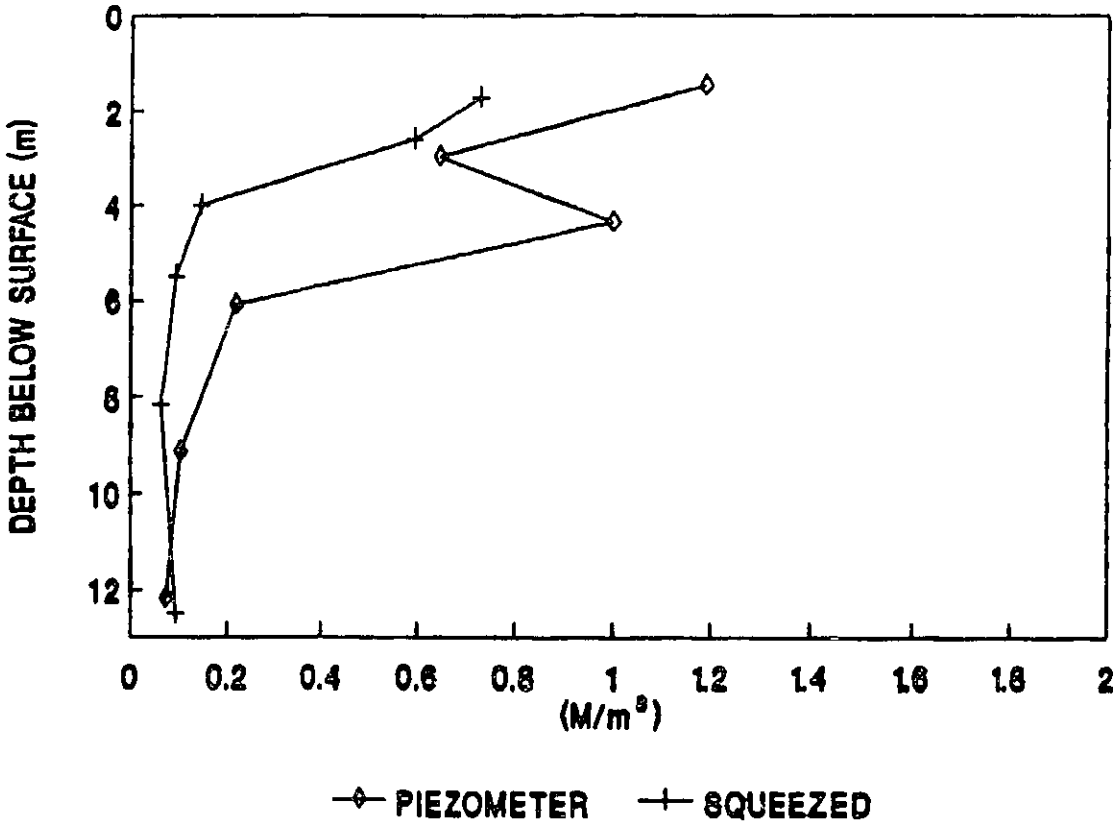

Figure 4.85. Comparison of sulfate profiles between squeezed and bailed piezometer porewater, NRC site.

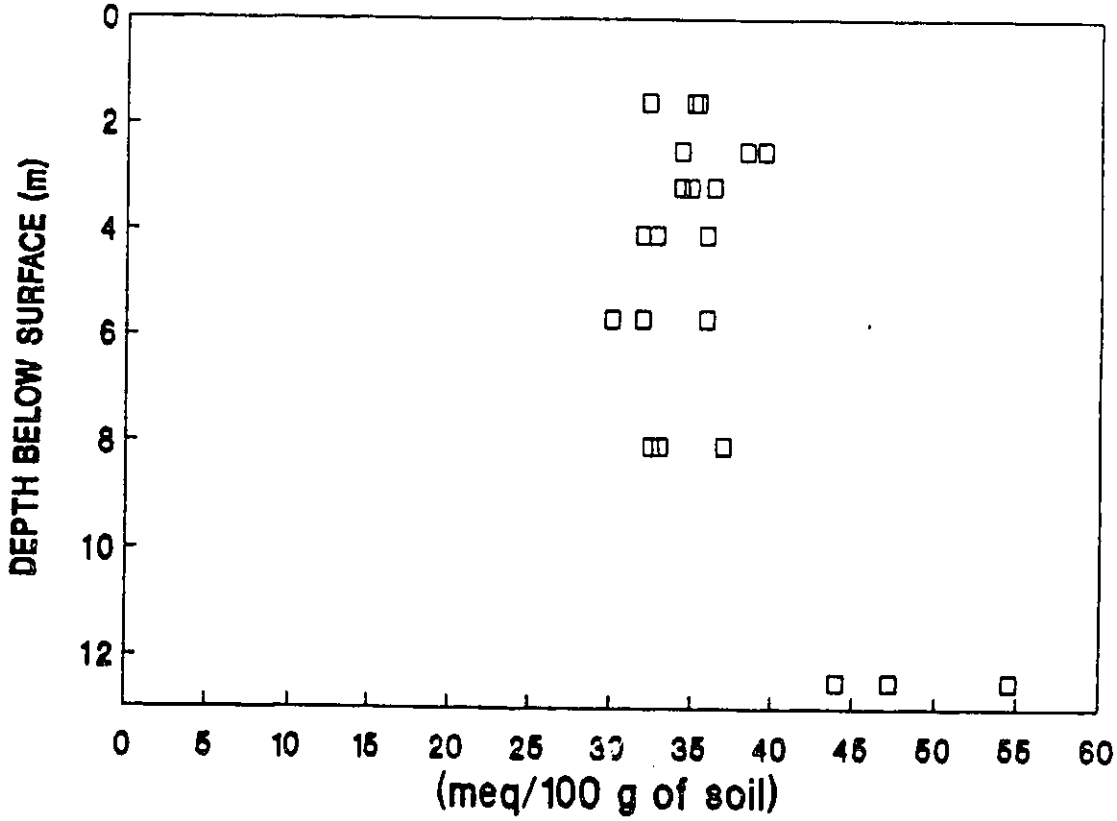

Figure 4.86. Cation exchange capacity profile at the NRC site.

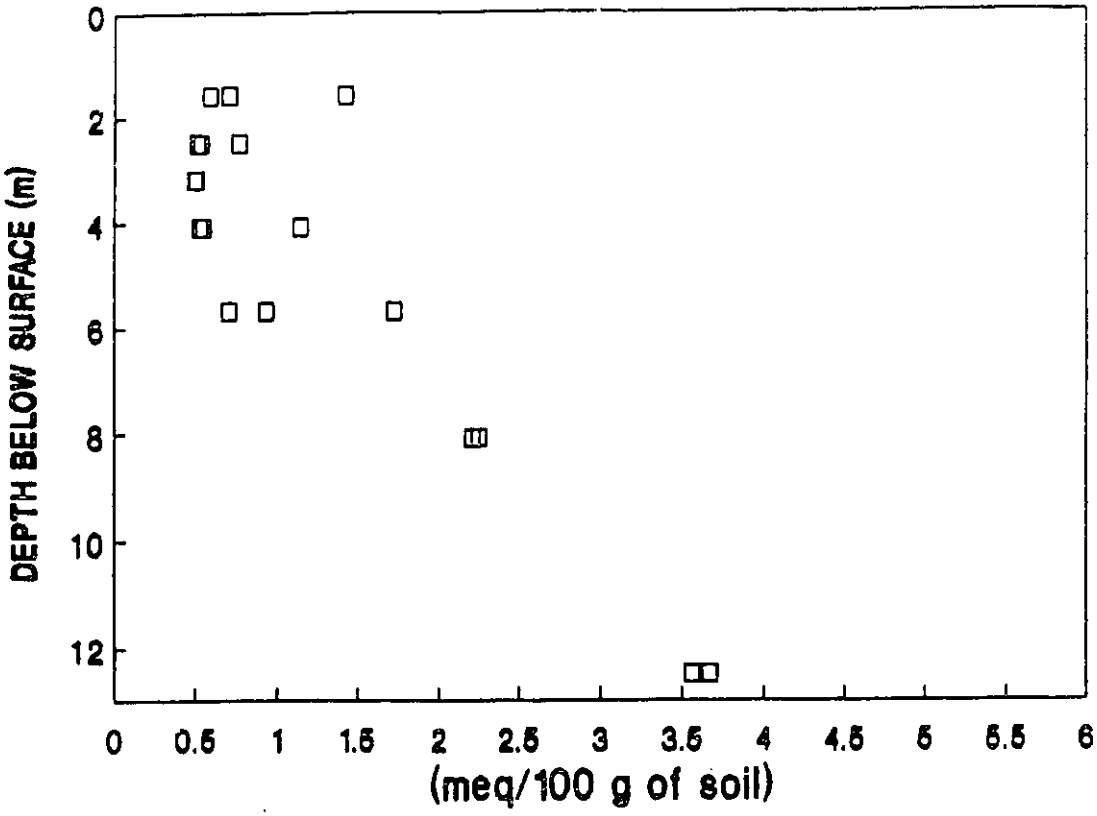

Figure 4.87. The extractable sodium profile at the NRC site.

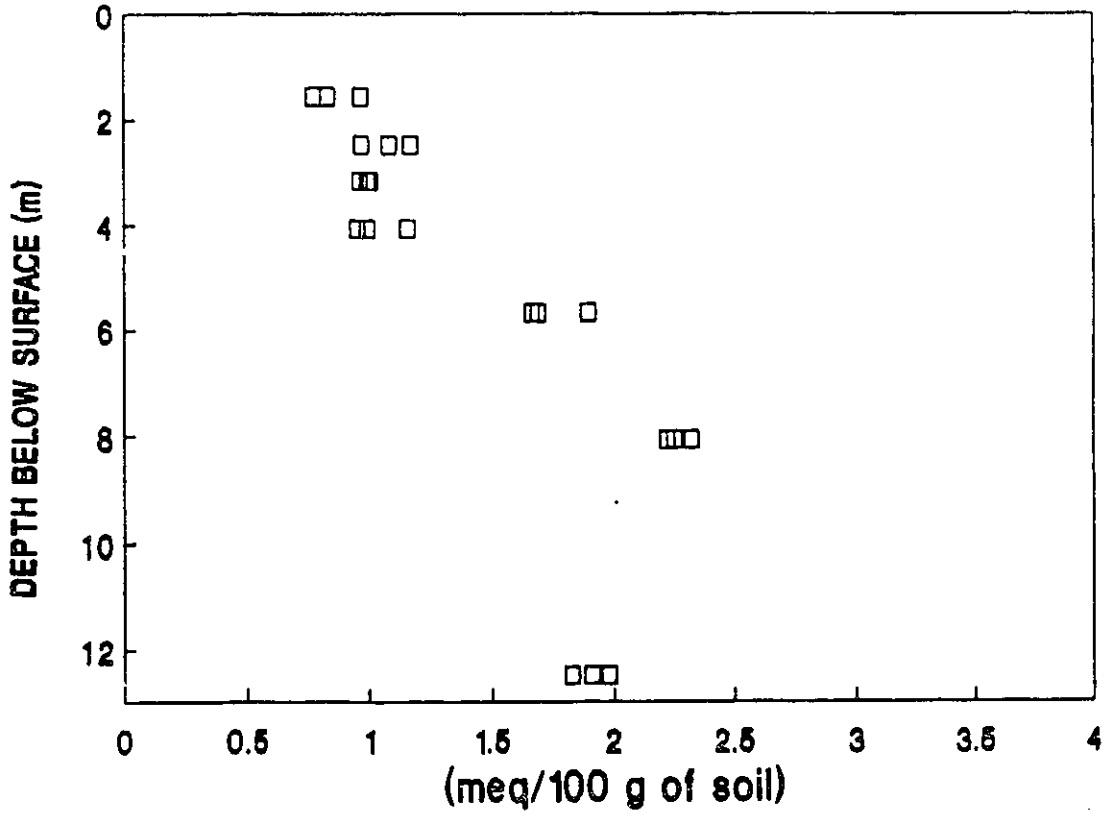

Figure 4.88. The extractable potassium profile at the NRC site.

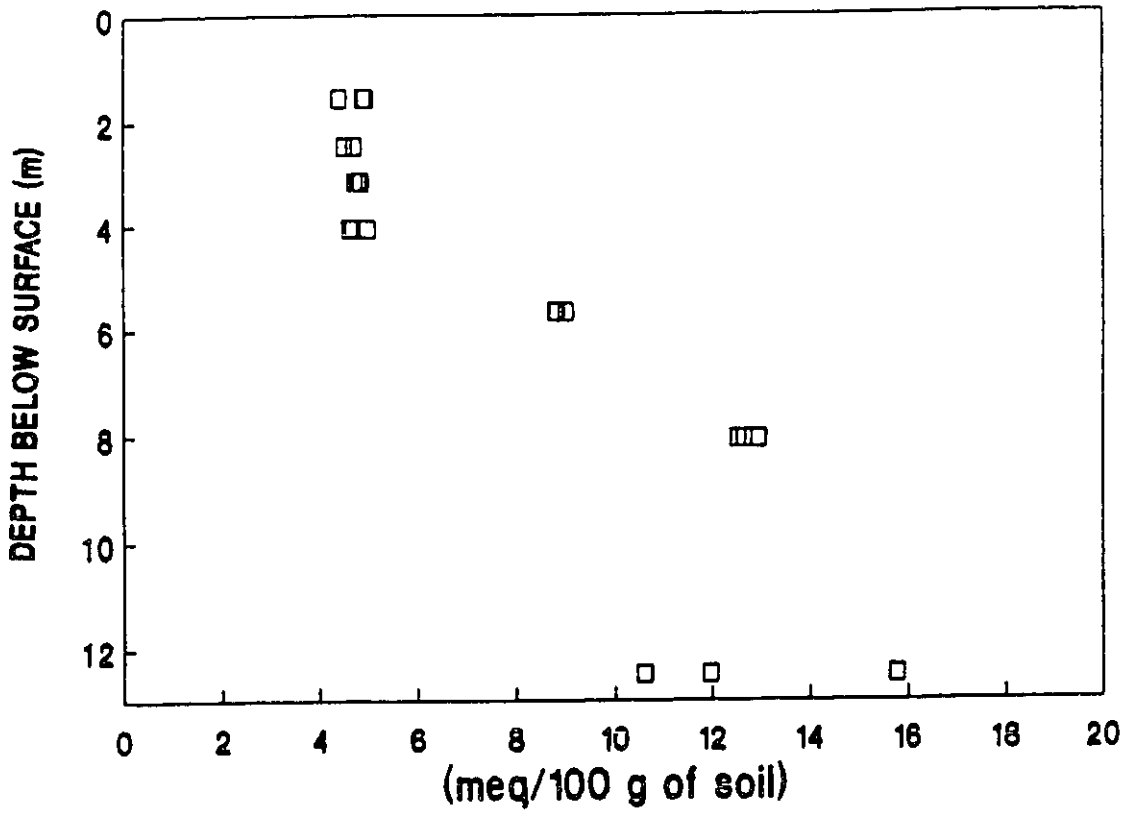

Figure 4.89. The extractable magnesium profile at the NRC site.

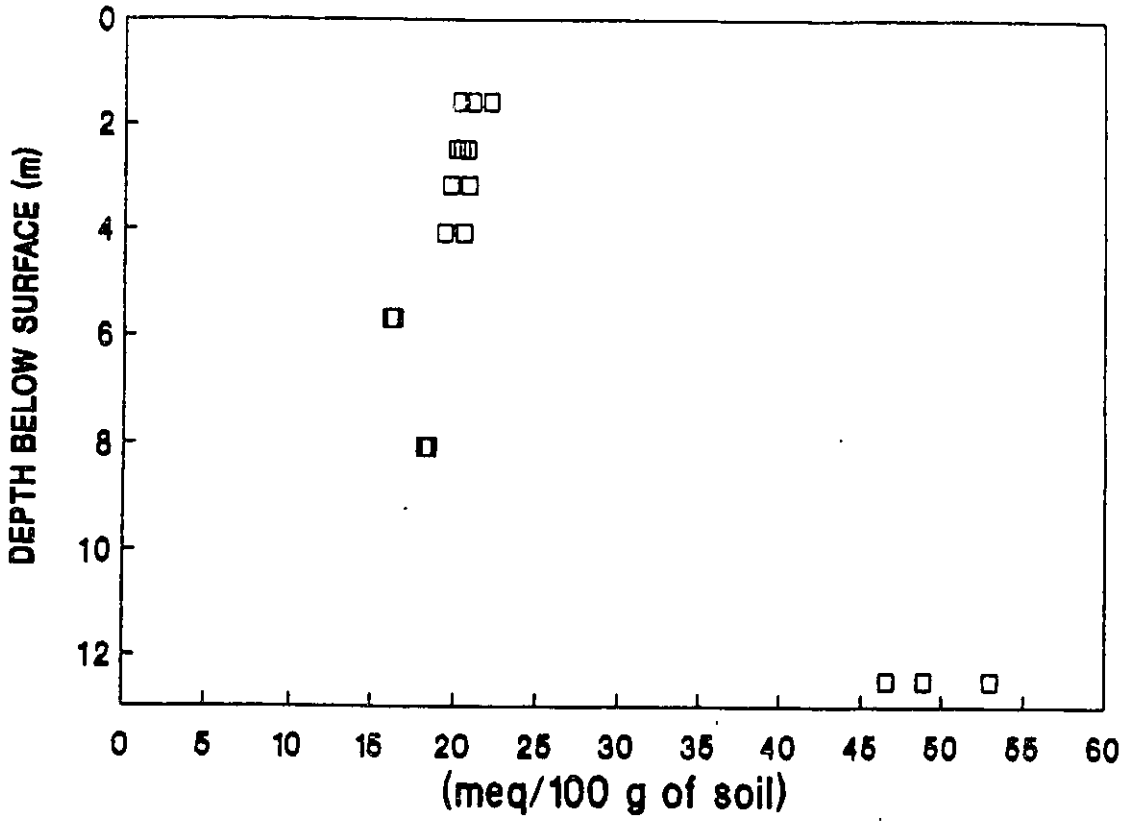

Figure 4.90. The extractable calcium profile at the NRC site.

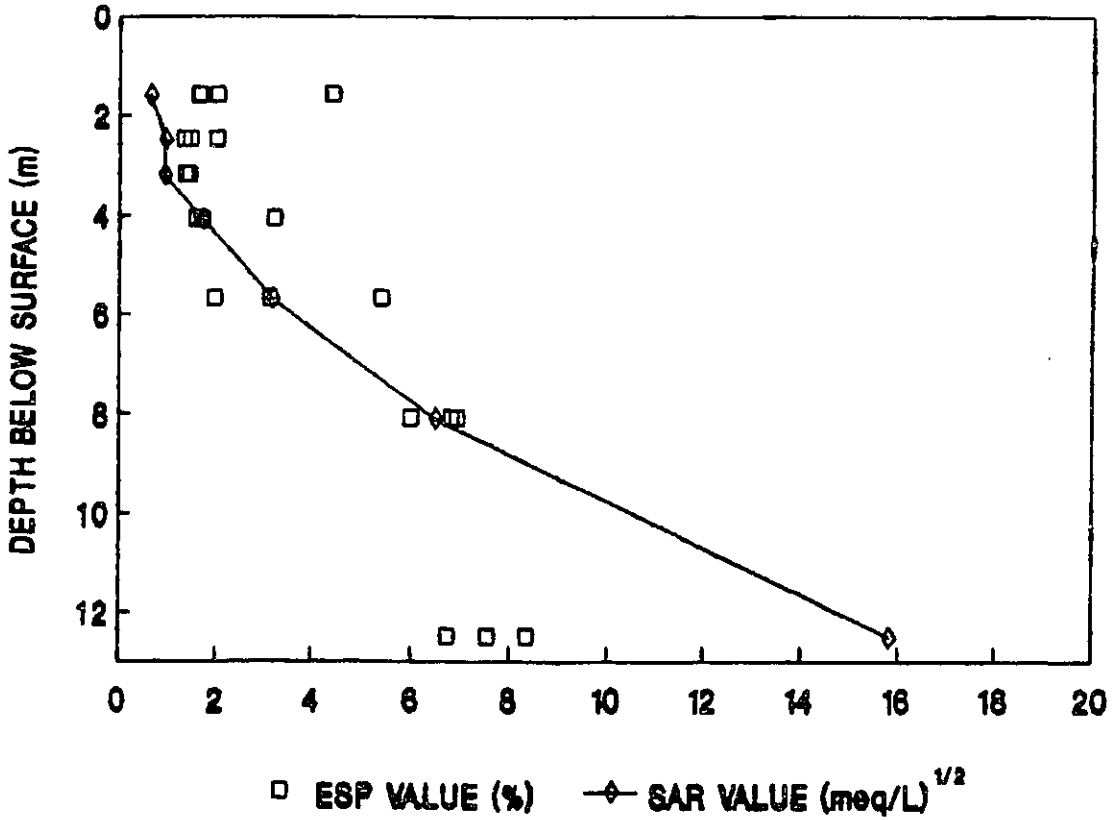

Figure 4.91. ESP and SAR profiles from squeezed clay samples at the NRC site.

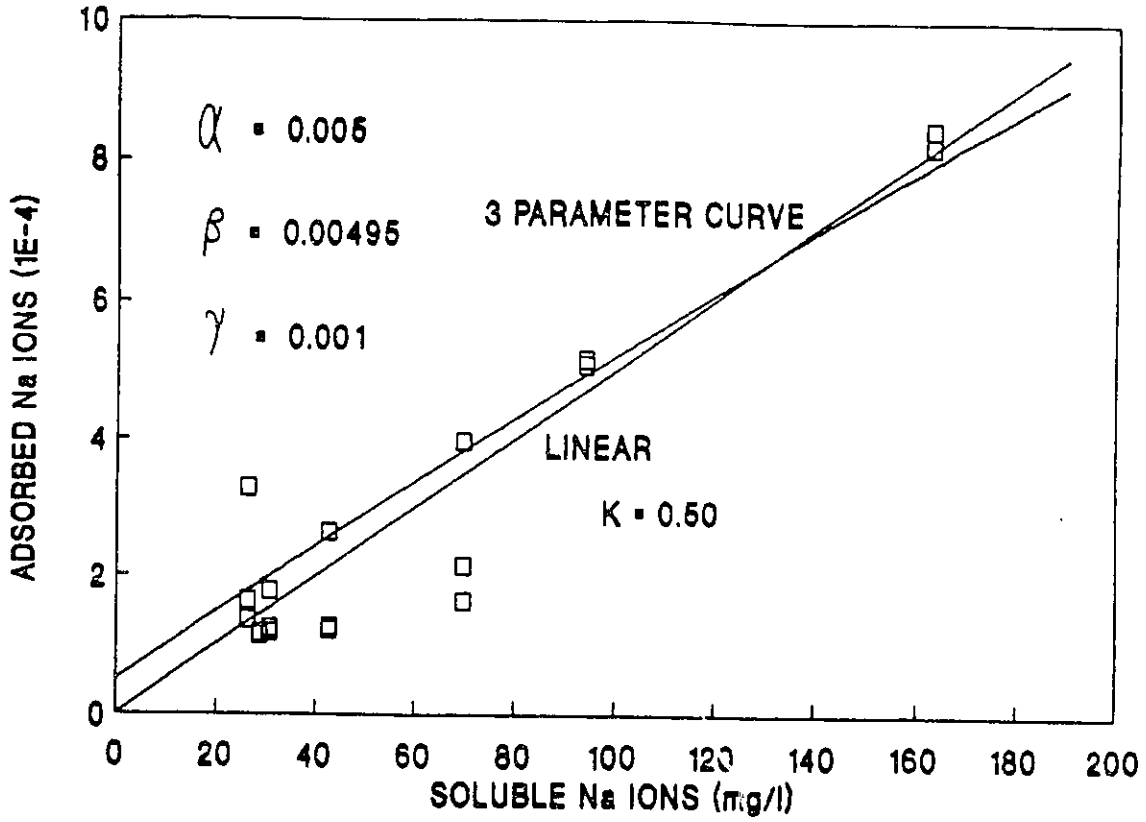

Figure 4.92. Relationship between soluble and adsorbed Na^+ cation from squeezed clay samples at the NRC site.

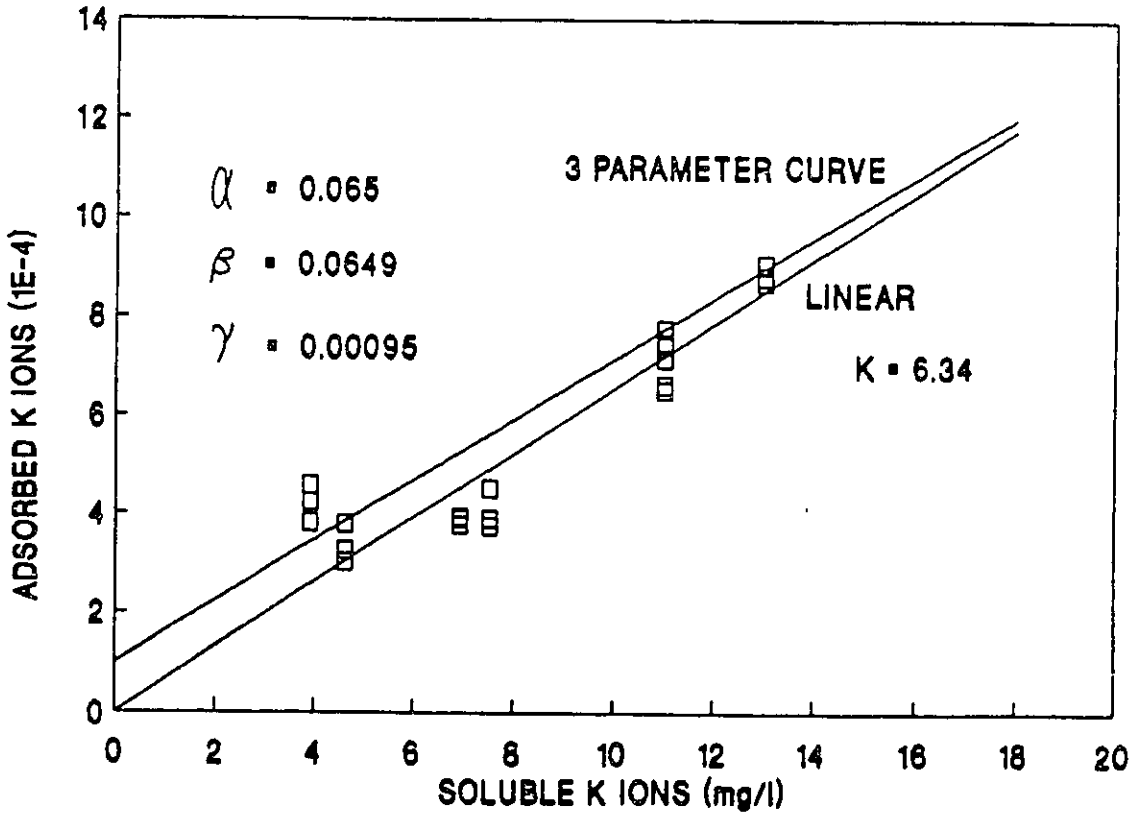

Figure 4.93. Relationship between soluble and adsorbed K^+ cation from squeezed clay samples at the NRC site.

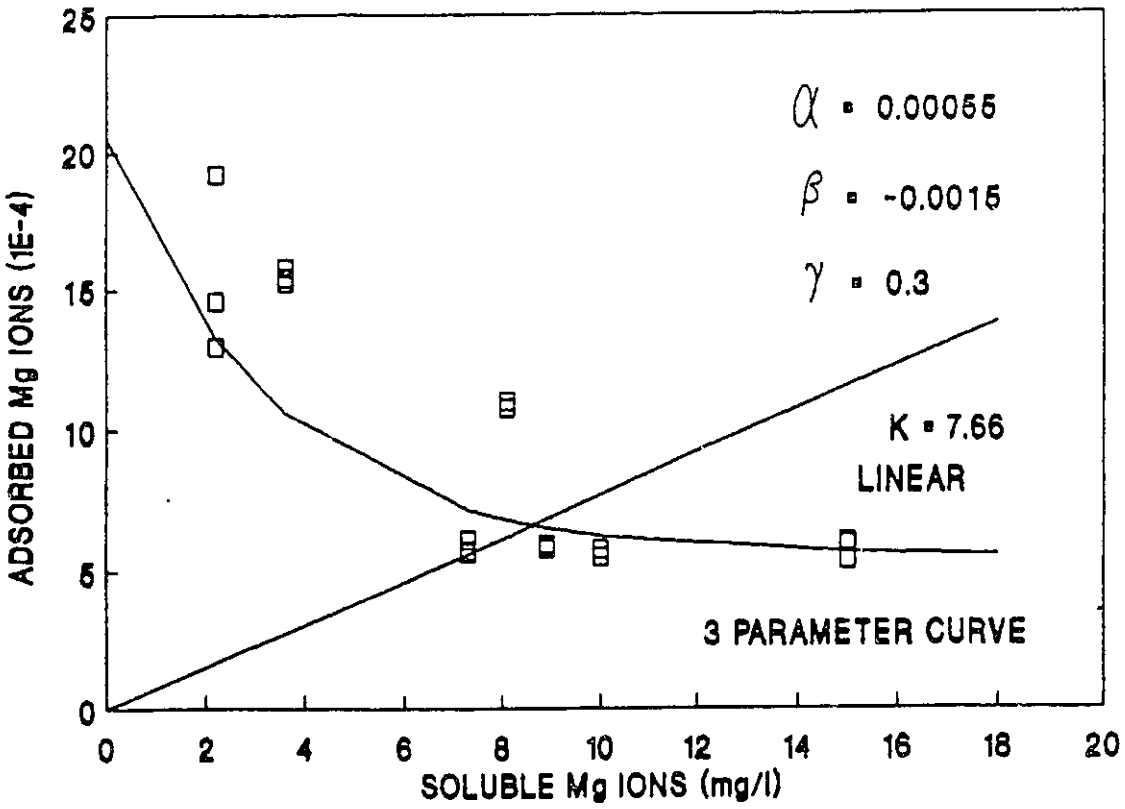

Figure 4.94. Relationship between soluble and adsorbed Mg^{2+} cation from squeezed clay samples at the NRC site.

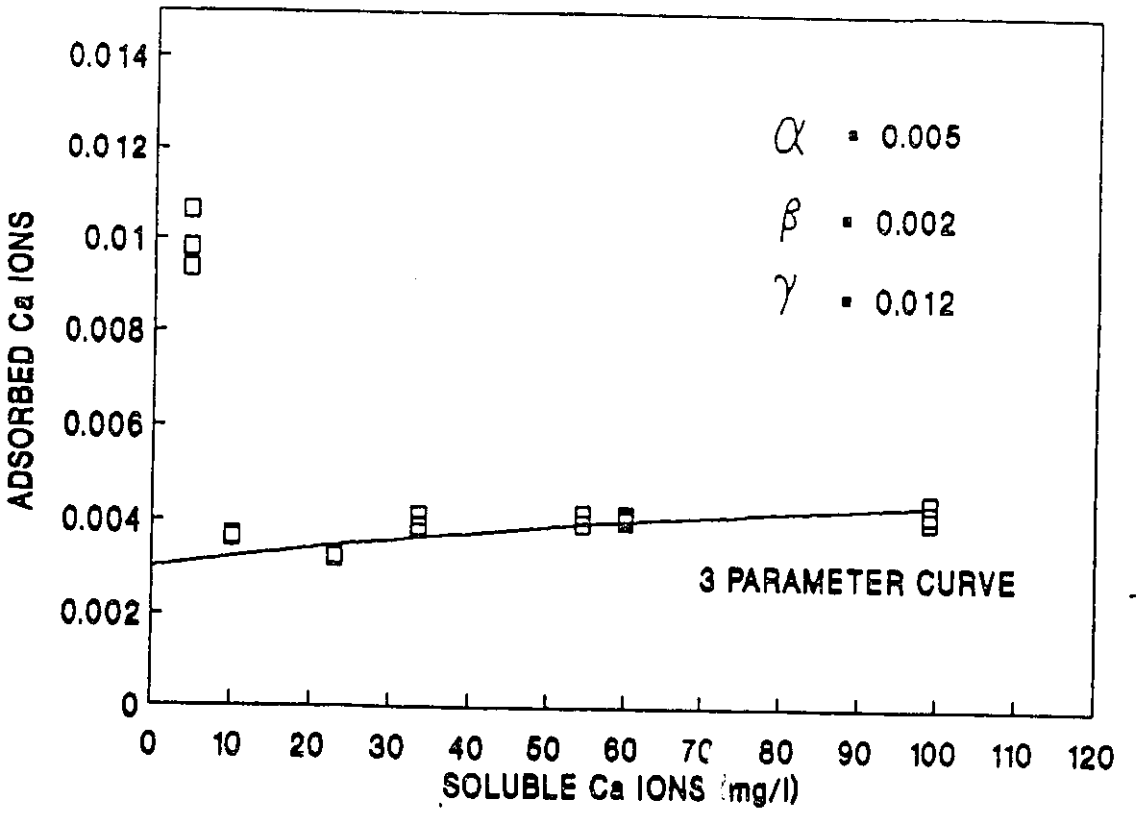

Figure 4.95. Relationship between soluble and adsorbed Ca^{2+} cation from squeezed clay samples at the NRC site.

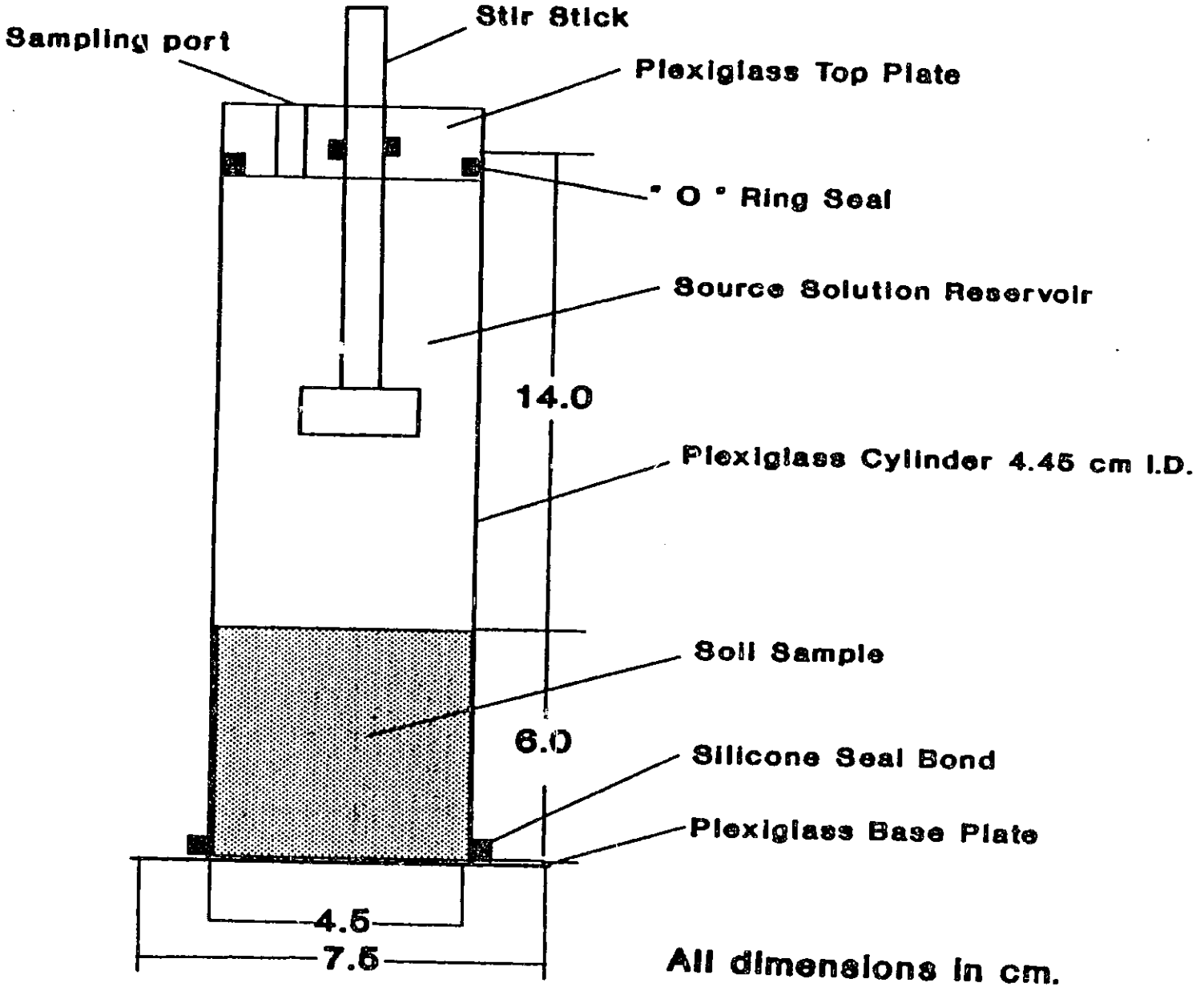

Figure 5.0. Schematic diagram of the diffusion apparatus.

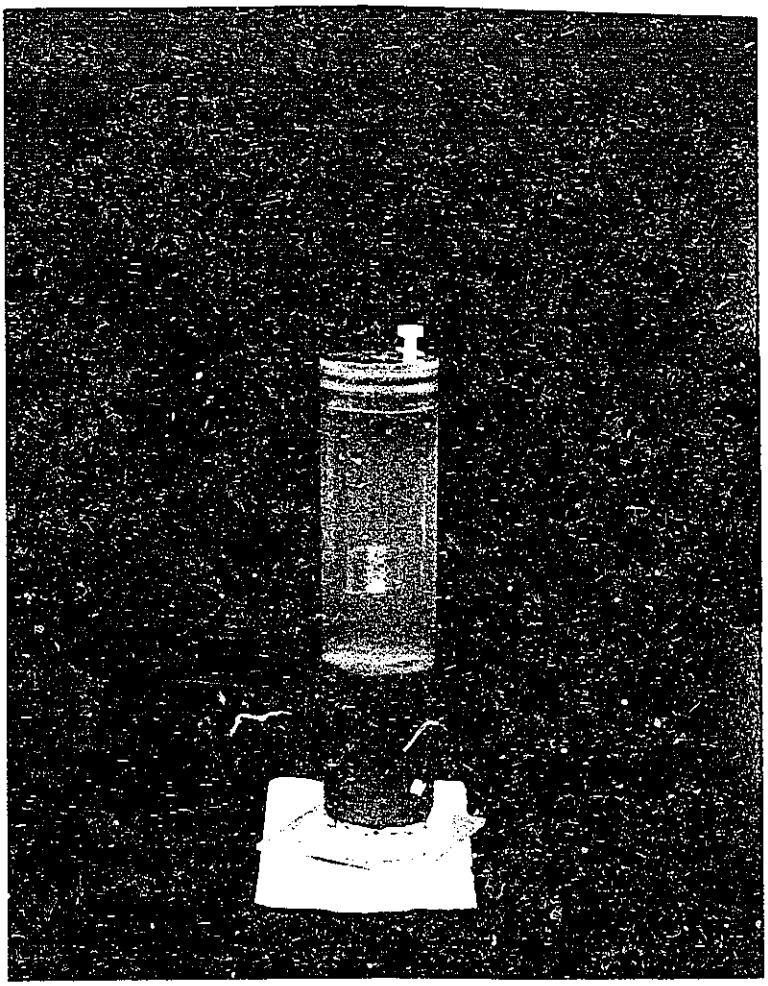

(A)

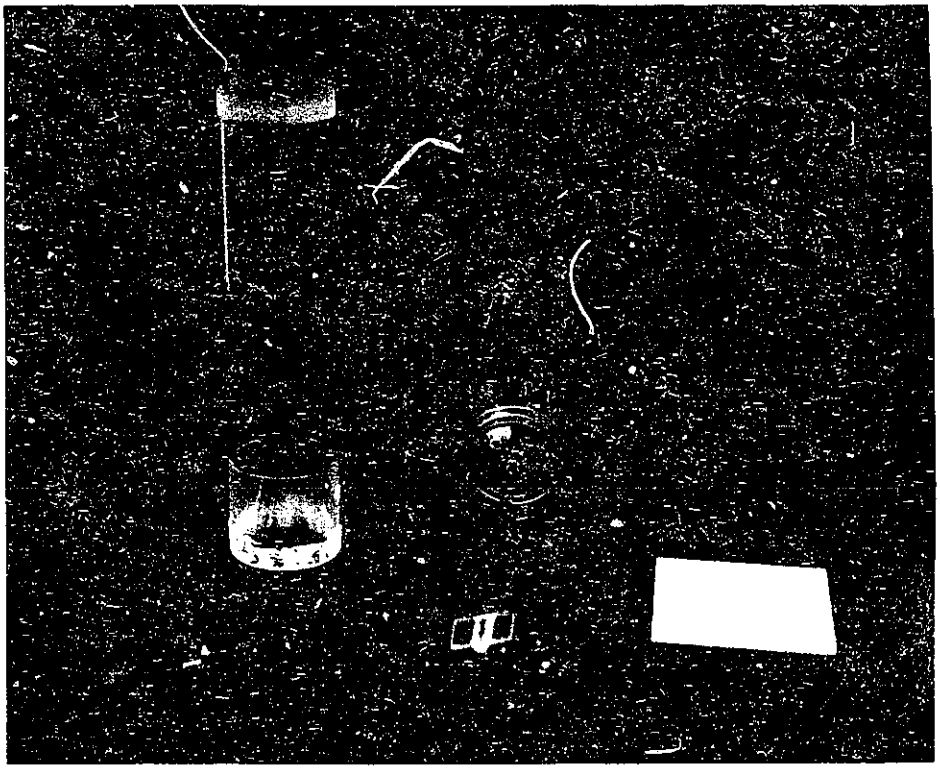

(B)

Figure 5.1. Photographs of diffusion experiment, (a) full experiment model, (b) the different diffusion cell parts.

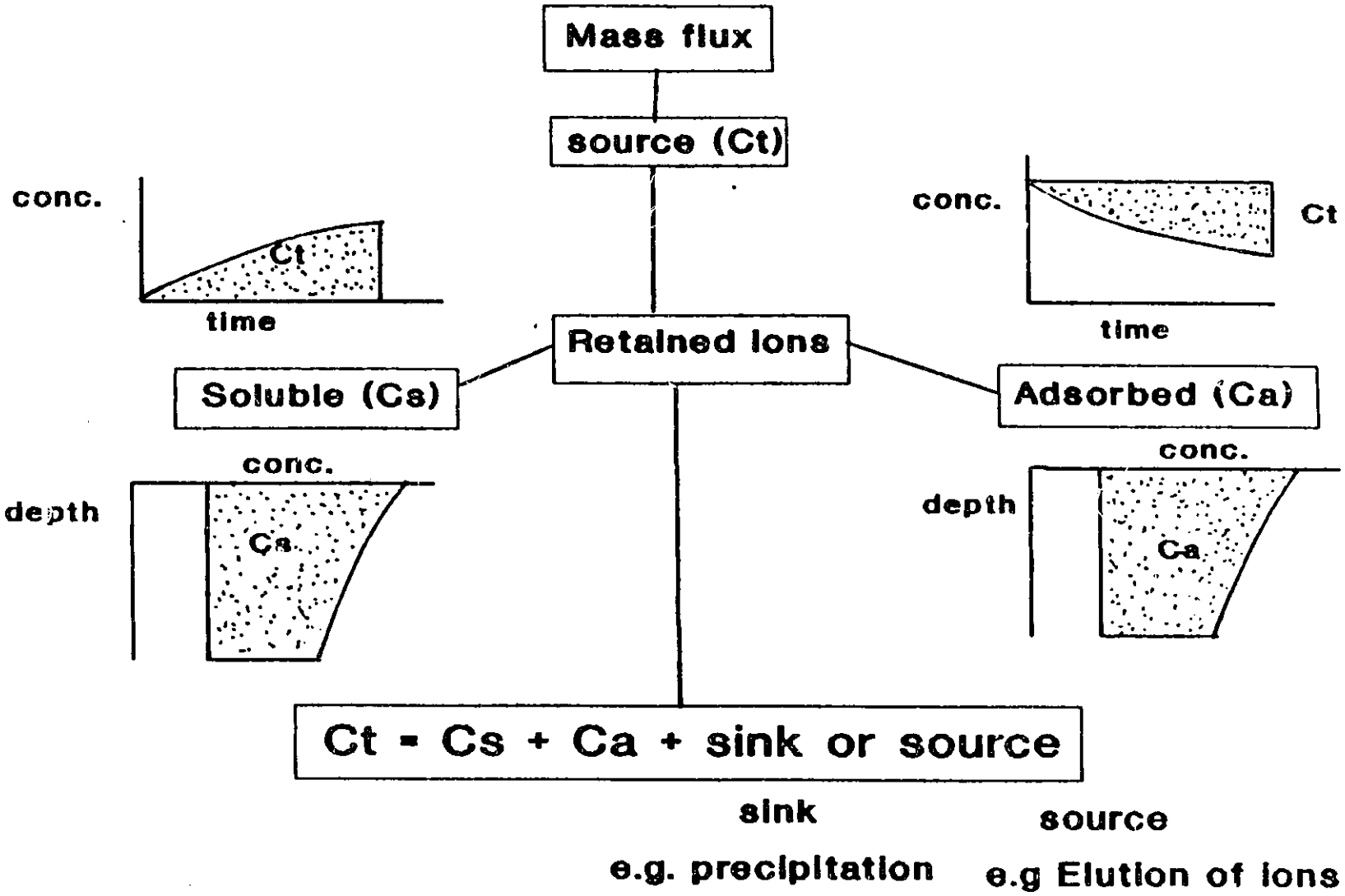

Figure 5.2. Schematic flow sheet of mass balance calculation.

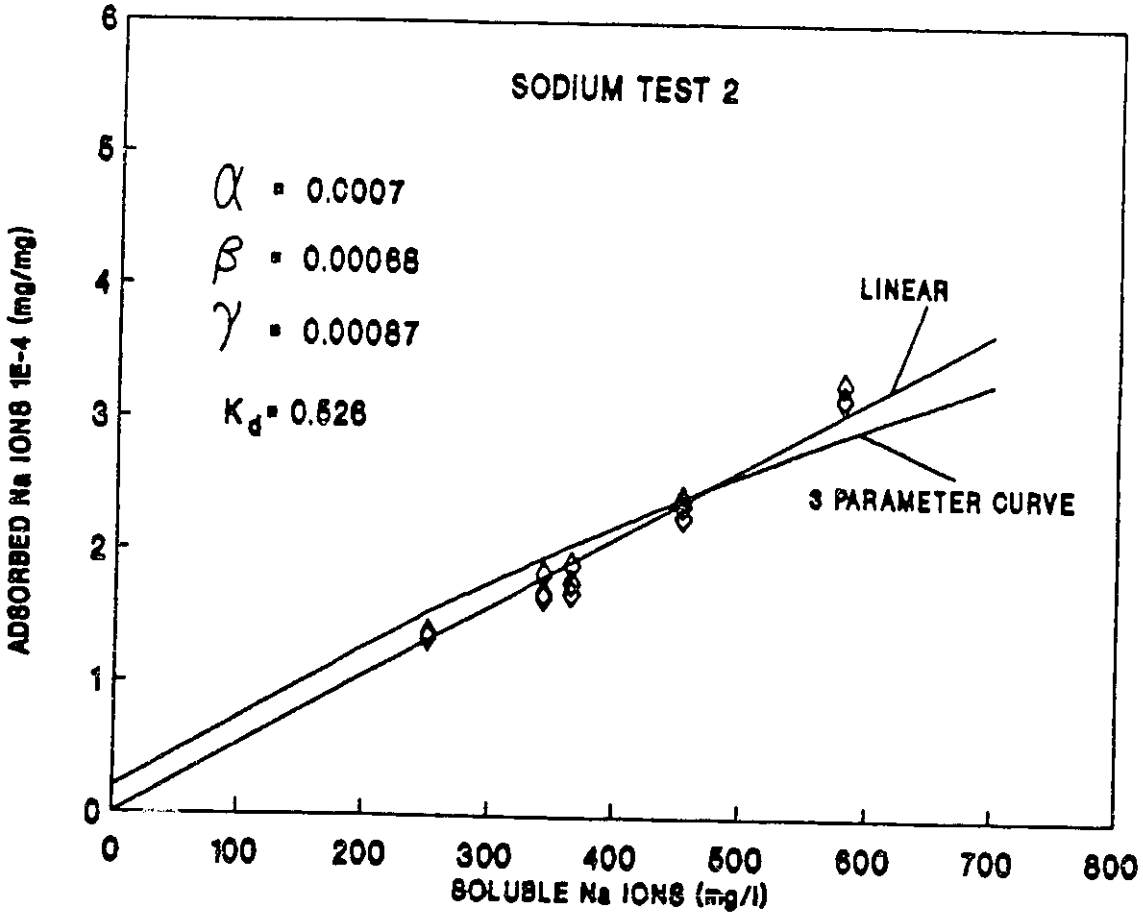

Figure 5.3. Relationship between soluble and adsorbed Na^+ cation for test 2, Fallowfield.

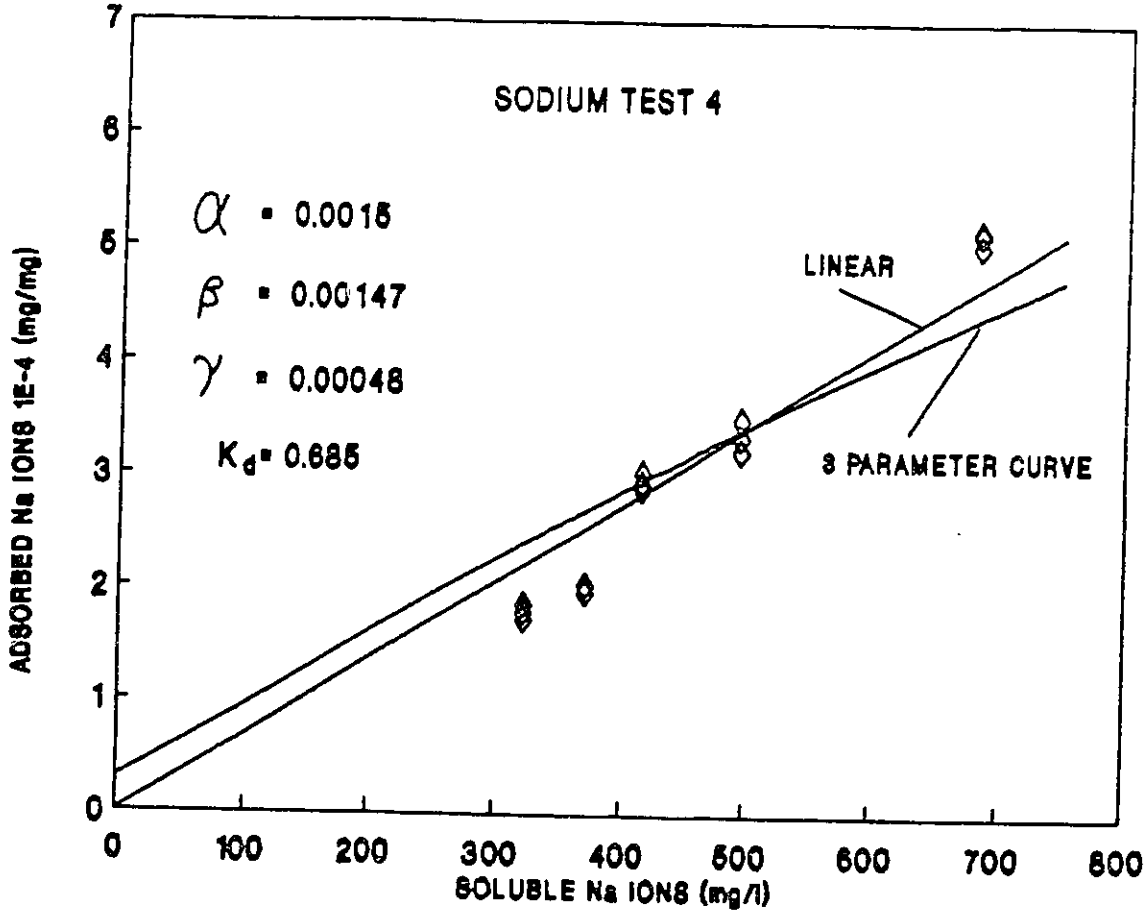

Figure 5.4. Relationship between soluble and adsorbed Na^+ cation for test 4, Fallowfield.

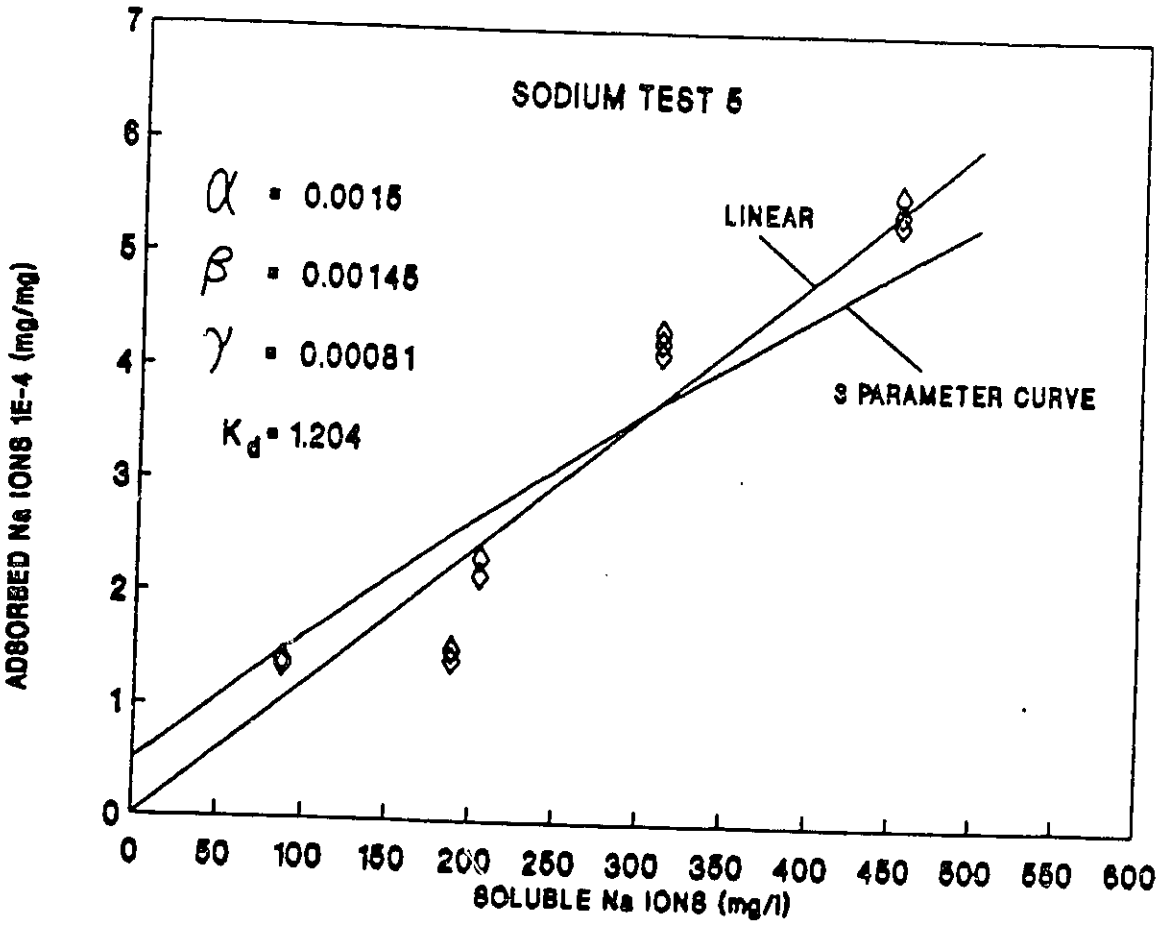

Figure 5.5. Relationship between soluble and adsorbed Na^+ cation for test 5, Casselman.

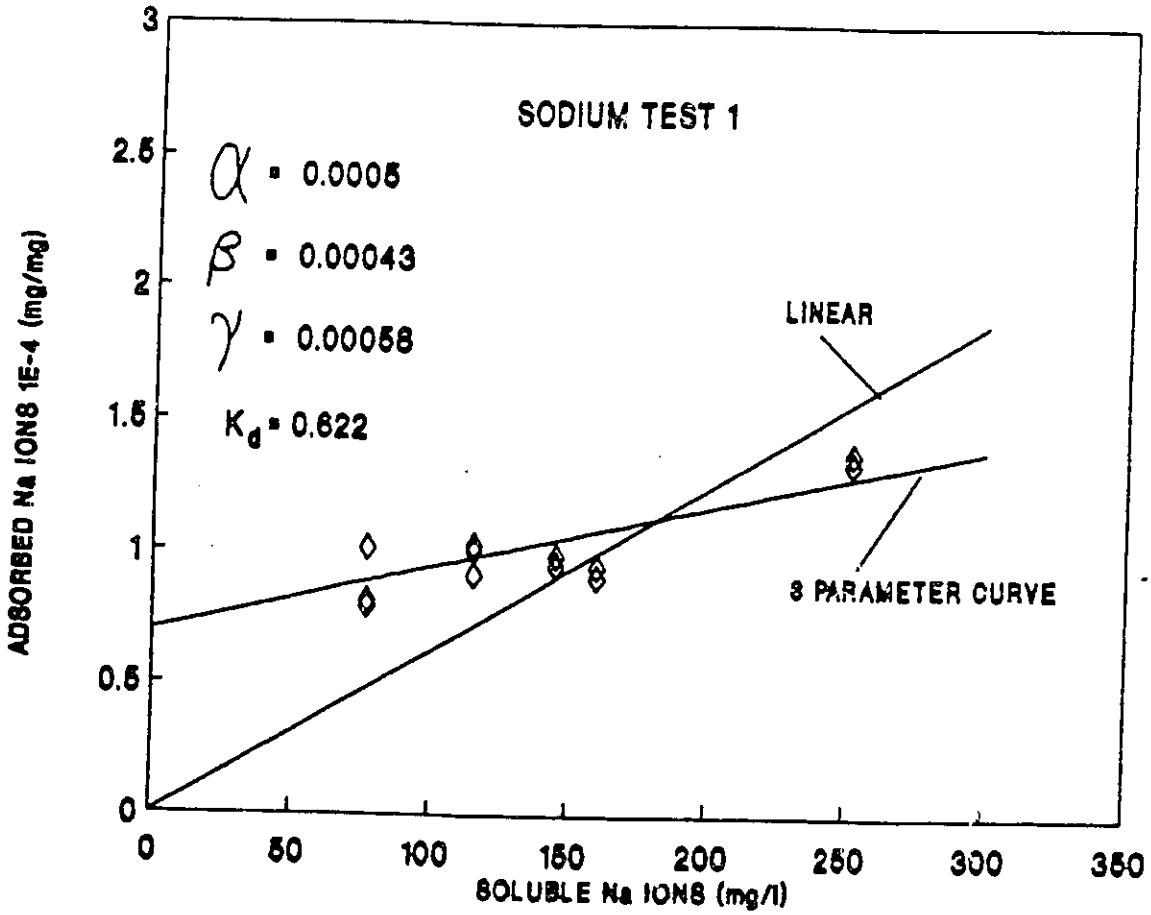

Figure 5.6a. Relationship between soluble and adsorbed Na^+ cation for test 1, Fallowfield.

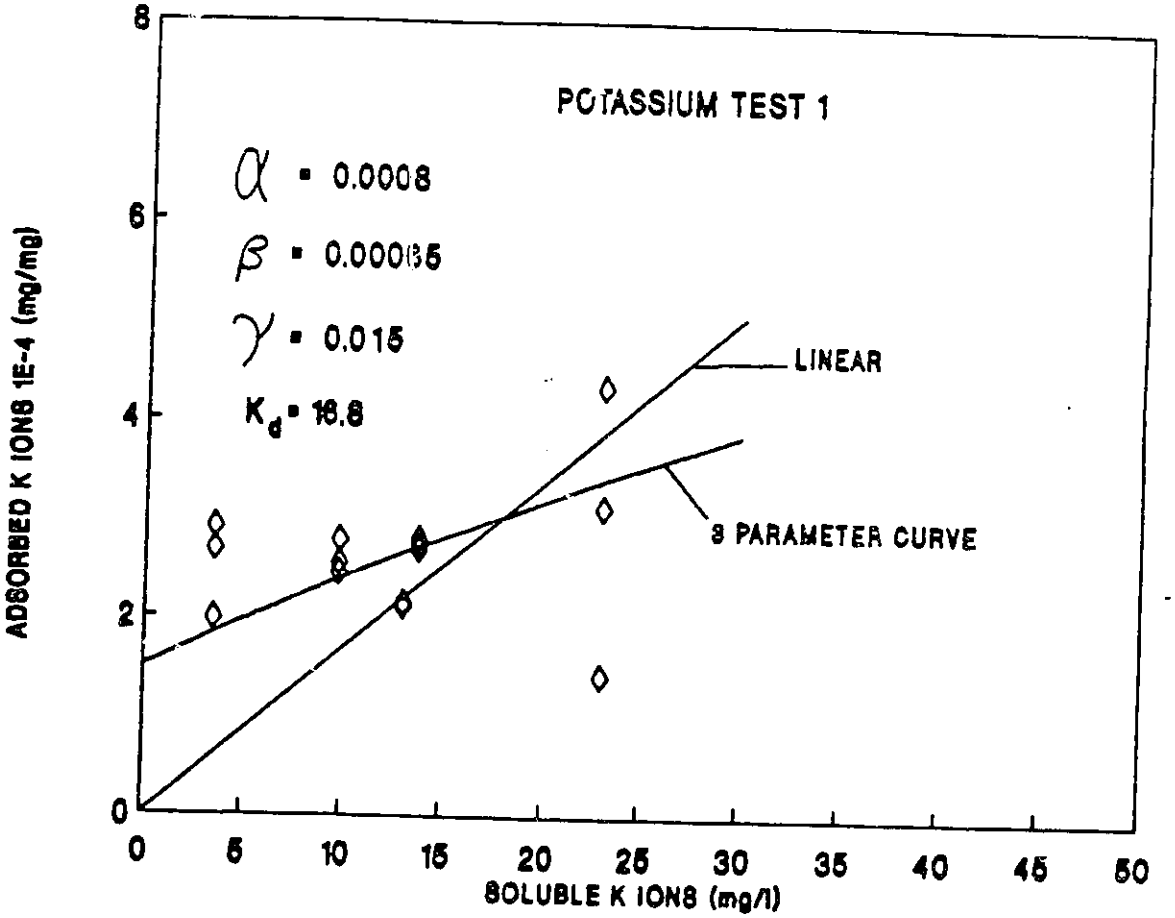

Figure 5.6b. Relationship between soluble and adsorbed K^+ cation for test 1, Fallowfield.

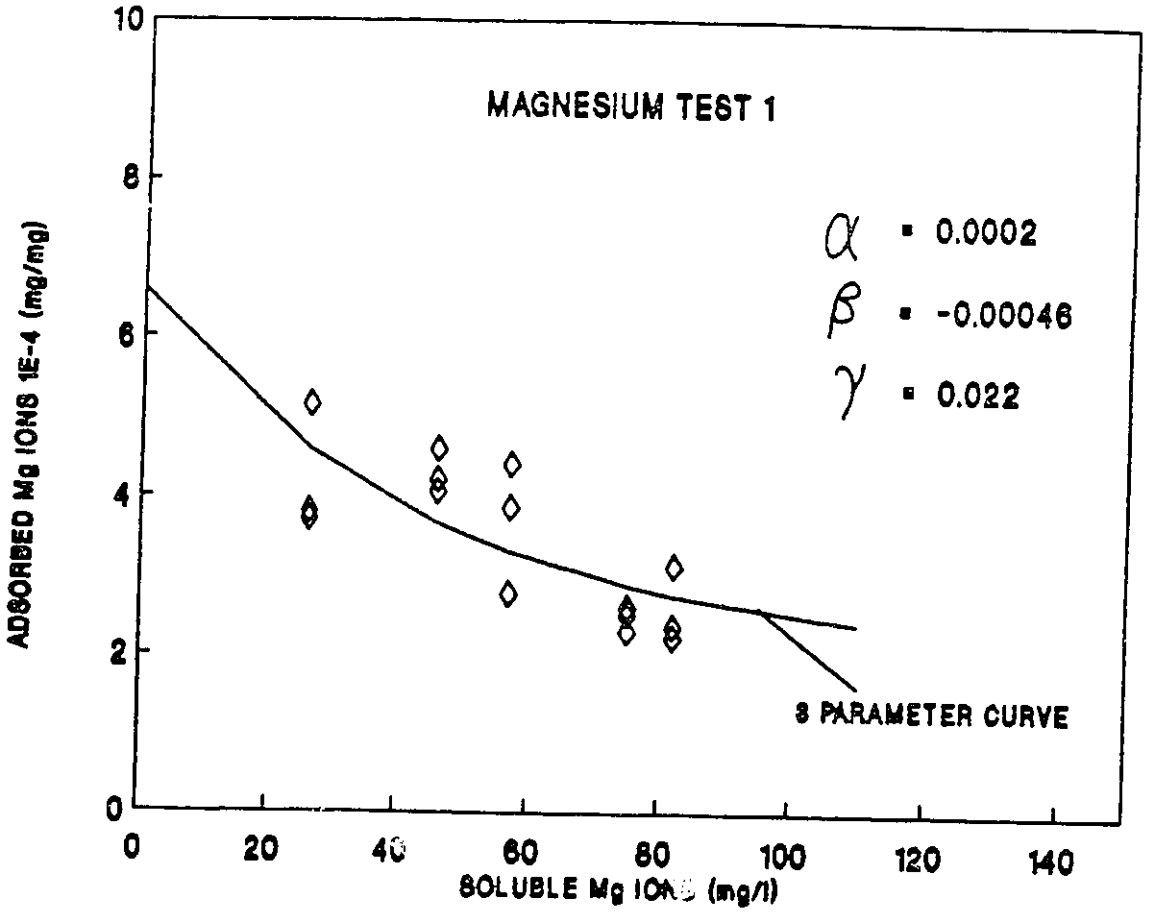

Figure 5.6c. Relationship between soluble and adsorbed Mg^{2+} cation for test 1, Fallowfield.

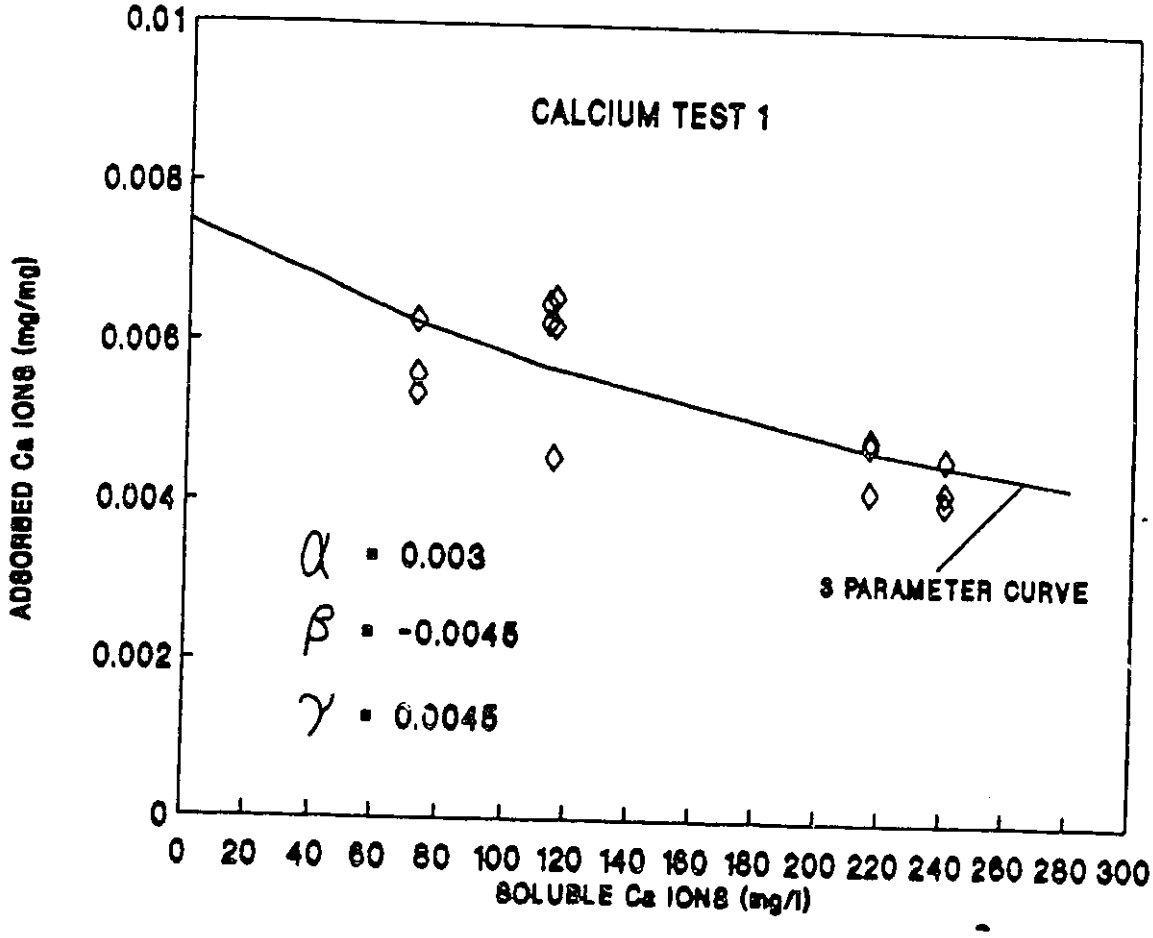

Figure 5.6d. Relationship between soluble and adsorbed Ca^{2+} cation for test 1, Fallowfield.

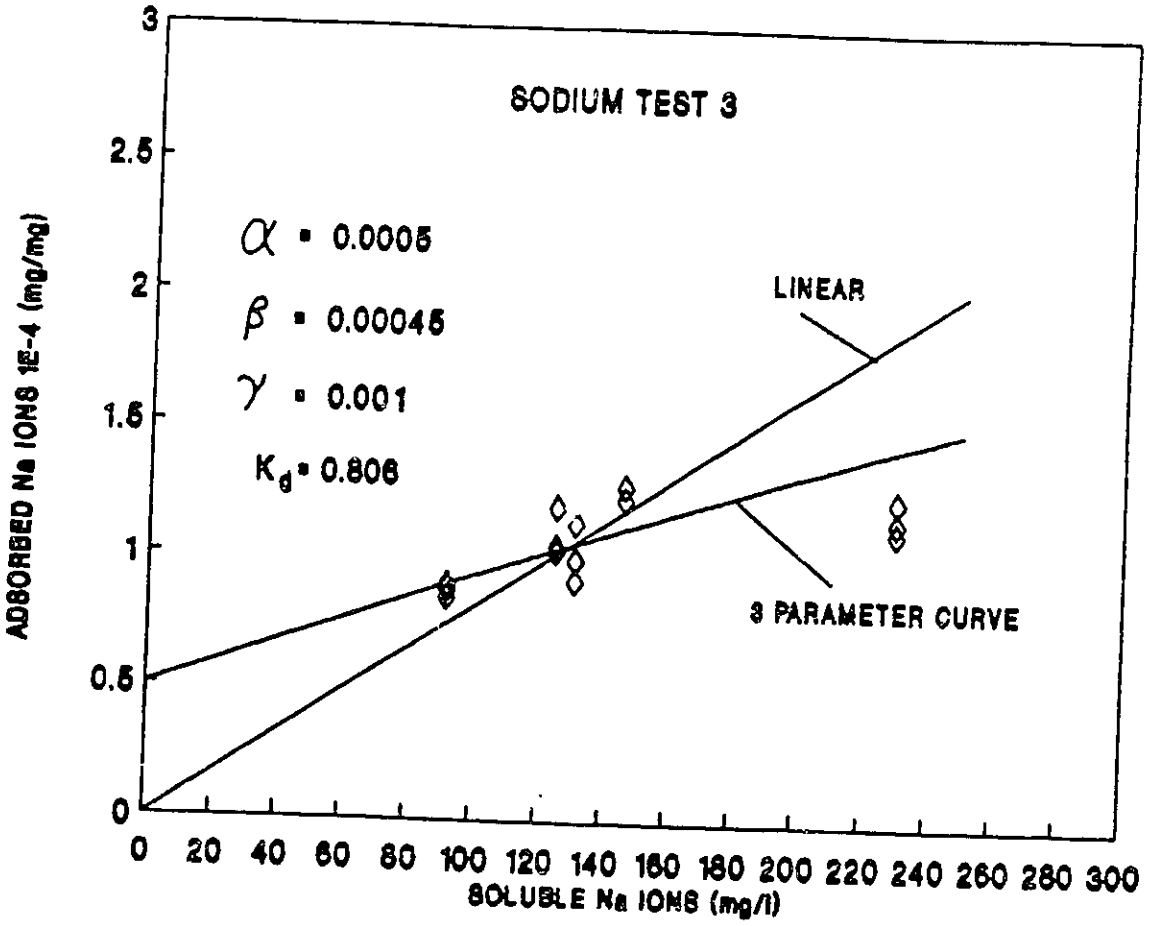

Figure 5.7a. Relationship between soluble and adsorbed Na^+ cation for test 3, Renfrew.

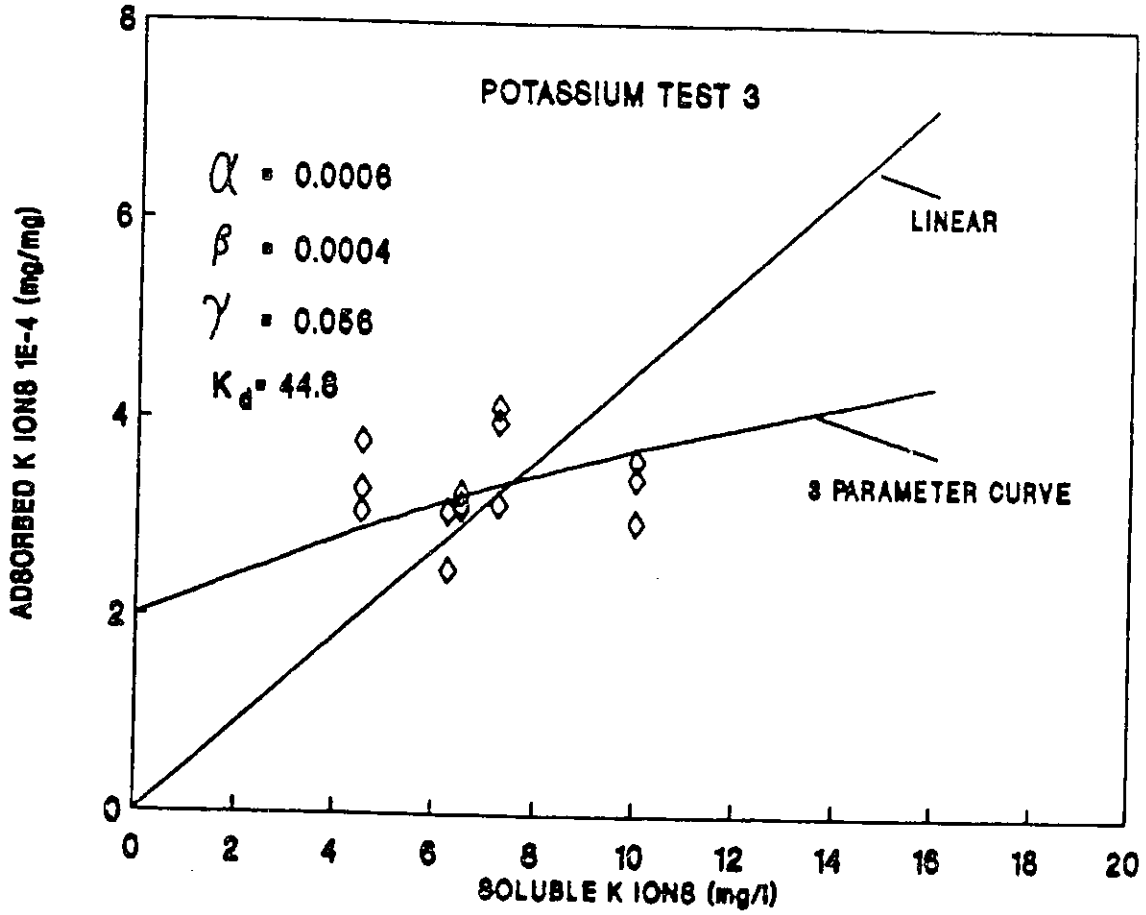

Figure 5.7b. Relationship between soluble and adsorbed K^+ cation for test 3, Renfrew.

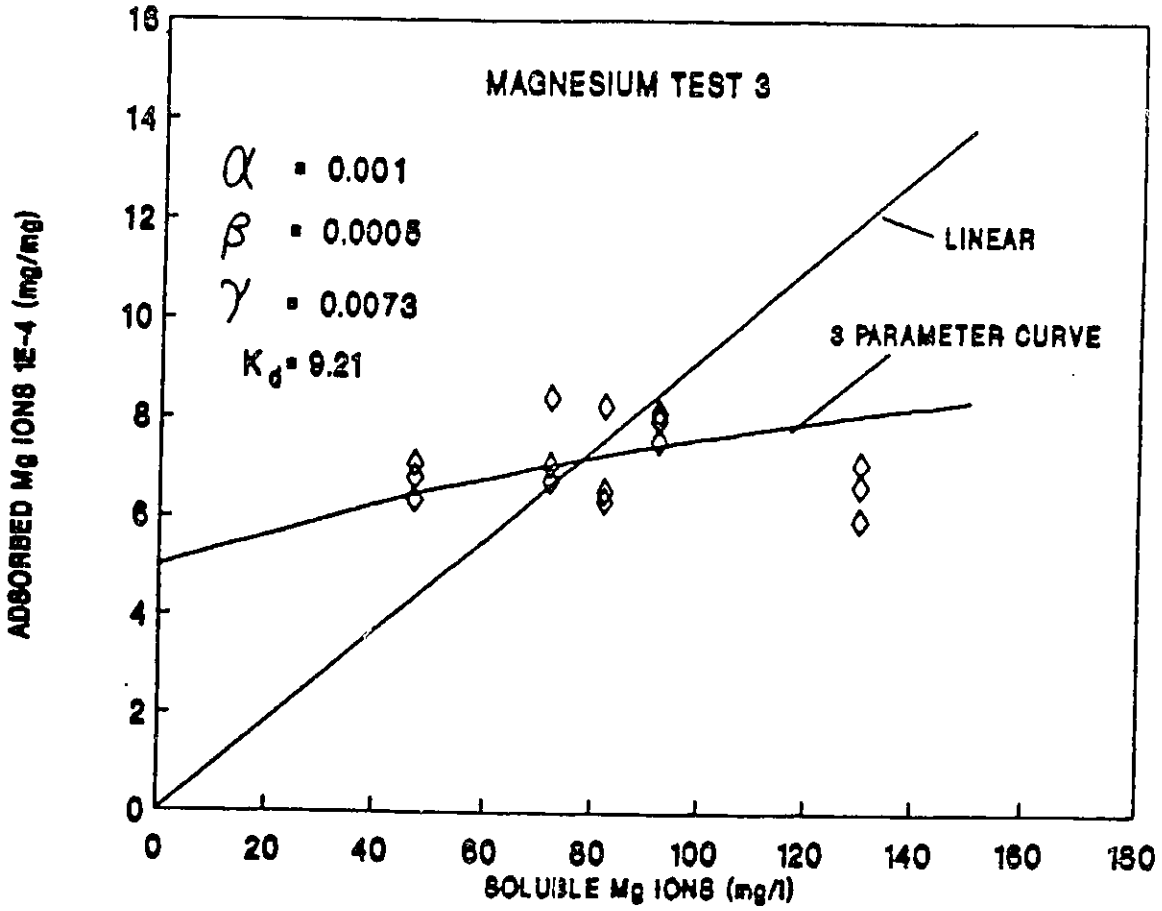

Figure 5.7c. Relationship between soluble and adsorbed Mg^{2+} cation for test 3, Renfrew.

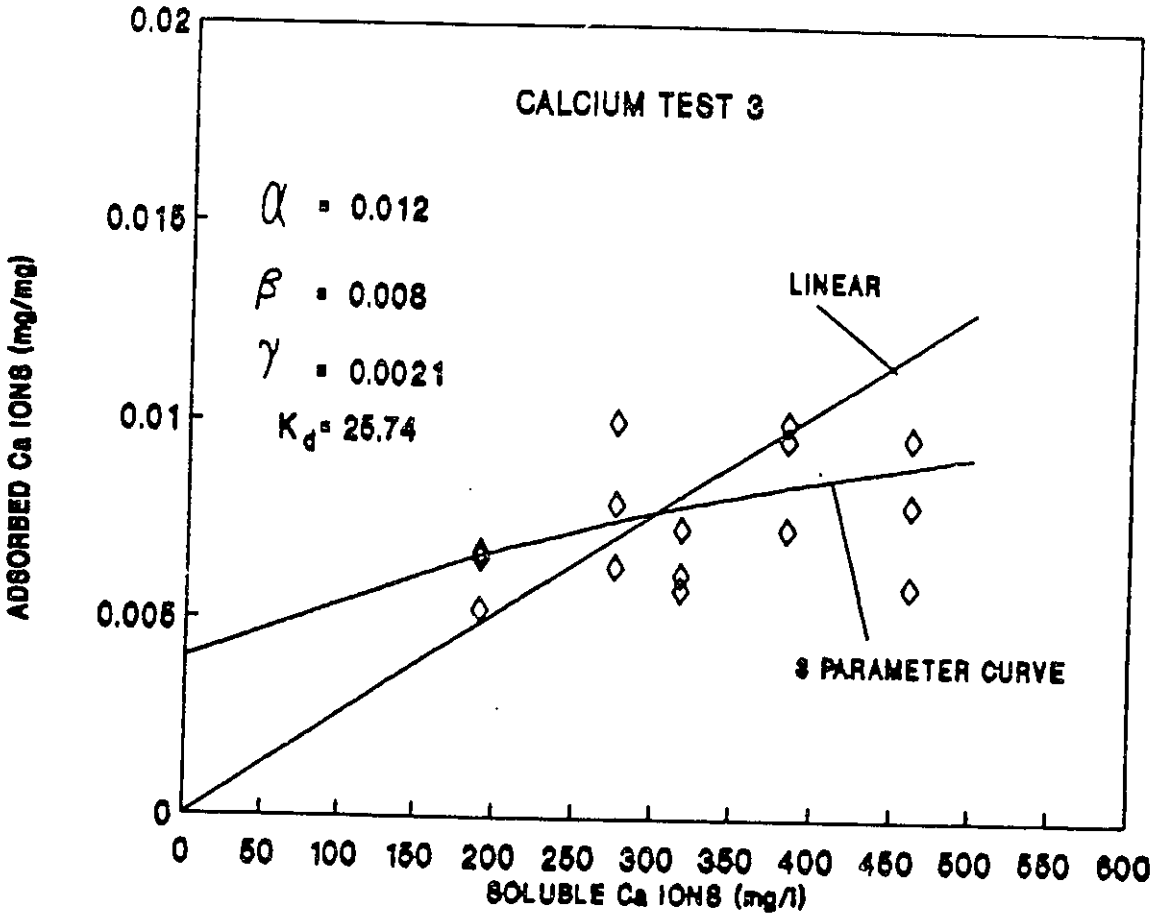

Figure 5.7d. Relationship between soluble and adsorbed Ca^{2+} cation for test 3, Renfrew.

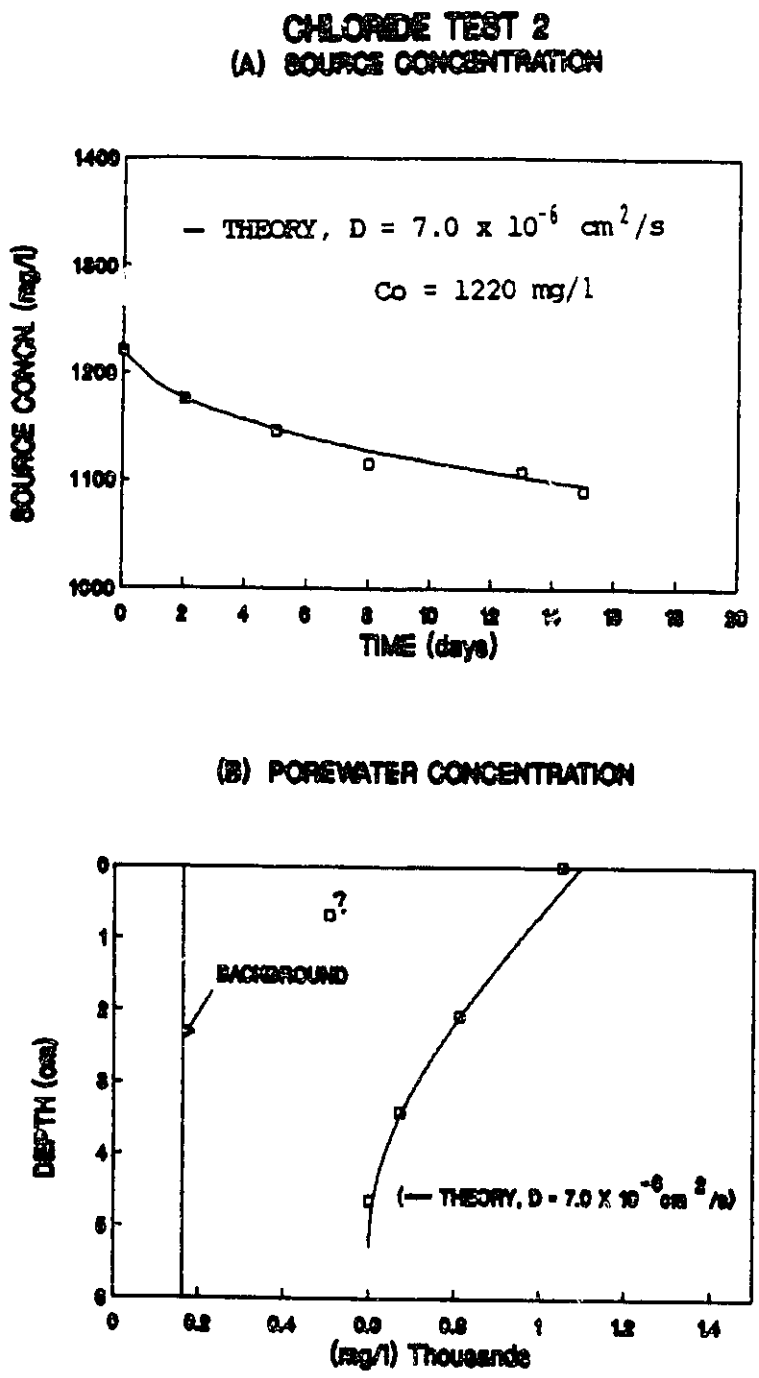

Figure 5.8a. Chloride, test 2: (a) source concentration vs. time; (b) porewater concentration vs. depth.

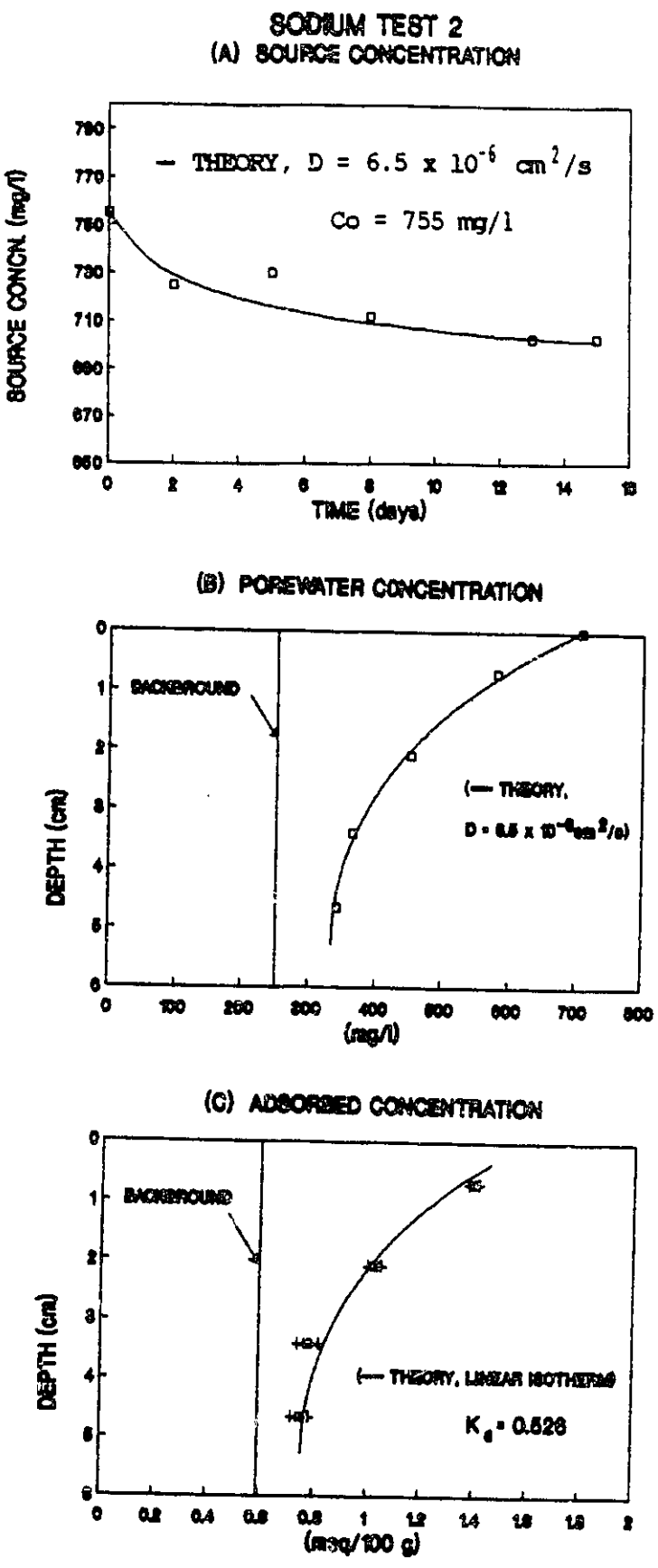

Figure 5.8b. Sodium, test 2: (a) source concentration vs. time; porewater concentration vs. depth; (c) adsorbed concentration vs. depth.

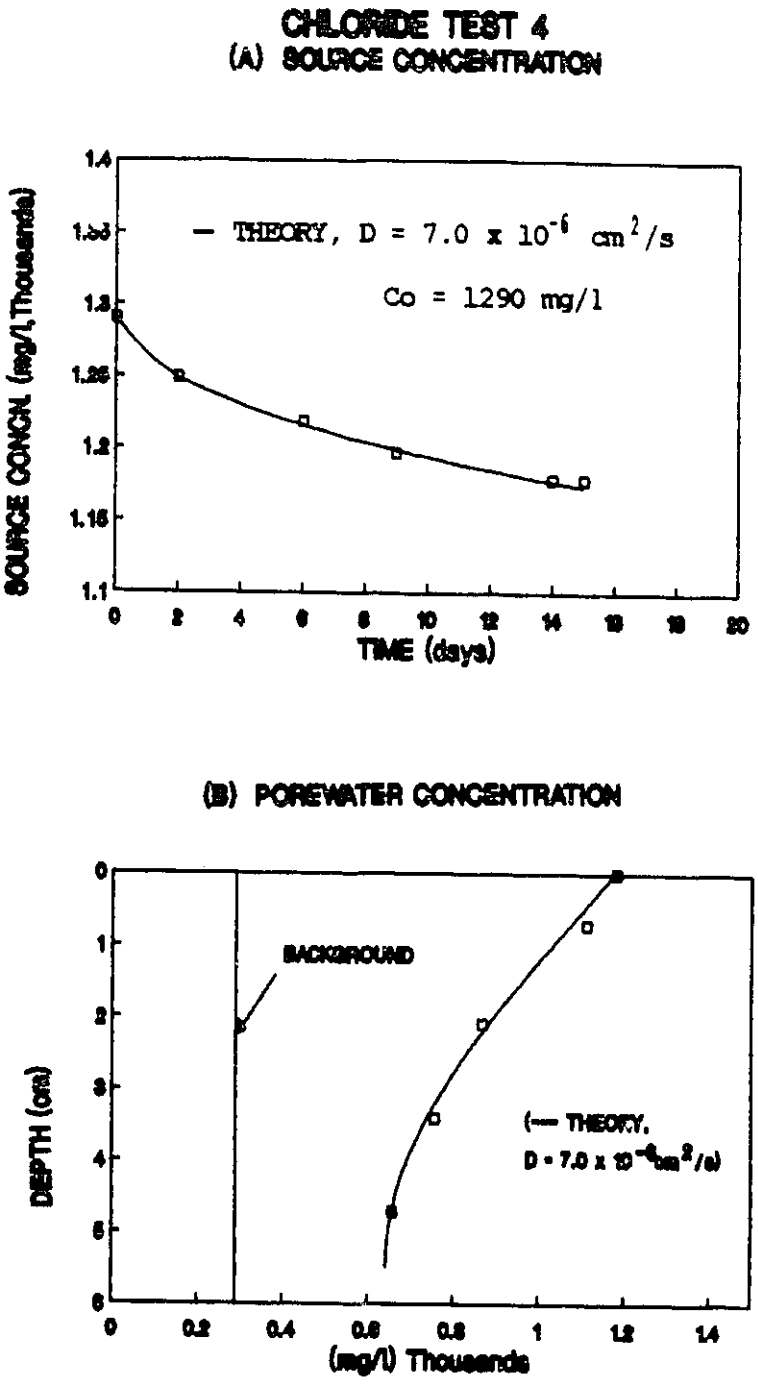

Figure 5.9a. Chloride, test 4: (a) source concentration vs. time; (b) porewater concentration vs. depth.

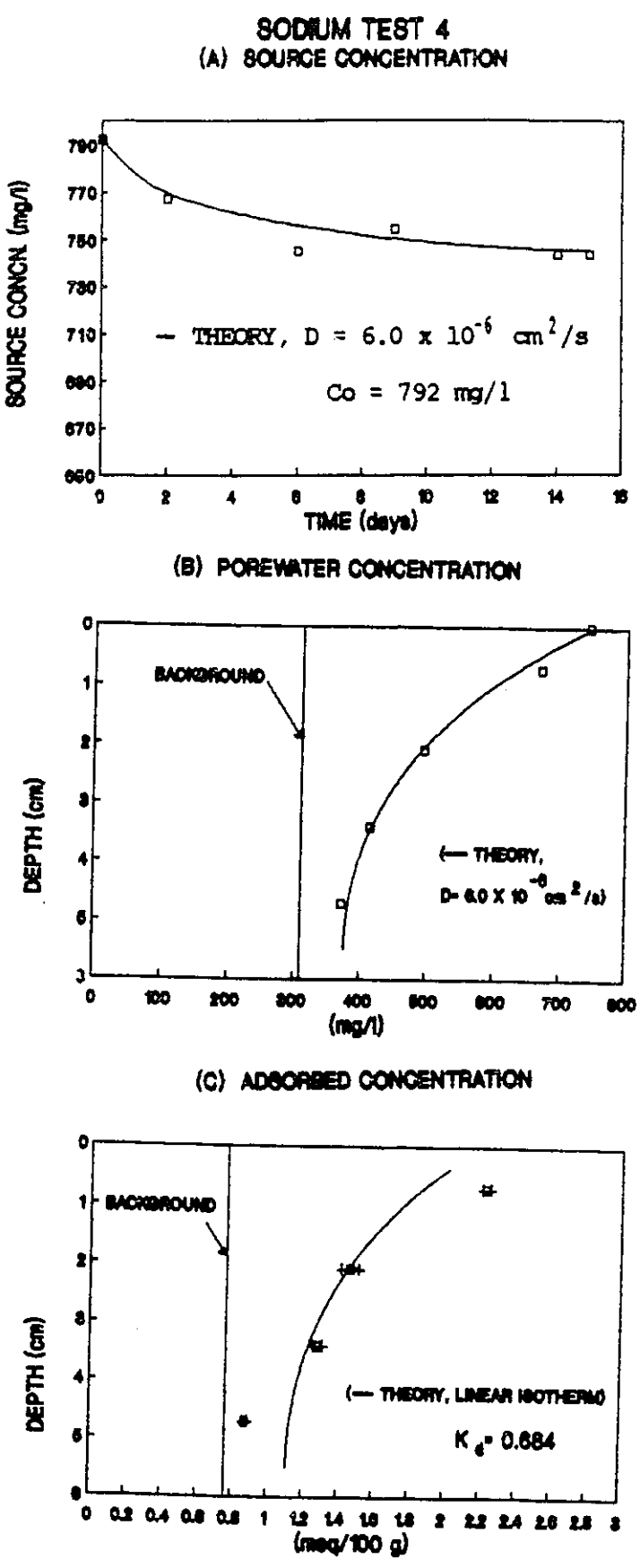

Figure 5.9b. Sodium, test 4: (a) source concentration vs. time; porewater concentration vs. depth; (c) adsorbed concentration vs. depth.

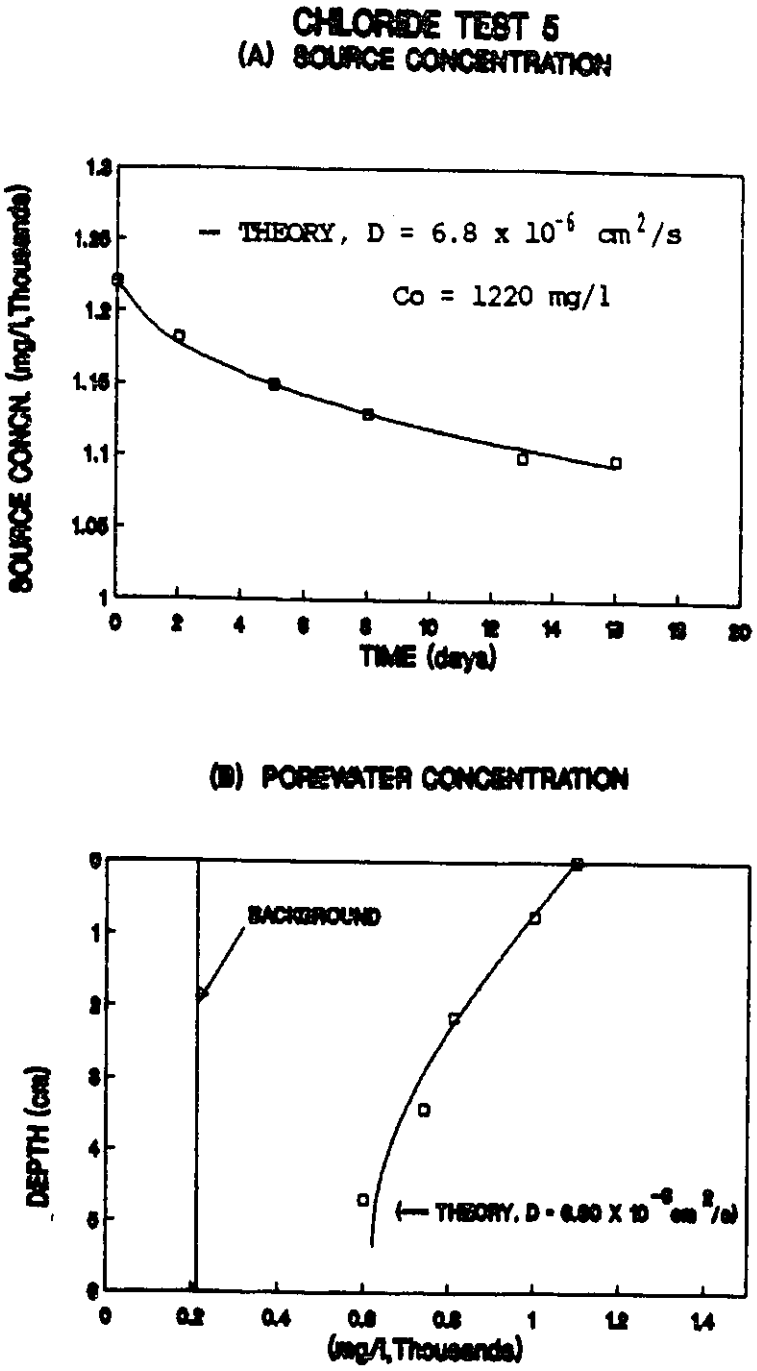

Figure 5.10a. Chloride, test 5: (a) source concentration vs. time; (b) porewater concentration vs. depth.

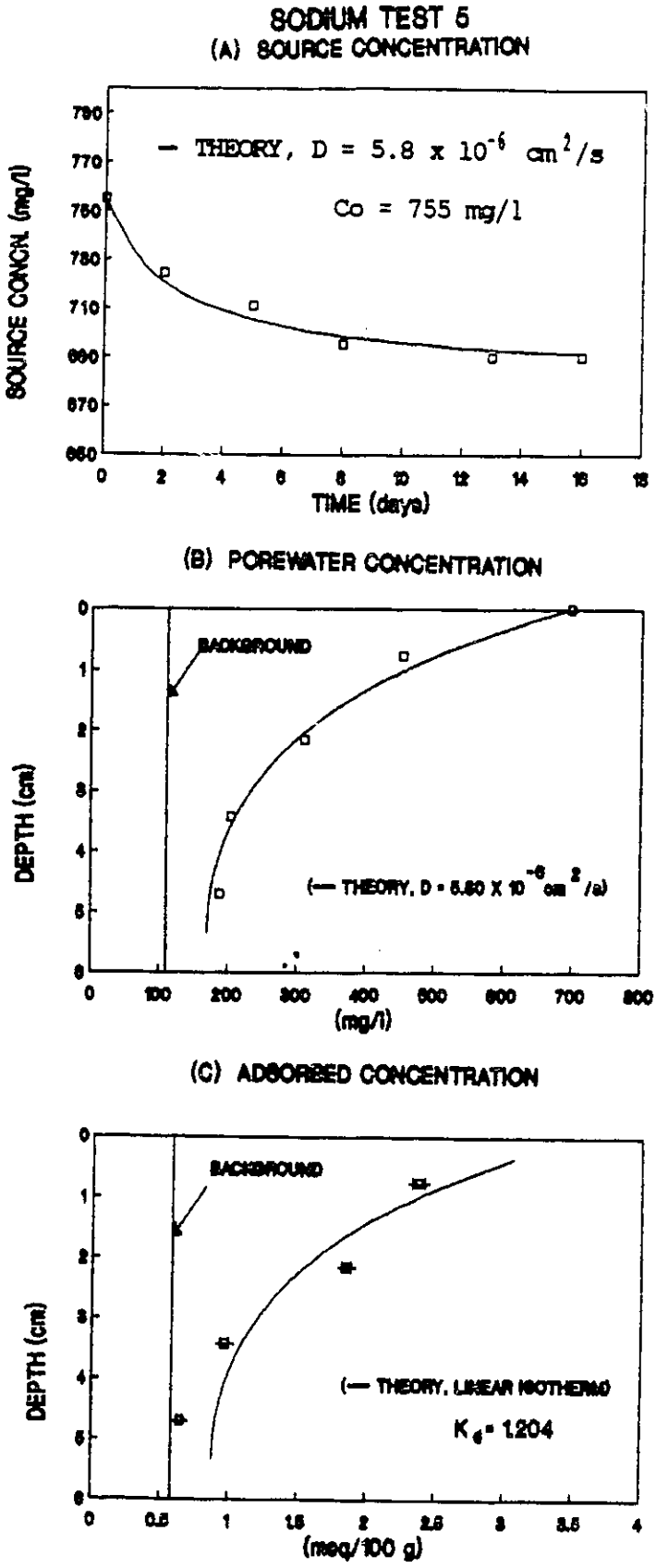

Figure 5.10b. Sodium, test 5: (a) source concentration vs. time; porewater concentration vs. depth; (c) adsorbed concentration vs. depth.

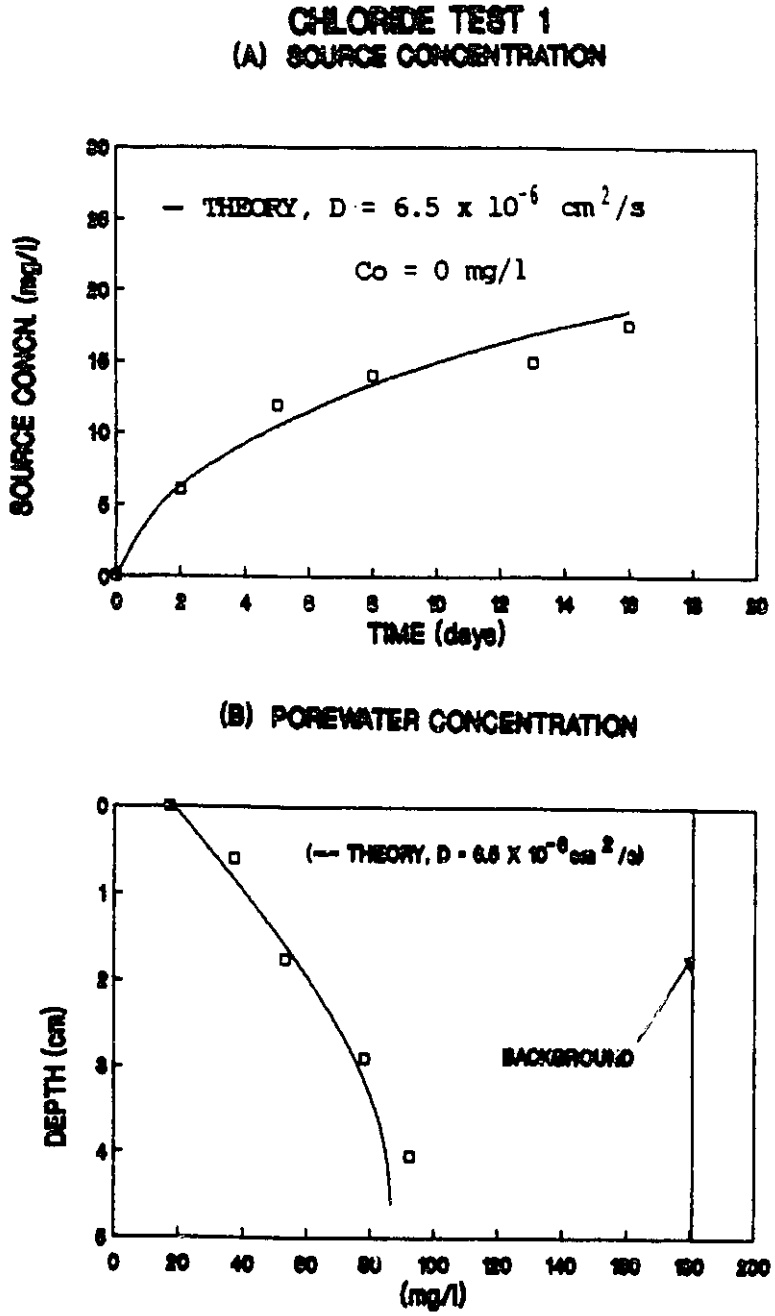

Figure 5.11a. Chloride, test 1: (a) source concentration vs. time; (b) porewater concentration vs. depth.

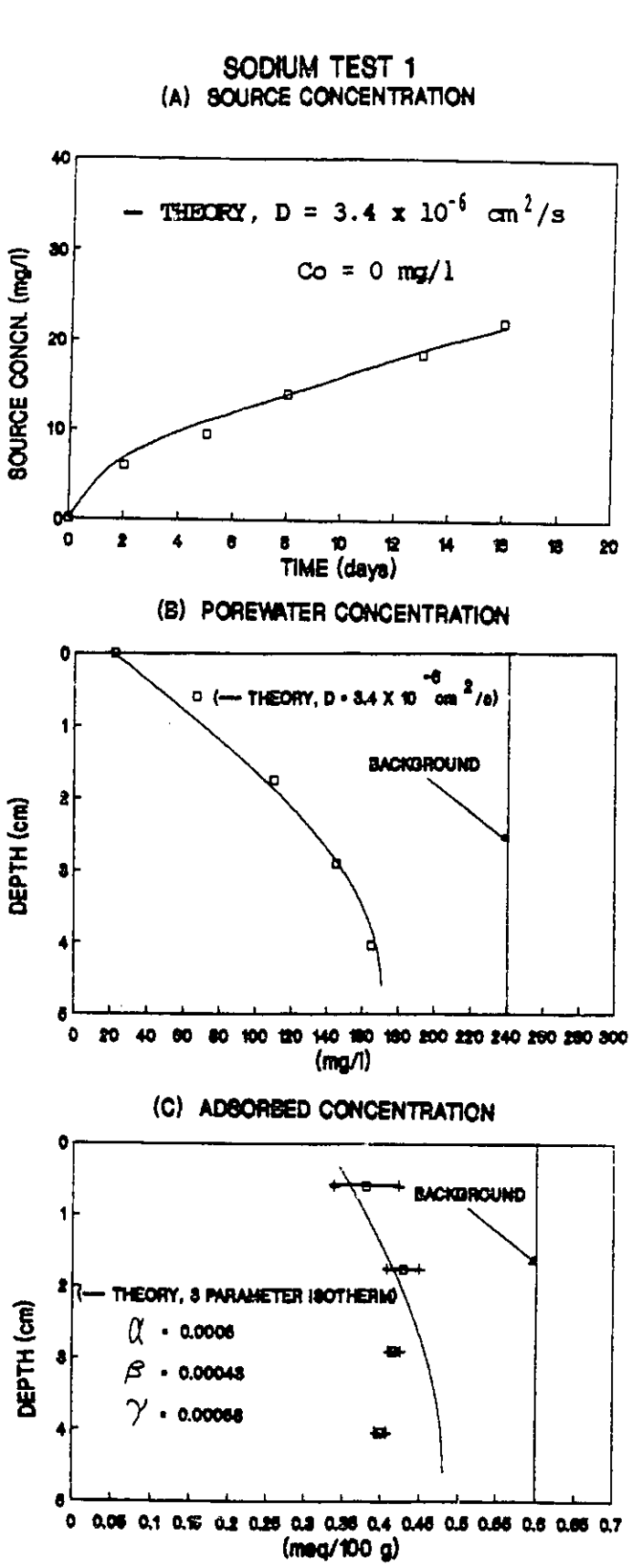

Figure 5.11b. Sodium, test 1: (a) source concentration vs. time; porewater concentration vs. depth; (c) adsorbed concentration vs. depth.

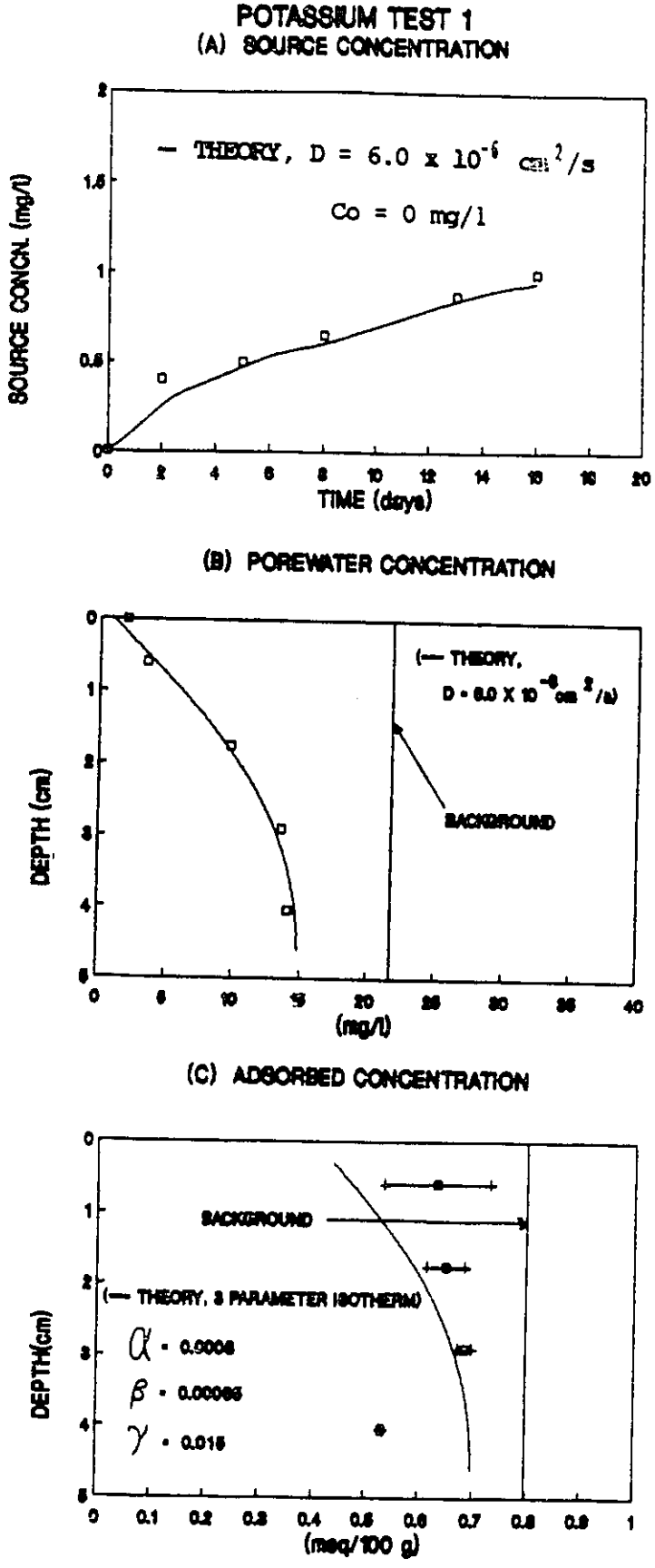

Figure 5.11c. Potassium, test 1: (a) source concentration vs. time; porewater concentration vs. depth; (c) adsorbed concentration vs. depth.

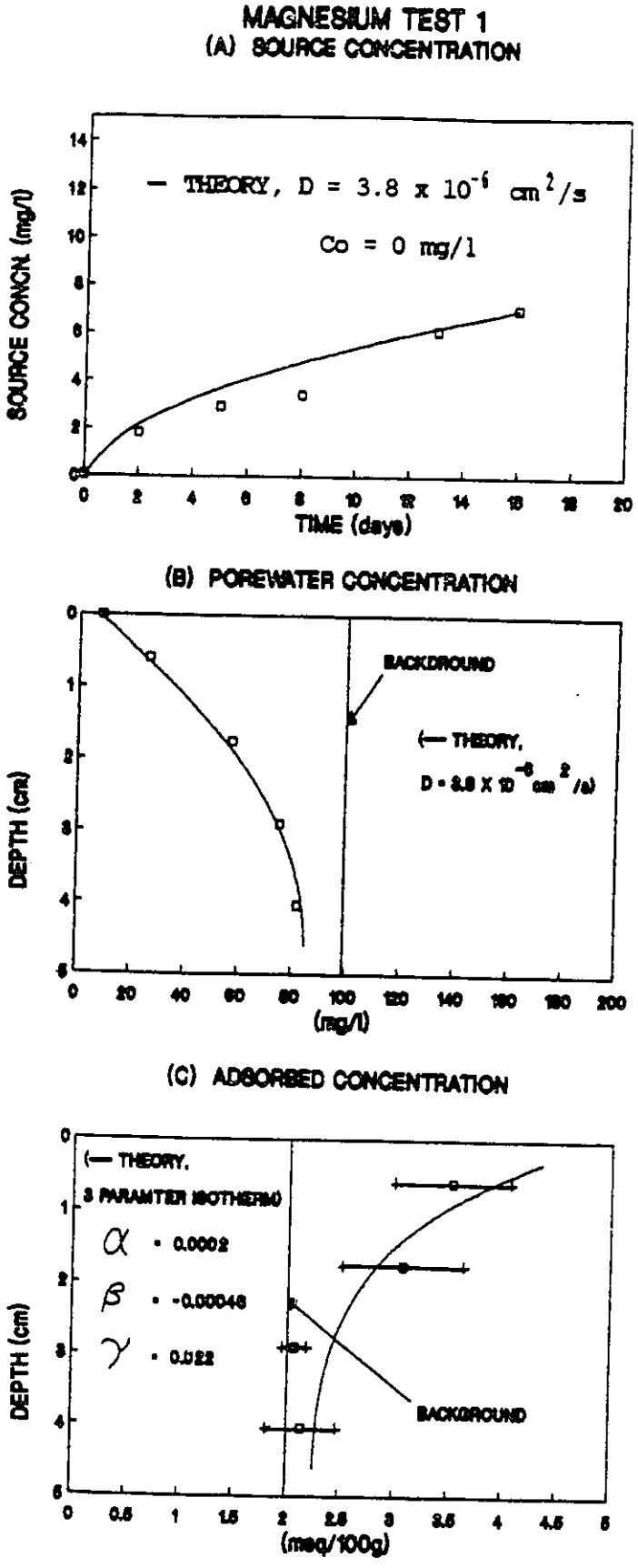

Figure 5.11d. Magnesium, test 1: (a) source concentration vs. time; porewater concentration vs. depth; (c) adsorbed concentration vs. depth.

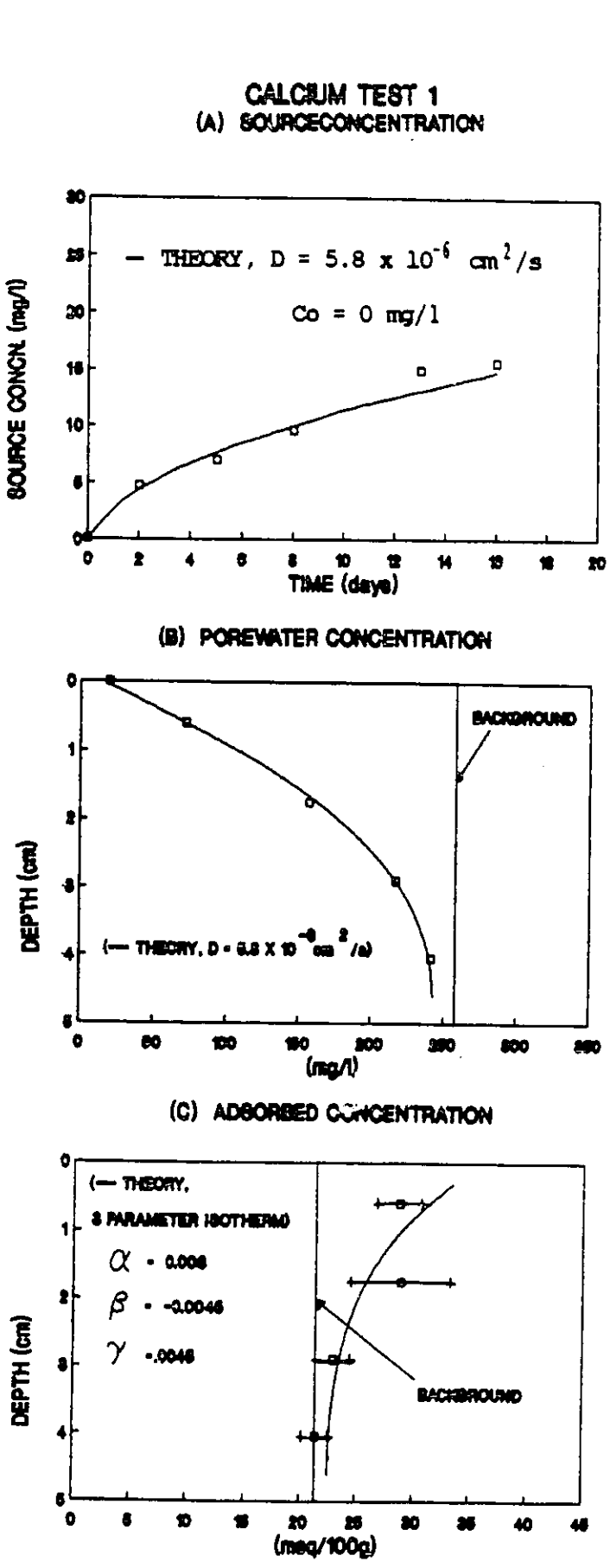

Figure 5.11e. Calcium, test 1: (a) source concentration vs. time; porewater concentration vs. depth; (c) adsorbed concentration vs. depth.

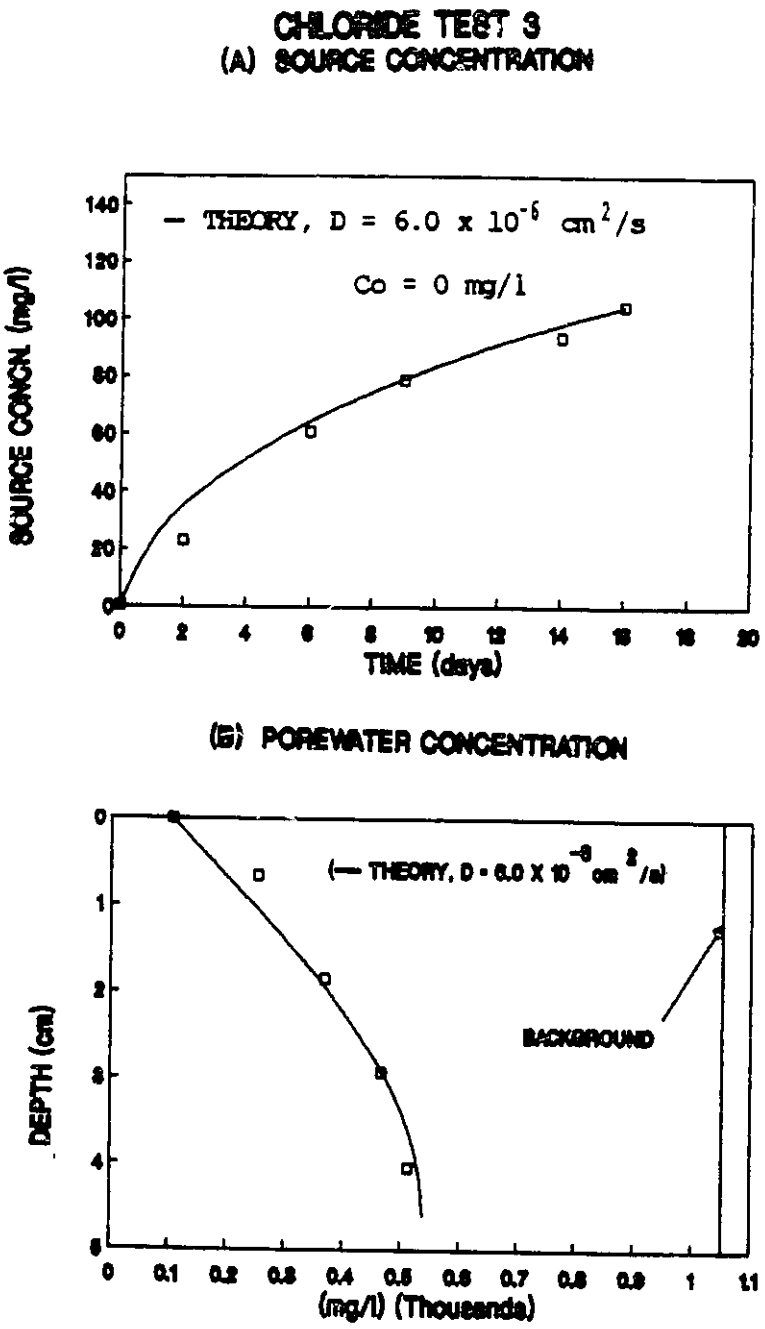

Figure 5.12a. Chloride, test 3: (a) source concentration vs. time; (b) porewater concentration vs. depth.

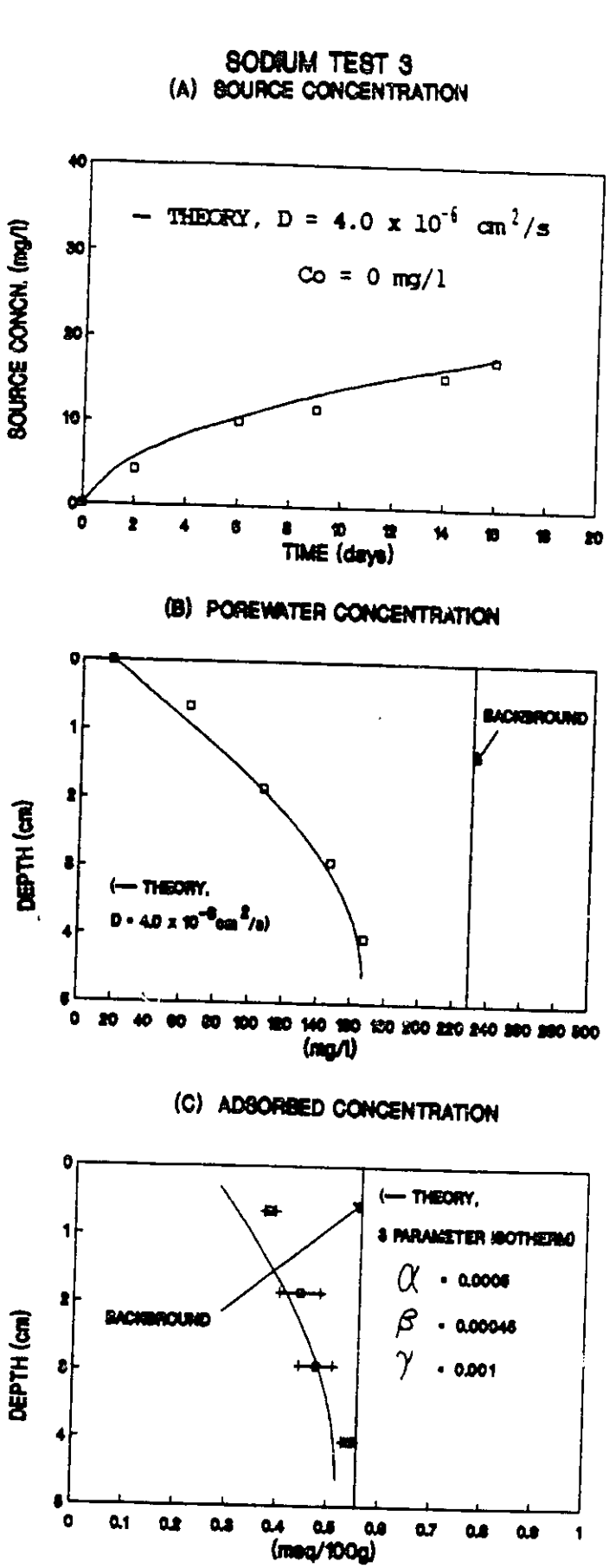

Figure 5.12b. Sodium, test 3: (a) source concentration vs. time; porewater concentration vs. depth; (c) adsorbed concentration vs. depth.

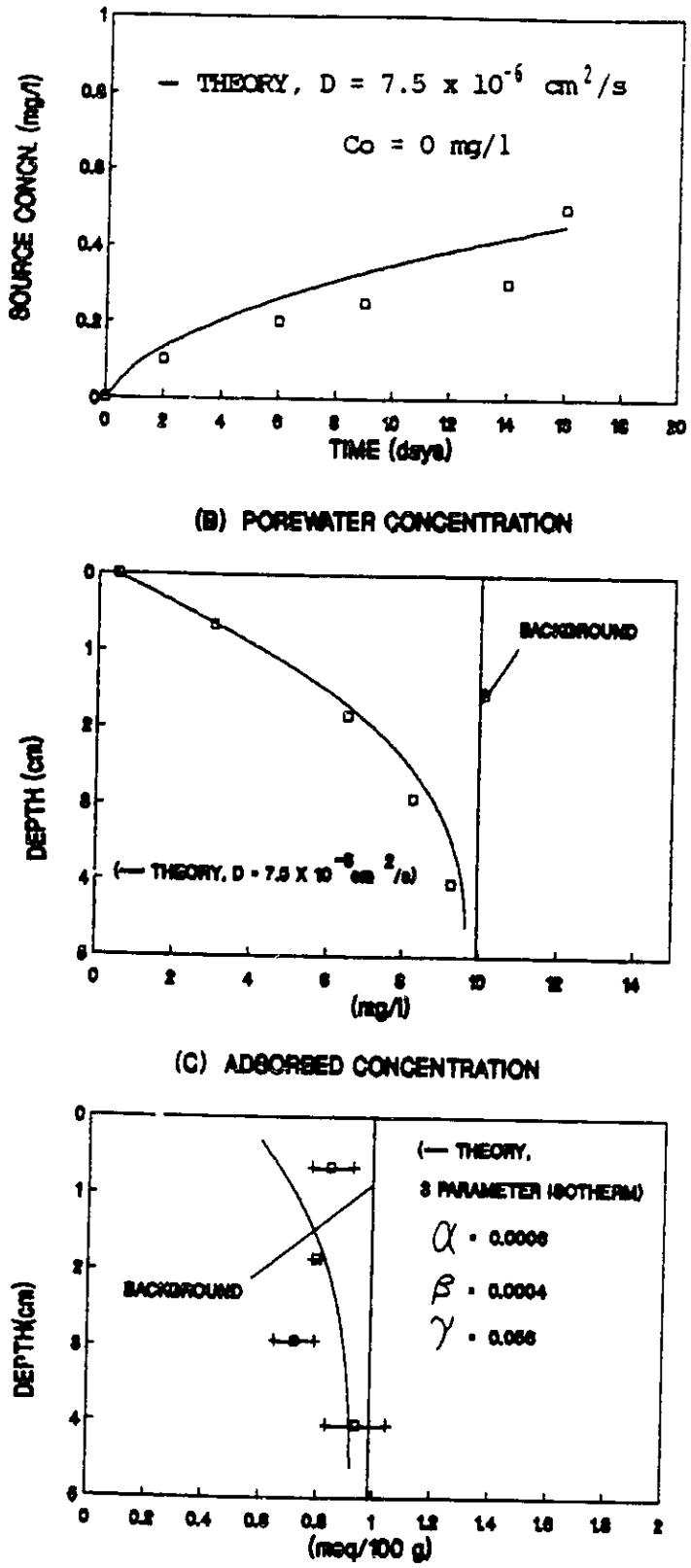

Figure 5.12c. Potassium, test 3: (a) source concentration vs. time; porewater concentration vs. depth; (c) adsorbed concentration vs. depth.

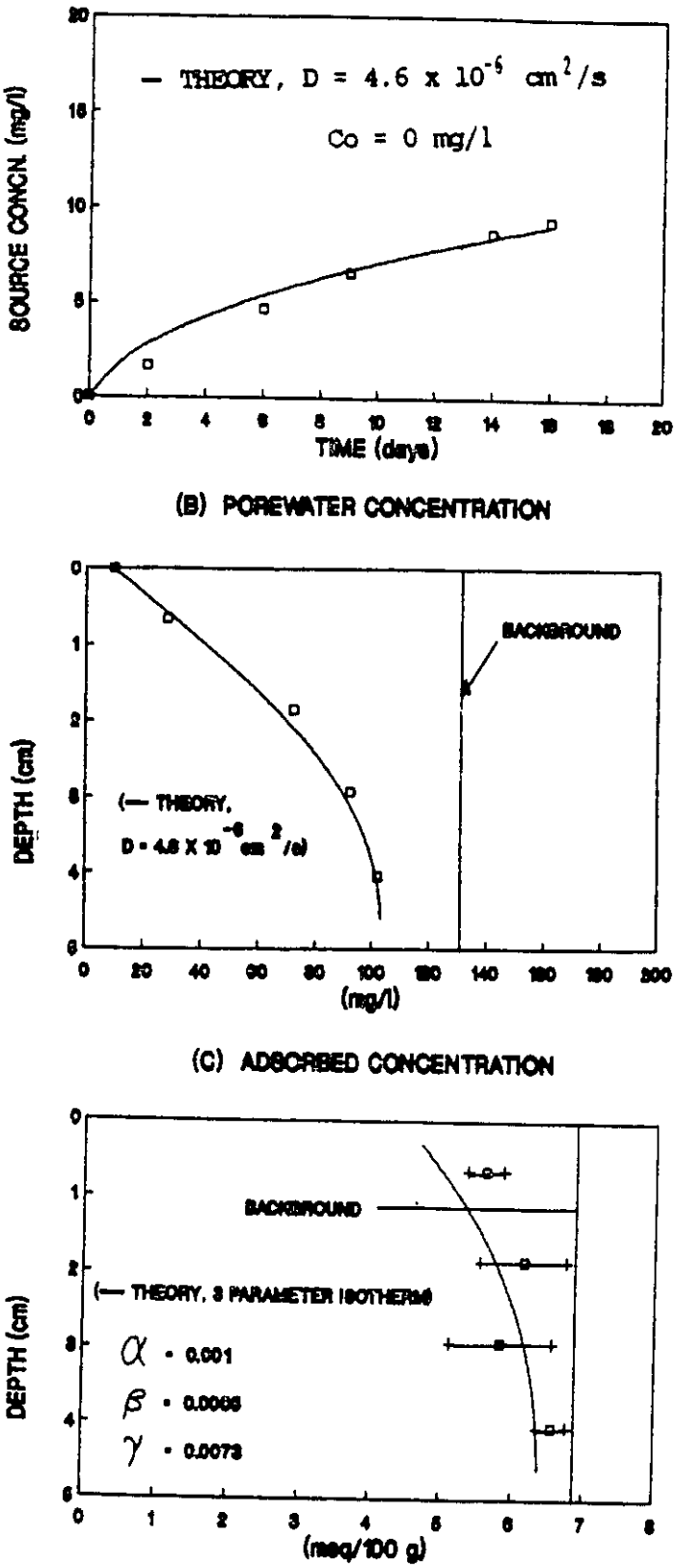

Figure 5.12d. Magnesium, test 3: (a) source concentration vs. time; porewater concentration vs. depth; (c) adsorbed concentration vs. depth.

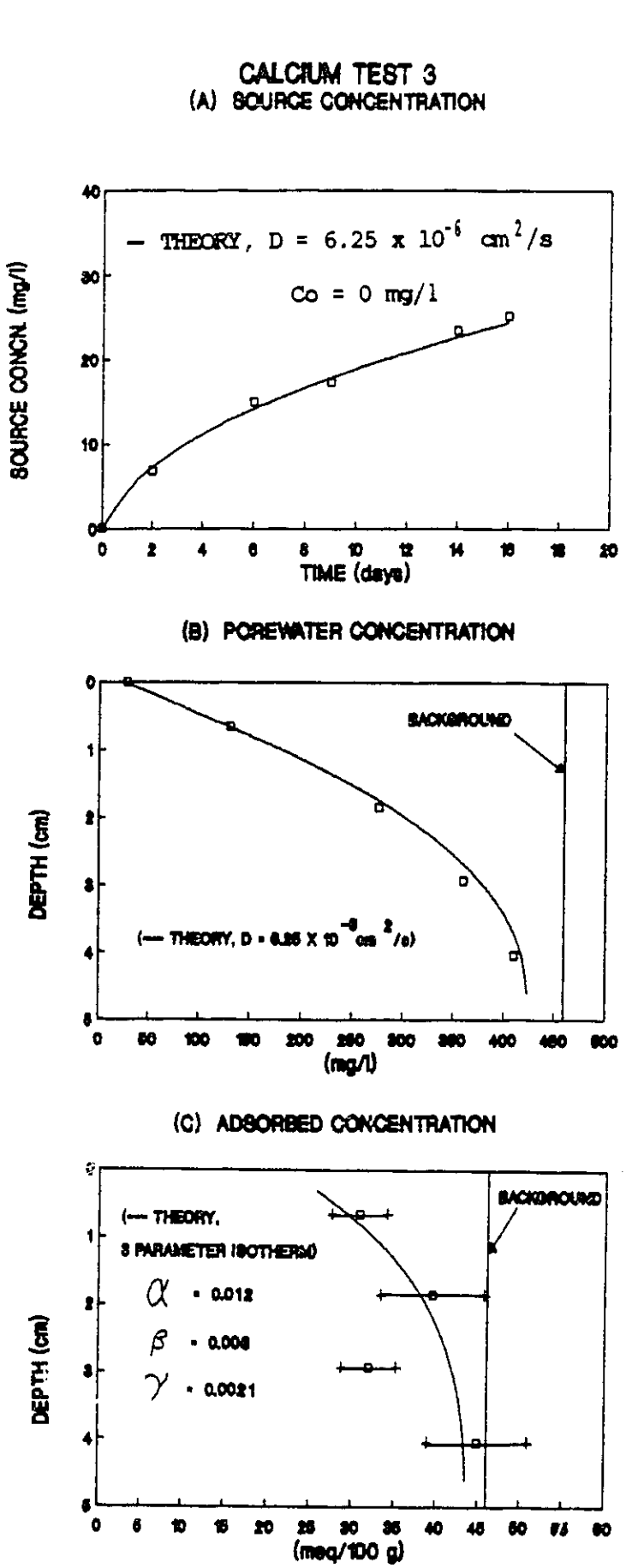

Figure 5.12e. Calcium, test 3: (a) source concentration vs. time; porewater concentration vs. depth; (c) adsorbed concentration vs. depth.

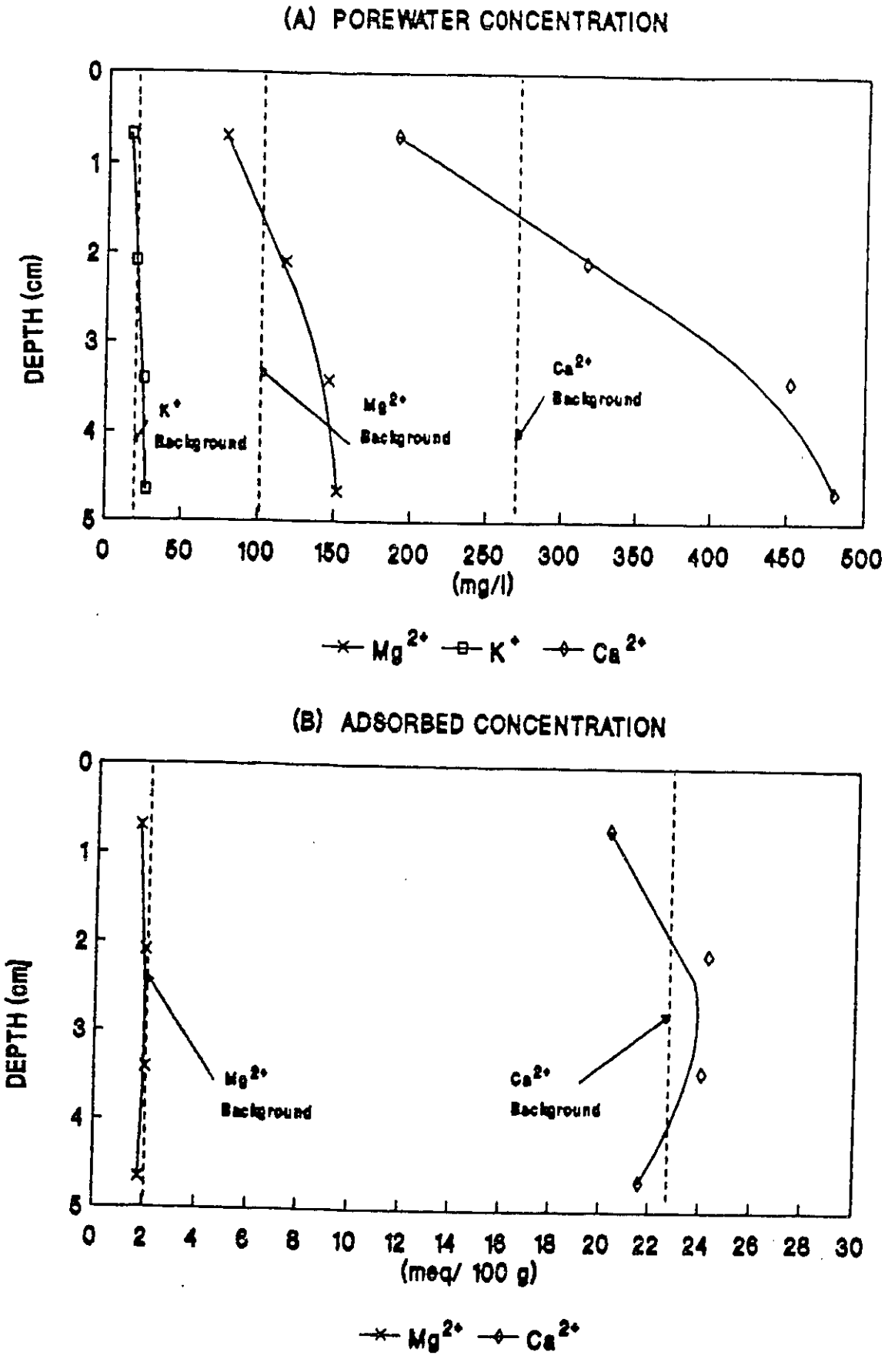

Figure 5.13. NaCl model, test 2: (a) porewater concentration vs. depth for K^{+}, Mg^{2+} and Ca^{2+}; (b) adsorbed concentration vs. depth for Mg^{2+} and Ca^{2+}.

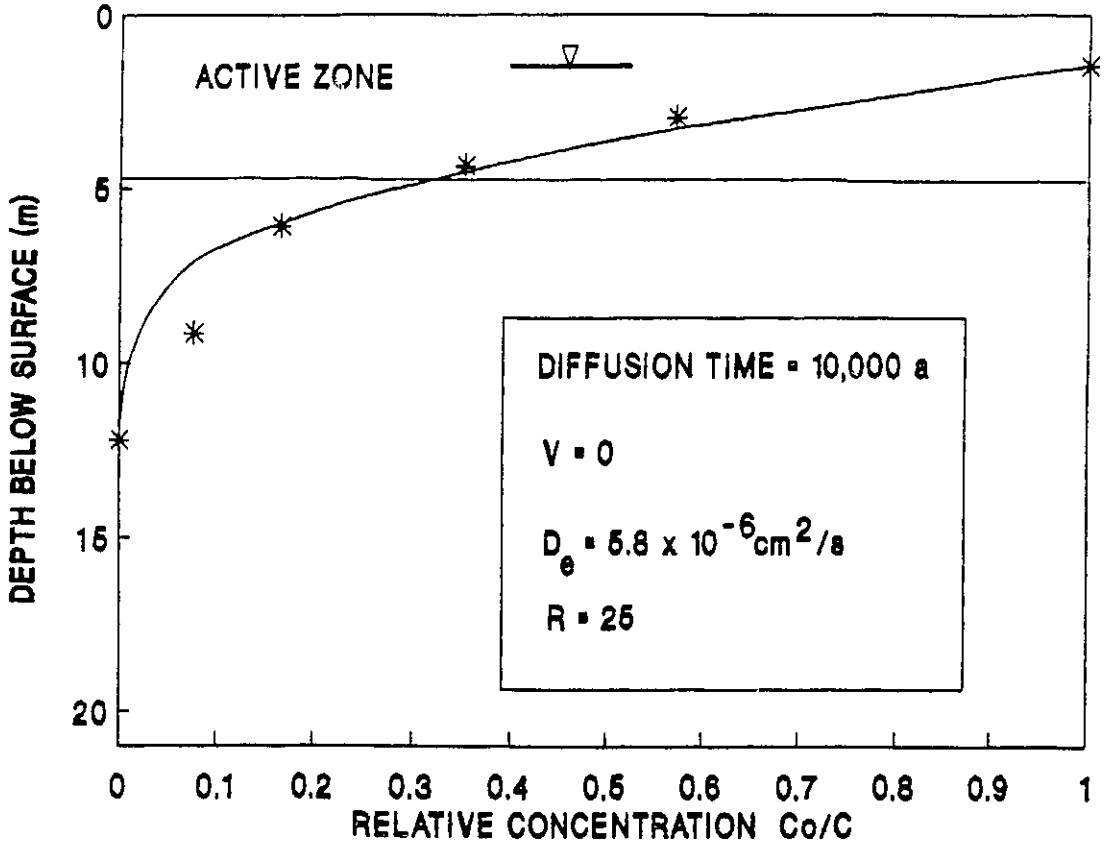

Figure 6.0. Simulation of calcium solute transport considering the silty clay deposit as a massive, unfractured porous medium at the NRC site.

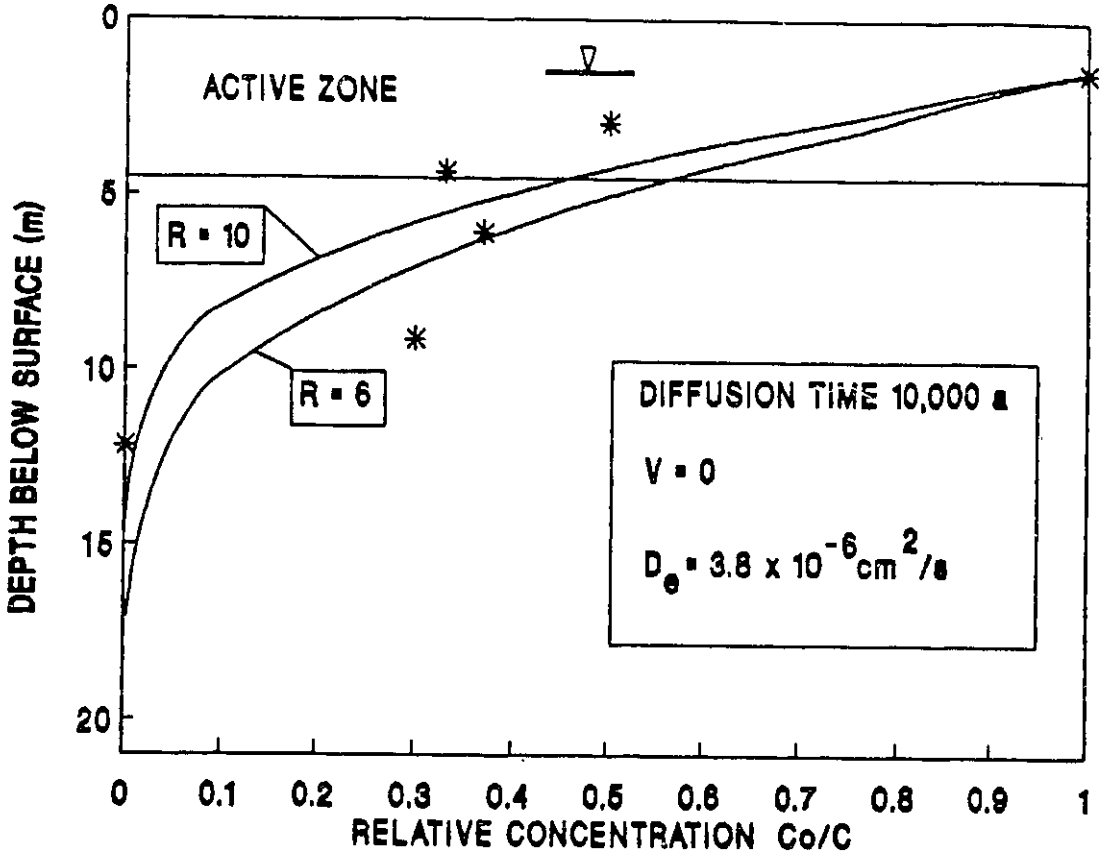

Figure 6.1. Simulations of magnesium solute transport considering the silty clay deposit as a massive, unfractured porous medium at the NRC site.

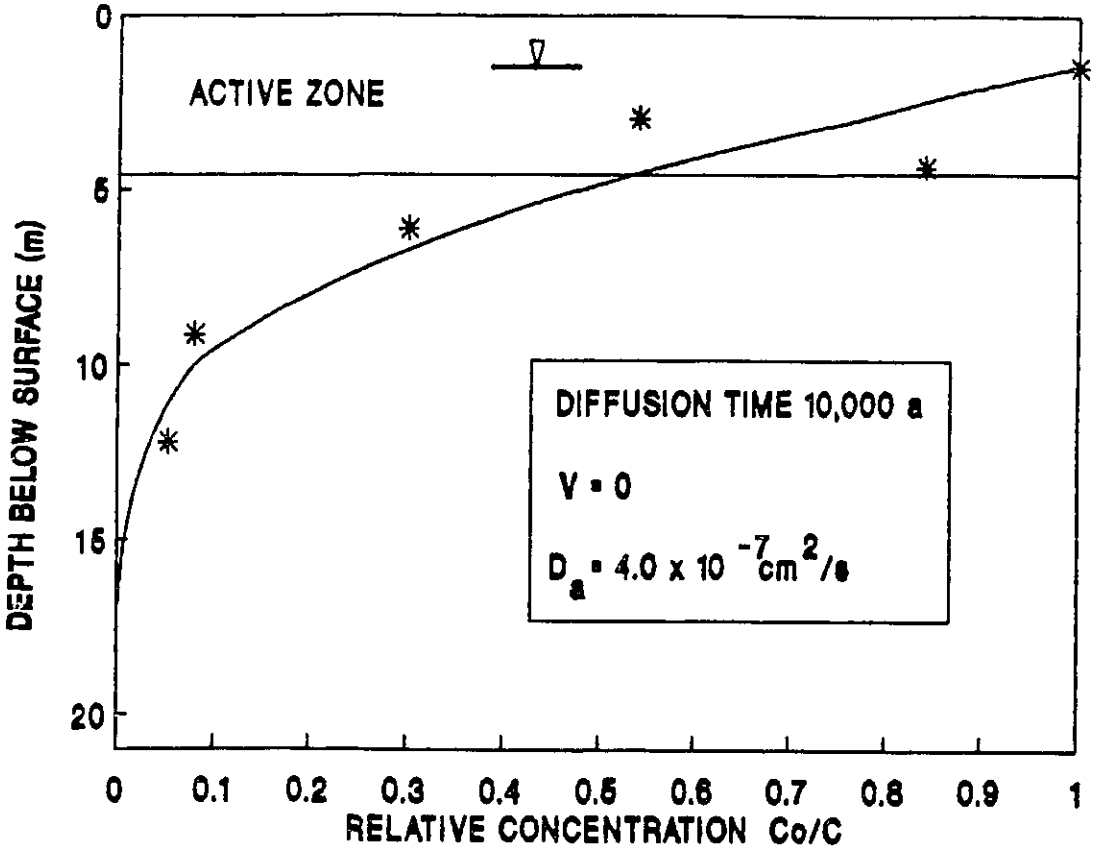

Figure 6.2. Simulation of sulfate solute transport considering the silty clay deposit as a massive, unfractured porous medium at the NRC site.

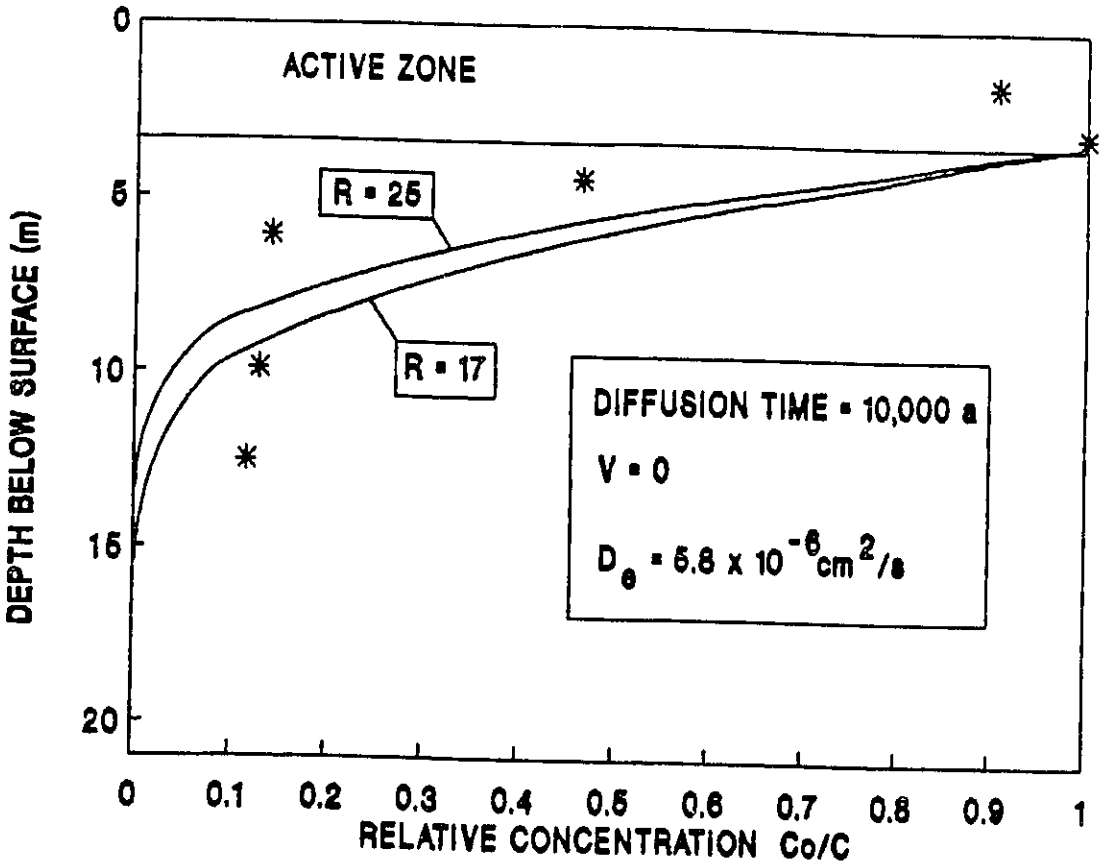

Figure 6.3. Simulations of calcium solute transport considering the silty clay deposit as a massive, unfractured porous medium at the Fallowfield site.

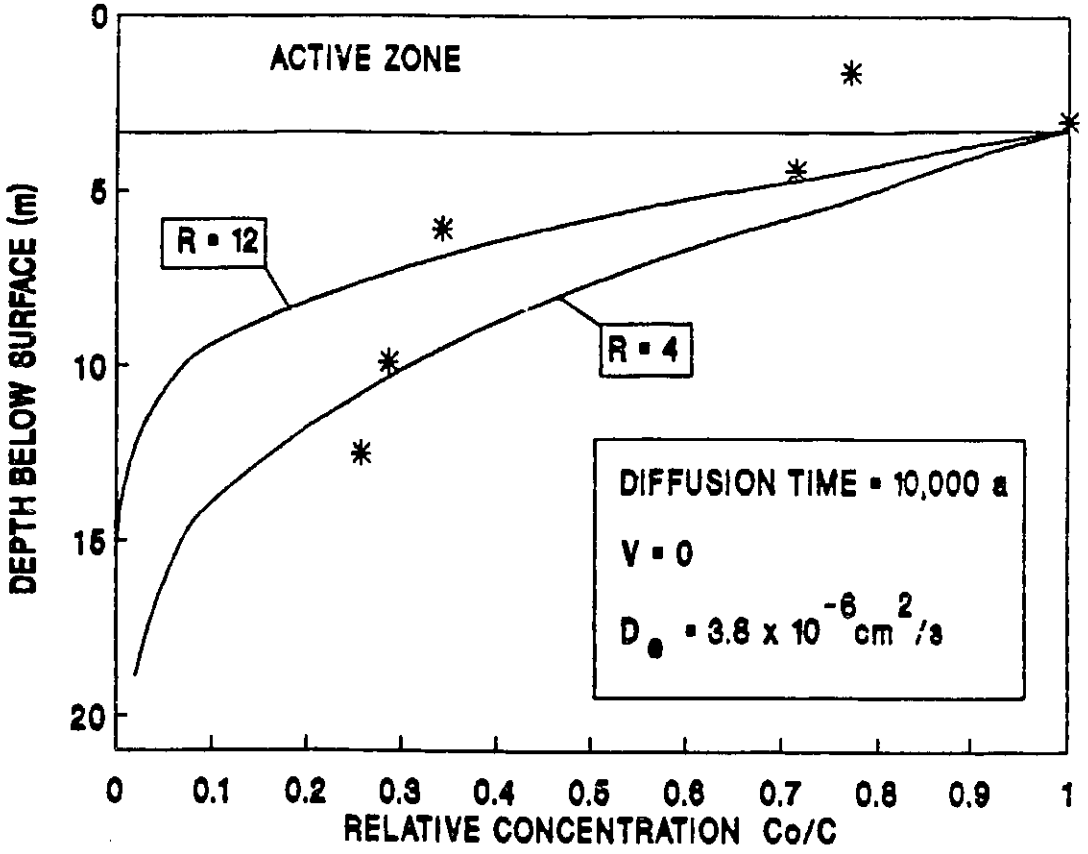

Figure 6.4. Simulations of magnesium solute transport considering the silty clay deposit as a massive, unfractured porous medium at the Fallowfield site.

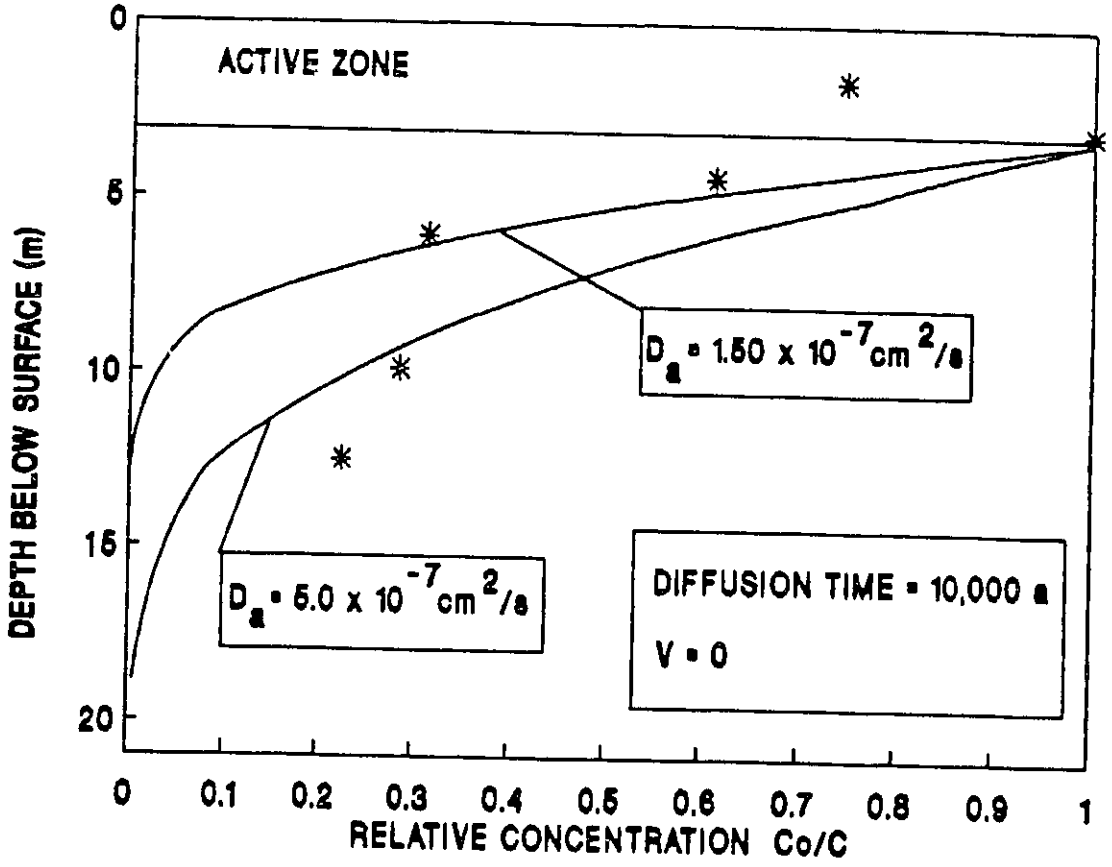

Figure 6.5. Simulations of sulfate solute transport considering the silty clay deposit as a massive, unfractured porous medium at the Fallowfield site.

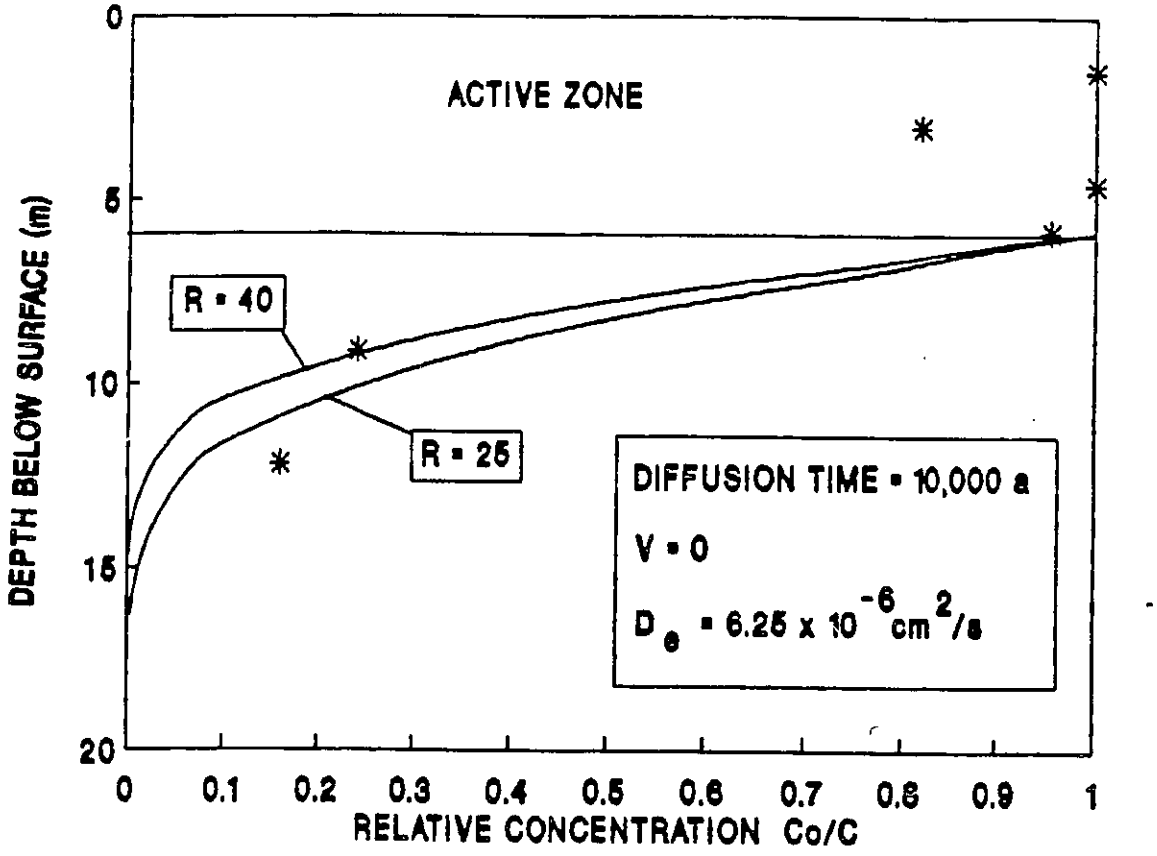

Figure 6.6. Simulations of calcium solute transport considering the silty clay deposit as a massive, unfractured porous medium at the Renfrew site.

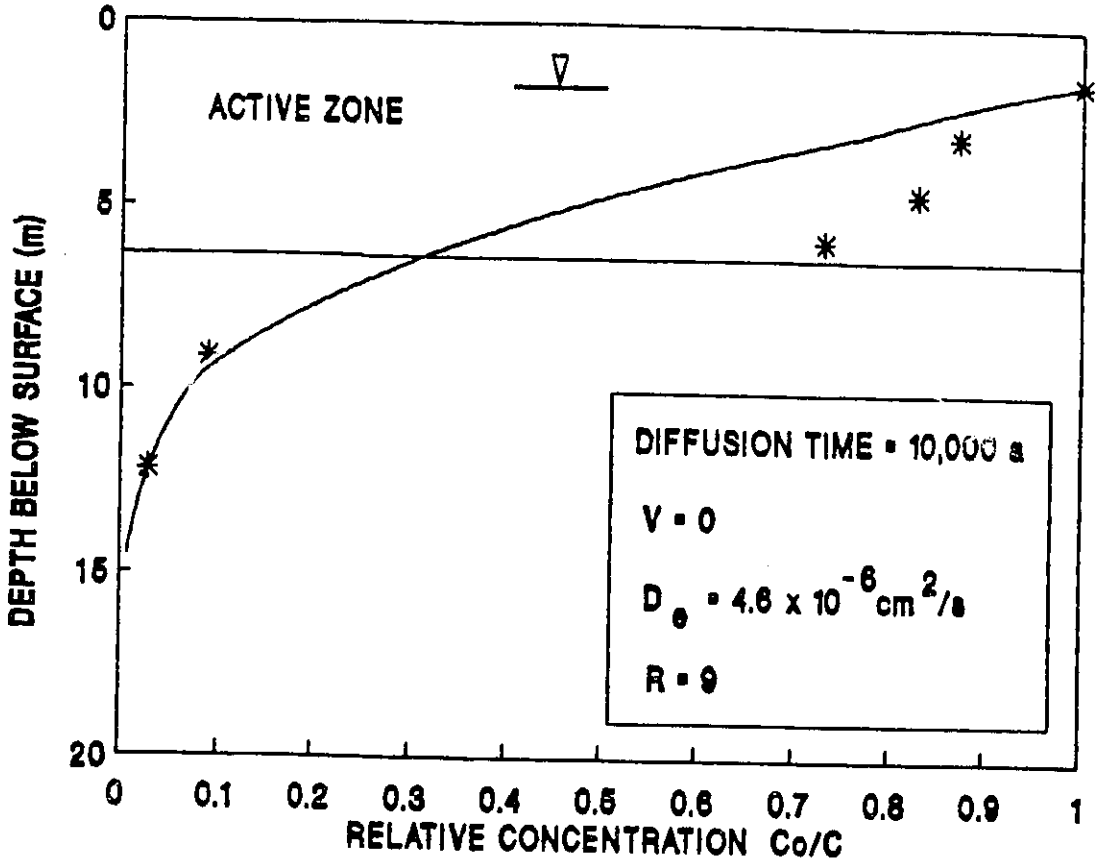

Figure 6.7. Simulation of magnesium solute transport considering the silty clay deposit as a massive, unfractured porous medium at the Renfrew site.

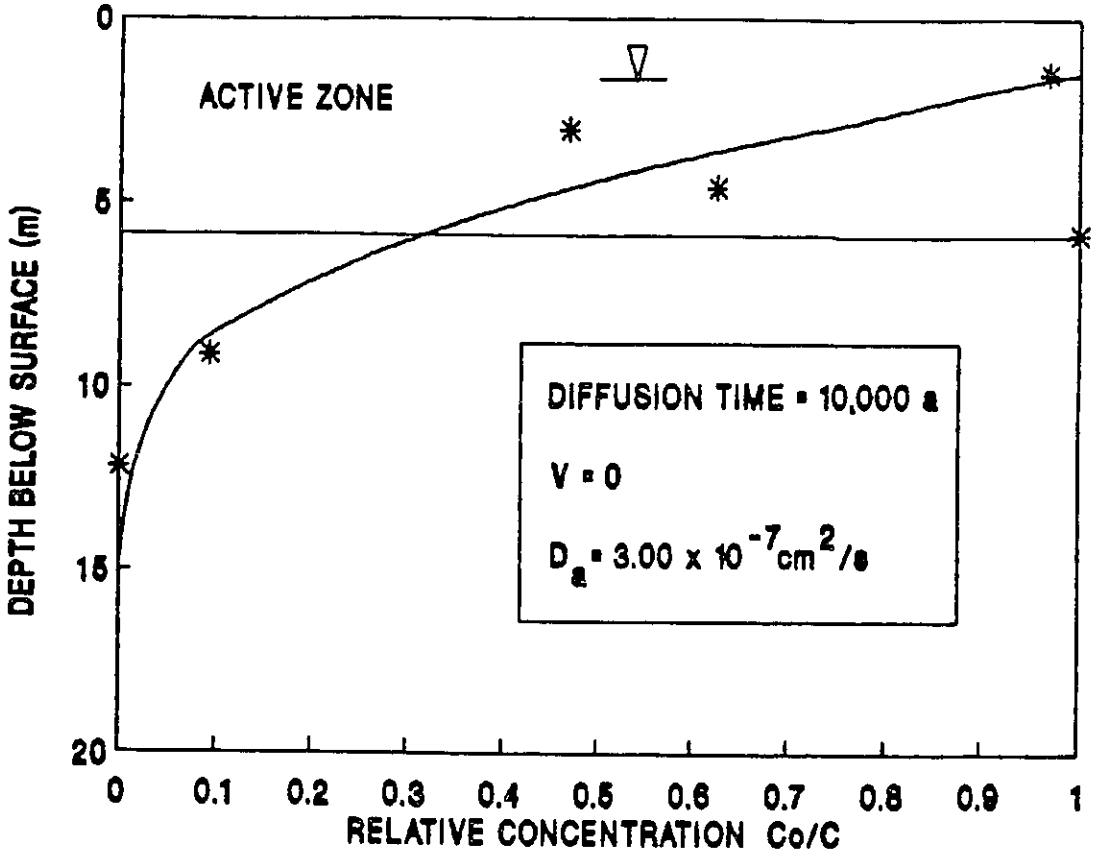

Figure 6.8. Simulation of sulfate solute transport considering the silty clay deposit as a massive, unfractured porous medium at the Renfrew site.

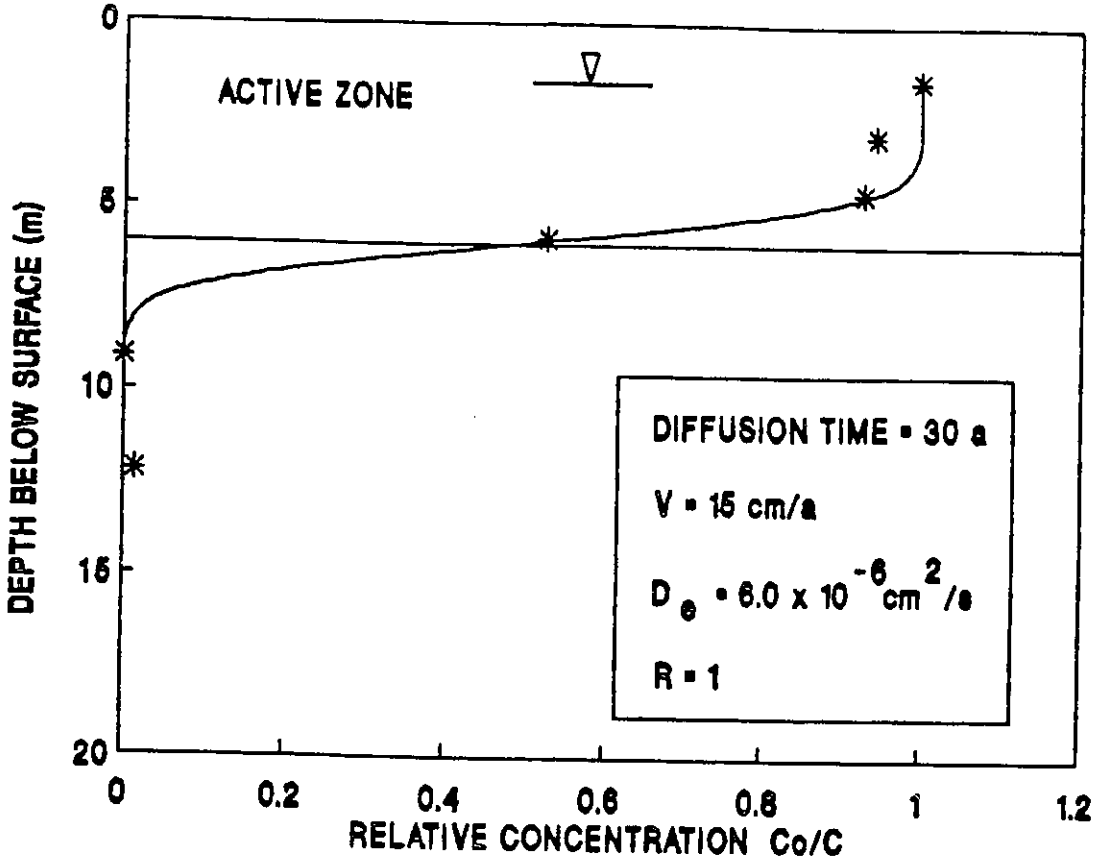

Figure 6.9. Simulation of chloride solute transport for 30 years considering the silty clay deposit as a massive, unfractured porous medium at the Renfrew site.

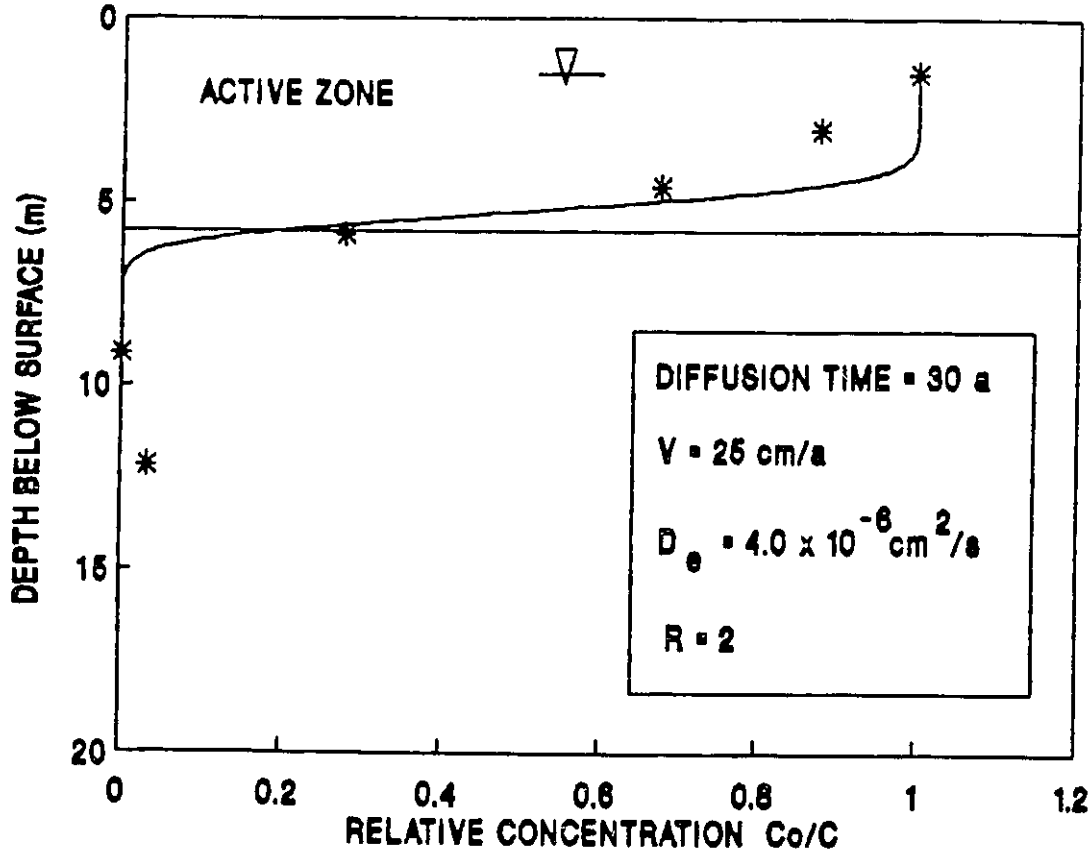

Figure 6.10. Simulation of sodium solute transport for 30 years considering the silty clay deposit as a massive, unfractured porous medium at the Renfrew site.

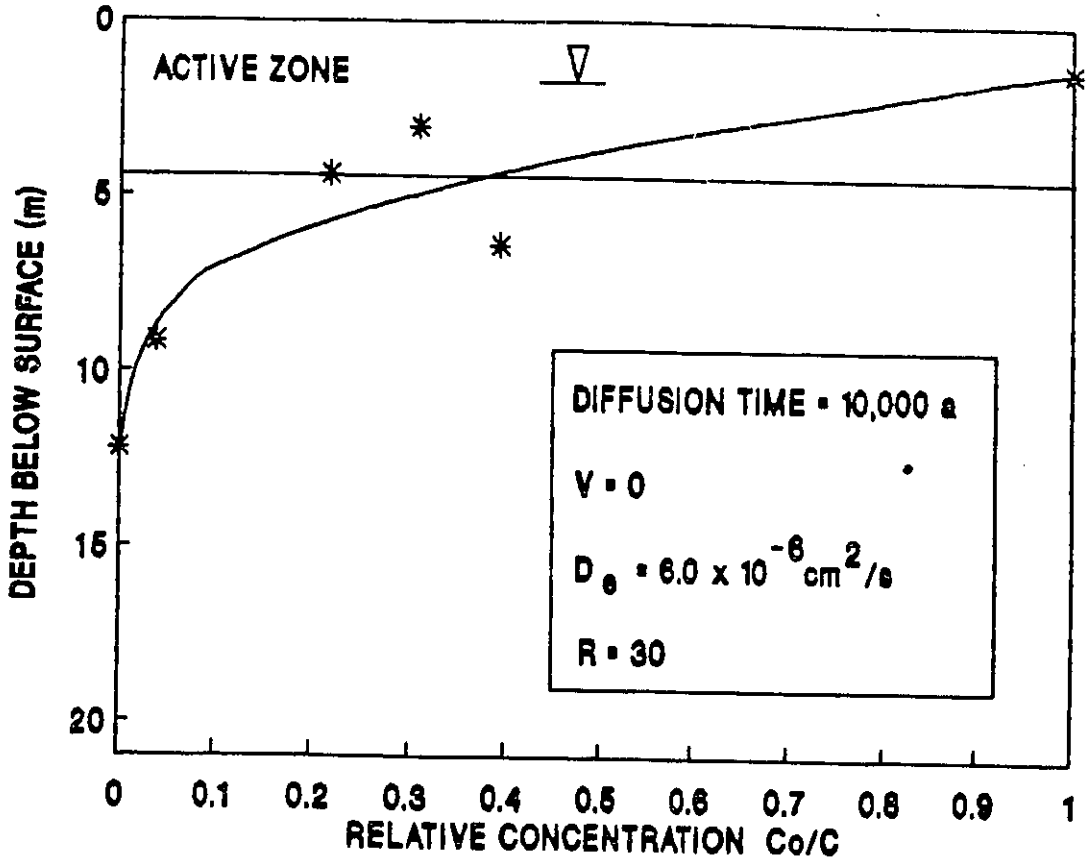

Figure 6.11. Simulations of calcium solute transport considering the silty clay deposit as a massive, unfractured porous medium at the Casselman site.

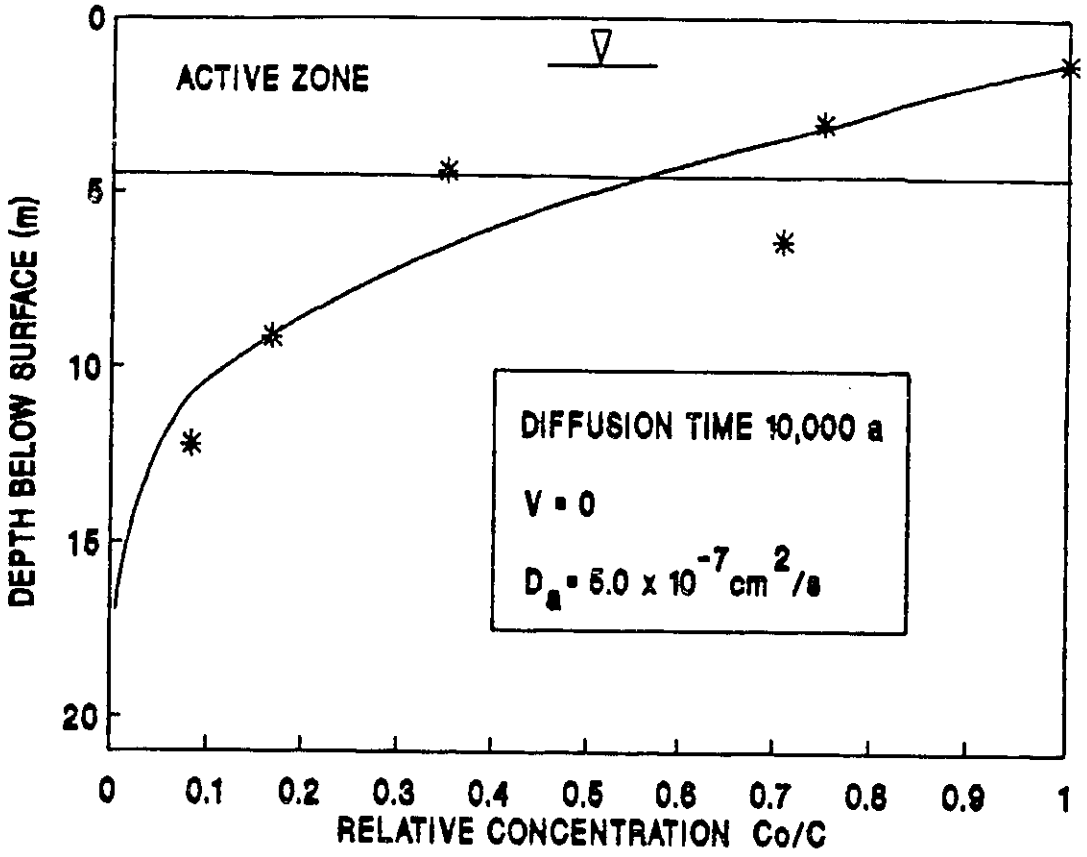

Figure 6.12. Simulation of sulfate solute transport considering the silty clay deposit as a massive, unfractured porous medium at the Casselman site.

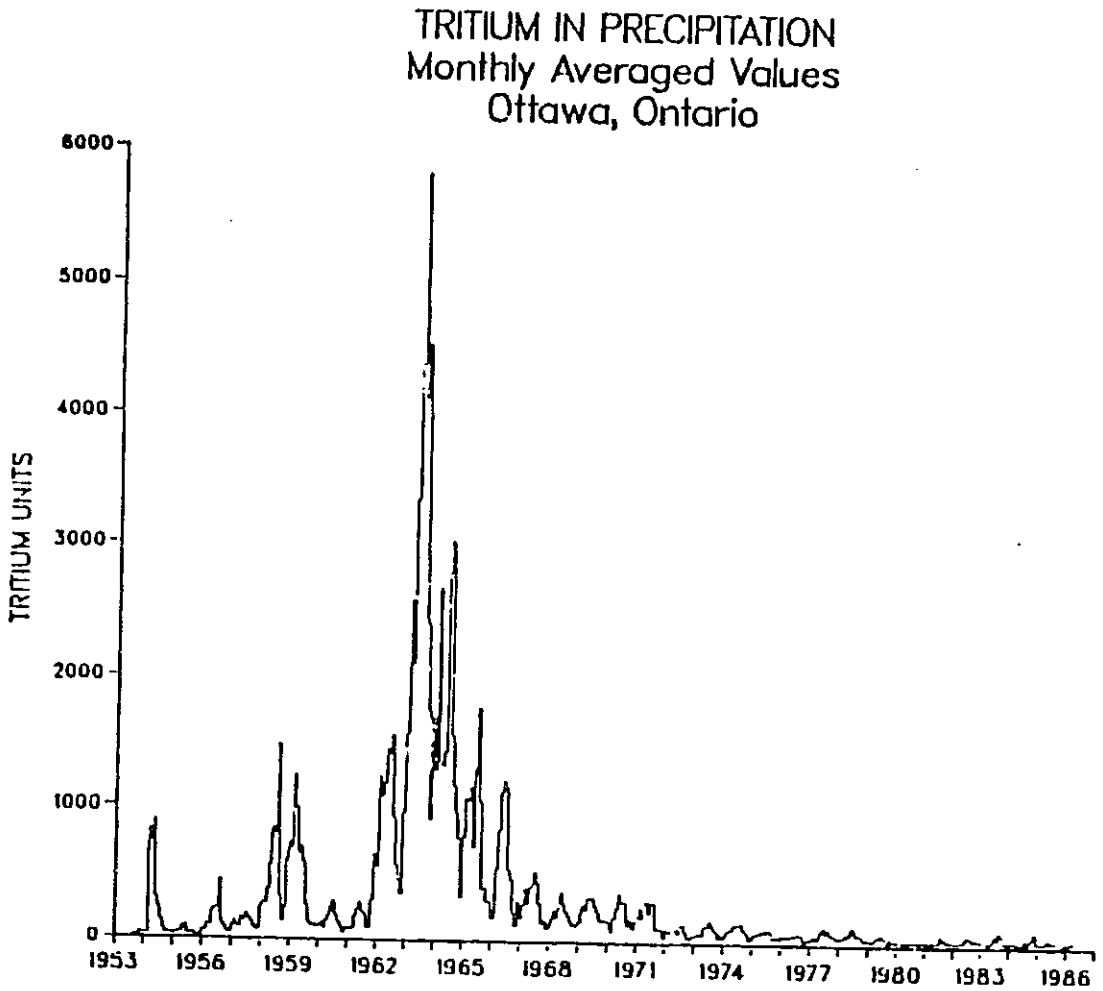

Figure 6.13. Monthly average tritium content of meteoric precipitation for Ottawa, Ontario from 1952 to 1986 (IAEA, 1986).

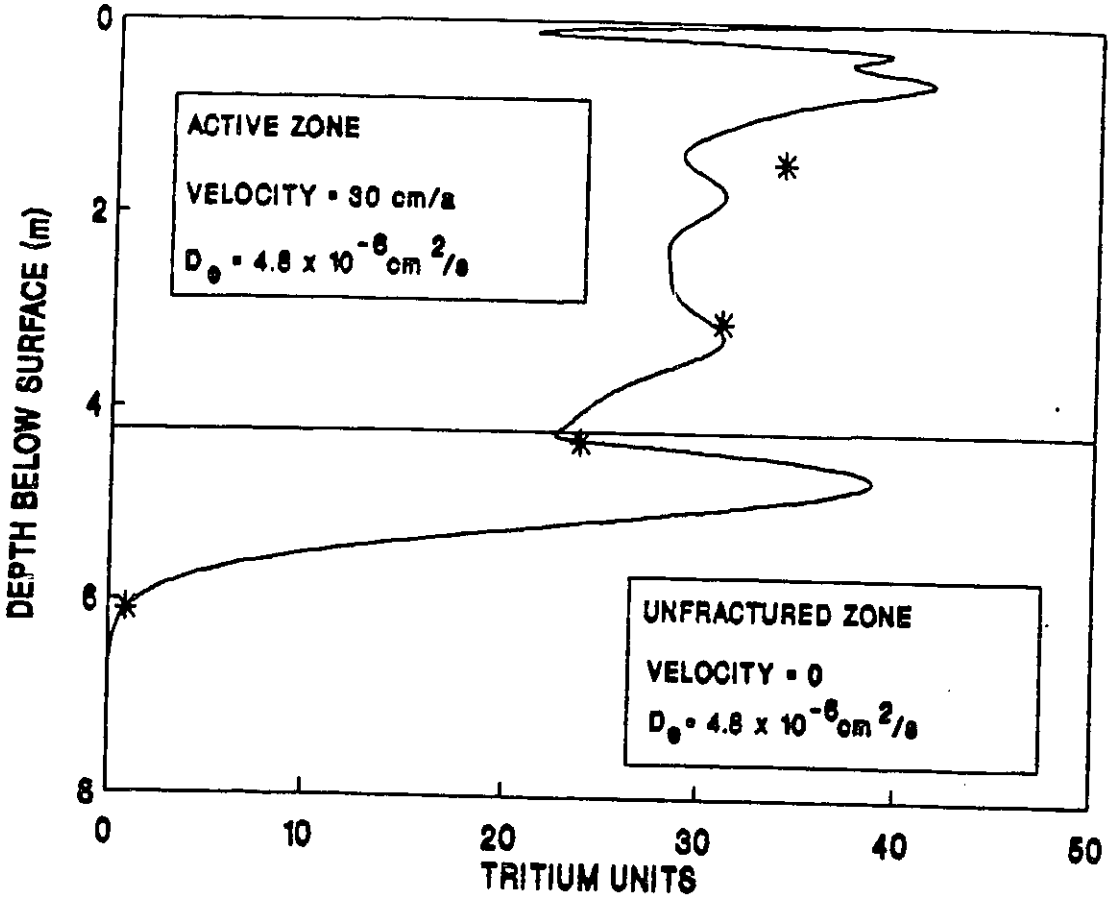

Figure 6.14. Simulation of tritium transport profile at the NRC site, considering the silty clay deposit as a massive, unfractured porous medium with the tritium input function at the ground surface.

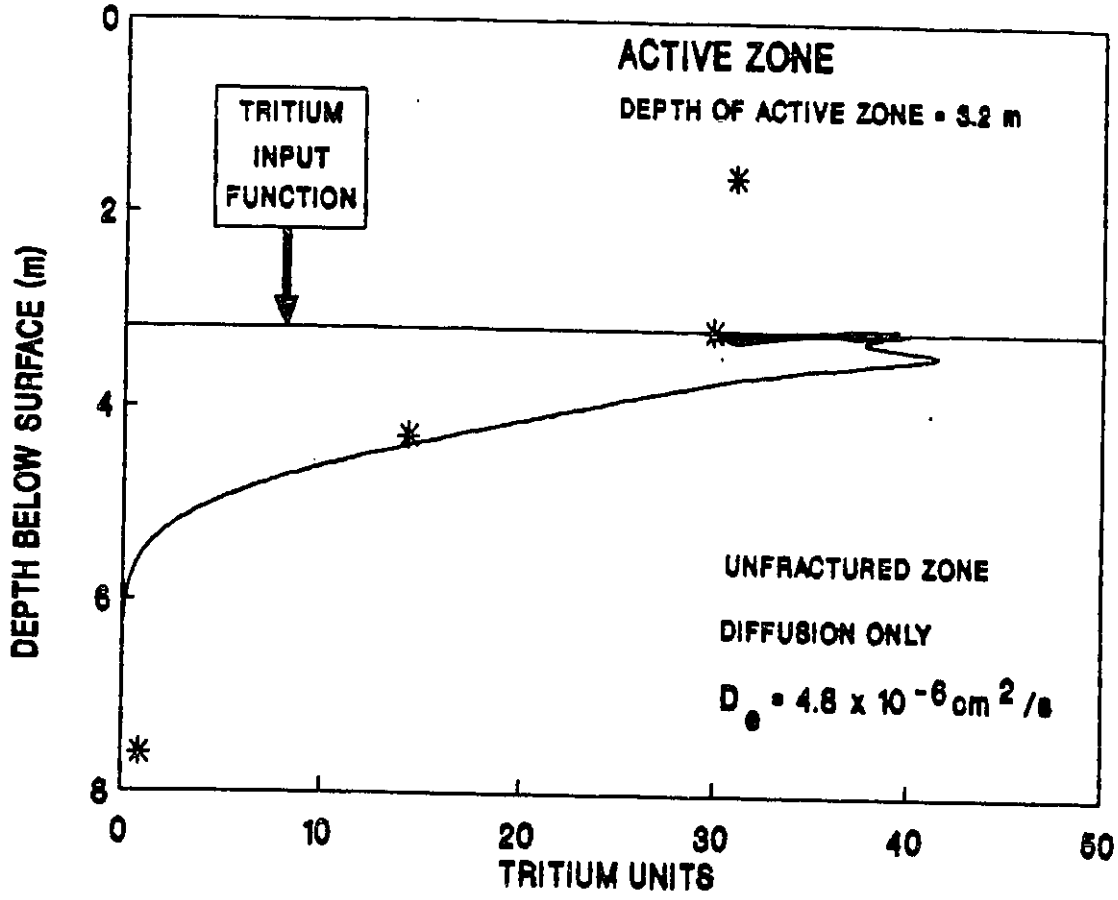

Figure 6.15. Simulation of tritium transport profile at the Fallowfield site, considering the silty clay deposit as a massive, unfractured porous medium with the tritium input function placed at a depth of 3.2 m.

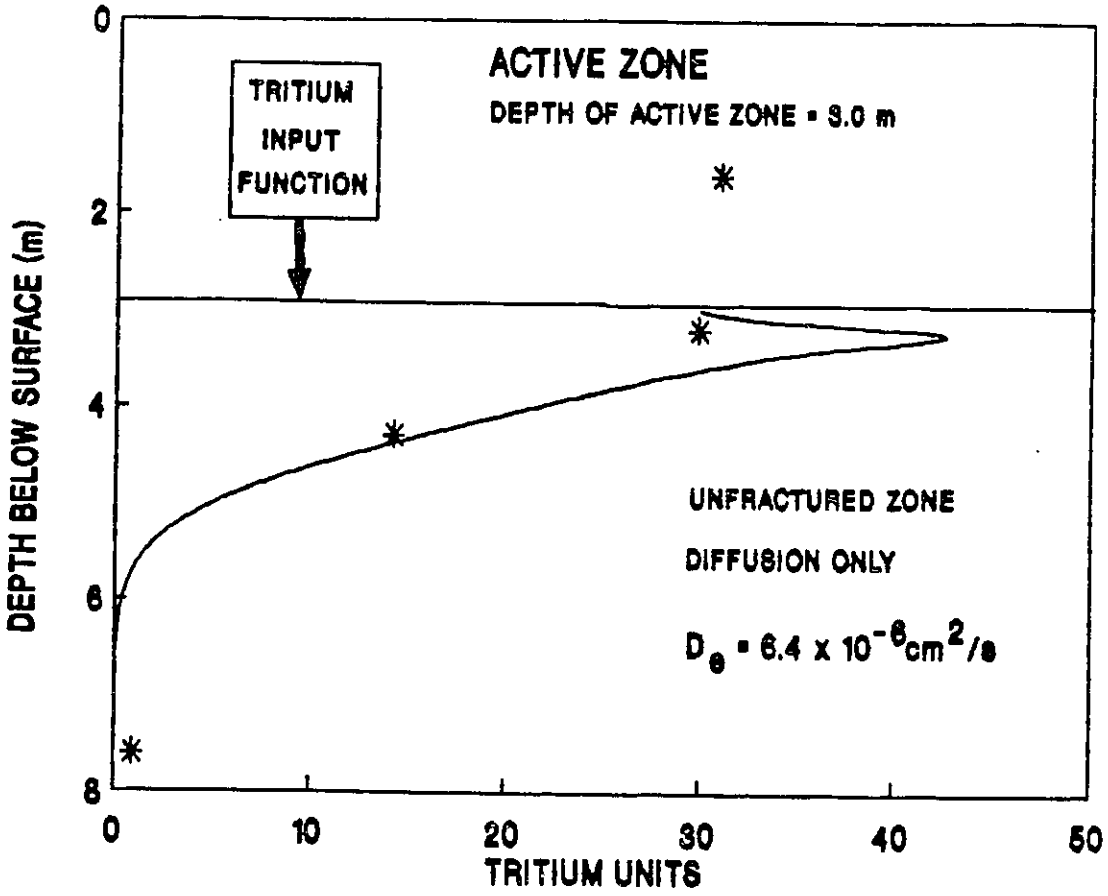

Figure 6.16. Simulation of tritium transport profile at the Fallowfield site, considering the silty clay deposit as a massive, unfractured porous medium with the tritium input function placed at a depth of 3.0 m.

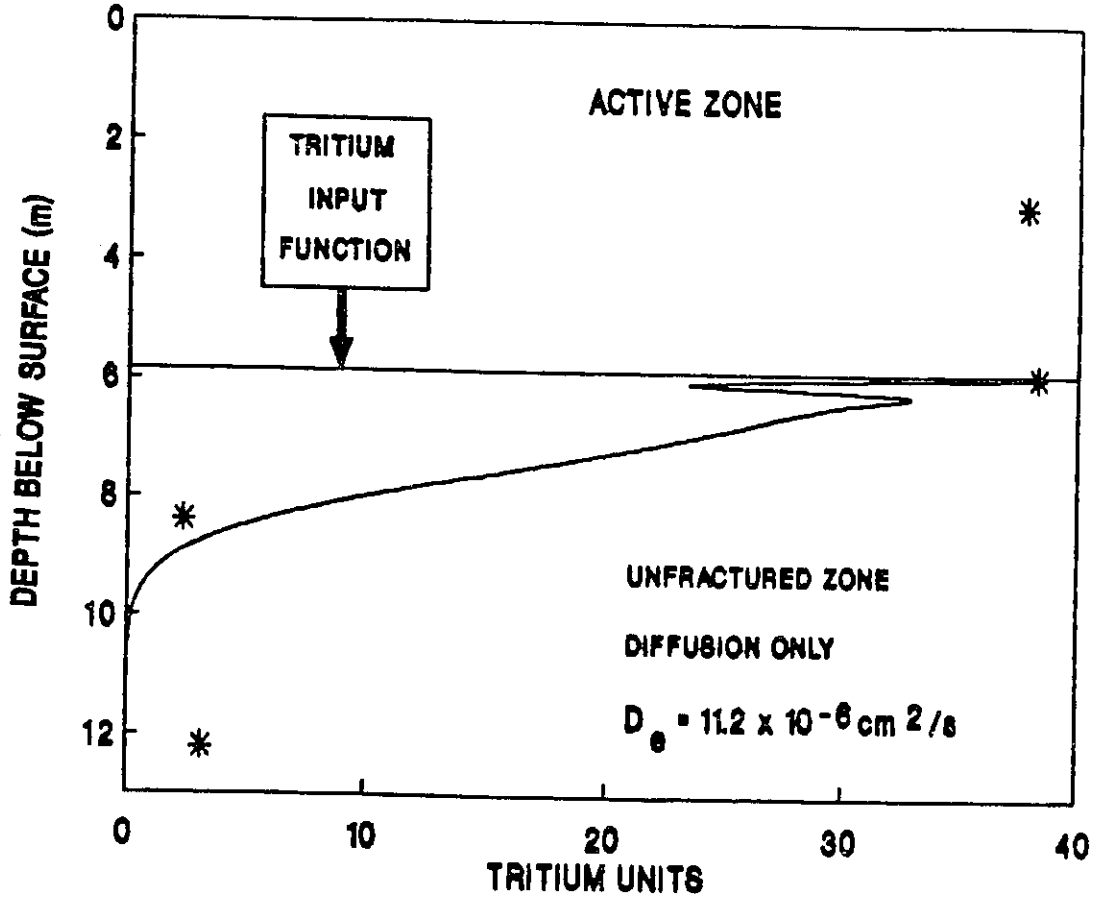

Figure 6.17. Simulation of tritium transport profile at the Renfrew site, considering the silty clay deposit as a massive, unfractured porous medium with an average groundwater velocity of 0 cm/a and the tritium input function placed at a depth of 5.9 m.

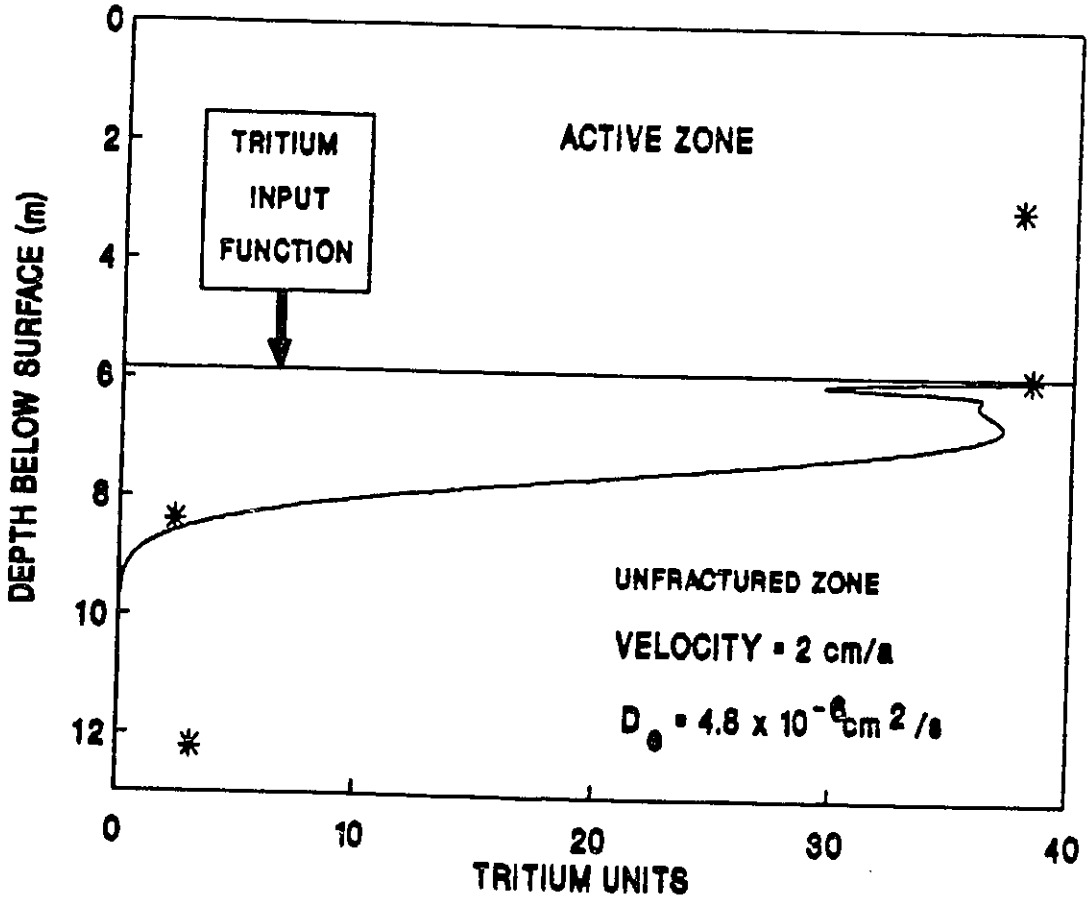

Figure 6.18. Simulation of tritium transport profile at the Renfrew site, considering the silty clay deposit as a massive, unfractured porous medium with an average groundwater velocity of 2.0 cm/a and the tritium input function placed at a depth of 5.9 m.

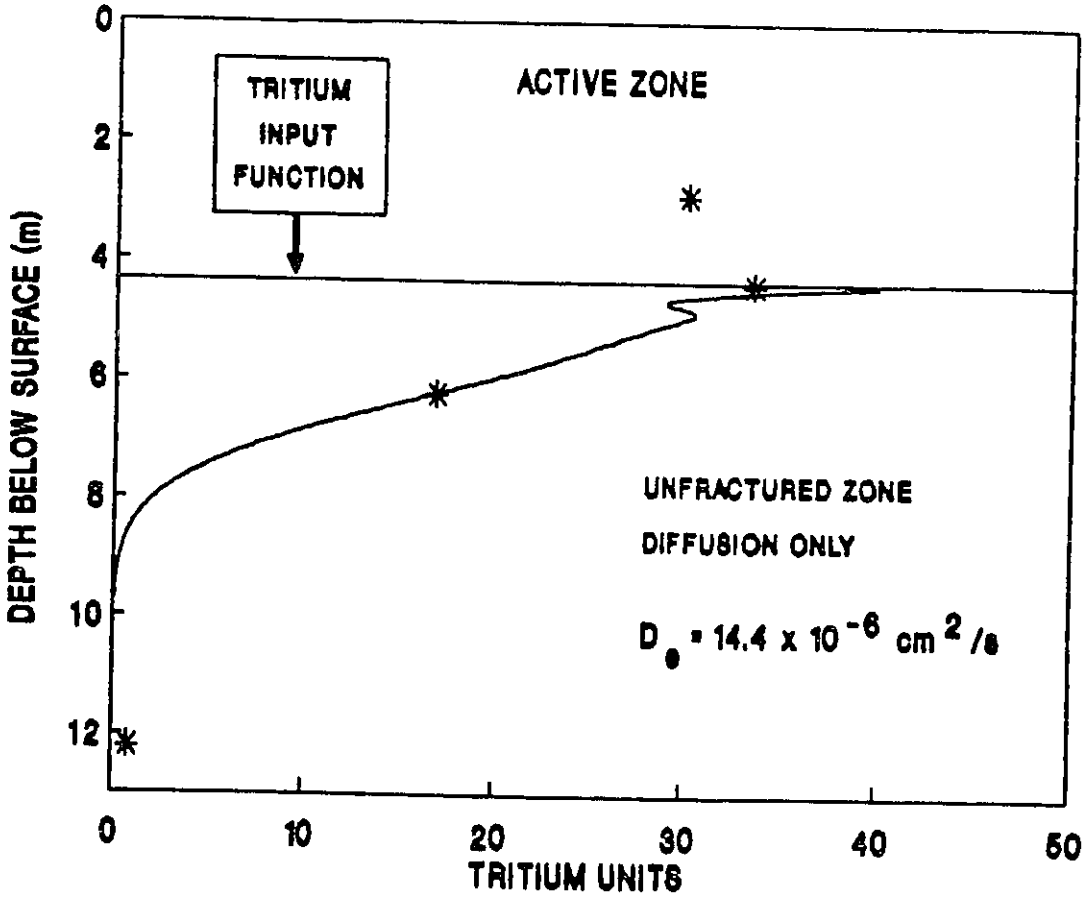

Figure 6.19. Simulation of tritium transport profile at the Casselman site, considering the silty clay deposit as a massive, unfractured porous medium with an average groundwater velocity of 0 cm/a and the tritium input function placed at a depth of 4.40 m.

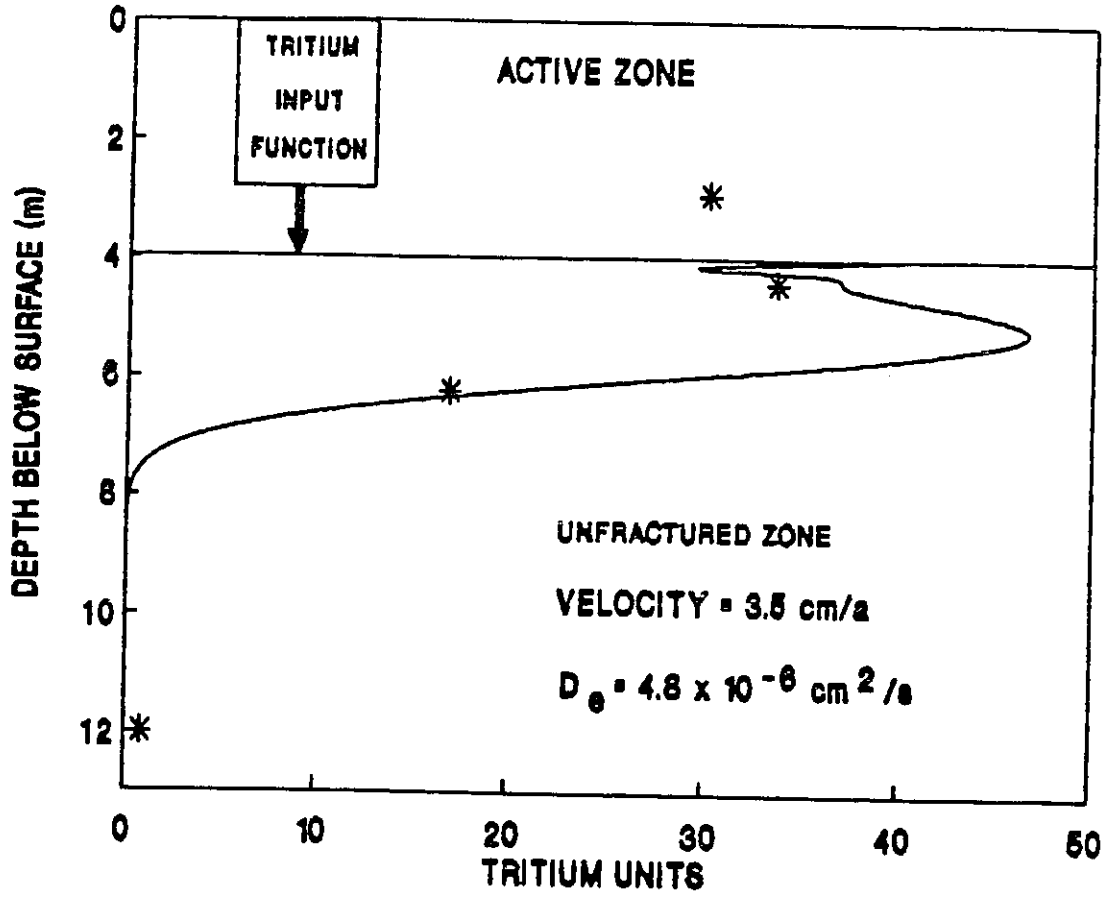

Figure 6.20. Simulation of tritium transport profile at the Casselman site, considering the silty clay deposit as a massive, unfractured porous medium with an average groundwater velocity of 3.5 cm/a and the tritium input function placed at a depth of 4.0 m.

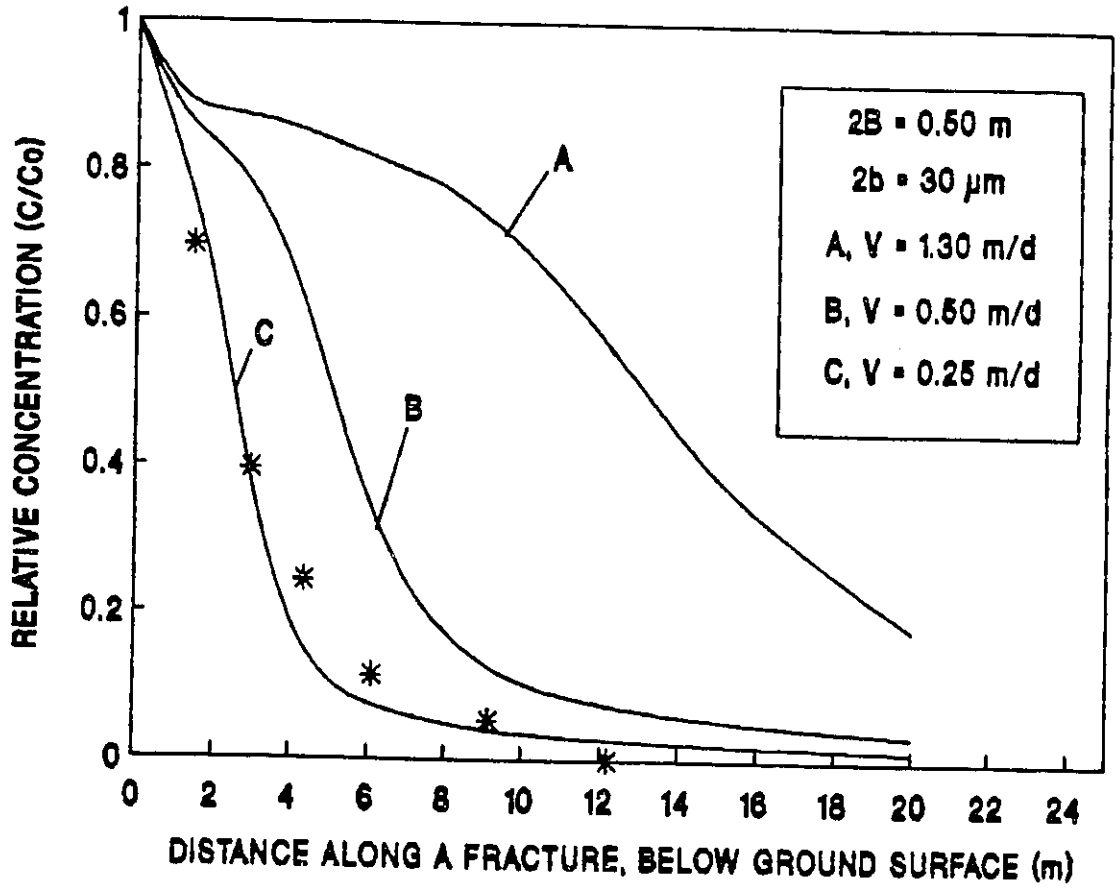

Figure 6.21. Simulation of calcium transport profiles at the NRC site, considering the silty clay deposit as a continuously fractured porous medium, with different fracture flow velocities.

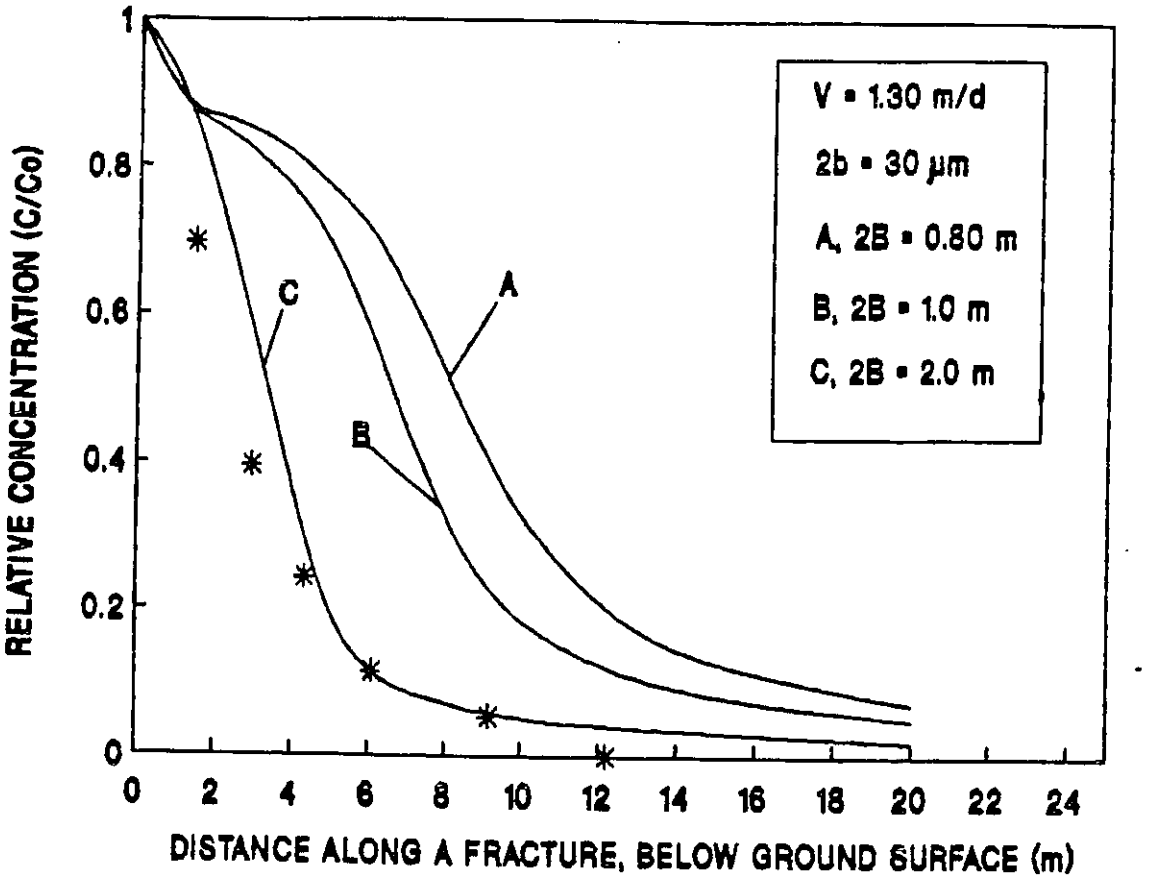

Figure 6.22. Simulation of calcium transport profiles at the NRC site, considering the silty clay deposit as a continuously fractured porous medium, with different fracture spacings.

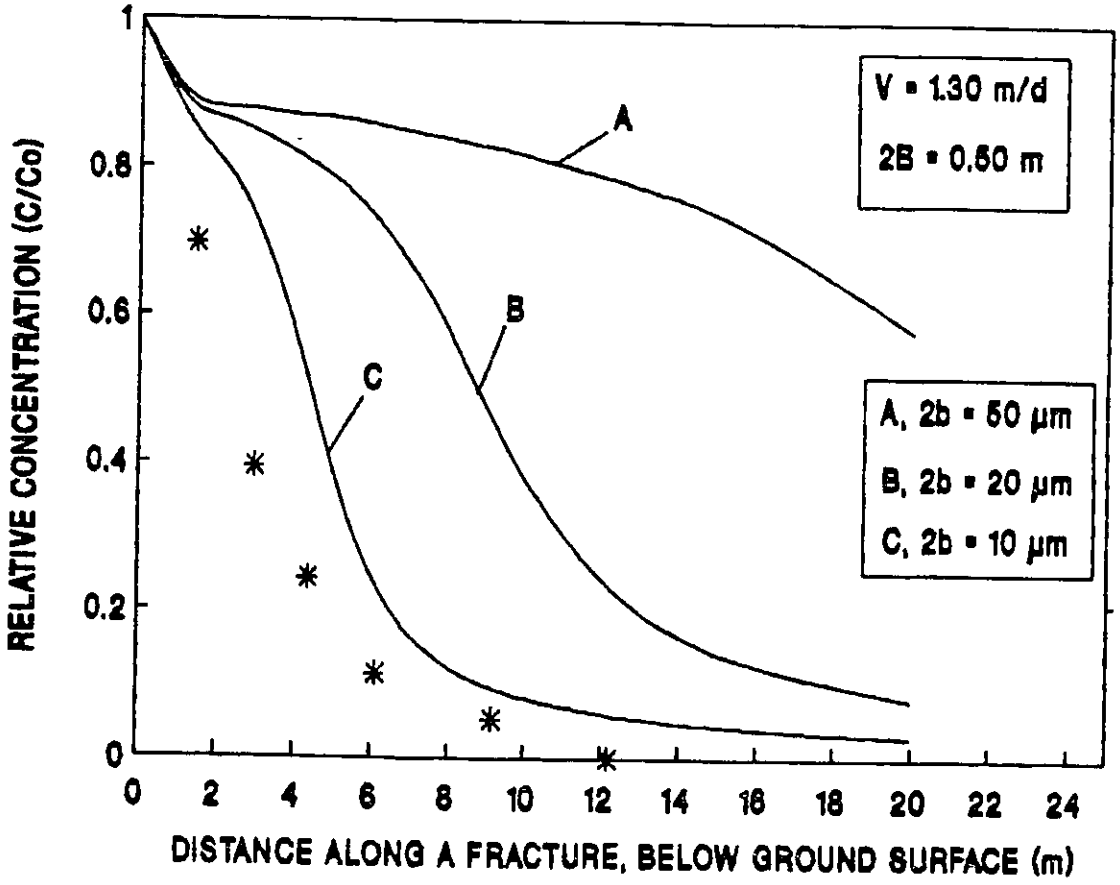

Figure 6.23. Simulation of calcium transport profiles at the NRC site, considering the silty clay deposit as a continuously fractured porous medium, with different fracture apertures.

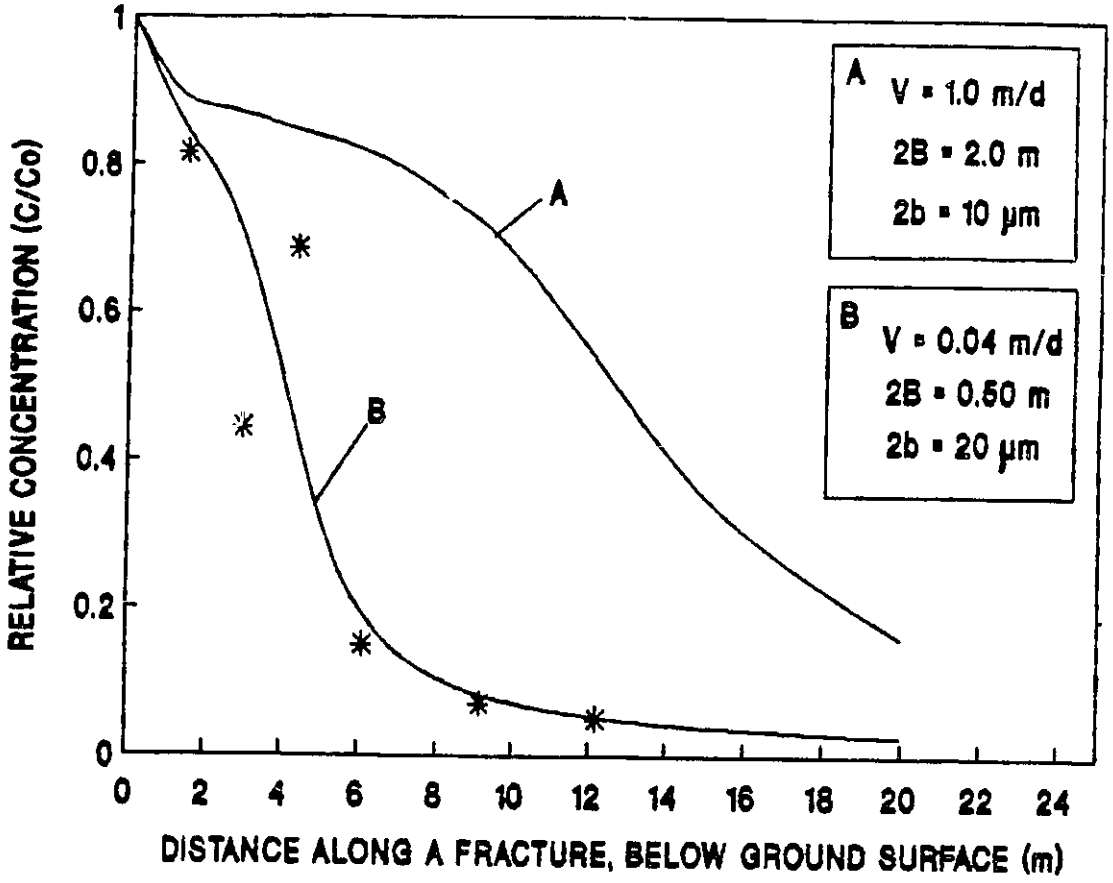

Figure 6.24. Simulation of sulfate transport profiles at the NRC site, considering the silty clay deposit as a continuously fractured porous medium.

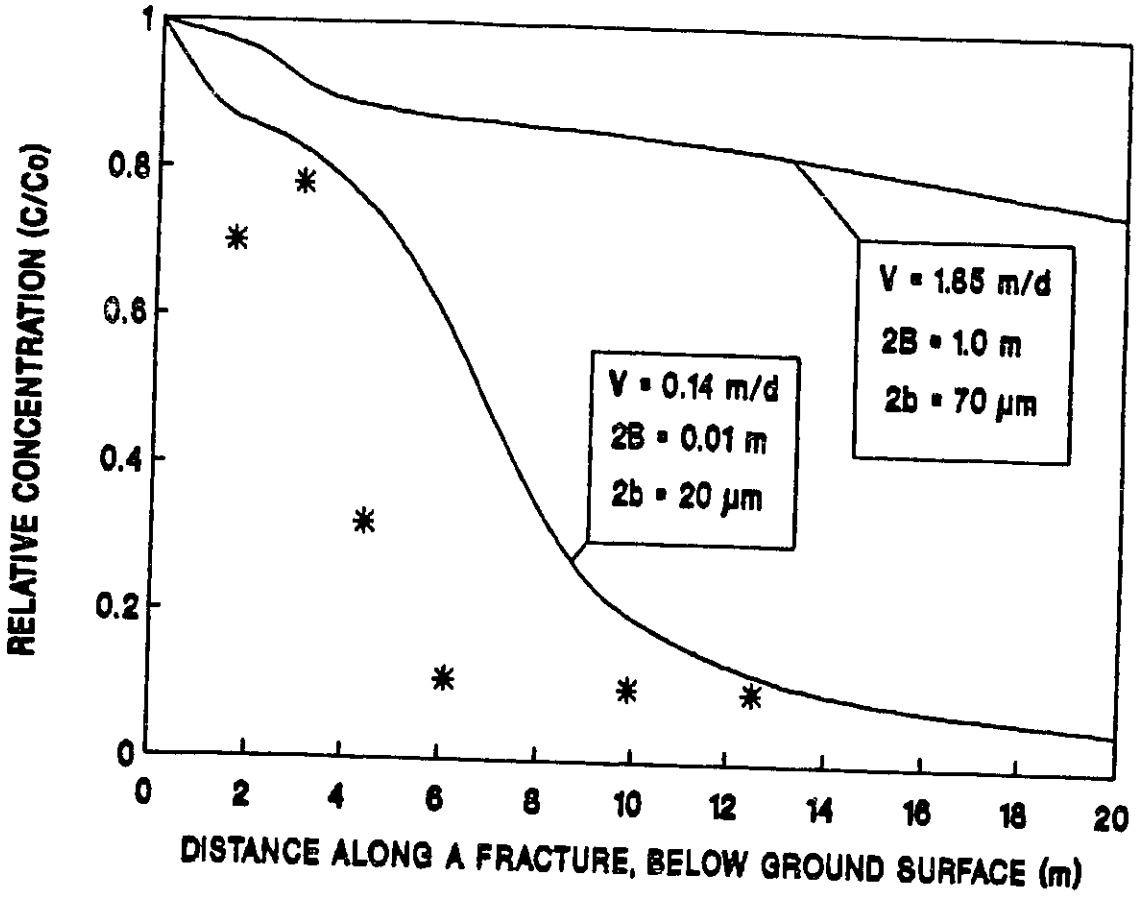

Figure 6.25. Simulation of calcium transport profiles at the Fallowfield site, considering the silty clay deposit as a continuously fractured porous medium.

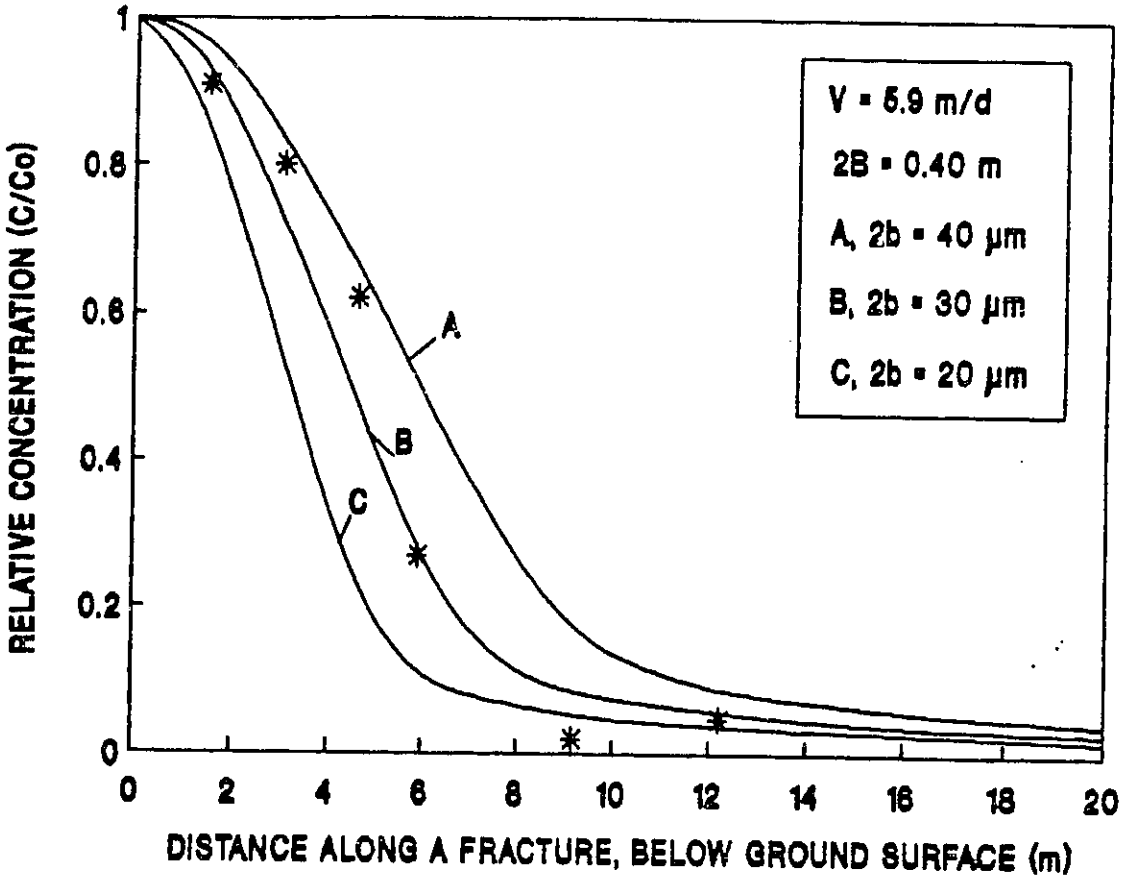

Figure 6.26. Simulation of sodium transport profiles at the Renfrew site, considering the silty clay deposit as a continuously fractured porous medium, for a time period of 30 years.

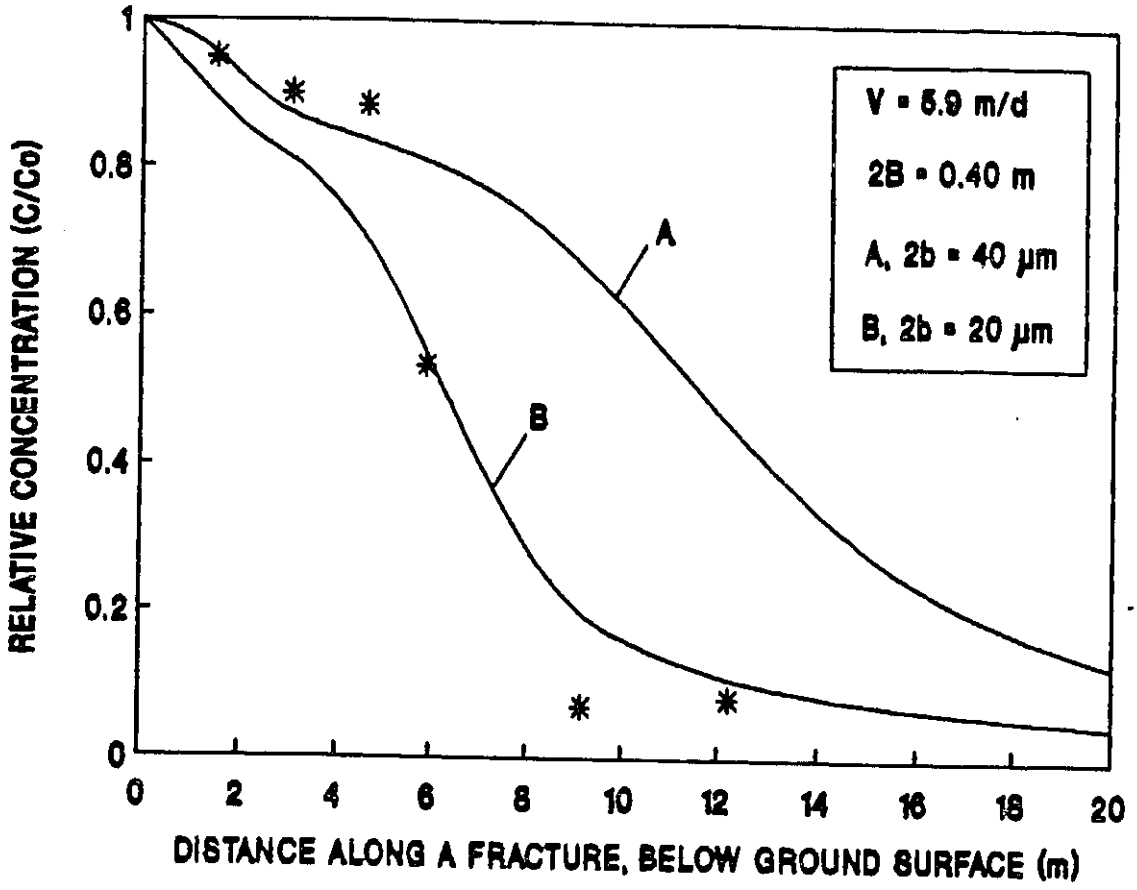

Figure 6.27. Simulation of chloride transport profiles at the Renfrew site, considering the silty clay deposit as a continuously fractured porous medium, for a time period of 30 years.

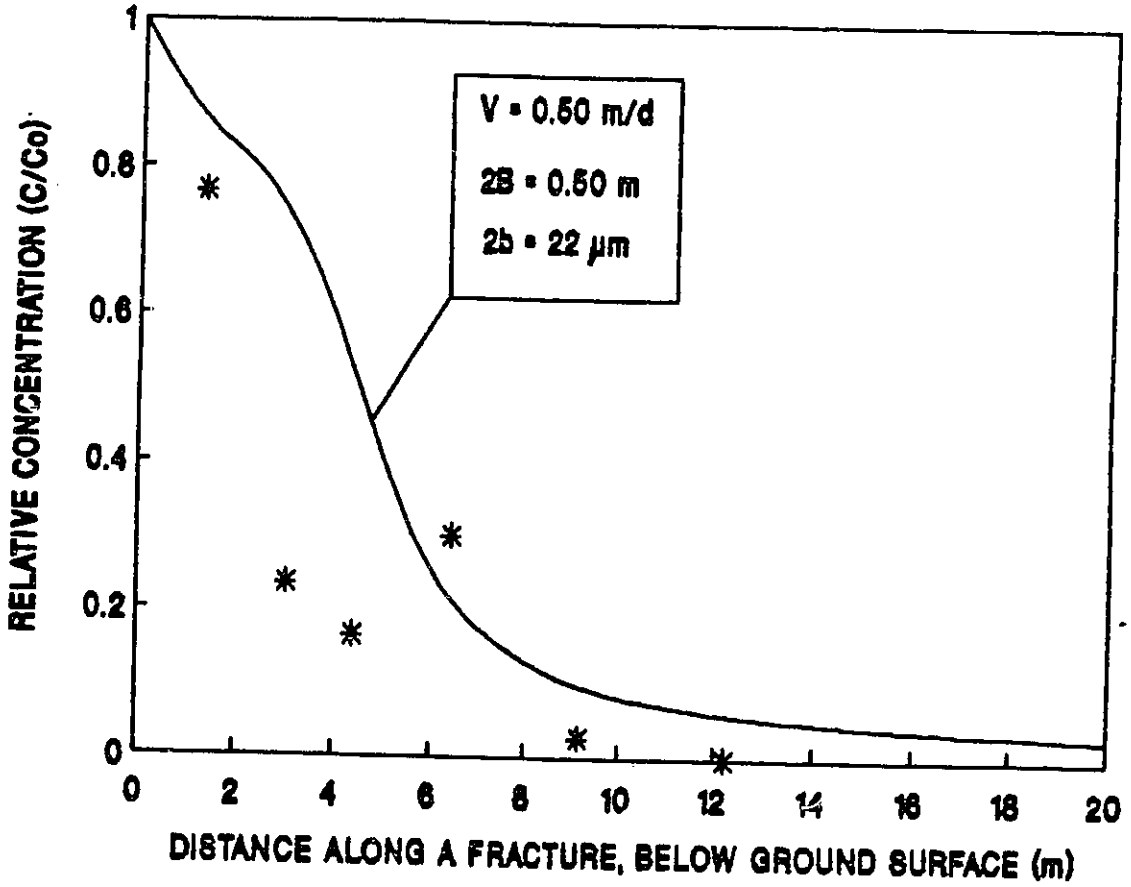

Figure 6.28. Simulation of calcium transport profile at the Casselman site, considering the silty clay deposit as a continuously fractured porous medium.

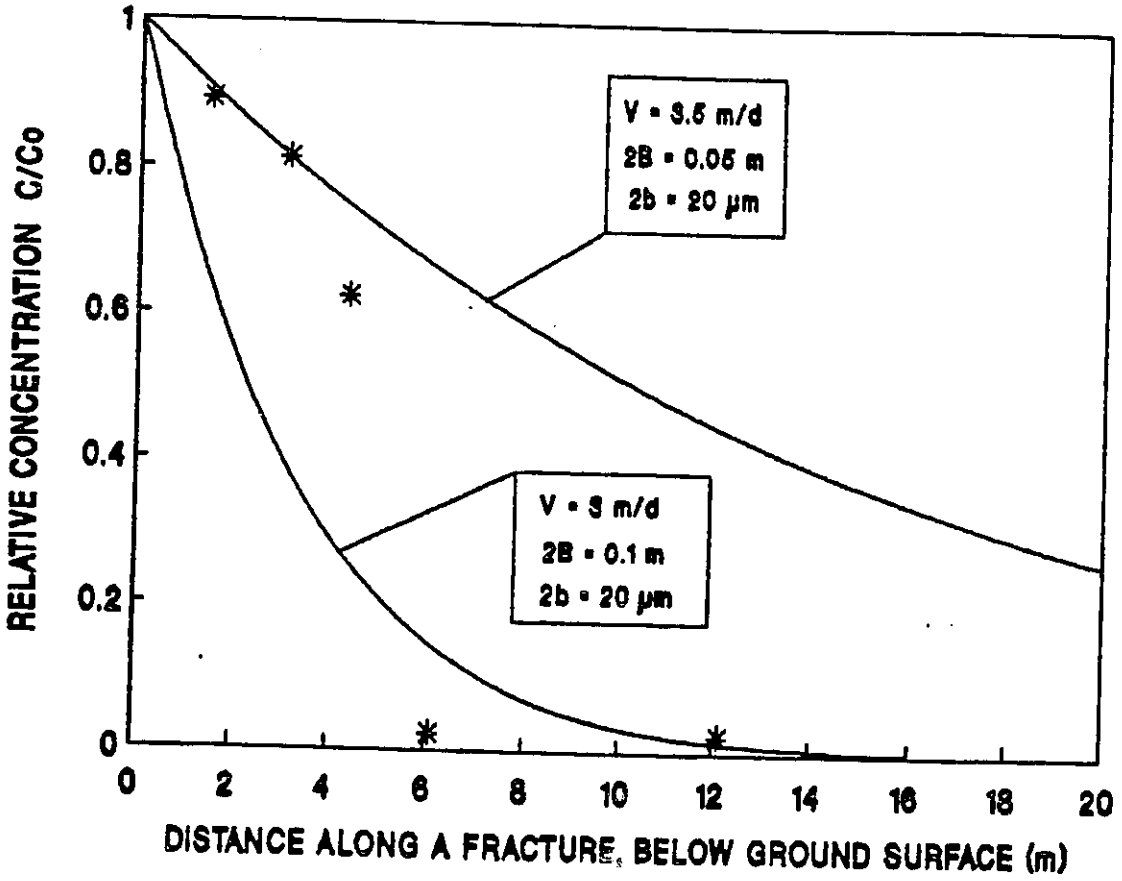

Figure 6.29. Simulation of tritium transport profiles at the NRC site, considering the silty clay deposit as a continuously fractured porous medium.

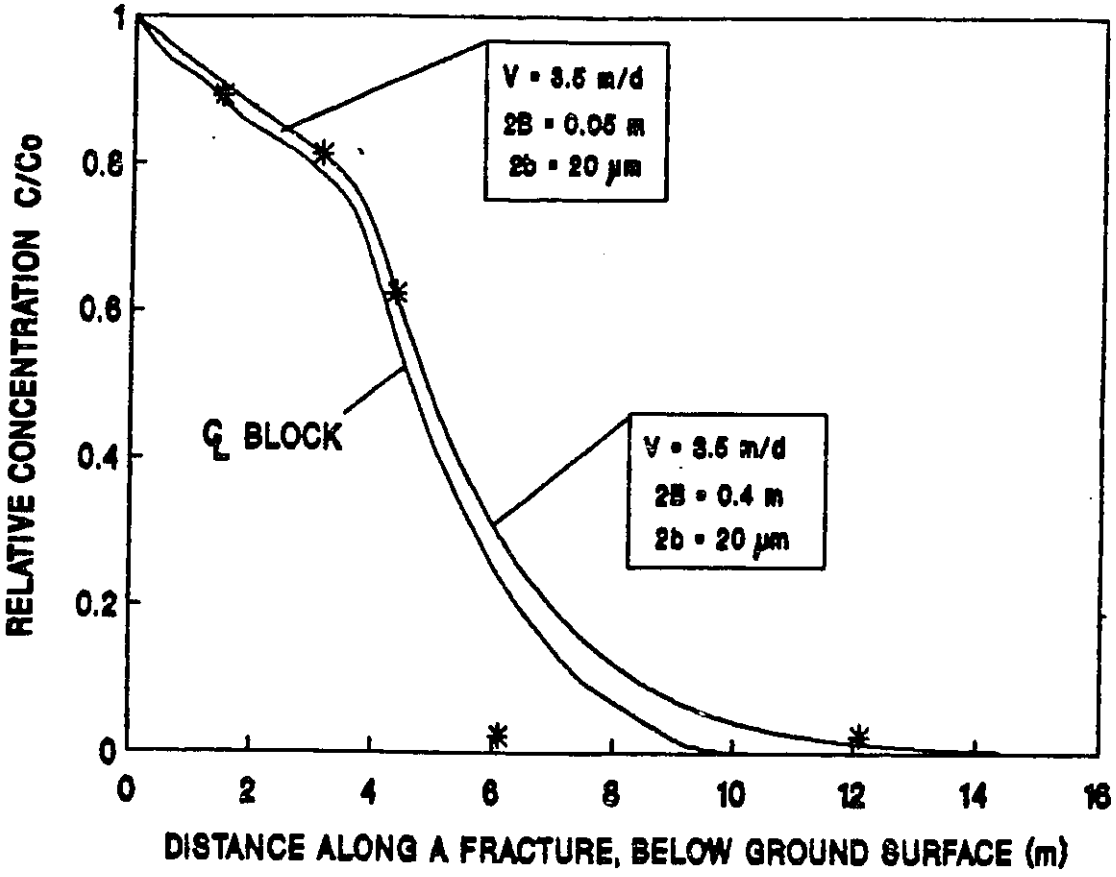

Figure 6.30. Combination of two theoretical tritium transport profiles at a depth of 3.5 m, considering the silty clay deposit at the NRC site as a continuously fractured porous medium. Also given is the centre line concentration profile of the clay matrix block.

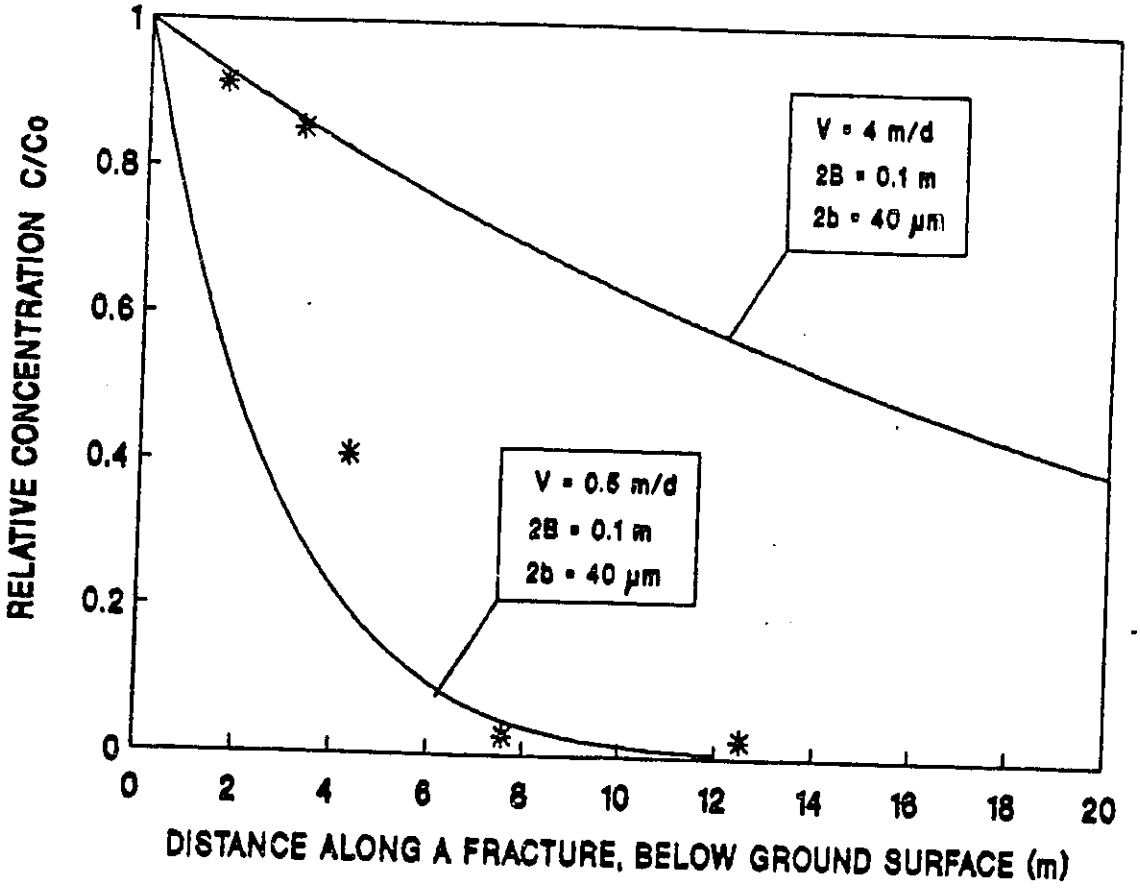

Figure 6.31. Simulation of tritium transport profiles at the Fallowfield site, considering the silty clay deposit as a continuously fractured porous medium.

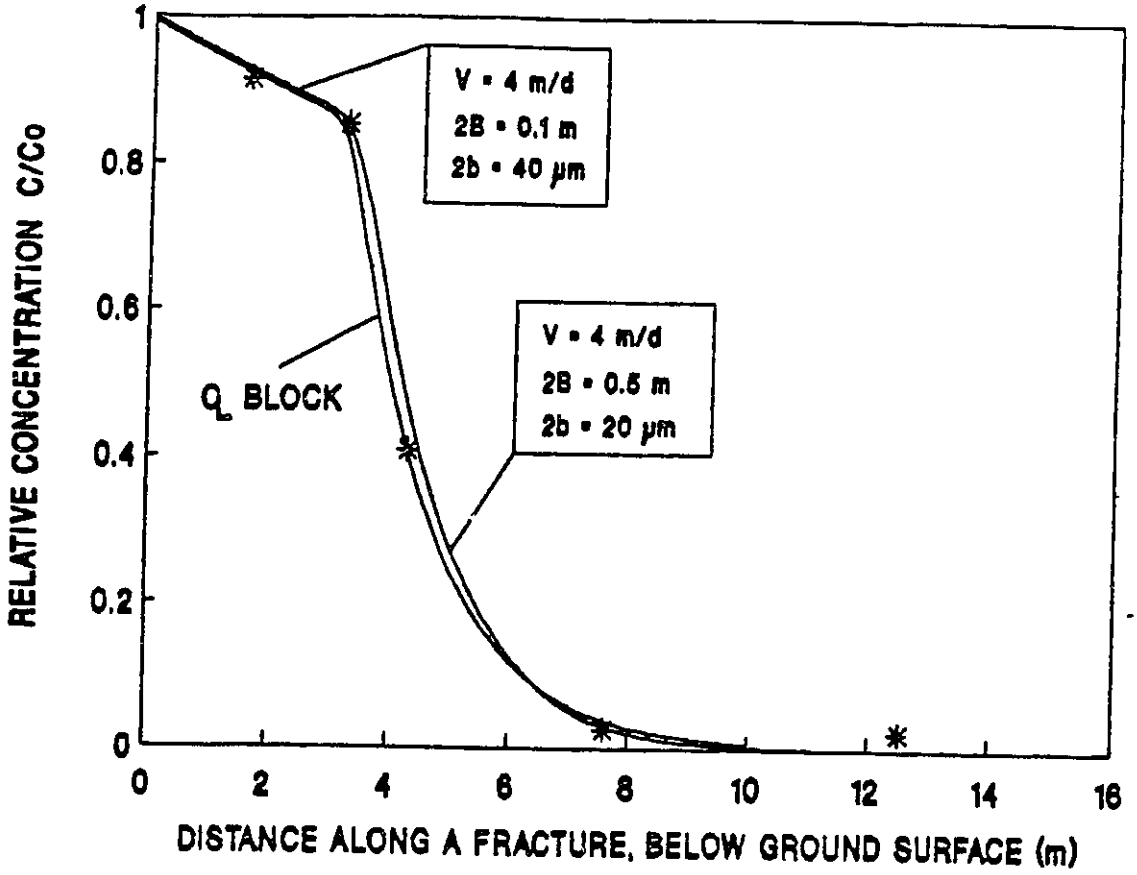

Figure 6.32. Combination of two theoretical tritium transport profiles at a depth of 3.2 m, considering the silty clay deposit at the Fallowfield site as a continuously fractured porous medium. Also given is the centre line concentration profile of the clay matrix block.

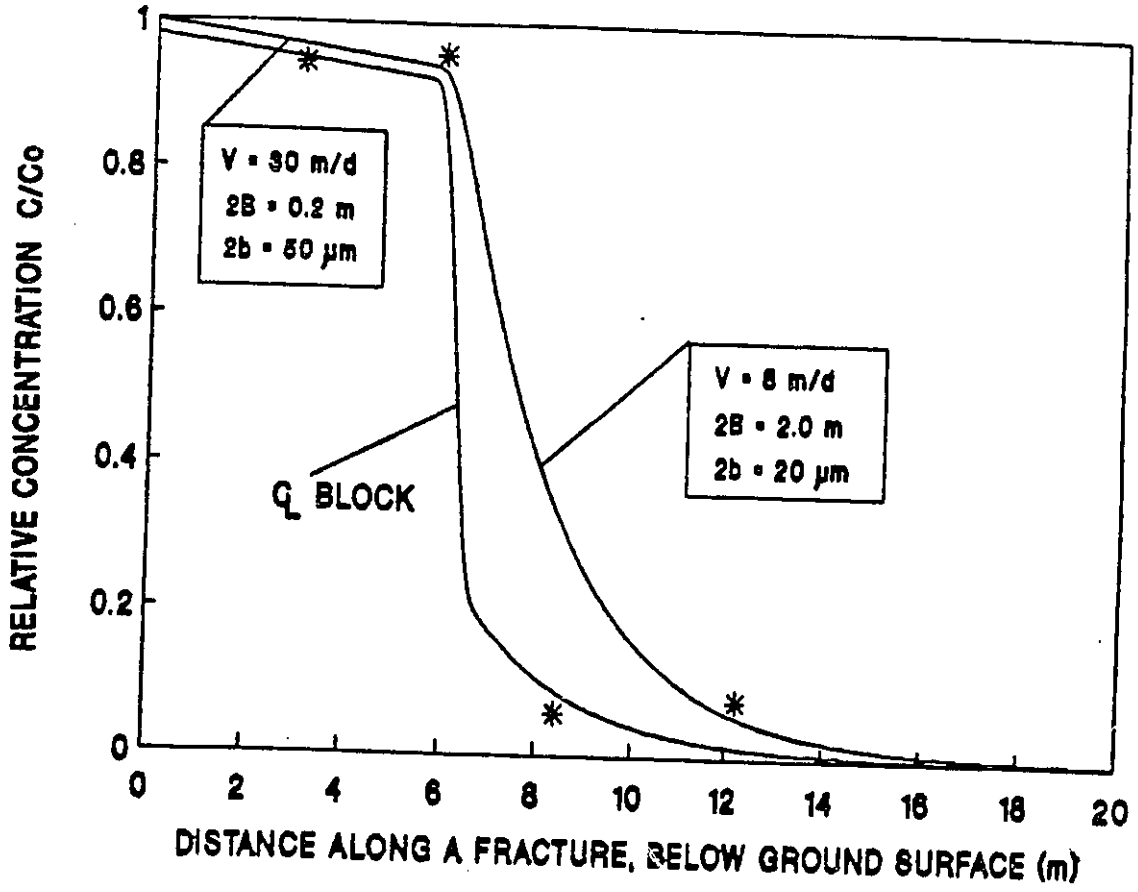

Figure 6.33. Combination of two theoretical tritium transport profiles at a depth of 6.0 m, considering the silty clay deposit at the Renfrew site as a continuously fractured porous medium. Also given is the centre line concentration profile of the clay matrix block.

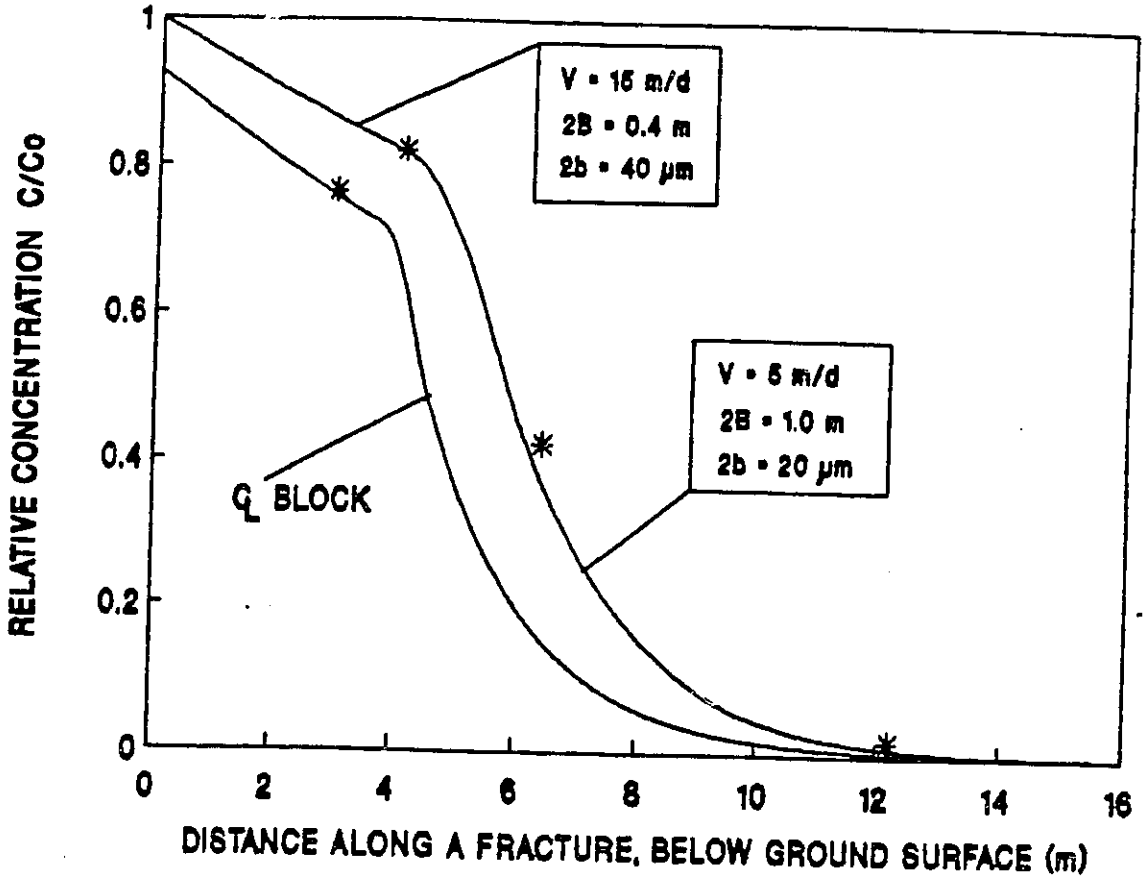

Figure 6.34. Combination of two theoretical tritium transport profiles at a depth of 4.40 m, considering the silty clay deposit at the Casselman site as a continuously fractured porous medium. Also given is the centre line concentration profile of the clay matrix block.

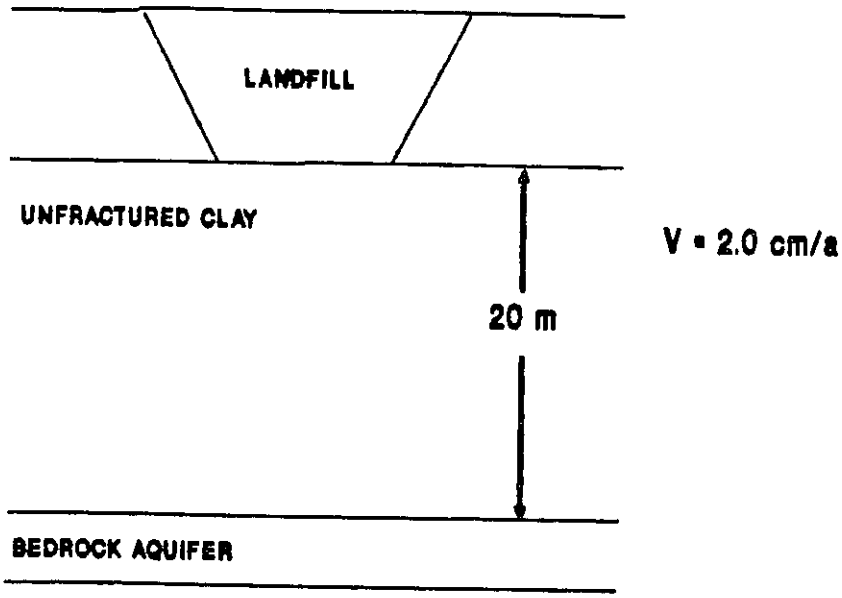

CASE 1

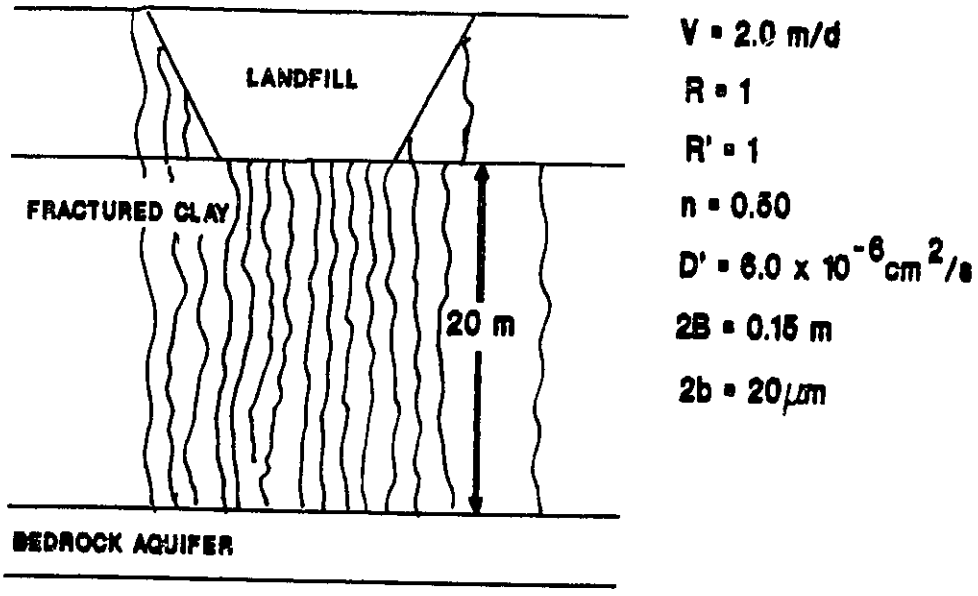

CASE 2

Figure 7.0. Physical representation of leachate migration prediction cases.

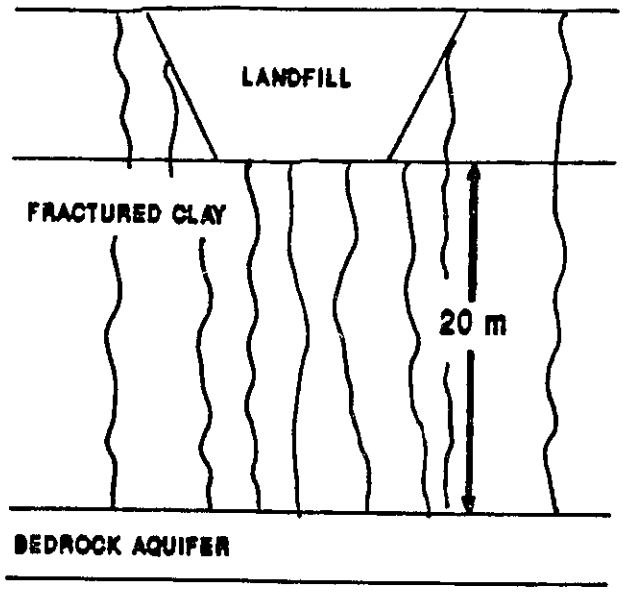

V = 2.0 m/d
R = 1
R' = 1
n = 0.50
$D' = 6.0 \times 10^{-6} cm^2/s$
2B = 0.40 m
2b = 20μm

CASE 3

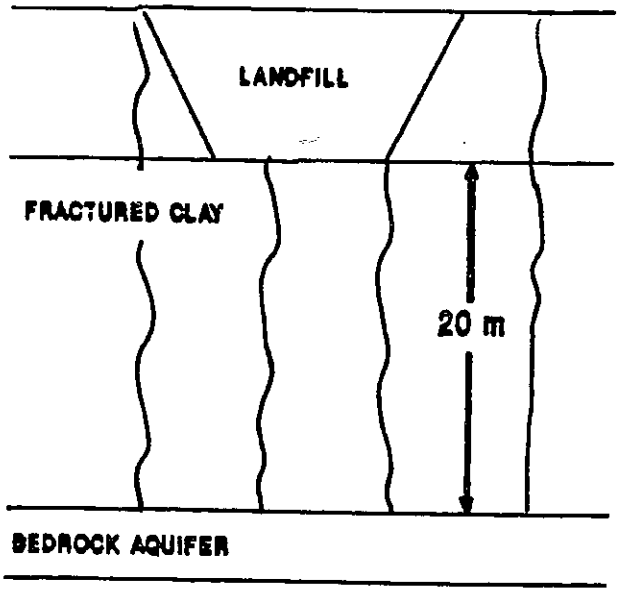

V = 2.0 m/d
R = 1
R' = 1
n = 0.50
$D' = 6.0 \times 10^{-6} cm^2/s$
2B = 1.0 m
2b = 50μm

CASE 4

Figure 7.0. Continued.

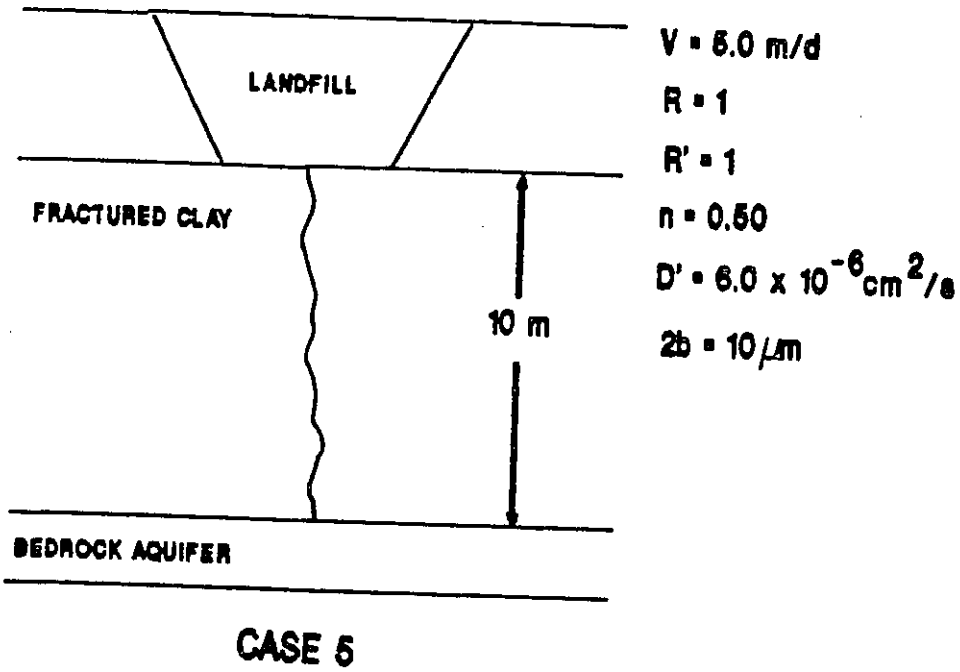

Figure 7.0. Continued.

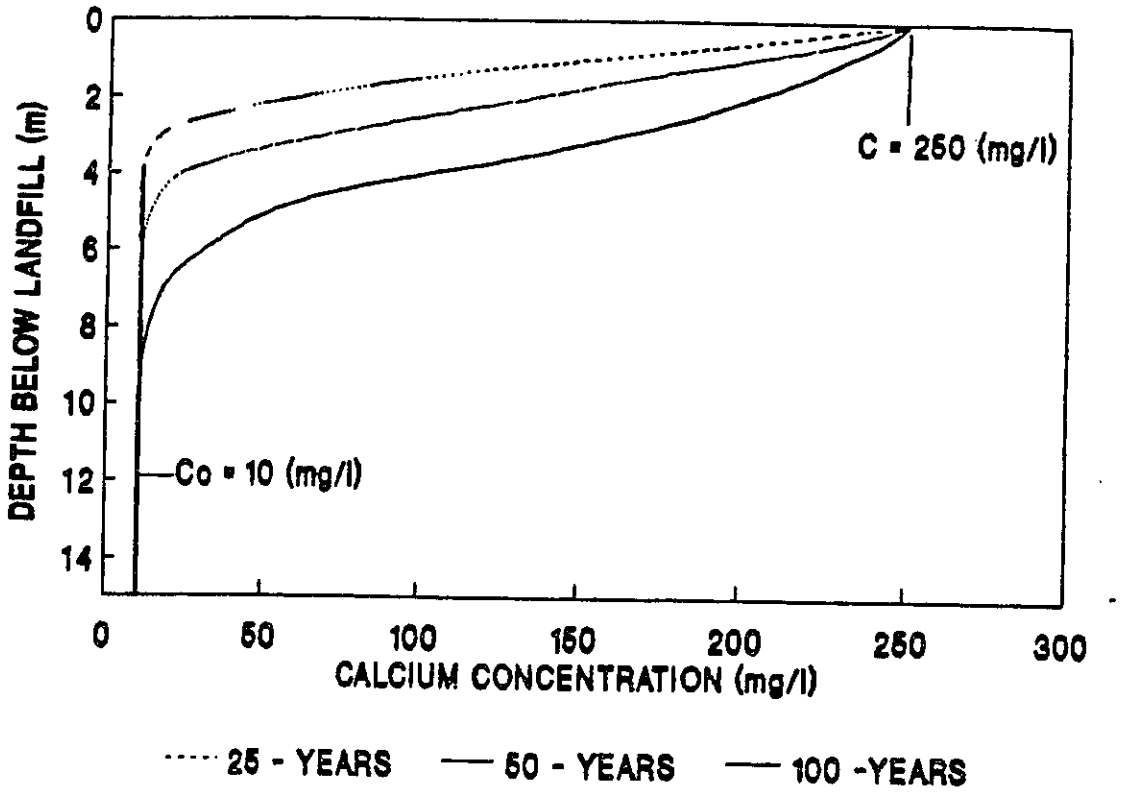

Figure 7.1. Calcium migration after 25, 50 and 100 years, for case 1.

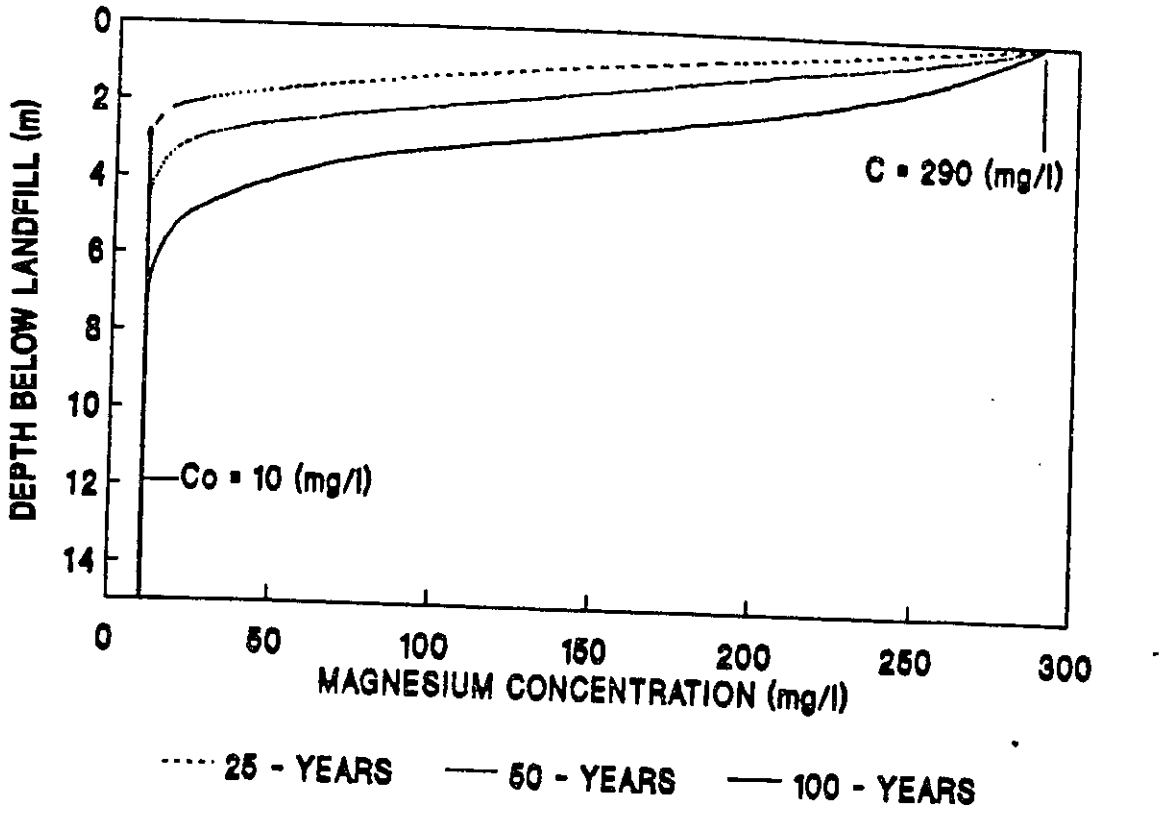

Figure 7.2. Magnesium migration after 25, 50 and 100 years, for case 1.

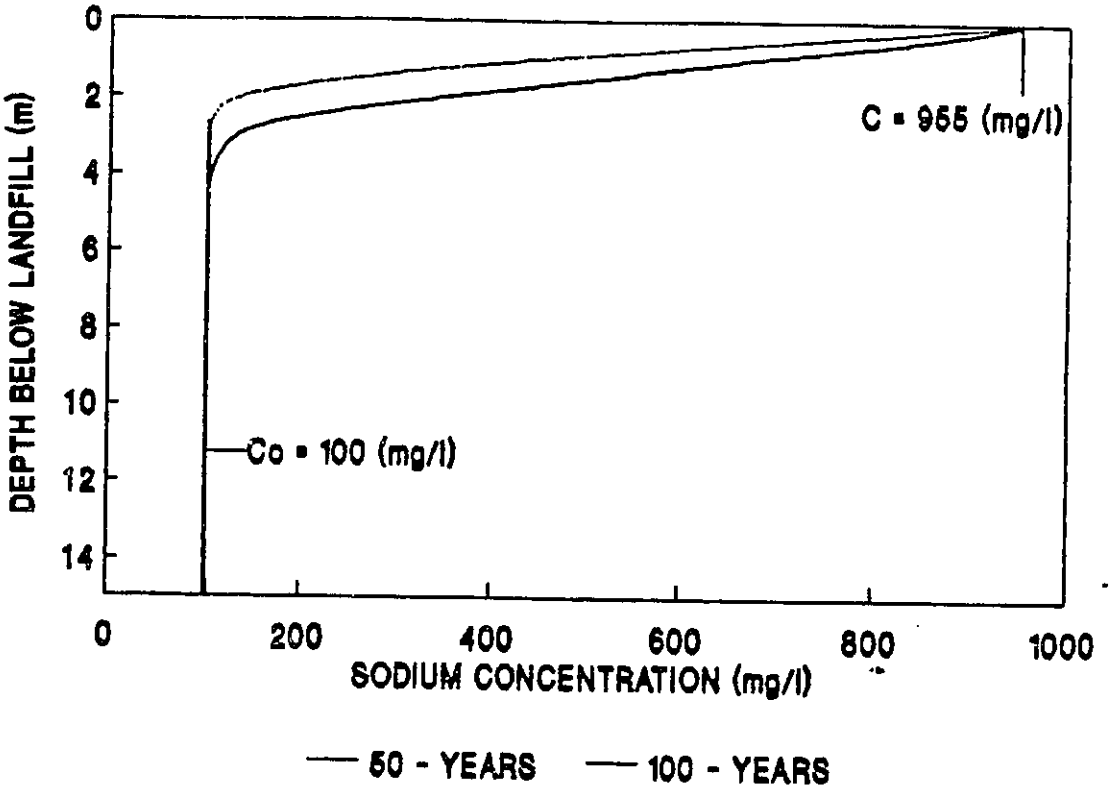

Figure 7.3. Sodium migration after 50 and 100 years, for case 1.

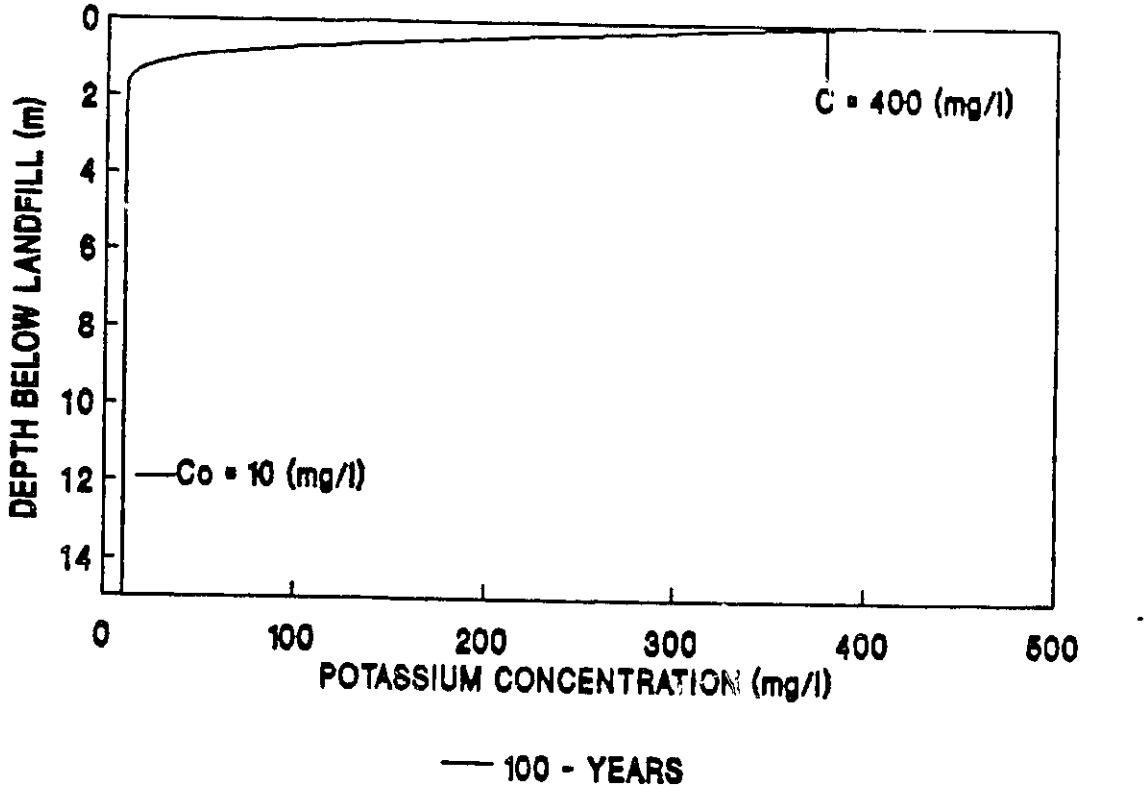

Figure 7.4. Potassium migration after 100 years, for case 1.

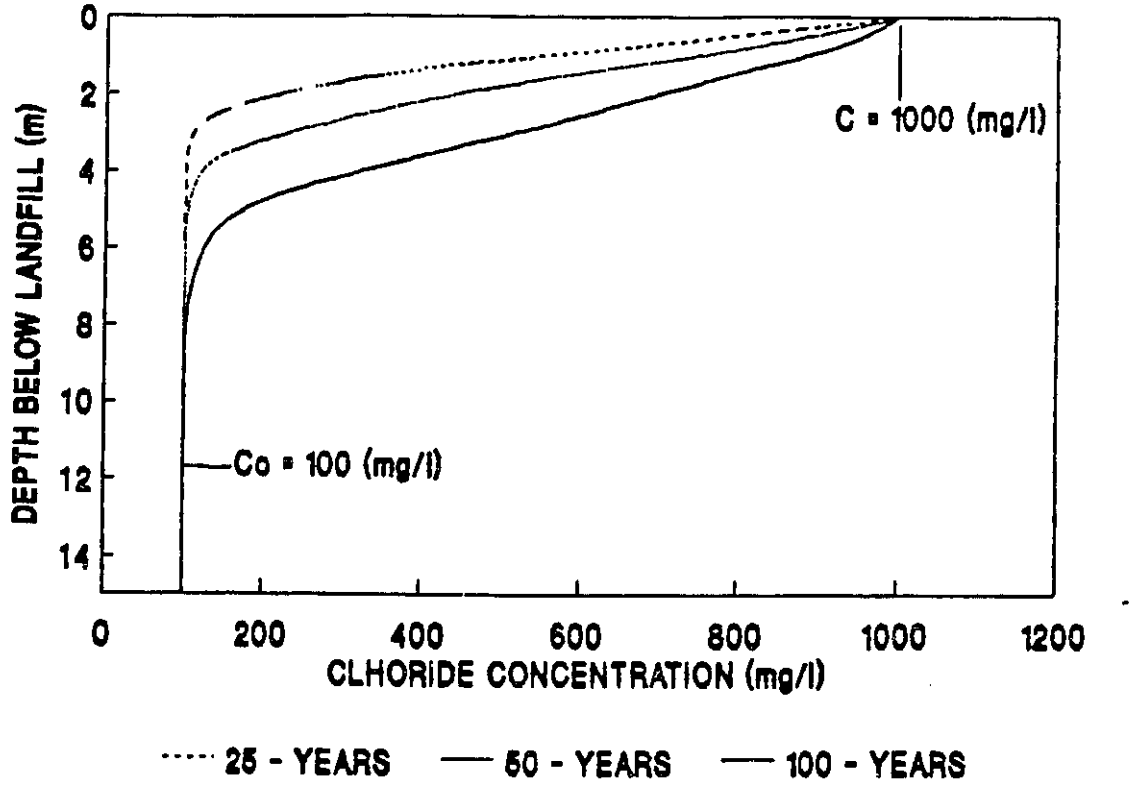

Figure 7.5. Chloride migration after 25, 50 and 100 years, for case 1.

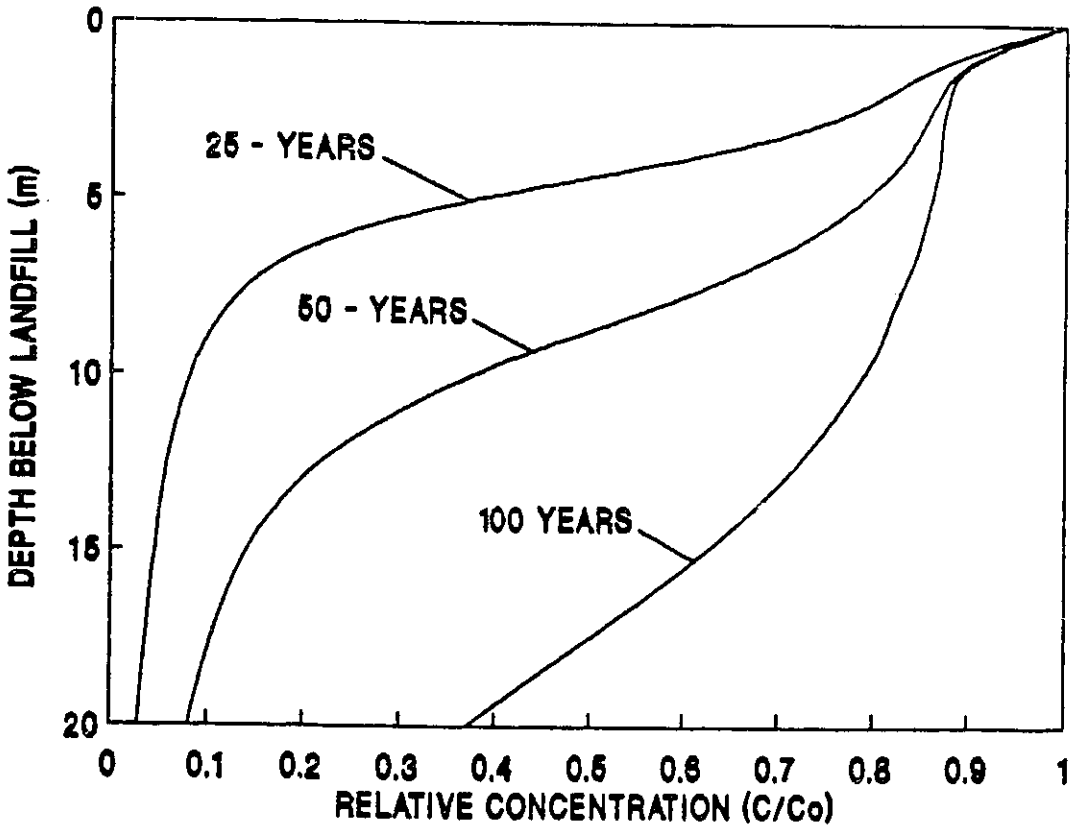

Figure 7.6. A non reactive solute migration through a fractured porous medium defined by case 2 after 25, 50 and 100 years.

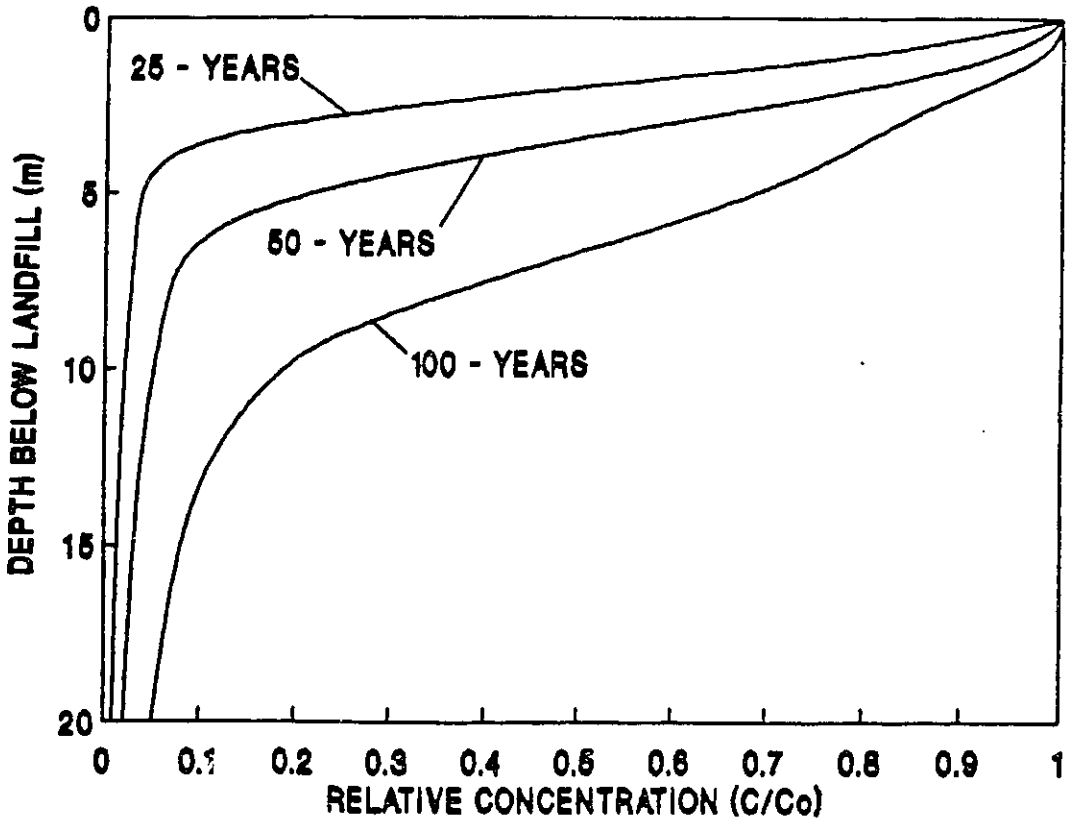

Figure 7.7. A non reactive solute migration through a fractured porous medium defined by case 3 after 25, 50 and 100 years.

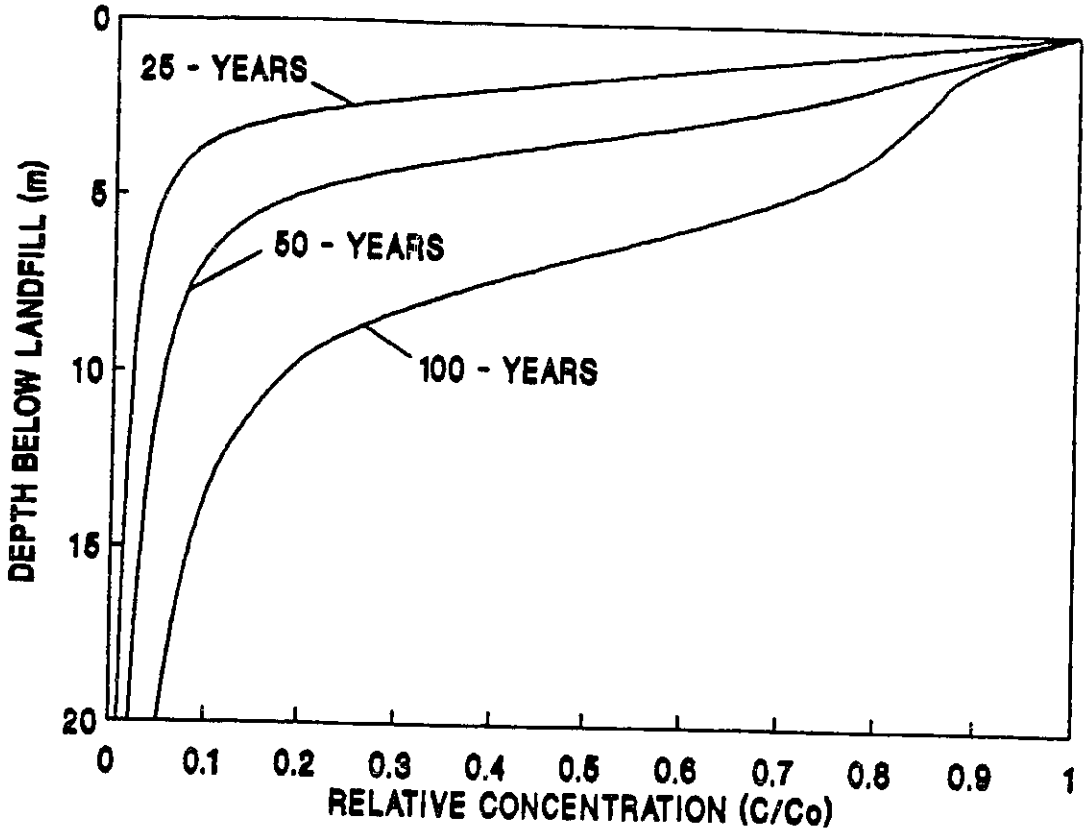

Figure 7.8. A non reactive solute migration through a fractured porous medium defined by case 4 after 25, 50 and 100 years.

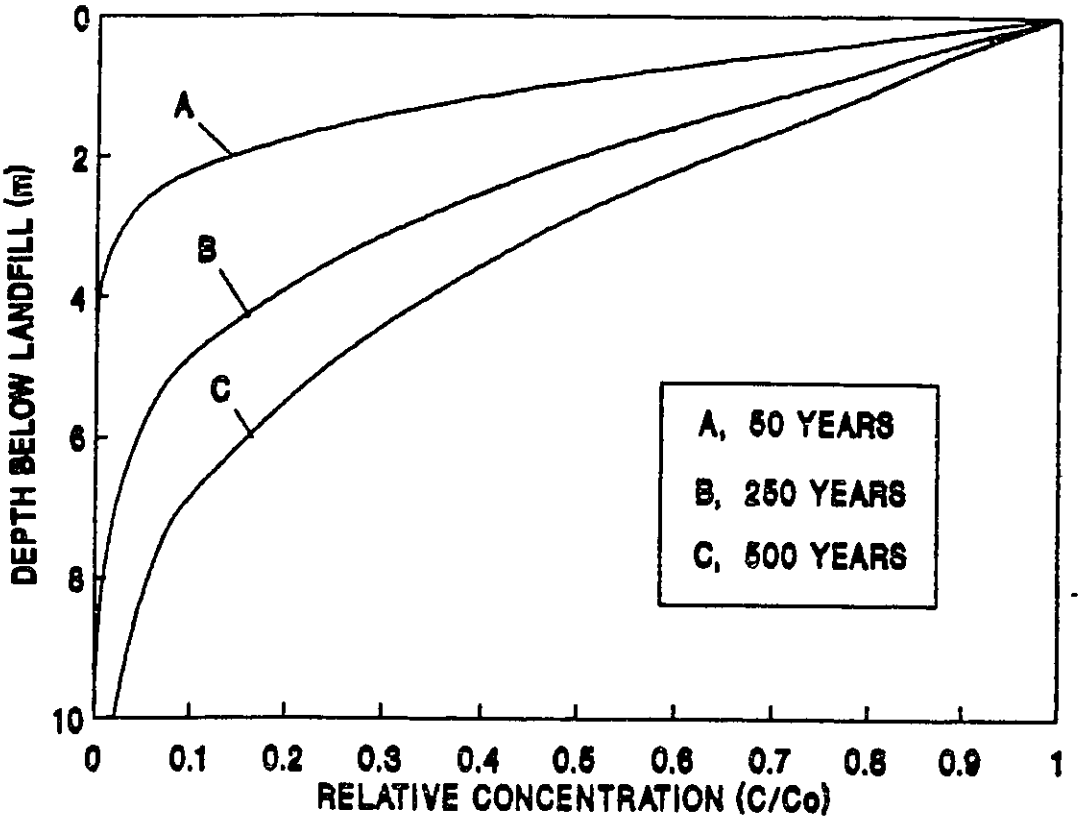

Figure 7.9. A non reactive solute migration through a fractured porous medium defined by case 5 after 50, 250 and 500 years.

APPENDIX A

DETAILS OF PIEZOMETER INSTALLATION

TABLE A-1, PIEZOMETER INSTALLATION: NRC.

Piezometer #	Depth (m)	Screen (m)	Sand pack (m)	Bentonite seal (m)	Type of installation
PZ-1	12.2	1.5	10.2 to 12.2	9.5 to 10.2	Conventional augering
PZ-2	9.1	1.5	7.0 to 9.1	3.7 to 7.0	Conventional augering
PZ-3	7.4	0.3	5.2 to 7.4	3.8 to 5.2	Double shelby
PZ-4	6.1	0.3	5.5 to 6.1	2.4 to 5.5	Conventional augering
Pz-5	6.4	0.3	5.8 to 6.4	4.7 to 5.8	Double shelby
PZ-6	4.4	0.3	4.0 to 4.4	3.1 to 4.0	Double shelby
PZ-7	3.5	0.3	2.9 to 3.5	2.1 to 2.9	Double shelby
PZ-8	3	0.3	2.6 to 3.0	0 to 2.6	Conventional augering
PZ-9	3.1	0.3	2.5 to 3.1	1.8 to 2.5	Double shelby
PZ-10	2.2	0.3	1.6 to 2.2	0.8 to 1.6	Double shelby
PZ-11	1.5	0.3	1.0 to 1.5	0.3 to 1.0	Double shelby
PZ-12	0.7	0.3	0.5 to 0.7	0 to 0.5	Double shelby

TABLE A-2, PIEZOMETER INSTALLATION: FALLOWFIELD.

Piezometer #	Depth (m)	Screen (m)	Sand pack (m)	Bentonite seal (m)	Type of installation
PZ-1	12.5	1.5	Backfill	5.5 to 6.4	Conventional augering
PZ-2	9.9	1.5	8.2 to 9.9	7.5 to 8.2	Conventional augering
PZ-3	7.6	1.5	6.1 to 7.6	0 to 6.0	Conventional augering
PZ-4	6.1	0.3	5.6 to 6.1	4.7 to 5.6	Double shelby
PZ-5	4.3	0.3	3.9 to 4.3	3.0 to 3.9	Double shelby
PZ-6	4.4	0.3	4.0 to 4.4	0 to 4.0	Conventional augering
PZ-7	3.7	0.3	3.1 to 3.7	2.0 to 3.1	Double shelby
PZ-8	3.2	0.3	2.6 to 3.2	1.6 to 2.6	Double shelby
PZ-9	3	0.3	2.5 to 3.0	0 to 2.5	Conventional augering
PZ-10	2.1	0.3	1.5 to 2.1	0.6 to 1.5	Double shelby
PZ-11	1.6	0.3	1.0 to 1.6	0.3 to 1.0	Double shelby
PZ-12	0.8	0.3	0.2 to 0.8	0 to 0.2	Double shelby

TABLE A-3, PIEZOMETER INSTALLATION: RENFREW.

Piezometer #	Depth (m)	Screen (m)	Sand pack (m)	Bentonite seal (m)	Type of installation
PZ-1	12.2	1.5	10.7 to 11.6	9.7 to 10.7	Conventional augering
PZ-2	9.15	1.5	7.6 to 9.1	0.8 to 9.1	Conventional augering
PZ-3	8.4	0.3	8.0 to 8.4	6.7 to 8.0	Double shelby
PZ-4	5.9	0.3	5.5 to 5.9	4.6 to 5.5	Double shelby
Pz-5	4.6	0.3	4.3 to 4.6	3.0 to 4.3	Double shelby
PZ-6	3.1	0.3	2.7 to 3.1	1.7 to 2.7	Double shelby
PZ-7	1.5	0.3	0.9 to 1.5	0.4 to 0.9	Double shelby

TABLE A-4. PIEZOMETER INSTALLATION: CASSELMAN.

Piezometer #	Depth (m)	Screen (m)	Sand pack (m)	Bentonite seal (m)	Type of installation
PZ-1	12.2	1.5	12.2 to 8.5	8.5 to 7.2	Conventional augering
PZ-2	9.2	1.5	7.2 to 9.2	6.4 to 7.2	Conventional augering
PZ-3	6.4	0.3	5.8 to 6.4	4.8 to 5.8	Double shelby
PZ-4	4.4	0.3	3.7 to 4.4	2.8 to 3.7	Double shelby
PZ-5	4.4	0.3	3.9 to 4.4	2.8 to 3.9	Conventional augering
PZ-6	3.1	0.3	2.6 to 3.1	1.7 to 2.6	Double shelby
PZ-7	2.9	0.3	2.2 to 2.9	0.6 to 2.2	Conventional augering
PZ-8	1.3	0.3	0.9 to 1.3	0.35 to 0.9	Double shelby

APPENDIX B

BOREHOLE LOGS

O-A248

FONDEX

BOREHOLE No NRC PZ-1

PROJECT MINISTRY OF ENVIRONMENT - ONTARIO

LOCATION RESEARCH PROJECT #466C

DATUM N/A BOREHOLE TYPE CME 55 (HOLLOW STEM)

DRILLING DATE 15-02-90

REPORT DATE NOV. 91

COMPILED BY N.C.

GEOLOGIC PROFILE			SAMPLE					DETAILS OF PIEZOMETER INSTALLATION	MOISTURE CONTENT (%)
Scale (m)	Elev. / Depth (m)	DESCRIPTION	STRATIGRAPHY	NUMBER	TYPE	BLOWS (N) / RQD	% RECOVERY		natural (W) liquid limit (w) l plastic limit (w) p 0 20 40 60 80 10
	0.0	TOPSOIL							
	0.15	LAMINATED SILTY CLAY : BROWN AND GREY BAND, VERY STIFF, TRACE OF RUST, ROOTS.							
1									
2									
3									
4	4.10	SILTY CLAY : GREY, SOFT.							
	4.60	SILTY CLAY : GREY, STIFF.							
5									
6									
7									
8									
9									
10		- TRACE OF ORGANIC MATTER AT A DEPTH OF 10.05m. - SHELLS.							
11									
12									
	12.20	END OF BOREHOLE							

O-A248

FONDEX

BOREHOLE No FFD PZ-1

PROJECT MINISTRY OF ENVIRONMENT - ONTARIO

LOCATION RESEARCH PROJECT #466C

DATUM N/A BOREHOLE TYPE CME 55 (HOLLOW STEM)

DRILLING DATE 12-12-89

REPORT DATE NOV. 91

COMPILED BY N.C.

Scale (m)	Elev. / Depth (m)	DESCRIPTION
	0.0	TOPSOIL
	0.15	SILTY CLAY : BROWN, FROZEN.
	0.45	SILTY CLAY : BROWN, SOFT PLASTIC, SOME PEBBLES, SAND LENSES, TRACE OF RUST, WET.
1		
2		
	2.30	LAMINATED SILTY CLAY : BROWN AND GREY BOND, SOFT, SPORADIC SAND LENSES, ROOTS, WET.
3		
4		
	4.50	SILTY CLAY : GREY, SOFT, ROOTS, WET.
5		
6		
7		
8		
	8.40	SILTY CLAY : GREY, HARD, HUMID.
9	9.00	SILTY CLAY : GREY, SOFT, WET.
10		
	10.50	SILTY CLAY : GREY, VERY SOFT, WET.
11		
12	12.00	END OF BOREHOLE

SAMPLE: STRATIGRAPHY | NUMBER | TYPE | BLOWS (N) / ROD | % RECOVERY

DETAILS OF PIEZOMETER INSTALLATION

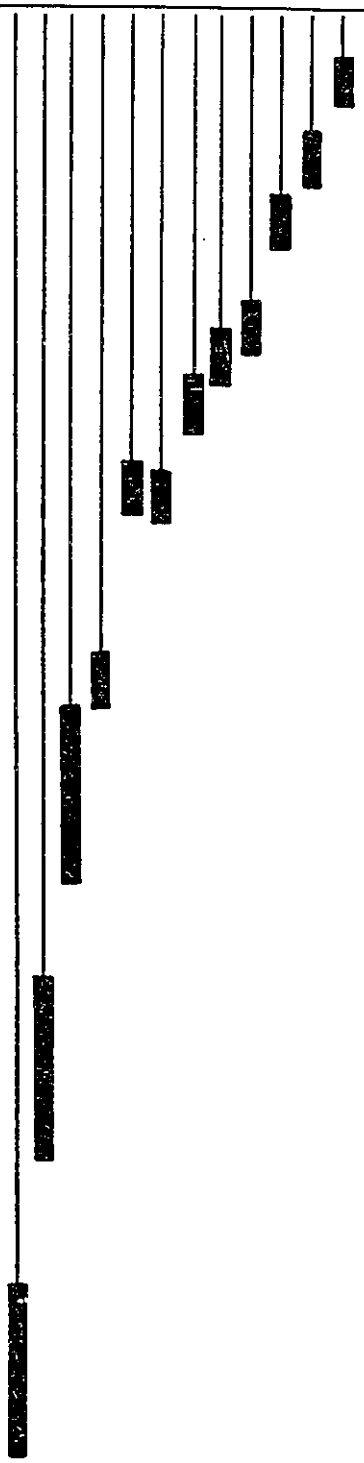

MOISTURE CONTENT (%)

natural (W)

liquid limit (w) l

plastic limit (w) p

0 20 40 60 80 100

O-A248

FONDEX

BOREHOLE No REN PZ-1

PROJECT MINISTRY OF ENVIRONMENT - ONTARIO

LOCATION RESEARCH PROJECT #466C

DRILLING DATE 15-02-90

DATUM N/A BOREHOLE TYPE CME 55 (HOLLOW STEM)

REPORT DATE NOV. 91

COMPILED BY N.C.

Scale (m)	Elev. / Depth (m)	DESCRIPTION
	0.0	TOPSOIL
	0.15	SILTY CLAY : BROWN, FROZEN
1		
	1.60	STRATIFIED SILTY CLAY : BROWN AND GREY BAND, SOME PEBBLES, HARD, DRY.
2		
3		
4		
5	5.00	GREY, HARD, WET.
6		
7		
		- BECOMING SOFT AT A DEPTH OF 7.6m.
8		- BECOMING HARD AT A DEPTH OF 8.3m.
9		
10		
11		
12		
	12.20	END OF BOREHOLE

SAMPLE: STRATIGRAPHY | NUMBER | TYPE | BLOWS(N)/RQD | % RECOVERY

DETAILS OF PIEZOMETER INSTALLATION

MOISTURE CONTENT (%)

natural (W)

liquid limit (w_l)

plastic limit (w_p)

0 20 40 60 80 1(

O-A248

FONDEX

BOREHOLE No. CSL PZ-1

PROJECT MINISTRY OF ENVIRONMENT - ONTARIO

LOCATION RESEARCH PROJECT #466C

DATUM N/A BOREHOLE TYPE CME 55 (HOLLOW STEM)

DRILLING DATE 28-03-90

REPORT DATE NOV. 91

COMPILED BY N.C.

Scale (m)	Elev. / Depth (m)	DESCRIPTION	SAMPLE: STRATIGRAPHY	SAMPLE: NUMBER	SAMPLE: TYPE	SAMPLE: BLOWS(N)/RQD	SAMPLE: % RECOVERY	DETAILS OF PIEZOMETER INSTALLATION
	0.0	TOPSOIL						
1	0.60	SILTY CLAY : BROWN, STIFF, DRY.						
2								
3		- BECOMING REDDISH BROWN AT A DEPTH OF 2.5m.						
4								
5		- BECOMING LIGHT BROWN, SOME SILT AND FINE SAND LENSES AT A DEPTH OF 4.5m.						
6	5.50	SILTY CLAY : GREY, STIFF, HUMID. - TRACE OF ORGANIC MATTER AT A DEPTH OF 6.0m.						
7								
8								
9		- OCCASIONALLY SOFT AND WET.						
10								
11								
12								
	12.20	END OF BOREHOLE						

MOISTURE CONTENT (%)

natural (W)

liquid limit (w_l)

plastic limit (w_p)

0 20 40 60 80 10

APPENDIX C

TEST PIT OBSERVATIONS

TABLE C-1 NRC GEOLOGY

SOIL	DEPTH (m)	DISCRIPTION
Top soil	0.0 to 0.30	Top soil - dark, granular with many small roots ranging from 1 to 4 mm in diameter
Lami-nated silty clay	0.30 to 0.55	Mixture of silty clay, red oxidized clay, and sand with many roots ranging from 2 to 3 mm in diameter
Orga-nic layer	0.55 to 0.56	Dark organic layer, seems to run the total length of the trench
Silty brown clay	0.56 to 1.3	Silty grey brown clay with some sand, very stiff, trace of gravel size granite, small roots, macropores or root holes with average diameter of 5 mm, fissures at this depth or well defined
Grey silty clay	1.3 to 1.8	Greyish silty clay with small oxydized bands (reddish in colour) - maximum with of 10 mm, very stiff roots and root imprints are still visible, large number of fissures - well defined with tight spacing which seperates the clay into small blocks
Stiff grey silty clay	1.8 to 3.5	Very stiff greyish silty clay with well defined fissures which are becomming long and planar, the fissures separate the clay into large blocks - monolithic in appearance, the contact zone between these blocks the clay has become granular in texture, roots, paleoroots are present in large amounts, oxidized clay band at a depth of 2.7 m
Stiff grey silty clay	3.5 to 3.9	Greyish silty clay, stiff, presence of only a few large fissures, the clay is becoming more massive, few paleoroot

TABLE C-2 NRC, FISSURE & ROOT DETAIL

DEPTH (m)	DISCRIPTION
0.5	No visible fissures, soiltexture is granular, large amounts of living roots, 10 roots for a horizontal distance of 40 cm, root holes
1.0	Fissures are not well defined, living roots are less frequent 3 to 4 for 40 cm, the observed root holes had the fallowing diameter 8, 5, 5 mm, with a corresponding vertical length of 13, 5, 5 cm
1.5	Fissures become distinctive after 1.1 m in depth, the fissures appear to be long and planar, the fissures face has a waxy appearance, the fissures divide the clay into small hexagonal blocks with the fallowing average dimensions: width - 0.5 to 1 cm, length - 2.0 to 5 cm, depth - 2 to 5 cm, four major fissure intersections - 8 fracture faces in the space of 60 cm, fissure length: 15, 20, 20, - 22 cm, orientation: 190/82, 280/81, 205/80, 300/87, 200/80, 305/90, 185/89, 280/88
2.0	one root of unknown origin - 20 cm in length, some fissures seem to continue from the above section, 5 fissure intersection - 10 faces with a measured length of 10, 130, 30, 30, 40 cm, the clay blocks fromed by the intersections of the fissures are becomming more massive, orientation: 205/83, 205/71, 320/86, 210/85, 315/81
2.5	Large fissure face exposed at a depth of 2.5 m witha length of 90 cm and a width of 50 cm - heavy network of paleoroots, on the roof of the exposed face - many root holes are visible (#20) with an average diameter of 1mm, the fissures are wet indicating hydraulic activity, 5 fissure intersections - 10 faces, orientation: 265/75, 175/80, 200/64, 275/69,between 2.6 and 2.75 meters in depth - two fissures: length 15 and 20 cm, openning of 2 and 1 cm,
3.0	Paleoroots on fissure faces, clay blocks becomming more massive, on these blocks smaller fissures are present - stress relief?, presence of water in the fissures indicating hydraulic activity, fissures are extensions from the above section, 4 fissure intersections - 8 faces, orientation: 165/85, 250/90, 170/80, 260/90, 215/86, 300/70, 180/79

TABLE C-2 CONTINUED, FISSURE & ROOT DETAIL

DEPTH (m)	DISCRIPTION
3.5	Decreasing number of paleoroots and fissures, the clay is becomming more massive, 2 fissure intersection - 4 faces, fissures extensions from those above, the fissures are becomming more active (observed more water in the fissures), the fissures have openings of 2 mm, less number of smaller fissures on the large blocks, orientation: 185/83, 260/90, 285/83, 210/83

TABLE C-3 NRC STEP INFORMATION

DEPTH (m)	GEOLOGY	FISSURE LENGTH	ORIENTATION strike / dip
STEP 1 1.5	Greyish silty clay with oxydized brown clay bands, 20 fissure intersection - 40 faces, length between 3 to >50 cm	# cm 4 50 2 20 1 15 1 12 1 10 1 7 2 5 2 3	160/84 215/90 210/80 200/70 195/68 130/85 180/70 210/70 220/86 175/75 260/76 305/7?
STEP 2 2.0	Greyish silty clay with oxydized red-brown clay, sand lenses found in fissures at 2.2 and 2.5 m, larger number of fissures over 50 cm in length, 12 fissure intersections - 24 faces, a good amount of water oozing out of the fissures	# cm 8 > 50 2 20 1 10 1 5	320/87 180/90 270/70 225/90 304/73 170/90 260/87 185/85 245/88 230/80

TABLE C-4 NRC ORIENTATION OF FISSURES TAKEN AT RANDOM

STRIKE / DIP	275/65, 328/90, 270/70, 260/85, 185/83, 210/50, 230/88, 300/78, 305/88

TABLE C-5 WATER FLOW INTO TEST PIT

VOLUME OF WATER (m^3)	TIME (sec.)	FLOW INTO PIT (l/s)
1.008	45000	0.022
0.864	52200	0.017

TABLE C-6 FALLOWFIELD GEOLOGY

SOIL	DEPTH (m)	DISCRIPTION
Top soil	0.0 to 0.2	Top soil - fairly granular, lots of roots
Silty brown clay	0.2 to 1.0	Light brown silty clay, plastic, dry, trace of rust/or oxidized clay, some sand, trace of cobbles lots of living roots, many root holes and small fissures, has a granular texture the fissures divides the soil into very small blocks observed many small pores in the soil ranging 1 mm in diameter or less above the water table (early September)
Silty brown clay	1.0 to 2.0	Light brown silty clay with sand lenses, some pebbles, wet, plastic, trace of rust, the soil is very soft, granular in texture, large # of rust spots, seem to be surround roots, root holes, fissures, and small pores, hard to distinguish fissures, many small pores are visible which seem to form small canals, the first observed sand lense, 2 to 3 mm in thickness, was at a depth of 1.4 m, these sand lense are a mixture of fine grey sand and silt.
Grey silty clay	2.0 to 3.25	Greyish silty clay with sand lenses, wet, soft, many root holes/ old roots, it is very hard to distinguish fissures due to the softness of the clay, observed many small pores or canals (just as above), this zone is hydraulicly active (water entering the trench is easily observed), most of this activty occurs in the small horizontal silty sand beds which can have a thickness of up to 12 mm.
Grey silty clay	3.25 to 3.80	Greyish silty clay with some dark organic bands, wet, soft, massive, no vissible fissures, some paleoroots and leaves are present, small and sort sand lenses with have no perferred orientation (1 to 3 mm in thickness & 4 to 6 mm in length, no living roots or small canals are observed

TABLE C-7 FALLOWFIELD, FISSURE & ROOT DETAIL

DEPTH (m)	DISCRIPTION
0.5	Many roots and root holes, in a distance of .5 m horizontally - 25 small roots with an avg. diameter of 1 to 2 mm, 8 root holes of 2 mm in diameter, 50 to 70 small fissures, in a vertical distance of 10 cm - 15 to 25 small fissures, fissures have a ramdom orientation
0.7	Large number of root holes, ranging from 2 to 10 mm in diameter and visible lengths of 5 to 70 mm, 10 measured root holes, diameters in mm: 8, 10, 3,4,3,5,2,3,4,5
1.0	Many roots and fissures, in a distance of .5 m horizontally - 15 to 20 small roots, 5 root holes with the fallowing diameters in mm: 3,8,5,4,2, and visible lenghts of 10 to 100 cm, 15 to 20 small fissures, in a vertical distance of 10 cm - 5 to 10 fissures, fissures have a ramdom orientation
1.5	Decreasing number of living roots, in a horizontal distance of .5 m - 10 small roots due to the wetness of the clay at this depth, fissures have become very hard to distinguish especially in the presence of small pores / or canals (these small canal can be actually fissures), in a 10 x 10 cm square - over 100 small canals with a diameter of 1 mm or less
2.0	5 living roots in a horizontal distance of .5 m, the number of small canals in a 10 x10 cm square is between 25 and 30, these small pore canals seem to be interconnected with themselfs and the small sand beds
2.5	No roots visible, the number of small canals in a 10 x 10 cm square is between 15 to 20, random orientation, no visible fissures
3.0	In a 10 x10 cm square - 10 to 20 small canals /or fissures ? , no roots, no visible fissures
3.5	Massive clay, no roots visible, no small canals, no fissures, some paleoroots visible

TABLE C-8 STRATIGRAPHIC SEQUENCE OF THE SAND / CLAY BEDS

SOIL TYPE	DEPTH (m)	THICKNESS of the BED (mm)
CLAY		1400
SAND	1.40	4
CLAY		196
SAND	1.60	2
CLAY		48
SAND	1.65	2
CLAY		88
SAND	1.74	2
CLAY		58
SAND	1.80	2
CLAY		68
SAND	1.87	2
CLAY		38
SAND	1.91	2
CLAY		38
SAND	1.95	2
CLAY		98
SAND	2.05	2
CLAY		28
SAND	2.08	1
CLAY		49
SAND	2.10	2
CLAY		48
SAND	2.15	2
CLAY		88
SAND	2.24	2
CLAY		58
SAND	2.30	2
CLAY		48
SAND	2.35	2
CLAY		58
SAND	2.41	2
CLAY		38
SAND	2.45	2
CLAY		48
SAND	2.50	8
CLAY		62
SAND	2.57	11
CLAY		69
SAND	2.65	10
CLAY		40
SAND	2.70	4
CLAY		46

TABLE C-8 CONTINUED, STRATIGRAPHIC SEQUENCE

SOIL TYPE	DEPTH (m)	THICKNESS of the BED (mm)
SAND	2.75	12
CLAY		88
SAND	2.85	6
CLAY		74
SAND	2.93	2
CLAY		120
SAND	3.05	2
CLAY		198
SAND	3.25	5
CLAY		

TABLE C-9 WATER FLOW INTO TEST PIT

VOLUME OF WATER (m^3)	TIME (sec.)	FLOW INTO PIT (l/s)
3.971	64800	0.061

APPENDIX D

Symbols and Terms Used in This Thesis

A = area (m^2)

2b = fracture aperture (m)

2B = Δ = fracture spacing (m)

C = concentration (M m^{-3})

CEC = cation exchange capacity of the soil's charged particles (a possible soil cation retention mechanism which can be totally reversible) (meq per 100 g of dry soil)

D = diffusion coefficient, movement of ions in solution from a region of high concentration to a region of low concentration (cm^2 s^{-1})

D_a = apparent diffusion coefficient (in a soil system) (cm^2 s^{-1})

D_e = effective diffusion coefficient (in a soil system) (cm^2 s^{-1})

D_o = molecular diffusion coefficient in water (cm^2 s^{-1})

D' = matrix diffusion coefficient (cm^2 s^{-1})

F = shape factor (Hvorslev 1951), a function of the piezometer intake area (dimensionless)

g = gravitational constant (m s^{-2})

G_s = specific gravity of soil particles

H = hydraulic head (m)

H_f = height of leachate in the source reservoir (m)

i = hydraulic gradient, dh/l (m m^{-1})

K = hydraulic conductivity (m s^{-1})

K_i = intrinsic permeability (m^2)

K_d = distribution coefficient, a measure of the soil's adsorption capabilities which is not influenced by solute concentration ($m^3\ kg^{-1}$)

K_f = fracture distribution coefficient (m)

K_m = Porous matrix distribution coefficient ($m^3\ kg^{-1}$)

L = length of the well screen (m)

L_w = depth of the confined aquifer (m)

N = Avogadro's number ($6.023 \times 10^{23}\ Mol^{-1}$)

n = total porosity, ratio of volume of voids over the total volume of soil ($m^3\ m^{-3}$)

n_e = effective matrix porosity, volume of interconnected pore spaces contributing to flow per unit bulk volume of soil ($m^3\ m^{-3}$)

n_{ef} = effective fracture porosity, the percentage of volumetric fractures contributing to the flow per bulk volume of soil ($m^3\ m^{-3}$)

Q = flow ($m^3\ s^{-1}$)

r = radius of the piezometer (m)

r_w = radial distance from undisturbed soil to the piezometer center line (m)

R = radius of the well screen (m)

R_e = effective radial distance over which the hydraulic head is dissipated (m)

R = Retardation Factor = the retardation factor represents the amount of adsorption of a specific contaminant onto the soil particles (dimensionless)

R' = matrix retardation factor (dimensionless)

R_g = universal gas constant ($8.134\ J\ Mol^{-1}\ K^{-1}$)

S = mass of contaminant adsorbed on solid mass of soil material ($kg\ kg^{-1}$)

S_r = degree of saturation

TL = Hvorslev (1951) hydrostatic time lag (s)

T = temperature (k)

t = time (s)

V_f = volume of leachate (m^3)

v = average linear velocity of water (advection) ($m\ s^{-1}$)

W = Boast and Kirkham (1971) shape factor for seepage into an augered hole (m)

x = distance perpendicular to the fracture's axis (m)

y = change in hydraulic head, slug test (m)

z = distance (m)

$|z|$ = ionic valence

α = maximum adsorption capacity of a soil system (dimensionless)

β = initial adsorption condition of the soil system at C=0 (dimensionless)

γ = the affinity capacity of adsorption sites on the soil particle surfaces ($m^3\ kg^{-1}$)

Γ = "complex tortuosity factor" ($m\ m^{-1}$)

θ = volumetric water content, volume of water over the total volume of voids ($m^3\ m^{-3}$)

η = viscosity of water ($N\ s\ m^2$)

λ = radioactive decay constant (s^{-1})

λ_o = limiting ionic conductance (cm^2/Ω equivalent)

μ = ionic mobility ($cm^2\ s^{-1}$)

ρ = fluid density ($kg\ m^{-3}$)

ρ_d = bulk density of the soil ($kg\ m^{-3}$)

τ = tortuosity, a measure of the degree of restriction imposed by the soil matrix on migrating ions (dimensionless)

υ = dynamic viscosity of the fluid ($m^2\ s^{-1}$)

Figure D-1. Water level elevations at the NRC site.

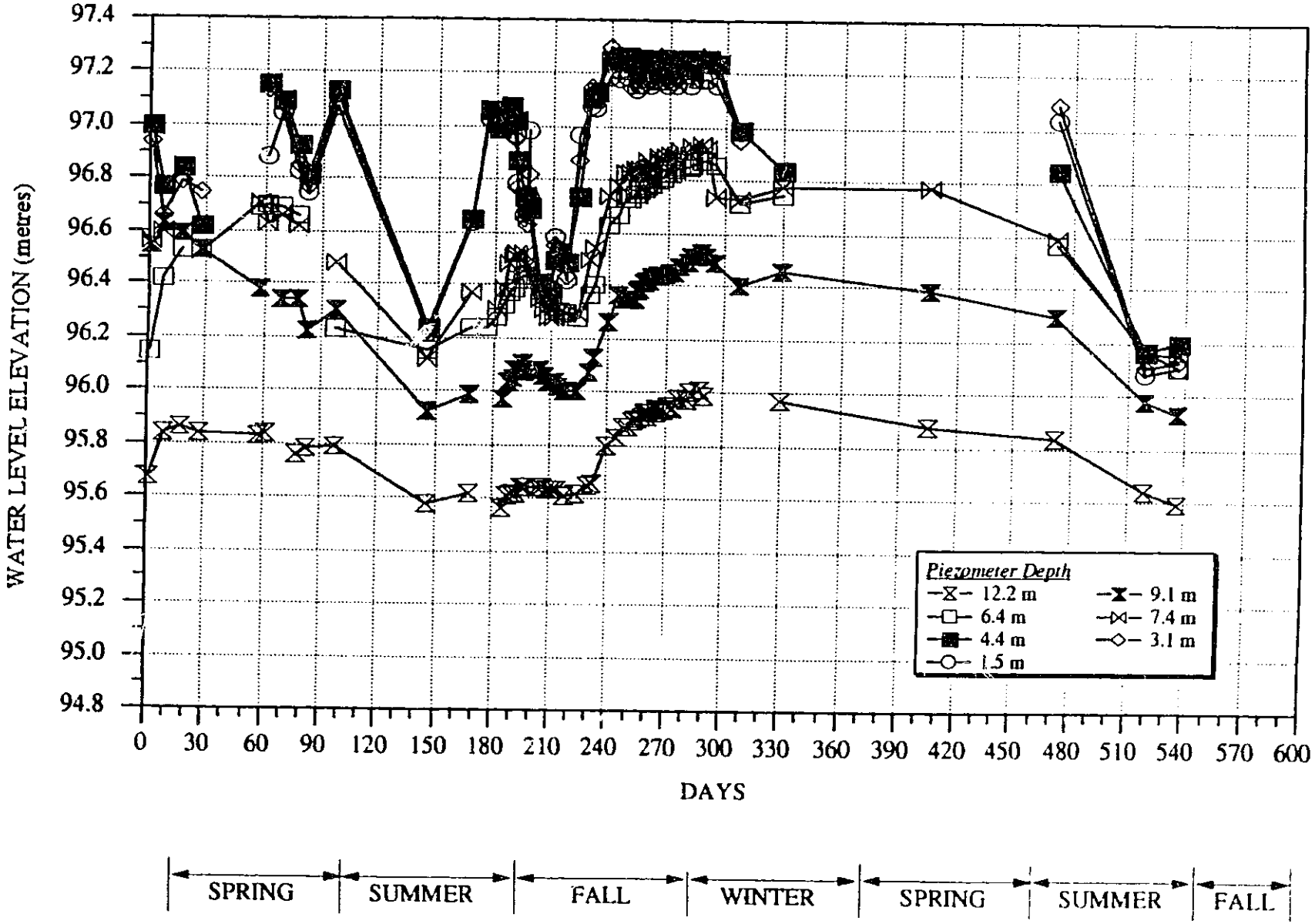

Figure D-2. Water level elevations at the Fallowfield site.

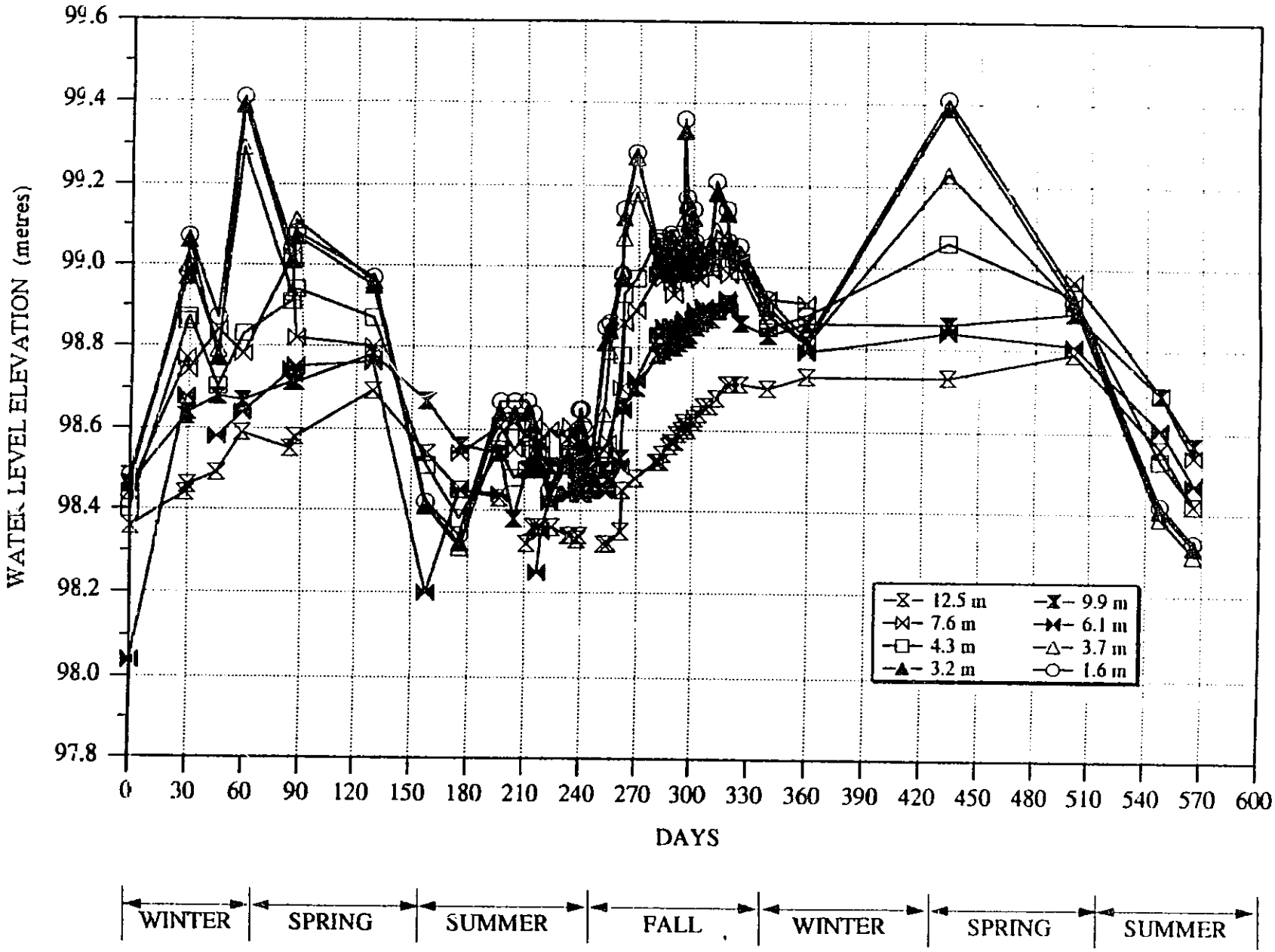

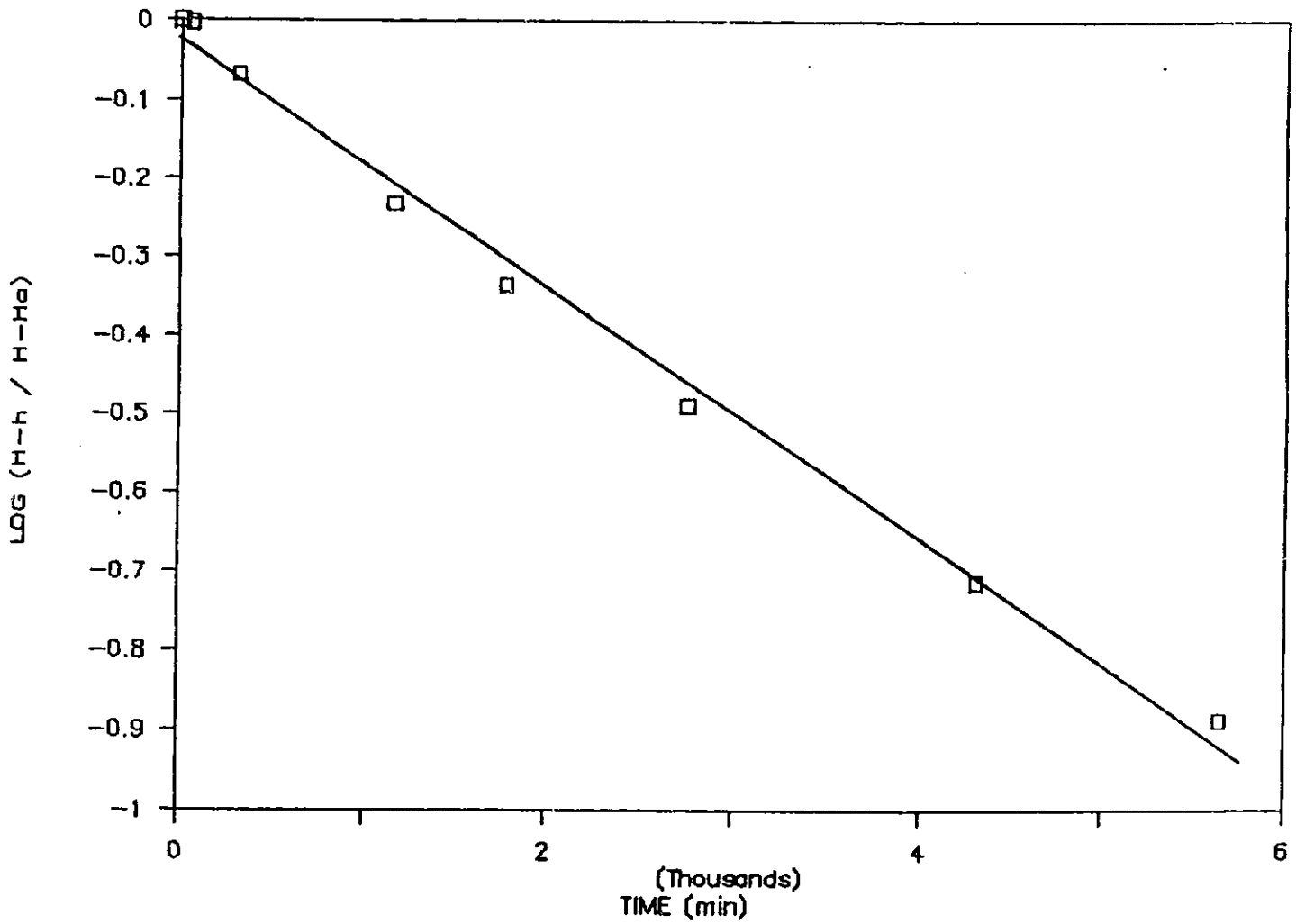

Figure D-3. Slug test result for NRC, piezometer #1, depth 12.2 m.

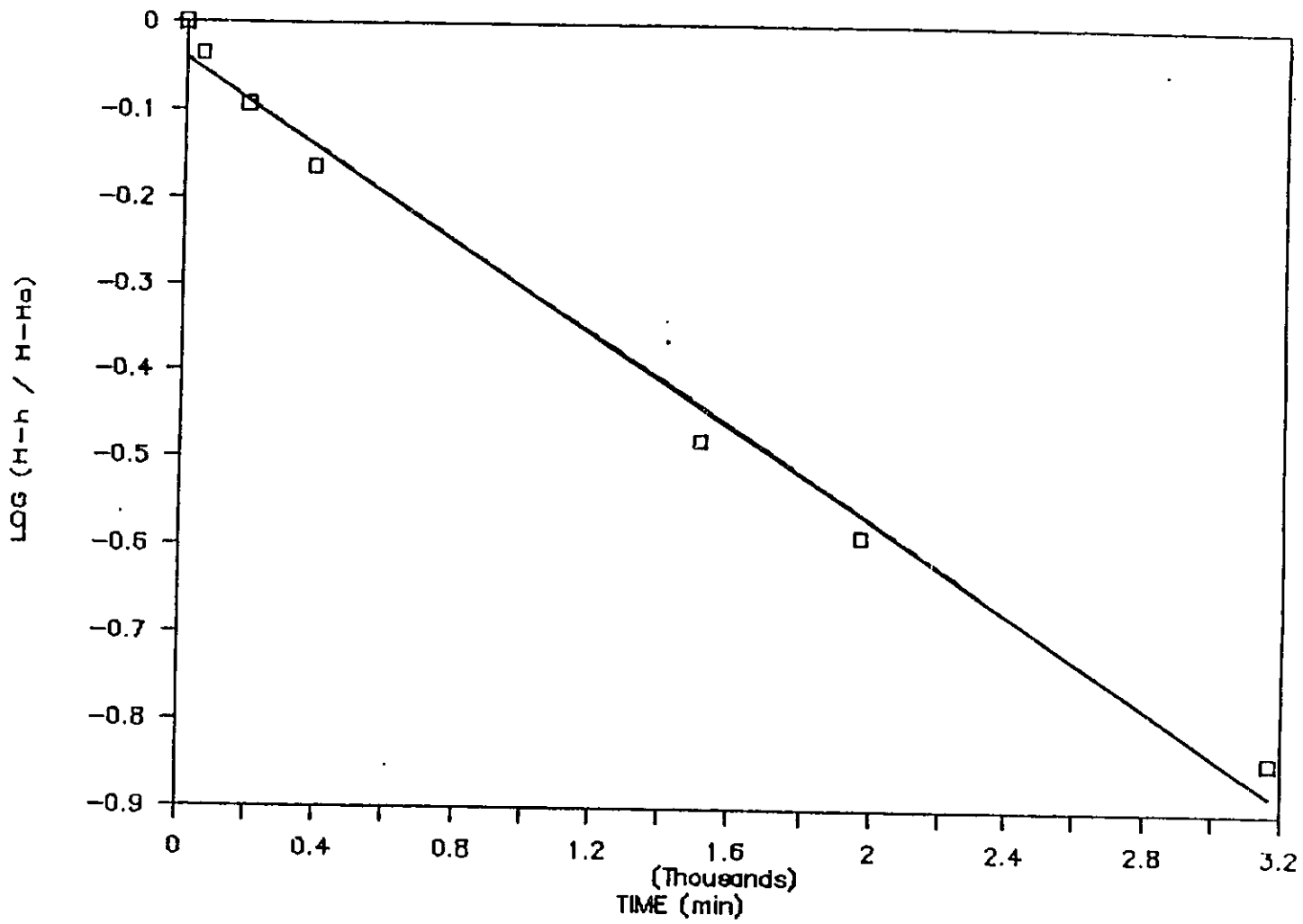

Figure D-4. Slug test result for NRC, piezometer #2, depth 9.1 m.

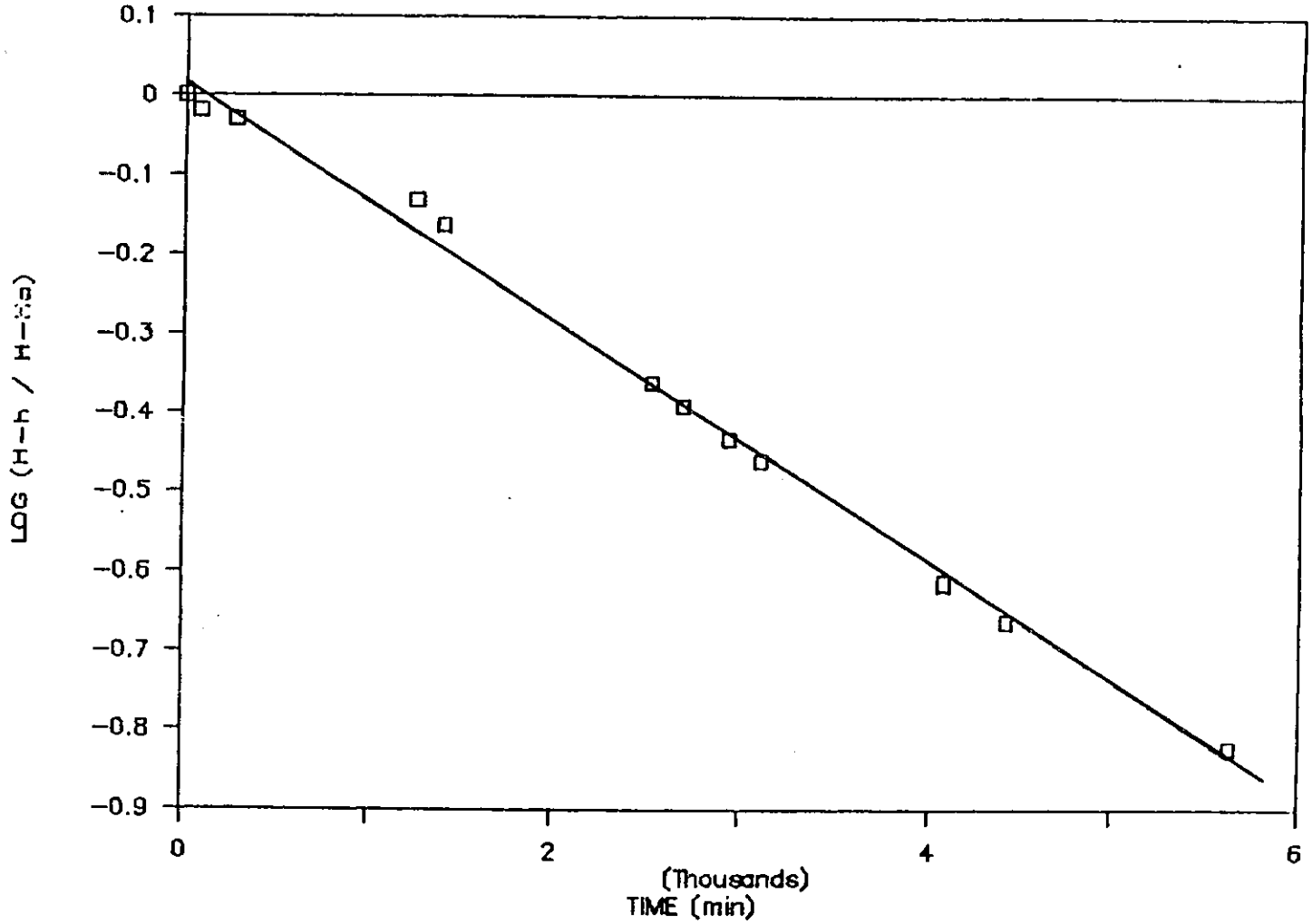

Figure D-5. Slug test result for NRC, piezometer #3, depth 7.4 m.

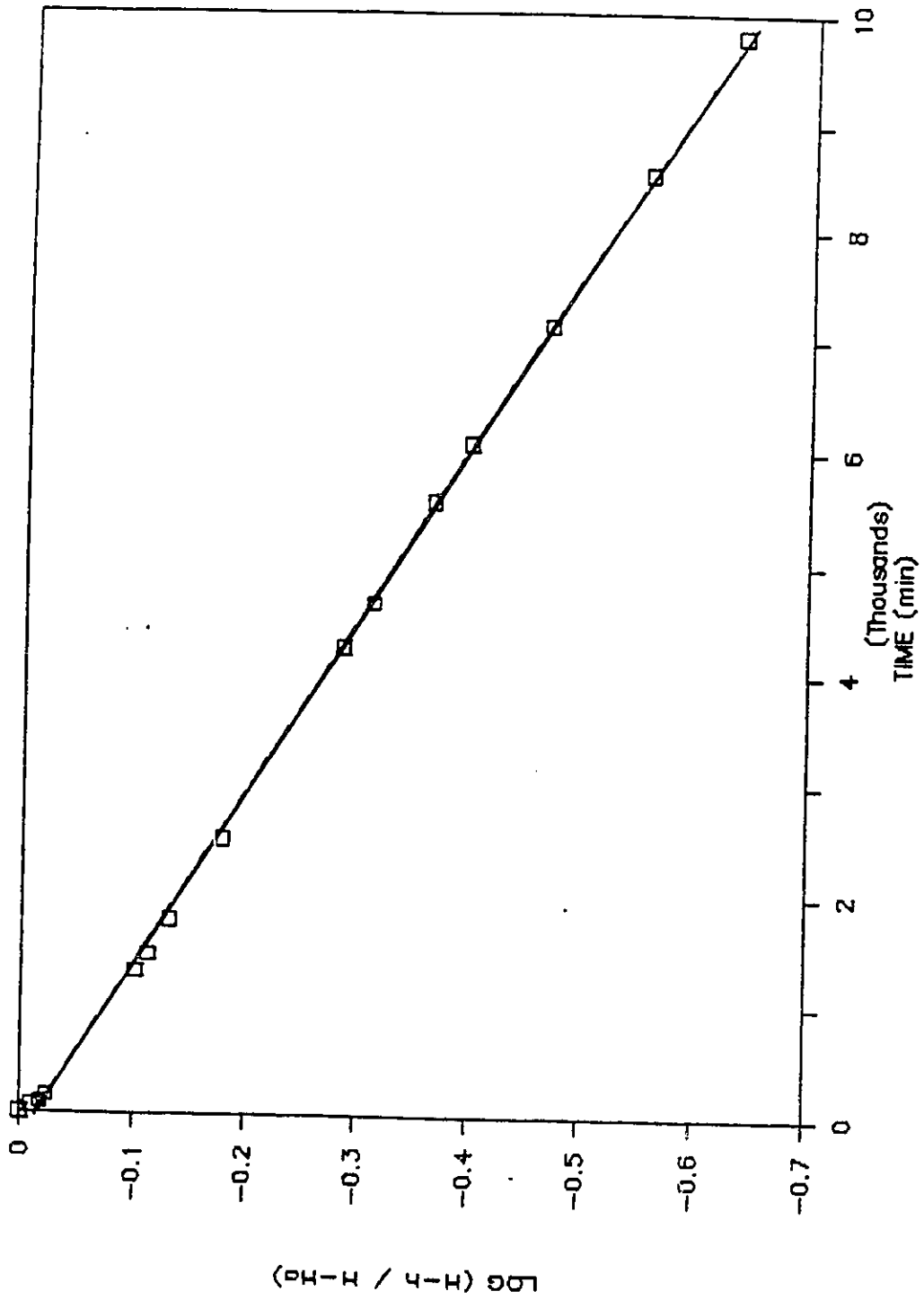

Figure D-6. Slug test result for NRC, piezometer #4, depth 6.1 m.

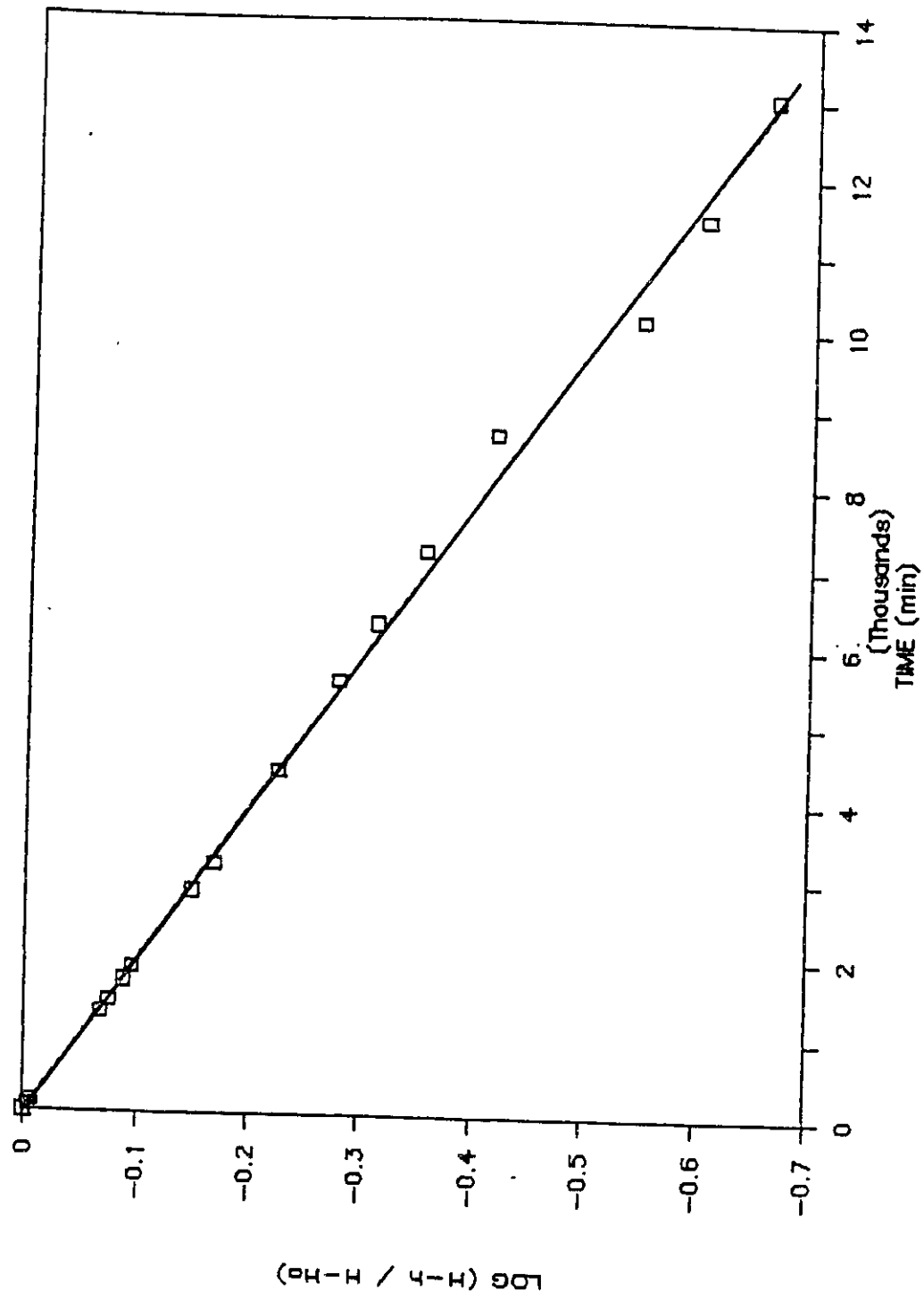

Figure D-7. Slug test result for NRC, piezometer #5, depth 6.4 m.

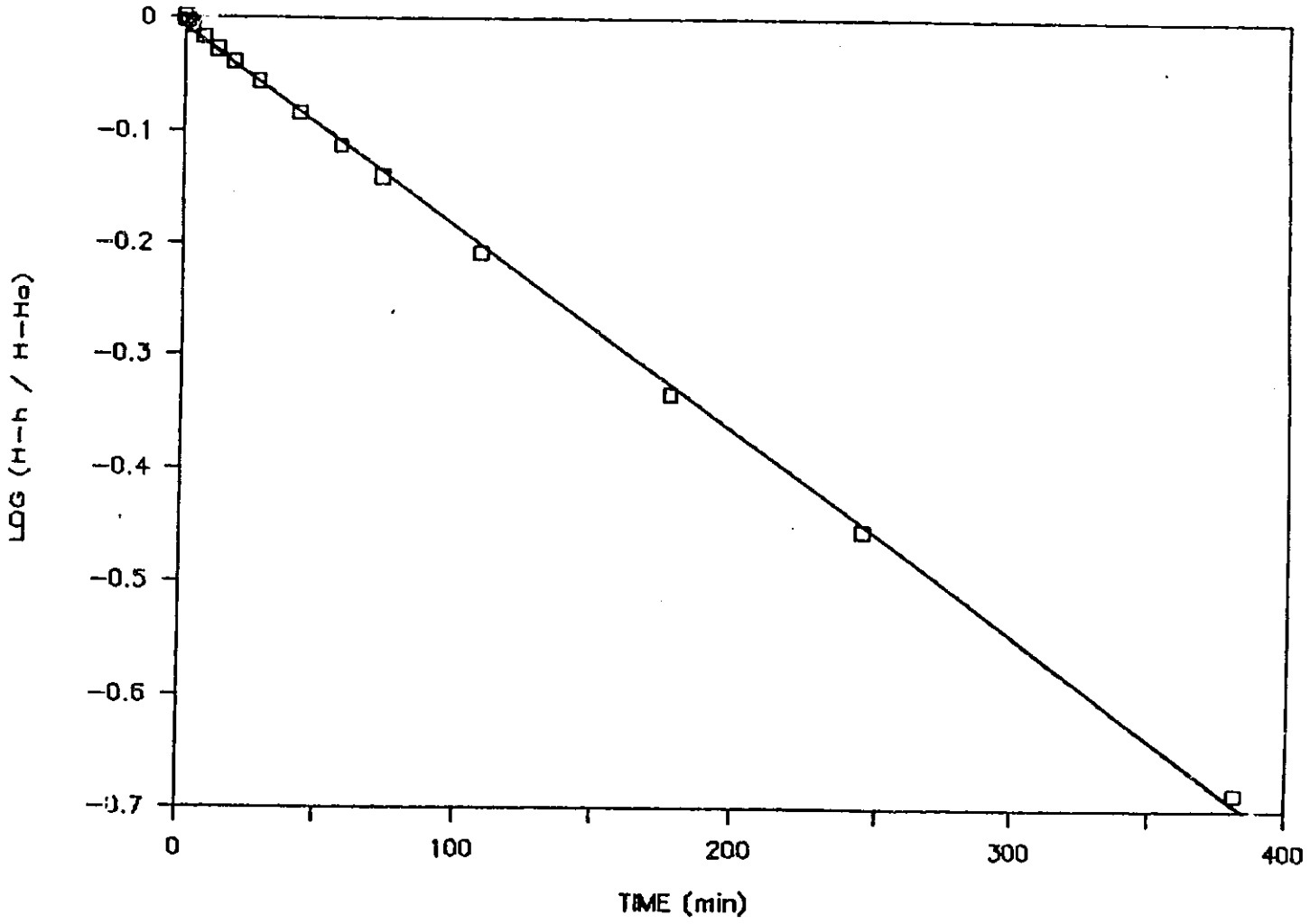

Figure D-8. Slug test result for NRC, piezometer #6, depth 4.4 m.

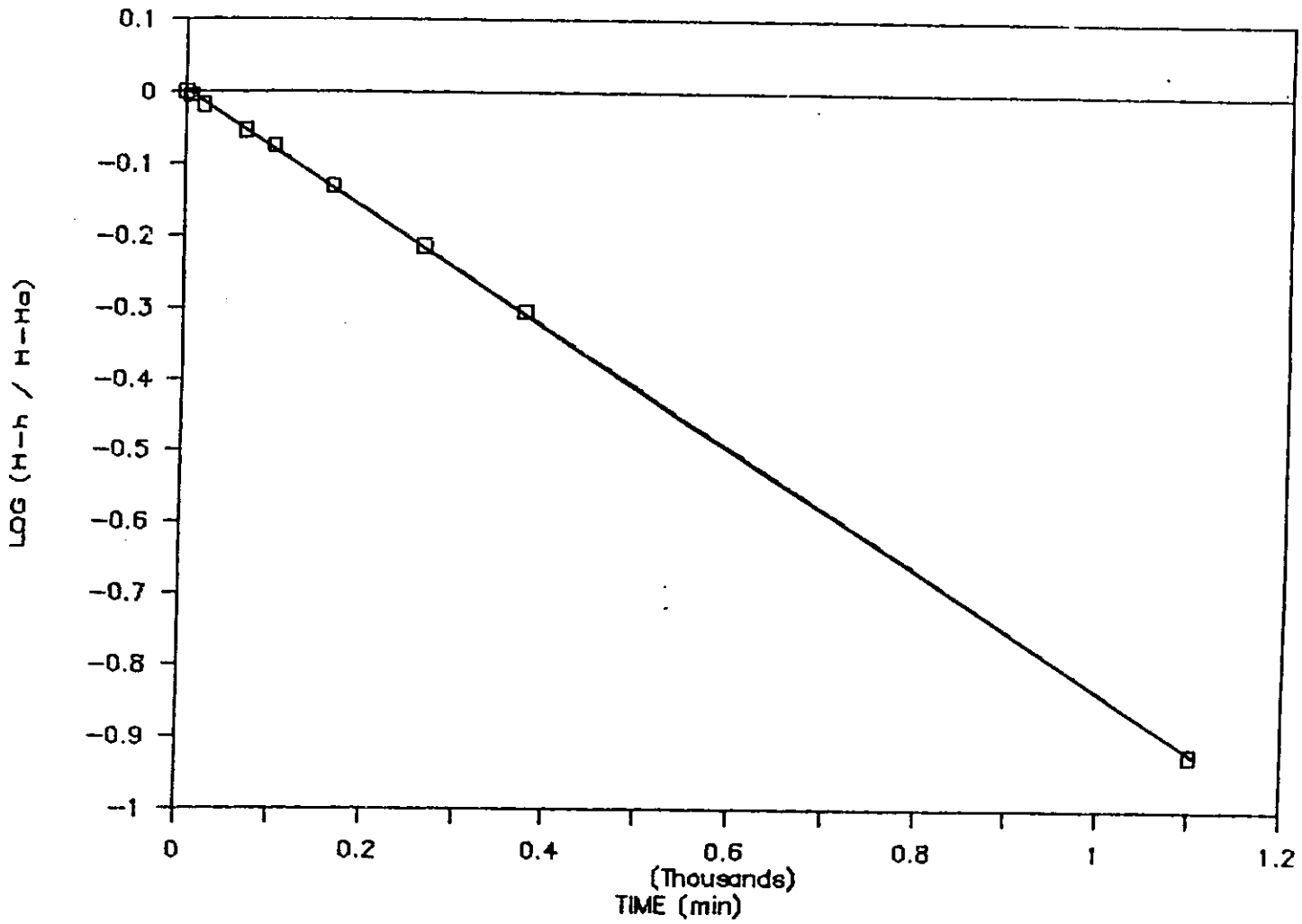

Figure D-9. Slug test result for NRC, piezometer #7, depth 3.5 m.

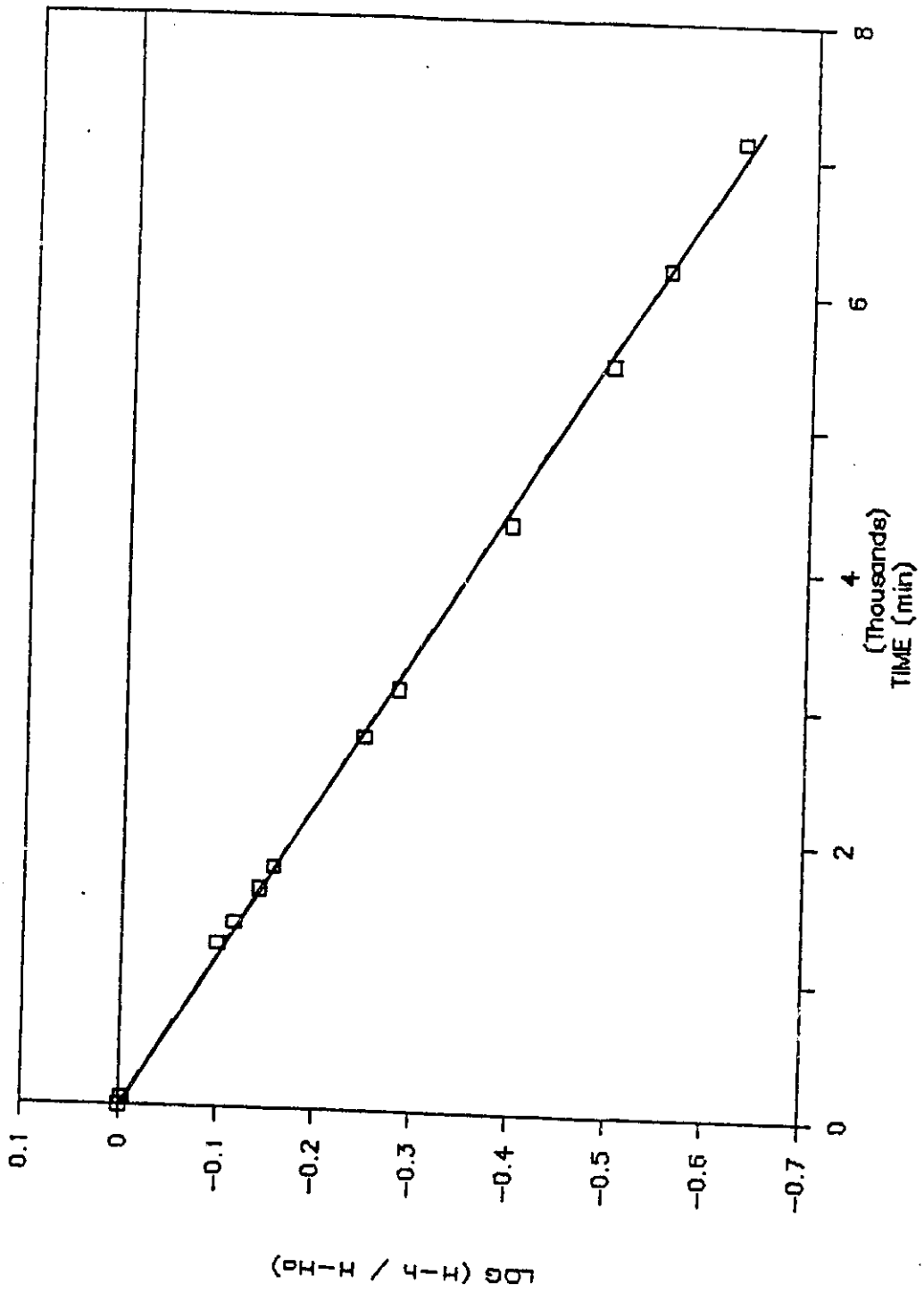

Figure D-10. Slug test result for NRC, piezometer #8, depth 3.0 m.

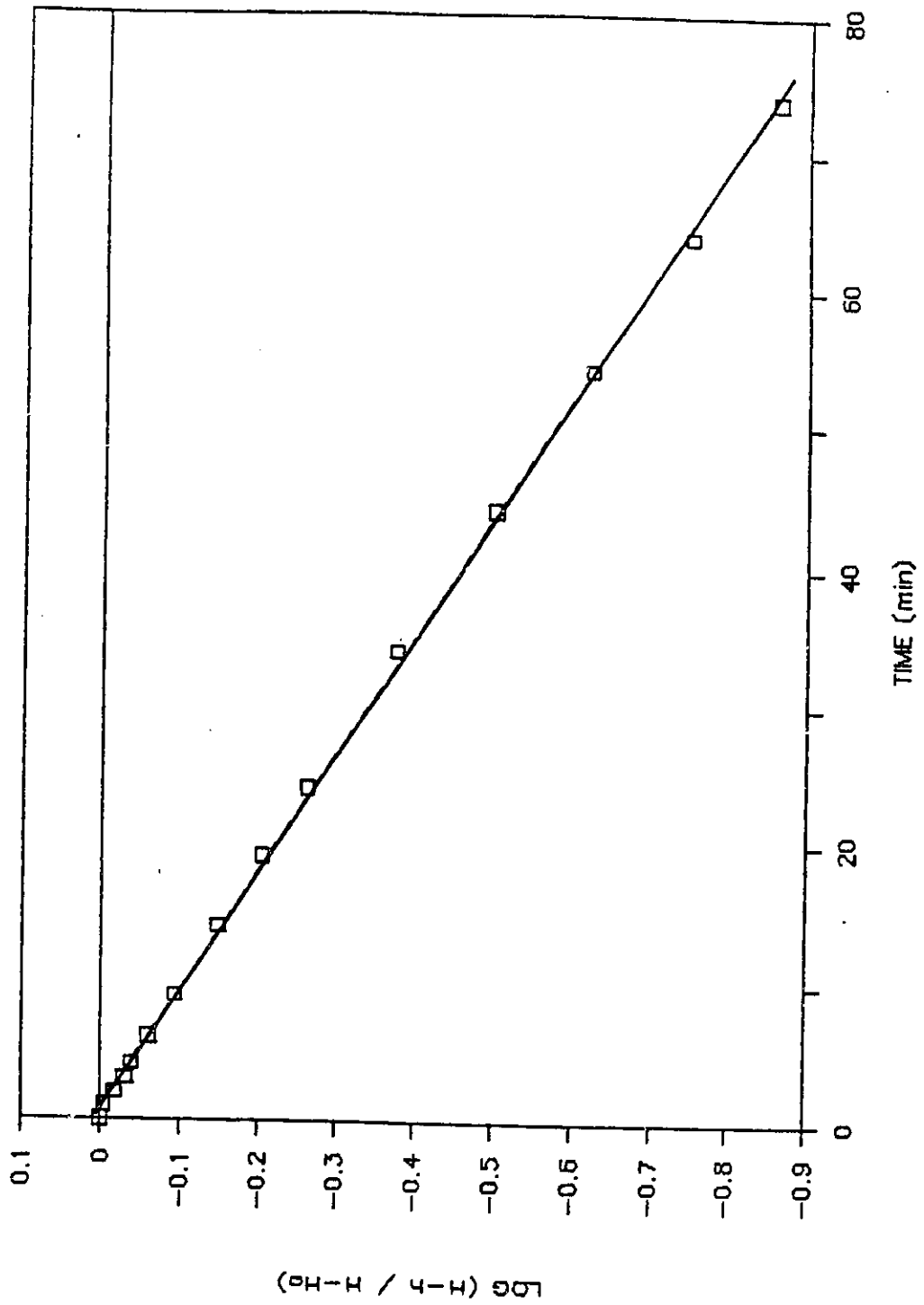

Figure D-11. Slug test result for NRC, piezometer #9, depth 3.1 m.

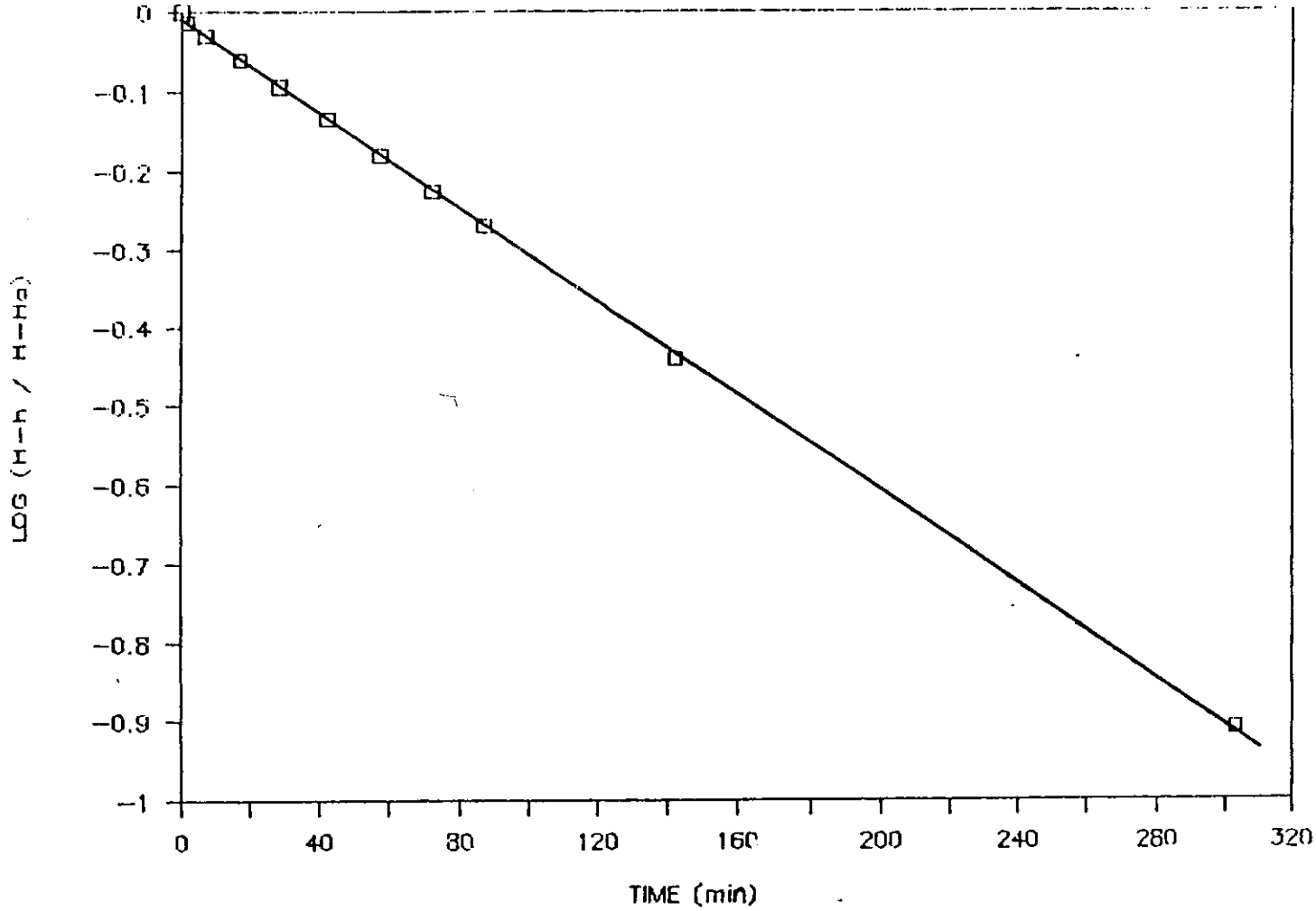

Figure D-12. Slug test result for NRC, piezometer #10, depth 2.2 m.

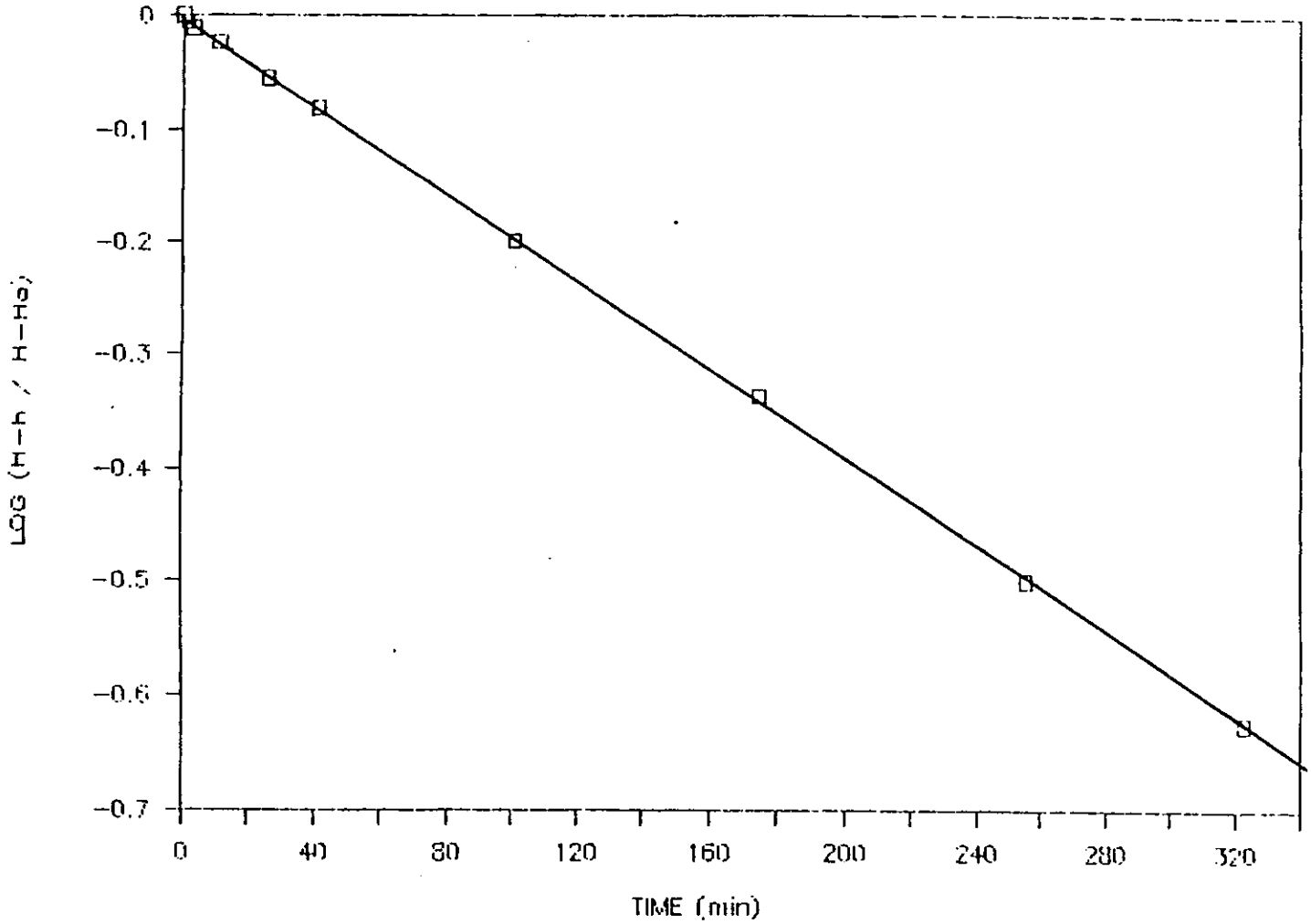

Figure D-13. Slug test result for NRC, piezometer #11, depth 1.5 m.

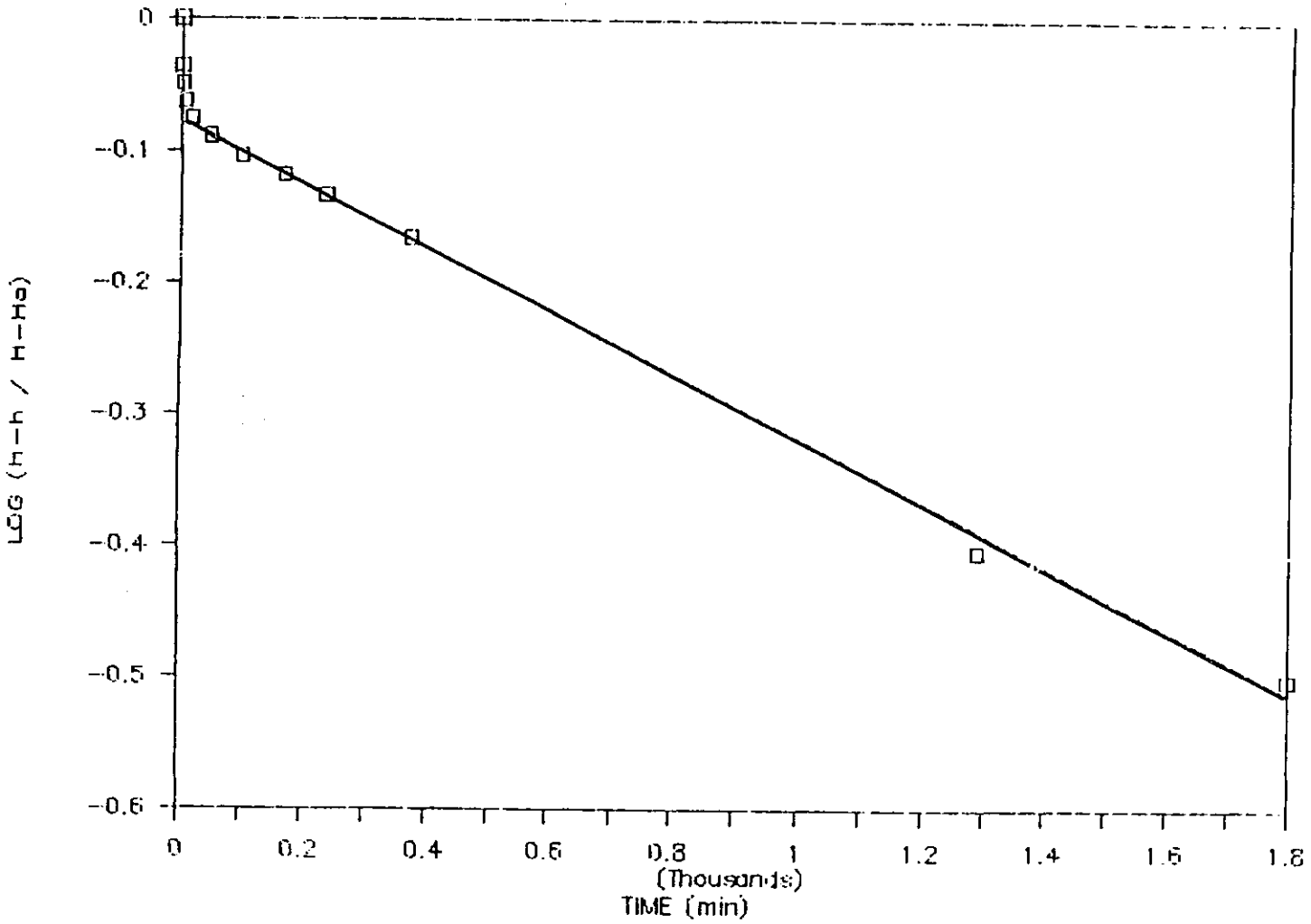

Figure D-14. Slug test result for NRC, piezometer #12, depth 0.70 m.

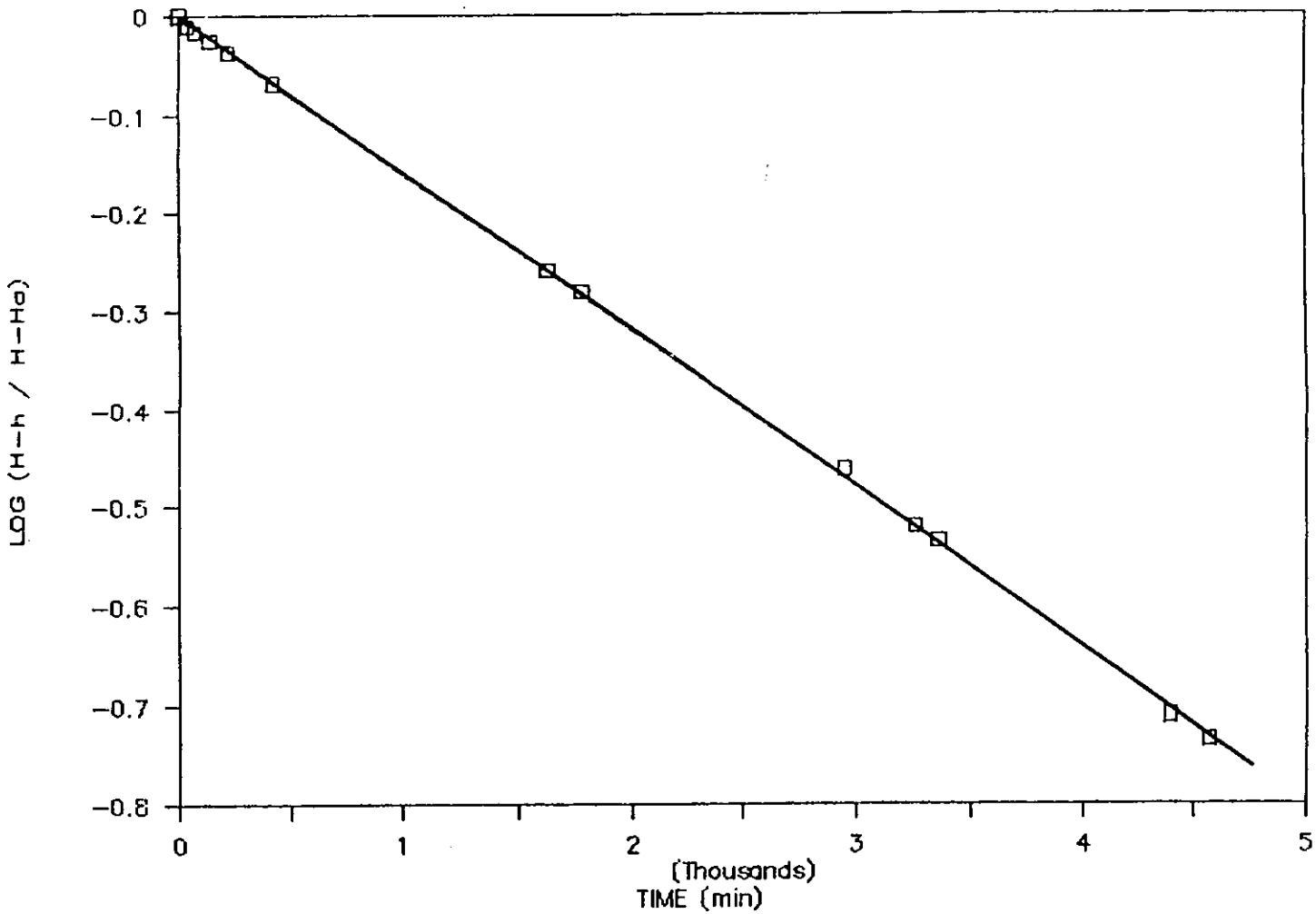

Figure D-15. Slug test result for Fallowfield, piezometer #1, depth 12.5 m.

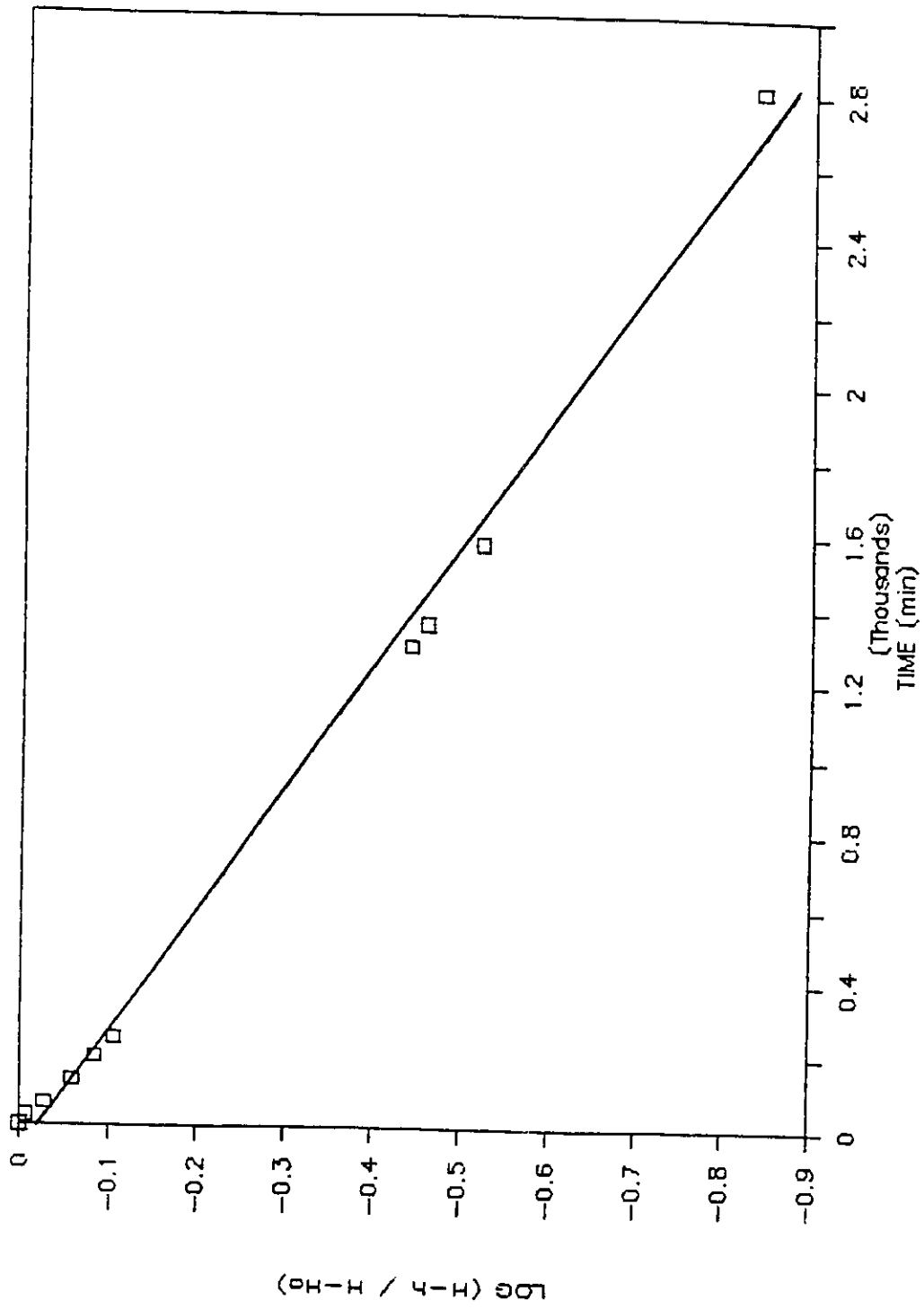

Figure D-16. Slug test result for Fallowfield, piezometer #2, depth 9.9 m.

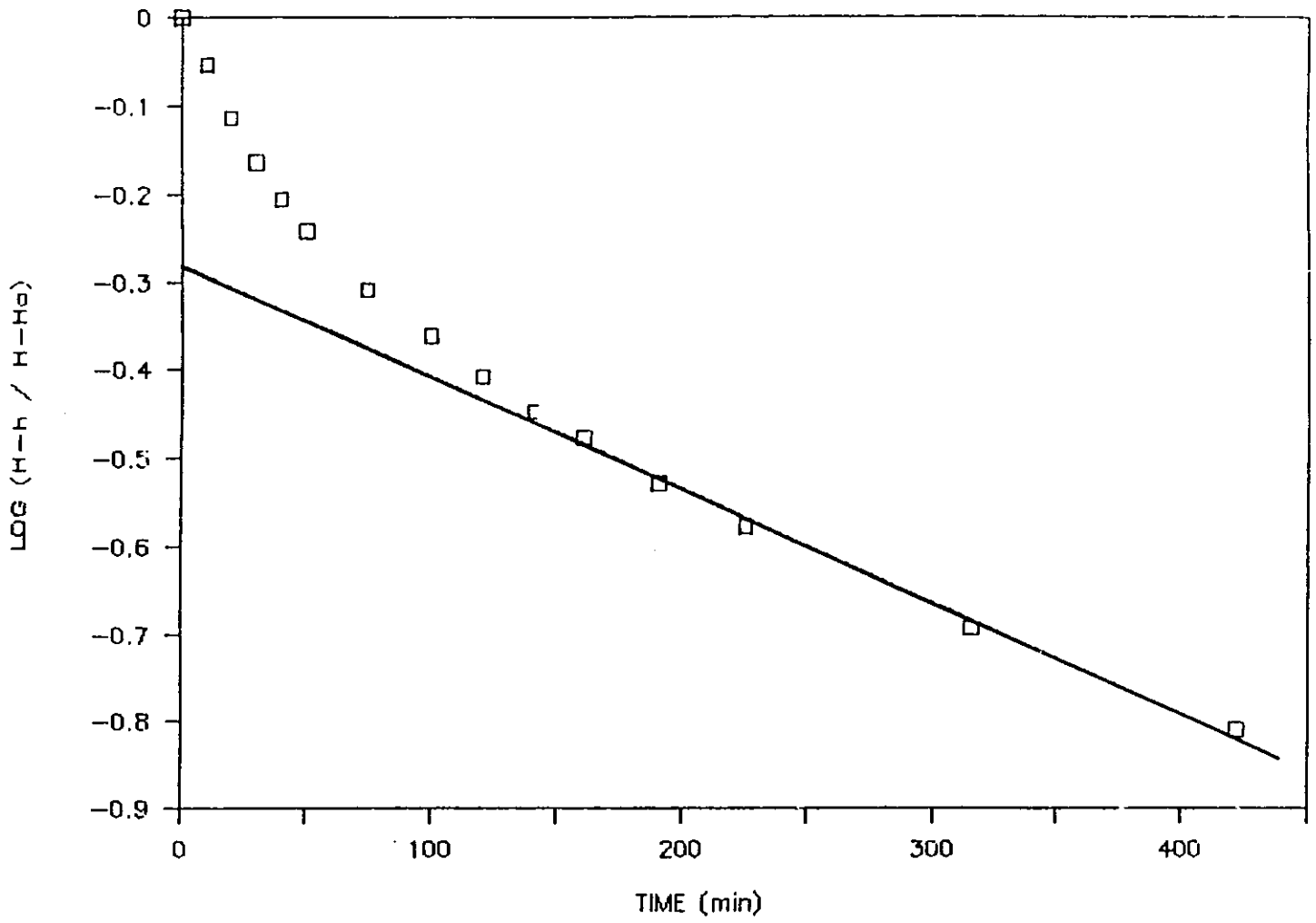

Figure D-17. Slug test result for Fallowfield, piezometer #3, depth 7.6 m.

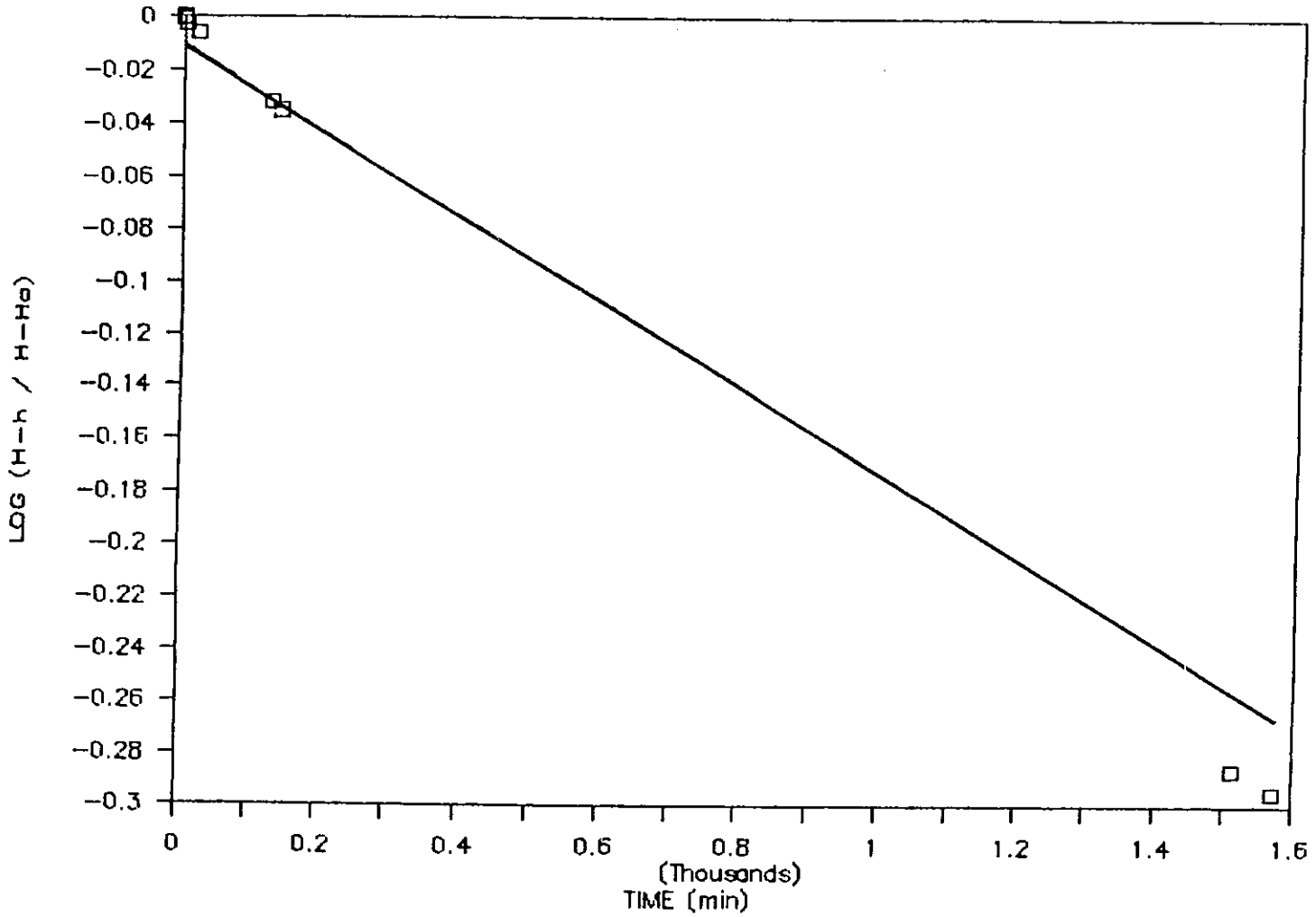

Figure D-18. Slug test result for Fallowfield, piezometer #4, depth 6.1 m.

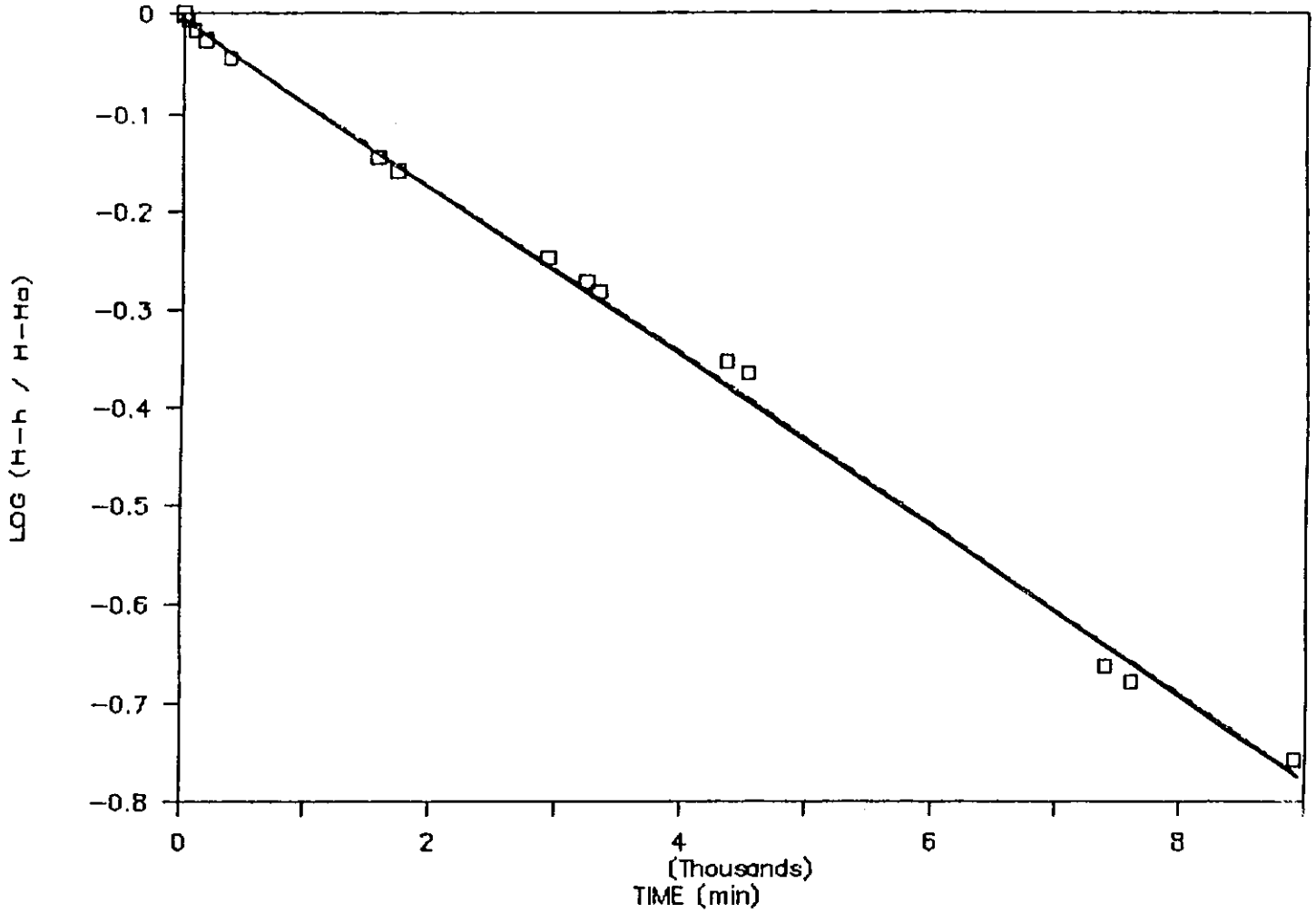

Figure D-19. Slug test result for Fallowfield, piezometer #5, depth 4.3 m.

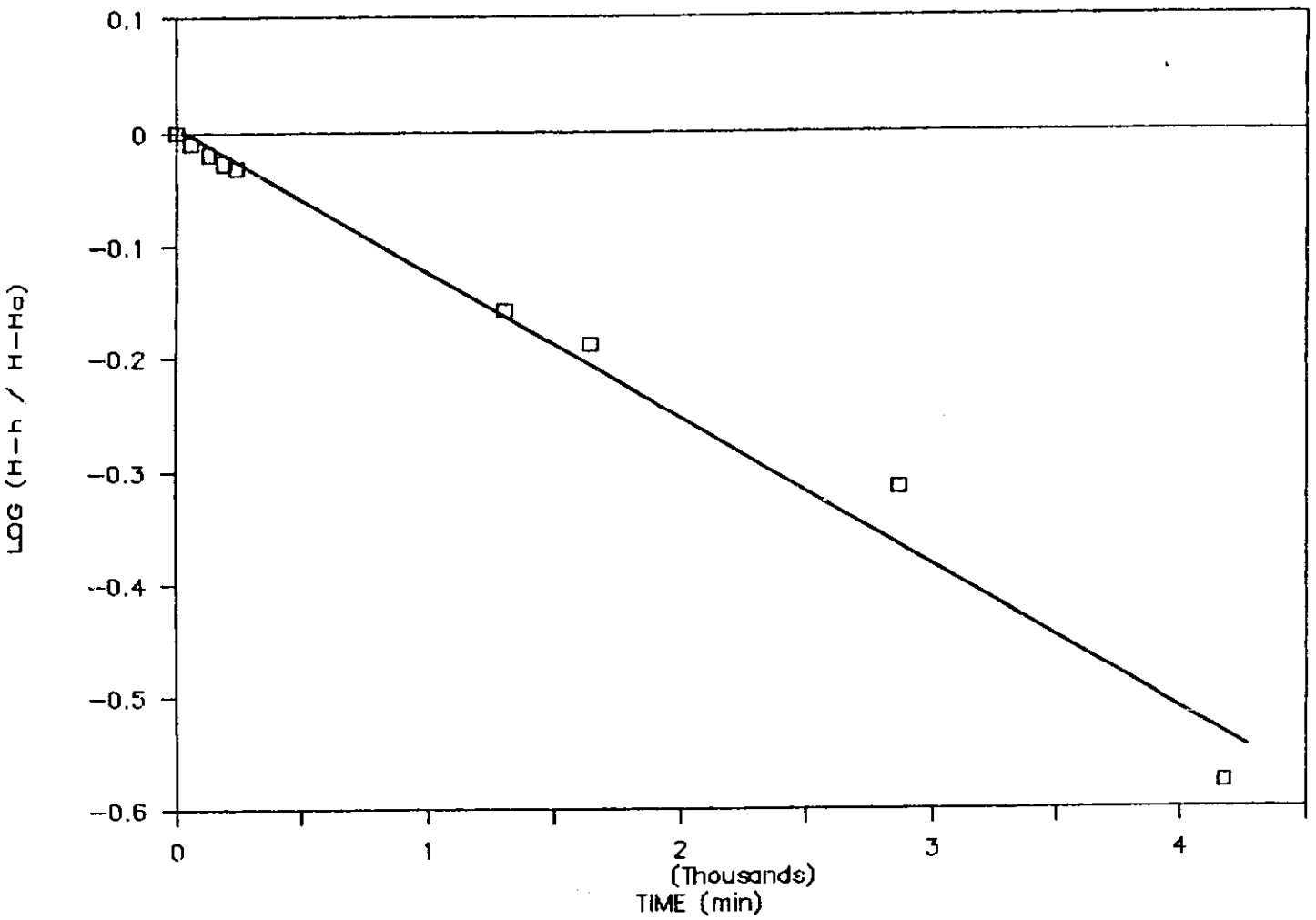

Figure D-20. Slug test result for Fallowfield, piezometer #6, depth 4.4 m.

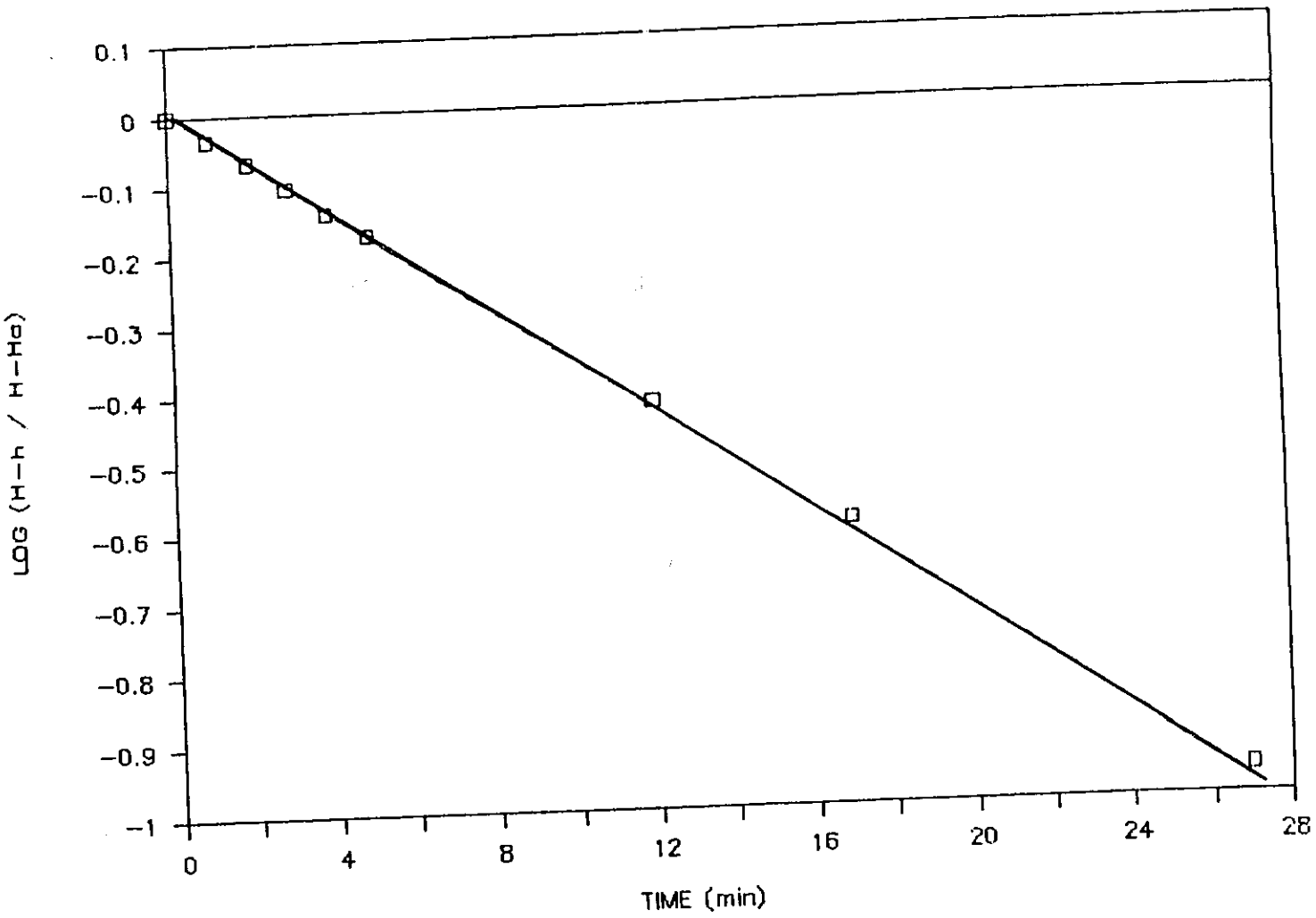

Figure D-21. Slug test result for Fallowfield, piezometer #7, depth 3.7 m.

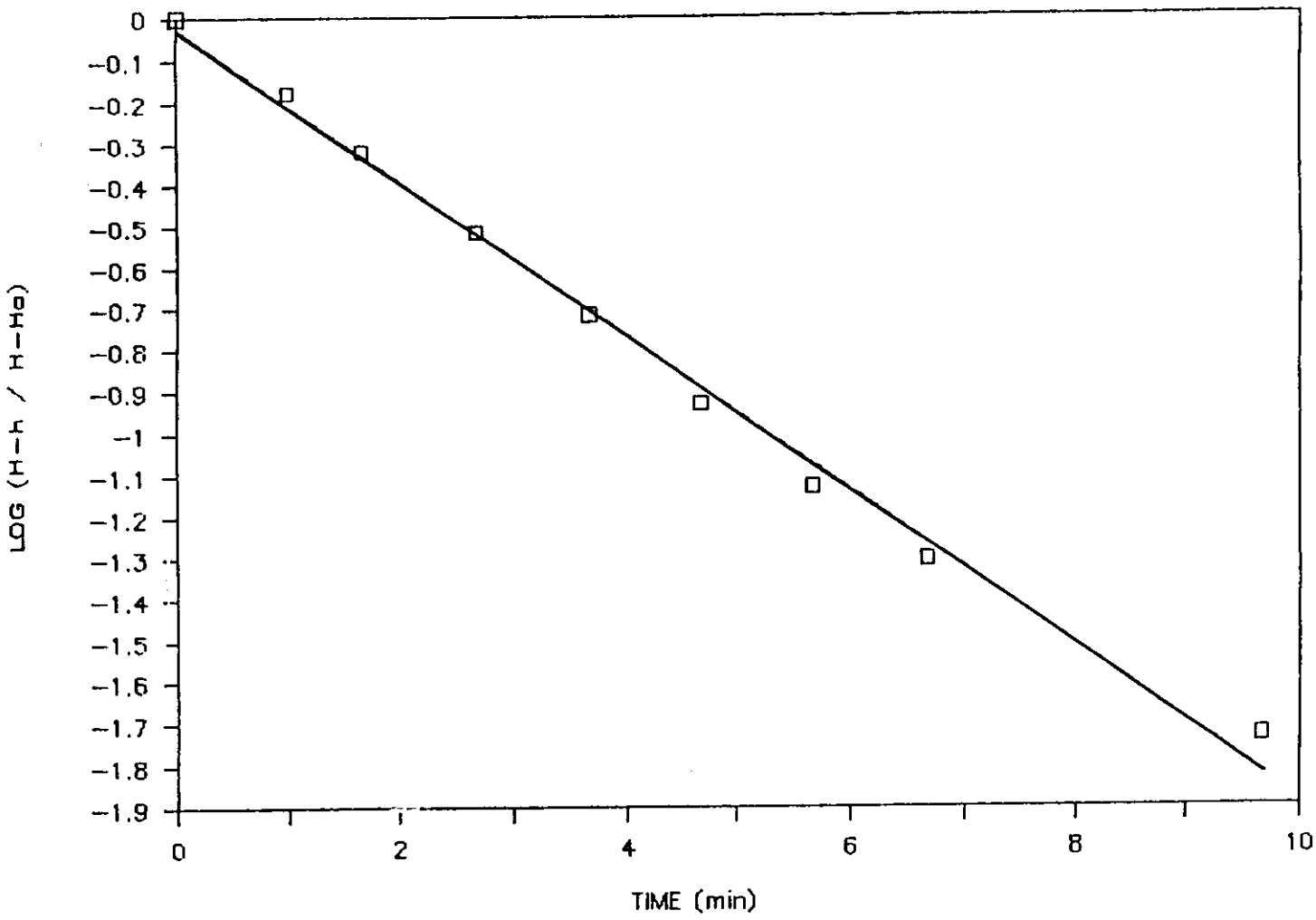

Figure D-22. Slug test result for Fallowfield, piezometer #8, depth 3.2 m.

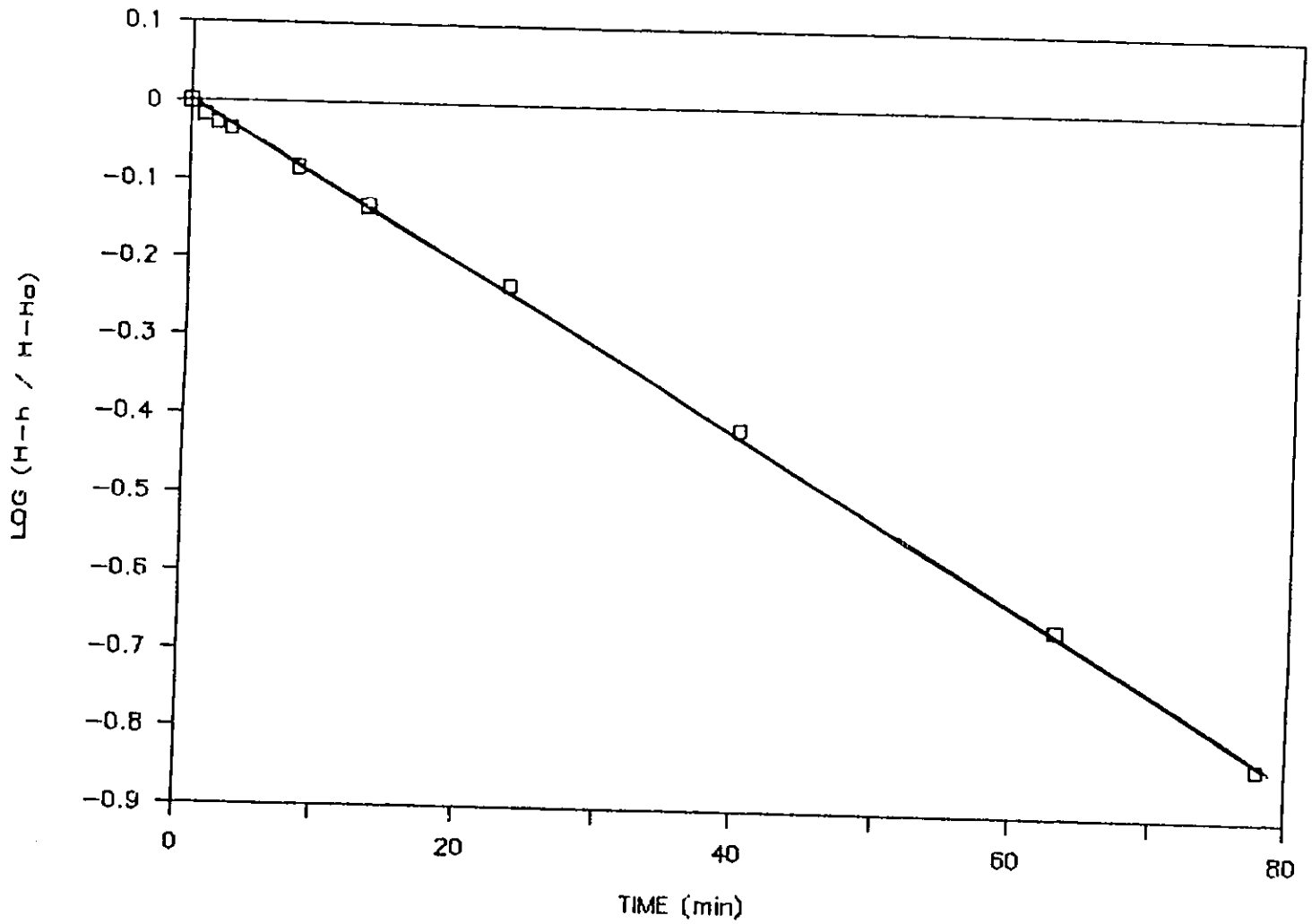

Figure D-23. Slug test result for Fallowfield, piezometer #9, depth 3.0 m.

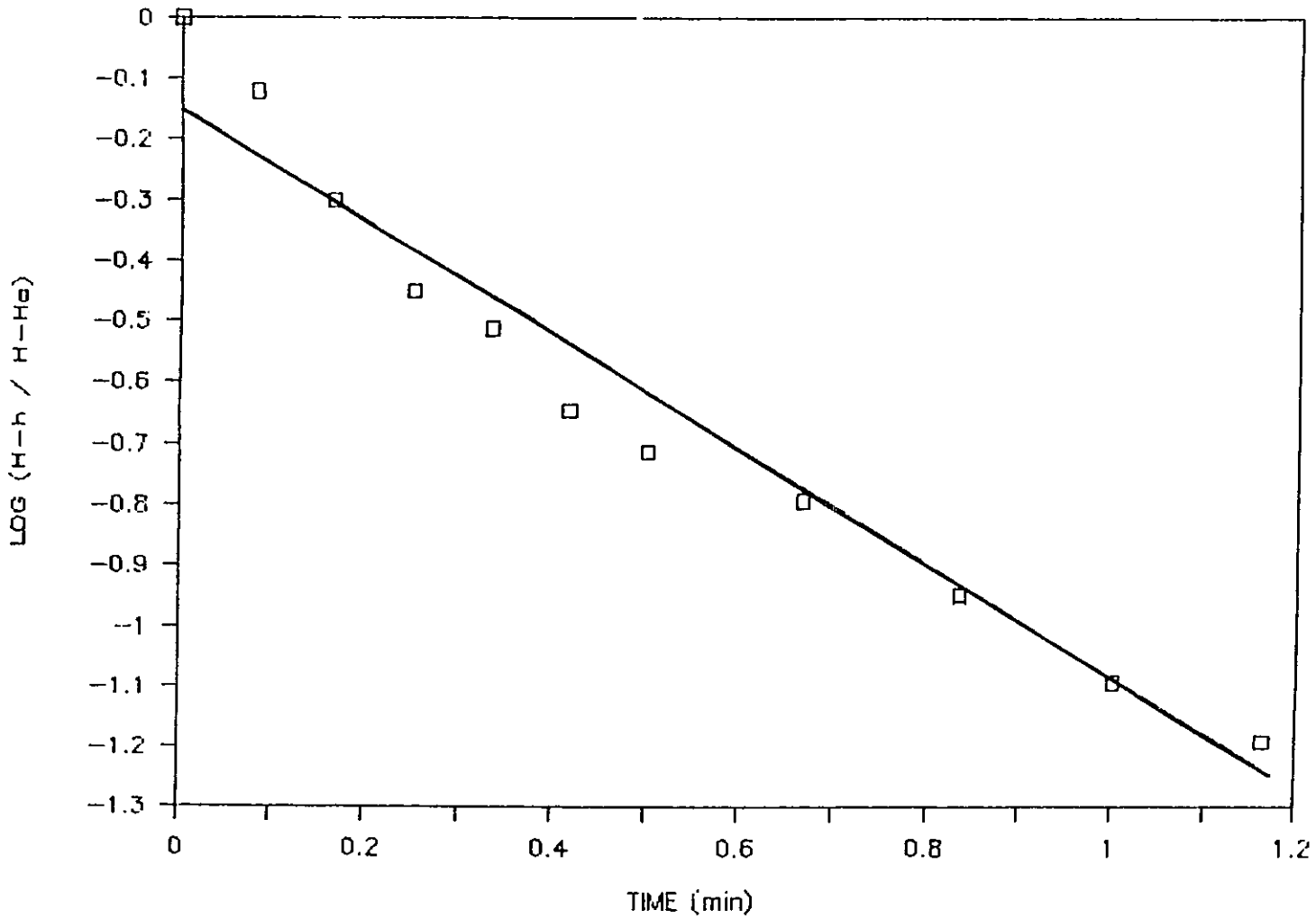

Figure D-24. Slug test result for Fallowfield, piezometer#10, depth 2.1 m.

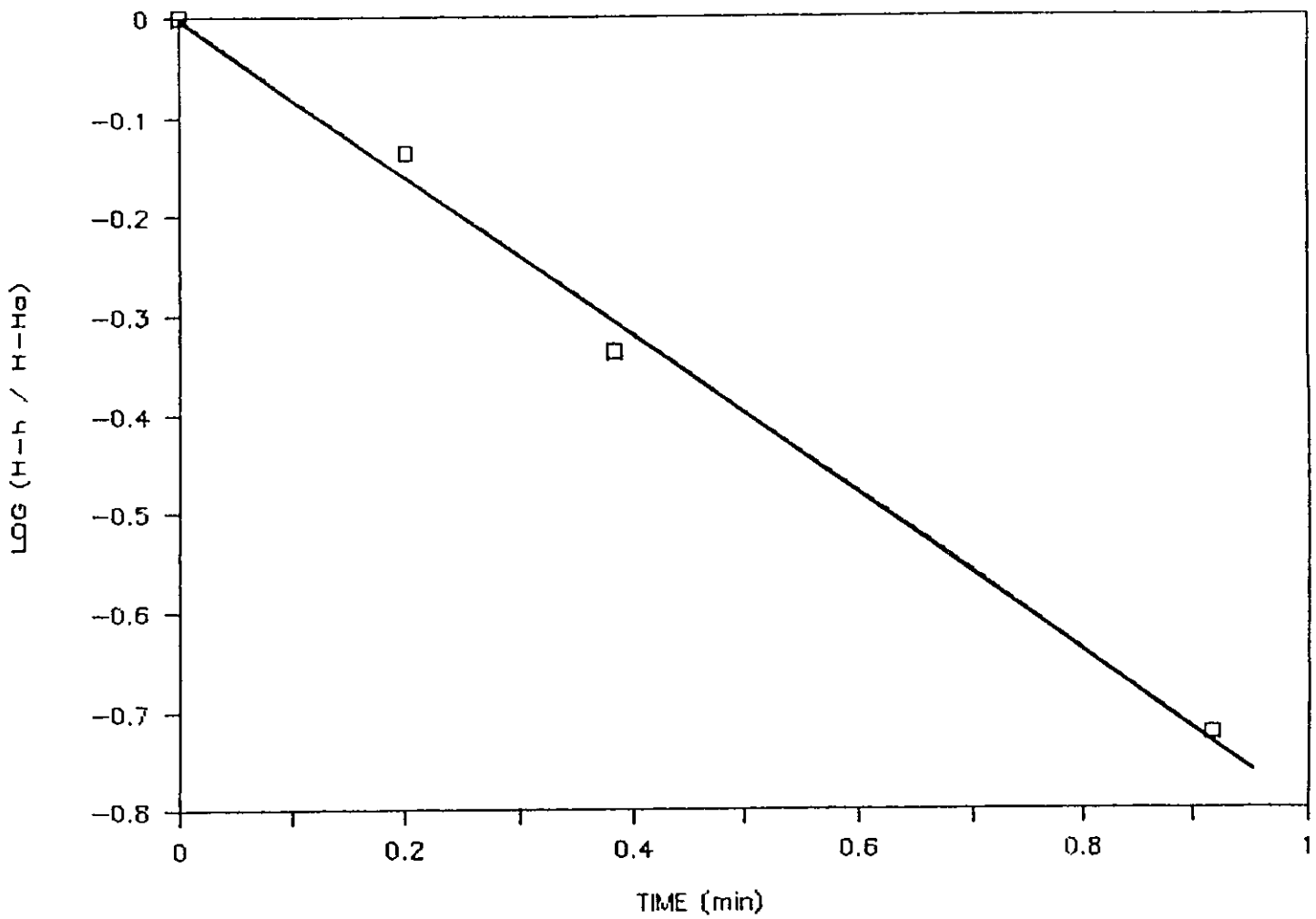

Figure D-25. Slug test result for Fallowfield, piezometer#11, depth 1.6 m.

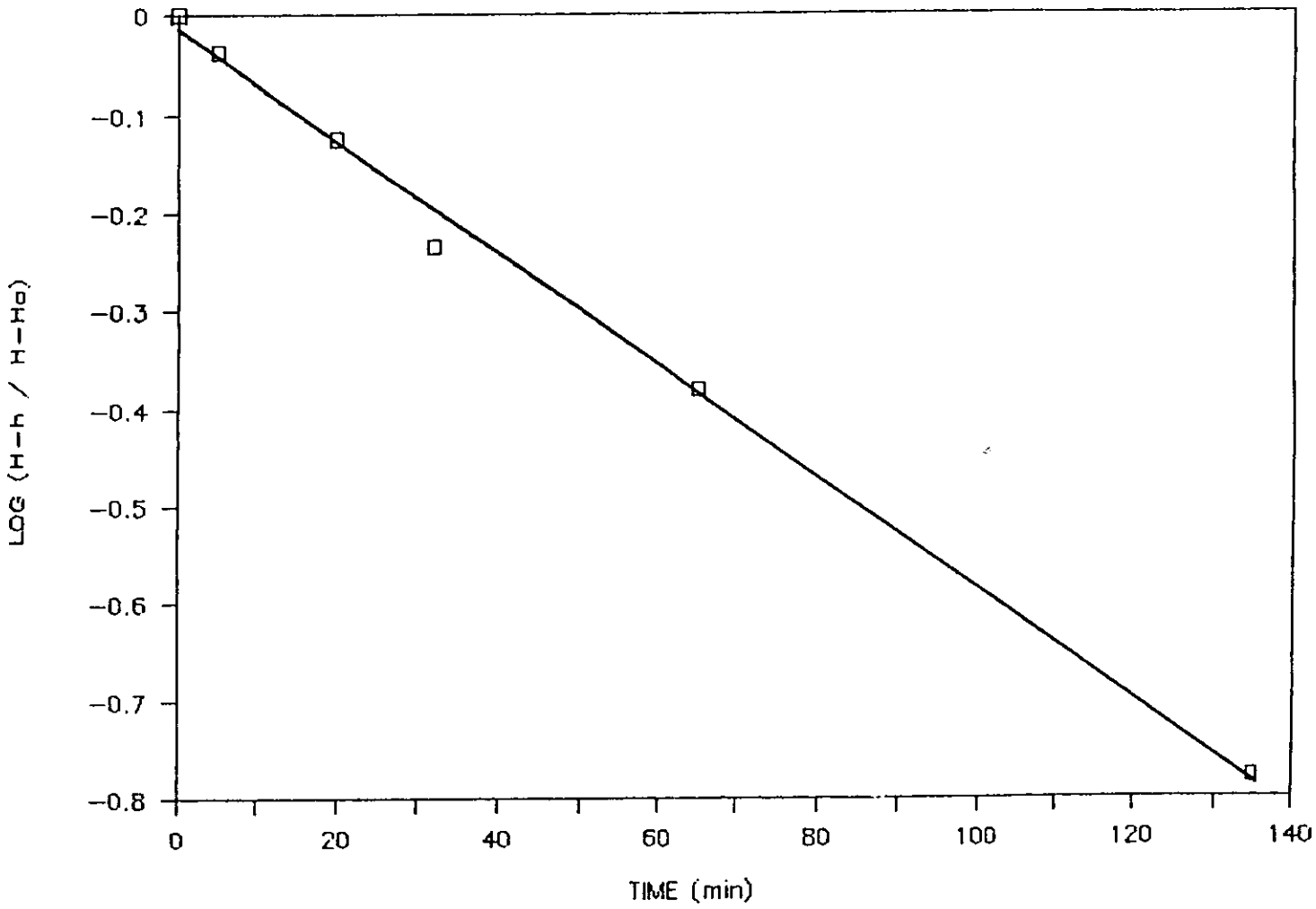

Figure D-26. Slug test result for Fallowfield, piezometer#12, depth 0.80 m.

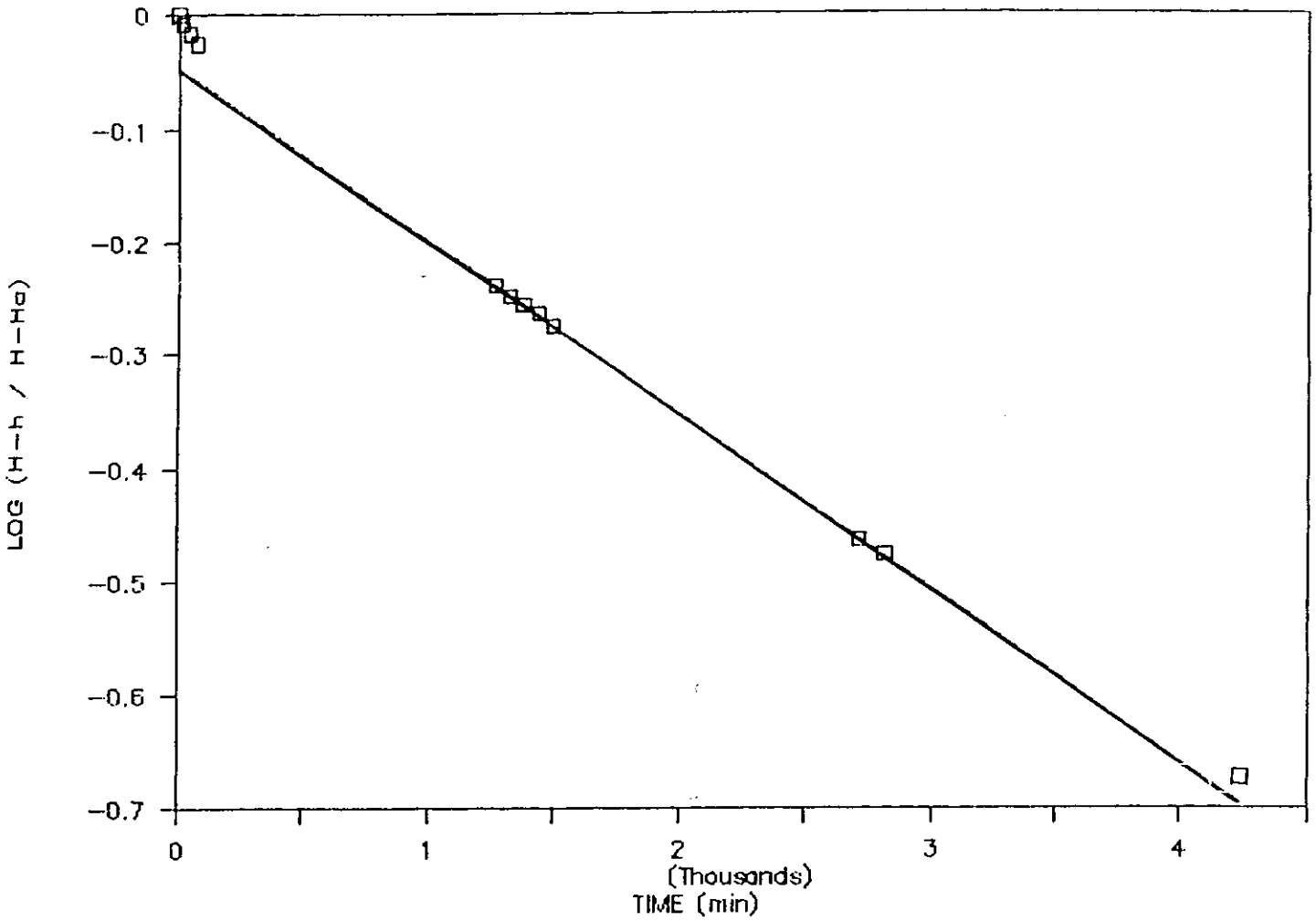

Figure D-27. Slug test result for Renfrew, piezometer #1, depth 12.2 m.

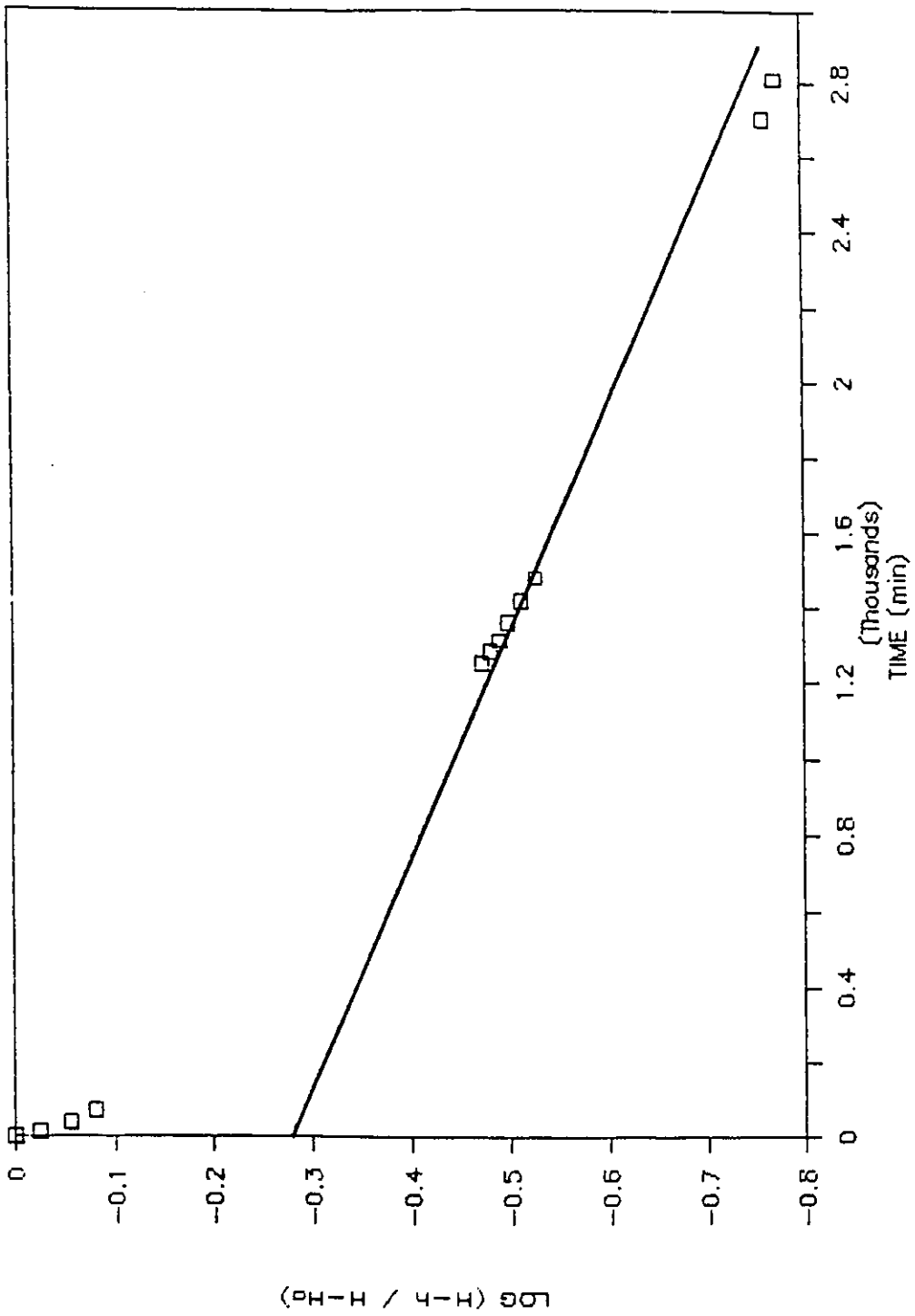

Figure D-28. Slug test result for Renfrew, piezometer #2, depth 9.15 m.

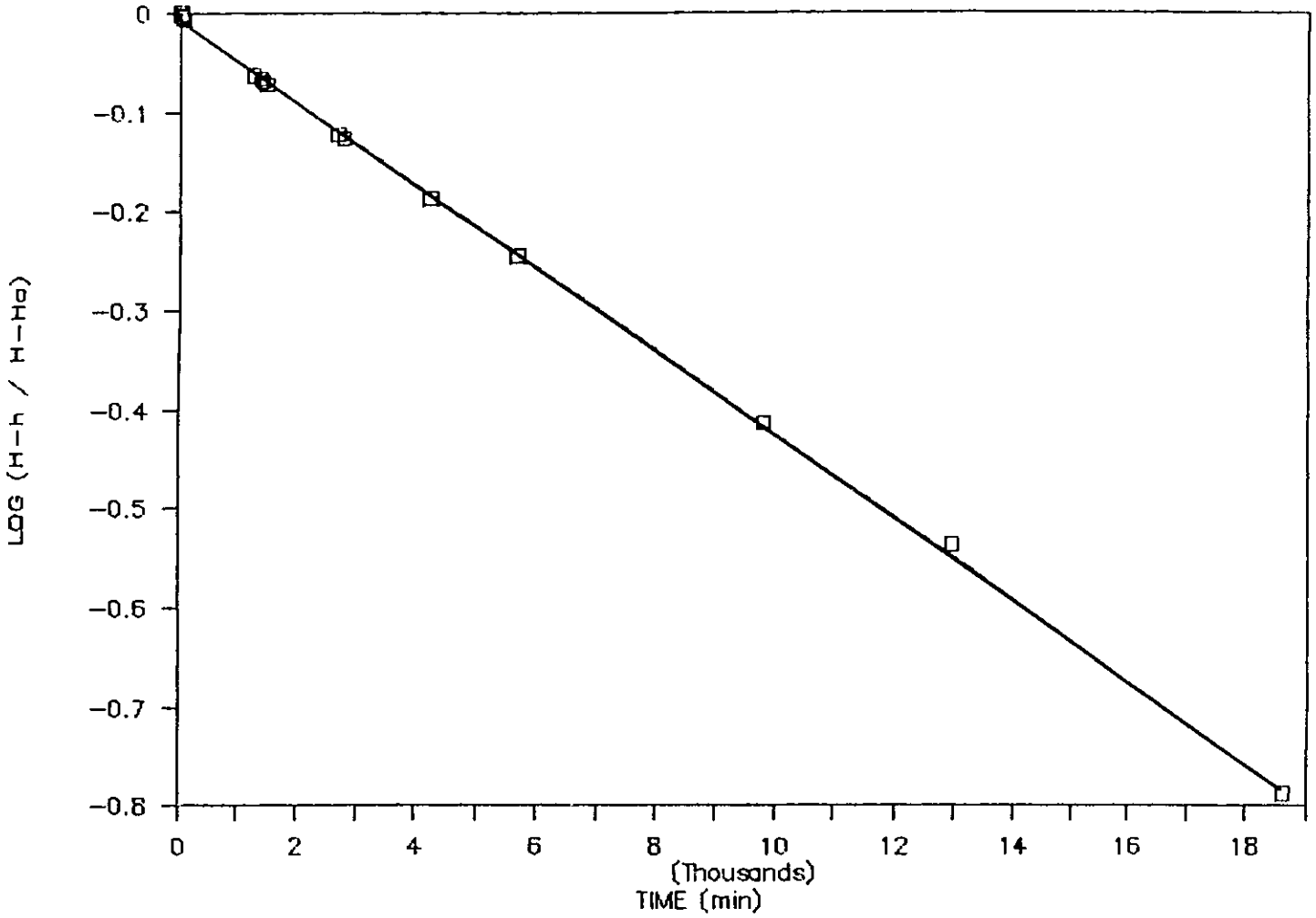

Figure D-29. Slug test result for Renfrew, piezometer #3, depth 8.4 m.

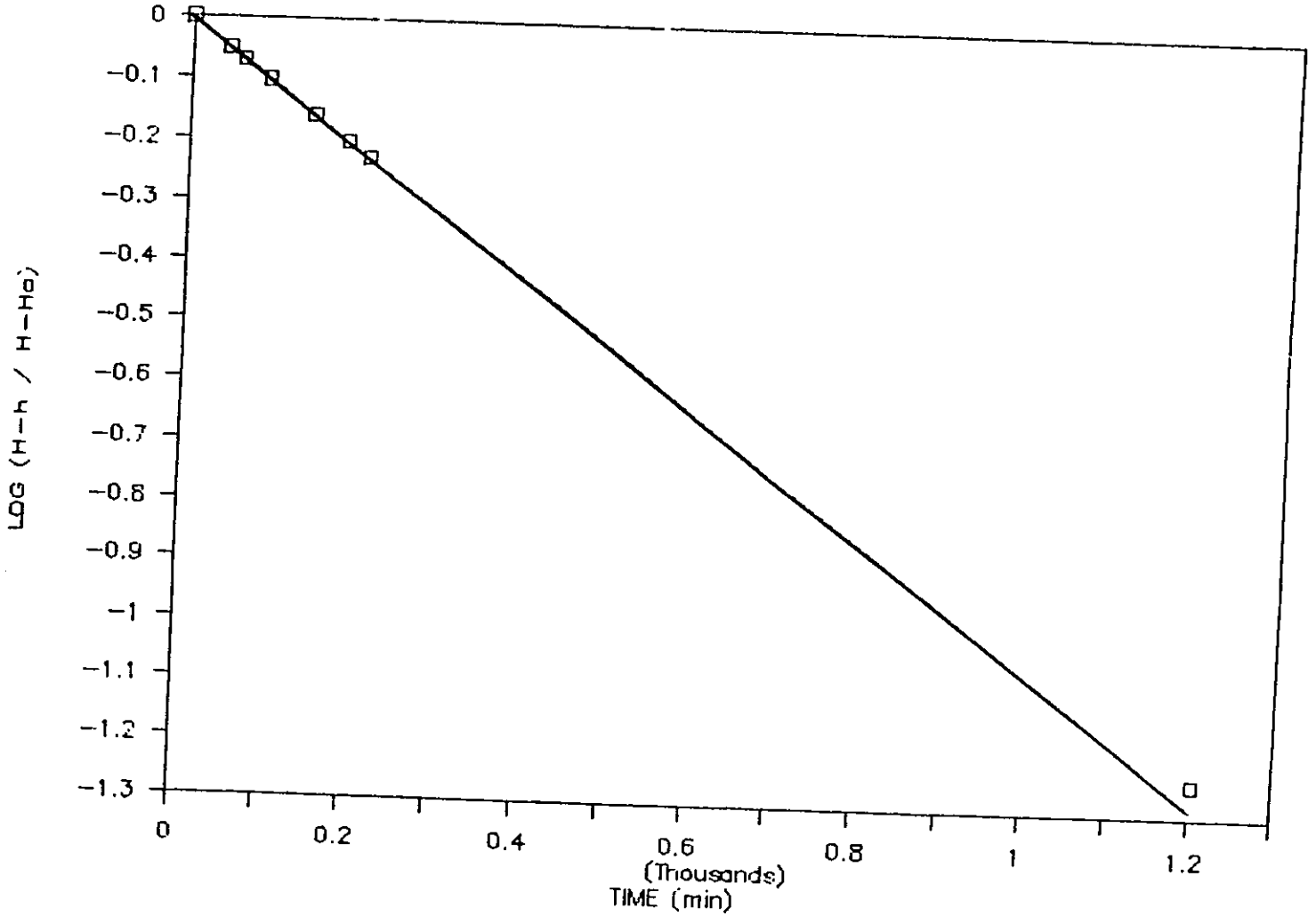

Figure D-30. Slug test result for Renfrew, piezometer #4, depth 5.9 m.

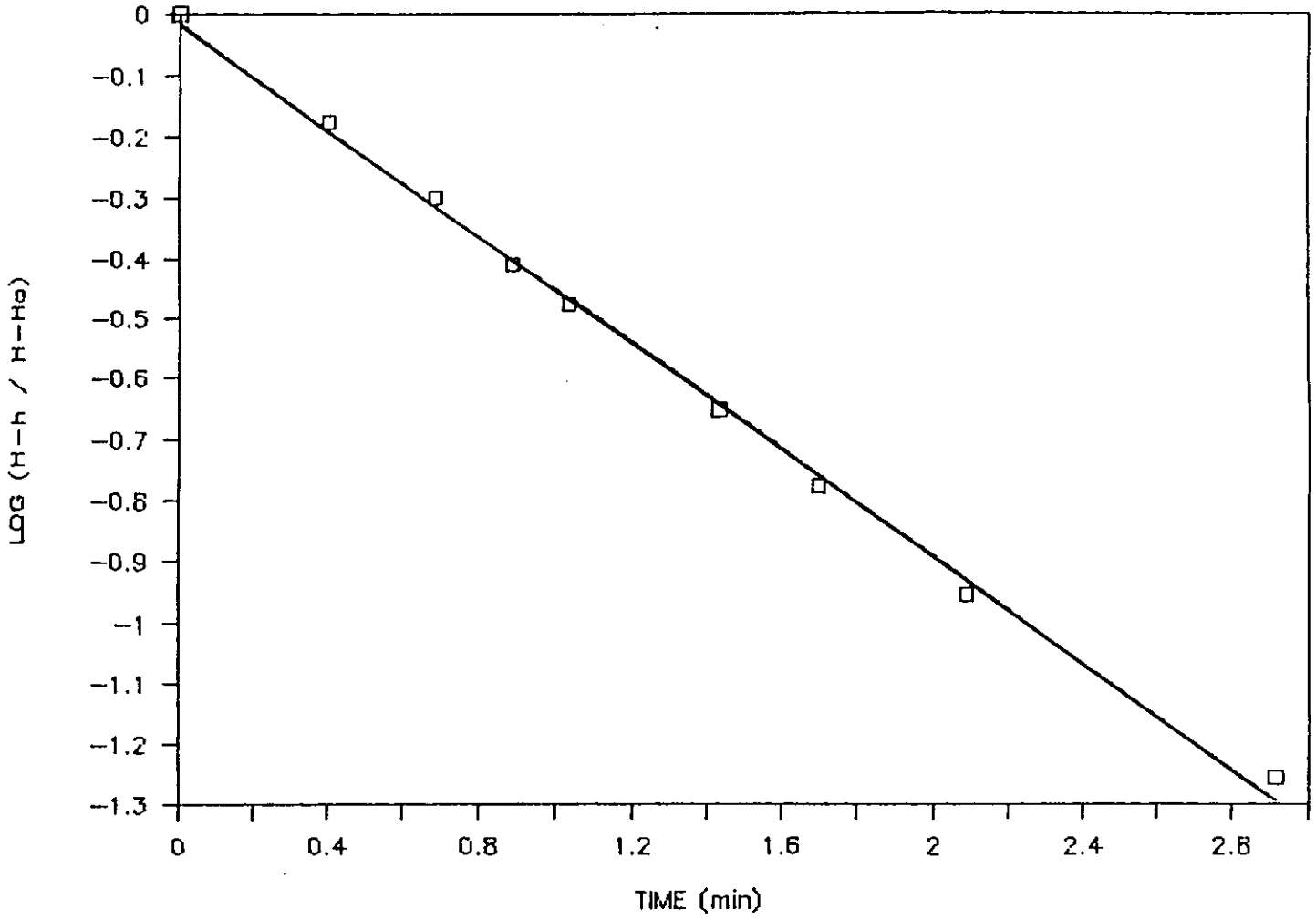

Figure D-31. Slug test result for Renfrew, piezometer #5, depth 4.6 m.

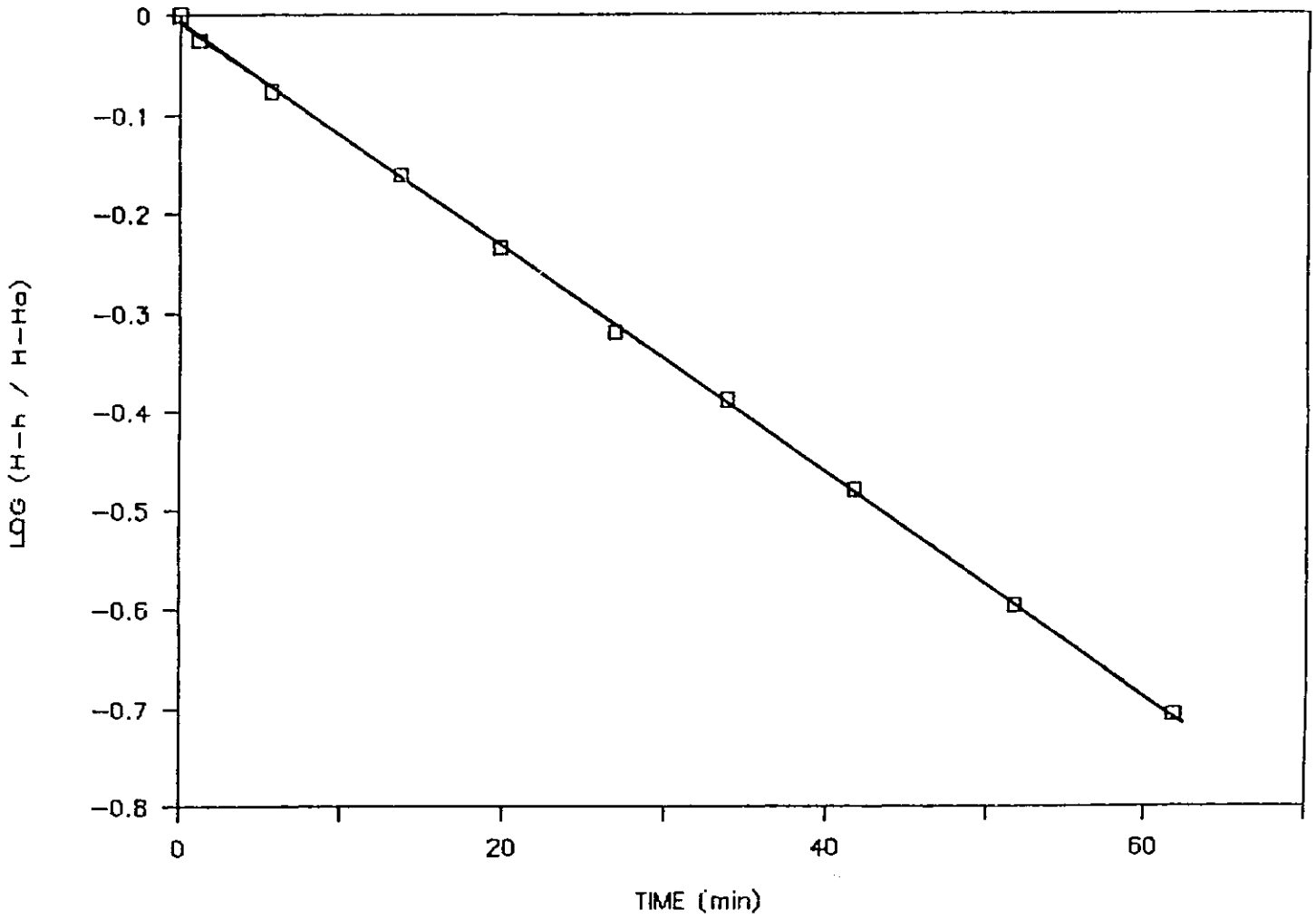

Figure D-32. Slug test result for Renfrew, piezometer #6, depth 3.1 m.

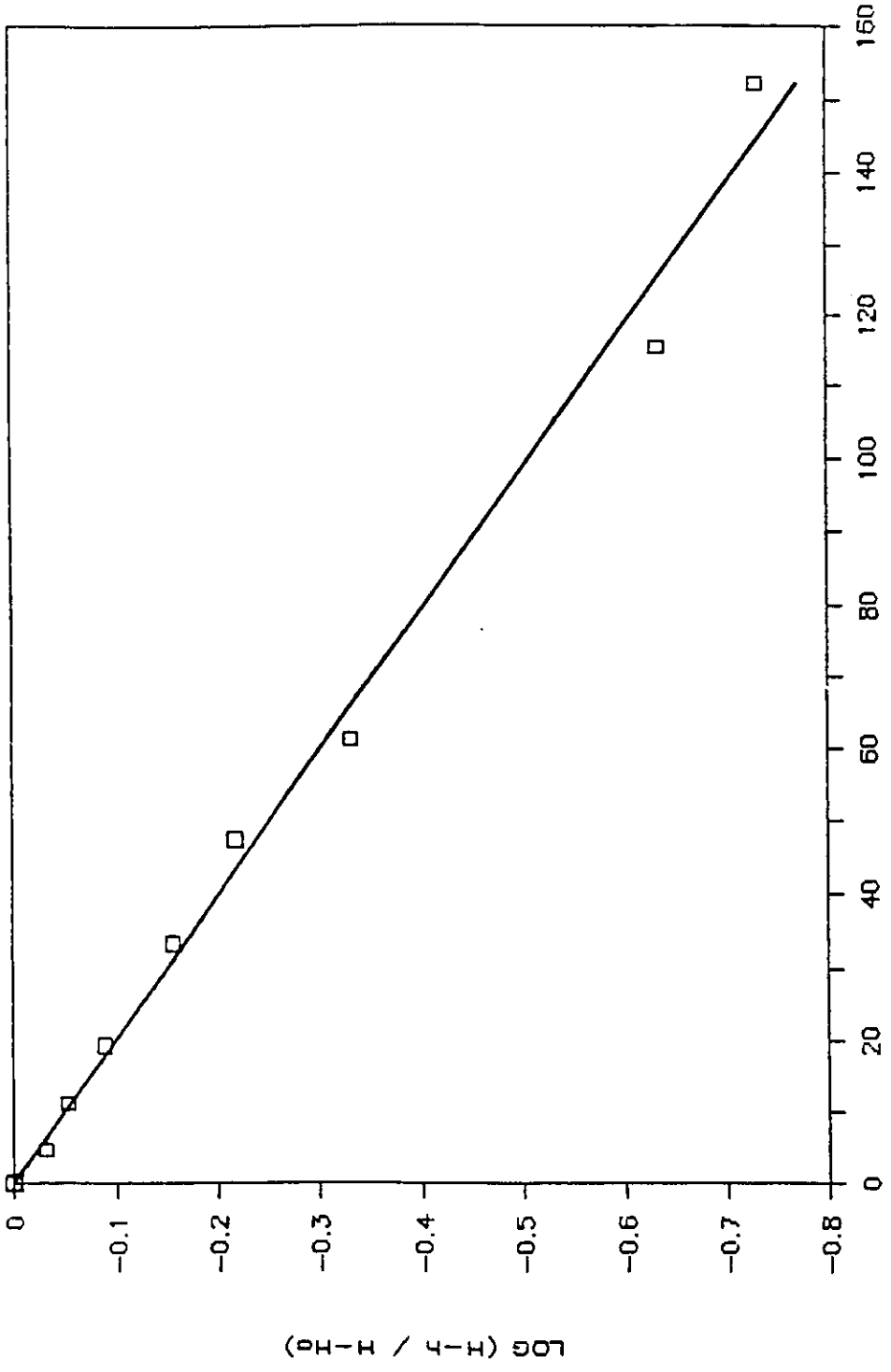

Figure D-33. Slug test result for Renfrew, piezometer #7, depth 1.5 m.

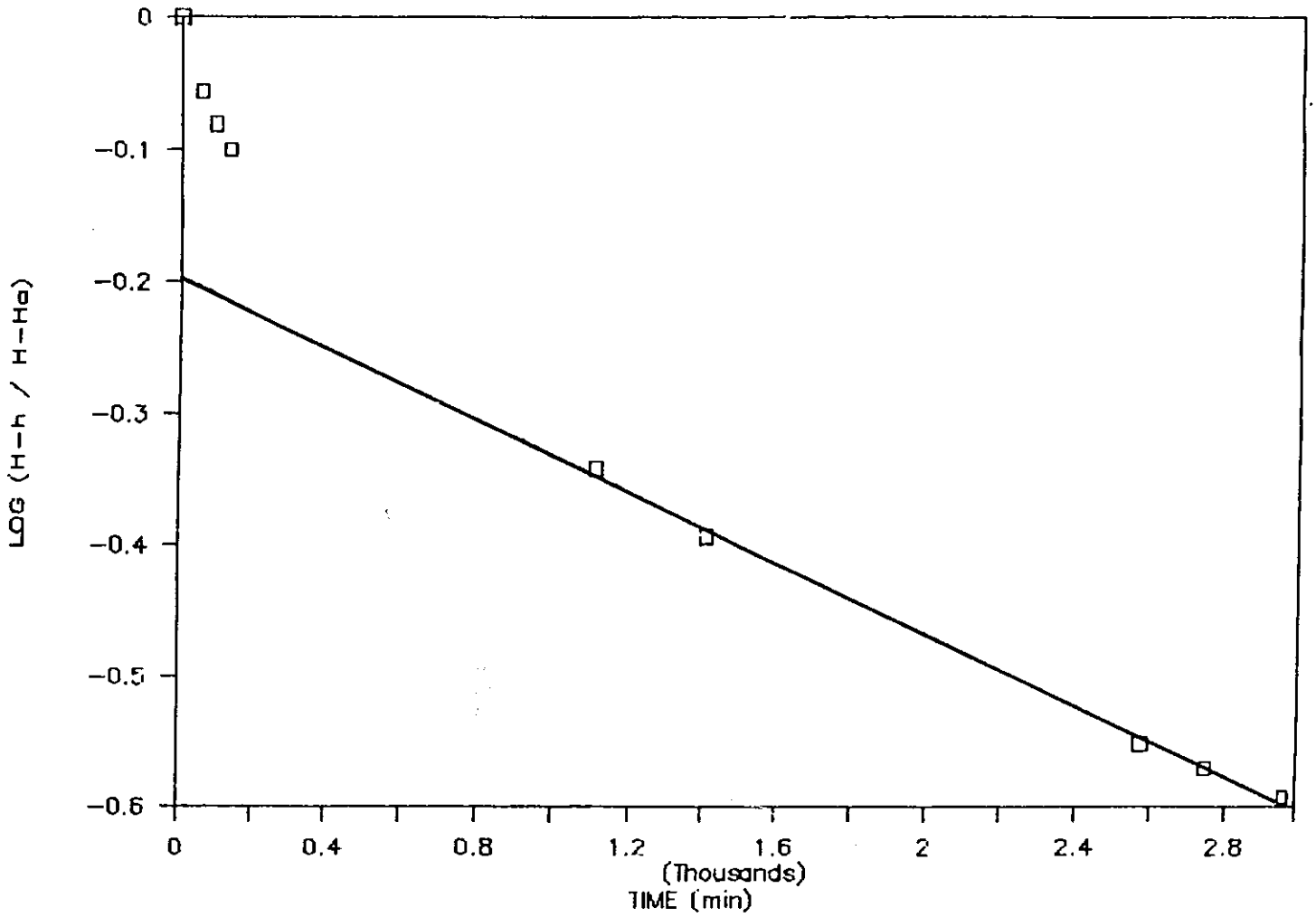

Figure D-34. Slug test result for Casselman, piezometer #1, depth 12.2 m.

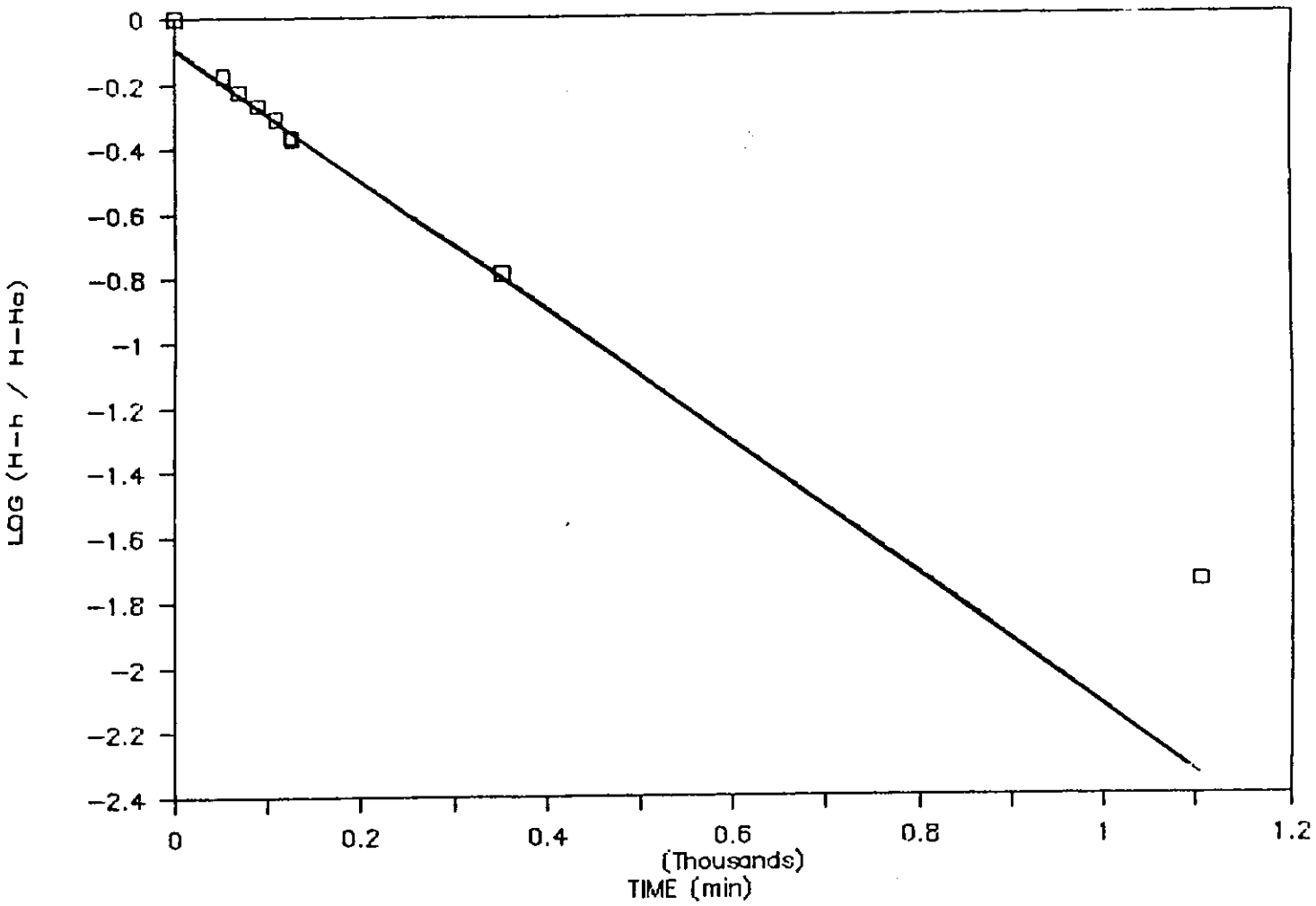

Figure D-35. Slug test result for Casselman, piezometer #2, depth 9.2 m.

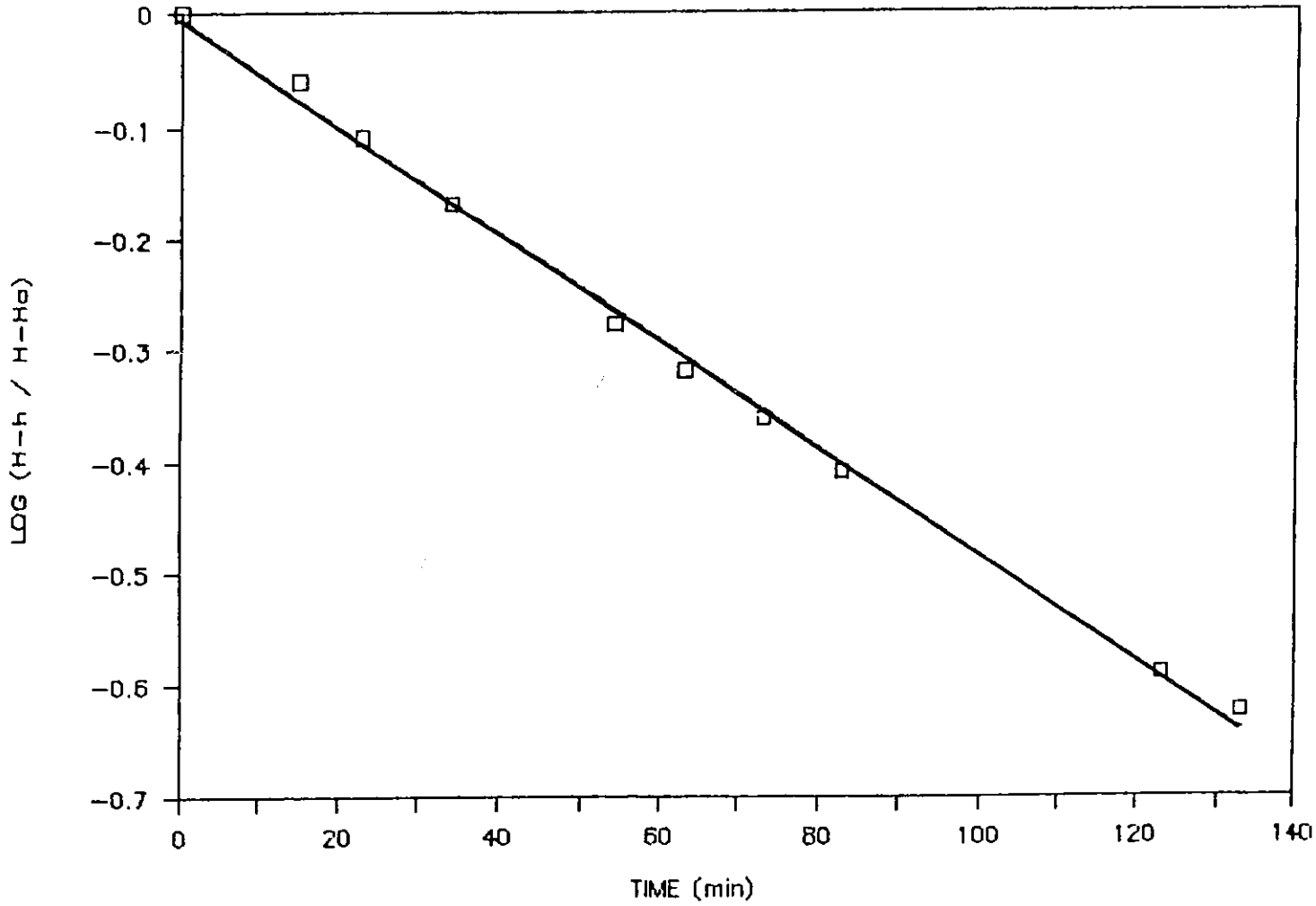

Figure D-36. Slug test result for Casselman, piezometer #3, depth 6.4 m.

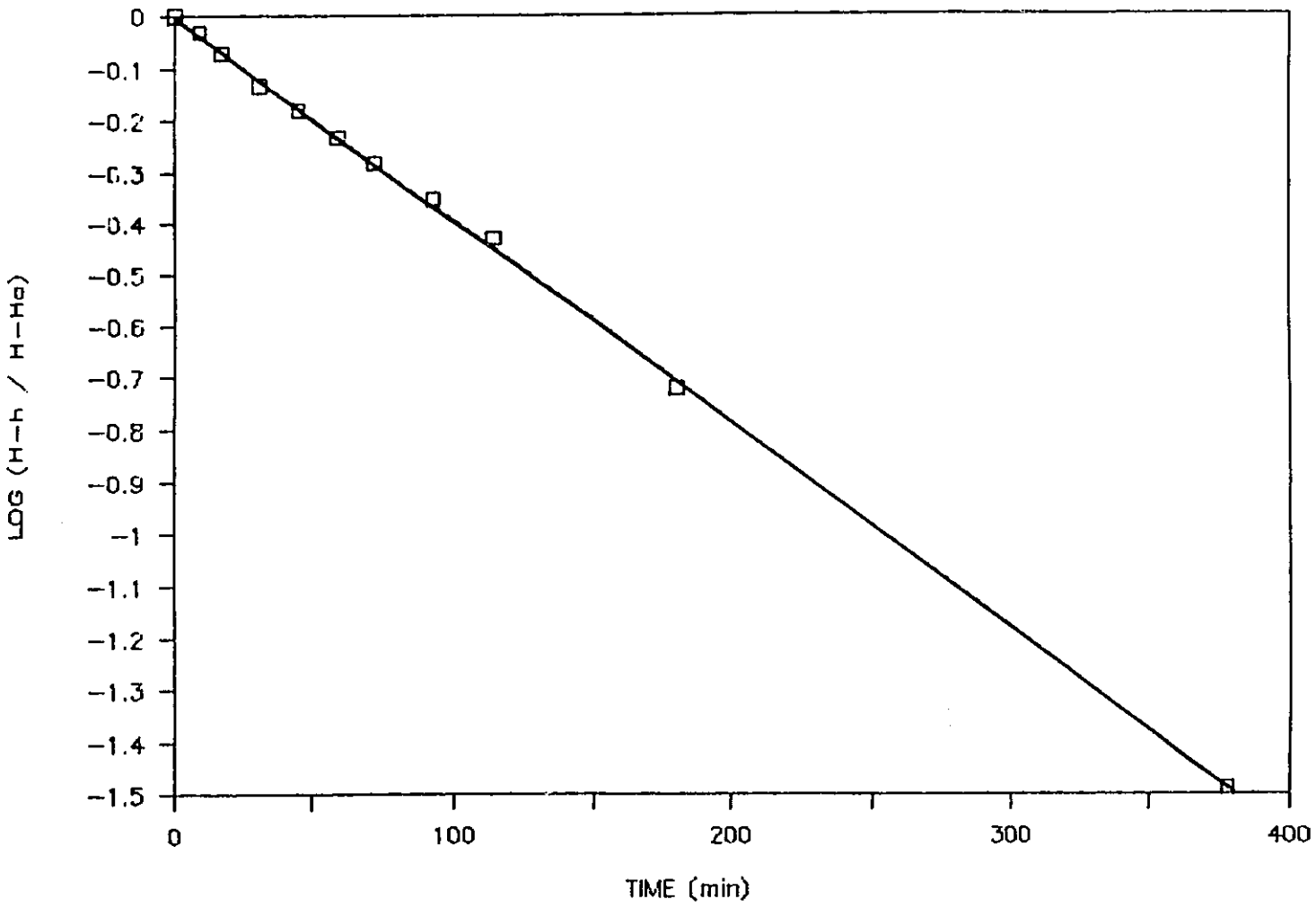

Figure D-37. Slug test result for Casselman, piezometer #4, depth 4.4 m.

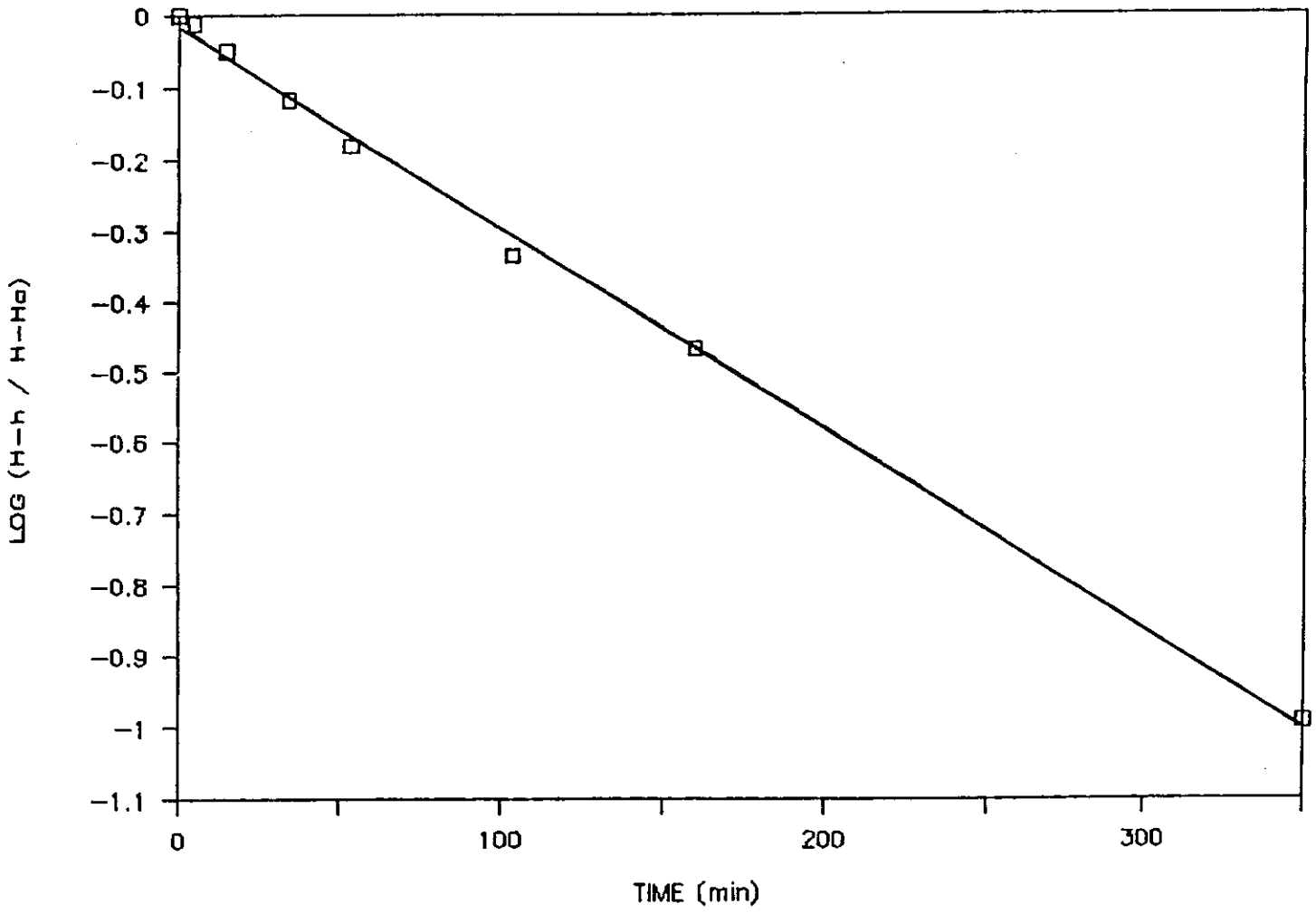

Figure D-38. Slug test result for Casselman, piezometer #5, depth 4.4 m.

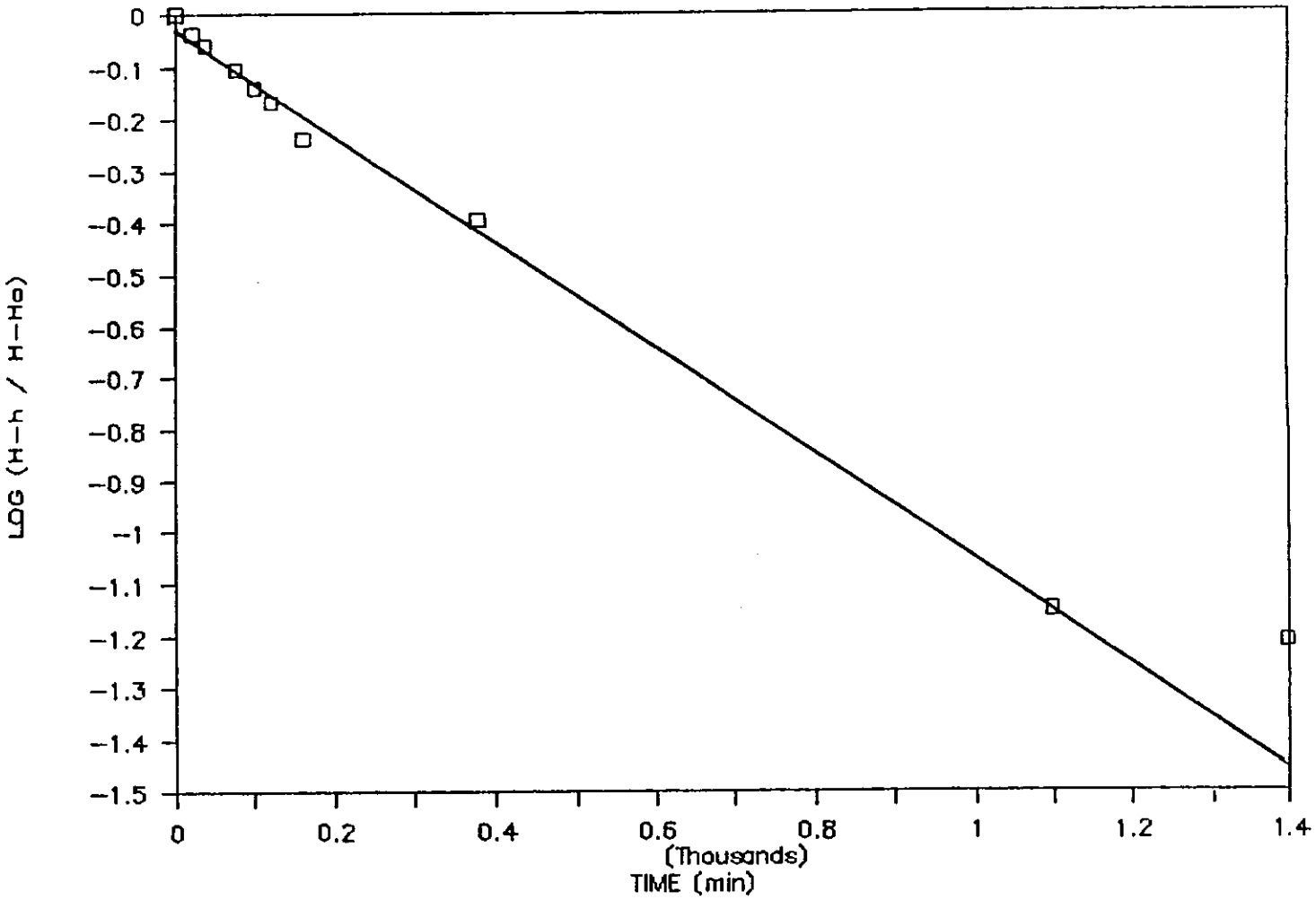

Figure D-39. Slug test result for Casselman, piezometer #6, depth 3.1 m.

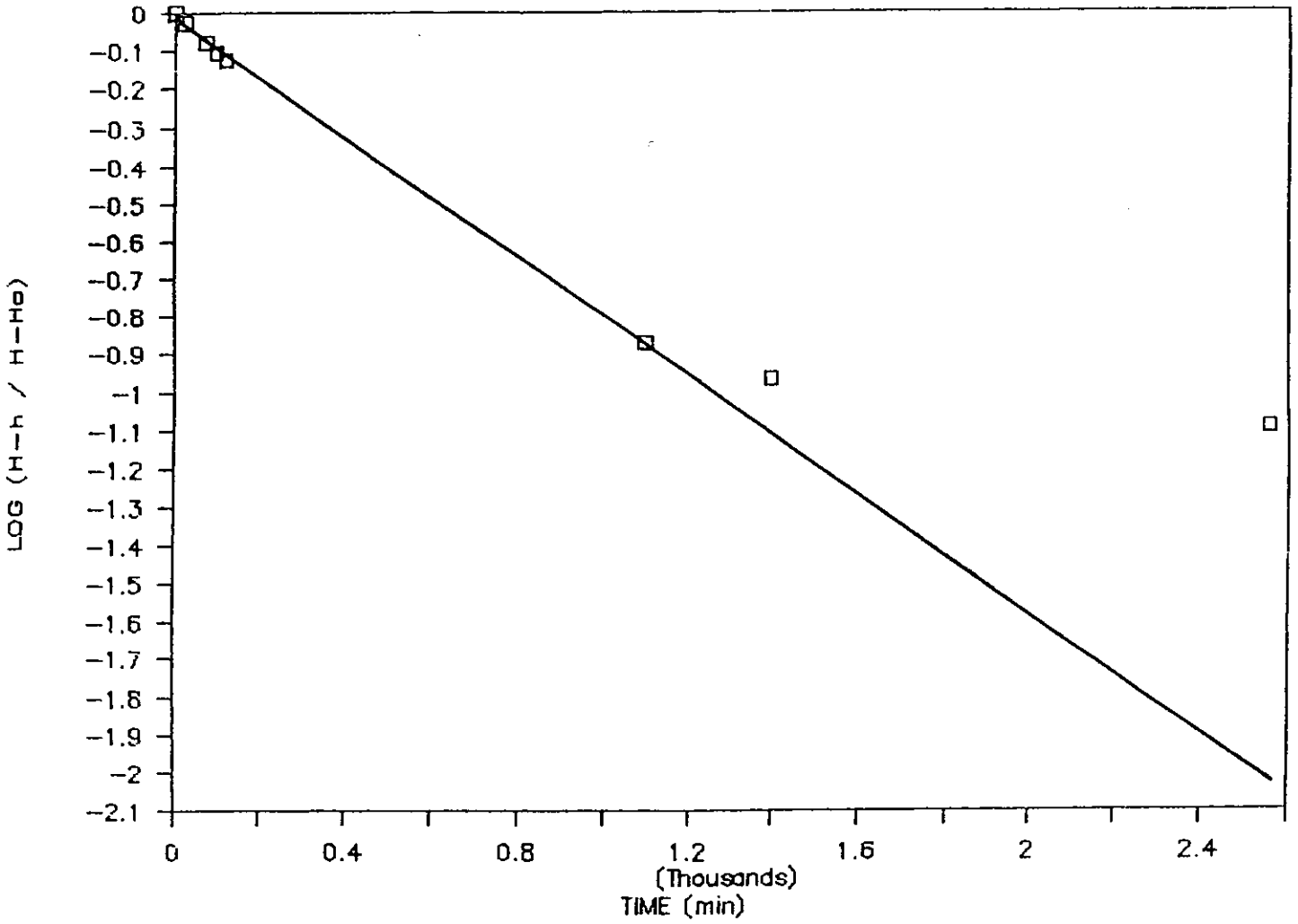

Figure D-40. Slug test result for Casselman, piezometer #7, depth 2.9 m.

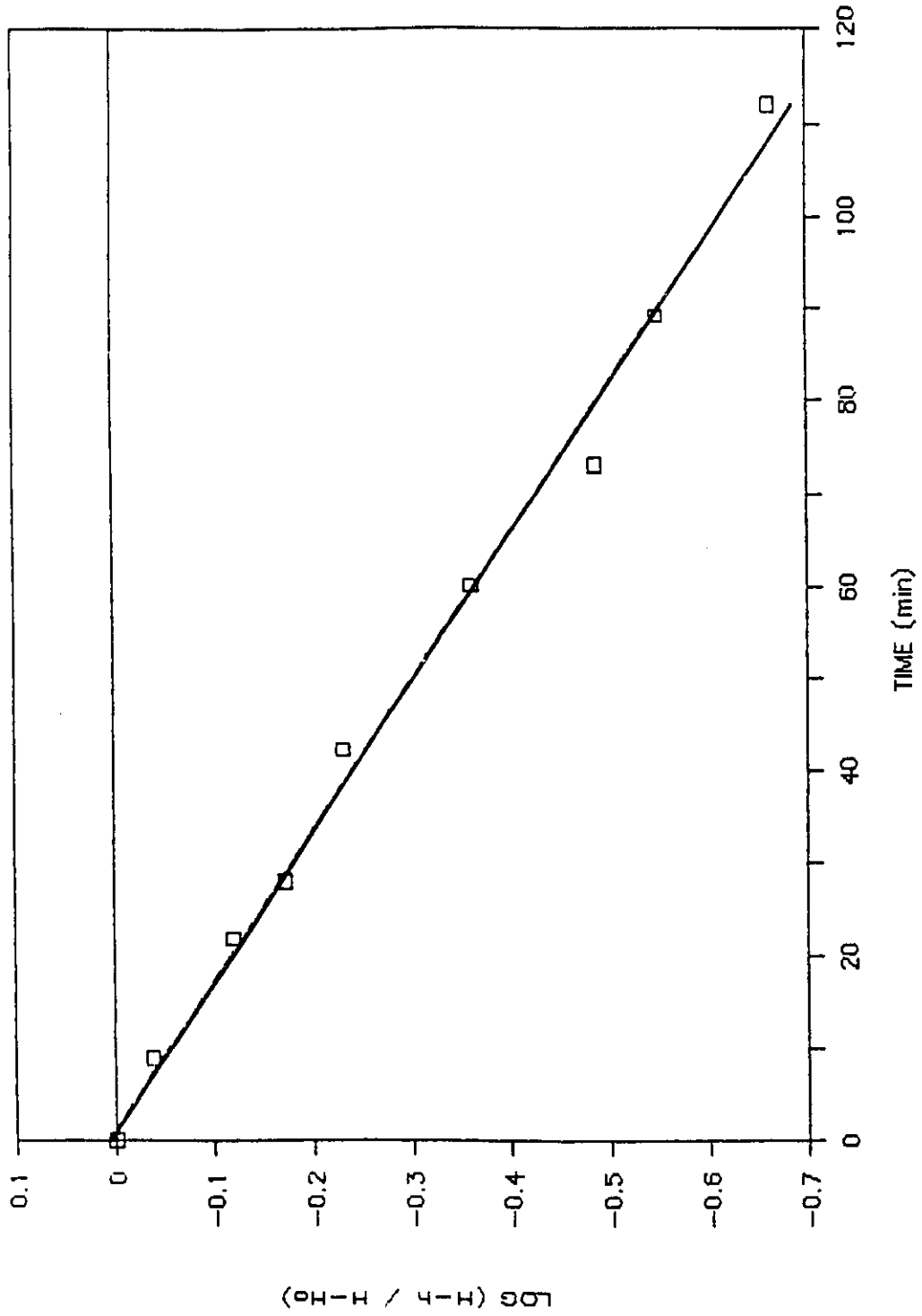

Figure D-41. Slug test result for Casselman, piezometer #8, depth 1.3 m.